Wilmington Harbor, North Carolina
Navigation Improvement Project

Integrated
Section 203 Study
&
Environmental Report

Appendix A

Engineering

February 2020

This page intentionally left blank

Table of Contents

Appendices

Table of Figures

List of Tables

This page intentionally left blank

1. Existing Conditions

1.1. Existing Project

The Cape Fear River Navigation Channel is a federally authorized and maintained navigation channel in southern North Carolina (NC), traversing the lower Cape Fear and Northeast Cape Fear Rivers. With approximately 38 miles of length, the channel connects the Atlantic Ocean at the mouth of the Cape Fear River to the Port of Wilmington (Figure 1-1). The Port of Wilmington is a major economic contributor to the region, providing facilities for general cargo and container vessels. The port is owned and maintained by the North Carolina State Ports Authority (NCSPA).

The channel is maintained by the United States Army Corps of Engineers (USACE) Wilmington District. Table 1-1 shows the authorized and currently maintained dimensions of the channel resulting from the Wilmington Harbor 96 Project improvements that began in the year 2000. Three main sections can be distinguished in this table: entrance channel (Baldhead Shoal to Battery Island), Wilmington Harbor (Lower Swash to Anchorage Basin), and northern reach (Cape Fear Memorial Bridge to just north of Hilton Railroad Bridge). Existing water depths along the northern reaches, however, are lower than the project dimensions, as these were not dredged due to lack of users (USACE, 2014). The reaches above the existing turning basin which is located in the lower section of the anchorage basin reach are not included in this proposed project.

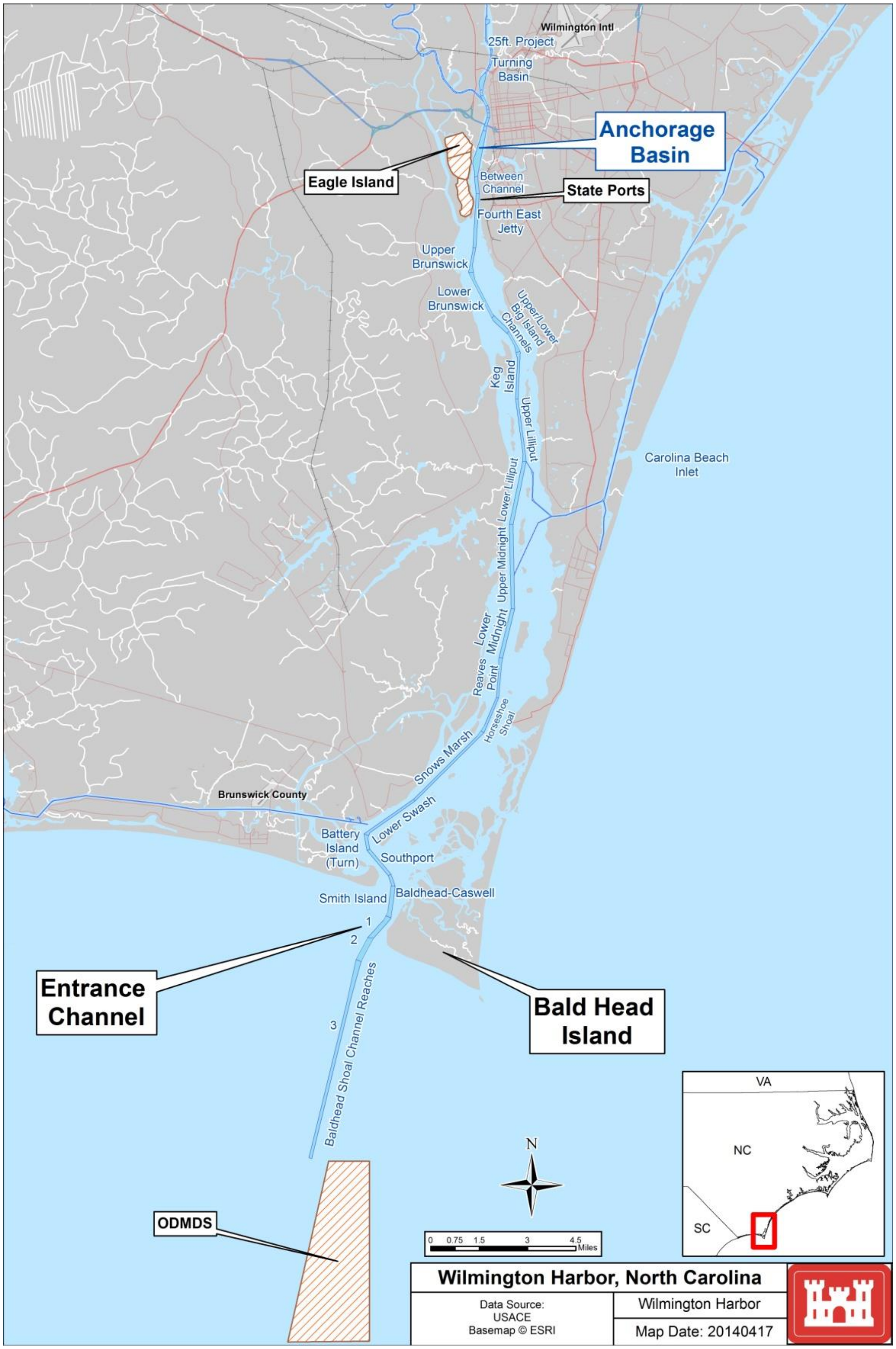

Figure 1-1: Cape Fear River Navigation Channel (USACE, 2014)

Table 1-1: Dimensions of Wilmington Harbor Navigation Channel (USACE, 2014)

Channel Name from Ocean to Upstream	Channel Length (ft)	Channel Width (ft)	Width at Turning Basin[1]	Maintained Channel Depth (ft)[2,3]	Authorized Channel Depth + Overdepth
Baldhead Shoal Reach 3	26,658	500 – 900		44	46
Baldhead Shoal Reach 2	4,342	900		44	46
Baldhead Shoal Reach 1	4,500	700 – 785		44	46
Smith Island	5,100	650		44	46
Baldhead-Caswell	1,921	500		44	46
Southport	5,363	500		44	46
Battery Island	2,589	500		44	46
Lower Swash	9,789	400		42	44
Snows Marsh	15,775	400		42	44
Horseshoe Shoal	6,102	400		42	44
Reaves Point	6,531	400		42	44
Lower Midnight[4]	8,241	600		42	44
Upper Midnight[4]	13,736	600		42	44
Lower Lilliput[4]	10,825	600		42	44
Upper Lilliput	10,217	400		42	44
Keg Island	7,726	400		42	44
Lower Big Island	3,616	400		42	44
Upper Big Island	3,533	510 – 700		42	44
Lower Brunswick	8,161	400		42	44
Upper Brunswick	4,079	400		42	44
Fourth East Jetty	8,852	500		42	44
Between	2,827	400		42	44
Anchorage Basin Station 8+00 to 84+81	7,681	550 – 1,400[5]	1,400[5]	42	44
Anchorage Basin Station 0+00 to 8+00	3,970	450 – 550		38	44
Memorial Bridge – Isabel Holmes Bridge	9,573	400	850	32	40
Isabel Holmes Bridge – Hilton RR Bridge	2,559	200 – 300		32	40
Hilton RR Bridge – Project Limit	6,718	200	700	25	36
Total Length in Feet	200,984				
Total Length in Miles	38.1				

1 Width shown is widest point at basins, and includes the channel width
2 Channel depths are at mean lower low water
3 Allowable Overdepth is two feet
4 This channel reach included the Passing Lane
5 Updated for 2016 Turning Basin Expansion

1.2. Physical Conditions

1.2.1. Water Levels

Water level measurements were available at Station 8658120 maintained by the Center for Operational Oceanographic Products and Services (CO-OPS) of the National Oceanic and Atmospheric Administration (NOAA). Information about the station is presented in Table 1-2 and its location is shown in Figure 1-2.

Table 1-2: Station Description and Tidal Datums for Station 8658120

Parameter	**Station 8658120**
Location	77.95°W, 34.23°N
Station name	Wilmington, NC
Period of available data	Jan 1936 to Sep 2017 (active)
Datum	
Mean Higher High Water	0.65 m (2.14 ft)
Mean High Water	0.57 m (1.87 ft)
Mean Sea Level	–0.03 m (–0.10 ft)
Mean Low Water	–0.72 m (–2.36 ft)
Mean Lower Low Water	–0.77 m (–2.54 ft)
NAVD88	0.00

Station 8658120 is located approximately at 25 miles from the river mouth. Figure 1-3 shows the percent exceedance of water levels at this location.

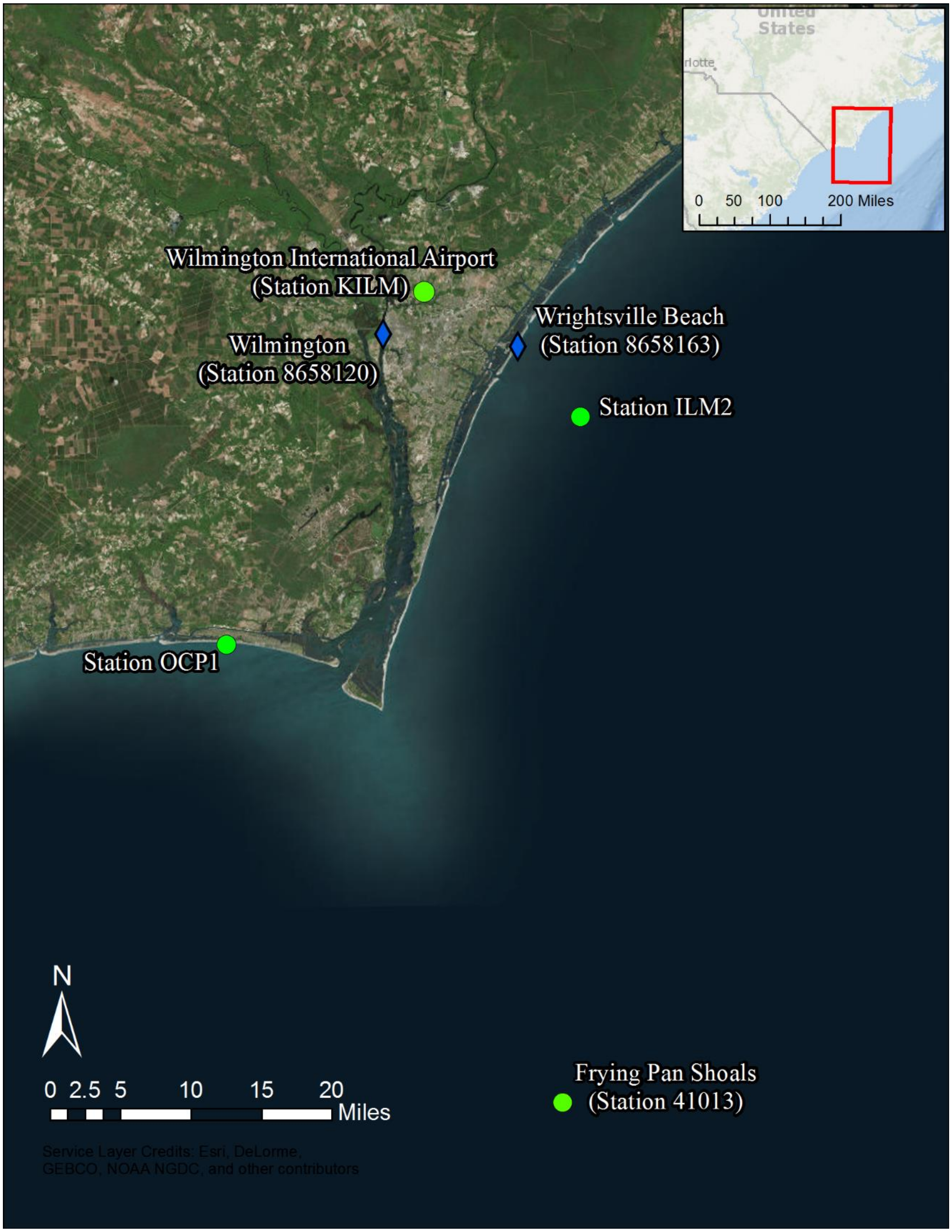

Figure 1-2: Location of water level and wind measurements

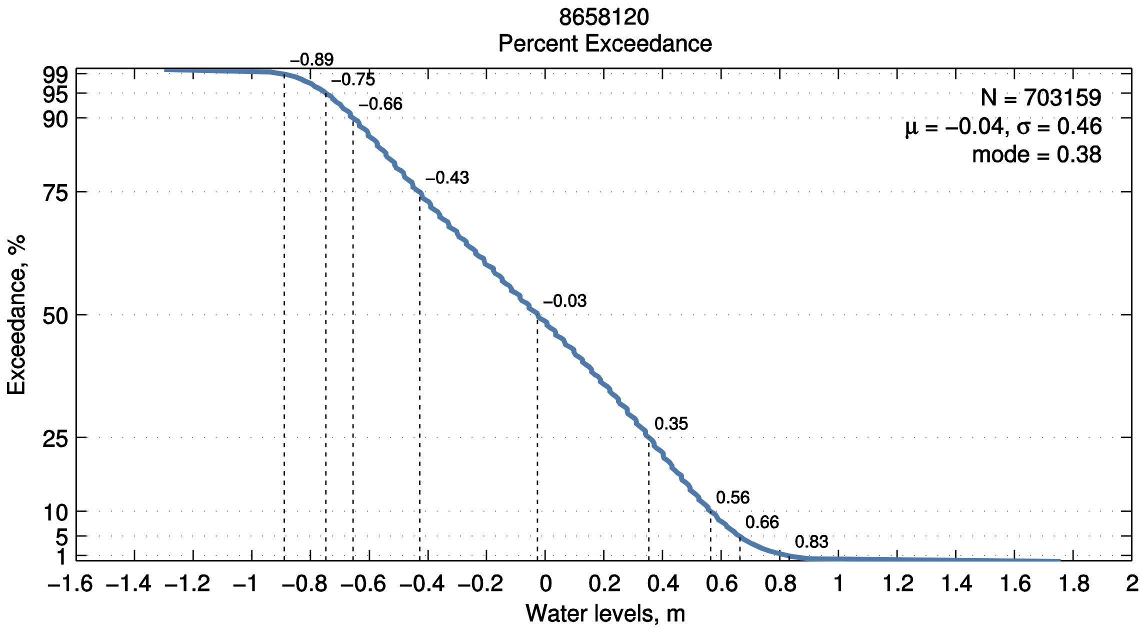

Figure 1-3: Percent exceedance of measured water levels (NAVD88) at Station 8658120

1.2.2. Wind

NOAA National Centers for Environmental Information (NCEI) hosts and provides access to comprehensive oceanic, atmospheric, and geophysical data. A wide range of data products such as topo-bathymetric data, satellite observations, ocean profile data, ocean climatology (satellite and in-situ), and water quality data are available from NCEI.

NOAA National Data Buoy Center (NDBC) designs, develops and operates a network of data collection buoys and coastal stations in the United States. Real-time and historical measurements are accessible online. The data consists of standard meteorological observations for ocean and atmospheric characteristics. Parameters such as wind speed, direction, sea-level air pressure, and temperature are measured at land stations. Floating buoys may record additional information such as wave height, wave period and directions, and sea surface temperature.

Weather observed using stations located at airports are available as Meteorological Terminal Air Reports (METAR). The historic records can be obtained, for example, from the Weather Underground website (www.wunderground.com). In general, data consists of hourly reports of wind speed, wind direction, wind gust speed, sea level air pressure, air temperature, and visibility.

Wind records were retrieved at NDBC Station 41013, METAR Station KILM at Wilmington International Airport, NC, and NCEI stations ILM2 and OCP1. The station locations are shown in Figure 1-2. The information of wind stations is listed in Table 1-3.

Table 1-3: Wind data stations

Source	Station	Anemometer elevation (ft)	Start date	End date	Frequency	Wind averaging
NCEI	ILM2	9.8	June 6, 2005	Dec 31, 2013	2 hr	Unknown
NCEI	OCP1	9.8	May 23, 2006	Dec 31, 2013	1 min before 2008 15 min after 2008	Unknown
NDBC	41013	13.1	Nov 10, 2003	Sep 19, 2017 (active)	1 hr	8-min
METAR	KILM	33	June 1, 1942	Sep 5, 2017 (active)	1 hr	2-min

Data analysis were done for wind measurements at these four stations. The annual and seasonal wind roses are shown from Figure 1-4 to Figure 1-11. Wind data plotted in the wind roses were converted to a standard 10 m (33 ft) elevation using ISO 19901-1:2005(E) formulation.

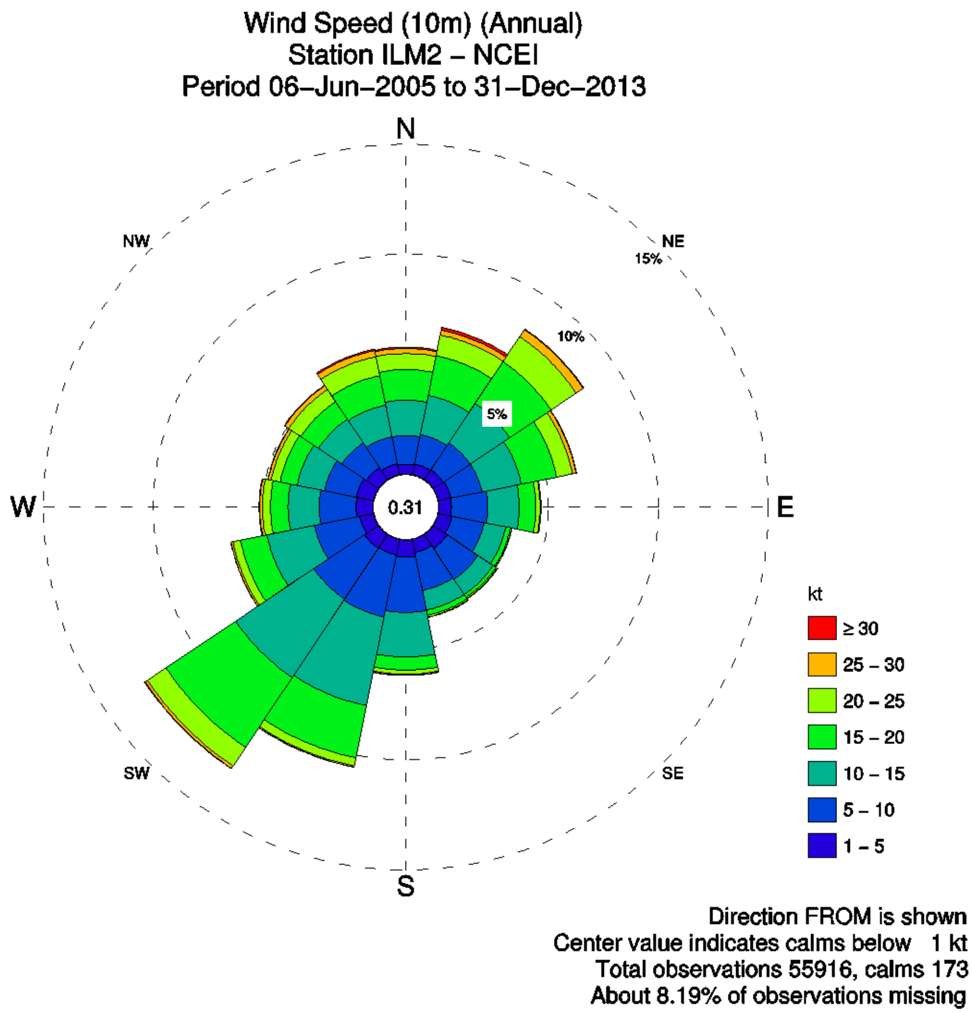

Percentage of Occurrence

Wind Speed (10m), kt	N	NNE	NE	ENE	E	ESE	SE	SSE	S	SSW	SW	WSW	W	WNW	NW	NNW	Total
Total	5.77	6.83	8.24	6.42	4.65	3.42	3.52	3.61	6.16	10.57	12.81	6.62	5.17	4.91	5.16	5.82	99.69
30+		0.13															0.51
25–30	0.23	0.23	0.38	0.18							0.13		0.12	0.14	0.21	0.28	2.14
20–25	0.73	0.95	1.37	0.73	0.19				0.18	0.38	1.02	0.35	0.36	0.42	0.66	0.89	8.44
15–20	1.39	1.85	2.28	1.64	0.76	0.22	0.17	0.24	0.60	2.42	3.82	1.23	0.80	0.78	0.97	1.36	20.52
10–15	1.60	1.81	2.16	1.83	1.43	1.01	0.83	0.90	2.02	4.11	4.28	2.21	1.42	1.27	1.29	1.47	29.63
5–10	1.30	1.36	1.47	1.44	1.65	1.49	1.68	1.76	2.52	2.87	2.77	2.09	1.67	1.47	1.34	1.26	28.14
1–5	0.45	0.50	0.55	0.58	0.58	0.63	0.76	0.61	0.78	0.72	0.76	0.65	0.77	0.80	0.67	0.50	10.31

Figure 1-4: Annual wind speed rose at NCEI Station ILM2

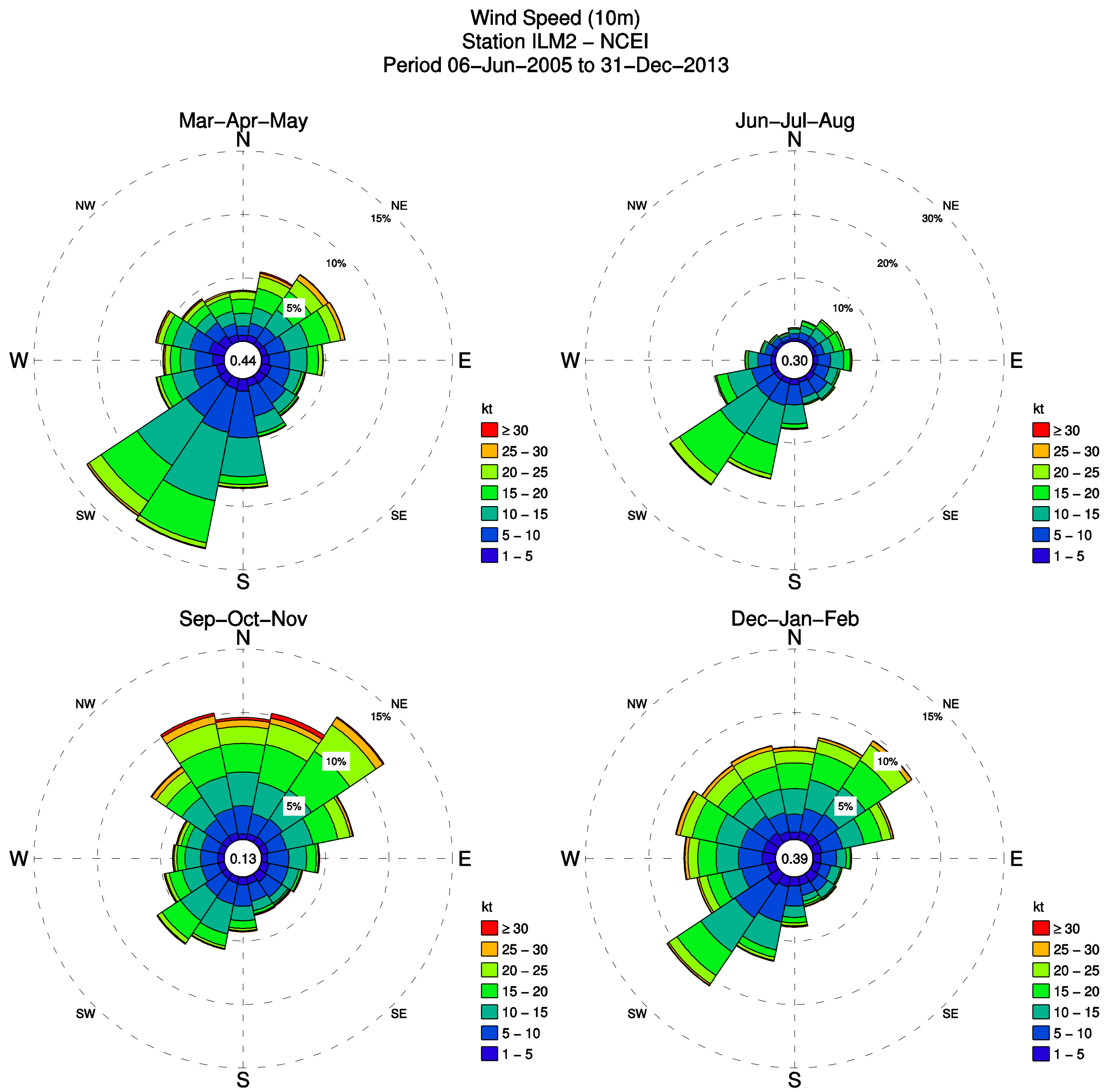

Figure 1-5: Seasonal wind speed rose at NCEI Station ILM2

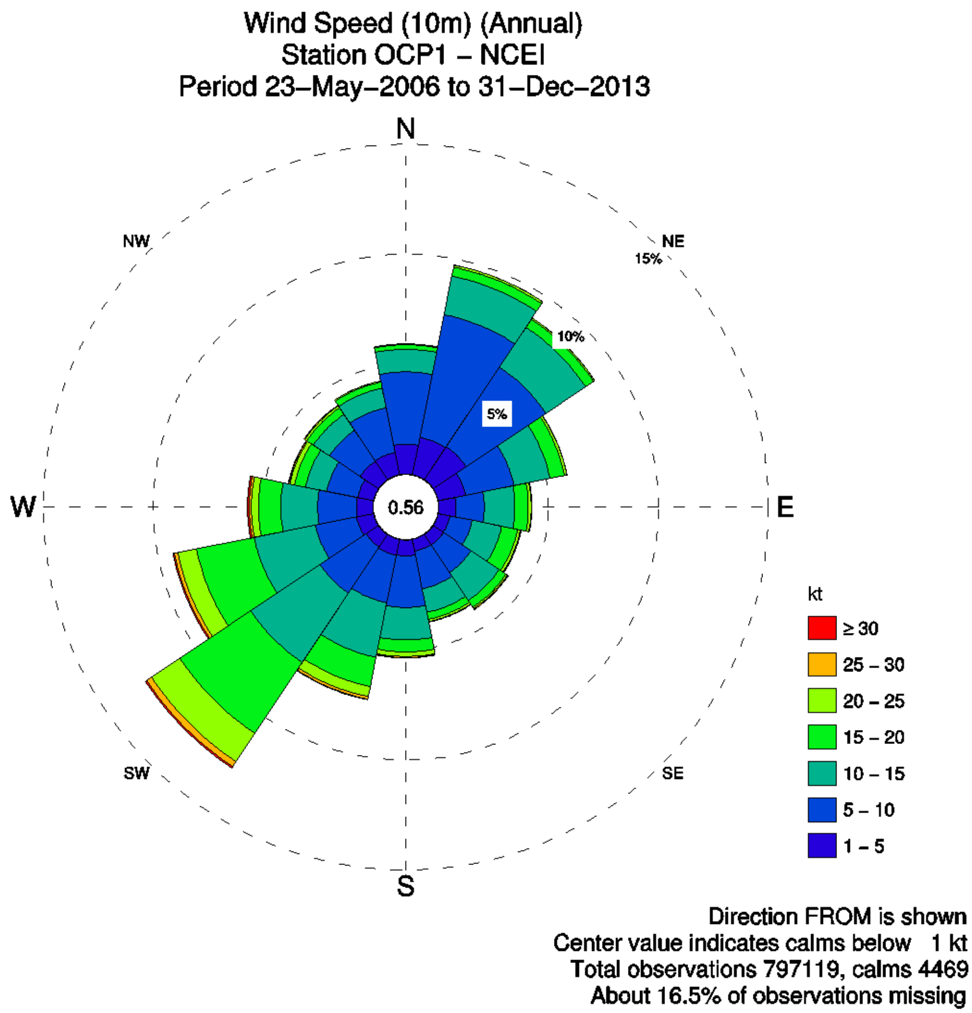

Percentage of Occurrence

Wind Speed (10m), kt	N	NNE	NE	ENE	E	ESE	SE	SSE	S	SSW	SW	WSW	W	WNW	NW	NNW	Total
Total	5.92	9.72	8.85	5.98	4.23	3.86	4.11	3.83	5.35	7.43	12.77	9.31	5.71	3.95	4.07	4.35	99.44
≥ 30																	0.35
25–30										0.12	0.28	0.16	0.10				0.94
20–25				0.11	0.13	0.13		0.10	0.21	0.47	1.55	0.87	0.33	0.21	0.11		4.53
15–20	0.21	0.42	0.44	0.67	0.61	0.74	0.38	0.32	0.54	1.36	3.88	2.67	1.01	0.52	0.35	0.28	14.40
10–15	1.02	1.78	2.17	1.68	1.39	1.37	1.53	1.09	1.47	2.52	3.78	2.85	1.67	0.98	0.88	0.91	27.10
5–10	3.28	5.68	4.36	2.25	1.29	1.03	1.50	1.74	2.36	2.20	2.53	1.90	1.77	1.44	1.68	2.07	37.09
1–5	1.36	1.74	1.80	1.26	0.78	0.54	0.57	0.55	0.71	0.73	0.68	0.79	0.76	0.73	1.01	1.03	15.04

Figure 1-6: Annual wind speed rose at NCEI Station OCP1

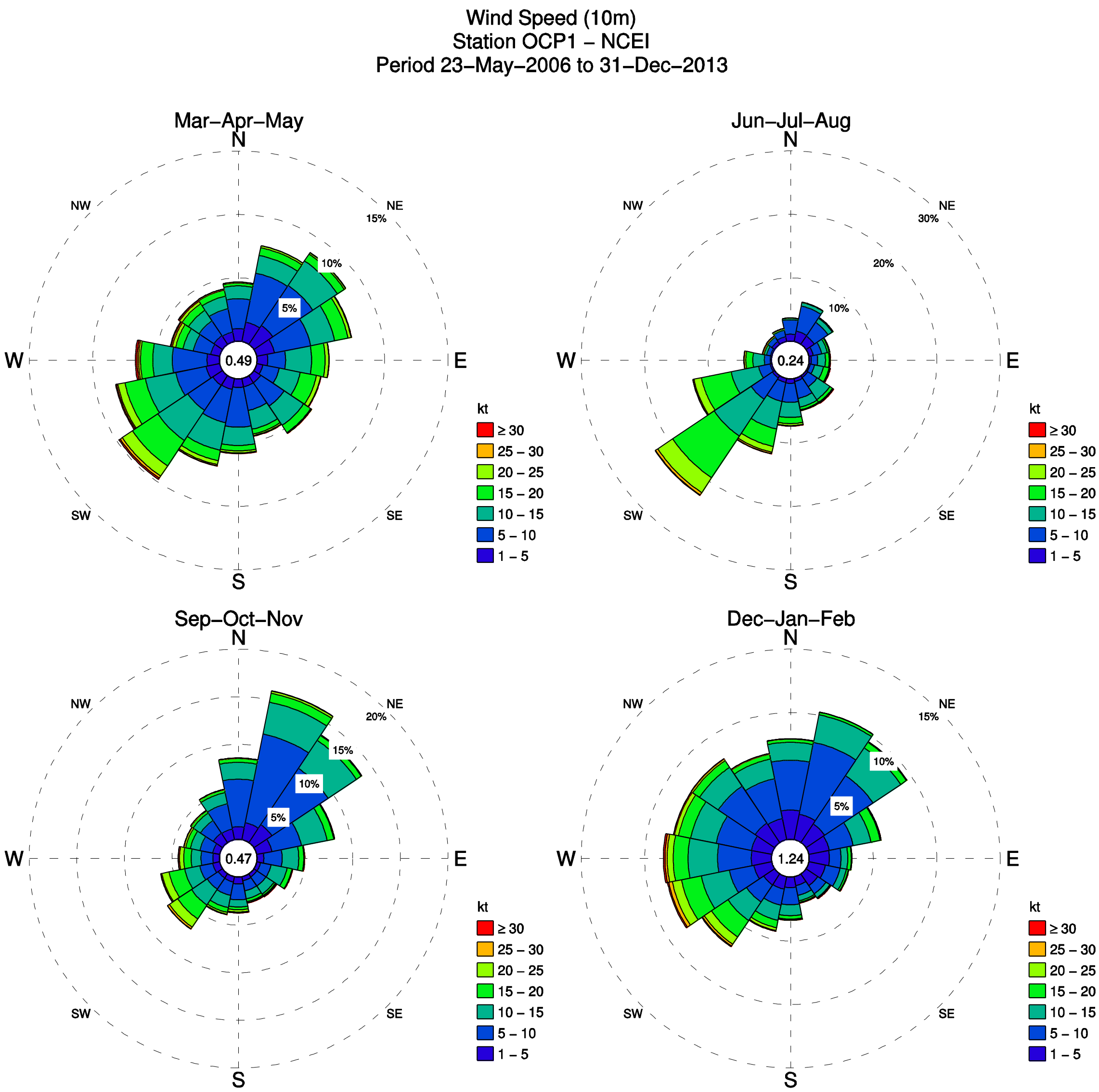

Figure 1-7: Seasonal wind speed rose at NCEI Station OCP1

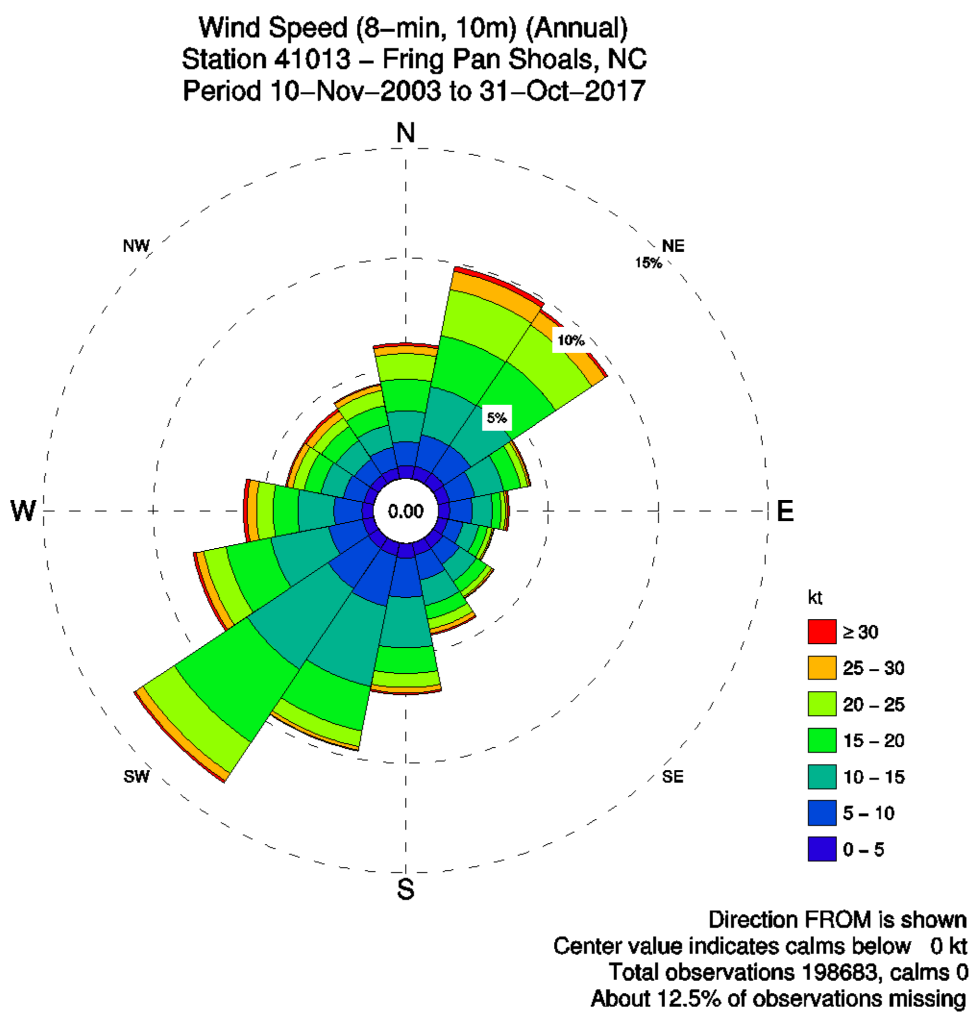

Percentage of Occurrence

Wind Speed (8–min, 10m), kt	N	NNE	NE	ENE	E	ESE	SE	SSE	S	SSW	SW	WSW	W	WNW	NW	NNW	Total
Total	6.14	9.84	9.54	4.31	3.21	2.59	3.32	4.28	6.87	9.65	13.40	8.37	5.89	4.08	4.09	4.40	100.00
30+	0.12	0.22	0.13									0.12	0.17		0.13		1.52
25–30	0.36	0.85	0.72	0.11				0.22	0.24	0.17	0.42	0.38	0.43	0.27	0.36	0.26	4.99
20–25	1.17	2.14	1.98	0.32	0.21	0.21	0.26	0.45	0.63	0.73	1.71	1.03	0.75	0.53	0.48	0.70	13.29
15–20	1.44	2.38	2.41	0.80	0.40	0.41	0.58	0.64	1.16	2.08	3.98	2.08	1.12	0.78	0.79	0.91	21.95
10–15	1.42	2.22	2.23	1.34	0.92	0.73	0.93	1.19	2.31	3.72	4.43	2.69	1.66	1.03	1.02	1.03	28.87
5–10	1.09	1.48	1.49	1.17	1.02	0.71	0.91	1.16	1.79	2.35	2.20	1.57	1.27	0.97	0.87	0.97	21.04
0–5	0.54	0.56	0.58	0.52	0.49	0.44	0.53	0.55	0.65	0.58	0.56	0.51	0.49	0.44	0.45	0.48	8.35

Figure 1-8: Annual wind speed rose at NDBC Station 41013

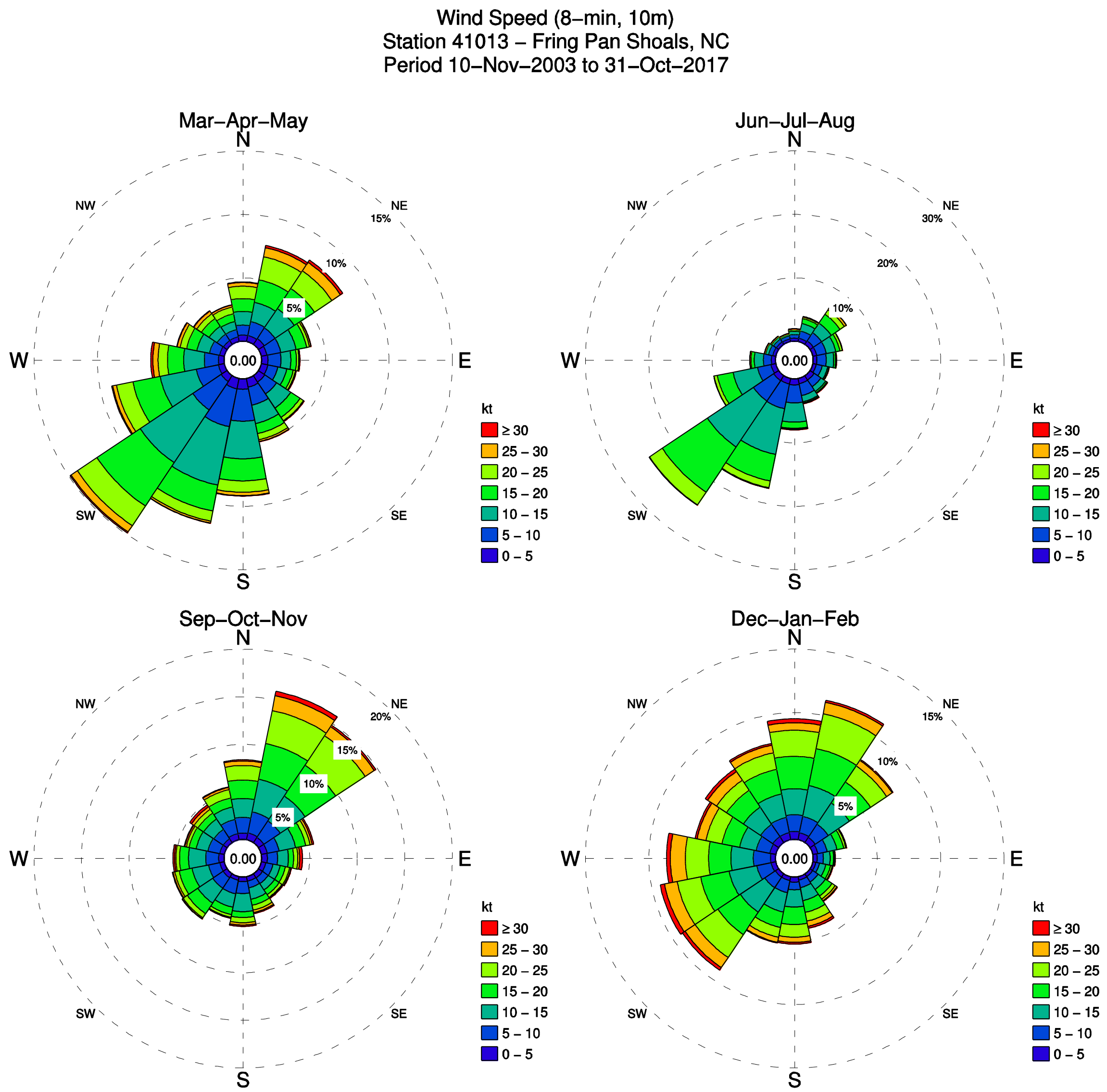

Figure 1-9: Seasonal wind speed rose at NDBC Station 41013

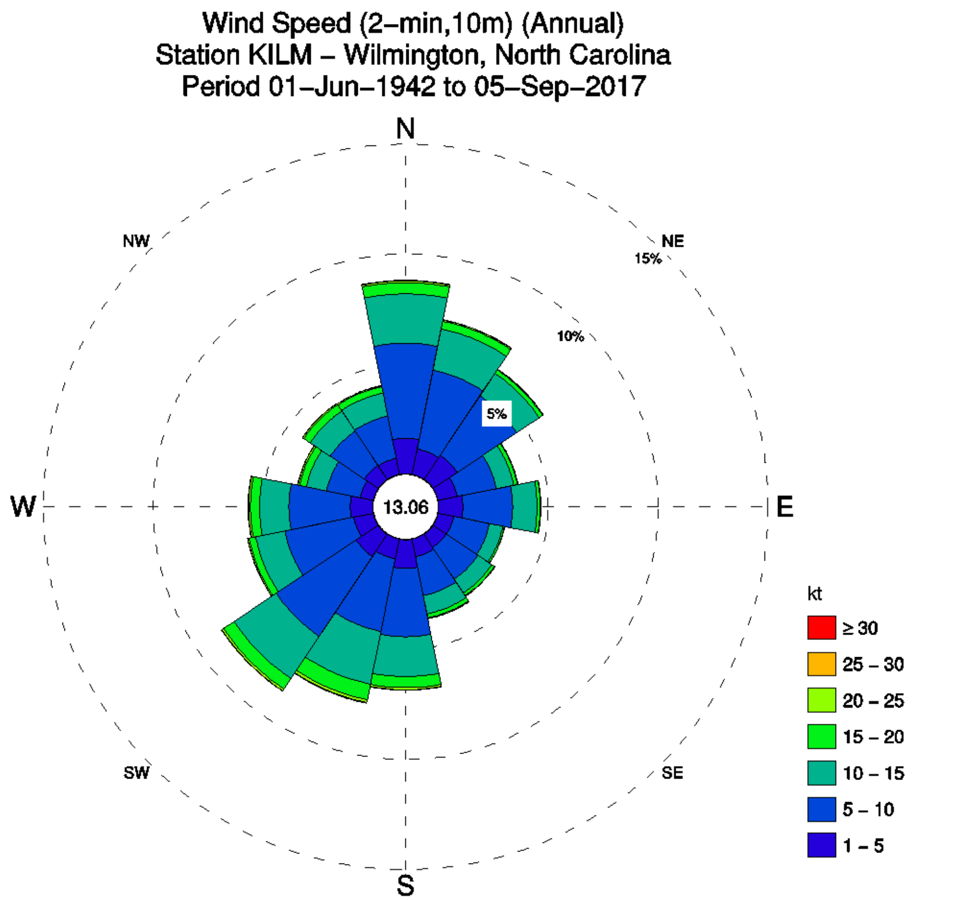

Direction FROM is shown
Center value indicates calms below 1 kt
Total observations 648211, calms 84645
About 5.18% of observations missing

Percentage of Occurrence

Wind Speed (2–min,10m), kt	N	NNE	NE	ENE	E	ESE	SE	SSE	S	SSW	SW	WSW	W	WNW	NW	NNW	Total
Total	8.80	7.18	6.04	3.72	4.65	3.10	3.40	3.69	6.85	7.61	8.59	5.84	5.68	3.52	4.16	4.13	86.94
30																	
25–30																	0.18
20–25										0.13							0.91
15–20	0.52	0.37	0.19	0.17	0.14		0.14	0.18	0.51	0.73	0.57	0.31	0.41	0.32	0.35	0.29	5.28
10–15	2.24	1.90	1.23	0.80	1.12	0.62	0.77	0.85	1.81	2.44	2.31	1.36	1.34	0.93	1.10	1.07	21.90
5–10	4.33	3.65	3.26	1.81	2.26	1.66	1.74	1.81	3.11	3.36	4.37	3.19	2.79	1.56	1.87	1.95	42.71
1–5	1.61	1.19	1.31	0.90	1.11	0.73	0.72	0.80	1.29	0.92	1.22	0.92	1.03	0.61	0.77	0.74	15.87

Figure 1-10: Annual wind speed rose at METAR Station KILM

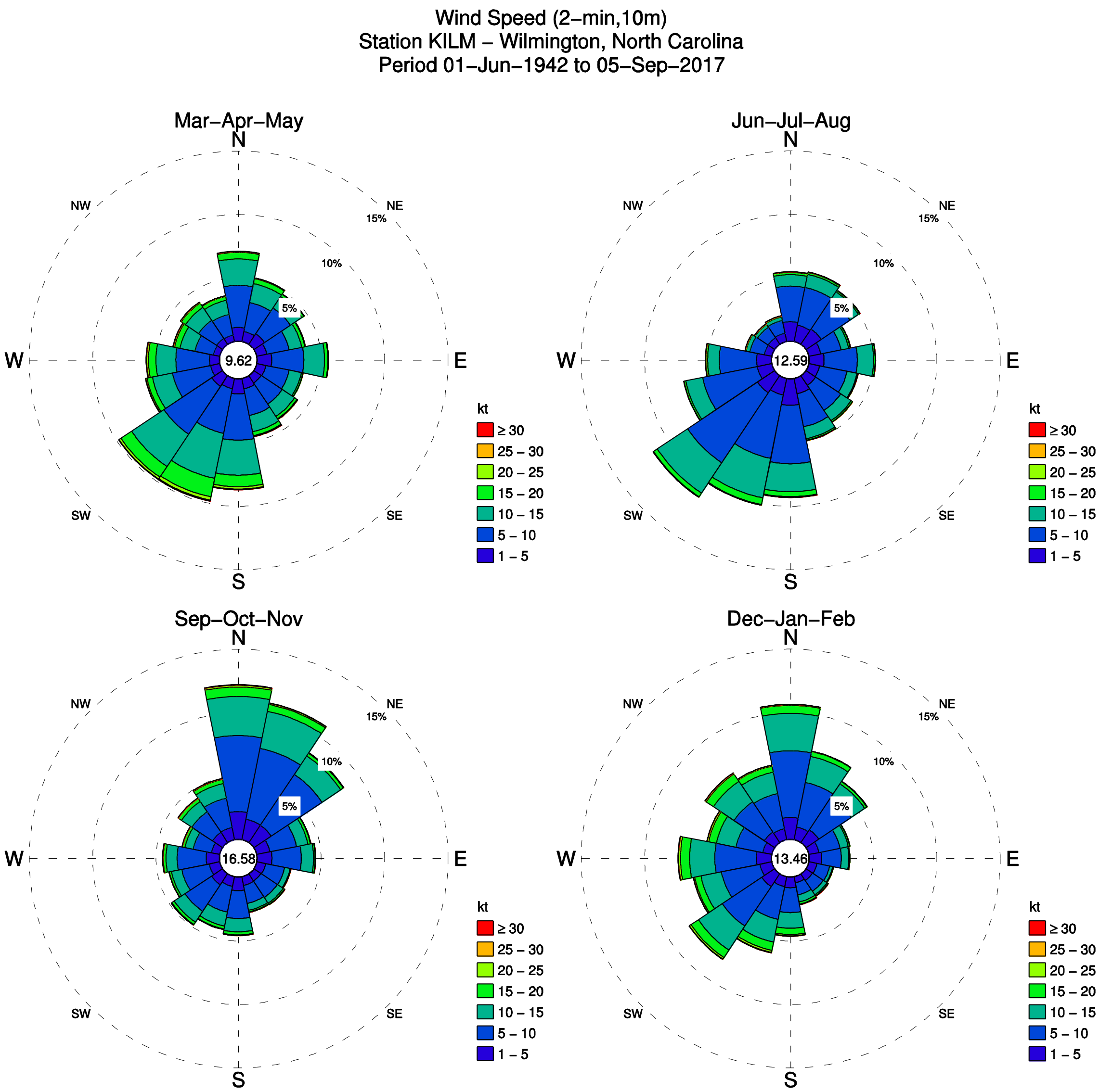

Figure 1-11: Seasonal wind speed rose at Station KILM

The wind roses show that the wind field in the estuary varies seasonally. Winds are predominantly from N–NE between September and December, while between March and August they are predominantly from S–SW. This indicates that during summer, the winds are from sea to land, during fall, the winds are from land to sea, winter months do not have a specific characteristic.

Annual wind roses at Station ILM2, OCP1, and 41013 show that the dominance of winds from S-SW directions is higher in the offshore area, primarily due to the fetch available.

Percent exceedance values of wind speeds at the four stations were calculated and are presented in Table 1-4.

Table 1-4: Statistics for wind speeds (knots)

Station	75%	50%	25%	10%	5%	1%	Max	Mean
ILM2	7.8	11.8	16.3	20.4	22.9	28.0	42.3	12.3
OCP1	6.3	9.6	13.9	18.1	20.5	25.9	47.9	10.5
41013	9.3	13.7	18.5	23.2	26.0	31.2	40.4	15.6
KILM	4.0	7.0	10.0	13.0	15.0	20.0	74.0	7.1

Analysis of percent exceedance plots show that, as it is generally observed, wind speeds over the land station (Station KILM) are lower than that of the stations that are located on the coast (Station OCP1), or offshore (Stations ILM2, 41013).

The highest wind speed recorded was 74 knots at Station KILM during Hurricane Helene, whose closest approach to the Cape Fear River estuary area was on September 27, 1958. The track of Hurricane Helen is shown in Figure 1-12.

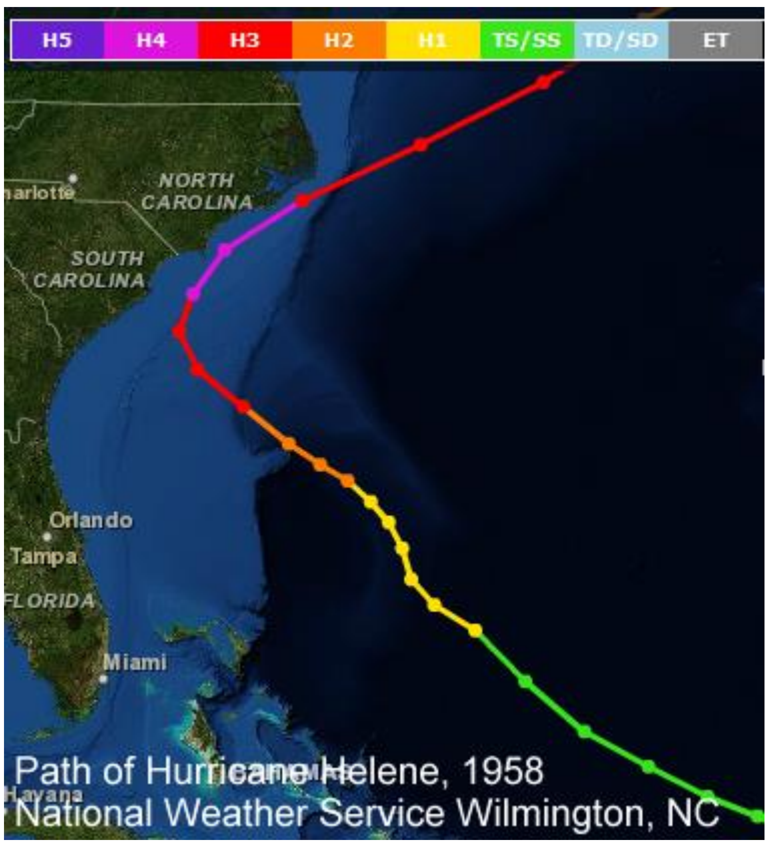

Figure 1-12: Track of Hurricane Helene (from National Weather Service)

Hindcast data from the NOAA Climate Forecast System (CFS) model and the USACE Wave Information System (WIS) are available in the project area. NOAA CFS data is available at a continuous spatial coverage.

1.2.3. Waves

There are five stations (as shown in Figure 1-13) with measured wave data available inside the wave model domains: one NOAA NDBC buoy – 41108; three USACE Acoustic Doppler Current Profiler (ADCP) gages – Eleven Mile, Bald Head and Oak Island; and one Coastal Ocean Research and Monitoring Program (CORMP) ADCP gage – OCP1 (Ocean Crest Pier, NC). Table 1-5 presents general information about these stations. The NOAA buoy 41108 is at the same location as the USACE Eleven Mile ADCP. The following bulk wave parameters are reported at both the NOAA buoys and the USACE ADCPs: significant wave height, peak and average wave periods, and peak wave direction. At the CORMP ADCP, the same bulk wave parameters except average wave period are reported. In addition, the directional wave spectra are also reported at the USACE ADCPs and NOAA buoy 41013.

Table 1-5: Information of offshore and nearshore wave measuring stations

Source	Station	Start Date	End Date	Frequency
NDBC	41108	02/2013	07/2017 (active)	30 min
NDBC	41013	11/2003	07/2017 (active)	1 hr
USACE	Eleven Mile	09/2000	05/2010	3 hr
USACE	Oak Island	09/2000	05/2010	1 hr
USACE	Bald Head	09/2000	01/2010	3 hr
CORMP	OCP1	05/2006	06/2013	1 hr

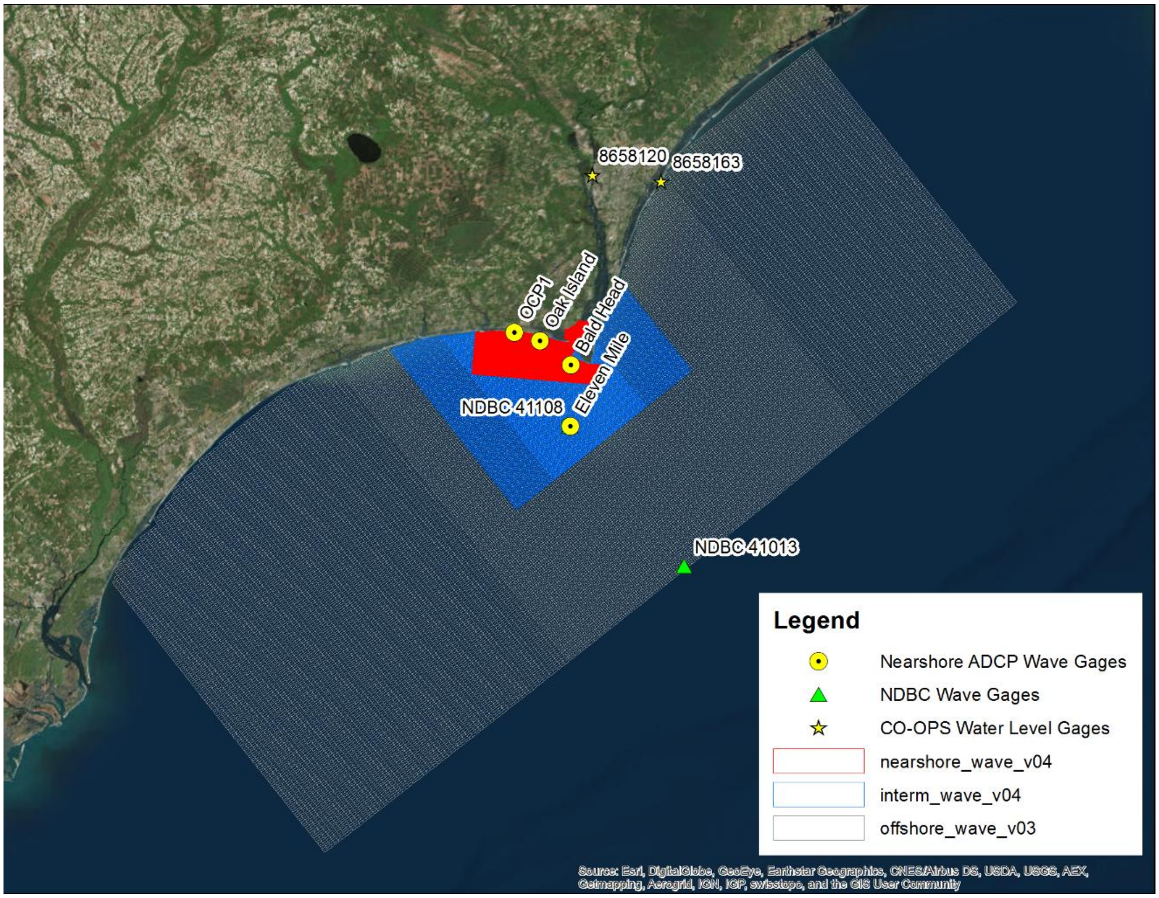

Figure 1-13: Wave Measurement Stations

In addition, reanalysis data from the NOAA Wave Watch III (WW3) and hindcast data from USACE Wave Information System (WIS) are available for the East Coast of America. The spatial coverage of WW3 reanalysis data is shown in Figure 1-14 and the location of the WIS station is shown in Figure 1-15. Table 1-6 lists the information of the hindcast data.

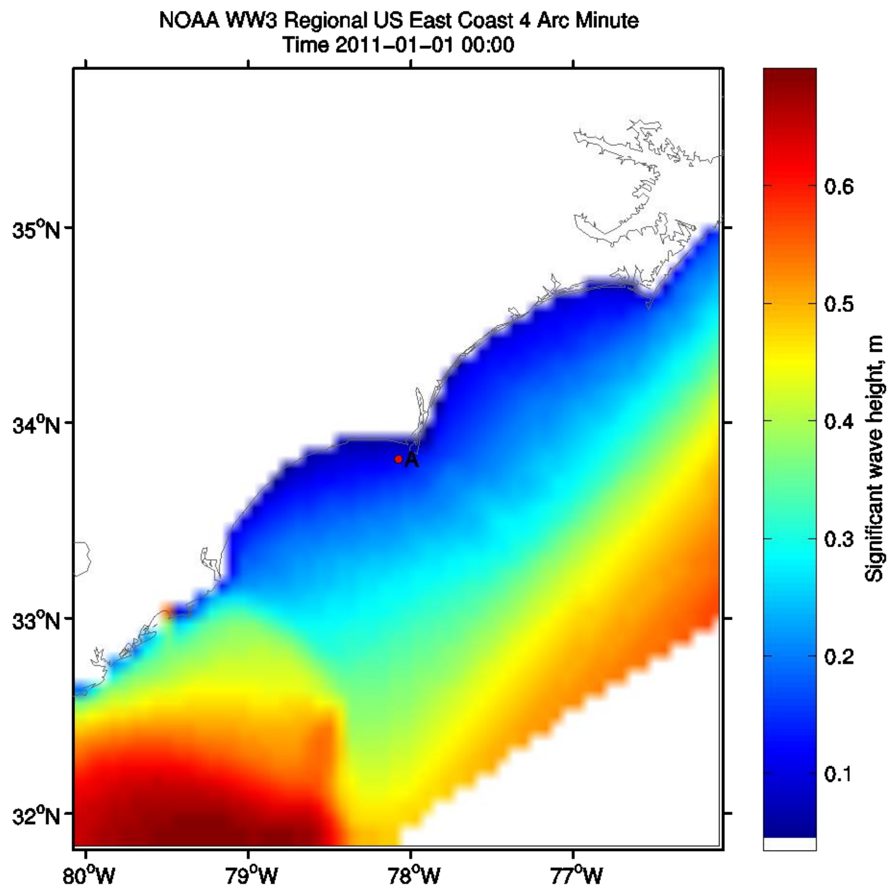

Figure 1-14: Coverage of WW3 reanalysis data

Figure 1-15: Locations of WIS stations

Table 1-6: Wave hindcast data

Source	Time Period	Frequency
WW3	1979-2007	3 hr
WIS	1980-2014	1 hr

1.2.4. Precipitation

Hourly precipitation data available at METAR Station KILM (Wilmington International Airport) was processed to calculate monthly minimum, mean and maximum precipitation for every month. The precipitation station is the same as the METAR wind station listed in Table 1-3 and the length of record analyzed here is from June 1, 1942 to Sep 5, 2017 (active). The monthly variation of precipitation is shown in Figure 1-16.

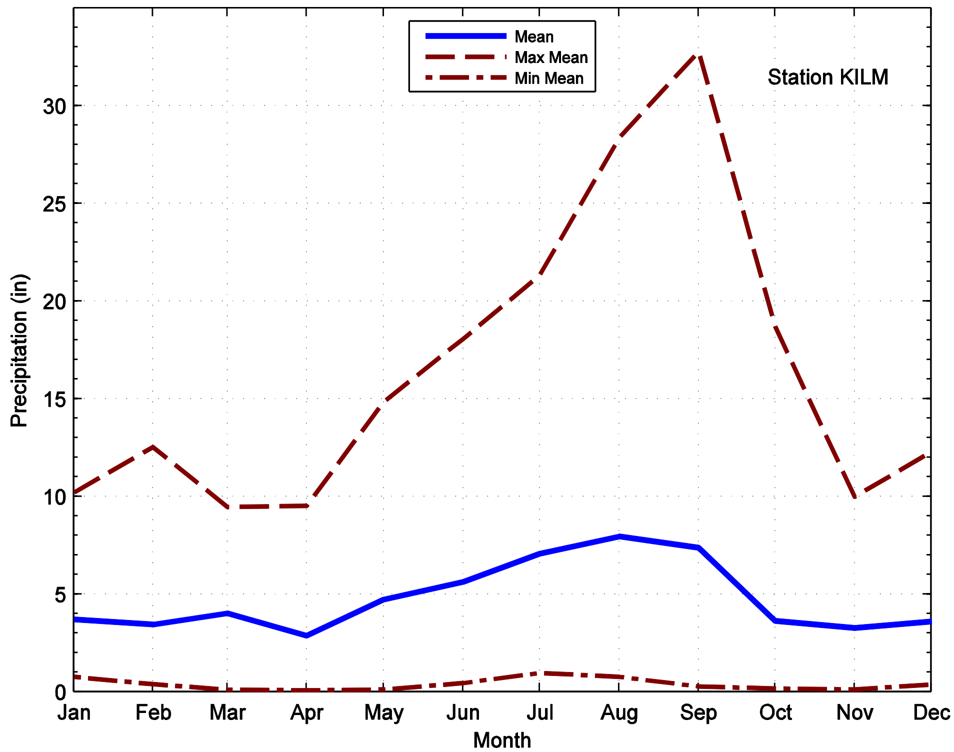

Figure 1-16: Monthly statistics of precipitation at Station 02105769

From Figure 1-16, it can be seen that the months between July and September are the wettest months.

1.2.5. River Discharge

River discharge data from three stations that are upstream of the Cape Fear estuary were collected from the United States Geological Survey (USGS) National Water Information System. The locations of the three stations and the drainage basin areas accounted by the respective stations are shown in Figure 1-17.

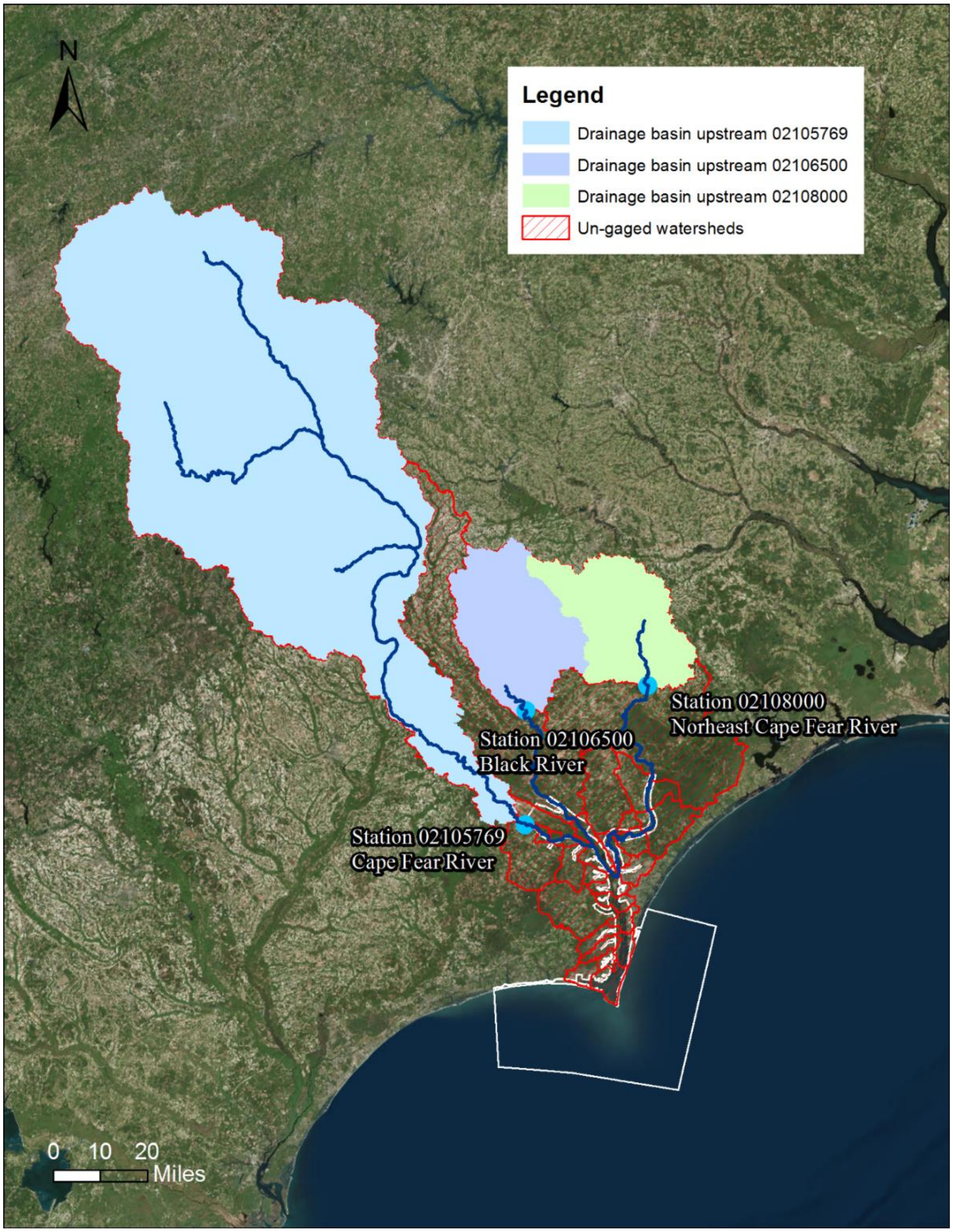

Figure 1-17: Location of USGS stations and respective drainage basins

The description of stations and the data available are given in Table 1-7, and the values of drainage basin area are from USGS StreamStats.

Table 1-7: USGS stations description

Station	Period of observations (15 min interval)	Period of observations (daily)	Drainage basin area (mi^2)
02105769 Cape Fear River at Lock 1 near Kelly	2007–2017	1969–2017	5,260
02106500 Black River near Tomahawk	2007–2017	1951–2017	677
02108000 Northeast Cape Fear River near Chinquapin	2007–2017	1940–2017	607

Statistical analyses were performed for both 15–min and daily records from the three stations. Percent exceedance values are listed in Table 1-8.

Table 1-8: Statistics for discharges at USGS stations (ft^3/s)

Station	Min	75%	50%	25%	10%	5%	1%	Max	Mean
15-min									
02105769	283	1190	2160	5160	11200	15500	22400	66600	4357
02106500	7	196	424	906	1580	2120	3870	39100	720
02108000	3	148	381	761	1610	2390	4970	19000	684
Daily									
02105769	179	1430	2780	6550	13600	18000	27200	66200	5255
02106500	7	229	496	1020	1730	2310	4310	34400	781
02108000	3	152	420	910	1690	2400	5000	29900	735

Monthly statistics of daily discharge data are shown in Figure 1-18 to Figure 1-20 for the three gage stations respectively. The mean value of the discharge data for each month was calculated for each year. For example, the daily data at Station 0210800 is available for 78 years from 1940 to 2017. Seventy-eight monthly mean values were calculated for the month of January. Then, the maximum, mean and minimum of these mean values were calculated for each month to show the statistics in these figures.

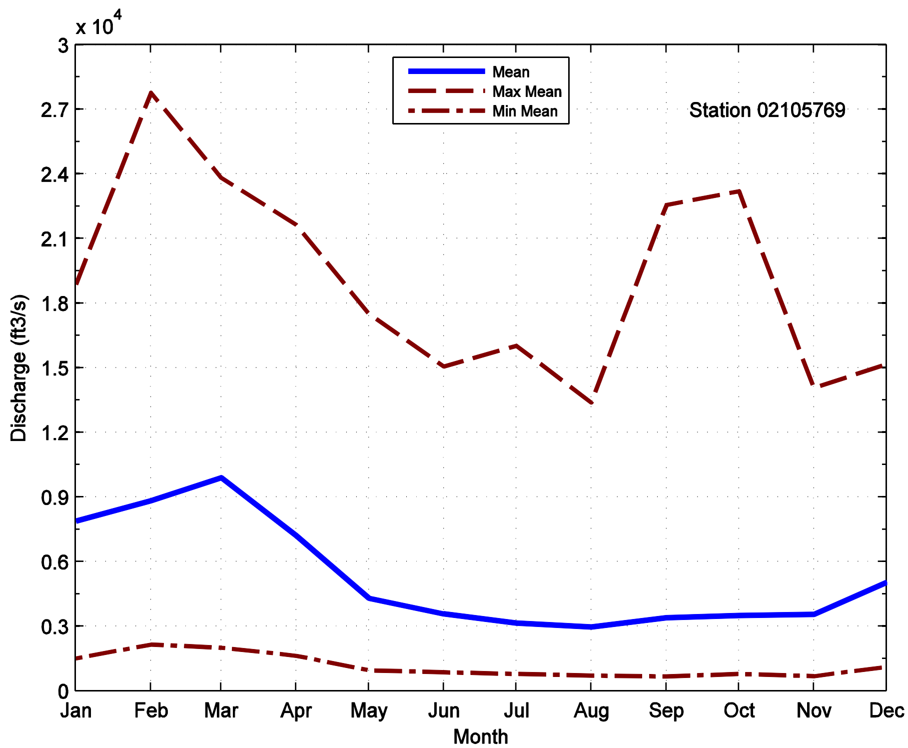

Figure 1-18: Monthly statistics of daily discharge data at Station 02105769

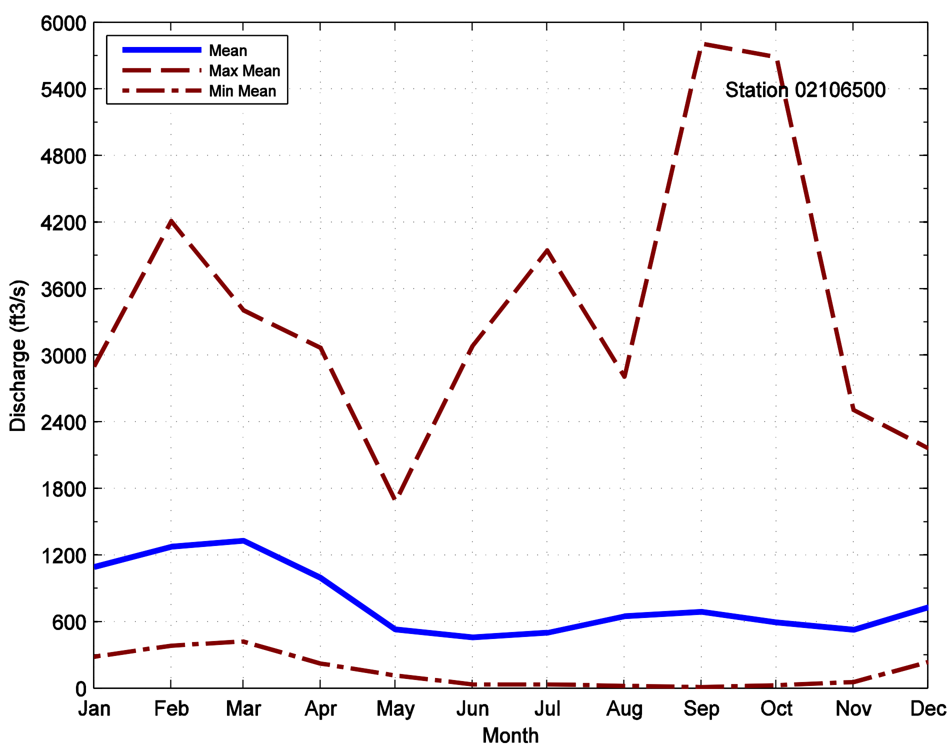

Figure 1-19: Monthly statistics of daily discharge data at Station 02106500

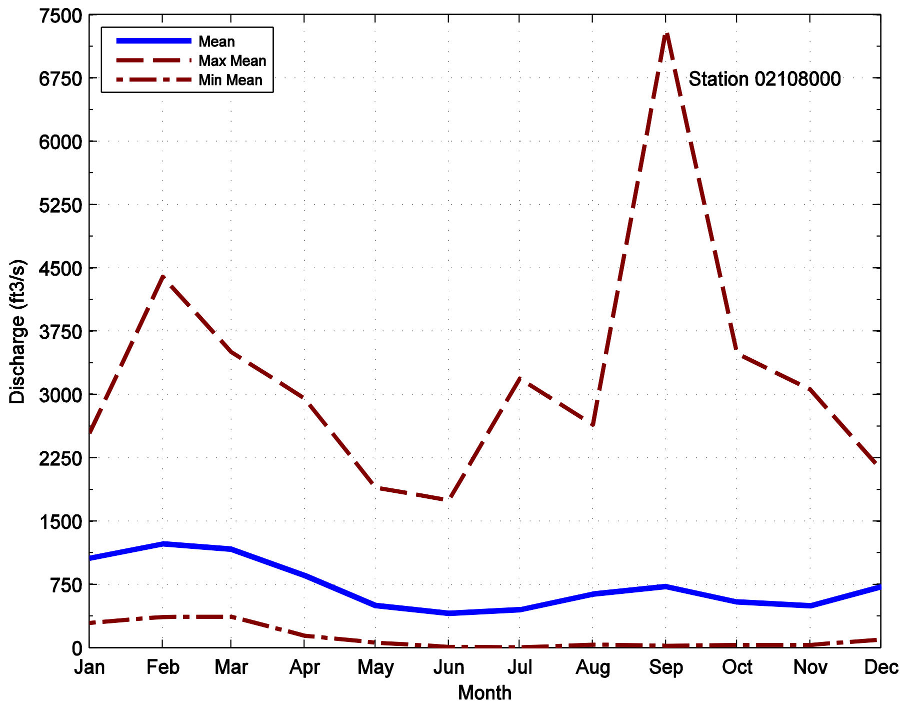

Figure 1-20: Monthly statistics of daily discharge data at Station 02108000

From these figures, it can be seen that the maximum mean values are between July and October at the three stations. It is observed that 80% of the hurricanes that affect North Carolina occur between August and October (NOAA NHC), precipitations from which could be causing this increase in discharge. From the means of the mean value, it is clear that the dry seasons are in the summer (May, June, and July) and flood seasons are in the winter (January, February and March), although analysis of precipitation at Station KILM does not show significant increase in rainfall during the winter. It is worth noting that the maximum value in September is very high comparing to the mean and minimum value. This is due to combined effect of Hurricane Dennis and Hurricane Floyd which produced heavy rainfall in eastern North Carolina. The rains caused widespread flooding over a period of several weeks in September; nearly every river basin in the eastern part of North Carolina exceeded 500-year flood levels.

1.2.6. Salinity

Salinity measurements in the Cape Fear River Estuary were obtained from three databases: National Centers for Environmental Information (NCEI) conducted by University of North Carolina - Wilmington (UNCW), Cape Fear Monitoring Coalition (CFMC), and EPA Storage and Retrieval (STORET) database. The data from NCEI contain surface and bottom salinity measurements, and the data from CFMC and STORET contain surface, middle and bottom salinity measurements. Figure 1-21 shows the spatial coverage of the salinity measurement stations. Among these three databases, only NCEI's data have continuous records; data from the other two databases are sparse. Table 1-9 lists the information of the salinity measurement stations from NCEI.

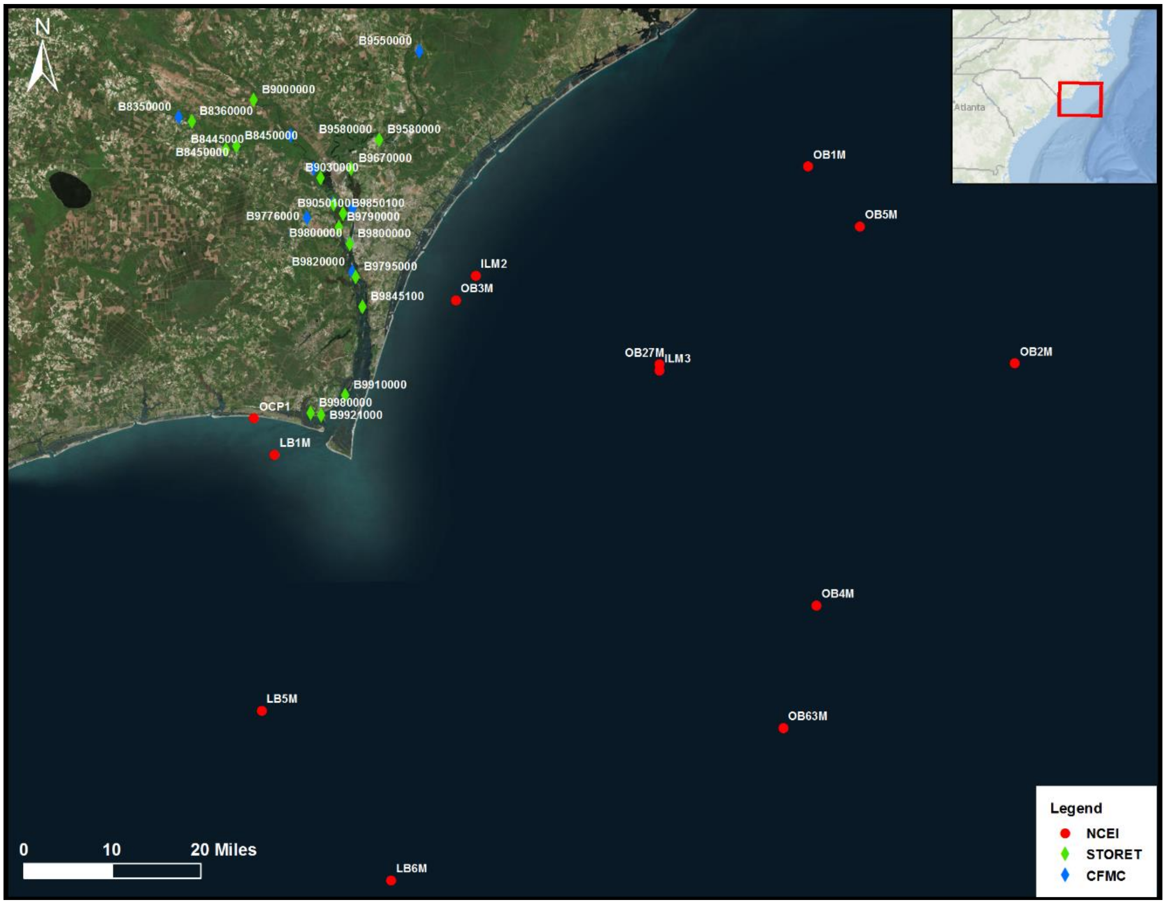

Figure 1-21: Locations of salinity measuring stations

Table 1-9: NCEI salinity measuring stations

Source	Station ID	Start Date	End Date	Frequency
NCEI	OB5M	7/19/2005	10/18/2005	30 min
NCEI	OB4M	10/19/2002	10/17/2003	15 min
NCEI	OB1M	10/18/2002	4/11/2005	15 min
NCEI	ILM3	6/6/2005	12/31/2013	2 hr before 2008 1 hr after 2008
NCEI	OB27M	4/20/2000	10/7/2004	5 min
NCEI	ILM2	6/7/2005	12/31/2013	2 hr before 2008 1 hr after 2008
NCEI	OB3M	10/20/2002	4/28/2003	15 min
NCEI	LB1M	12/3/2004	6/7/2007	15 min
NCEI	OCP1	5/23/2006	12/31/2013	15 min
NCEI	OB2M	4/25/2002	7/21/2004	15 min

1.2.7. Water Quality

The Lower Cape Fear River Program (LCFRP) is a water quality monitoring program covering the Cape Fear River Estuary and lower Cape Fear River watershed. Sampling and analysis are conducted by the University of North Carolina Wilmington's (UNCW) Aquatic Ecology Laboratory. The program includes 33 stations in the Cape Fear, Black, and Northeast Cape Fear watersheds. Data are collected under a Memorandum of Agreement between the State of NC and national pollutant discharge elimination system (NPDES) permittees in the lower Cape Fear. The State of NC also collects data under its Ambient Monitoring System (AMS).

LCFRP stations are shown in Figure 1-22. Parameters include temperature, DO, TSS, Chl *a*, TN, TKN, NH_4, NO_3 + NO_2 (referred to as simply NO_3), TP, and PO4.

1.3. Geotechnical

Data from previous geotechnical investigations along the navigation channel was collected. This included borings, washprobes, vibracore logs, lab data (including unconfined compressive strength and grain size) and top of rock picks from boring logs. The reports included in the Geotechnical Appendix document this data and a comprehensive GIS geotechnical database for the river was also developed.

Figure 1-22: Map of LCFRP stations within the model domain

1.4. Maintenance Dredging

Per USACE (2007): *The Wilmington Harbor navigation channel is divided into "reaches" or segments of river and dredging methods and disposal options vary depending on the reach location and quality of material to be dredged. Maintenance dredging in Wilmington Harbor is currently performed by varying methods depending on the location of the River reach and disposal of maintenance dredged material from the Harbor varies based on sediment quality and location.*

Table 1-10 contains a summary of all current maintenance dredging activities and includes dredging and disposal methods, sediment volumes, dredging frequency, and sediment classification. Sediment classification is based on the Engineering Unified Soil Classification System. Sand is described as a material where 50 % or more of the material lies between the number 4 sieve (4.76 mm) and the number 200 sieve (0.074mm). Silty sand is defined as a sand material with more than 12% of the material (silt) passing the number 200 sieve. Beach disposable sand is defined as sand material with less than 10% passing the number 200 sieve.

As shown in Table 1-10, material from the Outer Ocean Bar (Reach 3 of Bald Head Shoal) Channel is dredged annually by hopper dredge and deposited in the Ocean Dredged Material Disposal Site (ODMDS). Material from the Inner Ocean Bar Channel (Bald Head Shoal Channel reaches 1 and 2) and Smith Island Channel is dredged with an ocean certified pipeline dredge every other year and pumped to the beach at either Bald Head Island or Oak Island in accordance with the Sand Management Plan (SMP) that was incorporated in the Environmental Assessment, Preconstruction Modifications of Authorized Improvements, Wilmington Harbor, NC, 2000. The 2000 SMP is based on a 6-year cycle and remains in effect until the Phase III DMMP is completed.

Although the Phase III DMMP may not recommend any changes to the 2000 SMP, the Phase III DMMP will supersede the Sand Management Plan. Material from Bald Head-Caswell Channel, Southport Channel and Battery Island Channel is dredged about once every 4 years by hopper dredge and deposited in the ODMDS. Material from Snows Marsh Channel to Lower Big Island Channel is dredged once every 2 years by bucket and barge or by hopper dredge and deposited in the ODMDS. If nearby bird nesting islands, South Pelican Island and Ferry Slip Island, are in need of sand due to erosion, material from Snows Marsh Channel and Horseshoe Shoal Channel may be pumped to these islands by pipeline dredge. Also, DA-3 and DA-4 are alternative disposal areas available for disposal of dredged material by pipeline dredge from Bald Head-Caswell Channel through Horseshoe Shoal Channel. Upstream of Lower Big Island Channel to the upstream limits of the project, dredging is performed by pipeline dredge and material is pumped to the Eagle Island Disposal Area. Maintenance dredging in Upper Big Island Channel upstream through Fourth East Jetty Channel is performed every 2 years. Between Channel and the Anchorage Basin are dredged annually. The project area upstream of the Anchorage Basin to the upstream limits of the project is dredged about once every 5 years.

Table 1-10: Summary of Current Dredging and Disposal Practices (USACE 2007)

Reaches	Channel Reaches	Shoaling Cubic Yards Per Year	Frequency of Dredging (years)	Disposal Location	Dredge Type	Sediment Type
Upper	Upstream Limits of Project to 750 ft above Chemserve	12,600	5	EI Cells 2/3	pipeline	silt
Upper	750 ft above Chemserve to NC 133 Bridge	70,600	5	EI Cells 2/3	pipeline	silt
Upper	NC 133 Bridge to Cape Fear Mem Bridge	14,100	5	EI Cells 2/3	pipeline	silt
Upper	Anchorage Basin	1,168,100	1	EI Cells 1/2/3	pipeline	silt
Upper	Between Channel	84,200	1	EI Cells 1/2/3	pipeline	silt
Upper	Fourth East Jetty	19,600	2	EI Cells 1/2/3	pipeline	silt
Upper	Upper Brunswick	17,100	2	EI Cells 1/2	pipeline	silt
Upper	Lower Brunswick	29,800	2	EI Cells 1/2	pipeline	silt
Mid River	Upper Big Island	22,500	2	ODMDS / DA-10	B&B or Hopper, Pipe	sandy silt
Mid River	Lower Big Island	35,900	2	ODMDS / DA-10	B&B or Hopper, Pipe	sandy silt
Mid River	Keg Island	34,100	2	ODMDS / DA-10	B&B or Hopper, Pipe	sandy silt
Mid River	Upper Lilliput	48,900	2	ODMDS / DA-10	B&B or Hopper, Pipe	sandy silt
Mid River	Lower Lilliput	43,000	2	ODMDS / DA-10	B&B or Hopper, Pipe	sandy silt
Mid River	Upper Midnight	107,000	2	ODMDS / DA-8	B&B or Hopper, Pipe	sandy silt
Mid River	Lower Midnight	25,500	2	ODMDS / DA-8	B&B or Hopper, Pipe	sandy silt
Mid River	Reaves Point	21,200	2	ODMDS / DA-8	B&B or Hopper, Pipe	silty sand
Mid River	Horseshoe Shoal	45,900	2	Bird Island / DA-3/4	pipeline	sand
Mid River	Snows Marsh	21,800	2	Bird Island / DA-3/4	pipeline	sand
Mid River	Lower Swash	12,000	2	ODMDS/DA-3/4	B&B or Hopper, Pipe	sand
Inner OB	Battery Island	25,300	4	ODMDS/DA-3/4	B&B or Hopper, Pipe	sand
Inner OB	Southport	0	4	ODMDS/DA-3/4	B&B or Hopper, Pipe	sand
Inner OB	Baldhead-Caswell	11,000	4	ODMDS/DA-3/4	B&B or Hopper, Pipe	sand
Inner OB	Smith Island	257,800	2	BHI/CB/WOI beaches	pipeline	sand
Inner OB	Ocean Bar Entrance Channel	545,000	2	BHI/CB/WOI beaches	pipeline	sand & silt
Outer OB	Ocean Bar Outer Channels	538,000	1	ODMDS	Hopper	silt
	TOTAL	**3,211,000**				
EI=Eagle Island, ODMDS=Ocean Dredged Material Disposal, BHI=Bald Head Island, CB=Caswell Beach, WOI=West Oak Island, B&B=Bucket and Barge						

USACE (2014) also calculated the annual volume change rate in the existing Anchorage Basin based on the historic channel survey data taken by USACE ranging from January 2008 to July 2012 (Figure 1-23). The projected shoaling volume for the Anchorage Basin is approximately 1,251,804 cubic yards per year (cy/yr). The estimated annual shoaling rate was also calculated from the dredge records. The total dredged volume from the Anchorage Basin between 2004 and 2011(8 events) was 9,253,556 cy which corresponds to an annual dredging volume of 1,156,694 cy/yr (USACE 2014).

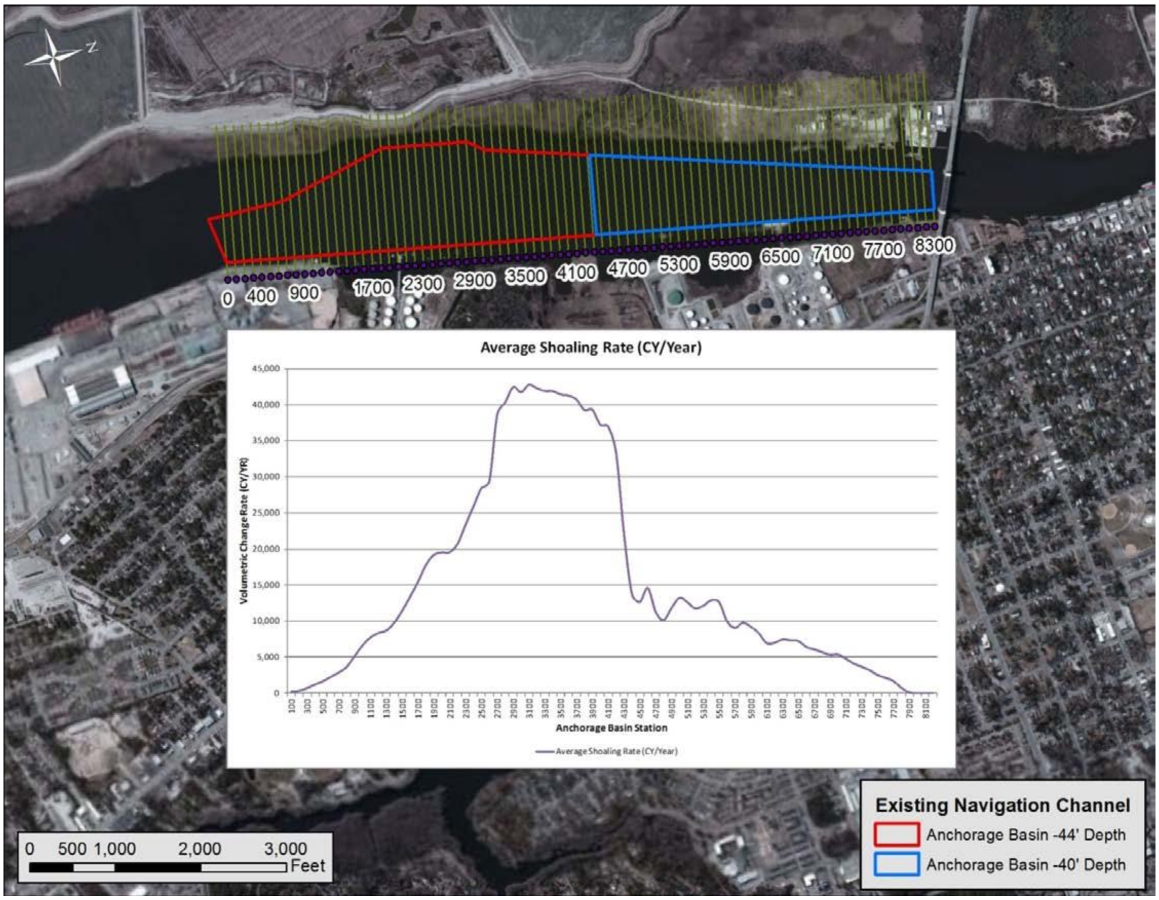

Figure 1-23: Annual volume change in Anchorage Basin (USACE 2014)

1.5. Sea Level Rise

NOAA's Center for Operational Oceanographic Products and Services has been measuring sea level for over 150 years, with tide stations of the National Water Level Observation Network operating on all U.S. coasts. Changes in RSL, either a rise or fall, have been computed at 142 long-term water level stations using a minimum span of 30 years of observations at each location. These measurements have been averaged by month which removes the effect of higher frequency phenomena in order to compute an accurate linear sea level trend. The trend analysis has also been extended to 240 global tide stations using data from the Permanent Service for Mean Sea Level (PSMSL).

The sea level trends measured by tide gauges are local relative sea level (RSL) trends as opposed to the global sea level trend. Tide gauge measurements are made with respect to a local fixed reference on land. RSL is a combination of the sea level rise and the local vertical land motion. A plot of historical water levels for Station 8658120 (see Figure 1-2) is presented in Figure 1-24.

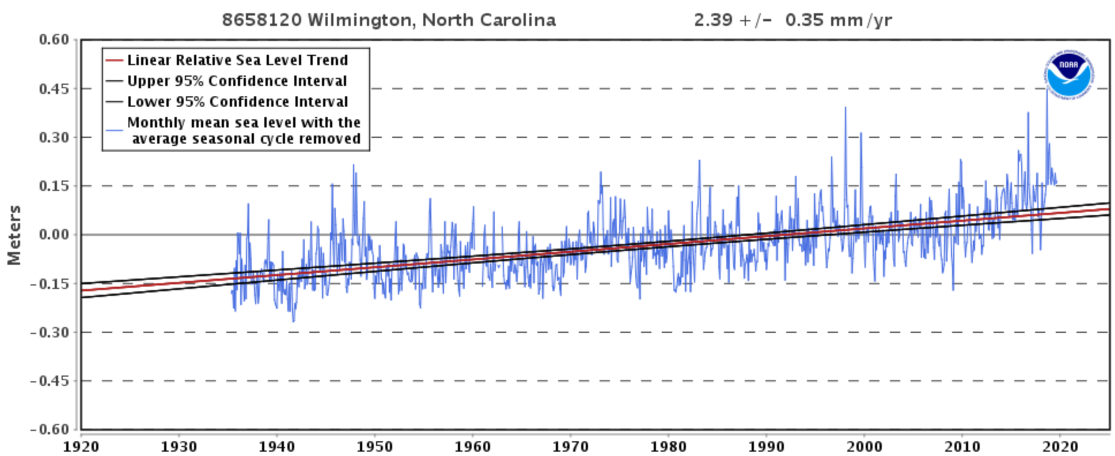

Figure 1-24: Historical Water Levels for Wilmington, NC

The relative sea level trend is 2.3 millimeters/year with a 95% confidence interval of +/- 0.34 mm/yr based on monthly mean sea level data from 1935 to 2017 which is equivalent to a change of 0.75 feet in 100 years.

The plot shows the monthly mean sea level without the regular seasonal fluctuations due to coastal ocean temperatures, salinities, winds, atmospheric pressures, and ocean currents. The long-term linear trend is also shown, including its 95% confidence interval. The plotted values are relative to the most recent Mean Sea Level datum established by CO-OPS.

United States Army Corps of Engineers (USACE) guidance ER 1100-2-8162, *Incorporating Sea Level Changes in Civil Works Programs*, requires consideration of projected future sea level changes and impacts. Since future sea level change rates are uncertain, project performance should consider a range of rates. Historic rates were used for the "low" sea level change rate while predictions of future "intermediate" and "high" sea level change rates were developed in accordance with USACE guidance by extension of rate Curve I and Curve III, respectively, from the National Research Council's 1987 report, *Responding to Changes in Sea Level: Engineering Implications*.

The proposed project was assumed to be completed by the year 2027 and to have a 50-year design life. The Relative Sea Level Changes presented in Table 1-11 were obtained through use of the USACE on-line sea level calculator at http://www.corpsclimate.us/ccaceslcurves.cfm through the end of project year 2077.

Table 1-11: Relative Sea Level Change to 2077 in Wilmington, NC

RSLR* Scenario	RSLR (ft)
Low	0.34
Intermediate	0.88
High	2.57

* Relative Sea Level Rise

1.6. Climate Hydrology Analysis

1.6.1. Introduction

The USACE's Engineering and Construction Bulletin (ECB) 2018-14, issued in September 2018, requires a qualitative climate hydrology analysis that discusses the relationships between climate, streamflows, and the USACE project, to ensure that changes in climate with the potential to significantly affect the project with respect to hydrology are identified, and the potential impacts are assessed with respect to the project over its life cycle.

The following analysis provides a discussion of past and future predicted climate and the nexus to the Port of Wilmington navigation improvement project. It relies on literature review and the application of analysis tools developed by USACE.

1.6.2. Methods

ECB 2018-14 was developed by the USACE as an update to ECB 2016-25, *Guidance for Incorporating Climate Change Impacts to Inland Hydrology in Civil Works Studies, Designs, and Projects*. The ECB provides guidance for incorporating climate change into the USACE planning process for long term projects. The analysis presented herein relies on literature review and two USACE tools in accordance with this guidance.

Literature reviewed for this qualitative analysis included:

1. National Climate Assessment (USGCRP, 2018),
2. Climate Change and Water Resources Management – A Federal Perspective by Brekke et al. (2009),
3. USACE Regional Climate Synthesis (USACE, 2015), and
4. US Environmental Protection Agency study which provides a modeling assessment of 20 watersheds in the US and their sensitivity to potential climate change (USEPA, 2013).

The ECB calls for application of analysis tools developed by the USACE including the Climate Hydrology Assessment Tool and the Nonstationarity Detection Tool (Friedman et al., 2018)). The Climate Hydrology Assessment Tool was used to investigate past and potential future trends in streamflow for the Cape Fear River and Hydrologic Unit Code (HUC) 0303. Further, the Nonstationarity Detection Tool was used to detect potential nonstationarity at the Cape Fear Lock and Dam 1 gage from USGS. Two additional tools are cited in the ECB: the Watershed Climate Vulnerability Assessment Tool and the Time Series Toolbox. These tools are not currently unavailable for use outside of USACE staff and have not been applied to the subject project.

Climate variables relevant to the project are temperature and precipitation. In addition, relevant hydrologic response variables include streamflow and sedimentation. Note that the focus of this section is on inland hydrology since a sea level rise analysis following USACE guidance ER 1100-2-8162 *Incorporating Sea Level Changes in Civil Works Programs* was discussed in Section 1.5.

1.6.3. Assessment of Existing Conditions

The following section focus on the existing conditions in the region and in the watershed including current climate and climate change already occurring. Information provided is derived from several literature sources along with analysis of data via the USACE tools.

1.6.3.1. Literature Review

The Fourth National Climate Assessment was prepared to comply with the Global Change Research Act of 1990 (USGCRP, 2018) with the purpose to help inform decision-makers and planners about the effects of climate change on the United States.

According to the report, the Southeast region of the US is experiencing a warming trend. The region has experienced a period of warming since the 1970s with the decade of 2010 through 2017 having been warmer than any previous decade on record. This holds true for average daily maximum and average daily minimum temperature. As a result, heatwaves are on the rise which has a detrimental effect on public health. In addition, agriculture can be impacted by decreased nighttime cooling. Moreover, evapotranspiration and evaporation may be affected resulting in changes to waterbody volumes and streamflow.

Figure 1-25 shows the variability and change in the annual number of hot days and warm nights up to 2016 for the region. Overall for the Southeast region, the annual number of hot days (maximum temperature above 95°F) has been lower in the second half of the century compared to the first half. However, in the lower Cape Fear portion of the Southeast region, hot days appear to have increased since the 1950s based on the map provided in the figure. The bottom chart in the same figure shows that the number of warm nights are on the rise and in the 2010's they were the largest in the century for the entire region. During the latter part of this century, most of the Cape Fear region has experienced large increases in warm nights.

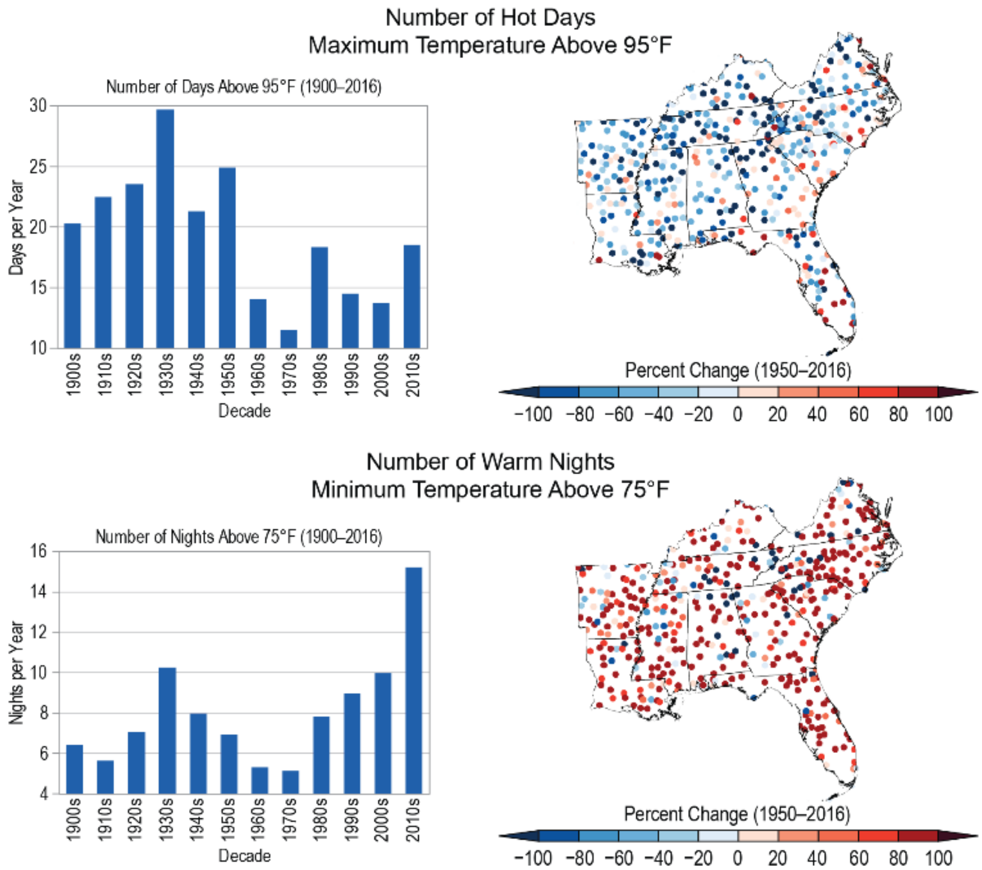

Figure 1-25: Historical changes in hot days and warm nights (USGCRP, 2018)

In addition to air temperature, the national climate assessment also presents data regarding precipitation changes. Again, focusing on the Southeast, the report presents the variability and change in the annual number of days with precipitation greater than 3 inches since 1900 and averaged over the Southeast. An overall rising trend is apparent. At individual precipitation station trends since 1950, the numbers of days with heavy precipitation has increased at most stations, including those in the lower Cape Fear river region.

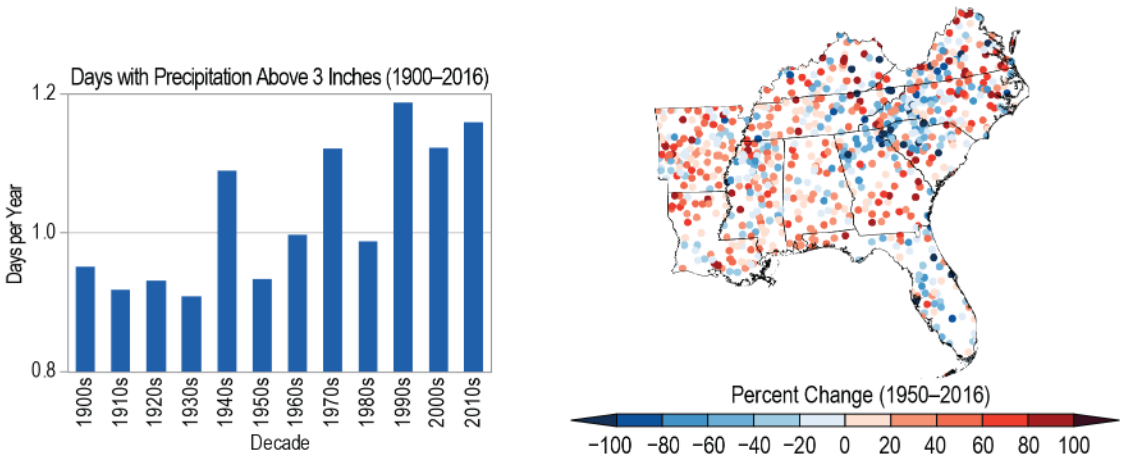

Figure 1-26: Historical changes in precipitation (USGCRP, 2018)

In addition to the National Climate Assessment, the interagency report by Brekke et al. (2009) provides further insight into the historical data concerning the climate. It was prepared on behalf of U.S. Geological Survey (USGS), USACE, and National Oceanic and Atmospheric Administration (NOAA). A number of key points were presented. The key point relevant to this section is that "the best available scientific evidence based on observations from long-term monitoring networks indicates that climate change is occurring, although the effects differ regionally." The report does not present evidence by region.

Next, USACE has developed a series of regional climate syntheses to address 2011 and 2014 policy statements on climate change by the Assistant Secretary of the Army for Civil Works and other plans, policy and guidance from the agency. The reports provide summaries of current climate change science and focus on regions at the scale of 2-digit USGS Hydrologic Unit Codes across the US. The following information is taken from the summary for the South Atlantic-Gulf Region 03 (USACE, 2015). This region includes the districts of Wilmington, Charleston, Savannah, Jacksonville, Atlanta, and Mobile USACE districts and a small section of the Mississippi Valley Division (Figure 1-27).

Figure 1-27: South Atlantic-Gulf Region (from USACE, 2015)

Climate trends presented in USACE (2015) focus on mean and extreme temperature and precipitation and well as mean streamflow. The key points for the region based on analysis of historical data are as follows:

- Air Temperature - there has been a warming temperature trend since the 1970s. The overall trend since the early 1900s, however, is unclear.
- Precipitation - a upward trend in precipitation in terms of both annual totals and occurrence of storm events, has been identified by multiple authors. However, the results vary in parts of the region, vary by season, and not all studies found the same trends. There is also some evidence for an increase in the year-to year variability in precipitation.
- Streamflow – there is a downward trend in mean streamflow, particularly since the 1970s, according to multiple authors. This paradox has been discussed by authors in light of generally increasing precipitation; they point to seasonal differences in the timing of changes in these two variables though temperature may also play a role.

While there were several studies reviewed and summarized for the regional synthesis, one study looked at historical climate data for NC at the Coweeta Laboratory. Data shows warming since the 1970s and a statistically significant trend in annual average air temperature. Another study at the regional scale based on data from 1950-2000 showed positive trends for most of the region in spring and summer and in the northern portion, some mild cooling in the fall. Another study using a different time period showed more cooling trends for the entire region, but summary results did not drill down to NC. For precipitation the Coweeta Laboratory data showed wetter wet years and dryer dry years.

1.6.3.2. Data Analysis

Nonstationarity Detection Tool

In addition to a review of the literature, two USACE tools were applied to understand the current climate in the region of the TSP. First, the USACE Nonstationarity Detection Tool was applied to the Cape Fear gage at Lock and Dam #1. Stationarity is the assumption that the statistical characteristics of hydrologic time series data are constant through time. This has been the foundation of most methods in water resources that assume the future based on the past. However, this assumption has now been called into question based on observed data showing a changing climate.

The Nonstationarity Detection Tool applies a series of statistical tests to assess the stationarity of annual instantaneous peak streamflow data series at USGS streamflow gages. The site must have more than 30 years of annual instantaneous peak streamflow records through Water Year 2014. In this application, the tool was used to detect whether there is nonstationarity in the record at the Cape Fear Lock and Dam 1 gage based on maximum annual flows.

The tool was applied for two conditions: the full record through Water Year 2014 and from Water Year 1983 through Water Year 2014. Since the upstream Jordan Reservoir was filled in 1983, this shorter time frame isolates the period when the dam would have had an effect on streamflows including at Lock and Dam 1.

For the post-1983 condition, there were no statistically significant nonstationarities found (Figure 1-28). They would be shown as black lines in the graph and colored lines in the heat map for the 12 statistical tests that the tool applies.

When the record is extended back to 1970, prior to the Jordan Reservoir construction, the tools suggests there is nonstationarity based on one of the statistical tests, the Lombard Wilcoxon (Figure 1-29). The pivot year was 1999. Before this year, streamflow was higher compared to the period after based on this test.

The next analysis looks for a monotonic trend in the gage record. Similarly, to the previous results, no trend was detected for the period 1983-2014 (Figure 1-30). An analysis based on the longer period beginning in 1970 is shown in Figure 1-31. The result is a statistically significant trend suggesting streamflow is declining.

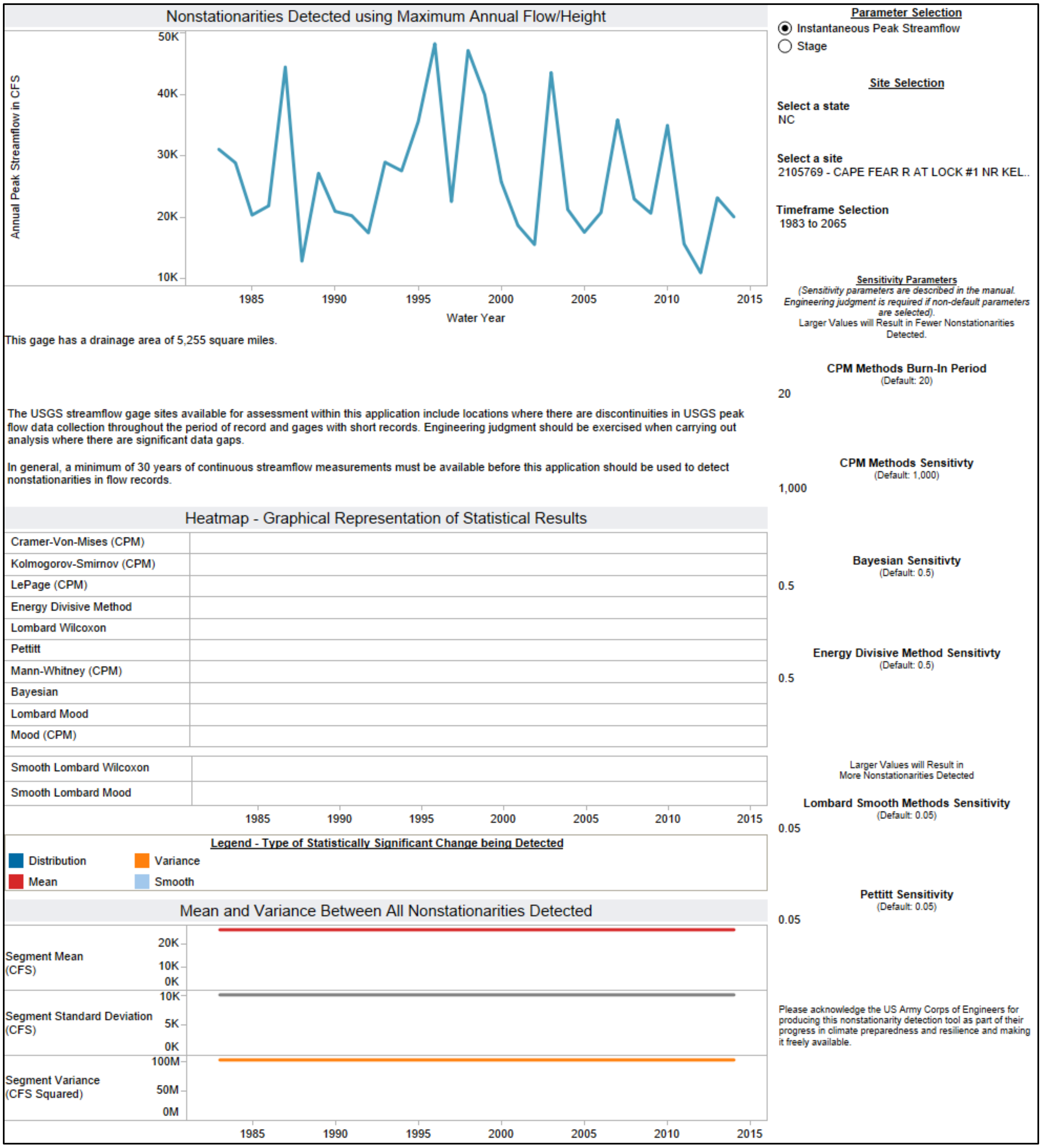

Figure 1-28: Nonstationarity analysis at Cape Fear River, Lock and Dam 1 (1983-2014)

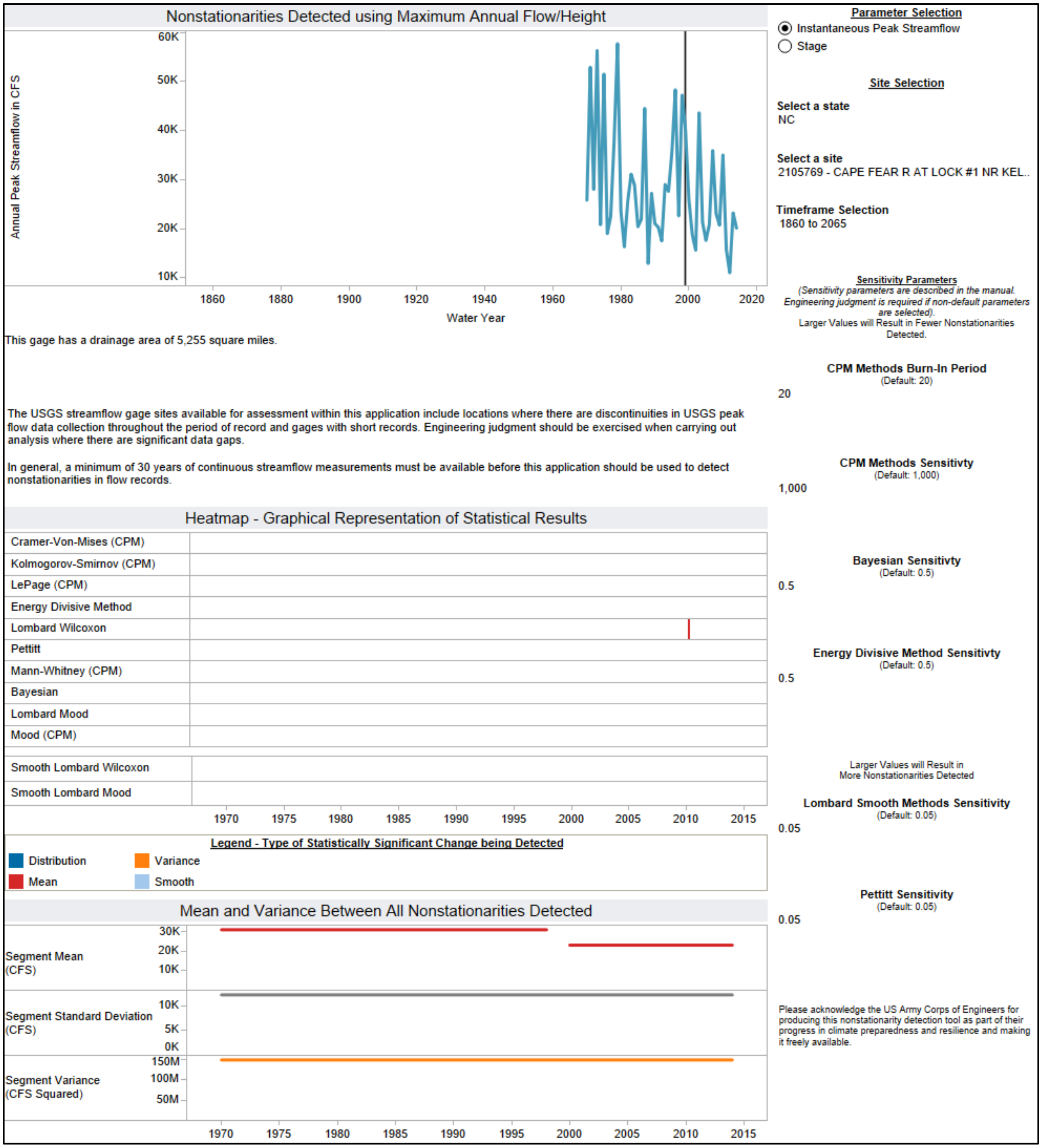

Figure 1-29: Nonstationarity analysis at Cape Fear River, Lock and Dam 1 (1970-2014)

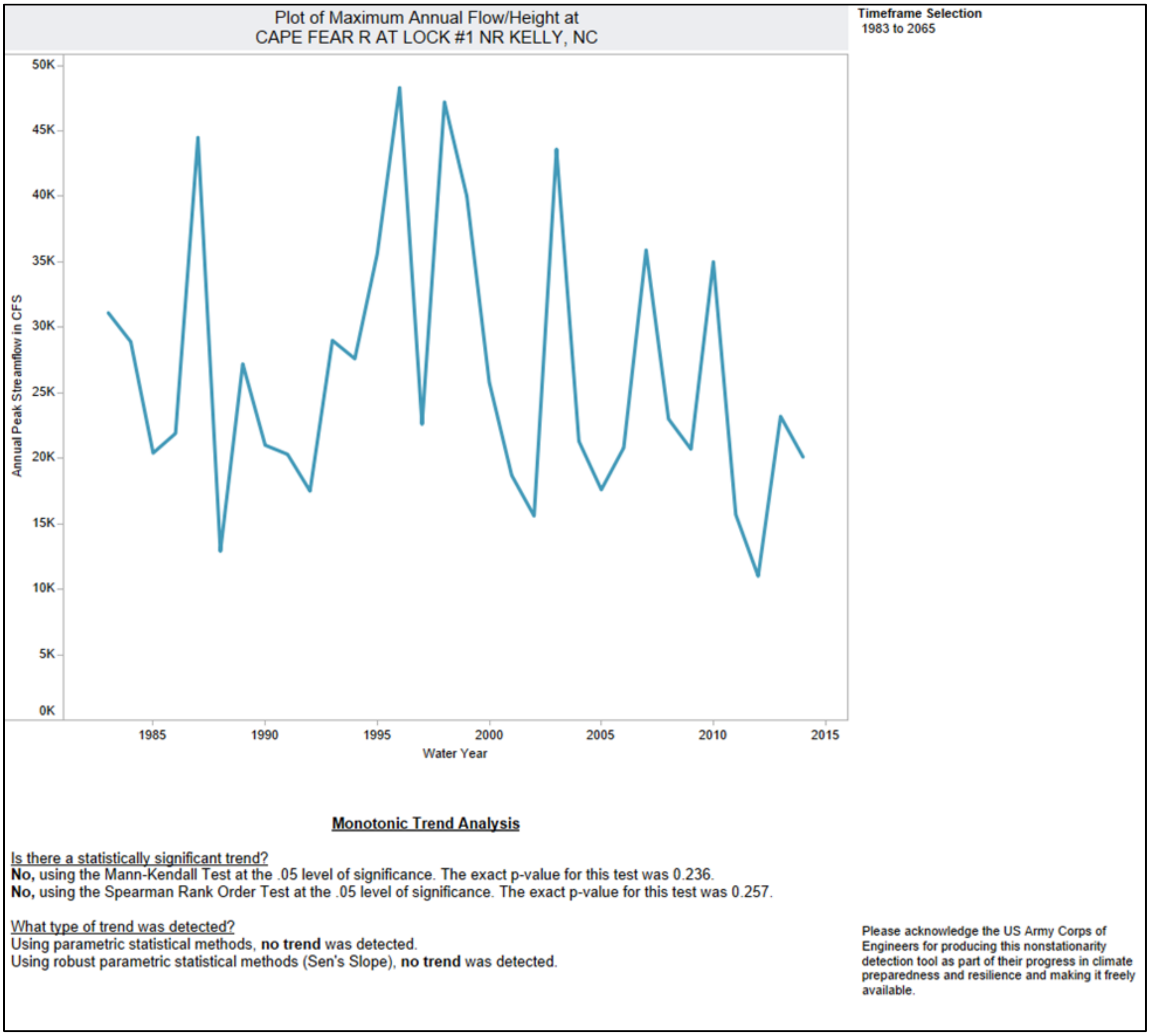

Figure 1-30: Monotonic Trend Analysis at Cape Fear River Gage at Kelly, NC (LD#1) since 1983

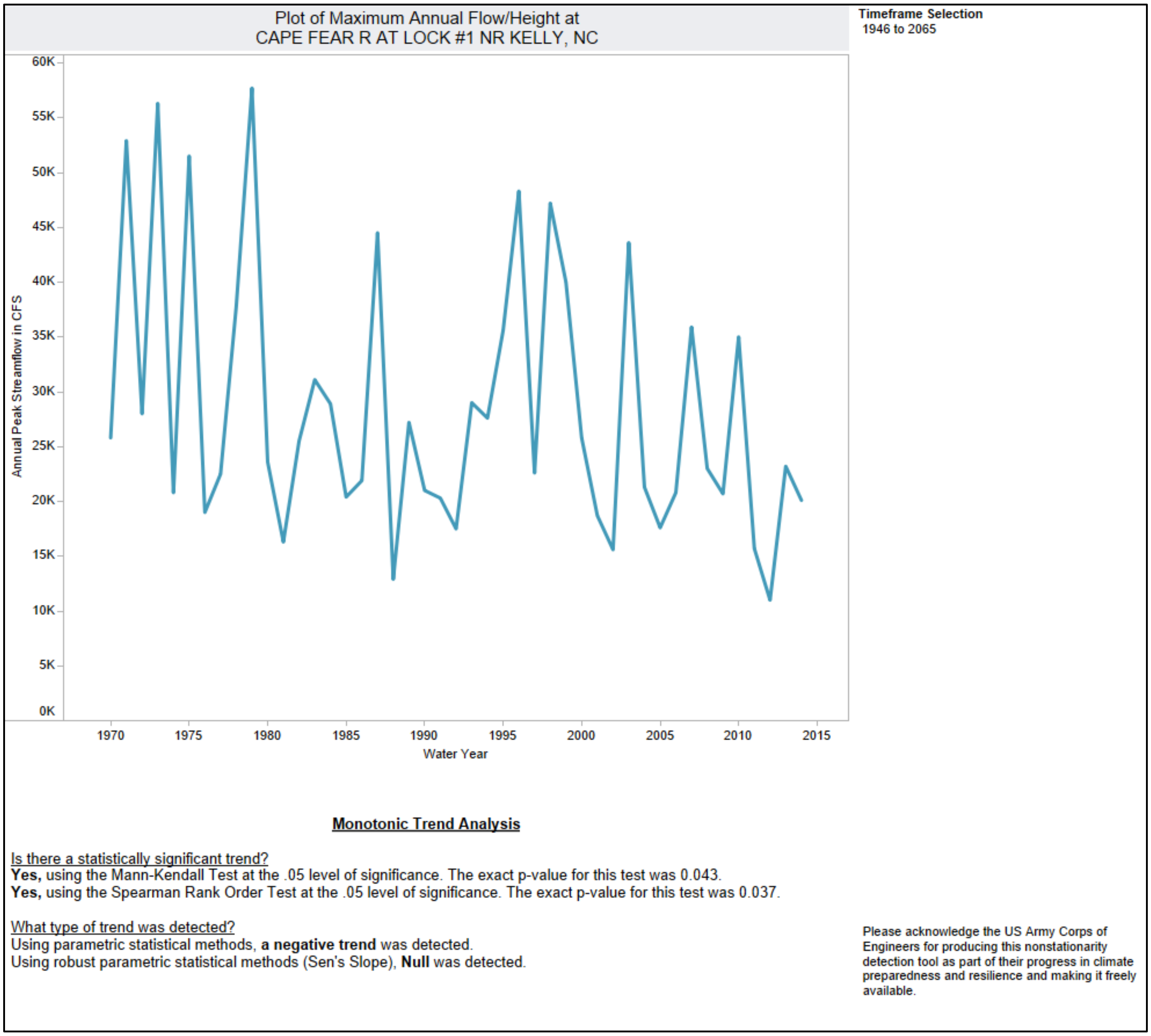

Figure 1-31: Monotonic Trend Analysis at Cape Fear River Gage at Kelly, NC (LD#1) since 1970

Climate Hydrology Assessment Tool

The USACE Climate Hydrology Assessment Tool was used to investigate trends in streamflow for the Cape Fear River and Hydrologic Unit Code (HUC) 0303. The observed trend in streamflow based on annual peaks from 1983 to 2017 (Jordan Lake normal pool filled in 1982) is shown in Figure 1-32 . Similar to the results of the Nonstationarity Detection Tool, there was no statistically significant trend found for the period 1983 through 2016 (p value of 0.34). When earlier data is added, back to 1970, a trend is found with p value of 0.03 (Figure 1-33).

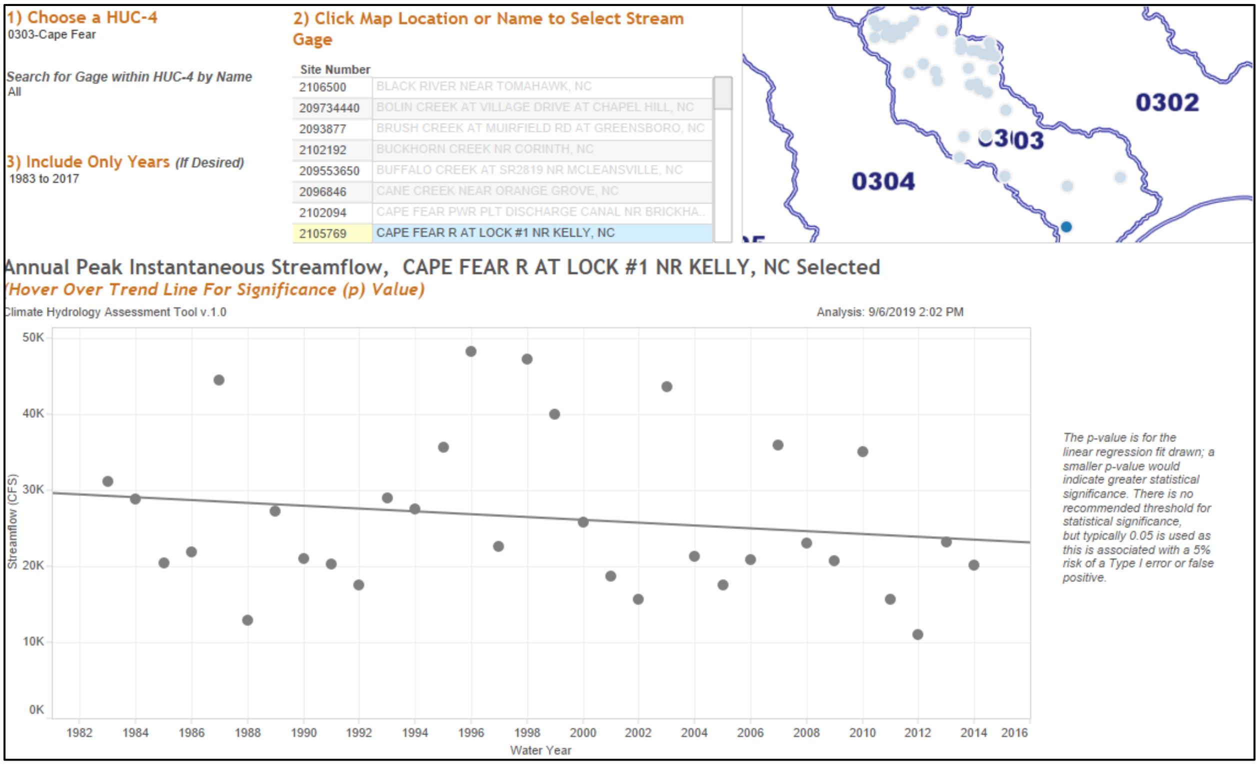

Figure 1-32: CHAT Trend Analysis for Cape Fear at Lock and Dam #1(1983-2016)

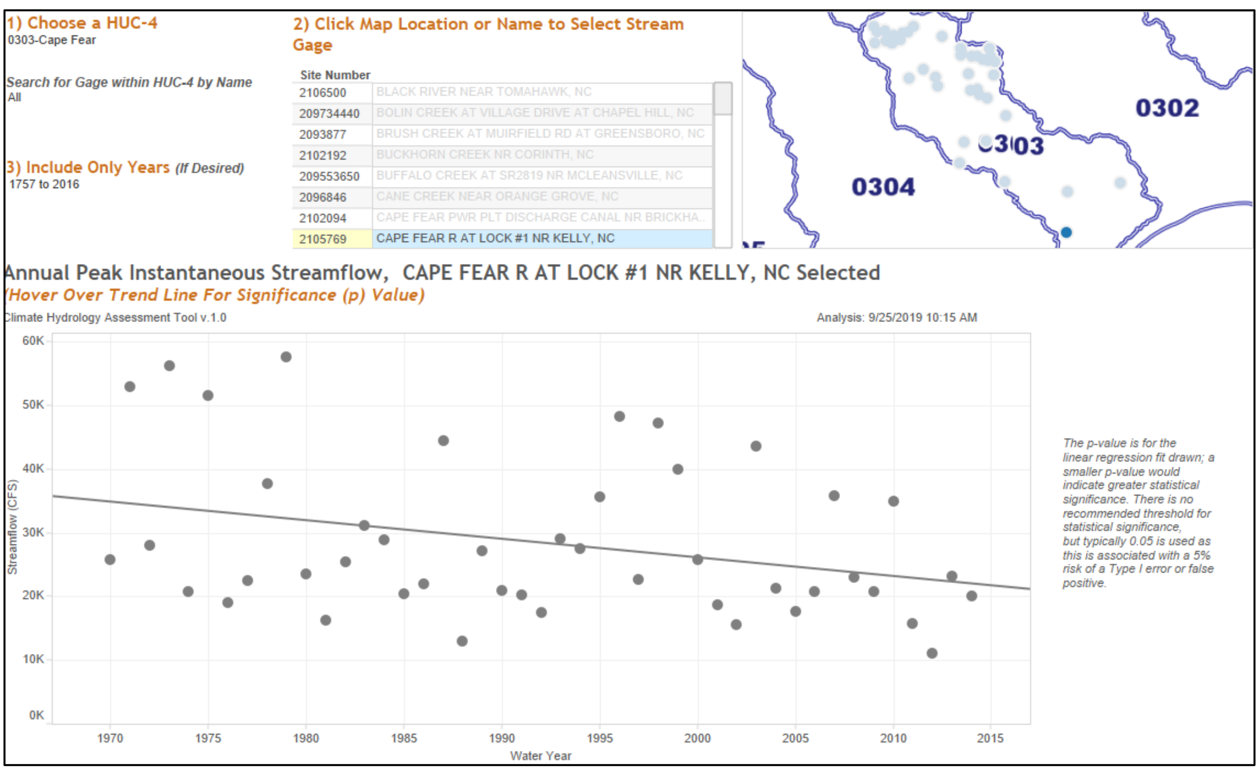

Figure 1-33: CHAT Trend Analysis for Cape Fear at Lock and Dam #1(1970-2016)

1.6.4. Projected Future Climate

Next, the qualitative analysis switches its focus to projected future climate. This would be expected to apply to the future without-project condition but also should be considered in the context of future with project.

1.6.4.1. Literature Review

The National Climate Assessment assembled data from numerous global climate models (GCMs) to understand the potential climate conditions in the future. As with past climate that has been measured, climate predictions are focused on the Southeast.

Climate model simulations of future conditions project increases in temperature and extreme precipitation for both lower and higher scenarios. Figure 1-34 shows the projected number of warm nights (i.e., days with minimum temperatures above 75°F) per year in the Southeast for the mid-21st century (2036–2065) and the late 21st century (2070–2099). Both the higher scenario and a lower scenario are provided. Compared to current conditions where only a few occur per year, the projections suggest increases are especially significant under the high scenario.

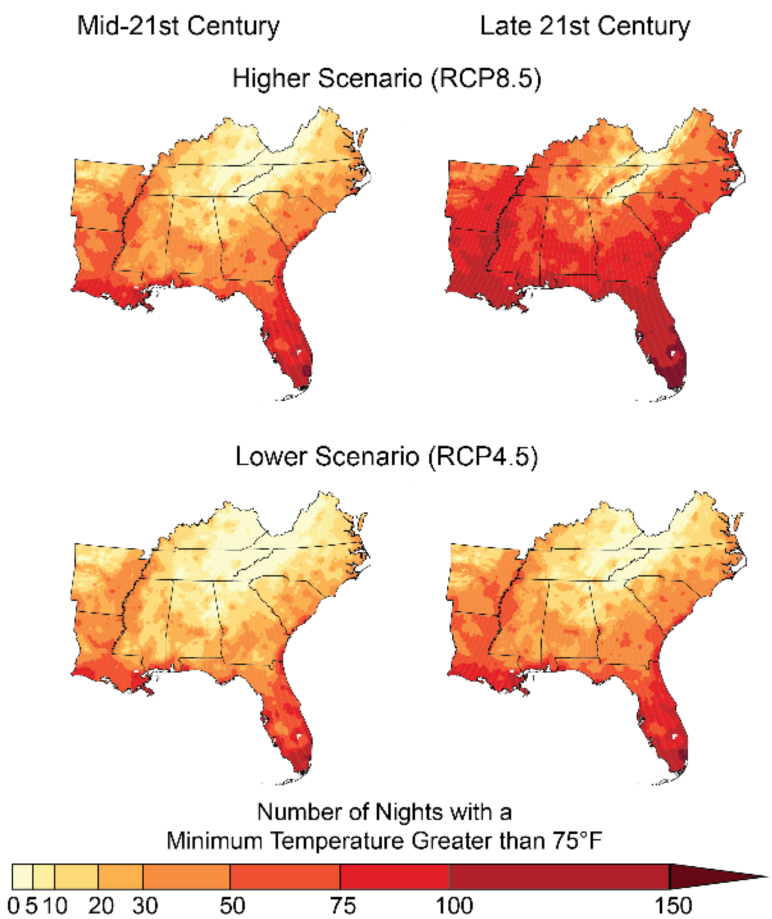

Figure 1-34: Projected number of warm nights for the mid and late 21st century

Extreme rainfall events have increased in frequency and intensity in the Southeast. The national climate assessment suggests there is a high likelihood that this will continue to increase in the future. By the end of the century under a higher scenario, projections indicate approximately double the number of heavy rainfall events (i.e., 2-day precipitation events with a 5-year return period) and a 21% increase in the amount of rain falling on the heaviest precipitation days.

In USACE's regional climate synthesis for the region, projected climate trends are provided based on studies using GCMs (USACE 2015). As the report suggests, non-stationarity or a changing climate requires use of more than historical data in the context of projects with long life spans.

The key points for the region based on projected climate trends are as follows:

- Air Temperature - There is strong evidence and consensus of increasing temperature over the next century for the region. Mean annual air temperature is expected to increase by about 2 to 4 degrees Celsius by the second have of the 21st century, particularly in the summer months.
- Precipitation – GCM projections suggest a "reasonable consensus" that the intensity and frequency of extreme storm events will increase across the region. There is less consensus on changes to total annual precipitation with the studies split on whether there will be increases or decreases. The northern portion is likely to exhibit increases.
- Streamflow – There is "no clear consensus" as to projected streamflow changes in the region.

Figure 1-35, taken from USACE (2015), summarizes the results for both observed and predicted variables in graphical form.

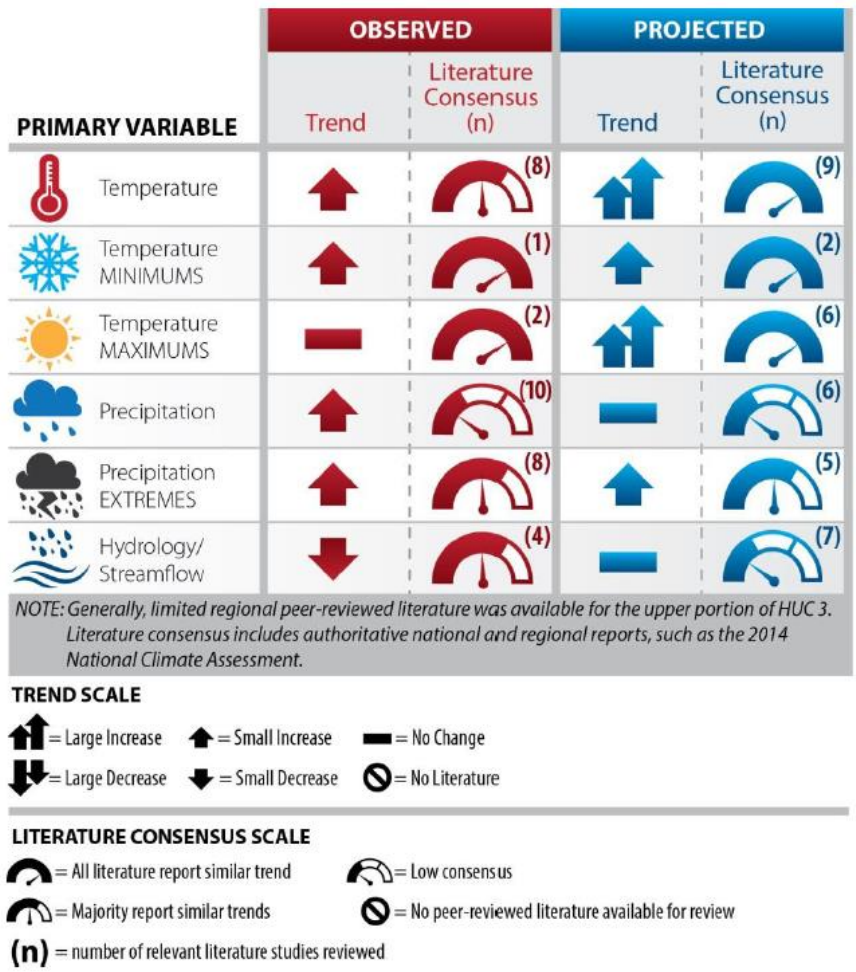

Figure 1-35: Summary of observed and projected climate trends and consensus from the literature (USACE, 2015)

In addition to these previous reports, USEPA (2013) was reviewed which provides a modeling assessment of 20 watersheds in the US and their sensitivity to potential climate change. The adjacent Tar River and Neuse River Basins were included in the set. These are located nearby to the northeast of the Cape Fear River Basin where the TSP is located.

The results suggest that there will be a potential for increased streamflow volume in these Southeastern watersheds. In addition, higher peak streamflows will likely lead to increases in erosion and sedimentation. The report also found that the simulated responses to streamflow and water quality to climate change varied based on different GCMs and downscaling methodologies. In the Tar Pamlico and Neuse, the results for select simulated parameters for mid-21st century climate relative to current conditions show the following:

- Average annual precipitation: 4 of 6 models showed increases
- Average annual temperature: All 6 models showed increases (median change of 4.16 degrees F)
- Total streamflow volume: 5 of 6 models showed increases
- 100-Year Peak Flow: 4 of 6 showed increases
- Total suspended solids: 5 of 6 models showed increases

1.6.4.2. Data *Analysis*

Climate Hydrology Assessment Tool

Figure 1-36 shows the range of projected annual maximum monthly streamflow for the HUC-4 and considering 93 combinations of downscaled climate model projections. The results are based on the Climate Hydrology Assessment Tool. The GCMs model precipitation and temperature in the future are based on various greenhouse gas emission scenarios (RCPs). Downscaling is needed to better understand the climate results at a more local scale. The climate model results are then used as input to the U.S. Bureau of Reclamation's Variable Infiltration Capacity (VIC) precipitation-runoff model to generate streamflow. The range is shown in yellow and the mean of the 93 projections is indicated by the blue line. The results suggest considerable uncertainty in streamflow changes indicated by the wide range in the projections.

In Figure 1-36, the trend in annual maximum monthly flow is shown for the mean of hydrology model output from 1983 to 2099. The trend of the mean is statistically significant in the upward direction with an R squared of 0.51 and p value of < 0.0001 (Figure 1-37). Adding the earlier data does not change the overall trend.

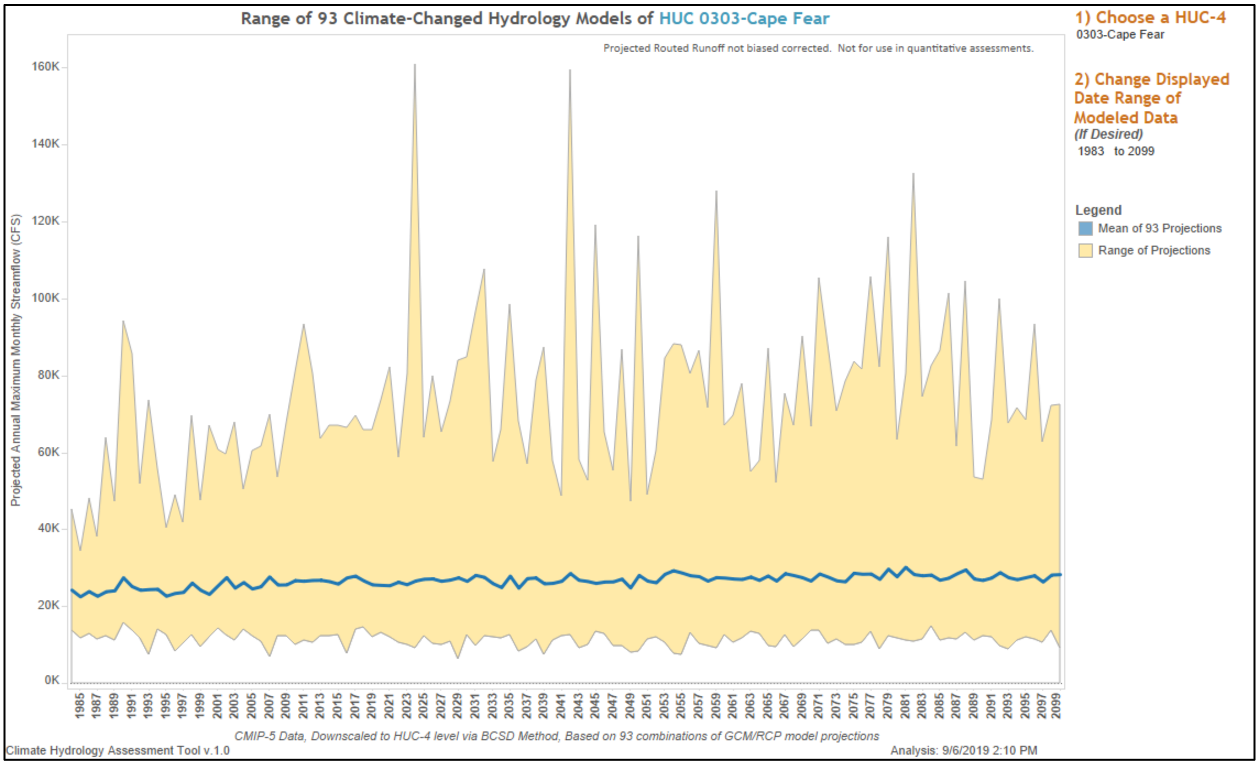

Figure 1-36: Range in projected annual max monthly flows using combinations of downscaled climate model predictions

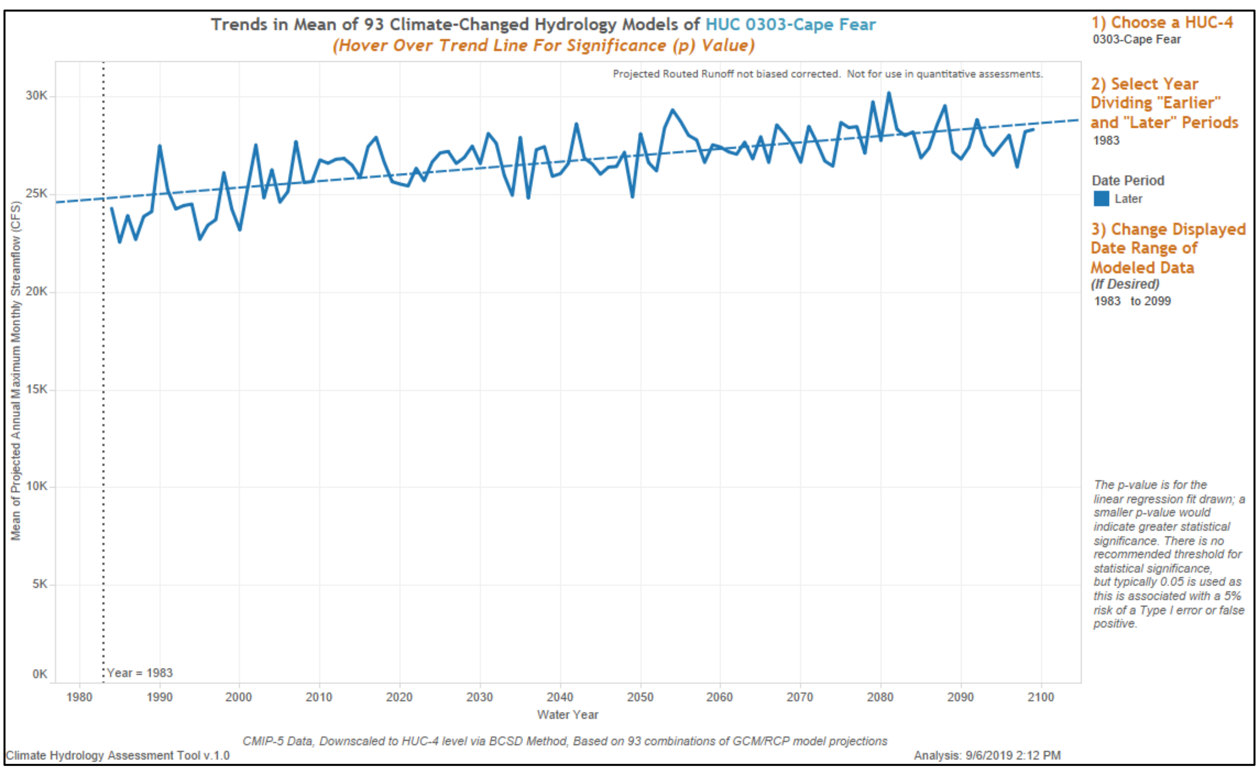

Figure 1-37: Trend in projected annual max monthly flow for HUC 0303

1.6.5. Vulnerability

The USACE recommends that projects be evaluated for potential vulnerabilities to planning, engineering and operational activities affected by climate change. Navigation and associated dredging projects like the TSP may be impacted. Figure 1-38 shows a summary of climate trends and impacts to USACE projects (USACE, 2015). In addition, the previous literature review and data analysis for current and future climate suggests the following general conclusions that should be considered in the context of the TSP:

Current Climate

1. Climate change is occurring, though the effects vary somewhat by region and within region.
2. In the lower Cape Fear portion of the Southeast region, air temperatures and days with heavy rainfall have increased since the 1950s based on the National Climate Assessment.
3. Likewise, the regional climate synthesis by USACE shows a warming trend since the 1970s. It also suggests an upward trend in precipitation, but this varies across studies and the region.
4. The regional synthesis also shows a downward trend in streamflow according to many studies. This paradox, if you consider an increasing trend in precipitation, can be explained by seasonal differences in rainfall and temperature with evapotranspiration also playing a role.
5. Analysis of gage data in the lower Cape Fear using two USACE tools shows nonstationarity and a statistically declining trend when analyzing data back to 1970. However, when limiting the analysis to the time that the watershed has been under active streamflow management from the Jordan Reservoir dam (since 1983), no significant trend is detected.

Future Climate

1. Climate change is expected to affect most sectors of water resources management, possibly requiring changes in design and operations (Brekke et al., 2009).
2. The National Climate Assessment describes how climate models point to increases in temperature and extreme rainfall events in the future for the Southeast.
3. The evidence for increased temperatures is strong based on the USACE synthesis for the region. Potential precipitation changes are less understood. There appears to be evidence that total volumes may increase or decrease depending on the location within the region. Stronger evidence exists for increases in intensity and frequency of extreme events over much of the region. However, streamflow changes in the future are less certain according to the synthesis.
4. A USEPA modeling study in nearby watersheds suggest that streamflow and sedimentation are likely to increase by mid-century. This conclusion should be coupled with analysis from the Climate Hydrology Assessment Tool which showed a wide range of streamflow projections for the hydrologic unit. The

overall mean of flow output from 93 model projections to the end of the century show a statistically significant trend of increasing streamflow.

CLIMATE VARIABLE	VULNERABILITY
Increased Ambient Temperatures	Increased ambient air temperatures throughout the century, and over the next century are expected to create the following vulnerabilities on the business lines in the region: • Loss of vegetation from increased periods of drought and reduced streamflows may have impacts on vegetation within the region, which is important for sediment stabilization in the watershed. Loss of non-drought resistant vegetation may result in an increase in sediment loading, potentially causing geomorphic changes in the tributaries to the river system. • Decrease in flows may result from periods of drought and reduced streamflow has implications for maintain water levels in the rivers. • Risk of wildfires during hot and dry conditions may cause an increased risk of wildfires, especially in heavily forested and dry areas. Flora and fauna that are not drought resistant can also be impacted by longer drought conditions, which may reduce opportunities for recreational wildlife viewing. **BUSINESS LINES IMPACTED:**
Increased Maximum Temperatures	Air temperatures are expected to increase 2-4°C in the latter half of the 21st century, especially in the summer months. This is expected to create the following vulnerabilities on business lines in the region: • Increased water temperatures leading to water quality concerns, particularly for the dissolved oxygen (DO) levels, growth of nuisance algal blooms and influence wildlife and supporting food supplies. • Increased evapotranspiration. • Human health risk increases from extended heat waves, impacting recreational visitors and increasing the need for emergency management. **BUSINESS LINES IMPACTED:**
Increased Storm Intensity and Frequency	Extreme storm events may become more intense and frequent over the coming century which are expected to influence the following vulnerabilities on business lines in the region: • Increased flows and runoff, which may carry pollutants to receiving water bodies, decreasing water quality. • Increased erosion with subsequent changes in sediment accumulation rates and creating water quality concerns. • Increased groundwater recharge rates, as residence times are shortened within areas where evapotranspiration takes place during high intensity events. • Increased flooding, which may have negative consequences for all infrastructure, habitats, and people in the area. **BUSINESS LINES IMPACTED:**
Sea Level Rise	Sea level rise may exacerbate saltwater intrusion into fresh water supplies. **BUSINESS LINES IMPACTED:**

NOTE: The Regulatory and Military Program business lines may be impacted by all climate variables

= Navigation = Flood Risk Management = Ecosystem Restoration = Hydropower = Recreation = Water Supply = Emergency Management

Figure 1-38: Summary of project climate trends and impacts to USACE projects (USACE, 2015)

1.6.6. Conclusions

The project itself is not expected to have a significant effect on climate change per se. Furthermore, potential climate change impacts do not impact the decision regarding the selection of the TSP. However, the project will be affected by the results of climate change. Increases in extreme precipitation events and resulting increases in streamflow have the potential to move more nutrients and sediment into the navigation channel. This combined with increases in air temperatures has the potential to impact water quality and dissolved oxygen (DO) levels through increases in oxygen demanding materials and nuisance algal blooms. Furthermore, increases in sediment transport may increase the need for channel maintenance in the future.

Review of the model results presented in Appendix A, though, indicates that the project impacts on water quality (DO) are most pronounced during the winter months when DO is at its highest levels (and temperature is lowest). Therefore, the potential impacts from increased temperatures and nutrients will likewise have the largest relative changes during the winter months when these impacts will not further adversely affect fishery resources under the with project conditions as compared to without project conditions.

With respect to the increase of salinity intrusion into the estuary due to the project (as well as future RSLR), increases in streamflow will actually be a mitigating factor reducing the potential impacts of the project on wetland vegetation composition and fishery resources.

Increases in streamflow and suspended sediment will likely increase potential maintenance dredging activities. If any changes in predicted future dredging volumes are observed, these will ultimately have to be incorporated into future Dredge Material Management Plan (DMMP) reports. However, given the project itself is expected to only increase these volumes by about 10%, climate change impacts should also be relatively minor and adaptive responses can be undertaken.

2. Data Collection

As a part of this project, RPS Evans-Hamilton (RPS EH) conducted water level, current, discharge, salinity and water quality measurements on the Cape Fear River in the spring and summer of 2017 (see Appendix A-1 and Appendix A-2 for full reports).

2.1. Water levels

Water level data was collected using HOBO water level sensors on fixed mounts at two stations near Southport and Wilmington. Location of the stations are shown in Figure 2-1. The measurements were collected during spring tide between March 27, 2017 and April 2, 2017, at 3-minute intervals.

Figure 2-1: Locations of water levels and current measurements

Figure 2-2 shows the measured water level data at the two stations along with water levels at CO-OPS Station 8658120.

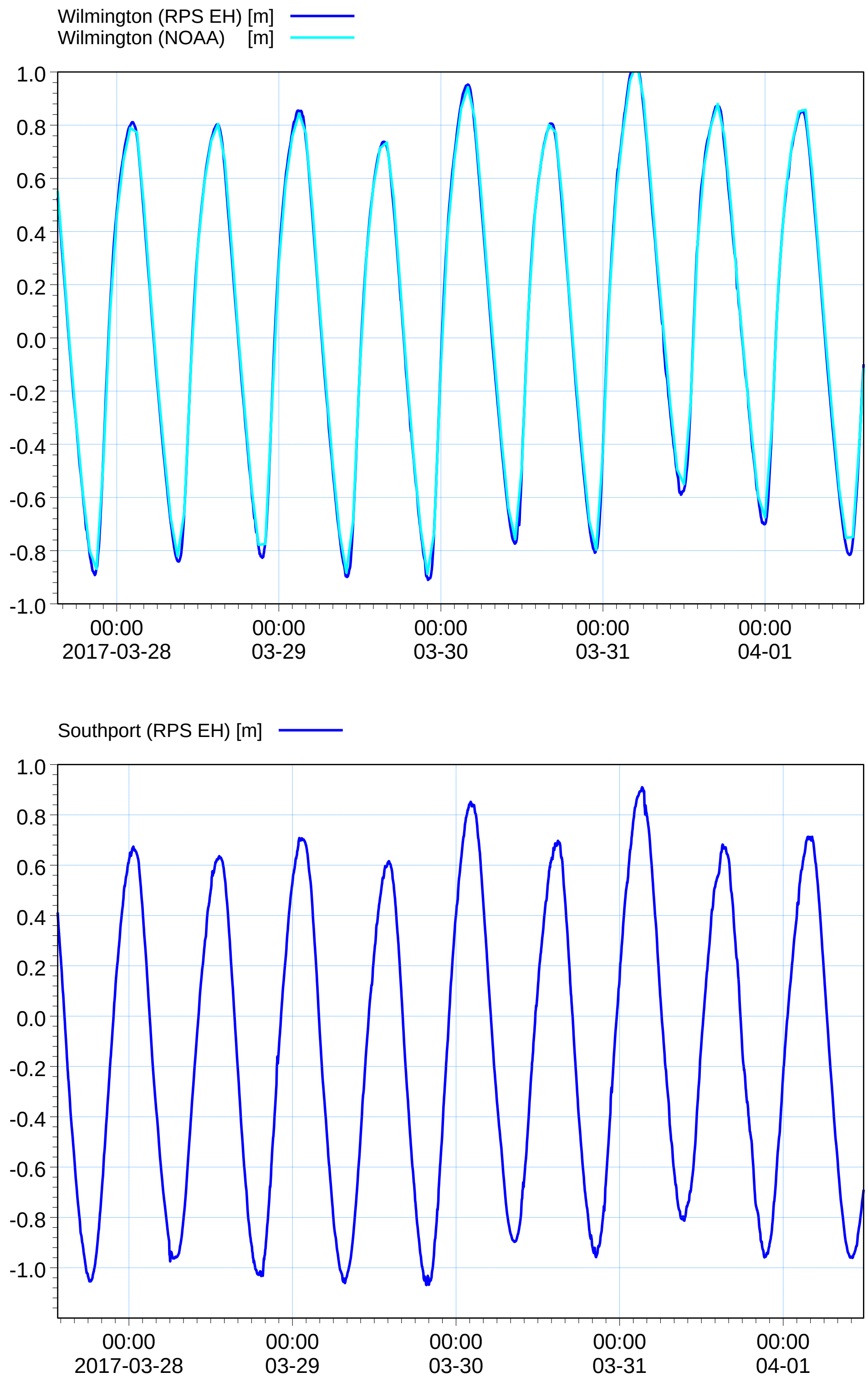

Figure 2-2: Measured water levels from RPS EH campaigns

2.2. Currents

Currents were measured at a location near Southport, NC (see Figure 2-1). A Trawl Resistant Bottom Mount was outfitted with a RDI Workhorse Sentinnel 600 kHz ADCP instrument. The number of depth cells was set to 45 and the bin size was 0.5 m. The mount was installed at a water depth of approximately 13.7 m (45 ft). The measurements were collected between March 27, 2015 and April 4, 2017.

The current measurements were processed to calculate depth-averaged current speed and direction, which is shown in Figure 2-3. Figure 2-4 and Figure 2-5 show vertical profiles of components of velocity at selected time steps. The time steps shown in Figure 2-4 and Figure 2-5 correspond to high tide during flooding stage, high tide during ebbing stage, low tide during flooding stage and low tide during ebbing stage respectively.

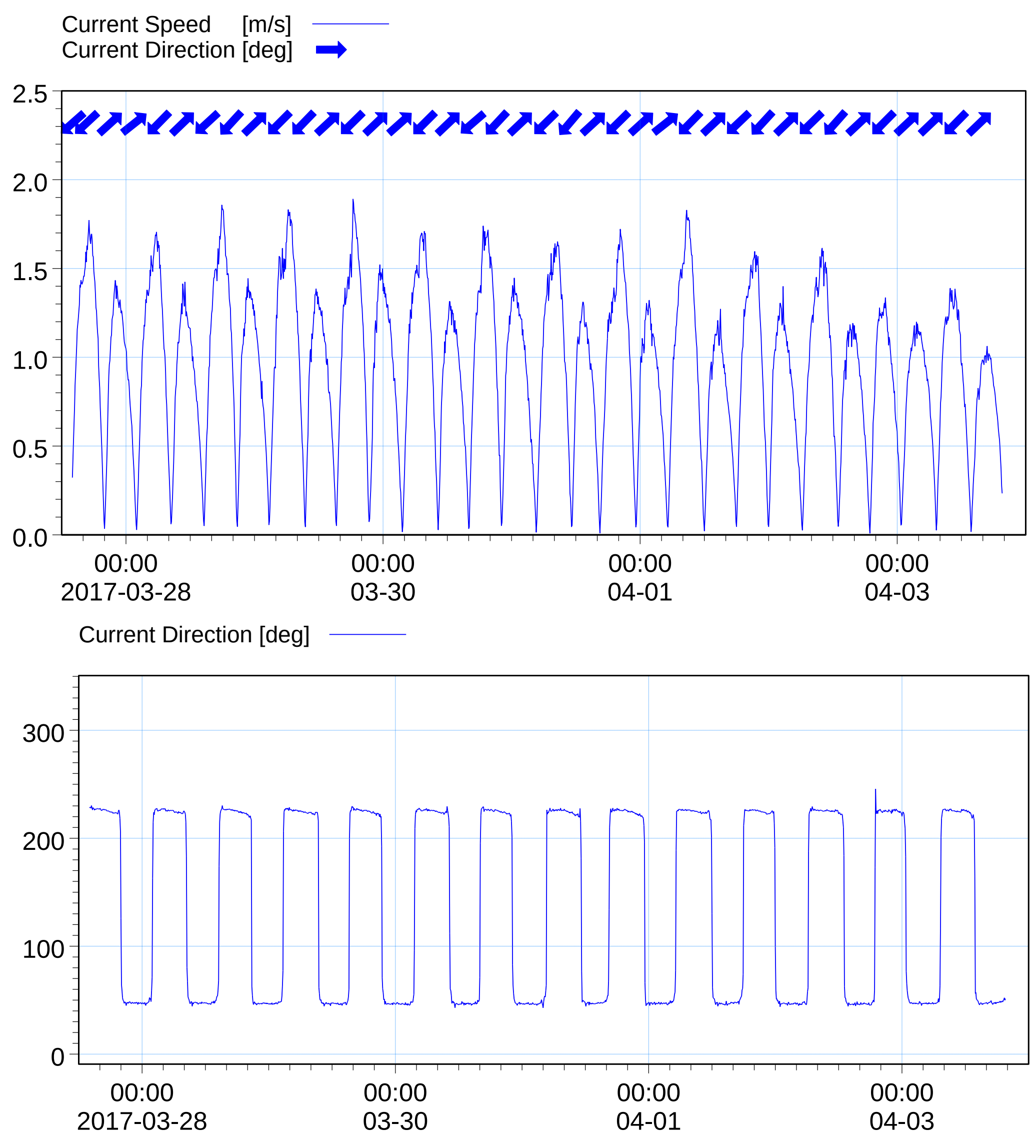

Figure 2-3: Depth averaged current speed and direction obtained from RPS EH site measurements

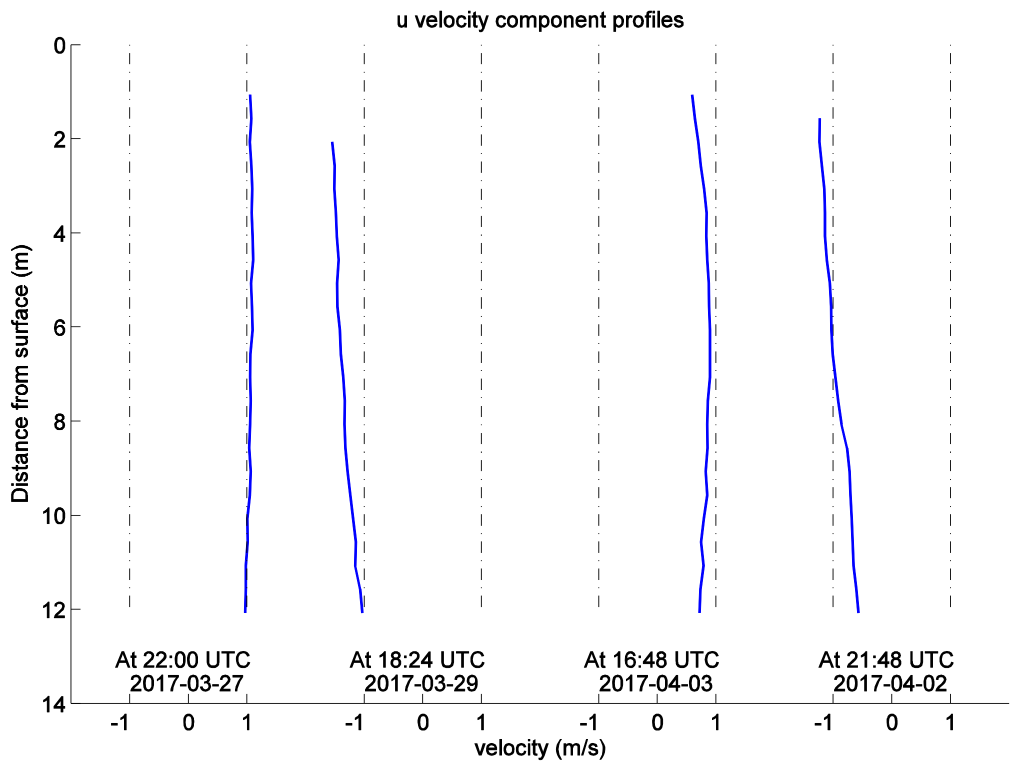

Figure 2-4: Profiles of u-velocity component at Southport

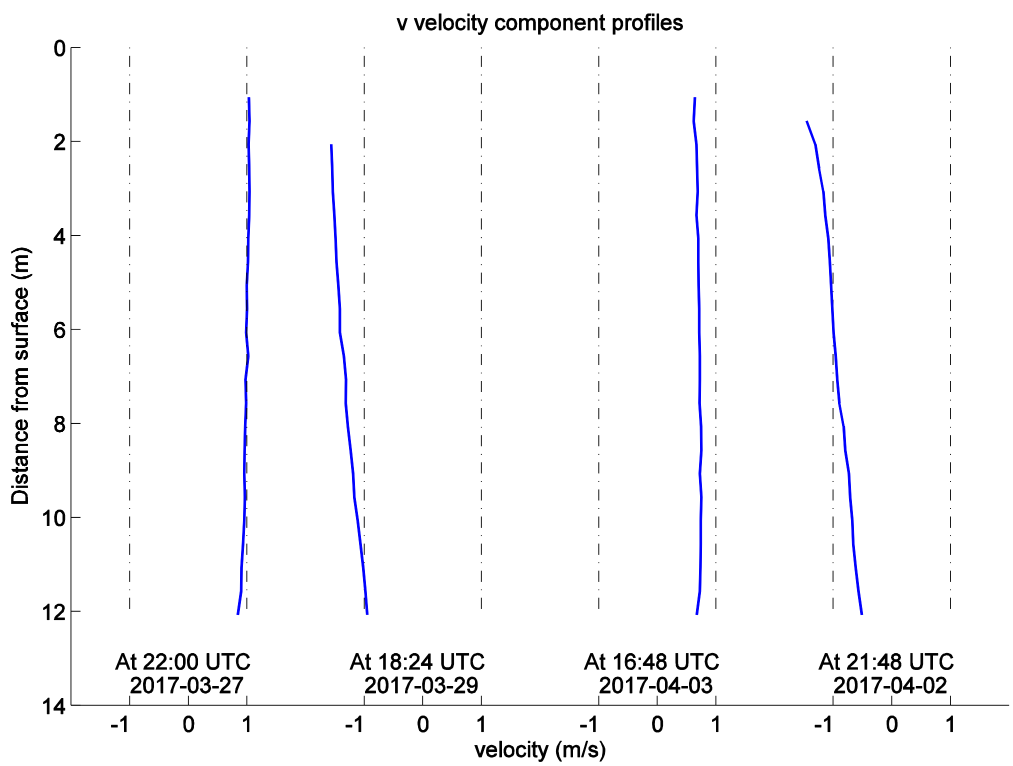

Figure 2-5: Profiles of v-velocity component at Southport

2.3. Discharges

Discharges and current velocities were measured at the same time in three areas of the Cape Fear River using three vessels equipped with downward looking ADCPs configured with bottom tracking. The three areas were Southport, Snows Cut, and Wilmington Harbor. In each area, measurements were performed along a series of transect lines across the channel. In total, there were 11 transects. Measurements were collected between March 29, 2017 and March 31, 2017. The locations of the transect lines are shown in Figure 2-6 to Figure 2-9.

Figure 2-6: Transects in Upper Wilmington area

Figure 2-7: Transects in Lower Wilmington area

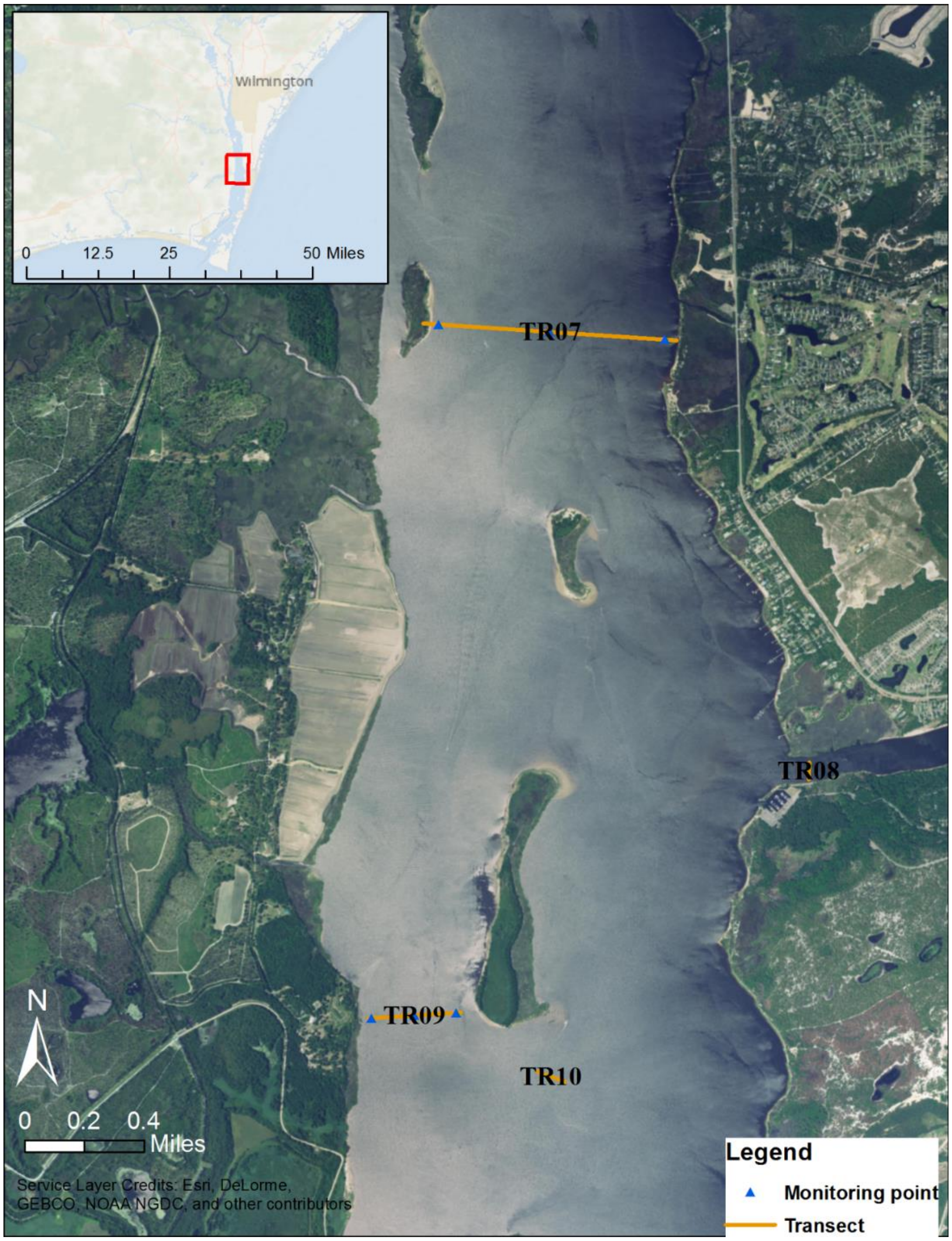

Figure 2-8: Transects in Snow's Cut area

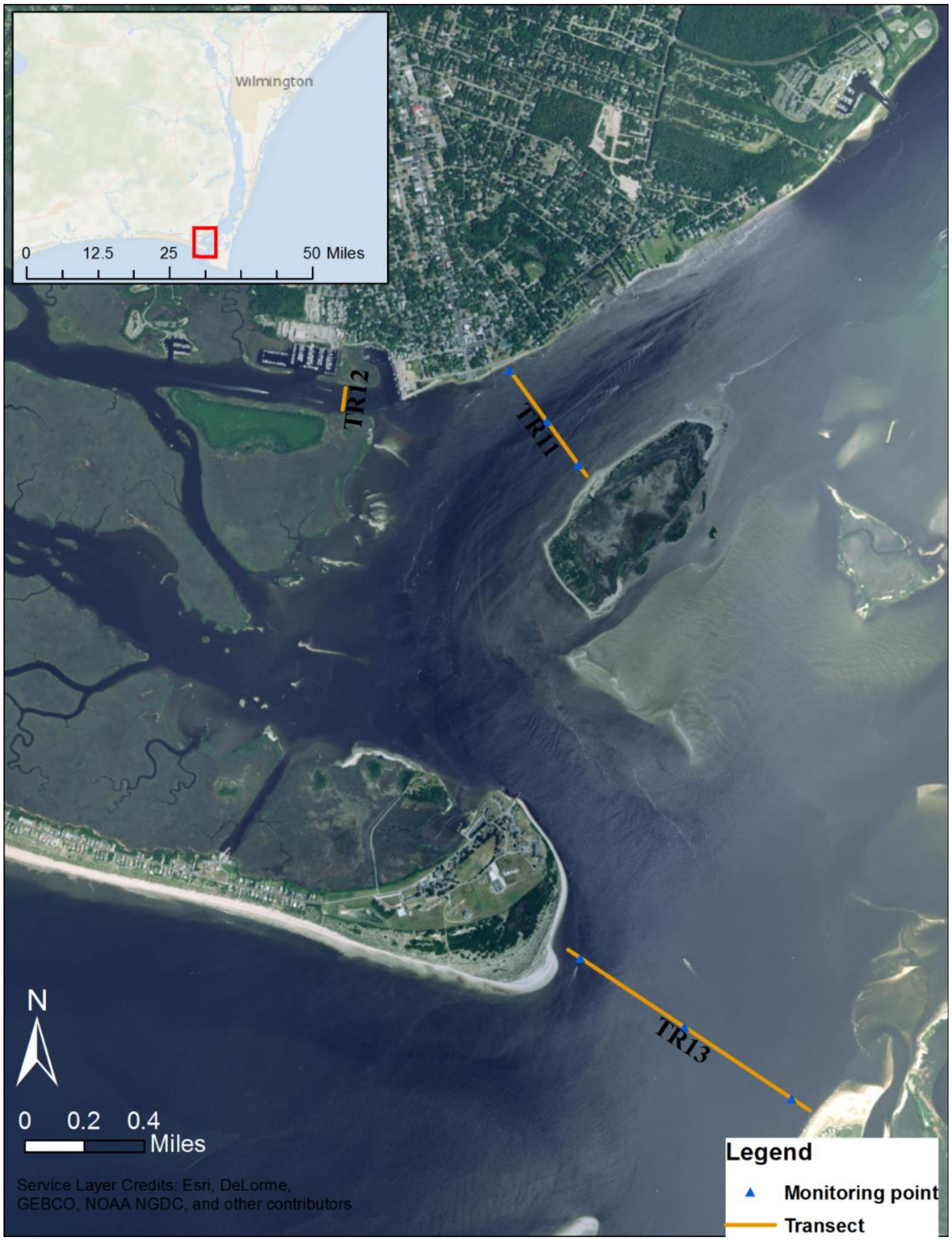

Figure 2-9: Transects in Southport area

The data collected during the current survey was processed using Teledyne RDI's WinRiver software to calculate discharge across each transect. Figure 2-10 to Figure 2-13 show the discharge measurements for all of the transects, and it can be observed that full flood and ebb tide cycles were captured inside the estuary from Wilmington to Southport during the field measurements.

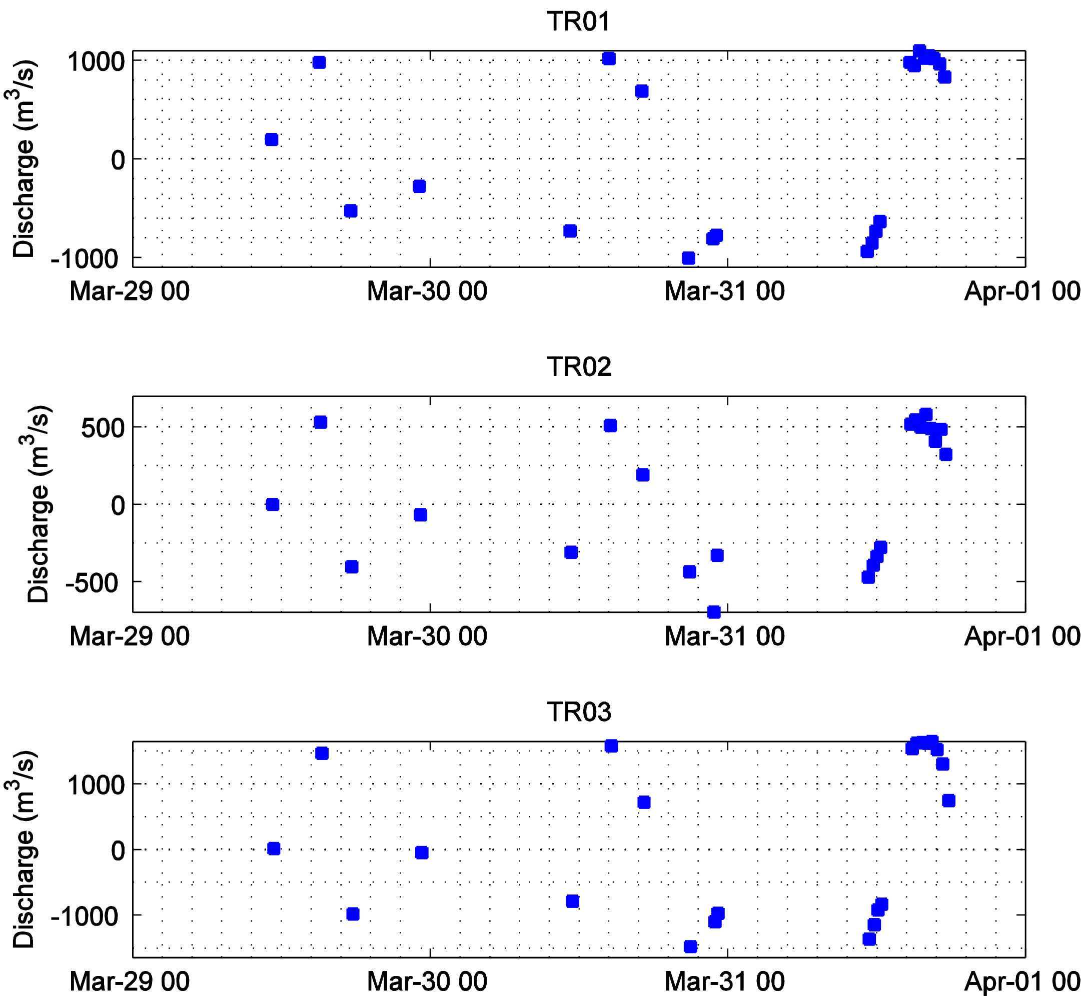

Figure 2-10: Measured discharges across transects in Upper Wilmington area

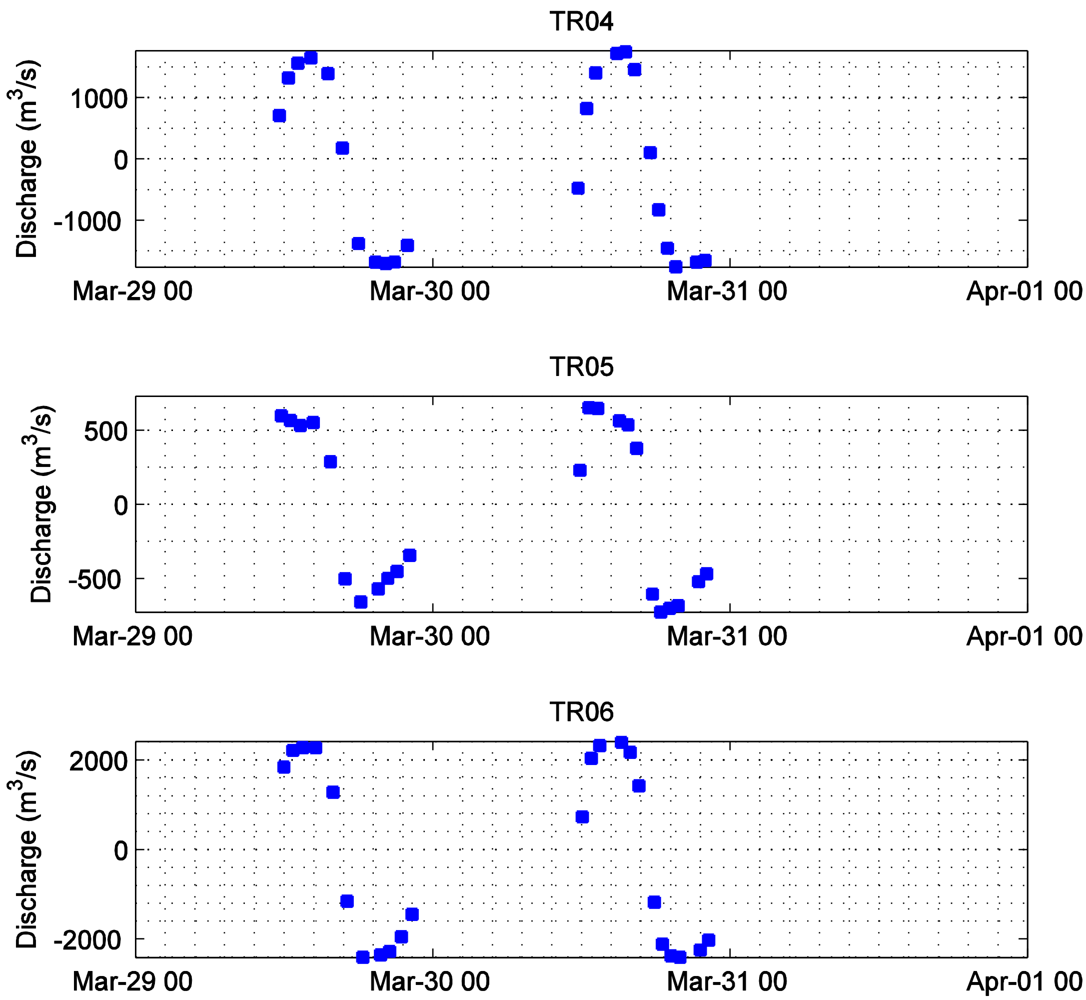

Figure 2-11: Measured discharges across transects in Lower Wilmington area

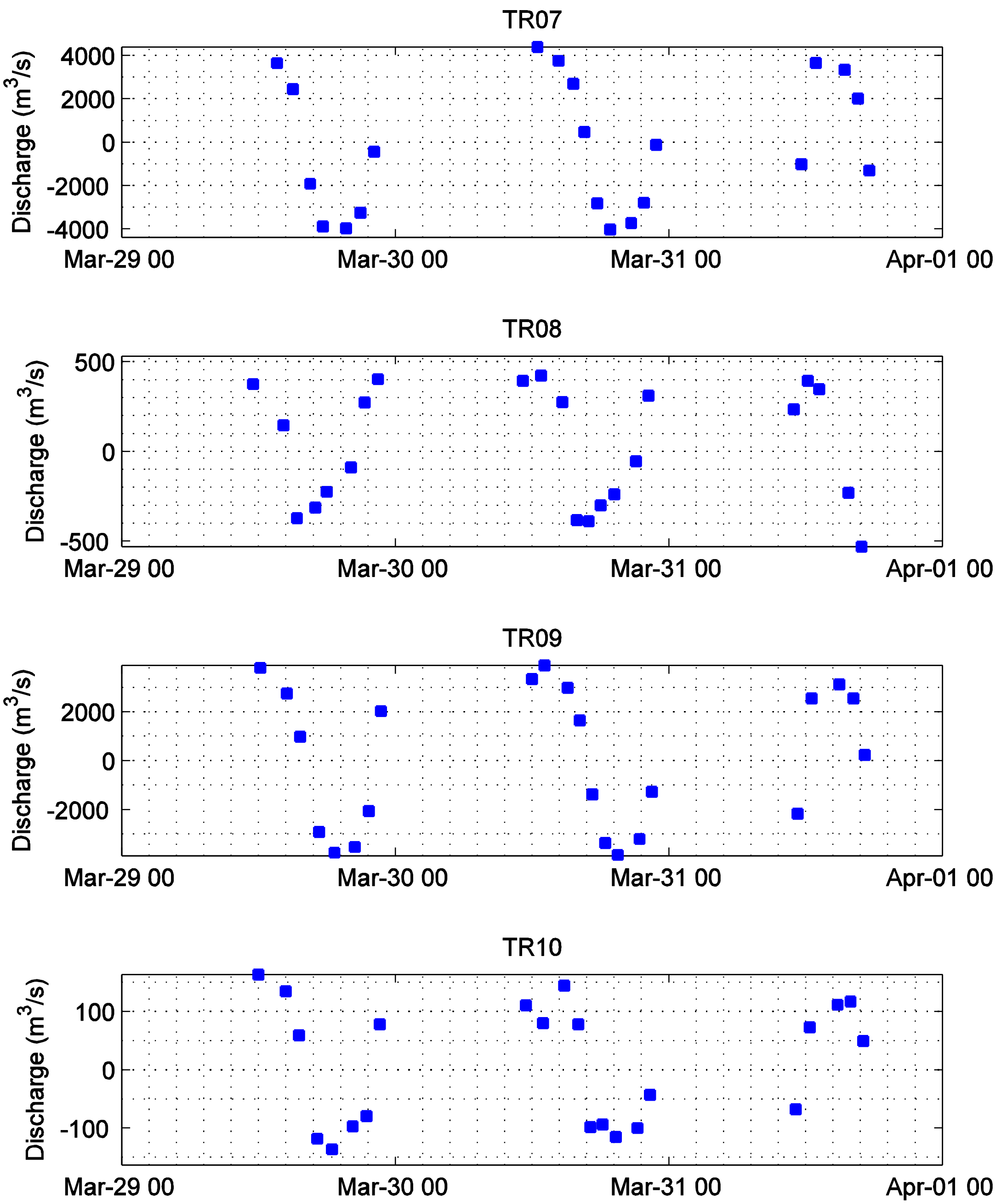

Figure 2-12: Measured discharges across transects in Snow's Cut area

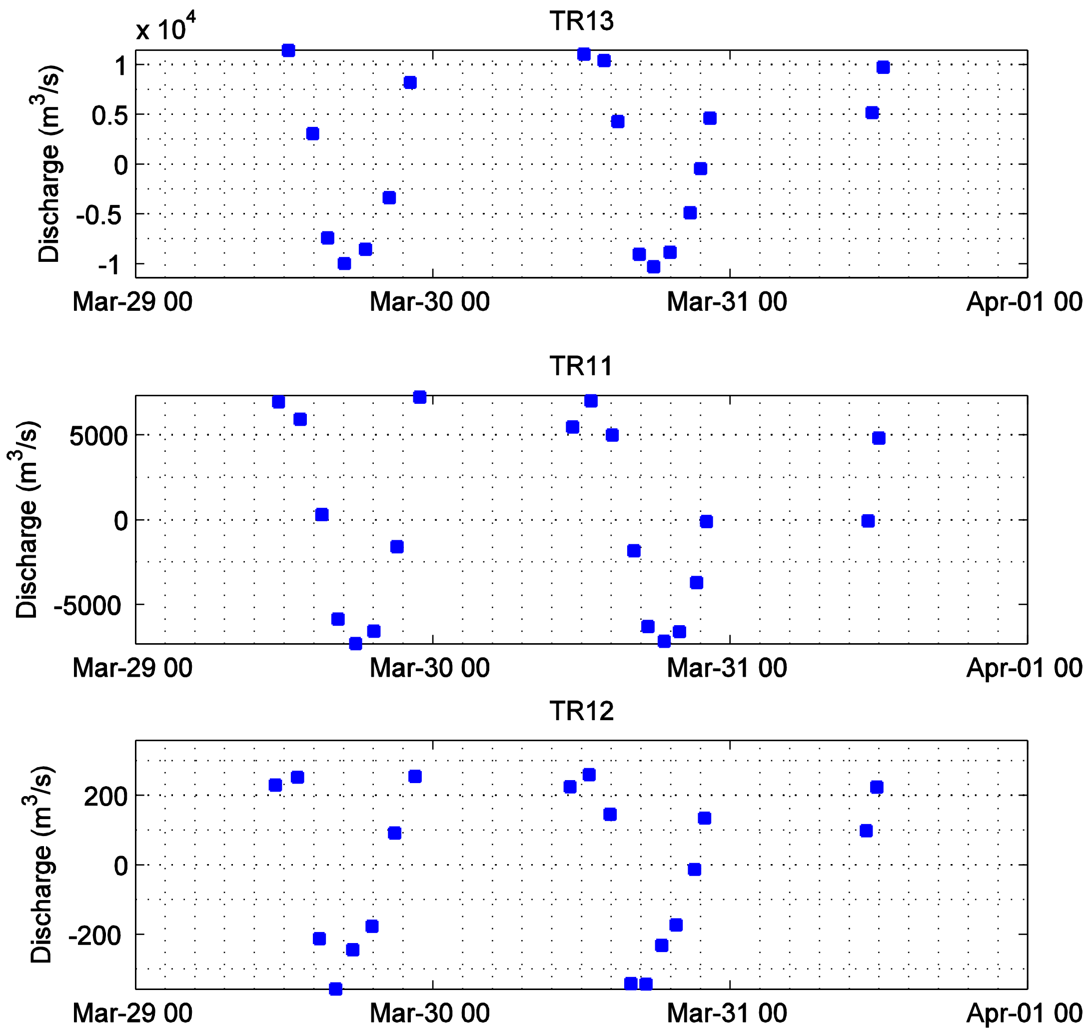

Figure 2-13: Measured discharges across transects in Southport area

2.4. Salinity

2.4.1. March 2017 Measurements

Long-term salinity measurements at two locations along the estuary were available from the March 2017 measurement period. At each of the two stations (see Figure 2-1 for locations of South and North stations), surface and bottom instruments, positioned approximately 3 ft above the water bottom and 3 ft below the average low water surface elevation, respectively, were deployed. Additional summary information for these stations is included in Table 2-1. Instruments collected data averaged over 8 seconds at 1-minute intervals during deployments of approximately one-week duration.

The surface and bottom instruments at each station were separately identified with the suffixes "_S" for surface and "_B" for bottom. Figure 2-14 shows an example of the measured data for the South surface and bottom instruments. The bottom instrument at the North station (identified as North_B in Figure 2-1) was completely submerged in the channel bottom mud, so did not collect any data.

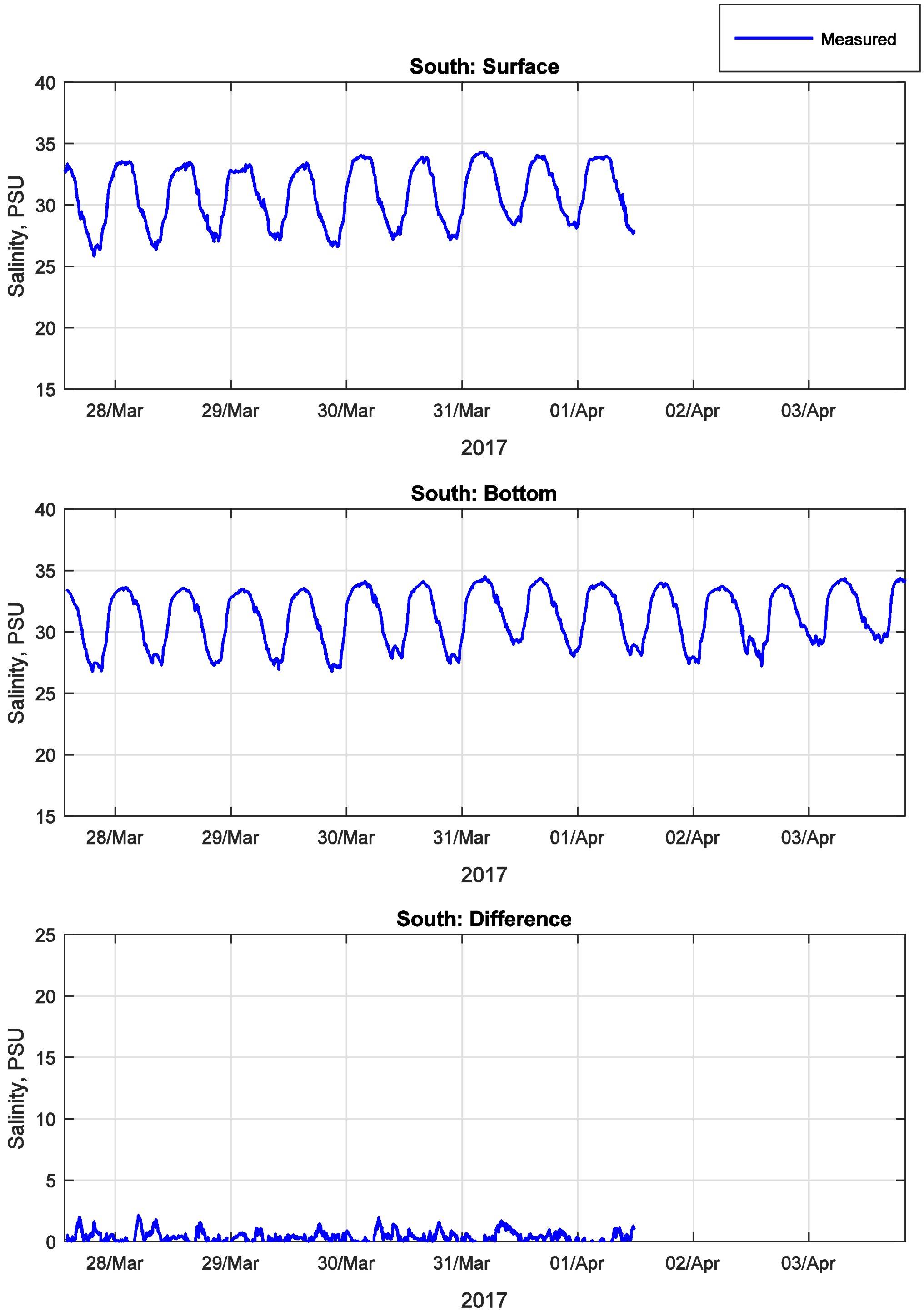

Figure 2-14: Measured surface and bottom salinity and computed difference at the South station in Late March 2017

2.4.2. August 2017 Measurements

Long-term salinity measurements at five locations along the estuary were available from the August 2017 water quality measurement campaign. At each location, surface and bottom instruments, positioned approximately 3 ft above the water bottom and 3 ft below the average low water surface elevation, respectively, were deployed. Instruments collected data averaged over 1 minute at 10-minute intervals during deployments of approximately one-month duration, so measurements were sufficient to characterize both the tidal and longer-term, subtidal salinity variations.

The locations of the August 2017 measurement stations are given in Figure 2-15 and are included in a table summarizing the fixed-station information in Table 2-1. The surface and bottom instruments comprising each station in some cases needed to be located a short distance from each other due to the availability of suitable mounting locations. To take this into account, the surface and bottom instruments at each station were separately identified with the suffixes "_S" for surface and "_B" for bottom. During this period, all upper-estuary stations (north of station Archer Daniels Midland, ADM) recorded a notable, sub-tidal freshening trend in early- to mid-August, indicating a substantial freshwater input, or freshet. Figure 2-16 shows an example of the measured data for the Kinder Morgan (KM) surface and bottom stations. The surface instrument at Cape Fear Boat Works (identified as CFBW_S in Figure 2-1) failed immediately after deployment so did not collect any data.

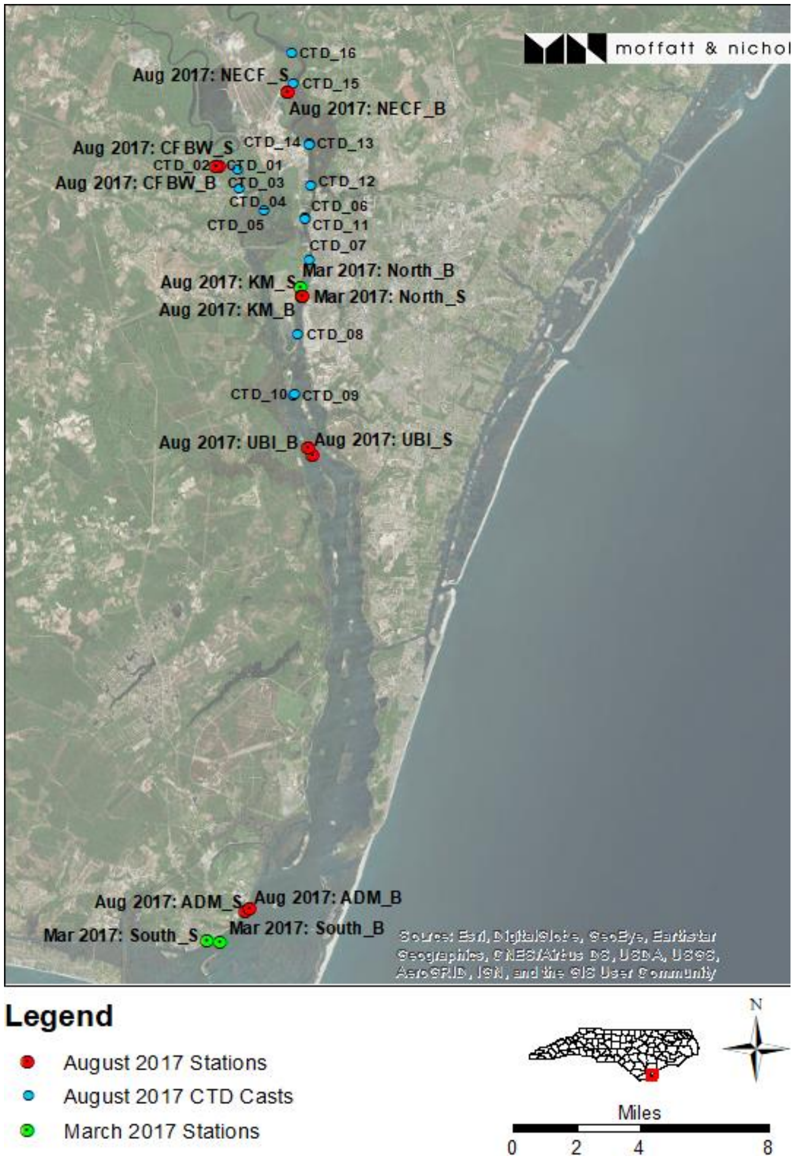

Figure 2-15: Salinity measurement locations for the August 2017 and March 2017 field campaigns.

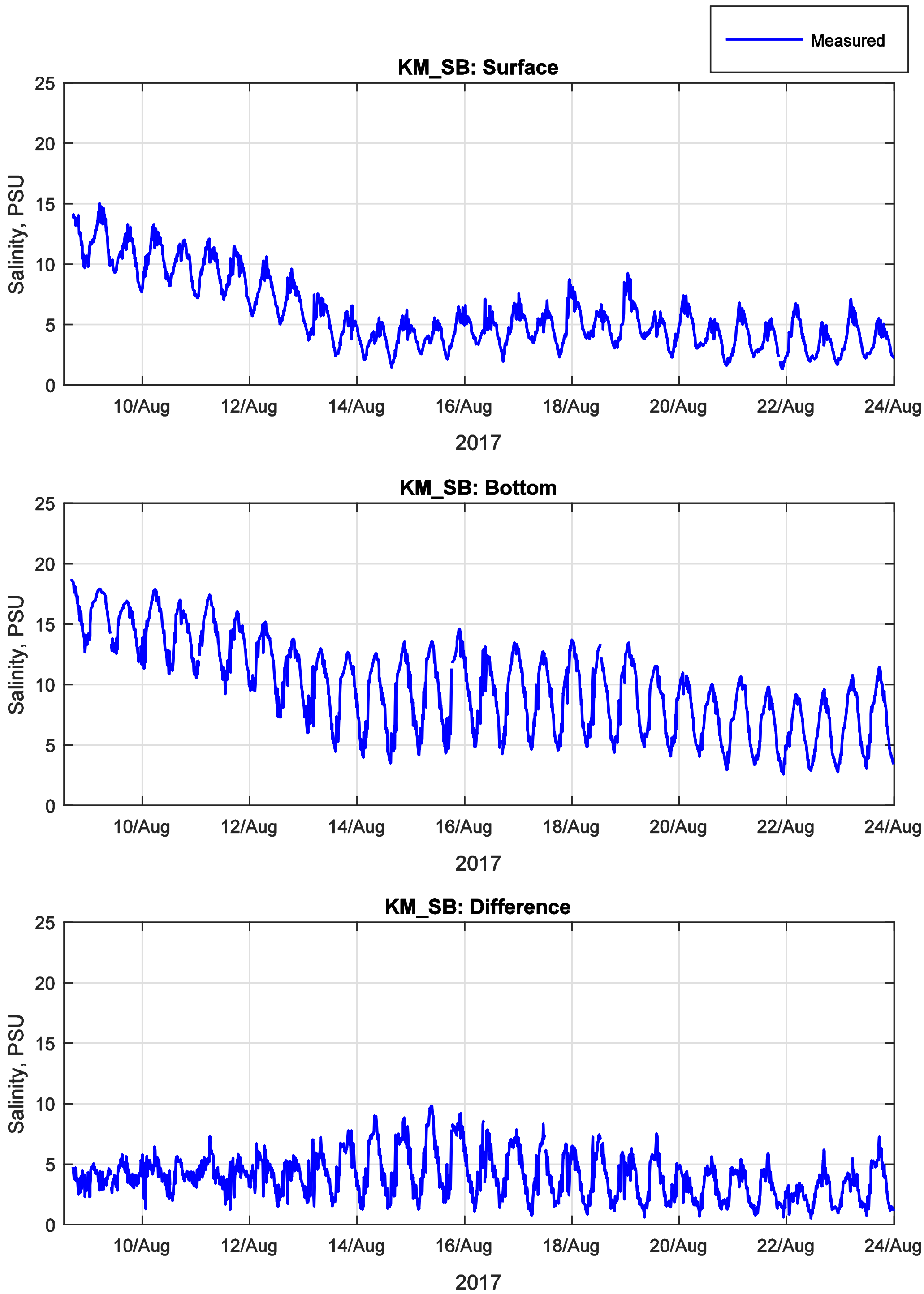

Figure 2-16: Measured surface and bottom salinity and computed difference at the Kinder Morgan station in August 2017

Table 2-1: Summary of fixed-instrument stations for salinity measurements

Station Name	Description	Latitude	Longitude	Water Depth at Station [ft]	Collected Parameters	Collection Interval [minutes]	Collection Period
ADM_S	Archer Daniels Midland Pier - Surface	33.93373°	-77.98843°	14	Salinity, Dissolved Oxygen (DO), Temperature, pH	10	8/9/2017 – 9/9/2017
ADM_B	Archer Daniels Midland Pier - Bottom	33.93465°	-77.98602°	32	Salinity, DO, Temperature, pH	10	8/8/2017 – 9/9/2017
UBI_S	Upper Big Island - Surface	34.13967°	-77.94943°	14	Salinity, DO, Temperature, pH	10	8/8/2017 – 8/29/2017
UBI_B	Upper Big Island – Bottom	34.14343°	-77.95183°	36	Salinity, DO, Temperature, pH	10	8/8/2017 – 8/28/2017
KM_S	Kinder Morgan Pier - Surface	34.21190°	-77.95469°	24	Salinity, DO, Temperature, pH	10	8/8/2017 – 9/2/2017
KM_B	Kinder Morgan Pier - Surface	34.21175°	-77.95472°	31	Salinity, DO, Temperature, pH	10	8/8/2017 – 9/7/2017
NECF_S	Northeast Cape Fear River - Surface	34.30452°	-77.96090°	27	Salinity, DO, Temperature, pH	10	8/8/2017 – 9/3/2017
NECF_B	Northeast Cape Fear River - Bottom	34.30452°	-77.96082°	27	Salinity, DO, Temperature, pH	10	8/8/2017 – 9/7/2017
CFBW_S	Cape Fear Boat Works - Surface	34.27100°	-77.99900°	20	-	-	-
CFBW_B	Cape Fear Boat Works - Bottom	34.27096°	-78.00043°	15	Salinity, DO, Temperature, pH	10	8/8/2017 – 9/7/2017
South_S	South Station - Surface	33.920601°	-78.009407°	-	Salinity, DO, Temperature, Turbidity, Currents, Water Levels	1	3/28/2017 – 4/2/2017
South_B	South Station - Bottom	33.919826°	-78.002425°	45	Salinity, DO, Temperature, Turbidity, Currents, Water Levels	1	3/28/2017 – 4/4/2017
North_S	North Station - Surface	34.211865°	-77.95445°	-	Salinity, DO, Temperature, Turbidity, Currents, Water Levels	1	3/28/2017 – 4/2/2017
North_B	North Station - Bottom	34.215695°	-77.954937°	-	-	-	-

2.4.3. August 2017 CTD Casts

After fixed instrument deployment for the Late Summer 2017 campaign, CTD casts were performed at sixteen (16) points along the upper estuary channel centerlines at 2 or 3 synoptic measurement times to measure vertical salinity profiles. The sixteen cast locations are shown in Figure 2-15 and labeled with the prefix “CTD_”. The locations are also shown in Figure 2-18 through Figure 2-21.

2.5. Water Quality

2.5.1. Spring 2017 Measurements

The spring measurements in March 2017 consisted of deployment of fixed instruments at two stations on the river to collect measurements of DO and temperature. At each of the two stations (see Figure 2-1 for locations of South and North stations), surface and bottom instruments, positioned approximately 3 ft above the water bottom and 3 ft below the average low water surface elevation, respectively, were deployed. Instruments collected data at 1-minute intervals during deployments of approximately one-week duration. Parameters included turbidity, DO, and temperature.

The surface and bottom instruments at each station were separately identified with the suffixes "_S" for surface and "_B" for bottom. The bottom instrument at the North station (identified as North_B in Figure 2-1) was completely submerged in the channel bottom mud, so did not collect any data.

2.5.2. Summer 2017 Measurements

RPS EH also sampled the Cape Fear River in August and September, 2017. For this period, surface- and bottom-mounted instruments were deployed at five locations along the estuary to measure DO, pH, and temperature, for a duration of approximately one month. At each location, surface and bottom instruments, positioned approximately 3 ft above the water bottom and 3 ft below the average low water surface elevation, respectively, were deployed. Instruments collected data at 10-minute intervals during deployments of approximately one-month duration, so measurements were sufficient to characterize both the tidal and longer-term, subtidal variations. Finally, water samples were collected at the five long-term stations for laboratory analyses. Samples were collected near surface and near bottom after deployment and prior to recovery. The parameters analyzed included total kjeldahl nitrogen (TKN), NO_3, total phosphorus (TP), total nitrogen (TN), BOD, DOC, DO, and Chl *a*.

The locations of the summer 2017 measurement stations are given in Figure 2-17. The surface and bottom instruments comprising each station in some cases needed to be located a short distance from each other due to the availability of suitable mounting locations. To take this into account, the surface and bottom instruments at each station were separately identified with the suffixes "_S" for surface and "_B" for bottom.

Additionally, Conductivity-Temperature-Depth (CTD) casts were performed at each of the long-term station locations shortly after deployment and before instrument recovery, and at various points along the Cape Fear River and Northeast Cape Fear River channel centerlines during the start of the campaign. Parameters included DO, salinity, temperature, pH, and Chl *a*. The sixteen cast locations are shown in Figure 2-17 and labeled with the prefix "CTD_". Overall, except for salinity, the data suggested little vertical stratification.

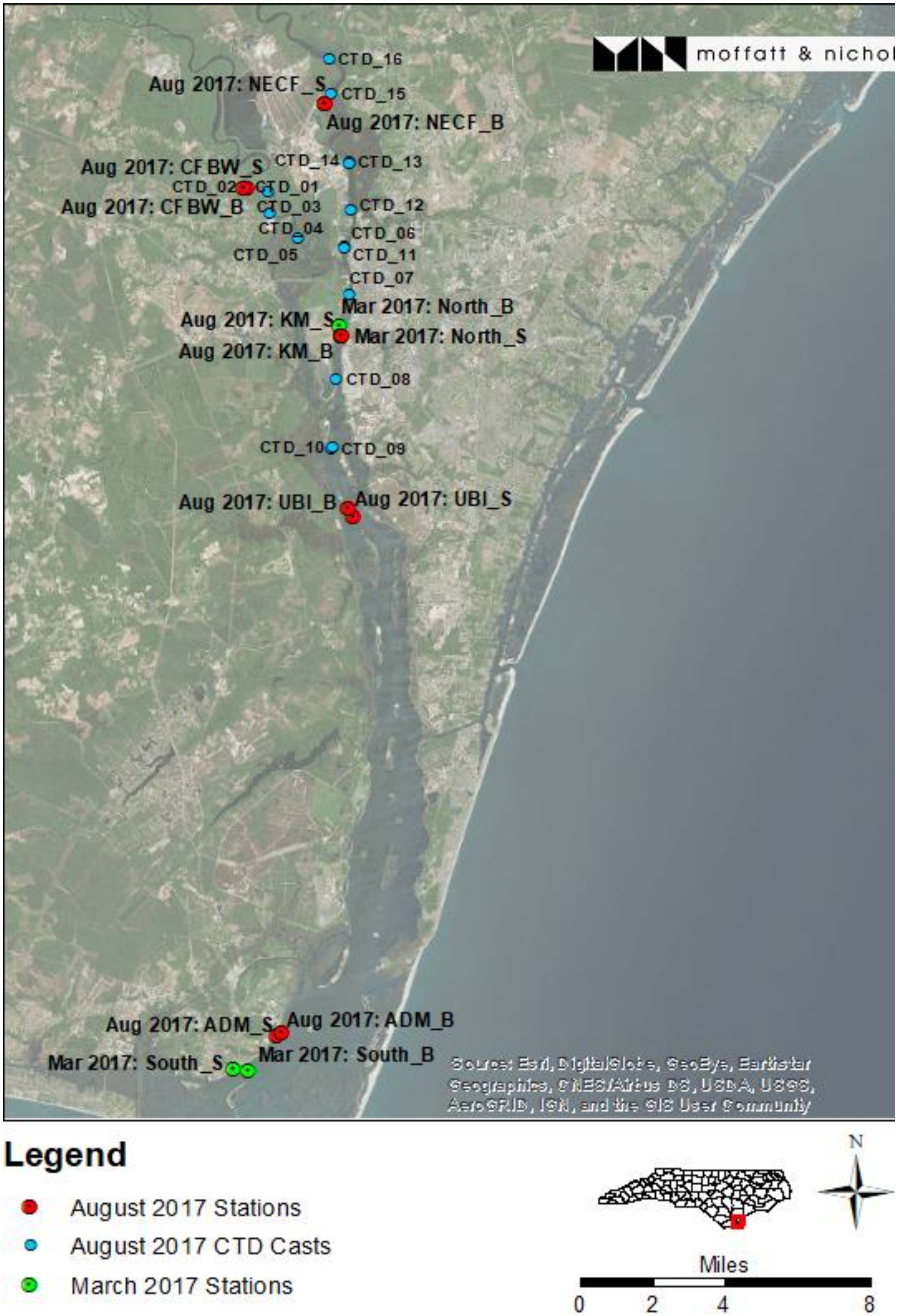

Figure 2-17: Measurement locations for the summer 2017 and spring 2017 field campaigns

2.6. Site Measurement of TSS

The cast measurements of water quality parameters over water depth were performed using an YSI EXO sonde with temperature, pressure, DO, and turbidity sensors which are referred to as “CTD casts”. The turbidity data and water samples were collected in the field and then TSS data was calculated from turbidity using calibration data. The casts and water samples were taken along transect lines TR03, TR06, TR09 and TR11 which are shown from Figure 2-18 to Figure 2-21. The casts were taken at the center of the channel except when water sampling was conducted, at which time casts were also done on the left and right sides of the channel approximately halfway up the side slope of the channel. The left and right sides were defined as the left and right sides when looking downstream of the channel. The measurement interval at the center of transect lines was approximately 30 min, and the measurement frequency at the left side and right side of transect lines was once per day.

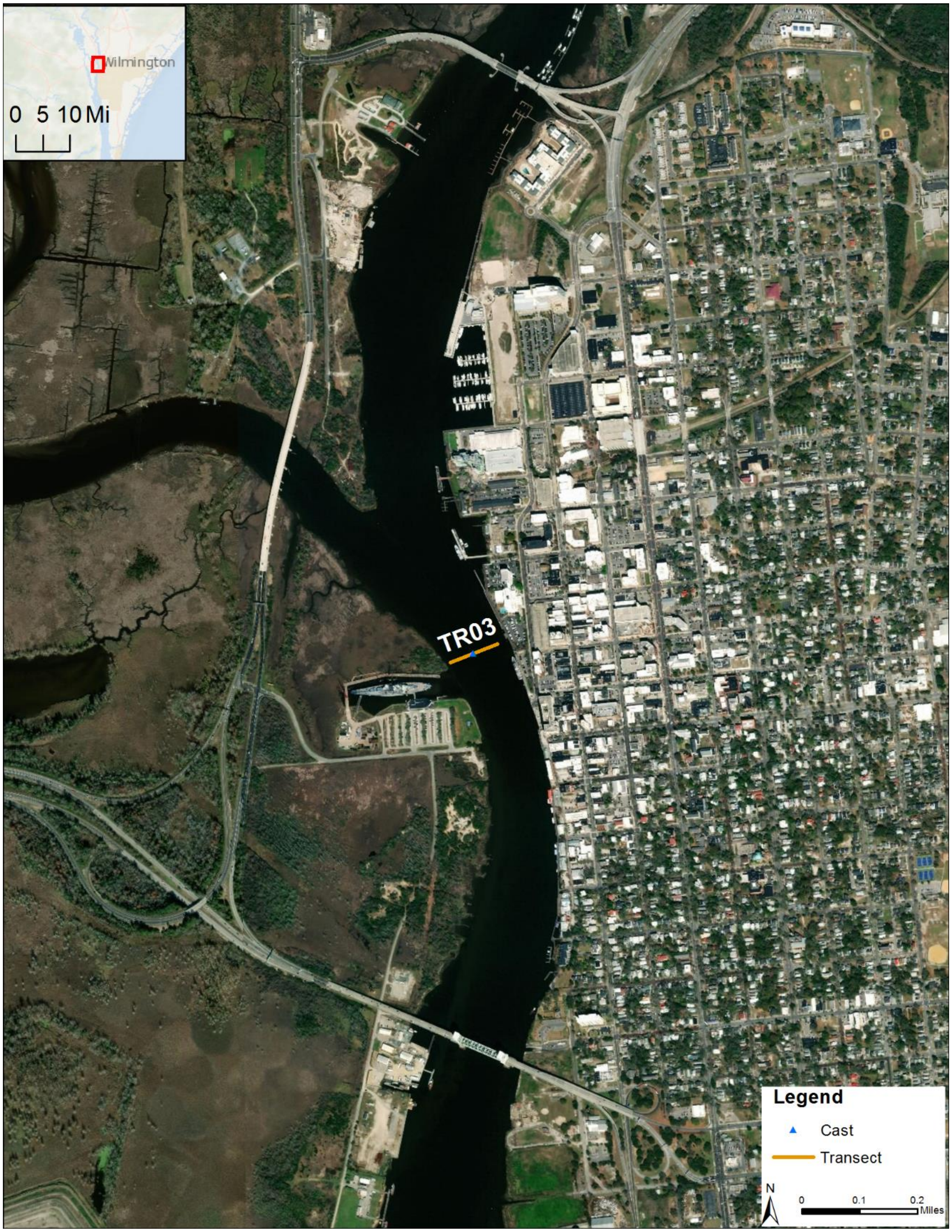

Figure 2-18: Cast and Transect in Upper Wilmington area

Figure 2-19: Cast and Transect in Lower Wilmington area

Figure 2-20: Cast and Transect in Snow's Cut area

Figure 2-21: Cast and Transect in Southport area

2.7. Bathymetry and Topography

Bathymetry and ground elevations were obtained from five datasets, which are listed below. The datasets are listed in order of increasing priority as datasets overlap in some areas.

- Navigational charts from C-MAP by Jeppesen for offshore areas
- North Carolina Department of Public Safety (NCDPS) ADCIRC grid data for upstream river channels and wetlands
- Topography from Flood Risk Information System (FRIS) for the wetlands adjoining Cape Fear river downstream of Wilmington harbor
- United Stated Army Corps of Engineers (USACE) survey data for the navigation channel
- National Ocean Service (NOS) estuarine bathymetry for the area outside the navigation channel
- Bathymetric survey from FUGRO for navigation channel bank and slope (see Geotechnical Appendix)
- Bathymetric survey from FUGRO for navigation channel in the offshore area (see Geotechnical Appendix)

For combining, all datasets were converted to reference geographic coordinates (WGS84). Vertical reference was converted to NAVD88 in meters using the NOAA VDatum software which can convert data from different horizontal/vertical references into a common system taking into the account spatial variance.

2.8. Geotechnical

A survey of the navigation channel was performed from April 25 to June 19, 2017. This survey collected low frequency and high frequency sub-bottom profiler data to image the shallow subsurface. The reports included in the Geotechnical Appendix evaluated the results of the survey and integrated the geophysical survey data with the existing geotechnical data to characterize the subsurface conditions along the Cape Fear River.

It is noted that the proposed channels will use the same side slopes as existing. Additionally, a preliminary analysis of the side slope in the Fourth East Jetty Reach indicated that widening the channel 50 ft towards the west (Eagle Island) and dredging to Elevation -50 ft-MLLW would result in the same factor of safety for stability as the existing slope.

3. Channel Design

3.1. Introduction

A real-time navigation, feasibility level, simulation study was conducted to evaluate the safety and navigability of design layouts for widening and deepening the Cape Fear River Navigation Channel. The conning of the vessels in the simulations was conducted by the Cape Fear River and Docking Pilots. This chapter documents the simulation procedures, set up, and feasibility results including recommendations for optimization of the design channel configuration.

3.1.1. Existing Navigation Channel

The existing navigation channel to the Port of Wilmington is approximately 33 miles long from the Cape Fear River pilot boarding area near 78.05°W, 33.77°N through 22 channel ranges to the Port of Wilmington facilities. The existing channel geometry is published in the current nautical charts for the Cape Fear River. Nautical charts published by the National Oceanic and Atmospheric Administration (NOAA) relevant to this area include the following:

- NOAA Nautical Chart number 11537.
- NOAA Electronic Nautical Chart (ENC) tile US5NC12M.

A summary of the existing channel ranges is provided in Table 3-1. The existing channel is shown on chart 11537 in Appendix B-1. For reference in discussion of channel locations throughout this report, channel stationing is provided on this figure. To facilitate discussion of the project geometry introduced in Section 3.2.1, the channel stationing starts offshore of the current pilot boarding area, where the new channel is expected to end. Table 3-1 provides approximate (i.e., +/- about 100 ft) range lengths based on the stationing shown in Appendix B-1.

The channel widths are provided in Table 3-1 for each range of the existing channel. Beginning offshore, the existing channel is 500 ft wide at the pilot boarding station and widens to 900 ft approaching the first bend at Bald Head Shoal. Through the following several ranges, the channel narrows back to 500 ft before entering the large turn around Battery Island. Upstream of Battery Island, the channel narrows to a typical width of 400 ft, with three exceptions:

- A 600 ft wide passing area extending from Lower Midnight Range to Lower Lilliput Range.
- Upper Big Island range, which is 660 ft wide.
- Fourth East Jetty Range, and the channel adjacent to the Wilmington terminal facilities, which are 500 ft wide.

The bearings of marked channel ranges are provided for reference in Table 3-1. Each bearing is reported as stated on the ENC, along with a precise measurement of the bearing from the range marker locations.

Recent (2014) ship traffic was studied using Automatic Identification System (AIS) data obtained from the United States Coast Guard to develop a baseline understanding of the current traffic in the channel. Appendix B-1 has a figure showing a traffic intensity map overlaid on chart 11537, which shows trends of traffic using the existing channel as well as a figure showing typical transit speeds for vessels along the length of the channel based on historic traffic.

Table 3-1: Summary of Existing Channel Ranges and Marked Range Headings

ID	Range Name	Begin Station	End Station	Approx. Length [ft]	Channel Width [ft]	Range Marker Description	Range Bearing Reported on ENC	True Geodetic Bearing of Range Shown on ENC
1	Bald Head Shoal Reach 3	494+00	803+00	30,900	500-900	Inbound	014	014.3
2	Bald Head Shoal Reach 2	803+00	846+00	4,300	900	No Range Markers		
3	Bald Head Shoal Reach 1	846+00	890+00	4,400	700	Inbound	043	043.5
4	Smith Island	890+00	943+00	5,300	650	Inbound	008	008.3
5	Bald Head Caswell	943+00	961+00	1,800	500	No Range Markers		
6	Southport	961+00	1015+00	5,400	500	Inbound	320	320.3
7	Battery Island	1015+00	1040+00	2,500	500	No Range Markers		
8	Lower Swash	1040+00	1138+00	9,800	400	Inbound	055	055.7
9	Snows Marsh	1138+00	1296+00	15,800	400	Inbound	045	045.9
10	Horseshoe Shoal	1296+00	1357+00	6,100	400	Outbound	204	203.7
11	Reaves Point	1357+00	1422+00	6,500	400	Outbound	185	185.3
12	Lower Midnight	1422+00	1505+00	8,300	600	Inbound	014	014.5
						Outbound	194	194.5
13	Upper Midnight	1505+00	1642+00	13,700	600	Inbound	359	359.5
						Outbound	179	179.6
14	Lower Lilliput	1642+00	1750+00	10,800	600	Inbound	012	012.5
15	Upper Lilliput	1750+00	1849+00	9,900	400	Outbound	173	173.0
16	Keg Island	1849+00	1927+00	7,800	400	Inbound	003	003.2
17	Lower Big Island	1927+00	1963+00	3,600	400	Inbound	331	332.1
						Outbound	151	151.4
18	Upper Big Island	1963+00	1998+00	3,500	660	Inbound	314	314.4
						Outbound	134	134.4
19	Lower Brunswick	1998+00	2080+00	8,200	400	Inbound	333	333.2
						Outbound	153	153.3
20	Upper Brunswick	2080+00	2121+00	4,100	400	Inbound	011	011.4
21	Fourth East Jetty	2121+00	2211+00	9,000	500	Outbound	184	184.1
22	Between Channel	2211+00	2238+00	2,700	500	No Range Markers		

3.1.2. Summary of Terminals Along Channel

A baseline understanding of the existing terminals along the Cape Fear River is provided here as a reference. This summary is intended to include terminals which contribute substantially to the vessel traffic and/or are located near the channel such that moored vessels may have an influence on the current channel widening efforts, or vice versa. Terminals along the Cape Fear River between the mouth of the river and the turning basin at Wilmington include:

- **Archer Daniels Midland (ADM) Terminal**: The ADM terminal is located on the green side of the Snows Marsh range (Station 1180+00). This terminal receives tankers up to Panamax size.

- **Military Ocean Terminal Sunny Point (MOTSP)**: This terminal is located on a restricted side channel on the Reaves Point Range (Station 1370+00). This terminal is located sufficiently far from the channel that moored vessels are not of concern to the channel widening project.

- **National Gypsum Terminal**: The National Gypsum Terminal is located on the red side of the channel approximately 1 mile south of the Port of Wilmington Berth 9 (Figure 3-1). This is the first of five private terminals encountered on the red side of the channel for inbound transit immediately south of the Port of Wilmington Berth 9. This terminal is not presently in use but can facilitate up to Panamax class vessels.

- **Kinder Morgan River Road Terminal**: This terminal (Figure 3-1) is immediately north of the National Gypsum Terminal and receives Panamax tankers.

- **Chemserve / Blue Knight Energy**: This terminal (Figure 3-1) is shared, with multiple users. Vessels calling at this terminal include Articulated Tug Barges (ATBs) and Panamax tankers.

- **Carolina Marine Terminal**: This is a bulk handling terminal (Figure 3-1), which takes vessels up to Panamax size.

- **Apex Oil Terminal**: The Apex terminal (Figure 3-1) takes tankers up to Panamax size.

- **Port of Wilmington Facility**: The Port of Wilmington facility consists of nine berths. Berths 1 to 7 are used for a combination of general cargo, bulker, and tanker traffic. Berths 8 and 9 are used for container vessels.

- **Kinder Morgan Terminal**: The Kinder Morgan Terminal is immediately north of the Port of Wilmington facility and was recently modified to make room for a larger turning basin. The vessels for this terminal now berth at Port of Wilmington Berth 1.

Figure 3-1: Identification of Terminals

3.1.3. Objectives

The objective of this simulation effort is to evaluate the critical navigation characteristics of design layouts (Section 3.2.1) for widening and deepening the Wilmington channel. These layouts were developed by M&N in consultation with the Cape Fear River pilots. In support of overall conclusions regarding the layouts, seven specific focus areas were identified in the simulation plan report to focus the efforts of this study. Each focus area is summarized as follows with the associated objective.

- **Entrance Turns**: Validate the channel geometry for the entrance turns, and evaluate alternative geometries at Battery Island, to provide sufficient room for navigation, while minimizing encroachment on Bald Head Island, Fort Caswell, and the town of Southport and minimizing the volume of new dredging required.

- **Turning Basin, Berthing Area and Adjacent Channel**: Evaluate/confirm the turning basin and channel width required for a 12,400 TEU design vessel navigating past a moored vessel of similar size in the Port of Wilmington and berthing at the port.

- **One-way Traffic Width in Channel**: Evaluate a channel width of 500 ft for one-way traffic in the river.

- **Two-way Traffic Width in Channel**: Evaluate a channel width of 800 ft for two-way traffic in the river.

- **One-way Traffic Width Offshore**: Evaluate a channel width of 600 ft for one-way traffic in the offshore portion of the channel (exposed to waves).

- **Two-way Traffic Width Offshore**: Evaluate a channel width of 900 ft for two-way traffic in the offshore portion of the channel (exposed to waves).

- **Aids to Navigation**: Confirm aids to navigation (ATON) and identify any modification or additions thereof.

3.1.4. Participants and Observers

The people listed in Table 3-2, participated or were present during all or part of the simulations at Moffatt & Nichol's Wilmington, NC office, January 24-30, 2018. Mariners from the project site are included in real-time simulation programs to take advantage of their local knowledge and expertise. This ensures that the simulations are conducted as close to real life as possible. Vessels transiting the federal channels in Wilmington NC typically use the services of both river pilots and docking pilots. The docking pilots typically dock and undock the ship, including the turning maneuver. The river pilots navigate all other portions of the federal channel. These Feasibility Simulations were conducted in the same manner.

Table 3-2: Simulation Participants

Participant	Organization	Role
Capt. Scott Aldridge	Cape Fear River Pilots Association	River Pilot
Capt. Bill Hue	Cape Fear River Pilots Association	River Pilot
Capt. Jason McDowell	Cape Fear River Pilots Association	River Pilot
Capt. Steve Phillips	Cape Fear River Pilots Association	River Pilot
Jerry Diamantides	David Miller Associates	Project Coordinator
Capt. Glenn Tuberville	McAllister Towing	Docking Pilot
Capt. Randy Bussey	McAllister Towing	Tug Captain & Docking Pilot
Jeff Shelden, P.E.	Moffatt & Nichol	Project Manager
Eric Smith, P.E.	Moffat & Nichol	Simulation Director
Gwen Lawrence	Moffat & Nichol	Simulation Operator
Mark Blake, P.E.	North Carolina State Ports Authority	Director of Engineering at North Carolina State Ports Authority - Observer
Dennis Webb, P.E.	Webb Simulation Consulting	Lead Observer

3.2. Simulation Inputs

3.2.1. Navigation Channel Design

The overall channel design effort for this project will consider depths between the existing 42-ft MLLW (mean lower low water, datum for all depths) channel depth and a 50-ft channel depth. A 2-ft wave allowance will be included for offshore areas of the channel (i.e., the offshore channel will be 2 ft deeper than the river channel depth). While a range of channel depths will be considered in the project design effort, only a single design depth (47 ft) was evaluated in this simulation effort. The evaluated depth represents a middle ground of potential channel depths. It is expected that the horizontal maneuvering characteristics of the design vessel in a 47-ft channel will be representative for other channel depths in the range being considered for the design. A full simulation program will be performed at a later stage of the project to verify maneuvering characteristics after the design depth is finalized.

The 47-ft-deep channel evaluated for this study applies for the Lower Swash and all ranges up-river from there. From Battery Island Range to the pilot station, the depth will be increased to 49 ft to allow for adequate under keel clearance in areas affected by ocean waves. The new channel is to extend farther out to sea than the existing channel to reach water that is consistently deeper than the maintained channel depth. The range offshore of the current pilot boarding station (Sta 490+00) will have a heading of approximately 30° (inbound), which, is approximately 16° shifted from Bald Head Shoal Reach 3 (14°). The purpose of this heading change is to reach deeper water in the most direct path and reduce dredging costs.

The widths for the new channel are in general terms as follows:

- One-way traffic width in the river (upstream of Sta 1140+00): 500 ft
- Two-way traffic width in the river (upstream of Sta 1140+00): 800 ft
- One-way traffic width offshore: 600 ft
- Two-way traffic width offshore: 900 ft

A more detailed summary of these channel widths applied to each range is shown in Table 3-3, which compares the simulated channel widths to the existing channel widths. In each case, a note is made regarding how the widening is proposed to be applied. In general, widening is proposed as a symmetric increase in width, moving the channel boundaries equally in both lateral directions. However, several of the ranges near the entrance of the river are widened asymmetrically either to avoid dredging very shallow areas or to improve navigability through the bends.

Dredge cut-slopes, based on previous USACE dredging of the channel, were assumed 3:1 horizontal to vertical for the river portion of the channel and 5:1 for offshore areas, which are similar to the slopes on the existing channel. These side slopes were used when developing the bathymetry for the hydrodynamic model. However, the side slopes were not incorporated in the simulation scene. Bank effects will be evaluated as part of a full simulation program during the Pre-Construction Engineering & Design (PED) Phase of the project.

A brief discussion of the modifications to existing ranges is provided below (see also Appendix B-1). Except where otherwise noted, only a single design configuration was considered for each channel range:

- **Bald Head Shoal Reach 3**: Two alternatives were evaluated for this range. The first provides a 900-ft-wide, two-way channel; the second provides a 600-ft, one-way channel, which widens out to the existing 900-ft width as it approaches the mouth of the river. Both of these alternatives were evaluated in this simulation study; however, the choice of which alternative to use for the new channel design will be made based on port planning analysis and dredging costs.

- **Bald Head Shoal Reach 2**: The width and orientation of this range remained unchanged from the existing channel design.

- **Bald Head Shoal Reach 1**: The red side channel boundary was maintained on the existing alignment and, the green side channel boundary was extended 200 ft. With this approach, the only increase in encroachment on Bald Head Island was from the daylighting of the cut slope of the deeper dredge depth. The additional channel width was claimed from the shallower areas toward the Jay Bird Shoals. The bearing of the range remained unchanged for this simulation effort.

- **Smith Island Channel**: The green side channel boundary was maintained on the existing alignment and the red side channel boundary was extended an additional 250 ft, for a total channel width of 900 ft. This channel width was consistent with the other ranges leading up to the main entrance turn around Battery Island. The preference for current traffic to use the red side of the channel in deep water, combined with the shallow banks on the green side, provide good justification for widening on the red side of the channel. The bearing of the range remained the same for this simulation effort.

- **Bald Head Caswell**: The Bald Head Caswell range was widened to 700 ft in an asymmetric manner (refer to layout details in Appendix B-1). The asymmetry results from a gradual transition along the range from the Smith Island Range, where widening was only provided on the red side, to a symmetric widening where Bald Head Caswell meets Southport Range. A range bearing for Bald Head Caswell changes from the existing channel; however, the range is short and there are no markers for the existing range.

- **Southport**: The Southport range widens from 700 ft to 800 ft while transitioning from a symmetric (100 ft on each side) widening at the downstream end to an asymmetric widening at the upstream end. The red side of the range meets up with the existing red side channel boundary before the turn at Battery Island. This angle slightly increases the total angle of the Battery Island turn, but it sets the channel up further to the southwest before the turn which allows for a more gradual turning radius while minimizing dredging volumes along the shore of Battery Island.

- **Battery Island**: The Battery Island range was eliminated (as a straight range) in the modified design for these navigation simulations. The range was replaced with a constant radius curve, with a width of 800 ft. This was a substantial change to the existing channel design; however, there was good justification for this configuration from the historic ship traffic around this turn. Vessels transiting this corner do not follow the shape of the existing channel; they proceed at a more-or-less constant radius path around the bend. Two different alternatives for the turn radius were considered in these navigation simulations: 4,000 ft radius, and 3,000 ft radius. The results of these navigation simulations determined the alternative to be included in the final channel design.

- **Lower Swash**: This range provides a transition out of the constant radius turn to the typical 500-ft, one-way channel width for the project. The red side of the channel begins on the existing channel red side boundary and transitions to a symmetric (50 ft per side) widening at the upstream end. The green side of this range runs relatively close to the shore at the town of Southport. For this simulation effort the bearing of the range remained the same.

- **Snows Marsh**: This range was widened from 400 ft to 500 ft. The widening is symmetric (50 ft on each side of the channel), so the range heading was not affected.

- **Horseshoe Shoal**: This range was widened from 400 ft to 500 ft. The widening is symmetric (50 ft on each side of the channel), so the range heading was not affected.

- **Reaves Point**: This range was widened from 400 ft to 500 ft. The widening is symmetric (50 ft on each side of the channel), so the range heading was not affected.

- **Lower Midnight**: This range is part of the existing two-way passing area. The existing channel is 600-ft wide, and the channel was widened to 800 ft symmetrically (100 ft on each side of the channel) for the simulation design. The range heading was not affected by this widening.

- **Upper Midnight**: This range is part of the existing two-way passing area. The existing channel is 600-ft wide, and the channel was widened to 800 ft symmetrically (100 ft on each side of the channel) for the simulation design. The range heading was not affected by this widening.

- **Lower Lilliput**: This range is part of the existing two-way passing area. The existing channel is 600-ft wide, and the channel was widened to 800 ft symmetrically (100 ft on each side of the channel) for the simulation design. The range heading was not affected by this widening.

- **Upper Lilliput**: Two alternatives were considered for Upper Lilliput. The first, provided an extension to the 800-ft, two-way passing area of the three adjacent ranges down-river. The second, provided only a one-way channel width of 500 ft. Both alternatives were included in the layouts evaluated for this simulation effort. However, the final decision regarding which alternative to include in the final design will be made based on port planning analysis and dredging cost, not navigation. In either case, the existing range bearings remain the same.

- **Keg Island**: This range was widened from 400 ft to 500 ft. The widening is symmetric (50 ft on each side of the channel), so the range heading was not affected.

- **Lower Big Island**: This range was widened from 400 ft to 500 ft. The widening is symmetric (50 ft on each side of the channel), so the range heading was not affected.

- **Upper Big Island**: This range is currently 660 ft wide. This range was not widened as part of this design effort.

- **Lower Brunswick**: This range was widened from 400 ft to 500 ft. The widening is symmetric (50 ft on each side of the channel), so the range heading was not affected.

- **Upper Brunswick**: This range was widened from 400 ft to 500 ft. The widening is symmetric (50 ft on each side of the channel), so the range heading was not affected.

- **Fourth East Jetty & Between Channel**: These two reaches run adjacent to the Port of Wilmington terminal and have been widened on the green side only (red side includes the terminal).

- **The Turning Basin**: The turning basin to the north of the Port of Wilmington terminal was widened from 1400 ft to 1,500 ft, with parallel east and west banks that provide an elongated turning area. This shape was designed based on the large percentage of the channel that the design vessel will block when turning. During peak flood and ebb tides, the currents may have a strong effect on the turning vessel.

Based on this summary of channel modifications, there were three specific areas where alternative configurations were explicitly evaluated in this study:

- **Bald Head Shoal Reach 1**: two different widths were considered for the potential addition of a passing area: 900-ft, two-way channel or 600-ft, one-way channel.

- **The Main Entrance Turn**: two different turn radii (4,000 ft and 3,000 ft) were considered for this entrance turn.

- **Upper Lilliput Range**: two different widths were considered for the potential addition of a passing area.

Because most of the simulations in this study focused on specific portions of the channel, the modifications were grouped into two different channel layouts for the simulations. These simulations are referred to in this report as Design Layout #1 and Design Layout #2 (see Table 3-3). The layouts are summarized as follows:

- **Design Layout #1**: This layout includes the most favorable alternatives from a navigation perspective, providing the wider channels on Bald Head Shoal Reach 1 and Upper Lilliput, and the larger turning radius on the entrance turn.

- **Design Layout #2**: This layout includes the most favorable alternatives from a perspective of minimizing dredging costs, providing the narrower channels for Bald Head Shoal Reach 1 and Upper Lilliput, and the smaller turning radius on the entrance turn.

Table 3-3: Summary of Existing and Simulated Channel Widths

ID	Range Name	Channel Widths [Ft]			Widening Approach
		Existing Channel	Design Layout #1	Design Layout #2	
1	Bald Head Shoal Reach 3	500 - 900	900	600 - 900	Symmetric
2	Bald Head Shoal Reach 2	900			-
3	Bald Head Shoal Reach 1	700	900		Green Side Only
4	Smith Island	650	900		Red Side Only
5	Bald Head Caswell	500	700		See Figures in Appendix B-1
6	Southport	500	700 - 800		See Figures in Appendix B-1
7	Battery	500	Replaced with 4000-ft Radius Curve	Replaced with 3000-ft Radius Curve	See Figures in Appendix B-1
8	Lower Swash	400	800 - 500		See Figures in Appendix B-1
9	Snows Marsh	400	500		Symmetric
10	Horseshoe Shoal	400	500		Symmetric
11	Reaves Point	400	500		Symmetric
12	Lower Midnight	600	800		Symmetric
13	Upper Midnight	600	800		Symmetric
14	Lower Lilliput	600	800		Symmetric
15	Upper Lilliput	400	800	500	Symmetric
16	Keg Island	400	500		Symmetric
17	Lower Big Island	400	500		Symmetric
18	Upper Big Island	660			-
19	Lower Brunswick	400	500		Symmetric
20	Upper Brunswick	400	500		Symmetric
21	Fourth East Jetty	500	550		Green Side Only
22	Between Channel	500	575		Green Side Only

3.2.2. Design Vessels

This section lists the vessels that were used in these simulations. Pilot cards are provided in Appendix B-2.

3.2.2.1. Deep Draft Vessels

A single deep draft vessel has been identified to serve as the design vessel for this channel improvement project: the MSC Lauren, a 12,400 TEU container vessel. The particulars of this design vessel are summarized in Table 3-4. Other containerships in the world fleet between 12,000 and 13,000 TEU capacity range have almost identical dimensions (+/- 1 ft in LOA and Beam) to the design vessel due to the size of the new Panama Canal locks. A TRANSAS software (Section 3.3.3) vessel model was identified to simulate the overall dimensions and performance characteristics of the design vessels.

Table 3-5 provides vessel particulars for the TRANSAS vessel model used for this study. The model vessel length matches the design vessel with the beam 10.7 ft (7%) wider. The slightly wider beam provides an additional factor-of-safety for the Feasibility Level Simulations. Full bridge simulations will include a vessel model that matches the design vessel. Partial load condition 3 was used for these simulations with an operational draft 2 ft (5%) less than the design vessel, which was sufficiently close for this feasibility-level channel validation. Partial load condition 1 was used for simulating the design vessel in the existing channel.

Table 3-4: Deep Draft Design Vessel

Attribute	12,400 TEU Container Vessel
Design Vessel	MSC Lauren
LOA [ft]	1,200
LBP [ft]	1,148
Beam [ft]	158.8
Operating Draft [ft]	43.0
Loaded Draft [ft]	49.2

Table 3-5: TRANSAS Deep Draft Vessel Models

Attribute	13,300 TEU Container Ship	
Vessel Model Designation	Container Ship 13 (CS13)	
Capacity [dwt]	106,896	
LOA [ft]	1,200	
Beam [ft]	169.46	
Operational Draft [ft] (fore/aft)	Partial Load 1	Partial Load 3
	37 / 38	41 / 41
Number of Propellers	1	
Max RPM	94.7	
Max Rudder Angle [deg]	35	

3.2.2.2. Tugs

Tugs were controlled in the simulator by the simulator operator and tug navigation was completed by the software autopilot. Even in the auto-controlled mode the tugs are active six-degrees-of-freedom vessels in the simulation and could run aground or collide with other vessels.

Typical tugs available in the Cape Fear River are summarized in Table 3-6. Docking pilot Glenn Turbeville of McAllister Towing Wilmington stated that four tugs would likely be needed to handle the larger 12,400 TEU vessels for docking maneuvers. TRANSAS vessel models used to simulate these tugs are summarized in Table 3-7. The completed testing matrix presented in Section 3.3.4 indicates the number of tugs used during each simulation.

Table 3-6: Typical Tugs Available in Wilmington

Name	Erin McAllister	Margaret McAllister	Maurania III	Annabelle Dorothy Moran	Cape May
Tug Type	Tractor	Tractor	Conventional Twin Screw	Tractor	Conventional Twin Screw
LOA [ft]	88	109	106	86	99
Beam [ft]	32	29	33.5	36	31
Draft [ft]	14.8	13.5	16.8	14.5	12.0
Bollard Pull [mt] or Horsepower [hp]	64 mt	52 mt	4,000 hp	5,100 hp	3,000 hp

Table 3-7: TRANSAS Tug Models

TRANSAS Vessel Model	Z-Drive Tug 1	Conventional Twin Screw Tug 5
Tug Type	Tractor	Conventional Twin Screw
LOA [ft]	82	105
Beam [ft]	34.1	32
Draft [ft]	12.8	14
Power	4,200 hp (53 mt)	2,961 hp (32 mt)

3.2.2.3. Passing Vessels

The channel was designed to support two-way traffic (passing) at specific locations along the channel. To verify the width of these passing areas, auto-piloted vessels were included in the model to simulate vessels passing in the opposite direction.

The design basis is a 12,400 TEU design vessel passing a similarly-sized vessel. The TRANSAS ship model shown in Table 3-5 for use as the design vessel was also be used as the passing vessel. The simulator includes representation of ship-to-ship interaction forces acting on the piloted vessel, but these forces were not validated or calibrated for the feasibility-level simulations. In TRANSAS the ship-to-ship interaction forces are calculated based on the pressure field induced by the passing vessel. The pressure distribution about the moving ship is approximated by three circular zones, bow, aft, and midship. If there is an intersection between the passing ships' zones, then a force is applied from the passing ship to the own ship along the line between the intersecting zones' center. For feasibility-level simulations these forces were used "as is" in the model and deemed acceptable by the pilots for preliminary channel width evaluations. Validation or calibration will be done for full bridge simulations.

The use of an auto-piloted vessel to simulate two-way traffic with a piloted ship was acceptable for feasibility level simulations. Two piloted ships will be used for the final design simulation program.

3.2.2.4. Moored Vessels

Moored vessels were included at several of the terminals within the model to provide a realistic representation of the maneuvering space available for the transiting vessels. Terminals on the Cape Fear River near the shipping channel between the mouth of the river and the Wilmington turning basin are summarized in Section 3.1.2.

Based on historic AIS data and local pilot input, typical vessels calling at the private terminals along the river, e.g., ADM, Apex Oil, and Carolina Marine Terminal, are Handysize and Panamax vessels. For this simulation effort the important factor was the beam of the vessel to evaluate the channel clearances and not the length or type. TRANSAS vessel models were identified (Table 3-8) to represent both the Handysize and Panamax vessel sizes. Both vessels had a beam of approximately 106 ft, which is the Panamax width. For all simulations the Chemical Tanker 7 vessel model was moored at the Archer Daniels Midland Terminal. For all port simulations a Handy Sized Tanker (Chemical Tanker 7) was moored at Apex Oil Terminal and Port of Wilmington Berth 3 and 5. A Panamax Oil Tanker (Oil Tanker 3) was moored at the National Gypsum Terminal and the Chemserve/ Blue Knight Energy Terminal for all port simulations.

Additionally, since the purpose of the overall channel improvement effort is to facilitate larger container vessels such as the 12,400 TEU design vessel used for this study, it was important to evaluate the clearances of the design vessel passing a moored container vessel at the Wilmington container terminal (Berth 8 or 9). For this purpose, an 8,500 TEU (Table 3-8) was moored at Port of Wilmington Berth 9 for all port simulations.

The berthed vessels were included as "target vessels" in the simulator, which means that they are represented visually and contribute a ship-to-ship interaction force to the transiting vessel. The ship-to-ship forces were present in the simulations but were not verified or evaluated in detail as part of this study.

Table 3-8: TRANSAS Vessel Models for Use as Moored Vessels

Attribute	Handy Sized Tanker	Panamax Oil Tanker	8,500 TEU Container Ship
Vessel Model Name	**Chemical Tanker 7**	**Oil Tanker 3**	**Container Ship 12**
Capacity (dwt)	50,161	59,708	125,696
LOA (ft)	600	797	1,138
Beam (ft)	105.6	105.6	148.3
Draft (ft)	42.7	36.1	50.9

3.2.3. Environmental Conditions

Environmental conditions considered in the simulations were tides, currents, waves, and winds. All simulations were performed during daylight with clear visibility. Night-time and low visibility transits were not included in this simulation effort but may be evaluated at a later stage in the design as part of a full mission bridge simulation.

The tides and currents were generated using a three-dimensional hydrodynamic model, Delft-3D-FLOW, and the offshore waves were generated using a spectral wave model, Delft-3D-WAVE, built by M&N for the Channel Improvement Project.

3.2.3.1. Tide and Current Fields

A full channel transit – inbound or outbound – typically takes 3 to 3.5 hours. Throughout this duration, the tidal currents vary during the transit. Time and space varying tidal currents were included in the simulator to account for these effects. However, the tide level was held constant at MLLW for all simulations representing a conservative under keel clearance. This is a common approach for feasibility level channel design studies. Extenuating circumstances, such as the need to "ride the tide", were not present in this effort.

The hydrodynamic model was calibrated for a period between March 27, 2017 and April 5, 2017. Comparison of the water levels from the model and the NOAA Wilmington gauge is shown in Figure 3-2. A 24-hour period (3.29.17 16:00 to 3.30.17 16:00) from the calibrated model representing the spring tide was extracted for the transit simulations. An example time series at the apex of Battery Island turn, Station 1030+00, is shown in Figure 3-3. The current magnitudes range from 0 kt to 3.5 kt along the Cape Fear River.

Both inbound and outbound transits of the 12,400 TEU vessel will be limited to flood tide around Battery Island, similar to the current protocol for the 8,500 TEU transits. Vessels do not transit during ebb tide due to complex cross currents that develop from tidal flows leaving the Intracoastal Waterway. As a result, all simulations excluding the port simulations were performed with flood tidal conditions. Because of the variation in currents along the channel a different starting time point was identified for each simulation according to simulation extent and desired tidal condition. The completed testing matrix presented in Section 3.3.4 indicates the starting current time.

Separate hydrodynamic models were developed for the different project alternatives. Although this is not typically considered necessary for feasibility level studies, this was considered appropriate for this study to characterize the significant changes to the channel around the Battery Island curves. Any modifications to the channel during the feasibility level study will be reflected in the hydrodynamic model for the full mission bridge simulations.

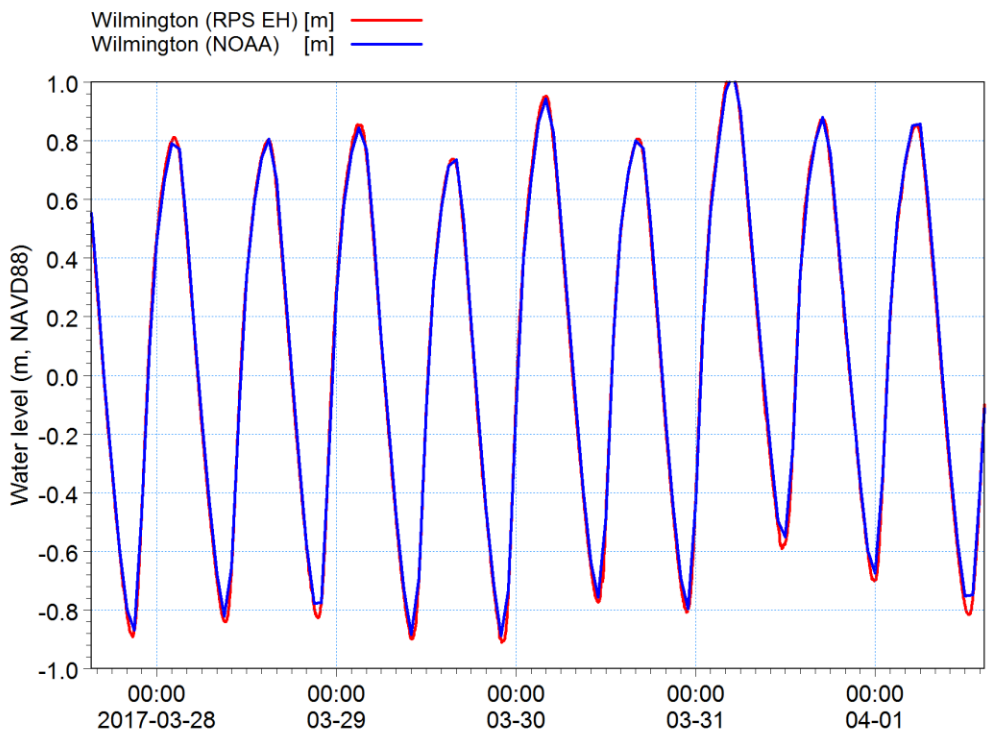

Figure 3-2: Hydrodynamic Model Comparison of Water Level Measurements to Model Results.

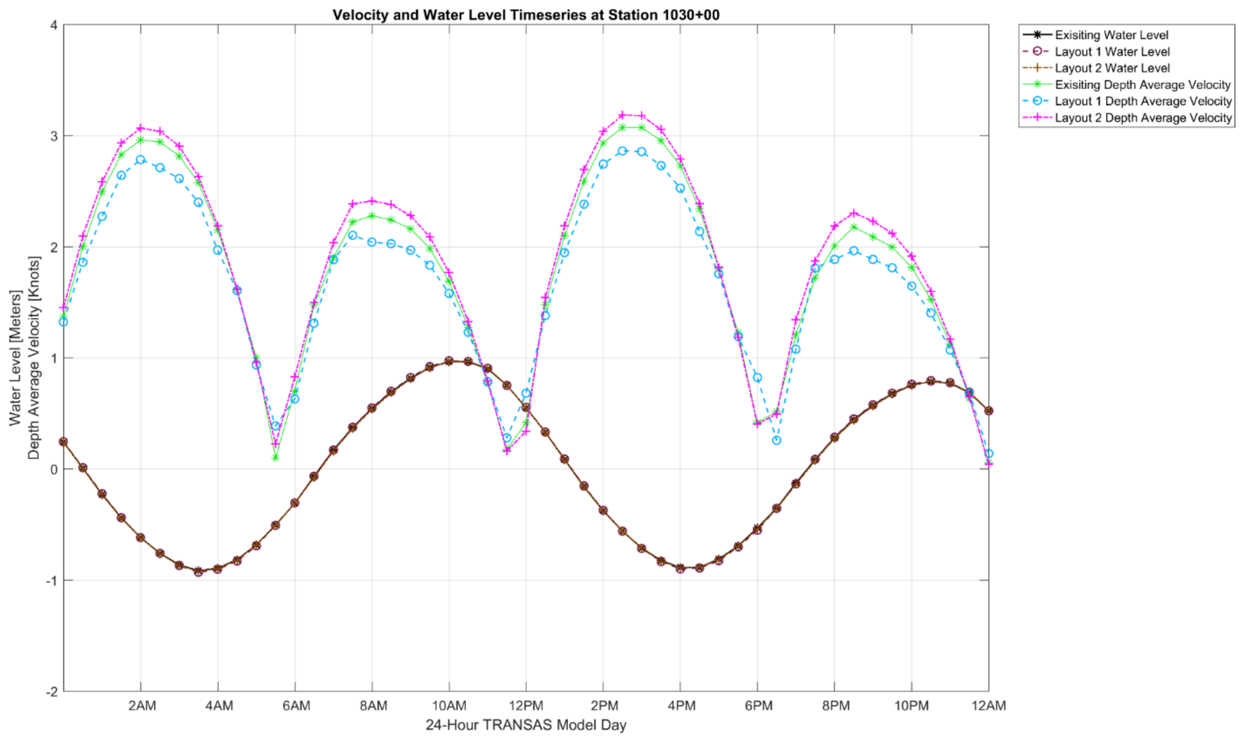

Figure 3-3: Hydrodynamic Velocity and Water Level Time Series at Station 1030+00

3.2.3.2. Wave Fields

A Delft-3D spectral wave model was developed and calibrated to provide a quantitative description of the wave climate at the channel entrance. From the spectral wave modeling the prevailing wave directions offshore of the Cape Fear River at the start of the designed navigational channel are from the southwest and southeast (Figure 3-4). As vessels transit inbound along Bald Head Shoal Reaches 2 and 1, Bald Head Island provides increasing sheltering of waves coming from the southeast. Waves from the southwest can propagate further up the channel, as can be seen on Figure 3-5, which summarizes the wave conditions where the Bald Head Caswell range meets the Southport range. Upriver beyond this point, the channel is protected almost entirely from ocean waves. However, even at the location shown in Figure 3-5, the waves have been significantly reduced.

The wave conditions (height, period, & direction) for the navigation simulations were developed from the roses at the offshore extent of the design channel (Figure 3-4 and Figure 3-6). Table 3-9 lists the design wave conditions used in the navigation simulations, along with a "typical" wave condition that was used for simulations of the existing channel. The design wave height for this study is 1.5 m. Wave conditions in the ship simulations are based on waves generated from a JONSWAP (Joint North Sea Wave Project) spectrum and therefore represent spectral variability in wave height and period. To account for the attenuation of the offshore wave as it progresses toward shore, two wave condition zones were created to represent the decreasing wave height from offshore to nearshore.

During the winter and fall months there are wind generated waves that come from the northeast. However, the entrance to the Cape Fear River is sheltered from the northeast waves by Bald Head Island. As a result, the local NE waves typically do not directly affect navigation in the entrance channel and were not included in this simulation effort.

Table 3-9: Deepwater Wave Conditions for use in Navigation Ship Simulations

Wave Condition	Deepwater Waves			Comment
	Significant Wave Height [m]	Peak Period [s]	Mean Wave Direction [deg]	
Design, SSW	1.5	8	202.5	Significant wave motion possible due to long wave period, penetrating into Cape Fear River up to the Southport Channel
Typical, SSW	1	8	202.5	Typical wave conditions used for evaluating existing channel.

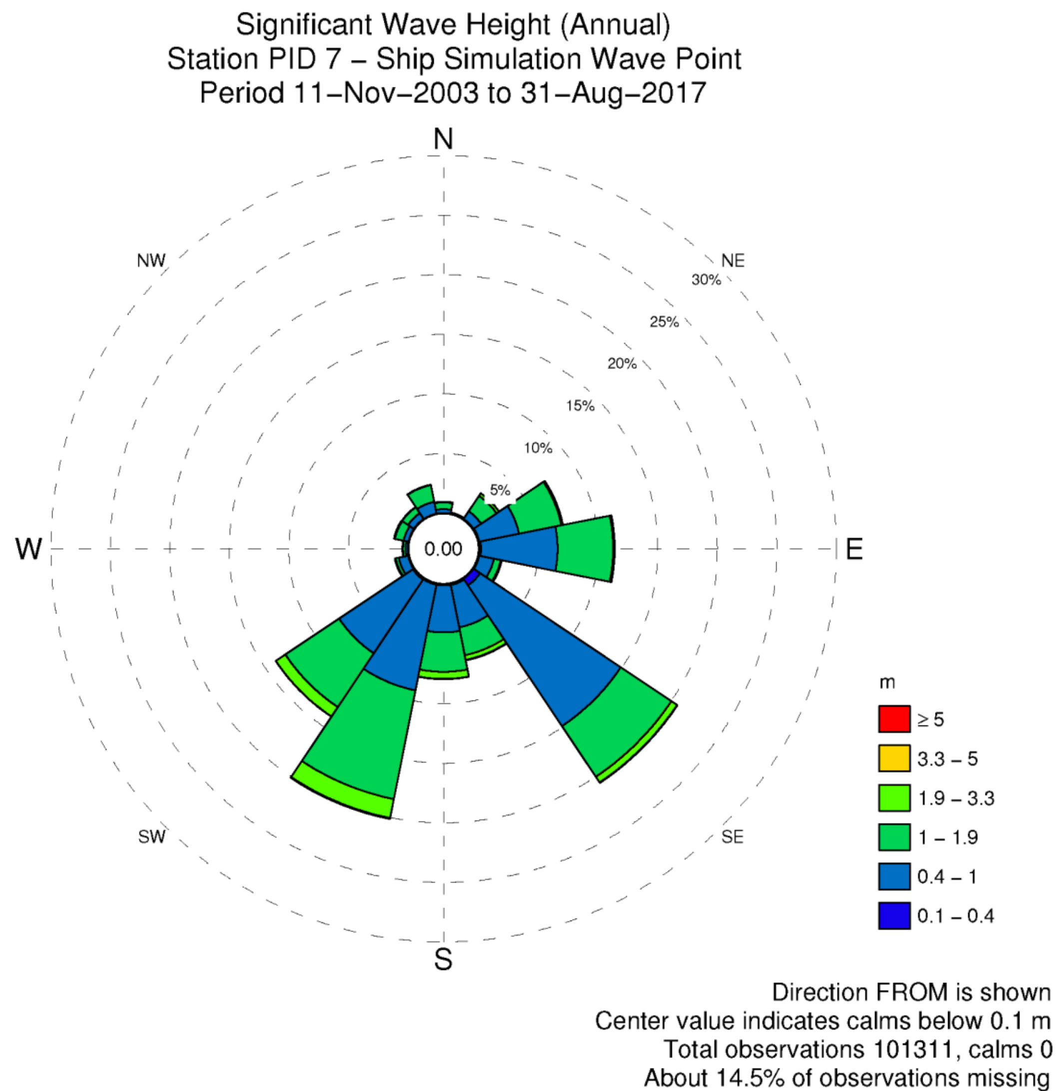

Percentage of Occurrence

Significant Wave Height, m	N	NNE	NE	ENE	E	ESE	SE	SSE	S	SSW	SW	WSW	W	WNW	NW	NNW	Total
Total	0.95		2.60	7.22	11.38	1.98	20.63	6.55	7.95	20.12	13.95	1.18	0.45	1.25	1.21	2.48	100.00
≥ 5																	
3.3 – 5																	0.19
1.9 – 3.3			0.26	0.13	0.13		0.58	0.40	0.59	1.62	0.96						5.11
1 – 1.9	0.56		1.56	3.63	4.66	0.58	5.11	2.38	3.31	9.31	5.43	0.26	0.23	0.75	0.60	1.43	39.83
0.4 – 1	0.32		0.78	3.41	6.44	1.25	14.22	3.62	3.95	9.05	7.46	0.82	0.18	0.42	0.58	1.01	53.55
0.1 – 0.4					0.14		0.68	0.10									1.31

Figure 3-4: Wave Height Rose at the Offshore End of the Design Navigation Channel

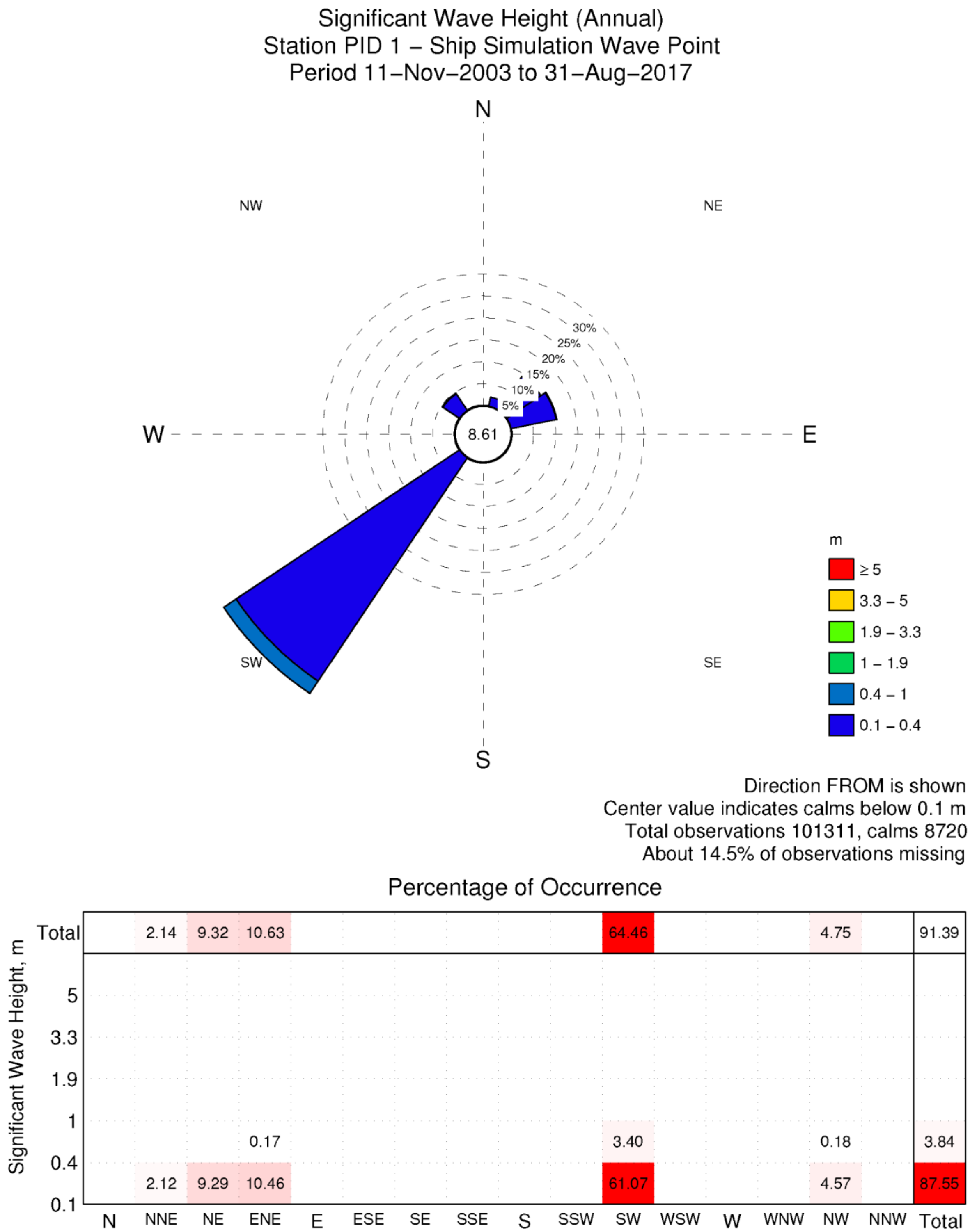

Figure 3-5: Wave Height Rose for between Southport Channel and the Bald Head Caswell

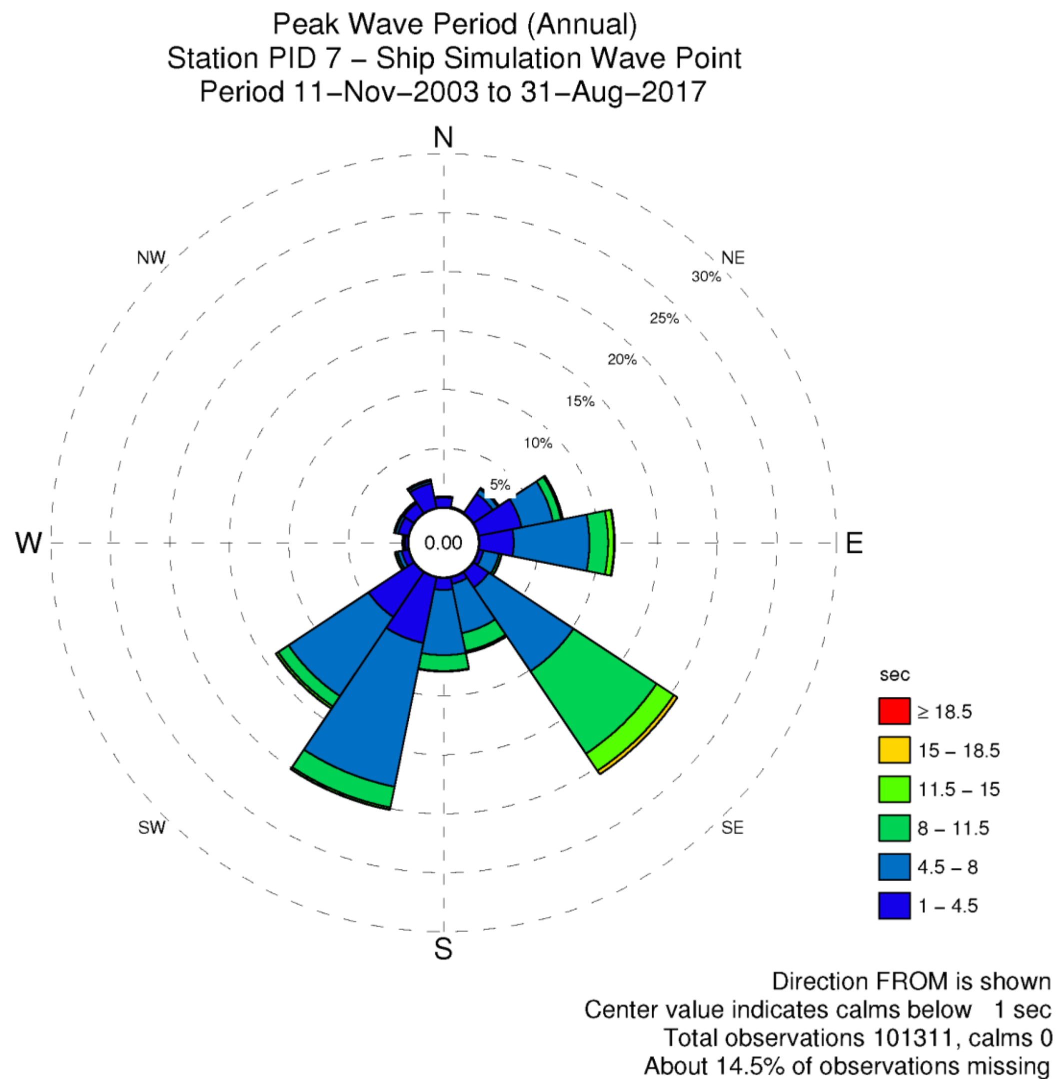

Percentage of Occurrence

Peak Wave Period, sec	N	NNE	NE	ENE	E	ESE	SE	SSE	S	SSW	SW	WSW	W	WNW	NW	NNW	Total
Total	0.95		2.60	7.22	11.38	1.98	20.63	6.55	7.95	20.12	13.95	1.18	0.45	1.25	1.21	2.48	100.00
≥ 18.5																	
15 – 18.5							0.36										0.56
11.5 – 15				0.15	0.49		1.74	0.14		0.18	0.23						3.22
8 – 11.5				0.69	1.57	0.21	8.41	1.55	1.33	1.80	1.05	0.19		0.11			17.23
4.5 – 8			0.49	2.70	6.35	1.34	8.56	4.25	5.53	12.43	8.08	0.35	0.15	0.24	0.11	0.21	50.91
1 – 4.5	0.82		1.98	3.66	2.89	0.40	1.56	0.57	1.01	5.68	4.58	0.58	0.23	0.87	1.03	2.13	28.09

Figure 3-6: Wave Period Rose at the Offshore End of the Design Navigation Channel

3.2.3.3. Wind Fields

Long term wind measurements are available at Wilmington (Station KILM). Winds along the Cape Fear River have strong northerly and southwesterly components. The winds tend to be more northerly in the fall and winter and more southwesterly in the spring and summer. Figure 3-7 shows the seasonal wind roses for Wilmington. Winds from the north are stronger in the fall than the typical winds from the southwest in the summer. Table 3-10 gives typical and high wind conditions (not extreme storms). Table 3-11 shows the primary wind conditions used for this simulation effort; additional wind conditions were tested to evaluate extreme conditions from a ship handling perspective and are listed in the completed testing matrix presented in Section 3.3.4. The Cape Fear River Pilots present-day procedure is to hold transits if the wind conditions are above 25 mph (21.7 kt). For reference, a sustained wind speed of 15 kt is exceeded approximately 7% of the time in Wilmington.

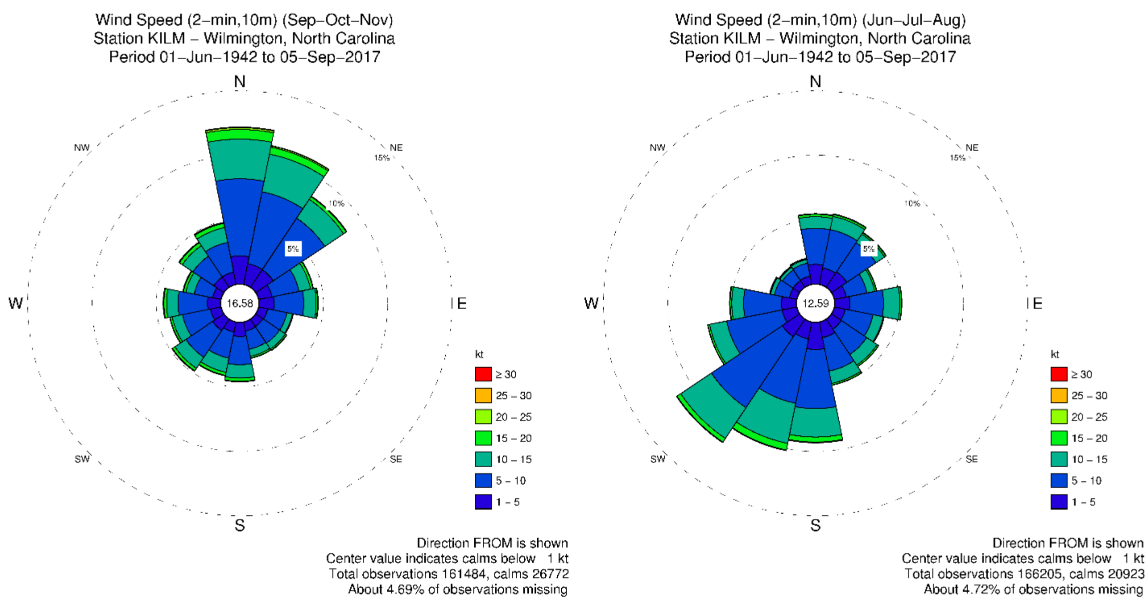

Figure 3-7: Wind Roses: September – November (left) and June – August (right)

Table 3-10: Typical Wind Conditions at Long-Term Anemometers

Wind Condition	2 Minute Wind Speeds / Direction
Typical spring/summer wind	5 to 15 kt S to SW
High spring/summer wind	15 to 20 kt S to SW
Typical fall/winter wind	5 to 15 kt N to NE
High fall/winter wind	15 to 20 kt N to NNE

Table 3-11: Wind Conditions Proposed for Ship Simulations

Sustained Wind Condition	Description
15-20 kt, NNE (022.5°)	Winter Wind
15-20 kt, SW (225°)	Summer Wind
10 kt, SW (225°)	“Calm” Wind

3.3. Basis of Maneuvers

The maneuvers identified for this simulation effort were developed to evaluate the critical navigation characteristics of the channel design for widening and deepening the Wilmington channel. The majority of the simulations were conducted for select channel segments, rather than transit of the entire channel, allotting more simulation time to evaluating areas of higher interest.

In support of overall conclusions regarding the design layouts, six specific objectives were identified for this study:

- **Entrance Turns**: Identify a feasible geometry for the entrance turns, which provides sufficient room for navigation, while minimizing encroachment on Bald Head Island, Fort Caswell, and the town of Southport and minimizing the volume of new dredging required.

- **Turning Basin, Berthing Area and Adjacent Channel**: Identify/confirm the turning basin size and channel width required for a 12,400 TEU design vessel navigating past a moored vessel of similar size and berthing at the port.

- **One-way Traffic Width in Channel**: Evaluate a channel width of 500-ft for one-way traffic in the river.

- **Two-way Traffic Width in Channel**: Evaluate a channel width of 800-ft for ranges designed to support two-way traffic in the river.

- **One-way Traffic Width Offshore**: Evaluate a channel width of 600-ft for one-way traffic in the offshore portion of the channel (exposed to waves).

- **Two-way Traffic Width Offshore**: Evaluate a channel width of 900-ft for two-way traffic in the offshore portion of the channel (exposed to waves).

3.3.1. Vessel Speeds

The starting vessel transit speed for each simulation was chosen as appropriate for the specified starting channel location and transit direction for the maneuver. The starting vessel speeds were chosen primarily based on the discretion of the pilot to align with his approach to the maneuver. Typical historic vessels speeds are summarized in Appendix B-1 based on historic AIS data.

3.3.2. Use of Tugs

The utilization of tugs was based on the pilots' discretion. No tugs were used for maneuvers offshore, around the entrance turn, or in the main river channel. In the vicinity of the Port of Wilmington, four tugs were available for the turning maneuver and docking, and two tugs were available for undocking.

3.3.3. Simulator Software & Facility

The simulations were performed by the M&N in-house simulator at the M&N Wilmington, NC office (Figure 3-8). The simulator consists of an operator console and a pilot console. A licensed pilot from the Cape Fear Pilots Association sat at the pilot console and was responsible for conning the simulations (no separate helmsman). The simulation operator (an M&N engineer) supervised the simulation (e.g., controlling environmental conditions) and operated the tugs as instructed by the pilot. For these simulations, the program's vector tugs were controlled by basic commands from the simulation operator (where to connect, how hard to pull, etc.).

The simulations were conducted using the navigation simulation software Navi Trainer Pro 5000 (NTPro), which was developed by TRANSAS to be used in training simulators for professional captains and pilots. While the NTPro software was developed for use in training simulators it is also suited for use by engineers to assist in the design of new terminals and the evaluation of channel modifications.

NTPro simulates real time vessel maneuvers through realistic 3D renderings of harbor geometry, accounting for vessel response to wind, waves, currents, bathymetry (shallow water effects), and vessel-structure and vessel-vessel interaction. The vessel hydrodynamics are incorporated with a full six degree-of-freedom model. Ship models used in the simulations were developed and verified by TRANSAS with data from basin tests and real-world collection schemes.

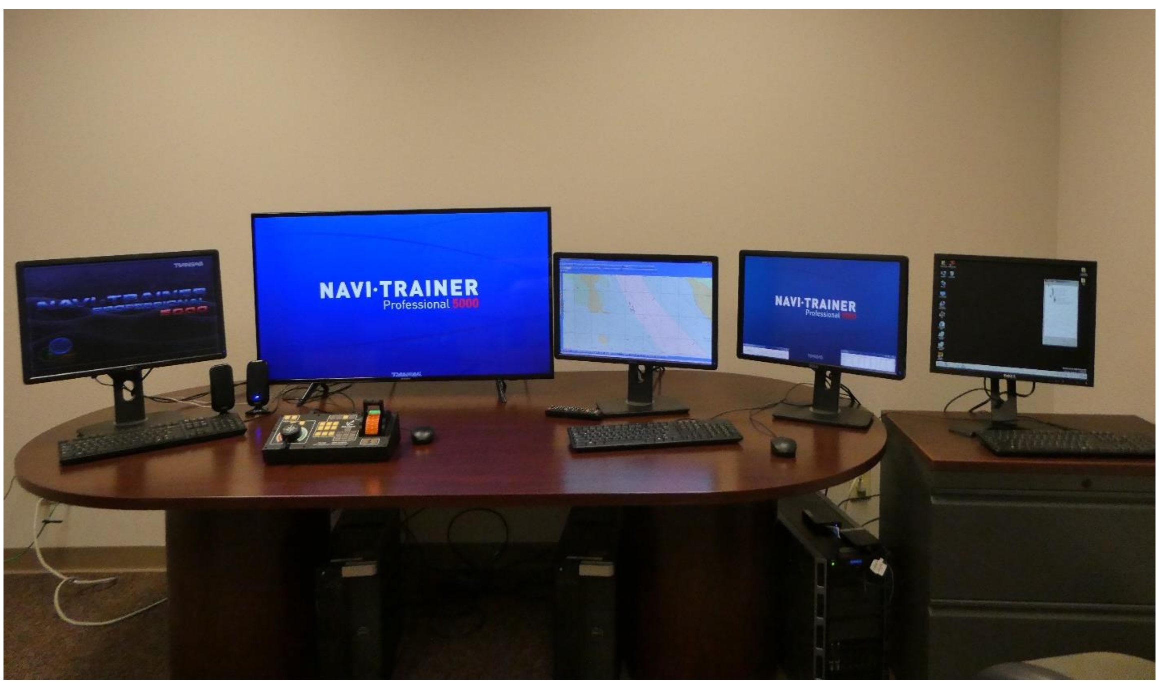

Figure 3-8: Moffatt & Nichol In-House Simulator at the Wilmington, NC office.

3.3.3.1. Model Area

A custom scene was developed for this Cape Fear River project. The scene included the channel geometry as included in the publicly available Electronic Nautical Charts (ENCs) for the Cape Fear River, with modifications to the channel to simulate the design geometries for this study. The simulator scene developed for this study included 3D renderings of selected shoreline structures (e.g., jetty terminals near the channel); however, the fidelity of the renderings is low and meant only to represent the navigationally significant objects in the river. Figure 3-9 and Figure 3-10 show a view of Southport and the Port of Wilmington, respectively, from a camera recording the simulations.

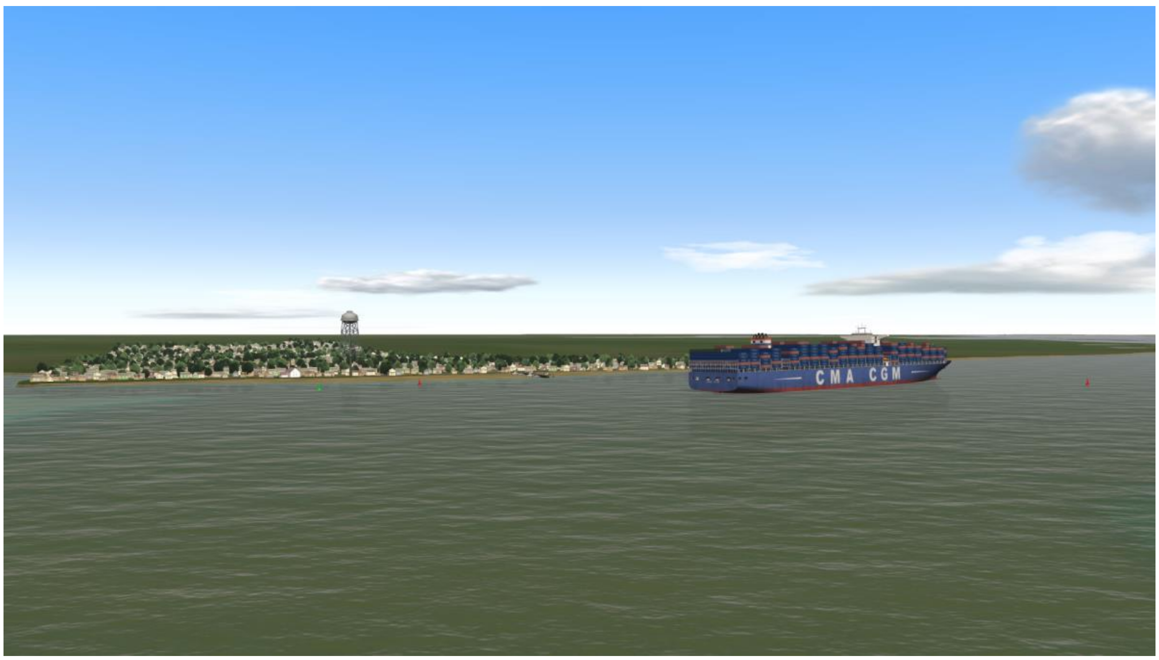

Figure 3-9: View of Southport inside the Cape Fear River scene.

Figure 3-10: View of Port of Wilmington inside the Cape Fear River scene.

3.3.3.2. Environmental Conditions

The simulation software incorporated the effects of the following environmental conditions:

- Tidal Currents: The model database imported space and time varying tidal currents in the Cape Fear River. The tidal currents were specified based on a 3D tidal model developed by M&N for this channel improvement project (see Section 3.2.3.1). The tidal currents used for the study incorporated the effects of the wider/deeper channels.
- Waves: The model incorporated a representative wave spectrum for the portion of channel outside of the Cape Fear River that are exposed to ocean waves. The spatially varying wave field was represented through two discrete regions with constant waves in each (see Section 3.2.3.2).
- Winds: The wind field was represented in the simulator as a sustained wind speed based on the conditions specified in the simulation matrix (Table 3-12).
- Other Weather Conditions: The model includes capability to simulate other weather conditions (e.g., rain and fog), as well as varied lighting (e.g., dusk and nighttime); however, these features were not used as part of this simulation effort.

3.3.3.3. Vessel Responses

The simulator provided the following dynamic modeling capabilities for the design vessels.

- Vessel Control: Real-time vessel response delays to rudder and speed commands.
- Tugs: Ability to visually and physically simulate and apply tug interaction. This includes the ability to specify tug attachment point locations and real-time movement of tugs during repositioning. Tugs were simulated in auto-tug mode and the simulator had the ability to provide a realistic response delay.
- Vessel Response: Real-time vessel response and location of vessel in terms of horizontal & vertical location with respect to the navigation channel limits and bottom elevations (under keel clearance).
- Mooring: Ability to specify mooring line locations. However, this effort did not call for vessel mooring to be simulated.
- Failures: Ability to specify dead ship and rudder failure conditions (not included in the feasibility studies).
- Other Vessels: The model included a hydrodynamic representation of moored vessels at terminals near the channel.

3.3.4. Testing Matrix

Table 3-12 shows the matrix of completed simulations. This matrix was based upon the test matrix included with the feasibility screening plan and modified based upon pilot input and observations during the simulations. In total, 64 simulations were conducted to evaluate the design layouts; 10 of these simulations were not analyzed due to either pilot familiarization or software malfunction.

Table 3-12: Simulation Matrix

Run No.	Purpose / Area of Study	Channel Layout	Piloted Vessel Start/End Stations	Direction of Transit	Wind	Waves	Current Stage	Water Level	No. Tugs	Bollard Pull [mt]	Piloted Vessel	Passing Vessel	Passing Vessel Start/End Stations	Pilot
1	Familiarization	Existing	750 - 1180	Inbound	10 kt, SW (225°)	1m, 8s, 202.5°	Slack	MLLW	0	--	CS19[b]	--	--	S. Aldridge
2	Familiarization	Existing	740 - 1190	Inbound	10 kt, SW (225°)	1m, 8s, 202.5°	Slack	MLLW	0	--	CS13 PL1[b]	--	--	S. Aldridge
3	Familiarization	Existing	990 - 1120	Inbound	10 kt, SW (225°)	1m, 8s, 202.5°	Slack	MLLW	0	--	CS19[b]	--	--	S. Aldridge
4	Familiarization	Existing	740 - 1080	Inbound	10 kt, SW (225°)	1m, 8s, 202.5°	Slack	MLLW	0	--	CS19[b]	--	--	B. Hue
5	Full Transit	Existing	490 - 2260	Inbound	10 kt, SW (225°)	1m, 8s, 202.5°	Flood	MLLW	0	--	CS13 PL1[b]	--	--	S. Aldridge
6	Entrance Turn	Existing	1200 - 670	Outbound	10 kt, SW (225°)	1m, 8s, 202.5°	Flood	MLLW	0	--	CS13 PL1[b]	--	--	S. Aldridge
7	Entrance Turn	Design Layout #1	750 - 1200	Inbound	15 kt, SW (225°)	1m, 8s, 202.5°	Slack	MLLW	0	--	CS13 PL3[b]	--	--	S. Phillips
8	Entrance Turn	Design Layout #1	800 - 910	Inbound	15 kt, SW (225°)	1.5m, 8s, 202.5°	Flood	MLLW	0	--	CS13 PL3[b]	--	--	S. Phillips
9	Entrance Turn	Design Layout #1	770 - 1200	Inbound	15 kt, SW (225°)	1.5m, 8s, 202.5°	Flood	MLLW	0	--	CS13 PL3[b]	--	--	S. Phillips
10	Entrance Turn	Design Layout #1	1210 - 920	Outbound	15 kt, SW (225°)	1.5m, 8s, 202.5°	Flood	MLLW	0	--	CS13 PL3[b]	--	--	S. Phillips
11	Entrance Turn	Design Layout #2	740 - 1190	Inbound	15 kt, SW (225°)	1.5m, 8s, 202.5°	Flood	MLLW	0	--	CS13 PL3[b]	--	--	S. Phillips
12	Entrance Turn	Design Layout #2	890 - 1150	Inbound	15 kt, SW (225°)	1.5m, 8s, 202.5°	Flood	MLLW	0	--	CS13 PL3[b]	--	--	S. Phillips
13	Entrance Turn	Design Layout #1	830 - 1140	Inbound	15 kt, SW (225°)	1.5m, 8s, 202.5°	Flood	MLLW	0	--	CS13 PL3[b]	--	--	S. Phillips
14	Entrance Turn	Design Layout #1	830 - 1170	Inbound	15 kt, SW (225°)	1.5m, 8s, 202.5°	Rising Flood	MLLW	0	--	CS13 PL3[b]	--	--	S. Phillips
15	Entrance Turn	Design Layout #1	830 - 1110	Inbound	20 kt, SW (225°)	1.5m, 8s, 202.5°	Rising Flood	MLLW	0	--	CS13 PL3[b]	--	--	S. Phillips
16	Entrance Turn	Design Layout #2	850 - 1110	Inbound	15 kt, SW (225°)	1.5m, 8s, 202.5°	Rising Flood	MLLW	0	--	CS13 PL3[b]	--	--	S. Phillips
17	Entrance Turn	Design Layout #1	1170 - 810	Outbound	20 kt, SW (225°)	1.5m, 8s, 202.5°	Rising Flood	MLLW	0	--	CS13 PL3[b]	--	--	S. Phillips
18	Two Way Channel Width	Design Layout #1	1460 - 1600	Inbound[a]	20 kt, SW (225°)	--	Flood	MLLW	0	--	CS13 PL3[b]	CS13 PL3[b]	1690 - 1550	B. Hue
19	Two Way Channel Width	Design Layout #1	1700 - 1570	Outbound[a]	20 kt, SW (225°)	--	Flood	MLLW	0	--	CS13 PL3[b]	CS13 PL3[b]	1150 - 1600	B. Hue
20	Two Way Channel Width	Design Layout #1	1460 - 1600	Inbound[a]	20 kt, SW (225°)	--	Flood	MLLW	0	--	CS13 PL3[b]	CS13 PL3[b]	1690-1550	B. Hue
21	Two Way Channel Width	Design Layout #1	1460 - 1590	Inbound[a]	20 kt, SW (225°)	--	Flood	MLLW	0	--	CS13 PL3[b]	CS13 PL3[b]	1690 - 1560	B. Hue
22	Two Way Channel Width	Existing	1450 - 1630	Inbound[a]	20 kt, SW (225°)	--	Flood	MLLW	0	--	CS13 PL1[b]	CS13 PL1[b]	1710 - 1600	B. Hue
23	Two Way Channel Width	Existing	1460 - 1620	Inbound[a]	20 kt, SW (225°)	--	Flood	MLLW	0	--	CS13 PL1[b]	CS13 PL1[b]	1710 - 1590	B. Hue
24	Two Way Channel Width	Design Layout #1	1700 - 1570	Outbound[a]	20 kt, SW (225°)	--	Flood	MLLW	0	--	CS13 PL3[b]	CS13 PL3[b]	1460 - 1590	B. Hue
25	Familiarization	Design Layout #1	--	Inbound	20 kt, SW (225°)	--	Flood	MLLW	0	--	CS13 PL3[b]	--	--	B. Hue
26	Entrance Turn	Design Layout #1	770 - 1200	Inbound	20 kt, SW (225°)	1.5m, 8s, 202.5°	Flood	MLLW	0	--	CS13 PL3[b]	--	--	B. Hue
27	Two Way Channel Width	Design Layout #1	--	--	--	--	--	--	0	--	CS13 PL3[b]	--	--	B. Hue
28	Channel Width	Design Layout #1	1240 - 1380	Inbound	20 kt, SW (225°)	--	Flood	MLLW	0	--	CS13 PL3[b]	--	--	B. Hue
29	Channel Width	Existing	1240 - 1360	Inbound	20 kt, SW (225°)	--	Flood	MLLW	0	--	CS13 PL1[b]	--	--	B. Hue
30	Channel Width	Existing	1240 - 1390	Inbound	20 kt, SW (225°)	--	Flood	MLLW	0	--	CS13 PL1[b]	--	--	B. Hue
31	Channel Width	Design Layout #1	360 - 540	Inbound	20 kt, SW (225°)	1.5m, 8s, 202.5°	Flood	MLLW	0	--	CS13 PL3[b]	--	--	S. Aldridge
32	Channel Width	Design Layout #1	370 - 530	Inbound	20 kt, NNE (22.5°)	1.5m, 8s, 202.5°	Flood	MLLW	0	--	CS13 PL3[b]	--	--	S. Aldridge
33	Channel Width	Design Layout #1	570 - 450	Outbound	20 kt, NNE (22.5°)	1.5m, 8s, 202.5°	Flood	MLLW	0	--	CS13 PL3[b]	--	--	S. Aldridge
34	Channel Width	Design Layout #1	570 - 470	Outbound	20 kt, SW (225°)	1.5m, 8s, 202.5°	Flood	MLLW	0	--	CS13 PL3[b]	--	--	S. Aldridge
35	Channel Width	Design Layout #1	570 - 450	Outbound	20 kt, NE (45°)	1.5m, 8s, 202.5°	Flood	MLLW	0	--	CS13 PL3[b]	--	--	S. Aldridge

Run No.	Purpose / Area of Study	Channel Layout	Piloted Vessel Start/End Stations	Direction of Transit	Wind	Waves	Current Stage	Water Level	No. Tugs	Bollard Pull [mt]	Piloted Vessel	Passing Vessel	Passing Vessel Start/End Stations	Pilot
36	Channel Width	Design Layout #2	410 - 620	Inbound	20 kt, SW (225°)	1.5m, 8s, 202.5°	Flood	MLLW	0	--	CS13 PL3[b]	--	--	S. Aldridge
37	Channel Width	Design Layout #2	410 - 540	Inbound	20 kt, NE (45°)	1.5m, 8s, 202.5°	Flood	MLLW	0	--	CS13 PL3[b]	--	--	S. Aldridge
38	Channel Width	Design Layout #2	560 - 420	Outbound	20 kt, NE (45°)	1.5m, 8s, 202.5°	Flood	MLLW	0	--	CS13 PL3[b]	--	--	S. Aldridge
39	Entrance Turn	Design Layout #1	770 - 1160	Inbound	20 kt, SW (225°)	11.5m, 8s, 202.5°	Flood	MLLW	0	--	CS13 PL3[b]	--	--	S. Aldridge
40	Two Way Channel Width	Design Layout #1	--	Inbound[a]	20 kt, SW (225°)	1.5m, 8s, 202.5°	Flood	MLLW	0	--	CS13 PL3[b]	--	--	B. Hue
41	Two Way Channel Width	Design Layout #1	520 - 600	Inbound[a]	20 kt, SW (225°)	1.5m, 8s, 202.5°	Rising Flood	MLLW	0	--	CS13 PL3[b]	CS13 PL3[b]	640 - 570	B. Hue / S. Aldridge
42	Two Way Channel Width	Design Layout #1	520 - 600	Inbound[a]	20 kt, SW (225°)	1.5m, 8s, 202.5°	Flood	MLLW	0	--	CS13 PL3[b]	CS13 PL3[b]	640 - 570	B. Hue / S. Aldridge
43	Two Way Channel Width	Design Layout #1	520 - 600	Inbound[a]	20 kt, SW (225°)	1.5m, 8s, 202.5°	Flood	MLLW	0	--	CS13 PL3[b]	CS13 PL3[b]	640 - 570	B. Hue / S. Aldridge
44	Channel Width	Design Layout #1	1240 - 1380	Inbound	20 kt, SW (225°)	--	Flood	MLLW	0	--	CS13 PL3[b]	--	--	B. Hue
45	Channel Width	Design Layout #1	1440 - 1260	Outbound	20 kt, SW (225°)	--	Flood	MLLW	0	--	CS13 PL3[b]	--	--	B. Hue
46	Entrance Turn	Design Layout #2	780 - 1150	Inbound	20 kt, SW (225°)	1.5m, 8s, 202.5°	Flood	MLLW	0	--	CS13 PL3[b]	--	--	S. Aldridge
47	Entrance Turn	Design Layout #1	970 - 1090	Inbound	20 kt, SW (225°)	1.5m, 8s, 202.5°	Flood	MLLW	0	--	CS13 PL3[b]	--	--	S. Aldridge
48	Entrance Turn	Design Layout #1	750 - 1120	Inbound	15 kt, SW (225°)	1.5m, 8s, 202.5°	Rising Flood	MLLW	0	--	CS13 PL3[b]	--	--	J. McDowell
49	Entrance Turn	Design Layout #1	750 - 1110	Inbound	20 kt, SW (225°)	1.5m, 8s, 202.5°	Rising Flood	MLLW	0	--	CS13 PL3[b]	--	--	J. McDowell
50	Entrance Turn	Design Layout #1	750 - 1110	Inbound	20 kt, SW (225°)	1.5m, 8s, 202.5°	Flood	MLLW	0	--	CS13 PL3[b]	--	--	J. McDowell
51	Entrance Turn	Design Layout #2	780 - 1110	Inbound	20 kt, SW (225°)	1.5m, 8s, 202.5°	Flood	MLLW	0	--	CS13 PL3[b]	--	--	J. McDowell
52	Two Way Channel Width	Design Layout #1	1460 - 1650	Inbound[a]	15 kt, W (270°)	--	Flood	MLLW	0	--	CS13 PL3[b]	CS13 PL3[b]	1700 - 1550	J. McDowell
53	Two Way Channel Width	Design Layout #1	1690 - 1540	Outbound[a]	15 kt, W (270°)	--	Flood	MLLW	0	--	CS13 PL3[b]	CS13 PL3[b]	1450 - 1600	J. McDowell
54	Entrance Turn	Design Layout #1	1160 - 810	Outbound	15 kt, NNE (22.5°)	1.5m, 8s, 202.5°	Rising Flood	MLLW	0	--	CS13 PL3[b]	--	--	J. McDowell
55	Entrance Turn	Design Layout #1	1160 - 790	Outbound	20 kt, SW (225°)	1.5m, 8s, 202.5°	Flood	MLLW	0	--	CS13 PL3[b]	--	--	J. McDowell
56	Port Familiarization	Design Layout #1	--	--	--	--	--	--	4	53/53/32/32	CS13 PL3[b]	--	--	G. Turbeville
57	Port Familiarization	Design Layout #1	2170 - TB[c]	Inbound	15 kt, NE (45°)	--	Slack	MLLW	4	53/53/32/32	CS13 PL3[b]	--	--	G. Turbeville
58	Port	Design Layout #1	2170 - 2230	Inbound	15 kt, NE (45°)	--	Slack	MLLW	4	53/53/32/32	CS13 PL3[b]	--	--	G. Turbeville
59	Port	Design Layout #1	2230 - TB[c]	Inbound	15 kt, SW (225°)	--	Flood	MLLW	4	53/53/32/32	CS13 PL3[b]	--	--	G. Turbeville
60	Port	Design Layout #1	2170 - B8[c]	Inbound	15 kt, NE (45°)	--	Slack	MLLW	4	53/53/32/32	CS13 PL3[b]	--	--	G. Turbeville
61	Port	Design Layout #1	2170 - B8[c]	Inbound	15 kt, SW (225°)	--	Flood	MLLW	4	53/53/32/32	CS13 PL3[b]	--	--	G. Turbeville
62	Port	Design Layout #1	B8[c] – 2180	Outbound	15 kt, NW (315°)	--	Ebb	MLLW	2	53/53	CS13 PL3[b]	--	--	G. Turbeville
63	Port	Design Layout #1	B8[c] – 2180	Outbound	15 kt, NW (315°)	--	Ebb	MLLW	2	53/53	CS13 PL3[b]	--	--	G. Turbeville
64	Port	Design Layout #1	2170 - B8[c]	Inbound	15 kt, NE (45°)	--	Ebb	MLLW	4	53/53/32/32	CS13 PL3[b]	--	--	G. Turbeville

Notes:
Grayed simulations results were not analyzed due to various reasons (e.g., Pilot Familiarization, Software Malfunction, etc.)
[a] Direction of transit is indicated for the piloted vessel. When present, a passing autopiloted vessel transits in the opposite direction as the piloted vessel.
[b] CS19 = Container Ship 19 (TRANSAS Vessel Model), CS13 = Container Ship 13 (TRANSAS Vessel Model), PL1 = Partial Load 1, PL3 = Partial Load 3.
[c] TB = Turning Basin & B8 = Port of Wilmington Berth 8

3.3.5. Evaluation Criteria

The primary criterion for the success of each run was pilot feedback during the simulations. A key component of the evaluation was the pilot assessment of overall safety and opinions as to whether specific maneuvers would be conducted in real life.

Additional variables that were used to critique the performance of the runs include but are not limited to:

- *Clearance to edge of channel*: The minimum clearance to the edge of the channel, structures and berthed vessels will be evaluated based on the swept path of the vessels. No minimum clearance is prescribed but will be used to compare runs. For example, if repeated runs result in small clearance, modifications to design may be considered.

- *Reserve engine and rudder*: The engine and rudder use during the simulation is evaluated with the aim of maintaining sufficient reserve for unanticipated maneuvering. Hard-over rudder for extended periods may indicate a lack of reserve.

- *Reserve tug power*: For the simulations near the terminal, where tugs were used, the tug power was tracked. Reserve tug power for emergency recovery should be available to the pilot when maneuvering in the Port. Tugs utilized at 100% power for extended periods will have little or no reserve to respond in an emergency.

- *Swept path density*: The use of the channel width is evaluated by looking at swept path density figure which illustrate which areas of the channel were used in more or fewer simulations. The density figures are developed by compositing the path of multiple runs and evaluating the number of tracks that use a particular area of the channel. This provides information on how vessels track around bends (e.g., inside of the curve vs. outside of the curve).

3.4. Results & Analysis

Vessel swept paths were developed for each simulation to illustrate clearance of the vessel to channel limits. The swept paths are illustrated in Appendix B-4. The vessel profiles are shown at two-minute intervals. Additional figures are included in Appendix B-5 to illustrate parameters such as use of the ship's engine and rudder.

Pilot feedback was recorded on pilot evaluation forms (Appendix B-3), along with notes and observations made by the engineers supervising the effort. For each simulation, the pilot was asked to rate the maneuver in three categories: Run Safety, Tug Adequacy, and Run Difficulty. These ratings are discussed in greater detail in the subsections below. Rating scales are as follows:

- Run Safety: 1 to 10 with "10" highest safety and "5" average safety;
- Tug Adequacy: 1 to 10 with "10" best and "5" average; and
- Difficulty: 1 to 10: with "10" most difficult and "5" average.

3.4.1. Entrance Turn

In total 20 simulations of the entrance turn were performed for this feasibility study. Of these simulations 16 were inbound while 4 were outbound. The ranges evaluated during the entrance turn simulations were:

- Bald Head Shoal Reach 1, 2, & 3
- Smith Island
- Bald Head Caswell
- Southport
- Battery Island Turn
- Lower Swash

The pilot safety and run difficulty ratings for all of the entrance turn simulations are summarized in Table 3-13. Note that four different pilots performed these simulations and performance ratings are subjective to each individual pilot.

Table 3-13: Pilot Ratings for Simulation Safety and Difficulty Entrance Turns Simulations

Simulation Number	Pilot	Run Safety	Run Difficulty
Inbound Design Layout #1 (4000-ft Battery Island Turn Radius)			
7	S. Phillips	10	3
9	S. Phillips	2	9
13	S. Phillips	7	6
14	S. Phillips	9	3
15	S. Phillips	9	3
26	B. Hue	8	5
39	S. Aldridge	6	7
47	S. Aldridge	8	3
48	J. McDowell	7	6
49	J. McDowell	8	5
50	J. McDowell	10	3
Inbound Design Layout #2 (3000-ft Battery Island Turn Radius)			
11	S. Phillips	7	6
12	S. Phillips	7	6
16	S. Phillips	7	6
46	S. Aldridge	6	6
51	J. McDowell	8	5
Outbound Design Layout #1			
10	S. Phillips	9	2
17	S. Phillips	9	2
54	J. McDowell	8	2
55	J. McDowell	10	2

3.4.1.1. Inbound Maneuvers

This section discusses the inbound maneuvers for the entrance turn. Of the 16 inbound simulations, 11 of them evaluated Layout #1, while the remaining 5 simulations evaluated Layout #2. The only difference between Layout #1 and Layout #2 for the entrance turn simulations is the radius of the turn at Battery Island. Layout #1 has a 4000-ft turn radius while Layout #2 has a 3000-ft turn radius. The other ranges for the entrance turn simulations had the same geometry.

Design Layout #1 – 4000 ft turn radius

Simulation 7 was the first simulation of Layout #1 to evaluate the entrance turn. This simulation was during slack tide with a wind of 15 kt from the SW. Typical procedure for the larger container ships is to transit during flood tide. However, slack tide was used for this first simulation to allow the pilot to become familiar with the new geometry specifically the 4000-ft turn radius at Battery Island. The vessel remained within the channel boundaries for the entire simulation with channel clearances of at least 50 ft on both the red and green sides of the channel.

Simulation 9 was the same as Simulation 7, but with peak flood tide currents. The pilot maintained his intended track until Smith Island Range. On Smith Island Range the stern of the vessel came within 70 ft of the red side of the channel. The pilot intended to be on the red side of the channel on Smith Island to set up the intended track line on the green of the channel for Bald Head Caswell and Southport Ranges. However, the flood current prevented the pilot from setting up on the green side of either range as he intended. During the turn from Bald Head Caswell into Southport, the stern of the vessel drifted outside the red side channel edge by 45 ft. The vessel corrected course into the Battery Island Turn. However, the stern exceeded the green side channel boundary (by 19 ft) at the apex of the turn.

Upon completing the turn in Simulation 9, the pilot began to slow down due to the vessel moored at the ADM terminal (green side at about station 1180+00). According to the pilot, vessels in the channel would reduce speed to 5 kt (in water) when passing a moored vessel at ADM. At this speed, the vessel has poor maneuvering characteristics. With this understanding, the pilot highly recommended the use of an assist tug when a vessel is moored at ADM. As denoted in the simulation ratings overall the pilot thought this maneuver was difficult with low safety because the vessel exceeded the channel limits.

The next Design Layout #1 simulation was Simulation 13, which was the same as Simulation 9, to evaluate whether the transit could be performed within the channel with greater familiarity. The pilot maintained his intended track through Bald Head Reaches 1 and 2. Similar to the previous simulation, the pilot intended to stay on the red side of the channel in Smith Island Range in effort to stay within the channel in Bald Head Caswell and Southport Ranges. In this attempt, the vessel's stern left the channel in Smith Island Range where the bathymetry is naturally deep but remained in the channel through Bald Head Caswell and Southport Ranges. The vessel had a minimum clearance of 66 ft on the red side of the channel in Southport. Similar to Simulation 9, the pilot was not able to set up the vessel on the green side of Southport Range as intended and the stern of the vessel left the channel by 62 ft on the green side at the apex of the Battery Island turn. In the simulation debrief the pilot indicated the tidal currents as the controlling factor for exceeding the channel boundaries in Simulation 9 & 13 (both performed with peak flood conditions). The vessel had remained in the channel for the duration of Simulation 7 (slack tide).

For the next two simulations (Simulation 14 & 15), the tidal currents were reduced from peak flood to rising flood conditions, which resulted in velocities approximately 30% less than the peak flood velocities. The other environmental conditionals remained the same for Simulation 14, while for Simulation 15 the wind velocity was increased to 20 kt. With the reduced currents, the vessel remained within the channel boundaries for both simulations. The clearance between the vessel and the channel boundary remained above 70 ft for the ranges approaching the turn at Battery Island for both simulations. For Simulation 14 the clearance in the apex of the turn at Battery Island remained above 100 ft while for Simulation 15 the clearance decreased to a minimum of 42 ft. As denoted by the pilot's ratings and by the vessel remaining within the channel, both of these simulations were successful and safe.

A second pilot performed the next Layout #1 entrance turn simulation, Simulation 26. This simulation was performed under peak flood currents with a wind from the SW at 20 kt. The vessel remained inside the channel for the entire simulation. In the apex of the turn at Battery Island the vessel had 74 ft of clearance to the green side of the channel. In the simulation debrief the pilot stated that he wanted the least amount of speed going into the turns between the ranges in which he could safely maneuver, approximately 8 to 9 kt. Overall, the pilot felt comfortable with the design and would perform a similar transit in a real-world simulation.

Comparing the vessel speeds around the Battery Island turn for Simulations 13 and 26, the vessel in Run 26 ran about 2 kt faster through the turn, Figure 3-11. This difference in speed may be the primary reason why the vessel for Simulation 26 was able to maintain the intended track through the turn during the peak flood.

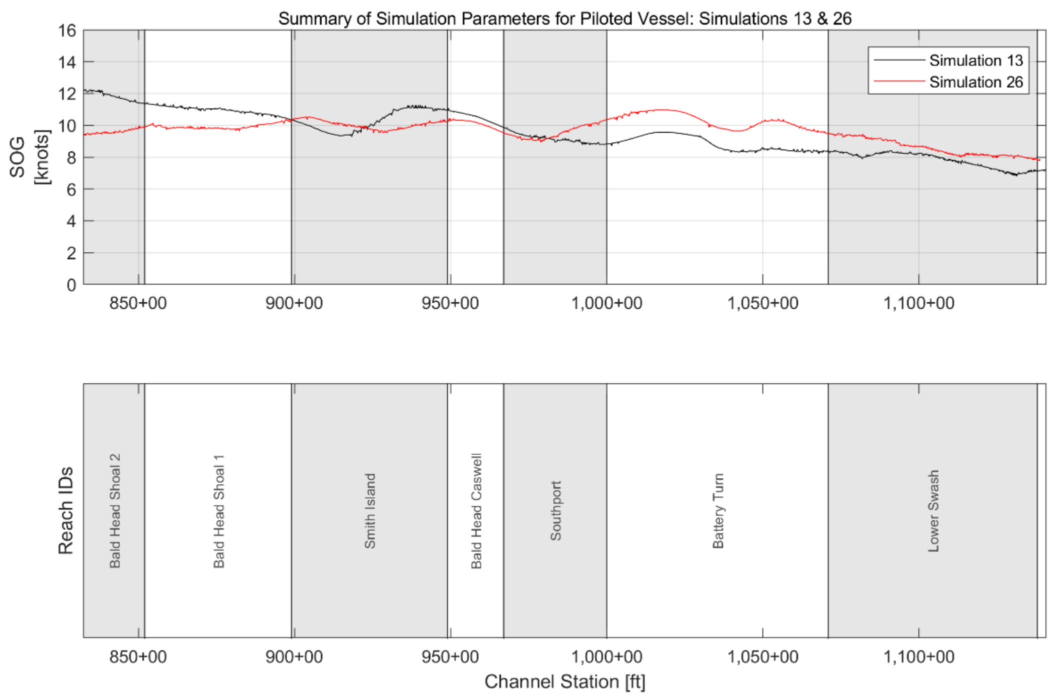

Figure 3-11: Summary of Vessel Speed Over Ground for Simulation 13 & 26.

An additional five simulations (Simulation 39, 47, 48, 49, 50, & 51) were performed on Layout #1 by the last two pilots. The first two simulations, Simulation 39 & 47, were performed on peak flood currents with 20 kt winds from the SW. The vessel remained within the channel boundaries for both simulations. However, for Simulation 39 the pilot had minimal to no clearance in the apex of the turn at Battery Island on the green side of the channel. Simulation 47 was a shorter simulation to give the pilot a second look at the 4000-ft turn at Battery Island. This simulation was started with the vessel in the desired position on Southport Range.

Simulations 48 & 49 were performed with rising flood currents and 15-kt and 20-kt winds from the SW, respectively. These simulations were this pilot's first look at the new design geometry and the reason why the reduced currents were used. In both of these simulations the vessel had over run or minimal clearance (-72 and 24 ft, respectively) in Bald Head Caswell Range on the red side of the channel. Additionally, in the apex of the turn at Battery Island for both simulations the vessel left the channel boundary on the green side by 21 and 70 ft, respectively. The pilot stated for Simulation 48 that he needed to use the maximum rudder angle throughout Bald Head Caswell. For Simulation 49 the vessel stayed within the channel in Bald Head Caswell; however, the resulting vessel alignment in Southport range prevented the pilot from setting up the turn at Battery Island as desired.

The same pilot then performed Simulation 50, which was the same as Simulation 49 but with peak flood conditions. The vessel remained within the channel up until the apex of the turn at Battery Island. At the turn, the stern of the vessel went slightly (6 ft) outside the channel on the green side. The pilot stated that he is inclined to be on the green side of the channel for the Battery Island turn due to the existing geometry but felt with more familiarization he could successful transit the turn inside the channel boundaries. The last two pilots both stated that they felt comfortable and would perform a similar transit in the real-world with design channel entering Cape Fear River and for the turn at Battery Island with a 4000-ft turn radius.

<u>Design Layout #2 – 3000 ft turn radius</u>

Five simulations (Simulation 11, 12, 16, 46, & 51) evaluated Design Layout #2 (3000-ft radius at Battery Island turn). The first two simulations, Simulation 11 & 12, were performed during peak flood tide with a wind of 15 kt from the SW. The pilot maintained his intended track throughout Bald Head Reaches 1, 2 & 3 and Smith Island Range for both simulations. However, for Simulation 11 the stern of the vessel was close (30 ft) to leaving the red side of the channel on Smith Island. Simulation 12 showed larger clearances for Smith Island; however, the vessel exceeded the red side channel boundary during the turn from Bald Head Caswell into Southport Range. The pilot indicated minimal reserve with respect to the rudder and engine capabilities during the turn from Bald Head Caswell into Southport.

During both of these simulations the stern of the vessel left the channel on the green side at the apex of the Battery Island turn. The pilot noted that he again had minimal reserve with respect to the rudder and the engine capabilities during the 3000-ft radius turn. The pilot stated that this turn felt more natural since it is closer to the existing geometry but that this turn overall was more difficult compared to the 4000-ft turn radius. When rating these simulations, the pilots acknowledged that their ratings may be biased more favorably toward the 3,000-ft radius layout due to the similarity to the existing conditions.

Similar to Layout #1, the pilot indicated the tidal currents as the controlling factor for exceeding the channel boundaries in both of the Layout #2 simulations. The next simulation, Simulation 16, evaluated this layout under rising flood conditions and 15 kt winds from the SW. The vessel remained in the channel with clearances above 70 ft. However, the pilot noted that to complete the turn at Battery Island he had to use the maximum rudder angle (35°) and full ahead on the engine. As a result of having to use additional rudder and engine for the 3000-ft turn radius the pilot felt more comfortable with the 4000ft turn radius, Layout #1.

Two additional simulations were performed on Layout #2, Simulation 46 & 51 by two different pilots. For both of these simulations, the vessel remained within the channel boundaries throughout the runs under peak flood currents and 20-kt winds from the SW. The vessel had 26 and 67 ft clearance, respectively, on the red-side channel in the Smith Island Range in these two simulations. Additionally, in Simulation 46 there was reduced clearance (41 ft) on the red side of the Channel on Bald Head Caswell. Both of the pilots performing these runs stated that for Layout #2 that they had to use the maximum rudder angle to be able to successfully complete the turn at Battery Island.

3.4.1.2. Outbound Maneuvers

In total, four outbound simulations (Simulations 10, 17, 54, & 55) were performed on the Layout #1 for the entrance turn. The outbound maneuvers were only performed on Layout #1 as a result of the pilot feedback preferring the 4000-ft turn radius. Two pilots, who also performed the inbound maneuver, simulated the outbound transit. The outbound simulations were all performed on varying environmental conditions with either rising flood or peak flood currents and either a wind speed of 15 or 20 kt from the SW or NNE. The pilots had sufficient clearance throughout the maneuver for all of the outbound simulations, with the exception Simulation 54. During Simulation #54 the vessel left the channel on the red side in Bald Head Caswell. In this simulation the channel boundary was overrun by 22 ft. This overrun would not have occurred in the improved channel alignment discussed below in Section 3.4.1.3. Both pilots found the outbound transit substantially easier than the inbound maneuver as denoted in their safety and difficult ratings (Table 3-13).

3.4.1.3. Discussion

In summary, all four pilots preferred design Layout #1 (4000-ft radius) over Layout #2 (3000-ft radius) because the four pilots felt that the vessel was maxed out in the 3000-ft turn radius and that there was room to correct unforeseen issues with the 4000-ft turn radius. Figure 3-12 shows how the Layout #1 channel was used in the ten inbound simulations. It should be noted that Simulation 47 was not included in this density figure due to the short extent of the transit. Figure 3-13 shows how the Layout #2 channel was used for inbound simulations.

From the discussion above and both density figures it is evident that the pilots remain on the green side of the channel in the turn at Battery Island and have minimal to no clearance in the apex of the turn. While this tendency is partially explained by the pilots' stated preference to use the green side because that results in a turn that feels similar to the existing geometry, it also seems to indicate that there would be value in providing additional maneuvering area on the green side of the channel. Layout #2 resulted in the need to correct on the exit of the turn and a tendency to slew from the green to the red side of the channel. The exit from the larger turn radius Layout #1 placed the vessel closer to the center of the channel.

Though the results presented above do not indicate precisely how much wider the turn should be, it seems reasonable to recommend adding somewhere between 100 and 300 ft at the apex of the turn. Figure 3-12Figure 3-12 shows an expanded channel that could be thought of as an upper bound for this expansion, with the channel being approximately 500 ft wider at the apex than the design tested. This design takes advantage of the naturally deep water on the green side of the turn which would require minimal dredging. This design is larger than necessary for safe navigation and could be reduced as needed later in the project. As with the rest of the channel, the final geometry selected for the entrance turn will be evaluated during with full mission bridge simulations.

The vessel traffic density figures also highlight the minimal clearance on the Bald Head Caswell and Southport Ranges on the red side of the channel. Both layouts tested, incorporated an asymmetric tapered widening for Bald Head Caswell and Southport Ranges. Based on the simulations' findings a design modification is recommended to widen Bald Head Caswell to a total of 800 ft wide with a 300 ft widening to the red side existing channel boundary and the green side of the channel remaining at the existing channel boundary. Similarly, for Southport Range the improved design would be to taper the red side channel boundary from the 300 ft widening in Bald Head Caswell Range to the simulated Layout #1 design at the turn at Battery Island. The green side of the channel for Southport Range would taper from the existing channel boundary at Bald Head Caswell Range to the simulated Layout #1 design at the turn at Battery Island. This updated alignment is shown in Figure 3-12.

For all of the inbound simulations a vessel was berthed at the ADM terminal. The four pilots all stated that with a vessel at ADM the transiting vessel's speed would need to be reduced to 5 kt through the water. Each pilot in the post-simulation debrief stated that they would highly recommend the use of an assist tug to pass a moored vessel at ADM with the design vessel. With the decreased speed the pilot loses effectiveness of the rudder, which significantly reduces the safety of the transit.

Upon viewing the vessel swept path figures (Appendix B-4) and the vessel use figures (Figure 3-12 and Figure 3-13), reduced clearance was observed on the red side of the channel of Lower Swash Range in the vicinity of green Buoy 19. This reduced clearance could have been a result of the reduced maneuverability due to the reduced speed previously discussed. However, it could also be a result of habit since the simulated paths align with the existing range line for Lower Swash (which was not modified in the simulations). Modifying alignment of the Lower Swash range may alleviate the trend to the red side of the channel and should be explored with future simulations with enough transits to ensure safety and reliability.

Following each simulation, the pilot was asked to evaluate the aids to navigation. Overall, the pilots thought that the buoys in the model were sufficient. The pilots particularly liked the red buoy that was added in the apex of the turn at Battery Island during the simulation and the shifting of R "16" and "18" to the beginning and end of the turn. The pilots stated that they did not want any buoys on the green side of the channel in the turn at Battery Island. As previously stated, the range markers in the model were kept at their existing headings. The pilots stated that the range headings should be located in the center of the channel based on the widened channel geometry. Based on the improved design alignment, four ranges would need to be updated near the entrance turn. These four ranges would be:

- Bald Head Shoal Reach 1 (range heading remains the same, but shifts to align with center of new channel),
- Smith Island (range heading remains the same, but shifts to align with center of new channel),
- Southport (range shifted/rotated for new alignment), and
- Lower Swash (range shifted/rotated for new alignment).

The evaluation of aids to navigation in this study was preliminary and provides insight for future modifications. These recommendations should be further evaluated and confirmed in future simulation efforts.

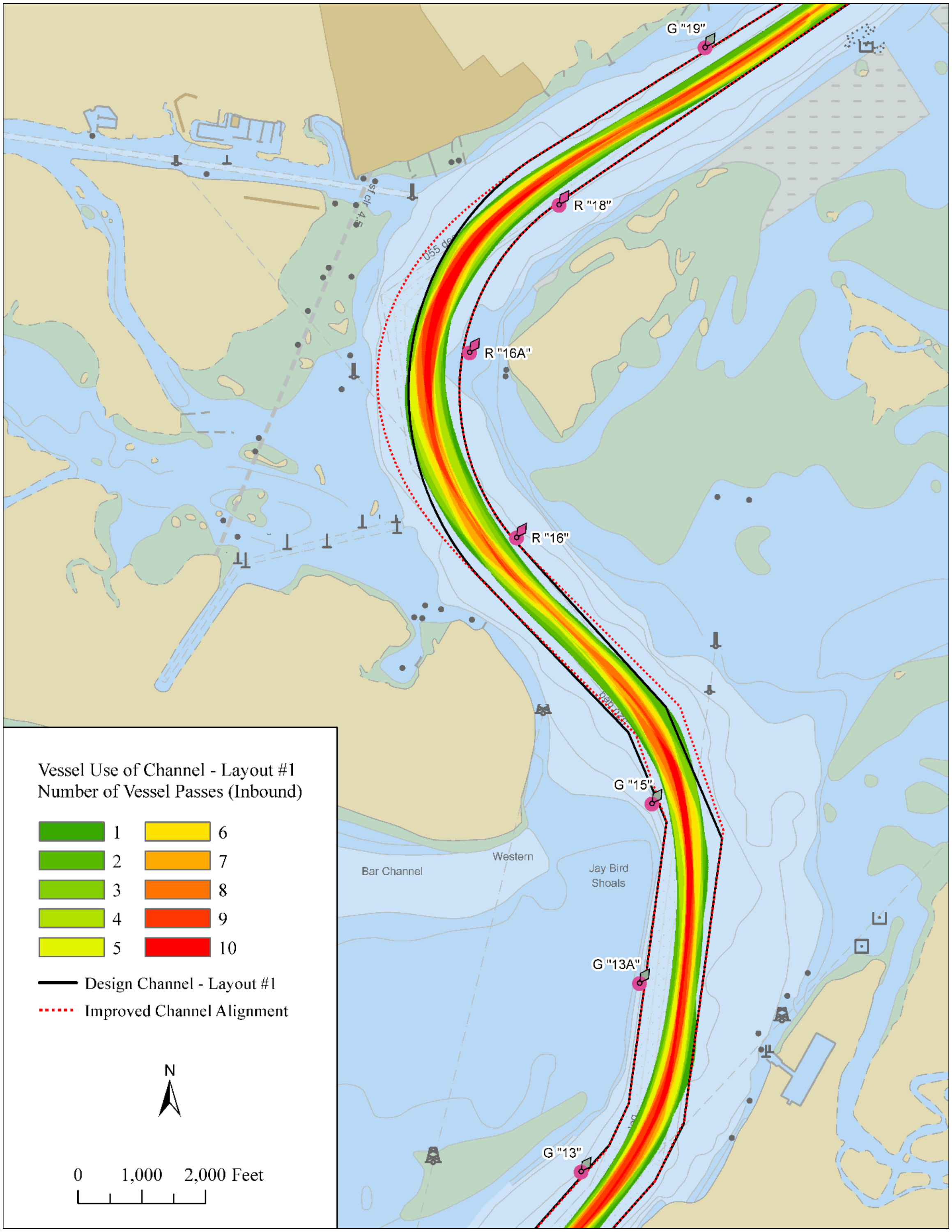

Figure 3-12: Swept Path Heat Map Layout #1 Inbound Entrance Turn Simulations

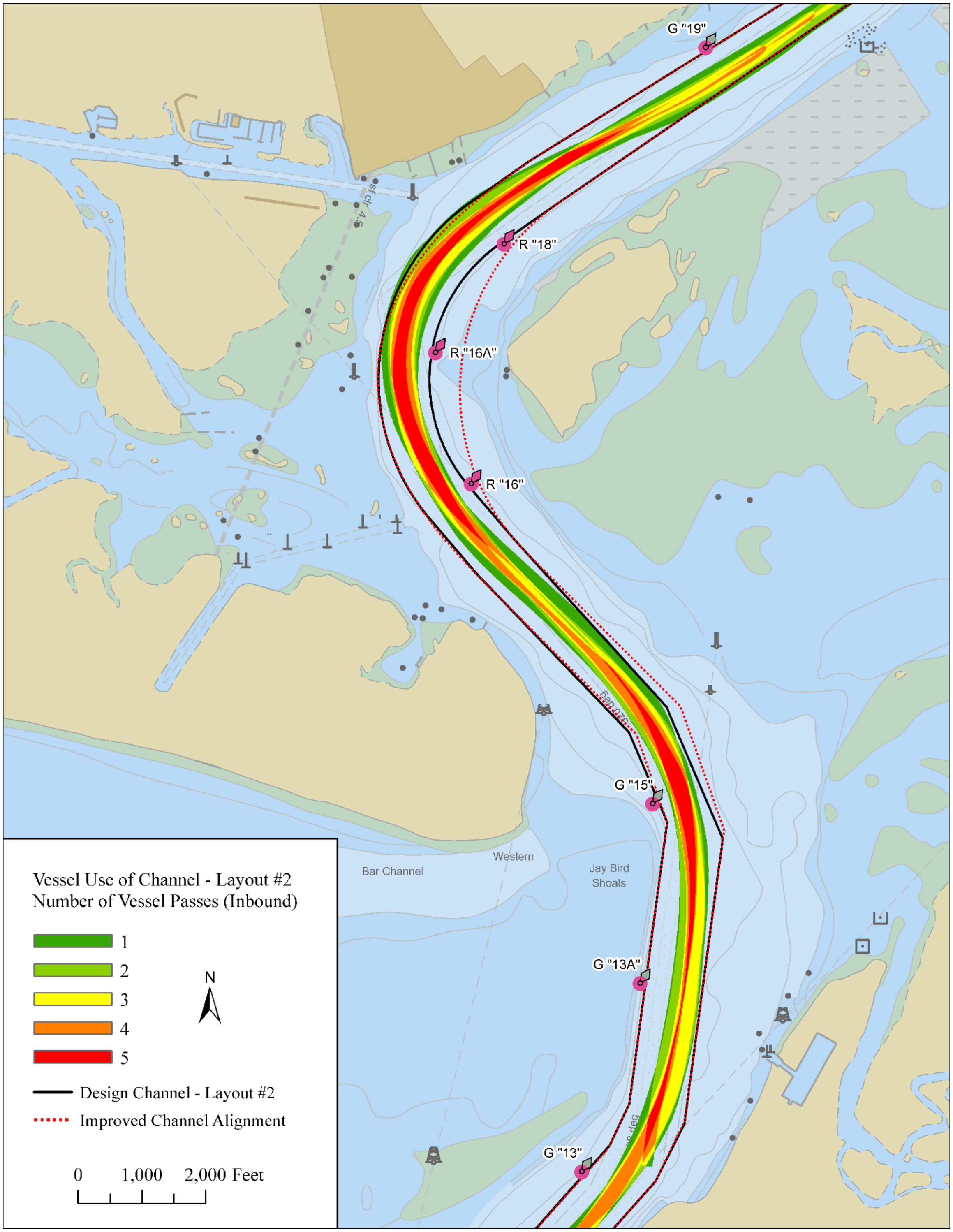

Figure 3-13: Swept Path Heat Map Layout #2 Inbound Entrance Turn Simulations

3.4.2. One-way Traffic Width in Channel

Of the simulations performed (Table 3-12), five simulations (28, 29, 30, 44, & 45) were performed with the explicit purpose of establishing an appropriate one-way channel width in the river. In addition to these simulations, Simulation 5 was a full-length transit with the existing channel, which provides insight into the required width for a one-way channel. Taken together, the simulations used to evaluate the one-way channel width are summarized in Table 3-14.

Table 3-14: One-way Channel Width Simulations – In River

Simulation Number	Pilot	Run Safety	Run Difficulty	Channel Width Considered [ft]
5	S. Aldridge	5	7	400
28	B. Hue	9	4	500
29	B. Hue	2	8	400
30	B. Hue	1	9	400
44	B. Hue	6	6	450*
45	B. Hue	7	6	450*

* Channel marker buoys were moved in 25 ft on both sides of the 500 ft channel to provide the pilot with some of the felt effect of a narrower (450 ft) channel.

Simulation 5 was performed as the first simulation after the pilot familiarization simulations (1 to 4). Appendix B-4 illustrates the vessel track followed in this simulation, from the pilot boarding station offshore all the way to the Port of Wilmington terminal. In order to operate in the existing channel, a lighter load condition vessel (37/38 ft draft) was used than what was used for subsequent simulations. The vessel exceeded the channel boundaries eight times (Smith Island into Baldhead Caswell; Battery Turn into Lower Swash; Snows Marsh into Horseshoe Shoal; Horseshoe Shoal into Reaves Point; Lower Big Island; Lower Brunswick; Upper Brunswick; and Fourth East Jetty into the Between Channel). However, in every case, the pilot indicated that the areas where the vessel swept outside of the channel were, in fact, deep enough that the vessel would not have grounded. In general, this was captured in the simulation scene; however, grounding was indicated in a few locations. The simulation was able to continue smoothly after each grounding incident without aborting the simulation.

The conclusion from Simulation 5, was that it may be feasible to bring a 1,200-ft vessel up the existing channel. However, the margin for error is very small, and any less-than-ideal weather conditions could greatly impact the safety of the maneuver. Additionally, it was noted that an assisting tug boat would be required for making the Battery Island turn in the existing channel.

After the full-length Simulation 5, the next simulation performed to evaluate the one-way in-river channel width was Simulation 28. Simulation 28 was considered the design channel width of 500 ft. Only a single simulation was performed because the pilot indicated immediately that he was comfortable with the 500-ft channel width and that a narrower channel width may be possible. This feedback from the pilot was considered substantial for the purposes of this feasibility level study, and subsequent simulations for the one-way channel width were spent testing the possibility of narrowing the channel further.

It is worth noting that Simulation 28 shows a relatively small bank clearance (approximately 10 ft) on the transition from Horseshoe Shoal Range to Reaves Point Range; however, the pilot indicated that this was due to loss of situational awareness rather than a restricting channel alignment. The pilot gave this simulation a safety rating of 9/10.

Following Simulation 28, Simulations 29 & 30 were performed for the same portion of the channel (Snows Marsh to Reaves Point), but with the existing channel width of 400 ft (the same lighter vessel load condition as Simulation 5 was used). The vessel exceeded the channel boundaries twice in each of these two simulations, and the pilot gave the simulations safety ratings of 2/10 and 1/10 for Simulation 29 & 30, respectively.

The pilot indicated that there was no margin for error with the 400 ft channel. Even if the environmental conditions were reduced from the 20 kt wind speed examined, the pilot did not think that he could make the turns. While a width of 400 ft in the straight away may be acceptable, providing extra width at each turn would be critical. The pilot indicated that he would not be willing to perform such a maneuver in the real world.

With the understanding from Simulation 28 that a 500-ft channel width is comfortable, and an indication from simulations 5, 29, & 30 that a 400-ft width is too narrow, the next natural question to explore was whether there is a width between 400 ft and 500 ft that would provide adequate maneuvering room, while minimizing required dredging volumes. Channel geometry had not been prepared to fully capture an intermediate channel width in the simulator scene; however, the simulator does allow for manual modification of certain aspects of the scene from the instructor console, including the channel marker buoys. To partially simulate the effect of an intermediate channel width (450 ft), the channel marker buoys were each moved in 25 ft (toward the center of the channel).

Simulations 44 & 45 were performed using this method of moving buoys to partially simulate the feel of a narrower 450-ft channel. In both simulations, the vessel maintained a minimum clearance of 25 ft to the Layout #1 (500 ft width) channel boundaries, indicating that it would have remained within a 450-ft channel. The pilot indicated that the 450 ft width is plausible in the straight reaches, but a width of at least 500 ft is necessary in turns. Both simulations were rated with above average safety 6/10 and 7/10 for Simulations 44 & 45, respectively. While it is not possible to draw firm conclusions from these simulations (because the channel line work was not actually in the model), these simulations do provide an indication that it may be possible to reduce the channel width below the design width of 500 ft.

Further simulation studies would be required to substantiate a narrowing of the channel. Such studies should include the side-slope geometry and ensure that bank-effects are captured appropriately. These effects would further limit maneuvering safety for narrow channels. Additionally, further simulations should evaluate the entire length of the channel.

Due to time constraints not all ranges (i.e., Keg Island or Lower Big Island Ranges) and turns were evaluated for the one-way traffic width.

Thus overall, these simulations provide feasibility level confirmation of the design 500-ft, one-way channel width, with an indication that some further optimization may be possible. In addition to confirming the basic width, the pilots suggested that bend wideners be included on the inside of the in-river bends to improve safety. The importance of bend wideners was noted explicitly by the pilots in their feedback for Simulations 44 & 45, as well as through informal conversation and in the debrief after the simulations. For example, in Simulations 28 and 44, the vessel passes close to Buoy G "27" from Horseshoe Shoal Range to Reaves Point Range. Providing a cut-off angle on the bend similar to the bend from Snows Marsh to Horseshoe Shoal would provide more clearance on the inside of the bend.

3.4.3. Two-way Traffic Width in Channel

Nine simulations (Table 3-15) were performed to evaluate the required width for passing two 1,200 ft container ships in the river portion of the channel. The two-way traffic width for testing in this simulation effort was 800 ft, which was reflected in both design Layout #1 and design Layout #2. In addition to the 800 ft channel width, the existing channel width of 600 ft was tested, along with an intermediate width of 700 ft.

Table 3-15: Two-way Channel Width Simulations – In River

Simulation Number	Pilot	Run Safety	Run Difficulty	Passing Distance Between Vessels [ft]	Piloted Vessel Bank Clearance* [ft]	Direction of Piloted Vessel	Passing Width
18	B. Hue	8	2	205	18	Inbound	800 ft
19	B. Hue	9	1	248	92	Outbound	
52	J. McDowell	10	3	236	86	Inbound	
53	J. McDowell	9	3	313	71	Outbound	
20	B. Hue	7	4	179	-1	Inbound	700 ft**
21	B. Hue	7	4	150	46	Inbound	700 ft***
24	B. Hue	9	4	157	127	Outbound	
22	B. Hue	3	7	76	-26	Inbound	600 ft
23	B. Hue	5	6	110	59	Inbound	

Notes:
* This bank clearance is during the active passing of the two vessels.

** Channel maker buoys were moved (75ft in on the red side and 25 ft on the green side) to provide the pilot with the sense of a narrower, 700 ft, channel.

*** The autopilot vessel track was moved over to simulate 700 ft channel.

As indicated in Section 3.2.2.3, the two-way passing simulations were performed with one vessel being conned by a CFR pilot and the other vessel being controlled by the simulator autopilot. For the autopiloted vessel, the intended track is specified, along with speed, turning radius and other parameters. The autopilot track was aligned so that the center of the autopiloted vessel would be offset one quarter of the available channel width from the channel boundary. Each simulation was set up so that the passing occurred on Upper Midnight; one vessel started the simulation in Lower Lilliput, and the other started in Lower Midnight.

The evaluation of two-way passing began with Simulations 18 and 19, which considered typical passing maneuvers with an 800 ft channel. For Simulation 18, the piloted vessel was transiting inbound; for Simulation 19, the piloted vessel was transiting outbound. Both simulations were rated high marks for safety (8/10 and 9/10) and low marks for difficulty (2/10 and 1/10). The pilot indicated that the 800 ft wide channel was comfortable for two ships passing and that he thought the channel could be narrower without compromising safety. In Simulation 19, the inbound vessel was traveling at a speed (over 12 kt), which would likely result in large interaction forces with the passing vessel, however this did not occur. It is likely the ship-to-ship interaction forces in the simulation are less than would be expected in reality.

Simulations 52 and 53 were performed later in the simulation effort but considered passing in the same 800-ft channel as Simulations 18 and 19. These simulations were performed by a different pilot under different environmental conditions, but received similar marks for safety and difficulty. The pilot for these simulations also indicated that 800 ft was more than adequate, and the he was open to the idea of a 700-ft wide channel.

The existing channel passing width of 600 ft was evaluated for two of the 1,200 ft vessels, each with a beam of 169 ft, in Simulations 22 and 23. These simulations were performed with minimal clearances between vessels and with channel boundaries. The piloted vessel exceeded the channel boundary in Simulation 22. Both simulations were given average to below-average marks for safety and above average marks for difficulty. The pilot indicated that he would not be willing to perform this maneuver in the real world without assist tugs, more practice, and/or restrictions. Additionally, the pilot indicated that the simulator was not fully capturing the bank effects and the ship-to-ship interaction, which would further complicate the maneuver. Overall, the 600 ft channel was not considered sufficient as a design width for these design vessels.

As was the case for the one-way channel width simulations, these scenes developed for this simulation effort did not include any intermediate channel widths between the existing width and the design width proposed for testing. However, since the pilots indicated that 800 ft was more than sufficient, it was clear that evaluating an intermediate width would be important.

A narrower, 700-ft, passing channel was evaluated two different ways. First, Simulation 20 provided some of the effects of a 700-ft channel by moving the channel marker buoys in toward the center of the channel 75 ft on the red side and 25 ft on the green side. Moving the buoys in this manner allowed the autopilot ship track to maintain the same alignment as for Simulation 18. The pilot performed this maneuver with adequate passing clearance, but essentially zero bank clearance. If clearance is taken between the piloted vessel and the hypothetical red-side channel boundary that was simulated by moving the buoys, the vessel exceeded the boundary by one foot. The pilot indicated that it was difficult to perceive the narrowing of the channel when simulated by moving the buoys.

Simulations 21 and 24 applied a second approach for simulating the effect of a 700-ft channel. These simulations still used the base scene for the 800-ft design channel but simulated the effect of a narrower channel by moving the autopilot track over 75 ft toward the piloted vessel, which simulates the maneuvering area that the piloted vessel would expect in a 700-ft channel. This method was determined to be more effective at simulating the narrower channel than moving buoys; however, the method is imperfect. For example, the autopilot tracks are only a target track for the autopiloted vessel; they are not followed exactly. In Simulation 24, the autopiloted vessel was off course while the two vessels passed, such that the available space for the piloted vessel was similar to the space expected in a 750-ft wide overall channel. This uncertainty in channel width is reasonable for a feasibility level analysis, but it is clear that the simulations performed only provide a general indication that a 700-ft channel might be acceptable for passing. A 700 ft channel was not fully tested in this study.

Overall, this study confirmed that the design channel width of 800 ft is sufficient for two-way passing of two 1,200-ft container ships with a beam of 169 ft. Additional simulations indicated that a narrower, 700-ft channel may be feasible, but should be tested further with proper hydrodynamic flow field and interaction with channel banks. It should be noted that the channel is being design for passing two 12,400 TEU vessels. This design criteria will need to be re-evaluated in PED phase of the project based on the economic analyses. As previously discussed, for this simulator effort the vessel was 10 ft wider than the project design vessel.

The pilots indicated repeatedly throughout these simulations that the passing vessel effects and bank effects were not accurately captured in the simulator. These limitations introduce some uncertainty in the simulations. However, much of this uncertainty can be made up for by the intuition and experience of the local pilots. For testing in full mission bridge simulations, the ship-to-ship and ship-to-bank interactions should be tested and validated prior to the testing program to make sure the vessel models will reproduce the effects anticipated in the real world.

3.4.4. One-way Traffic Width in Offshore

Eight simulations (Table 3-16) were performed to evaluate the design offshore one-way traffic width of 600 ft. Five of these simulations (31-35) considered the design channel width of 600 ft for the New Sea Range in conjunction with a wider, 900 ft, Baldhead Shoal 3. While it is not certain that a two-way passing width on Baldhead Shoal Reach 3 would reach all the way to the pilot station (if it is included in the design), the wider transition provided an opportunity for the pilot to familiarize himself with this area of the scene, especially with the proposed ATONs. After these five simulations, three simulations were performed with the design 600 ft channel width on both sides of the bend where the current pilot boarding station is located.

All eight simulations for the one-way channel width were rated above average for safety and below average for difficulty. It was determined that the width of 600 ft is sufficient for offshore maneuvers in the straight channel (Simulations 31 to 35), as well as for the bend (Simulations 36 to 38). No recommendations were made regarding changes to the channel width or alignment in this area.

The pilot did provide recommendations regarding ATONs in the offshore area:

- The New Sea Range will require range markers.
- The pilot liked the location of Buoy "E", the green-side channel marker buoy at the bend between Baldhead Shoal 3 and the New Sea Range.

Table 3-16: One-way Channel Width Simulations - Offshore

<table>
<tr><th>Simulation Number</th><th>Pilot</th><th>Run Safety</th><th>Run Difficulty</th><th>Direction of Transit</th><th>Channel</th></tr>
<tr><td>31</td><td>S. Aldridge</td><td>9</td><td>2</td><td rowspan="2">Inbound</td><td rowspan="5">Transition between 900 ft wide Baldhead Shoal 3 and 600ft wide New Sea Range</td></tr>
<tr><td>32</td><td>S. Aldridge</td><td>10</td><td>1</td></tr>
<tr><td>33</td><td>S. Aldridge</td><td>8</td><td>2</td><td rowspan="3">Outbound</td></tr>
<tr><td>34</td><td>S. Aldridge</td><td>9</td><td>2</td></tr>
<tr><td>35</td><td>S. Aldridge</td><td>9</td><td>2</td></tr>
<tr><td>36</td><td>S. Aldridge</td><td>7</td><td>3</td><td rowspan="2">Inbound</td><td rowspan="3">Transition between 600 ft wide Baldhead Shoal 3 and 600 ft wide New Sea Range</td></tr>
<tr><td>37</td><td>S. Aldridge</td><td>7</td><td>3</td></tr>
<tr><td>38</td><td>S. Aldridge</td><td>6</td><td>4</td><td>Outbound</td></tr>
</table>

3.4.5. Two-way Traffic Width in Offshore

Three simulations (Table 3-17) were performed to evaluate the two-way traffic width that would be required in Baldhead Shoal Reach 3 if the relevant economic analyses indicate that it is necessary to have a passing area in that range. These simulations were performed differently than the two-way in-river passing simulations. These simulations were performed with two pilots (no autopilot). One vessel was conned by a pilot on the simulator bridge controls (used for all other simulations), and the other vessel was conned by a pilot using the basic vessel controls available through the instructor station. These controls allow for specification of basic engine orders and rudder, which was sufficient for these simulations.

Table 3-17: Two-way Channel Width Simulations – Offshore

Simulation Number	Pilot	Run Safety	Run Difficulty	Passing Distance Between Vessels [ft]	Bank Clearance of Inbound Vessel [ft]	Bank Clearance of Outbound Vessel [ft]	Passing Width [ft]
41	S. Aldridge / B. Heu	8	3	241	110	100	900
42	S. Aldridge / B. Heu	8	3	217	70	195*	900
43	S. Aldridge / B. Heu	7	4	233	75	48	800**

Notes:
* Bank clearance excludes the final portion of the track, where the pilot (thinking the simulation was over) stopped controlling the vessel, which ran aground.

** Channel maker buoys were moved to provide the pilots with the sense of a narrower, 800 ft, channel.

Simulations 41 and 42 considered the design 900 ft wide channel that was prepared for evaluation in this study. Both simulations received high marks for safety (8/10) and low marks for difficulty (3/10), and the pilots indicated that 900 ft is sufficient width for two-way passing in Baldhead Shoal Reach 3.

After testing the 900 ft wide channel, an additional simulation (43) was performed with the channel marker buoys moved in 50 ft on the red and green side toward the center of the channel to simulate a narrower, 800 ft channel. While this method only provides part of the effect of a narrower channel, the pilots were very comfortable with how the simulation went and indicated that their opinion was that an 800 ft channel would be sufficient, and that they would even be open to testing a 700 to 750 ft channel in future testing.

Overall, the offshore two-way passing width of 900 ft was validated and determined to be more than adequate. The preliminary testing of an 800 ft channel provided a strong indication that an 800 ft channel would be sufficient as well. As mentioned previously, the channel is being design for passing two 12,400 TEU vessels. This design criteria will need to be re-evaluated in PED phase of the project based on the economic analyses. As previously discussed for this simulator effort the vessel was 10 ft wider than the project design vessel.

3.4.6. Turning Basin, Berthing Area and Adjacent Channel

Seven simulations were performed in the vicinity of the Port of Wilmington. Of these simulations five were inbound transits to evaluate the turning basin, berthing area and adjacent channel. The other two simulations were outbound maneuvers that evaluated the berthing area and adjacent channel. The pilot safety and run difficulty ratings for the port simulations are summarized in Table 3-18. All of the port simulations were performed by Glenn Turbeville, a McAllister Docking Pilot.

Table 3-18: Pilot Ratings for Simulation Safety, Difficulty, and Tug Adequacy for Port Simulations

Simulation Number	Direction of Transit	Pilot	Run Safety	Tug Adequacy	Run Difficulty
58	Inbound	G. Turbeville	8	6	7
59		G. Turbeville	9	9	3
60		G. Turbeville	9	8	4
61		G. Turbeville	8	8	5
64		G. Turbeville	7	8	7
62	Outbound	G. Turbeville	5	8	8
63		G. Turbeville	8	10	7

As previously discussed in Section 3.2.2.4, for all port simulations the transiting vessel had to pass the following moored vessels:

- Handy Sized Vessel at Apex Oil Terminal and Port of Wilmington Berth 3 & 5
- 8,500 TEU Vessel at Port of Wilmington Berth 9

In each simulation, vessel maneuvers were performed to/from Port of Wilmington Berth 8. The channel and turning basin geometry was the same for both design Layout #1 and design Layout #2. The geometry that was evaluated was a 50 ft and 75 ft widening on the green side only for Fourth East Jetty Range and Between Channel Reach, respectively. The turning basin alignment that was evaluated was an enlargement of the existing turning basin to 1500 ft in width and 1,000 ft along the river on both the west and east sides, as shown in Figure 3-14. Additionally, the design layout for the turning basin included a tapered widening on the green side of the channel. This design assumes that the derelict Chevron pier will be removed.

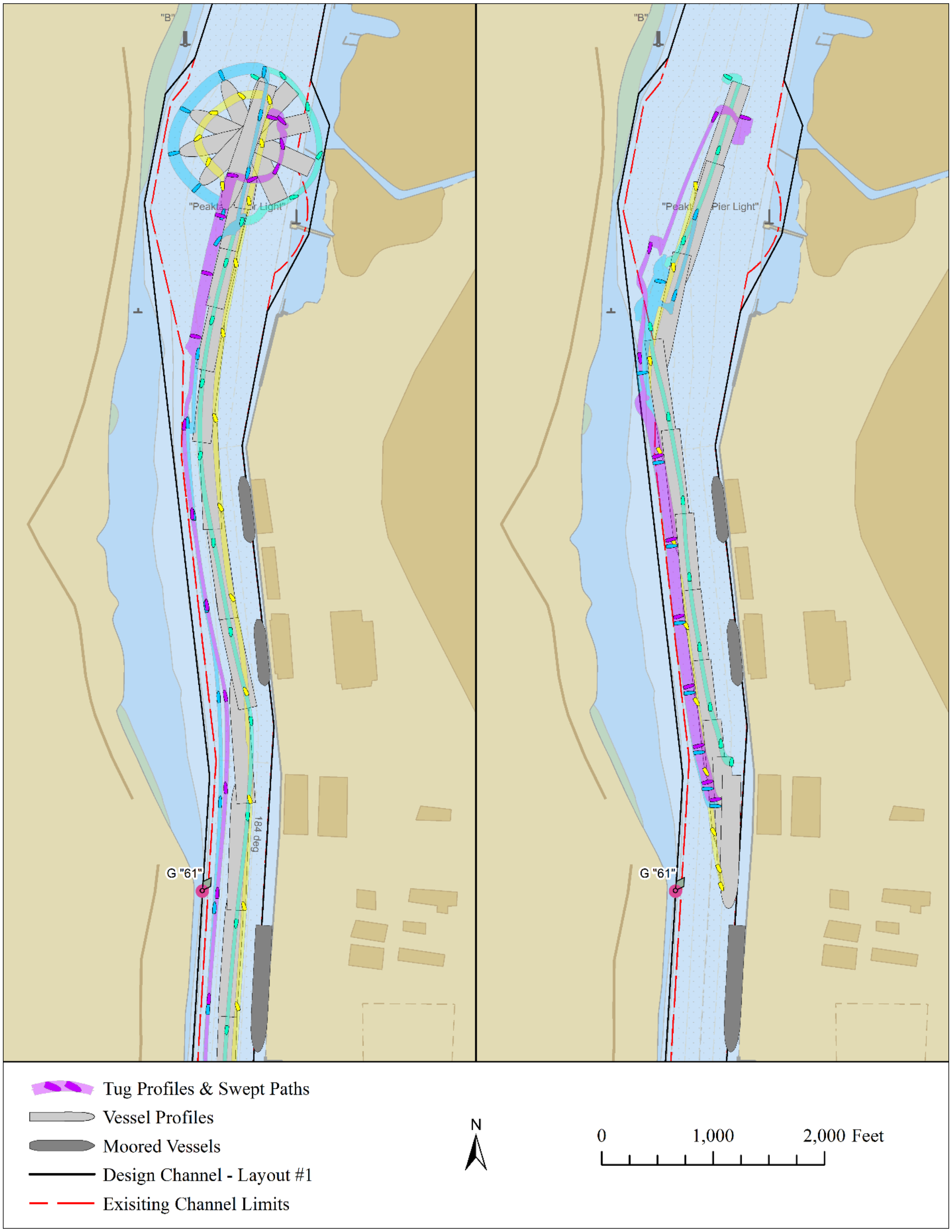

Figure 3-14: Simulation #61 Tug Swept Path Summary with Profiles & Channel Geometry

The first inbound simulation, Simulation 58, evaluated the transit under slack tide with a wind of 15 kt from the NE. Due to a limitation in the TRANSAS software the pilot only had the option to start the transit at either 0.0 kt or 6.6 kt, dead slow ahead. The pilot decided to start the transit at 0.0 kt at a distance from the turning basin such that he could increase the speed to a typical transiting speed in the channel approaching the basin. All of the inbound simulations assessing the turning basin followed this same methodology.

For Simulation 58 the pilot used four tugs, two 53 mt Z-Drive tugs and two 32 mt Conventional Twin Screw tugs. The pilot stated that the docking pilot typically takes over from the river pilot at red Buoy 58 at which point at least one tug is fastened. Due to time constraints the simulation was started between green Buoy 59 and 61. As the pilot approached the turning basin and as he passed the moored vessels, he had the first Z-drive tug positioned with the center lead aft in line with the vessel and the second Z-drive tug attached at the starboard shoulder. During the inbound transit to the turning basin the pilot had minimal clearance to the green side of the channel; first in the turn from Fourth East Jetty Range into the Between Channel Reach and secondly at the northern end of the Between Channel Reach. This minimal clearance highlights the importance of the widening on the green side of the channel. In the simulation debrief the pilot also emphasized the desire to have this widening.

In Simulation 58 the pilot successfully completed the turning maneuver in the turning basin with the utilization of the four tugs. For the turning maneuver the pilot had the following alignment of the tugs:

- 53 mt Z-Drive Tug 1 – center lead aft at 90 degrees to starboard,
- 53 mt Z-Drive Tug 2 – starboard shoulder,
- 32 mt Conventional Tug 1 – port quarter,
- 32 mt Conventional Tug 1 – bow pushing inline.

The two aft tugs were utilized at 100% for the entire maneuver in the turning basin, approximately 10 minutes. The other two tugs on the bow were utilized at 50% for the majority of the turn. Tug power use in Simulation 58 is summarized in Figure 3-15. The pilot also used the bow thruster from 50 to 100% to assist in the maneuver. During this maneuver the pilot had reserve tug power in the two bow tugs. The pilot maintained over 100 ft of clearance to both the red and green side channel banks and had an average rate of turn of 20 degrees/min. Upon completing the turn the stern tug went back in line and the two conventional tugs attached at the starboard quarter. While going to berth the pilot grounded the vessel on the green side of the channel in the Between Channel Reach. The pilot stated that this grounding occurred due to a lack of familiarity with the ship model and simulator. The pilot did not consider the grounding of the vessel when rating this simulation.

Simulation 59 evaluated the approach and the maneuver in the turning basin under peak flood currents with a wind from the SW at 15 kt. Due to time constraints this transit started at the entrance to the turning basin and only evaluated the turn. The pilot had the same configuration of the four tugs as Simulation 58. The two bow tugs were utilized at 100% for the majority of the maneuver in the turning basin. The two aft tugs were utilized between 50 and 100% during the turn. The pilot also used the bow thruster at 100% during the turn in the turning basin to assist the maneuver. During this maneuver the pilot at one point had no reserve tug power. The pilot maintained over 100 ft clearance to both channel banks during the turning maneuver. The pilot gave this simulation a relatively high safety rating of 9/10 even though he maxed out his tug power. The pilot stated that the flood tide assisted the maneuver. During the simulation debrief the pilot stated that the width and length of the design turning basin was sufficient.

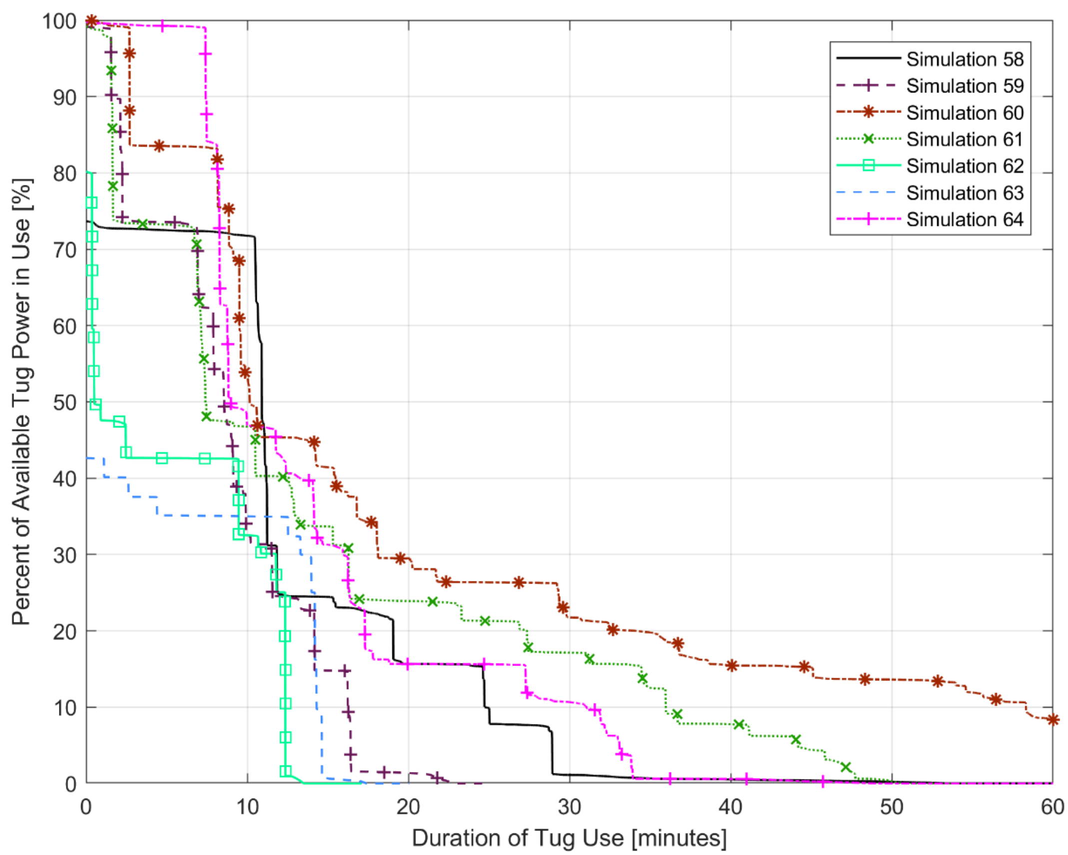

Figure 3-15: Summary of Tug Usage

The next simulation, Simulation 60, evaluated the same conditions as Simulation 58 (Slack tide & 15 kt wind from the NE). The pilot took the same approach to the tug use as he maneuvered past the moored vessels as Simulation 58. However, for this simulation he maintained larger clearances on the green side of the channel comparatively to Simulation 58. For the maneuver in the turning basin the pilot adjusted the tug alignment that he had used in the previous two simulations in that the second conventional tug was pushing next to the other conventional tug on the port quarter. The Z-Drive tugs remain on the center lead aft at 90 degrees to starboard and on the starboard shoulder. During the turning basin maneuver the pilot used the three aft tugs at 100%. The bow tug was used at 100% twice but primarily utilized at 50% power. When the bow tug utilization was at 100% the pilot had no tug reserve power and limited to no bow thruster reserve. Following the turning maneuver, the pilot re-aligned the starboard bow tug to the port shoulder and the center lead aft tug to be in line with the vessel. The pilot safely docked the vessel at Port of Wilmington's Berth 8. In the simulation debrief the pilot stated that he prefers to use the full tug power to get momentum and then eases off. He stated that if there was a problem with one of conventional tugs during the maneuver, he would be able to still safely complete the maneuver. He did not state the same for the loss of one of the Z-Drive tugs.

Simulation 61 evaluated the same environmental conditions as Simulation 59 (Peak flood currents & 15 kt wind from SW). The pilot used the same alignment of the tugs as he transited by the moored vessels, performed the turning maneuver, and berthed the vessel as in Simulation 58. An example inbound tug maneuver is shown in Figure 3-14. The pilot maintained a clearance of at least 60 ft from the moored vessels. In the turning basin the stern of the vessel came within 70 ft of the red side of the channel. The pilot used the main engine at dead slow ahead twice during the turning maneuver to keep 60-70 ft clearance on the red side of the channel. The pilot stated that a clearance of 60-70 ft in the turning basin routinely occurs today. Similar to the previous simulations, at one point during the turning maneuver the pilot utilized 100% of the tug power and the bow thruster, leaving no reserve power aside from the vessel's engine. The pilot did not seem concerned that there was no reserve power in the tugs. In the simulation debrief the pilot again stated the desire for the 1000 ft length of the turning basin.

The last inbound maneuver, Simulation 64, evaluated peak ebb currents with a wind from the NE at 15 kt. For this simulation the pilot only had the Z-Drive tug at the center lead aft in line with the vessel as the transiting vessel passed the moored vessels. The pilot was able to maintain his intended track line as he approached the turning basin. For the turning maneuver the stern tug swung out 90 degrees to starboard and the other Z-drive tug and two conventional tugs were all pushing the port quarter of the vessel. All four tugs were utilized at 100% power for the majority of the turn, leaving no reserve power. The bow thruster did not exceed 25% power during the turn. The stern of the vessel came within 40 ft of the red side of the channel at which point the pilot used half ahead of the engine. After completing the turn the vessel passed near the green side channel boundary (minimum clearance of 13 ft) while maneuvering toward the berth. At this point, the pilot used the stern tug for steering which he did not anticipate. The pilot safely docked the vessel at Berth 8 after correcting course with the stern tug. In the simulation debrief the pilot stated that with peak ebb currents the transit would require a minimum of four tugs.

Two outbound maneuvers were performed from Berth 8, Simulation 62 & 63. Both simulations were performed during peak ebb currents with 15 kt winds from the NW. Two 53 mt Z-Drive tugs were used to perform this transit per the pilot's request, one each at the bow and stern. Coming off the berth the maneuvers felt as expected. However, once off berth in Simulation 62 the pilot thought he would feel more ship-ship interaction with the vessel at Berth 9. As a result, the stern of the vessel left the channel slightly on the green side of the channel. Knowing this the pilot left the tugs attached until the vessel cleared Berth 9 for Simulation 63. Overall the pilot felt comfortable with the off-berth maneuver. In simulation debrief the pilot did state he would like green Buoy 61 removed.

In summary, the pilot was content with the design channel for the port and turning basin even with the minimal reserve tug power shown in these simulations. Future simulations should evaluate the ability to perform this maneuver with handicapped tug power, lack of bow thruster, and loss of a tug, to ensure safety during unforeseen conditions. The pilot stated the need for the design 75 ft widening in the Between Channel Reach and the 1000 ft length on both sides turning basin. The pilot was open to a slightly narrower, 1450 ft, turning basin. However, a narrower basin was not evaluated in this simulation effort and would be difficult to justify as a design due to the limited reserve power in the maneuver.

3.5. Summary and Conclusions

The primary findings of this simulation study are summarized in this section, structured around the main objectives for the study. The proposed design layout and new stationing from this simulation effort are shown in Appendix B-1.

3.5.1. Entrance Turn

The channel geometry for the entrance turn was evaluated with the following specific conclusions:

The 4,000-ft radius entrance turn around Battery Island is preferred over the 3,000-ft radius alternative. However, a hybrid alternative seems most appropriate, taking the 4,000-ft radius alignment (Layout #1) and adding some additional width on the outside of the bend through the Battery Island turn, Figure 3-12. An upper bound on the entrance bend channel width could be composed by including all the areas in both Layout #1 and Layout #2, which expands the apex of the bend to approximately 1300 ft width (500 ft wider than Layout #1). The width at the apex of the turn will be finalized during the PED phase of the study.

- The design alignment of Bald Head Caswell range should be modified from the alignment tested to include additional area on the red side of the channel resulting in a design channel width of 800 ft. The green side of the channel for Bald Head Caswell will remain at the existing channel.

- For Southport Range the design alignment should be modified to taper the red side from a 300 ft widening at Bald Head Caswell Range to Layout #1 design at Battery Island turn. The green side of the channel for Southport Range would taper from the existing channel boundary at Bald Head Caswell Range to the simulated Layout #1 design at the turn at Battery Island.

- The pilots had preliminary recommendations regarding the ATONs. For the proposed channel the range markers for Bald Head Shoal Reach 1, Smith Island, Southport, and Lower Swash would need to be updated to align with the center of the channel. Additionally, the pilots would like to see a red buoy at the apex of the turn at Battery Island and have R "16" and "18" shifted to the beginning and the end of turn.

3.5.2. One-way Traffic Width in Channel

The channel geometry for the one-way traffic width in-river was evaluated with the following specific conclusions:

- The design 500-ft one-way channel width was validated at a feasibility level, with an indication that some further optimization may be possible.
- Cut off angles on all bends in the river are recommended and should be consistent for the run of the channel to improve clearance on the inside of the in-river bends.

3.5.3. Two-way Channel Width in Channel

The channel geometry for the two-way traffic width in-river was evaluated with the following specific conclusions:

- The design channel width of 800-ft was confirmed to be sufficient for two-way passing of two, 1200-ft container ships. There is a possibility that a narrower, 700-ft or 750-ft channel is also feasible, which should be confirmed through additional simulations with the channel geometry and side slopes modified and modeled accordingly.
- Additional simulations should include validation of ship-to-ship and ship-to-bank interaction for passing scenarios, particularly for narrowing the channels.
- Based on the economic analyses additional simulations may necessary to evaluate the design criteria of a 12,400 TEU vessel passing a Panamax sized vessel, as the economic analyses may find the passing of two 12,400 TEU vessels unlikely.

3.5.4. One-way Channel Width Offshore

- The channel geometry for the one-way channel width offshore of 600-ft was confirmed to be sufficient.

3.5.5. Two-way Channel Width Offshore

- The offshore two-way passing width of 900-ft was confirmed to be adequate. Preliminary testing indicated that an 800-ft wide channel would likely be sufficient as well.

3.5.6. Turning Basin, Berthing Area and Adjacent Channel

The geometry for the port and turning basin area was confirmed feasible as simulated, with the following specific conclusions:

- The 50 and 75 ft widenings on the Fourth East Jetty and Between Channel ranges, respectively, are important for maneuvering past vessels moored at the Port.
- The increased turning basin length to 1,000 ft on both sides of the channel is sufficient, but not excessive for turning these larger vessels.
- The turning basin width of 1,500 ft was sufficient for berthing the design containership for wind speeds up to 15 kt; wind speeds higher than 15 kt were not

examined. It should be noted that the tugs were operated up to 100% of the available capacity for extended periods (10 minutes) of the berthing maneuvers at the pilot's discretion. Additionally, the vessel's bow thruster was required to complete the turning maneuver.

3.5.7. Aids to Navigation

The evaluation of aids to navigation in this study was preliminary and provided the following recommendations for future study:

- The range markers should be modified as necessary to align with the center of each channel segment. In some cases, this requires modifying the range heading; in other ranges, this results in a lateral shift of both range markers to align with the widened channel geometry. This recommendation was specifically stated for Bald Head Shoal Reach 1, Smith Island, Southport, and Lower Swash Ranges, but it applies to all ranges.
- At the turn at Battery Island the pilots particularly liked the red buoy added at the apex of the turn and the shifting of R "16" and "18" to the beginning and end of the turn. The pilots stated that they did not want any buoys on the green side of the channel in the turn.
- For the New Sea Range the pilot stated that new range markers would be required. Additionally, the pilot liked the location of Buoy "E", the green-side channel marker buoy at the bend between Baldhead Shoal 3 and the New Sea Range.
- Additional ATONs may be required to mark the bend wideners recommended in Section 3.5.2 and will be evaluated during the Full Bridge Mission Simulations.

3.6. Proposed Channel Layout

Based on this simulation study, the widths for the proposed channel to be carried through the feasibility stage of this project are as follows:

- One-way traffic width in the river (upstream of Sta 1140+00): 500 ft
- Two-way traffic width in the river (upstream of Sta 1140+00): 700 ft[1]
- One-way traffic width offshore: 600 ft
- Two-way traffic width offshore: 800 ft[1]

The proposed deign layout and new stationing from this simulation effort are shown in Appendix B-1. These channel widths and configurations will be confirmed during Full Mission Bridge Simulations during the PED phase of the project. From Battery Island Turn to the pilot station, the final channel depth will be increased by 2 ft over the depth in the river channel to allow for adequate under keel clearance in the areas affected by ocean waves.

[1] Two-way traffic widths are preliminary and need to be confirmed with additional simulations that include the modified channel geometry and side slopes, and ship-to-ship and ship-to-bank interaction.

4. Estuarine Numerical Modeling Development

4.1. Framework

Several numerical models were identified that would be potentially suitable for this project's required modeling efforts. These models are approved by the U.S. Army Corps of Engineers (USACE) for coastal modeling, as indicated by the designations CoP (Community of Practice) Preferred and Allowed for Use. A screening process was performed and examined model capabilities, integration/coupling of modules, availability (commercial vs public domain), user interface, widespread usage and acceptance.

The Delft3D model suite developed by Deltares was identified as the preferred system for this project. This model is well suited for the requirements of the study in terms of its capabilities to model the required processes, ease of use, and recognition in the U.S. and abroad. The USACE designates this model as Allowed for Use. Compared to other qualified coastal model suites such as Mike 21, Delft3D is of public domain, which is a significant advantage considering the potential need for the model to be reviewed by third parties. The Delft3D model suite is recommended to model hydrodynamics in three dimensions, waves, sediment transport, morphology, and water quality.

The model GenCade, developed by the USACE, is proposed to model shoreline morphology around the mouth of the estuary. This model is capable of modeling longshore sediment transport taking into account waves. Figure 4-1 shows the proposed modeling framework. The effort begins with the collection and analysis of all the metocean data and definition of the channel alternatives, as these two impact the development of grids and model setups. This is followed by the development of the 3-D hydrodynamic model and spectral wave model. The results of these two models are, to varying degrees, used in the rest of the models.

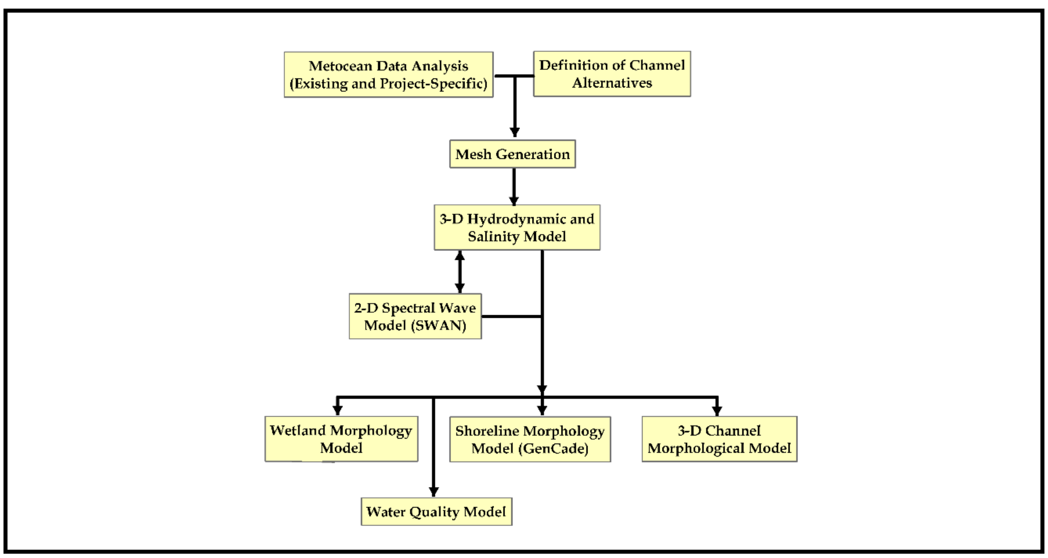

Figure 4-1: Proposed modeling framework

4.2. Hydrodynamics

A Delft3D three-dimensional hydrodynamic model (hereinafter referred to as HD model) was developed to simulate hydrodynamic conditions in the Cape Fear River estuary. The model is capable of predicting time dependent flow parameters such as free surface elevation and current velocity at each point in the computational domain. The model can be forced with either constant or time dependent boundary conditions, which in general may include tides, river discharges, wind, and other parameters. The model utilizes a curvilinear grid.

4.2.1. Model Grid and Bathymetry

The model domain included the Cape Fear River estuary from upstream of the Cape Fear, Black, and Northeast Cape Fear Rivers to twenty miles offshore from the mouth of Cape Fear River near Southport, NC. The grid cell sizes were variable throughout the domain. In the offshore area the resolution was approximately 90 meters. For upstream Cape Fear, Black, and Northeast Cape Fear River areas, the resolution was approximately 30 meters. The resolution along the upstream river areas was selected and varied so that most of the meanders and oxbow sections were resolved as judiciously as possible. Along the channel the resolution was approximately 5 meters, which is sufficient to resolve the proposed changes in channel width and channel slopes. The vertical grid is also very fine with 25 uniform layers each having a 1.28m thickness. Considering the large 3-dimensional domain size, the model resolution reached the practical limits for runtimes while adequately capturing the processes modeled. The model domain and grid are shown in Figure 4-2. Figure 4-3 and Figure 4-4 show the model grid near Wilmington Harbor and the mouth of the Cape Fear River, respectively.

Figure 4-2: Model domain and grid

Figure 4-3: Model grid near Wilmington Harbor

Figure 4-4: Model grid near the mouth of the Cape Fear River

Bathymetry and ground elevations were combined from the previously discussed five datasets and the resulting model bathymetry is shown in Figure 4-5 to Figure 4-7. For representational purposes, the bathymetry is shown in feet.

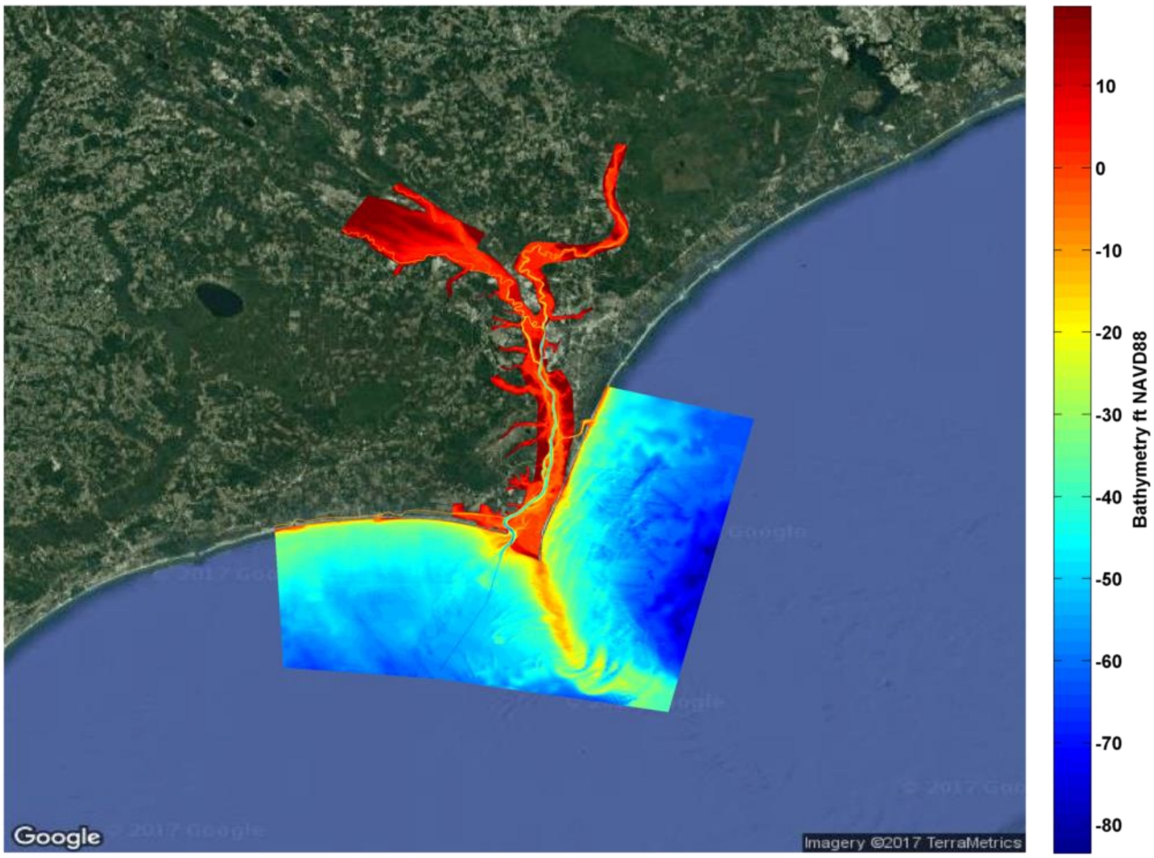

Figure 4-5: Model bathymetry

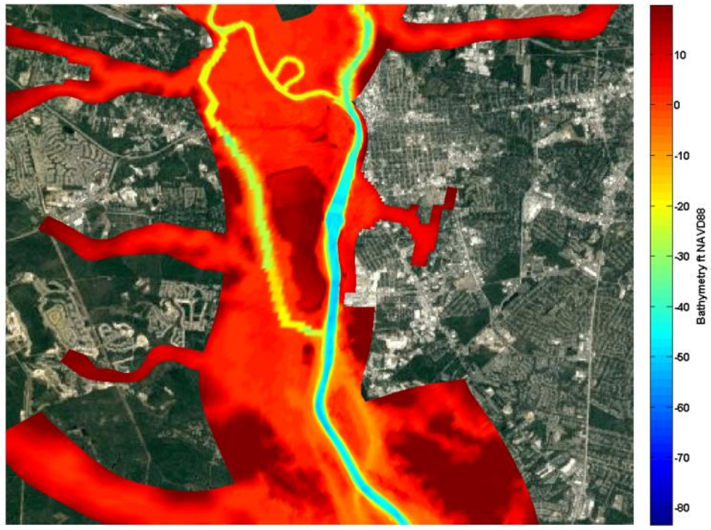

Figure 4-6: Model bathymetry near Wilmington Harbor

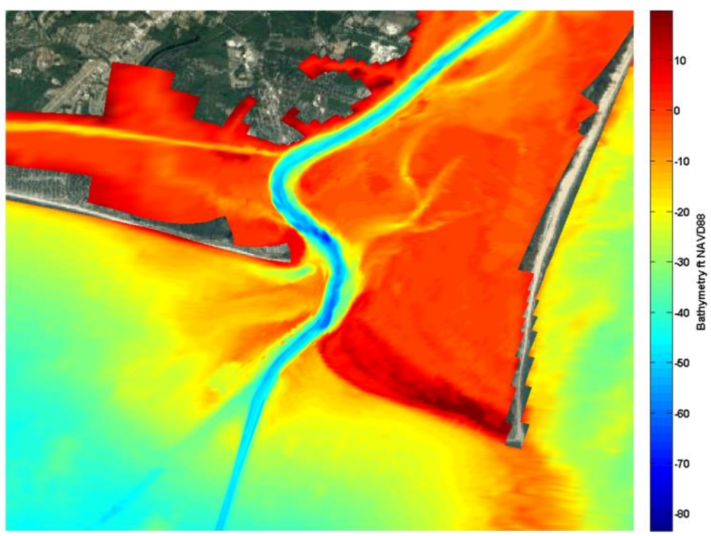

Figure 4-7: Model bathymetry at the mouth of Cape Fear River

4.2.2. Boundary Conditions

The model has seven open boundaries: four offshore—West, South, East, and North; and three upstream—NE Cape Fear River, Black River, and Cape Fear River. Locations of the boundaries are shown in Figure 4-2. The model was forced using tidal water levels at the offshore boundaries and river discharges at the upstream boundaries. Winds were applied uniformly over the entire domain.

4.2.2.1. Tidal Boundary Conditions

Astronomical tidal constituents for water levels were extracted from the Oregon State University (OSU) tidal database which is based on TOPEX/Poseidon satellite altimetry data (Egbert et al., 1994; Egbert and Erofeeva, 2002). The global model with a resolution of 1/6°, with high resolution along coastal areas was used. North and West open boundary were specified as Neumann boundaries, and South and East open boundary were specified as water level boundaries. Amplitudes and phases of astronomical tidal constituents were extracted at two end points of the South and East open boundaries, respectively. Amplitudes and phases between those two end points along South and East open boundaries were calculated by linear interpolation.

4.2.2.2. Winds

From the analysis of available wind data, it was found that the wind field in the Cape Fear River estuary is very seasonal in nature, i.e., predominant wind direction changes according to the season. Winds recorded at Stations ILM2, OCP1, 41013, and KILM show similar trends, also wind speeds vary depending on the location of the station. Stations that are offshore indicate higher wind speed than stations located on the coast or on land.

Wind data from Station KILM was used to force the model. Station KILM is located on the land and is considered to better represent wind over the estuary compared to the offshore stations.

4.2.2.3. River Discharges

The time series of discharges from the rivers measured at the USGS stations shown in Figure 1-17 were used at the three upstream open boundaries. Discharge data at Station 02105769 was used at the upstream boundary at the Cape Fear River, Station 02106500 data was used at the Black River, and Station 02108000 data was used at the Northeast Cape Fear River.

In Figure 1-17, dashed polygons indicate the un-gaged drainage area where there are no discharge measurements. Methods to estimate discharge of those un-gaged drainage area have been developed during salinity model calibration and the same approach was applied in the hydrodynamic study here.

4.2.2.4. Precipitation

Precipitation rates were calculated from the data available at METAR Station KILM (Wilmington International Airport). The precipitation was applied uniformly over the domain.

4.2.3. Model Calibration

4.2.3.1. Calibration Metrics

Several statistical parameters were used to assess model calibration and validation results. These include the mean error (*ME*), root mean square (*RMS*) error, normalized *RMS* error, mean absolute error (*MAE*), correlation coefficient (*R*), index of agreement (*d*), and time delay or lag (ΔT). These parameters are briefly described here.

If x and y are the measured and calculated data respectively, then the following statistics can be calculated:

Mean error (*ME*):

$$ME = \bar{y} - \bar{x} \tag{1}$$

Where "bar" denotes the sample mean.

Root mean square (*RMS*) error:

$$\varepsilon_{RMS} = \sqrt{\overline{(x-y)^2}} \tag{2}$$

To reduce the effect of measurement error and possible outliers, a one-hour low-pass filter was applied to the measured data to compute trend x_f. Then the normalized error is calculated as

$$\varepsilon_{norm} = \frac{\varepsilon_{RMS}}{x_{f,\max} - x_{f,\min}} \cdot 100\% \tag{3}$$

Where $x_{f,\max}$ and $x_{f,\min}$ are the maximum and minimum values of the trend x_f. The residual in the denominator defines the range of measured data.

The root mean square error of measured data was estimated as:

$$\varepsilon_{meas} = \sqrt{\overline{(x-x_f)^2}} \tag{4}$$

Mean absolute error (*MAE*):

$$MAE = \overline{|x-y|} \tag{5}$$

The correlation coefficient R was calculated using standard method and represents a non-squared value.

The model prediction capability was estimated with an index of agreement between measured and calculated data (after Willmott, 1982 and Willmott et al., 1985):

$$d = 1 - \frac{\overline{(x-y)^2}}{\overline{\left(|x-\bar{x}| - |y-\bar{x}|\right)^2}}, 0 \le d \le 1 \tag{6}$$

The time delay ΔT shows expected time difference between corresponding events in measured and calculated data. To estimate the delay, the cross-correlation function between measured and calculated data is computed and the smallest time lag at which a maximum occurs is found. Because the cross-correlation function is calculated from discrete data, resulting time resolution may not be sufficient to accurately define the maximum. Therefore, computed values of the cross-correlation function were interpolated with a piecewise polynomial of 5^{th} order, which was then used to determine the maximum.

4.2.3.2. Model Configuration

The model was calibrated for the period of available measurements between March 27, 2017 and April 5, 2017 and then validated for Hurricane Matthew between October 4, 2016 and October 14, 2016. For the calibration period, water level measurements were available at Southport and Wilmington (Figure 2-1); current measurements were available at Southport (Figure 2-1); and discharge measurements were available at the eleven transects between Wilmington and Southport (Figure 2-6 to Figure 2-9). The model was calibrated to match the measured water levels, discharges, and currents. For the validation period of Hurricane Matthew, water level measurements were available at NOAA CO-OPS Wilmington station (Figure 1-2).

The model was forced with astronomical tidal constituents at the offshore boundaries and time series (15 min interval) of river discharges at the upstream boundaries. The bottom roughness was the main calibration parameter. A variable bottom roughness was used over the domain (Figure 4-8). The Manning number selected in the model domain was based on Manning number for Channels (Chow, 1959) with modification after several calibration tests. Manning numbers used in the simulation ranged from 0.018 to 0.028 with smaller values in the offshore area and along main navigation channel and larger values in the upstream areas. An arbitrary large value of Manning number of 0.03 was used near the offshore boundaries to improve model stability.

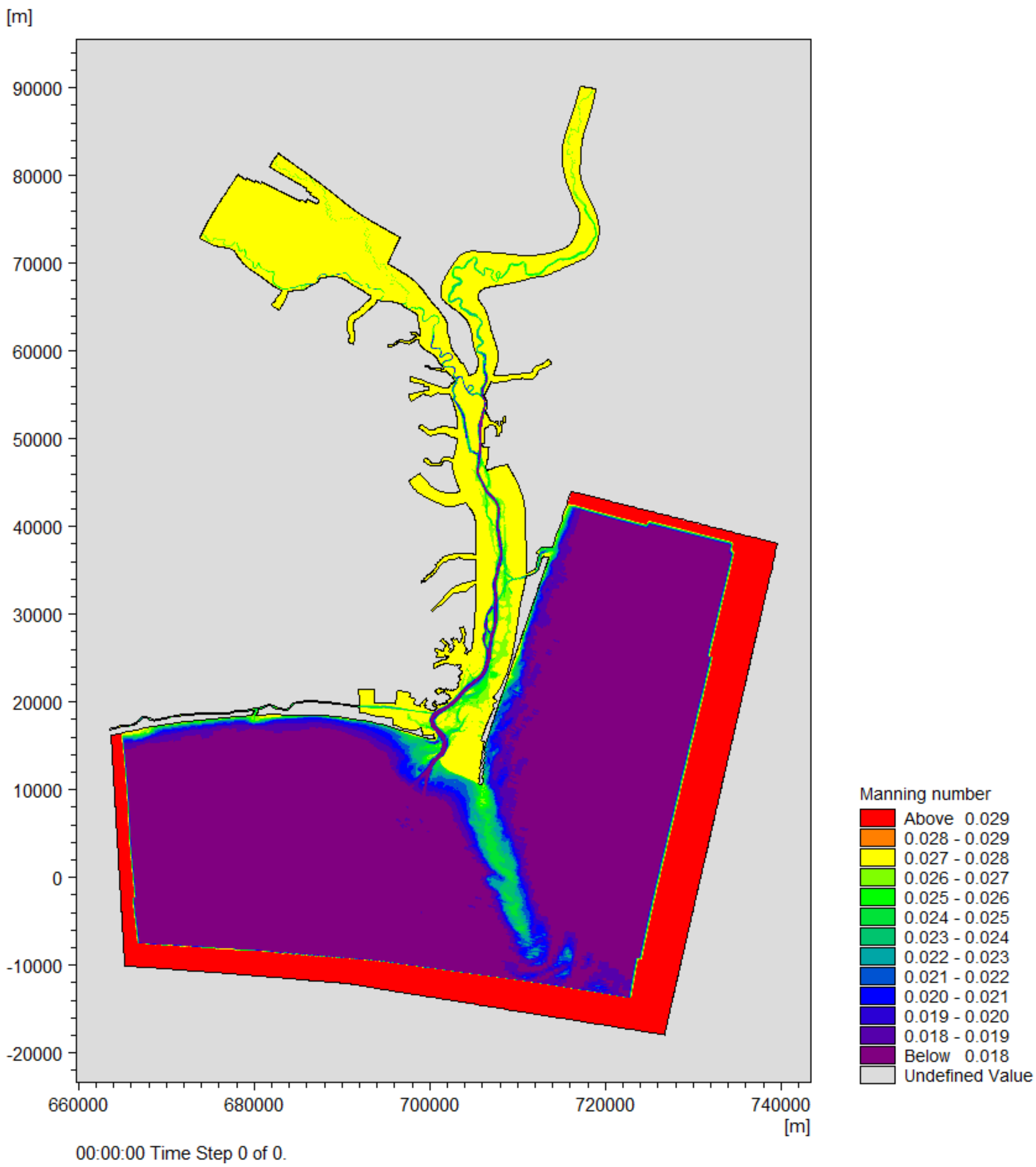

Figure 4-8: Manning number used in the model domain

4.2.4. Calibration and Validation Results

Water levels, currents, and discharges obtained from the model results were compared with measurements available at various locations. Figure 4-9 shows the comparison of water level time series. It can be seen that the model replicates the water levels well with a small over prediction for most of the time (Station Wilmington (NOAA) in Figure 4-9). Figure 4-10 shows the comparison of depth averaged currents and the model replicates the currents at Southport well.

Figure 4-11 to Figure 4-15 show comparisons of the discharge measurements. The statistics shown in those figures were calculated by comparing the model and measurement values at corresponding times. The positive and negative discharge correspond to ebb current and flood current direction, respectively. The calibration results match well at all the transects in the main channel. It needs to be pointed out that TR01, TR02, TR05, TR08 and TR12 are not in the main channel, so the following discussion will not be focused on those transects. At TR13, TR11, TR09, TR07, TR06, TR04 and TR03, model results and measurement match well. As a result, the calculated discharge matches the measurement from the river mouth to the area upstream of Wilmington.

Vertical current profiles were also compared at the main channel transects TR04, TR06, TR07, TR09, TR11, and TR13. The results were compared in the middle of the channel, and on the right and left banks of the channel (looking downstream) (Figure 2-7 to Figure 2-9). The results are shown from Figure 4-16 to Figure 4-33. It is noted that in order to show the maximum component of the currents, the currents compared here for both the measurements and the model calculations were converted into the current component along the channel direction. In addition, model results are not always compared at the exactly same instantaneous time step with measurements because the measurement usually takes 10 – 15 min to finish and the model output interval is 1 min. So the model results at the nearest matching time step were extracted to show the comparison. By comparing the current profiles, it can be seen that the measurements and 3-D model results do capture the overall vertical current structure in the navigation channel.

For the validation period of Hurricane Matthew, the water level calibration result is shown in Figure 4-34. The model was forced with time series of measured water levels at Wrightsville beach (from CO-OPS station 8658163, location shown in Figure 1-2), and wind from KILM station. It can be seen that the model captures the more extreme water levels well during this hurricane event.

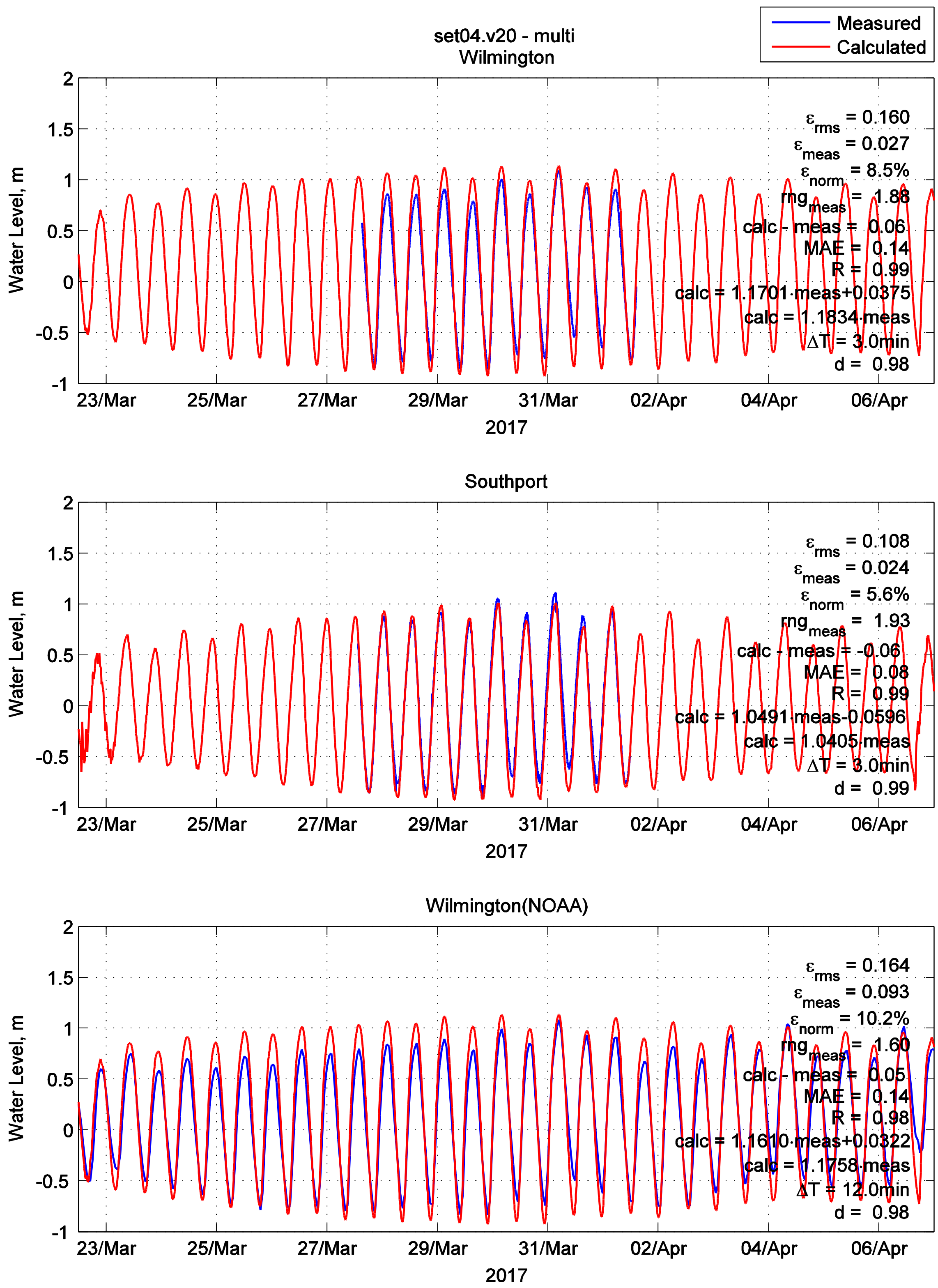

Figure 4-9: Comparison of water level measurements to model results

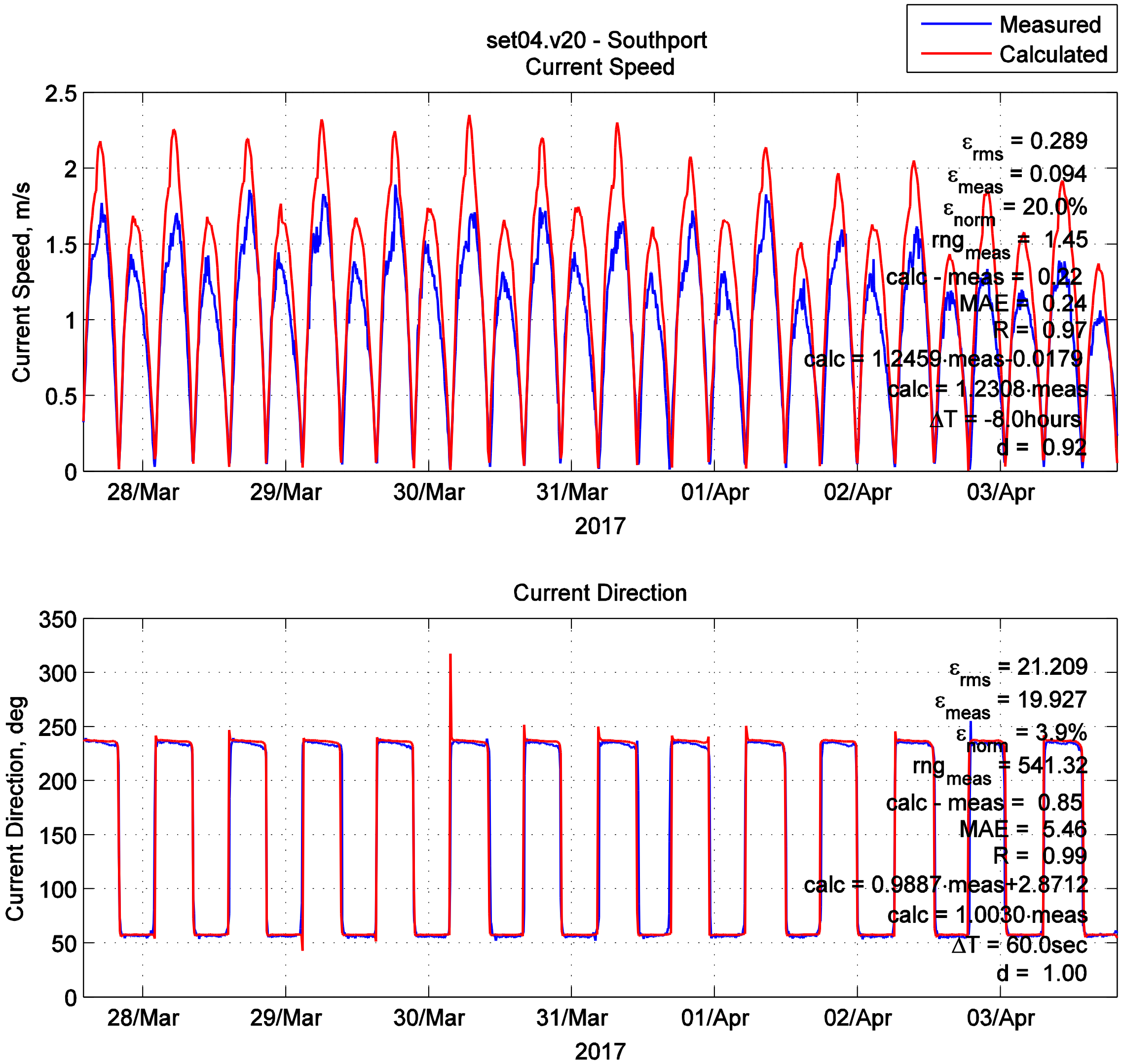

Figure 4-10: Comparison of depth averaged current measurements with model results

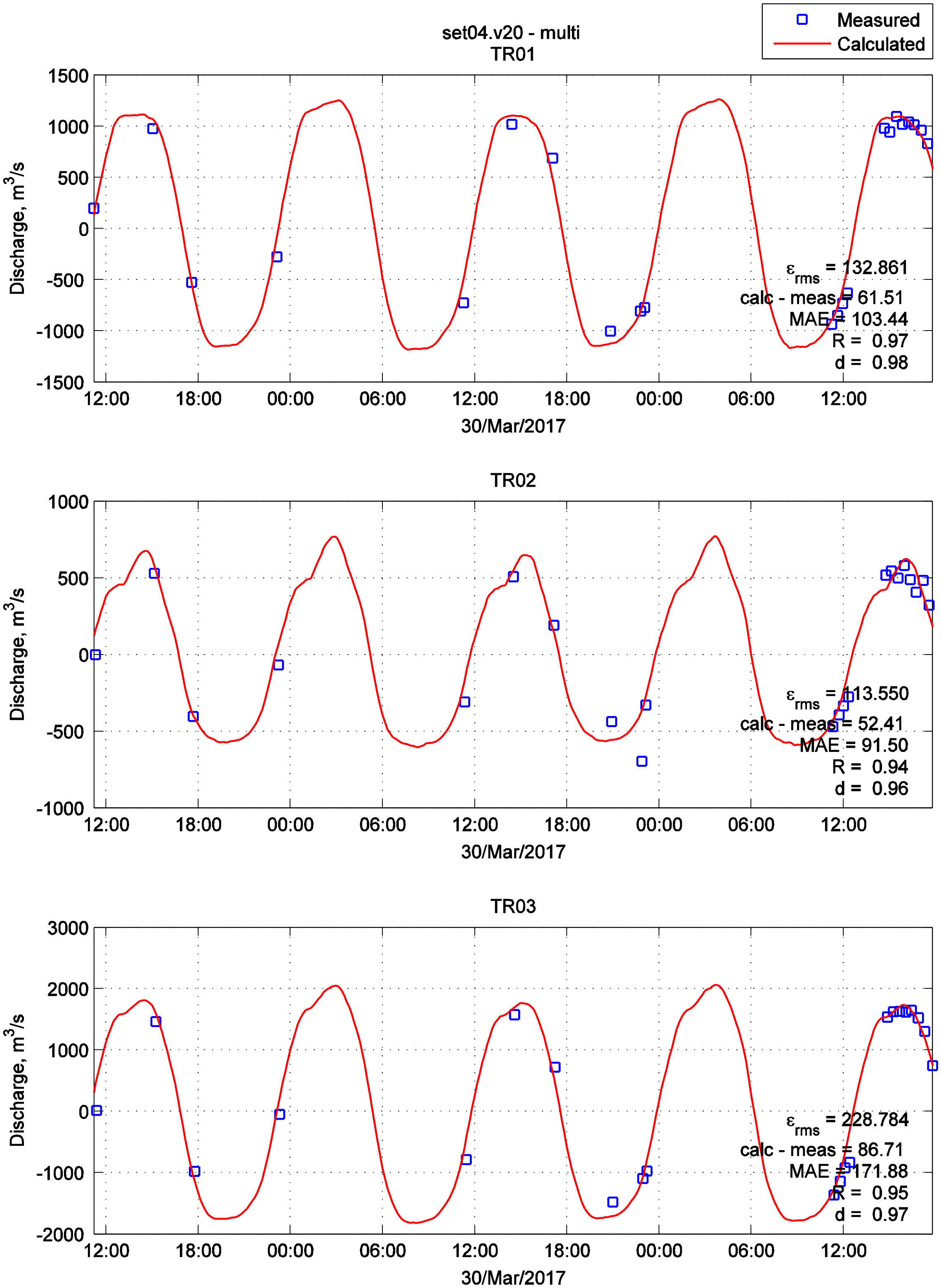

Figure 4-11: Comparison of discharge measurements to model results

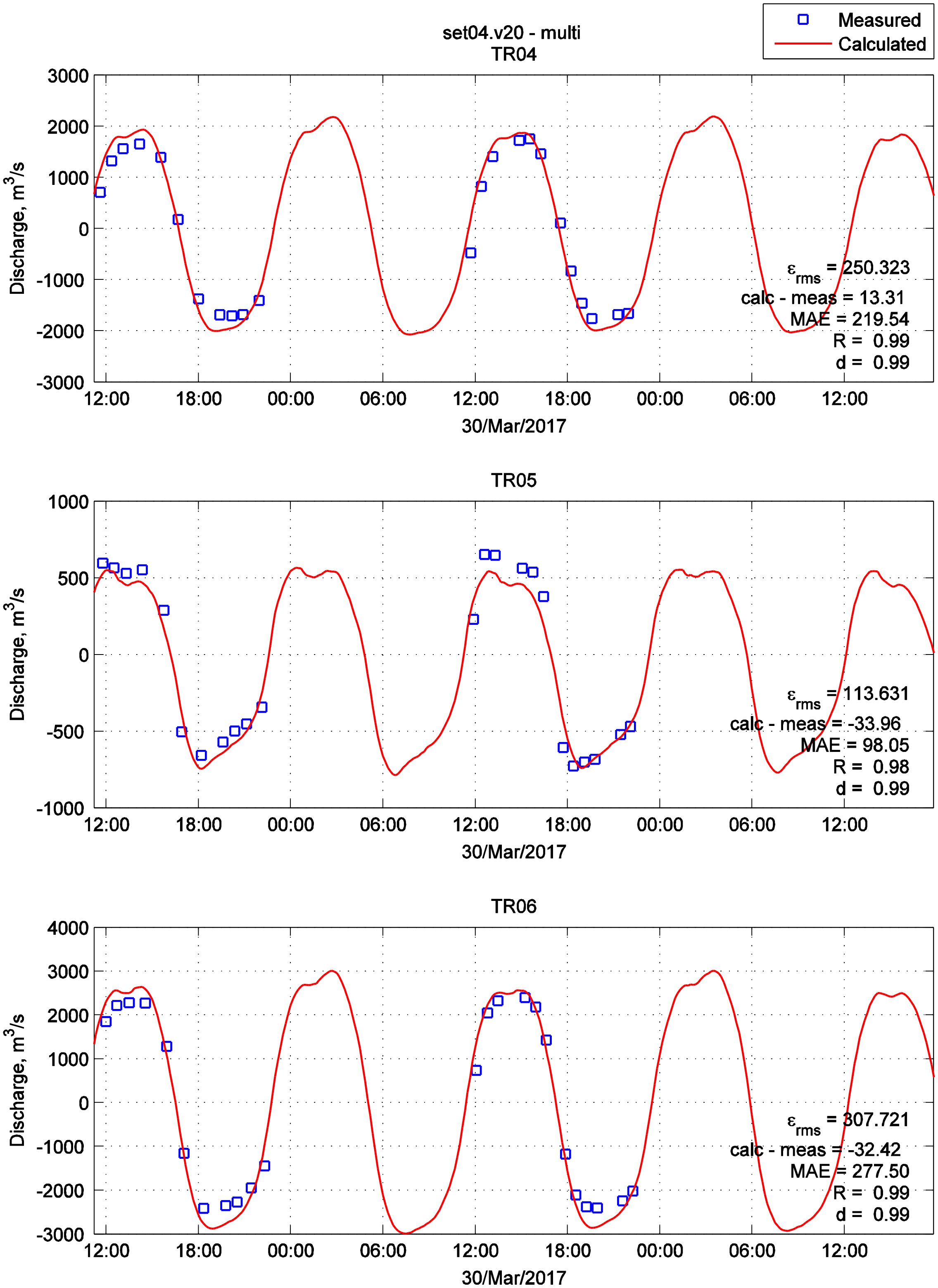

Figure 4-12: Comparison of discharge measurements to model results

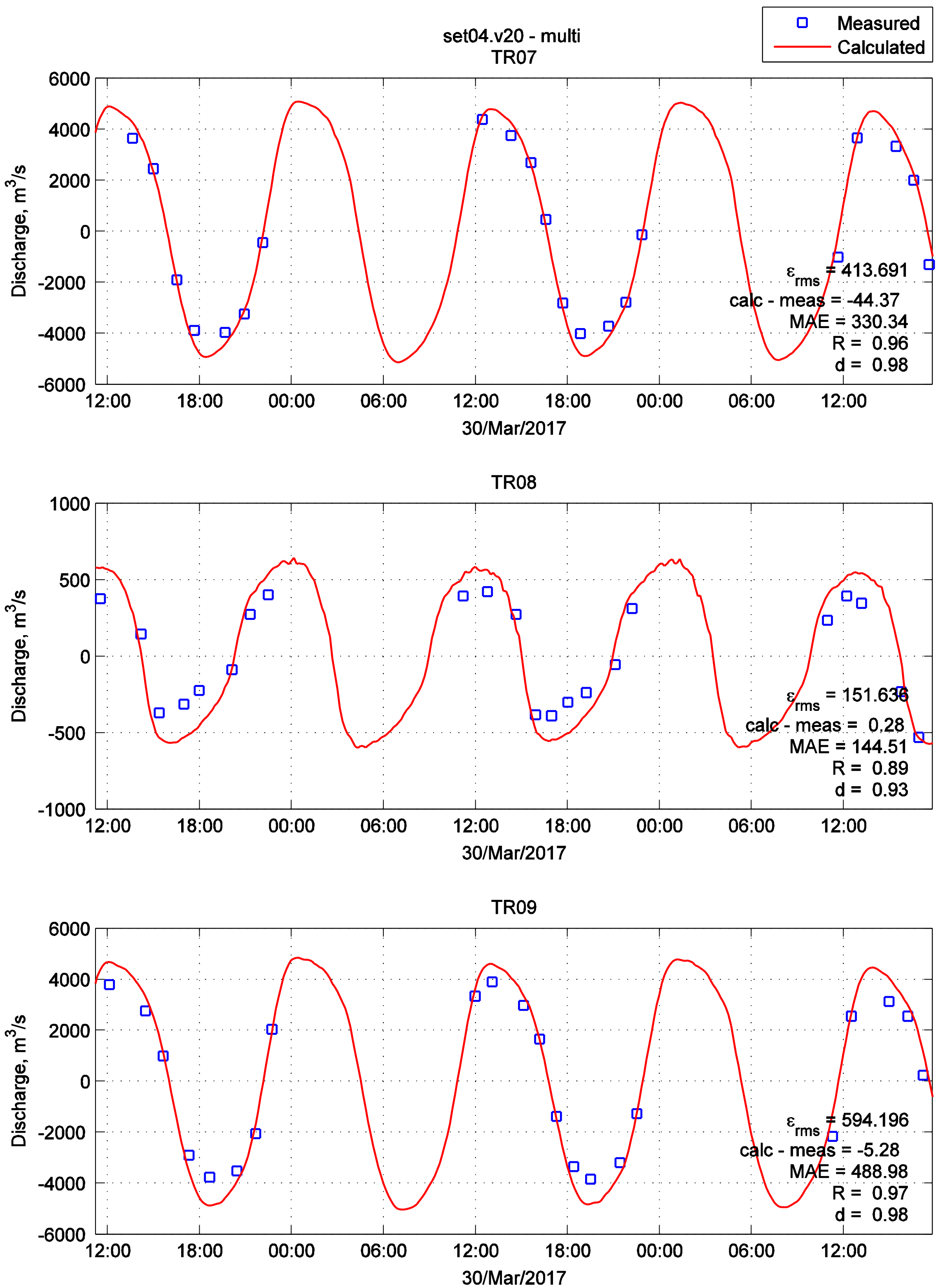

Figure 4-13: Comparison of discharge measurements to model results

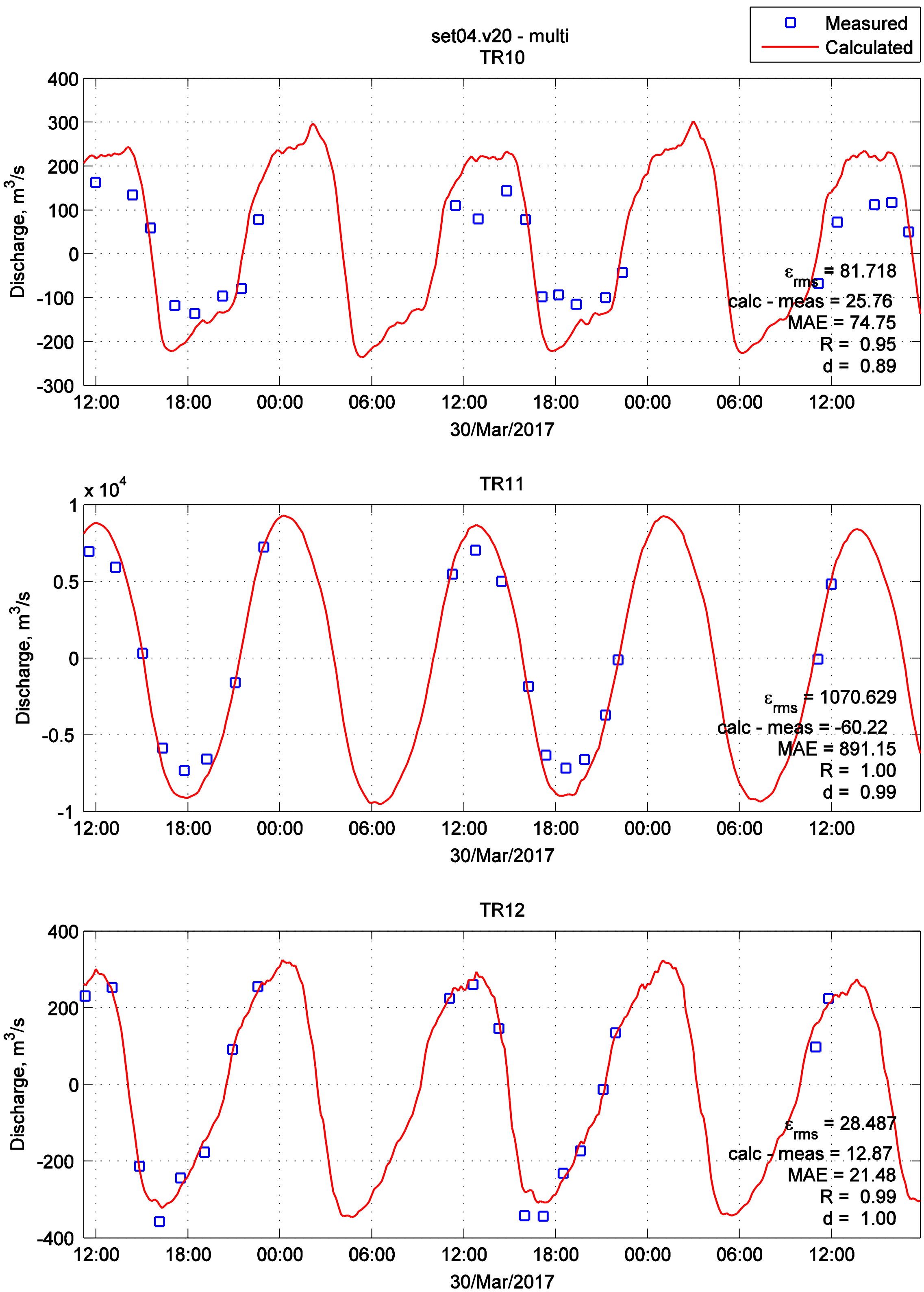

Figure 4-14: Comparison of discharge measurements to model results

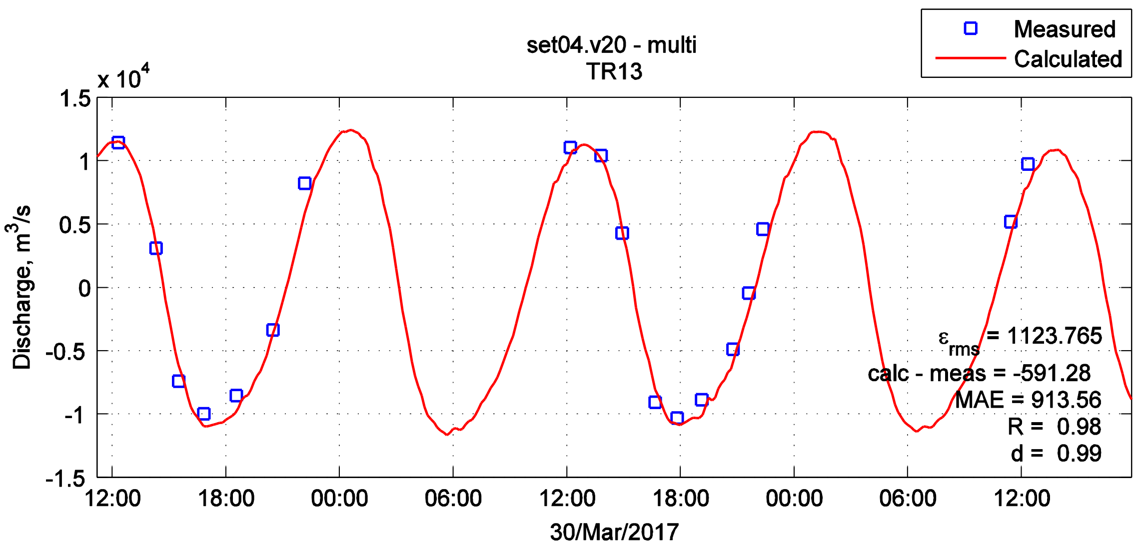

Figure 4-15: Comparison of discharge measurements to model results

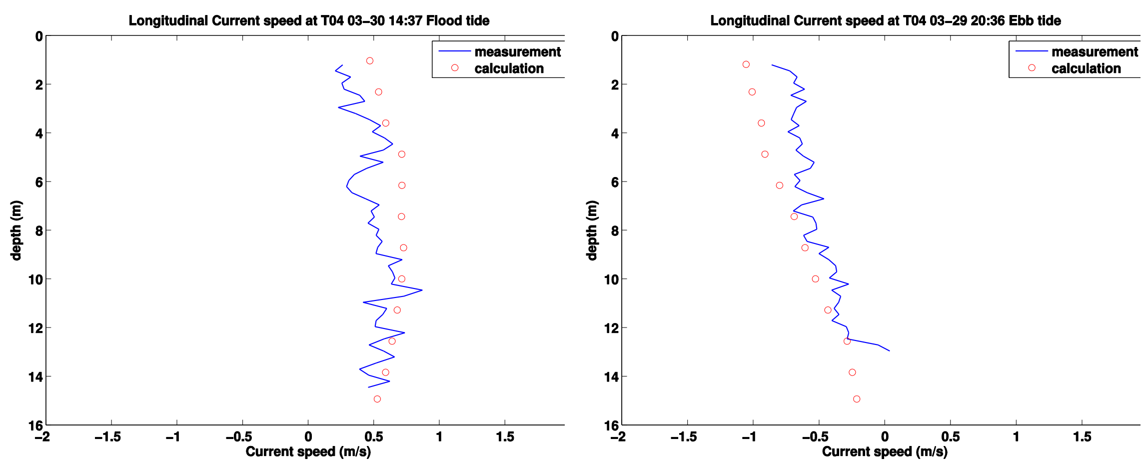

Figure 4-16: Comparison of vertical current profile at middle of TR04 during flood and ebb tide

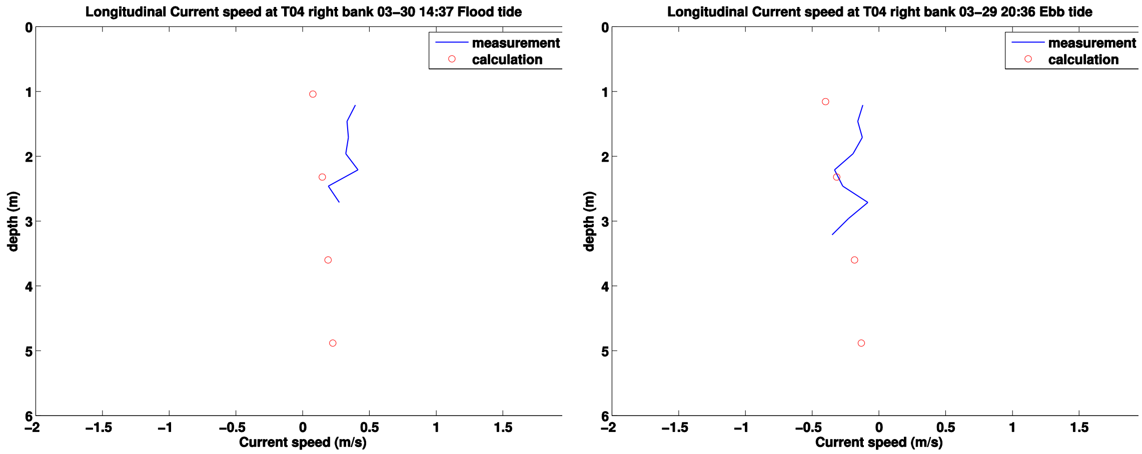

Figure 4-17: Comparison of vertical current profile at right bank of TR04 during flood and ebb tide

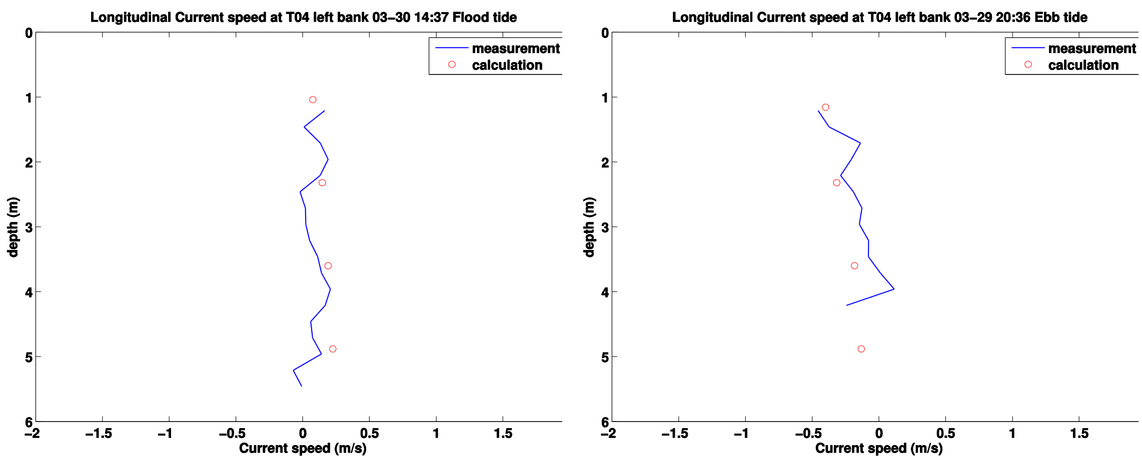

Figure 4-18: Comparison of vertical current profile at left bank of TR04 during flood and ebb tide

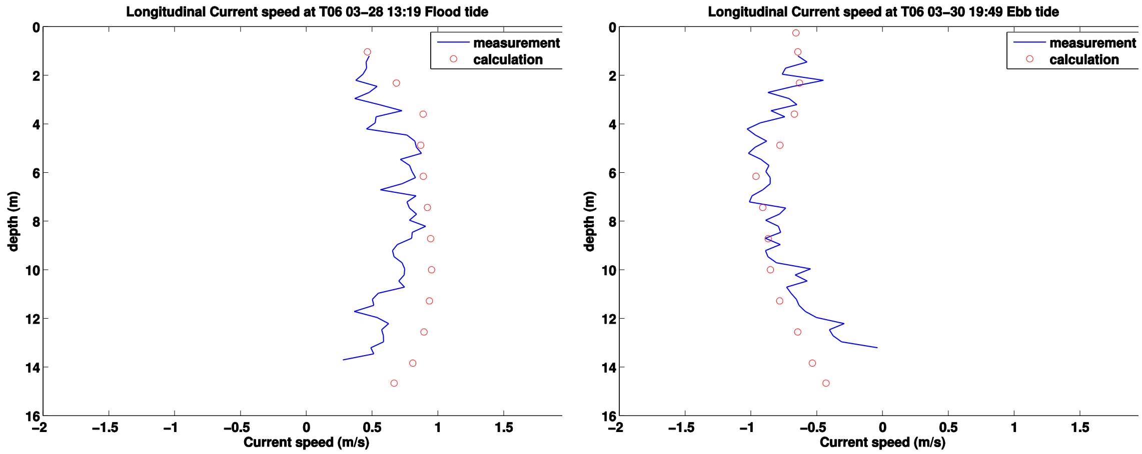

Figure 4-19: Comparison of vertical current profile at middle of TR06 during flood and ebb tide

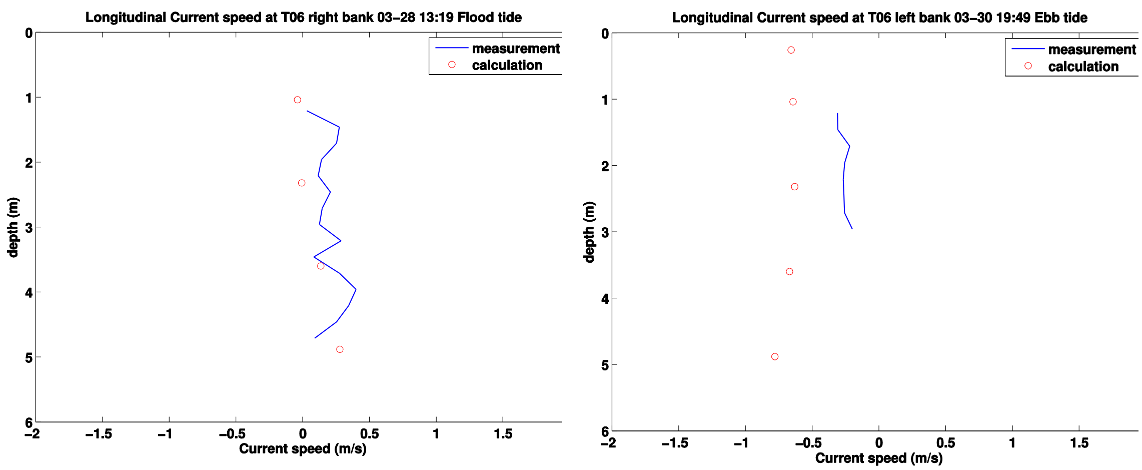

Figure 4-20: Comparison of vertical current profile at right bank of TR06 during flood and ebb tide

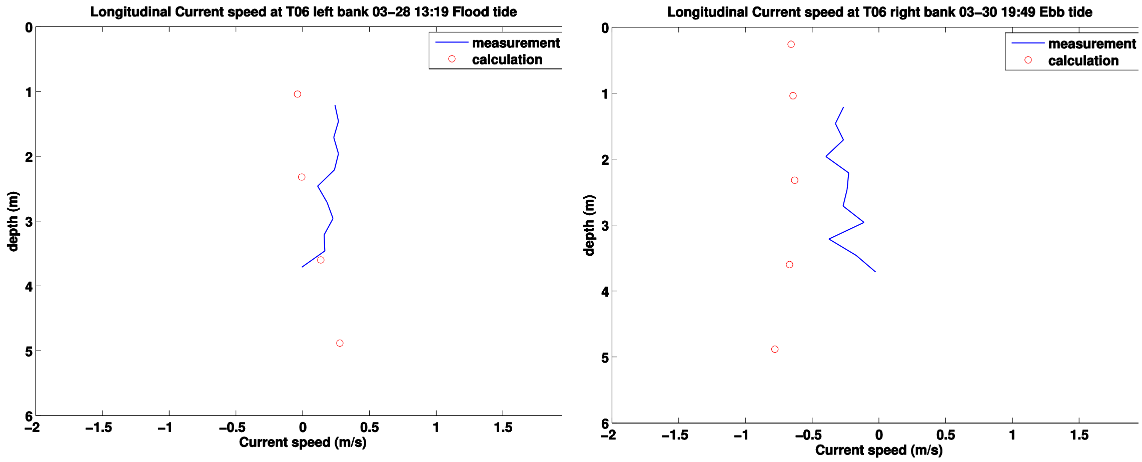

Figure 4-21: Comparison of vertical current profile at left bank of TR06 during flood and ebb tide

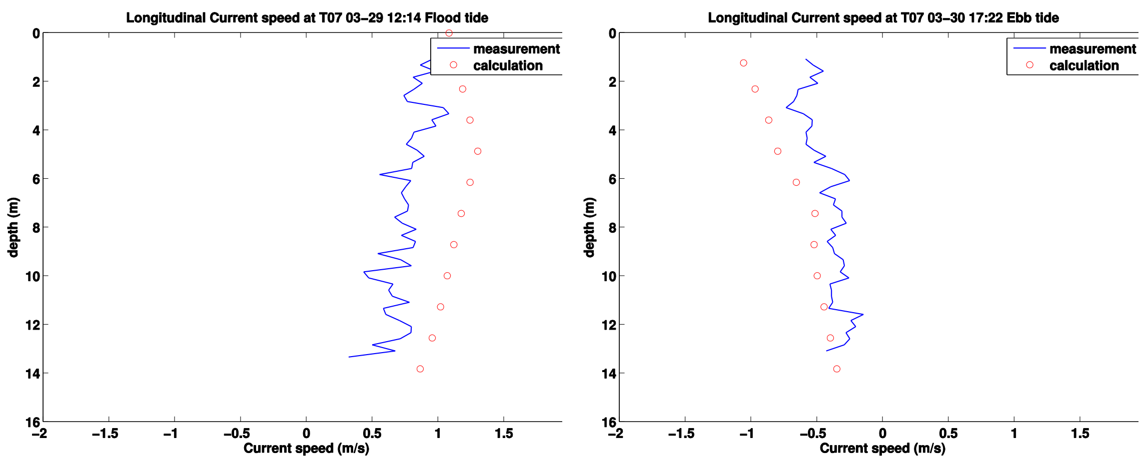

Figure 4-22: Comparison of vertical current profile at middle of TR07 during flood and ebb tide

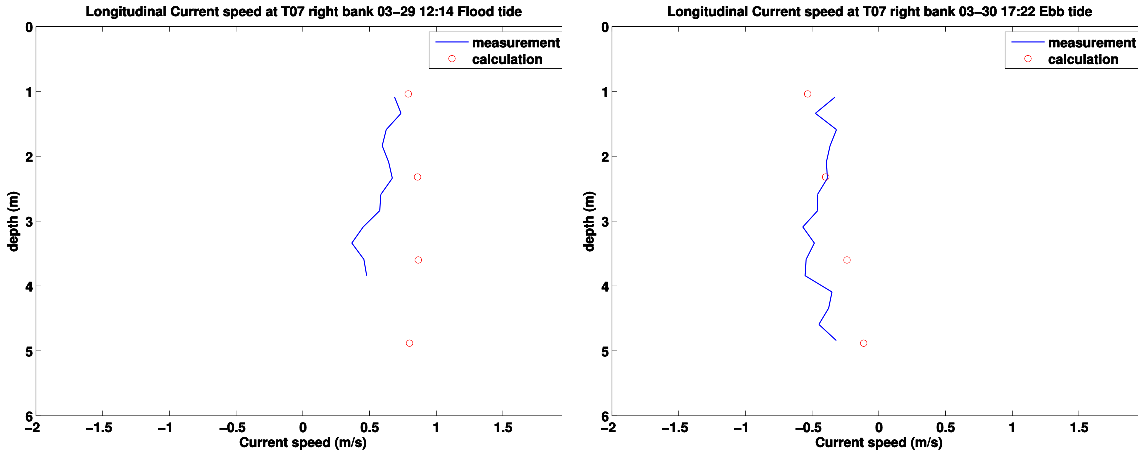

Figure 4-23: Comparison of vertical current profile at right bank of TR07 during flood and ebb tide

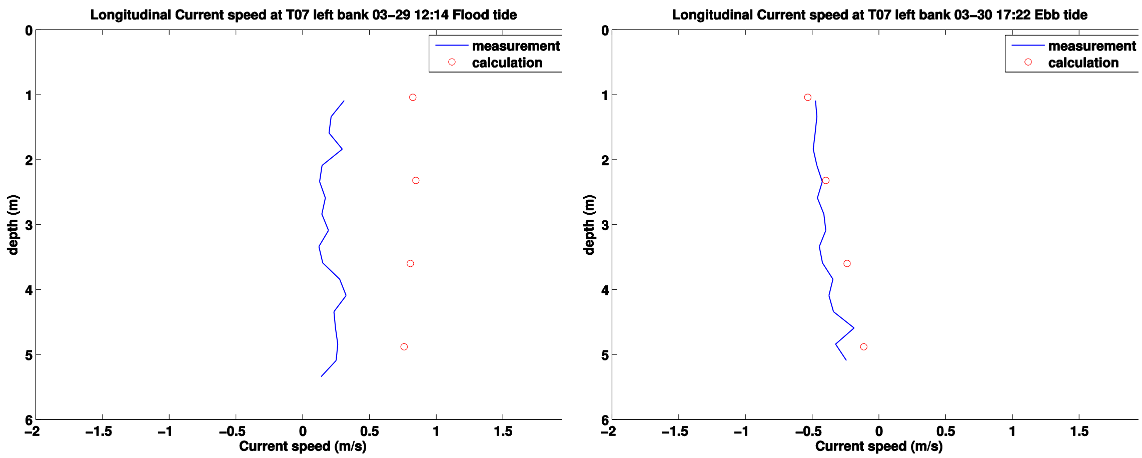

Figure 4-24: Comparison of vertical current profile at left bank of TR07 during flood and ebb tide

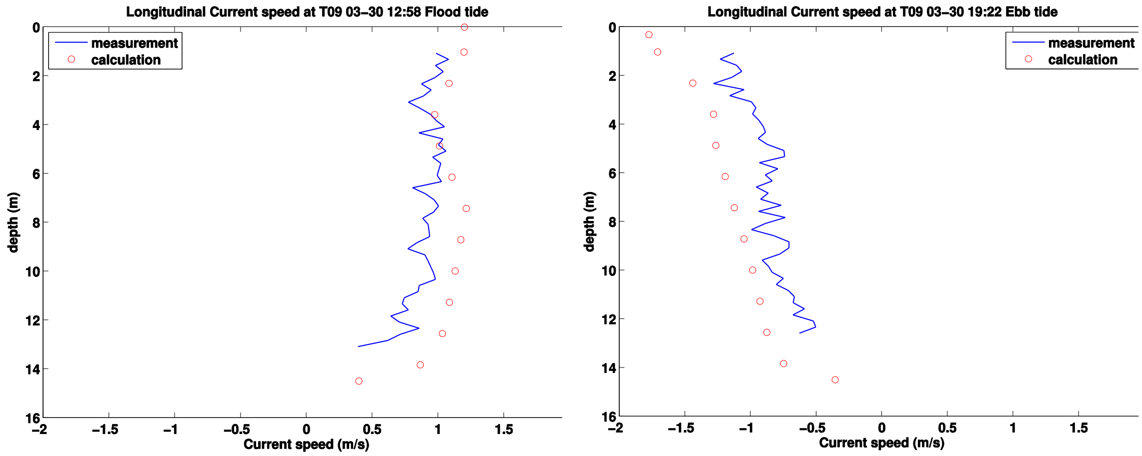

Figure 4-25: Comparison of vertical current profile at middle of TR09 during flood and ebb tide

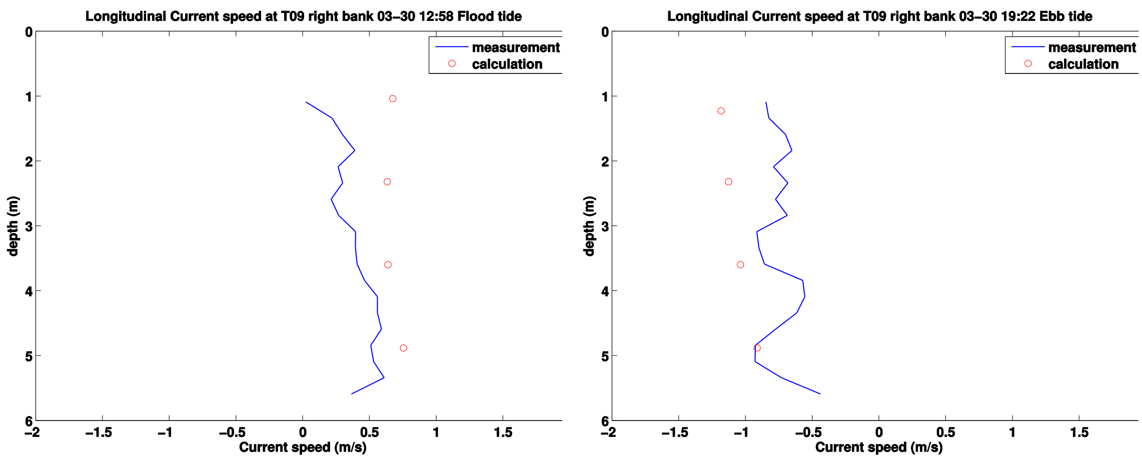

Figure 4-26: Comparison of vertical current profile at right bank of TR09 during flood and ebb tide

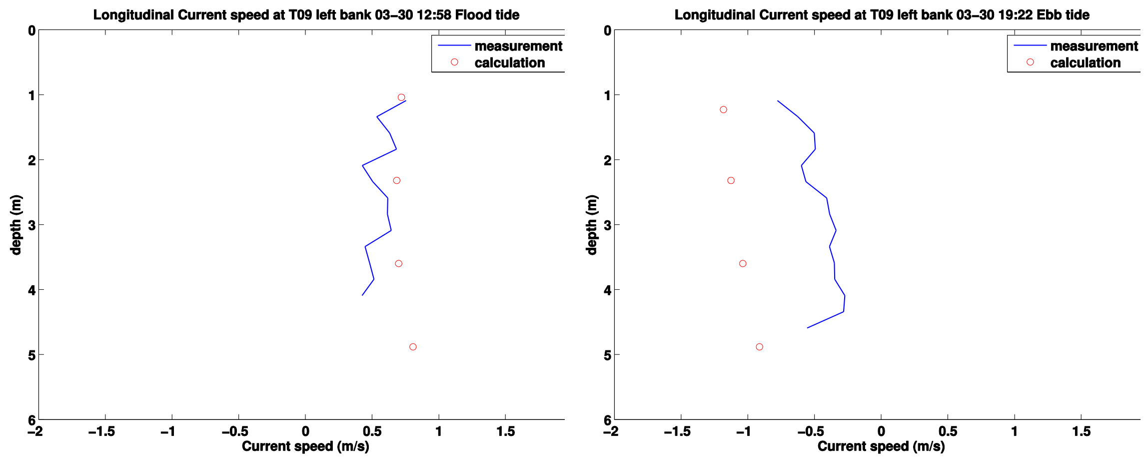

Figure 4-27: Comparison of vertical current profile at left bank of TR09 during flood and ebb tide

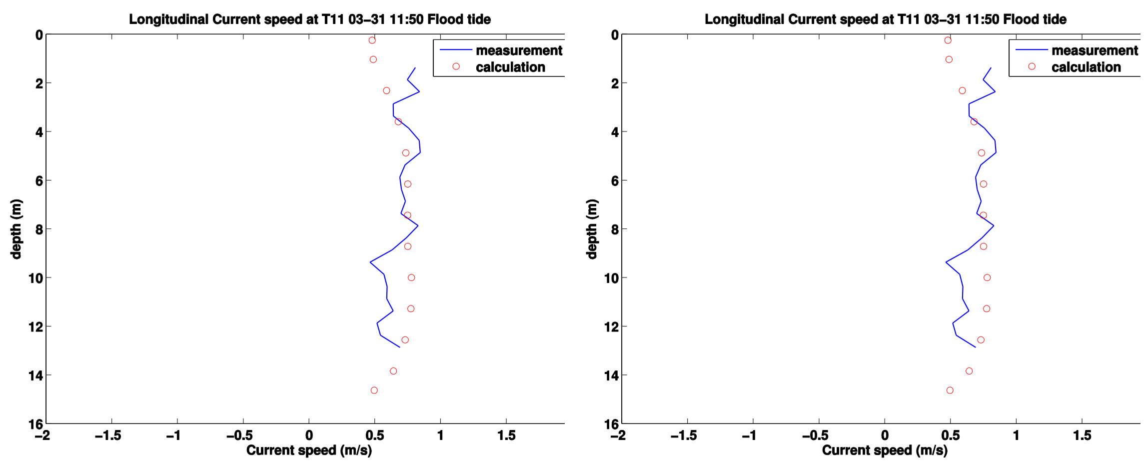

Figure 4-28: Comparison of vertical current profile at middle of TR11 during flood and ebb tide

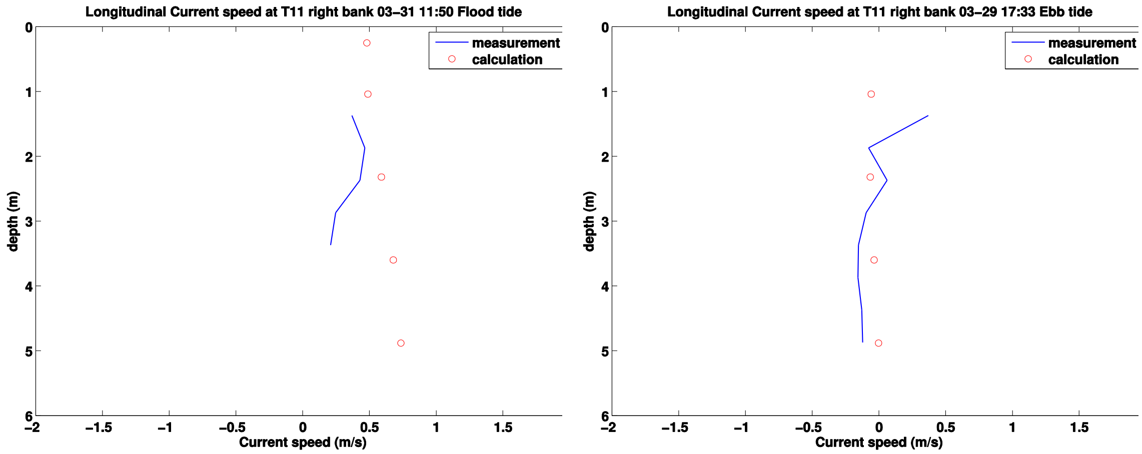

Figure 4-29: Comparison of vertical current profile at right bank of TR11 during flood and ebb tide

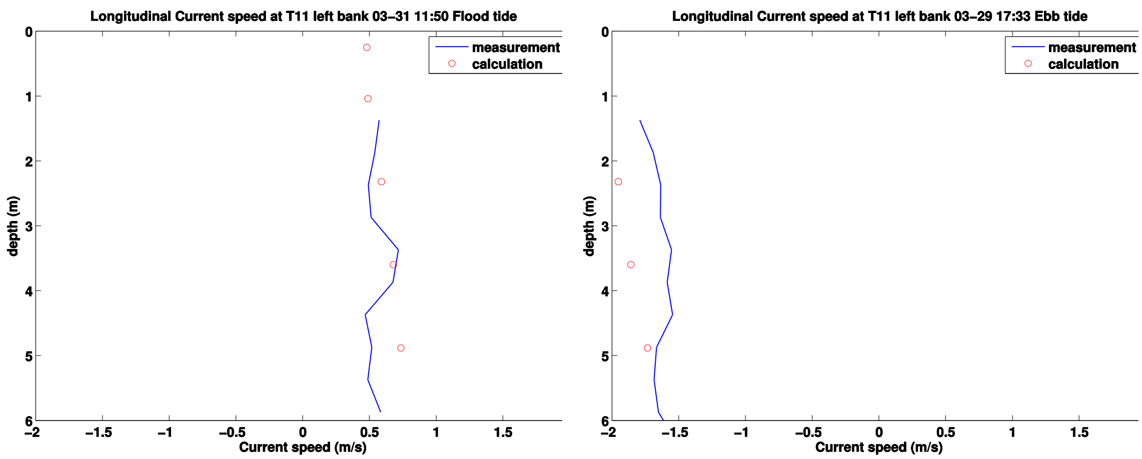

Figure 4-30: Comparison of vertical current profile at left bank of TR11 during flood and ebb tide

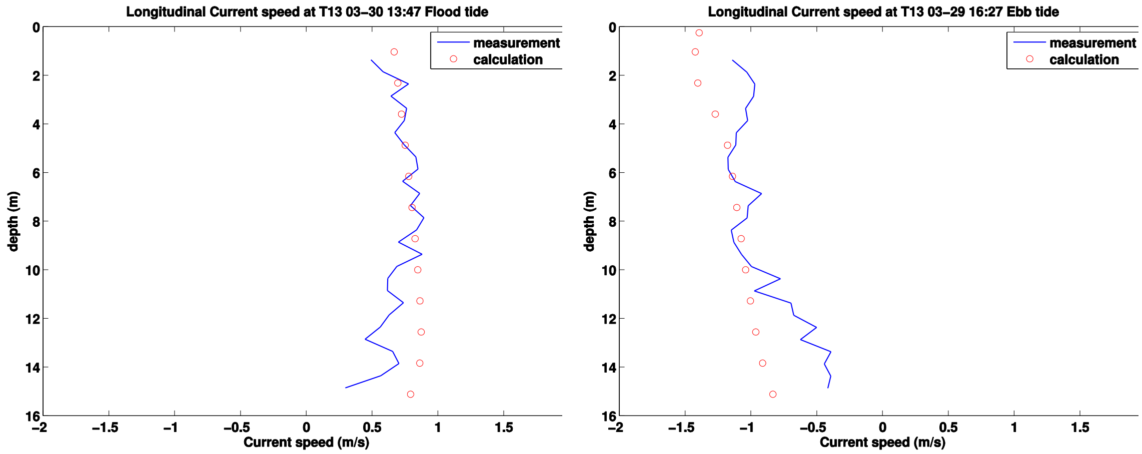

Figure 4-31: Comparison of vertical current profile at middle of TR13 during flood and ebb tide

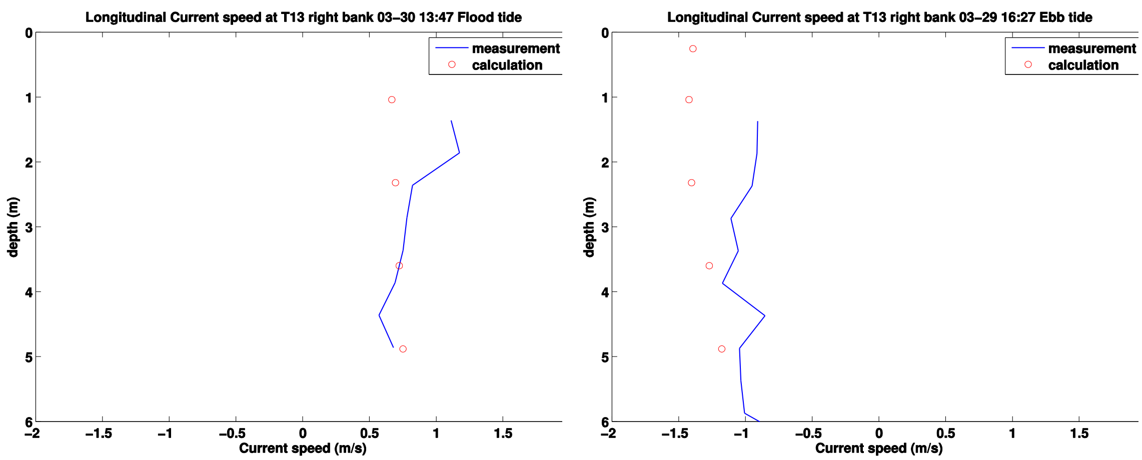

Figure 4-32: Comparison of vertical current profile at right bank of TR13 during flood and ebb tide

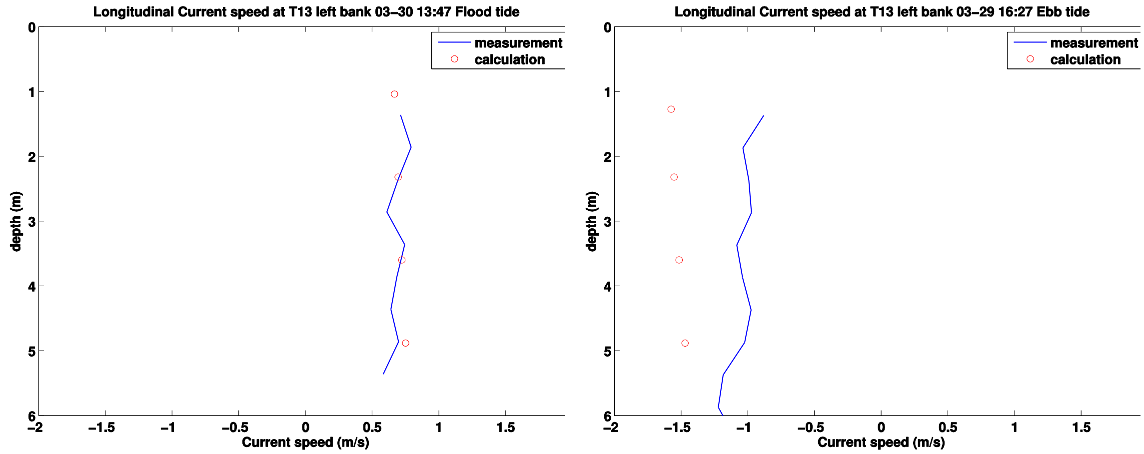

Figure 4-33: Comparison of vertical current profile at left bank of TR13 during flood and ebb tide

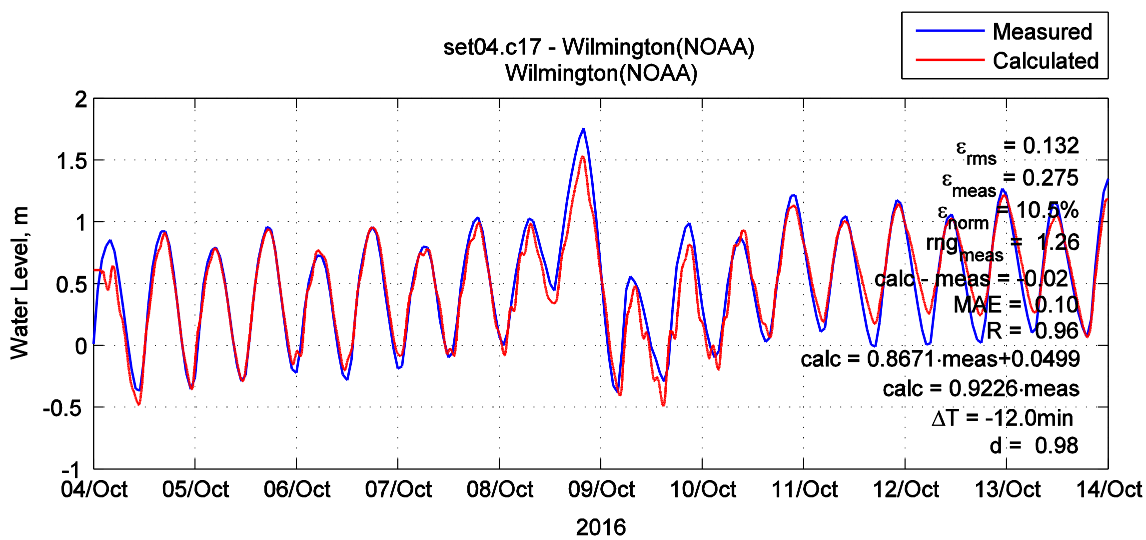

Figure 4-34: Comparison of water level measurements to model results during Hurricane Matthew

4.2.5. Conclusion

In summary, the 3-D hydrodynamic model is well calibrated in terms of water levels, currents and discharges. Water levels match well in the Wilmington and Southport areas between the model results and the measurements with a small over prediction for much of the time. The model also predicts the currents accurately in the channel in Southport, and discharges are accurately predicted at the transects in the river mouth and in the upstream Wilmington area which fully captures the tidal prism.

4.3. Salinity

With development, calibration, and validation of the Cape Fear River estuary hydrodynamic model completed, this section focuses on the additional model development tasks necessary to extend the HD model to simulate salinity.

4.3.1. Model Grid

The model domain included the Cape Fear River estuary from upstream of the Cape Fear, Black, and Northeast Cape Fear Rivers to twenty miles offshore from the mouth of Cape Fear River near Southport, NC. Grid resolution varies from approximately 90 meters in offshore areas to approximately 5 meters along the navigation channel, which is sufficient to resolve the proposed changes in channel width and slopes. The grid was discretization vertically with 25 z-type layers with a uniform resolution of approximately 1.3 m.

4.3.2. Boundary Conditions

Boundary conditions for the salinity model were kept the same as in the HD model to the greatest extent possible. Salinity boundary conditions were added to each of the model open boundaries. Additional freshwater point sources were added throughout the model domain to better simulate the estuary freshwater input; while inconsequential to the estuary hydrodynamics, these additional sources were necessary to adequately simulate the fresh water inflows and resulting subtidal salinity trends.

4.3.2.1. Offshore Boundary Conditions

The original HD model had seven open boundaries: four offshore—West, South, East, and North; and three upstream—NE Cape Fear River, Black River, and Cape Fear River. With the addition of salinity transport and salinity boundary conditions, it was found that elimination of the North boundary (i.e. reformulating into a closed boundary) eliminated stability issues along that boundary. As the North boundary is far removed from the mouth of the Cape Fear River where the majority of tidal exchange occurs, this was considered an acceptable adjustment that would not impact the hydrodynamics within the estuary. The locations of the remaining tidal boundaries are shown in Figure 4-35. To enhance dispersion of the relatively-fresh plume of water exiting the river mouth with each ebb-tide, a constant, alongshore current offshore of the mouth was added to the tidal boundary conditions to move the freshwater plume from the mouth and to allow ocean water with higher salinity to enter the estuary during flood tide. The imposed alongshore current mimics the effect of natural processes, which are not included in the model, such as currents due to wind and waves. These offshore processes were not included in the model as their effects are insignificant for estuarine hydrodynamics and salinities. The imposed current (intended to be approximately 0.5 m/s magnitude) was implemented by adding a small alongshore slope at the offshore boundaries. The low magnitude of the imposed slope and current had a negligible impact on the hydrodynamic calibration. The imposed slope had the intended effect of improving the salinity calibration at the most-downstream calibration point, without negatively impacting the calibration of points further upstream. The imposed slope did not create any model instabilities.

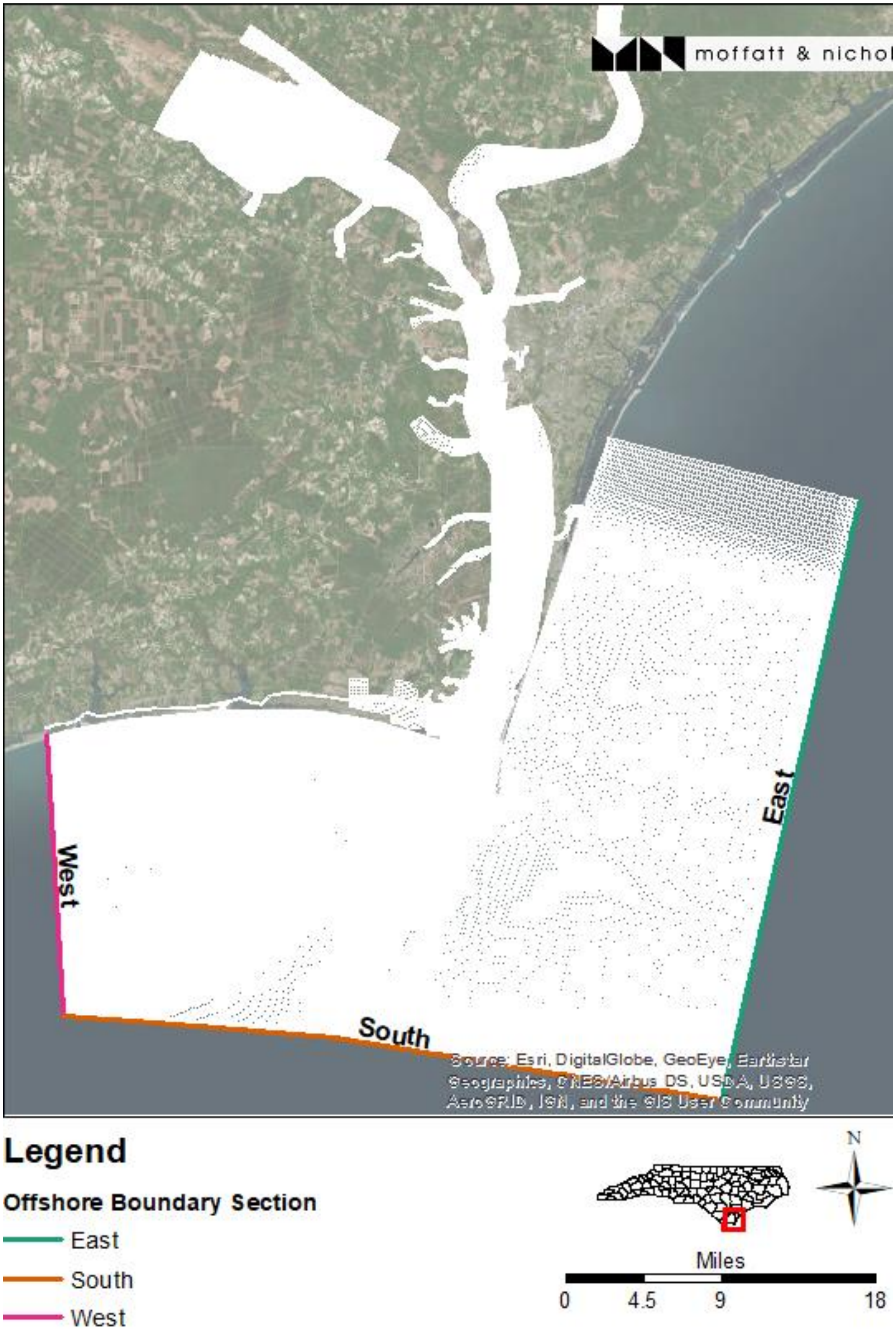

Figure 4-35: Model grid and offshore tidal boundaries

Offshore salinity boundary conditions were specified at each boundary segment end with an assumed linear interpolation along the boundary. Salinity data were derived from the Global Hybrid Coordinate Ocean Model (HYCOM) three-dimensional hind cast simulations, with model output available on a 0.08-degree grid (with approximately 7 to 9 km spacing). Each offshore boundary segment corner was assigned salinity at the closest HYCOM model grid point. While three-dimensional data were available from the HYCOM output and could be specified for the Delft3D boundary condition, HYCOM-simulated conditions at the boundaries did not vary significantly along the vertical dimension. As such, vertically-uniform salinity boundary conditions were imposed.

4.3.2.2. River Discharges and Point Sources

In the HD model, discharge boundary conditions for the three river inputs (Cape Fear, Black, and Northeast Cape Fear) were derived from USGS measurements, with appropriate scale factors to account for the ungaged drainage area for each branch.

Over the course of the salinity calibration, it became apparent that the method of freshwater input into the model domain should be altered to increase the flow delivered to the entire estuary, not just the upstream reaches. Upstream river boundaries continued to use measured discharge from USGS stations as described in the HD model calibration report; however, they were no longer scaled to account for ungaged drainage areas. Instead, freshwater flows from all ungaged drainage areas draining into the Cape Fear River estuary were applied as point sources.

Based on a combination of HU10- and HU12-level delineated watersheds, M&N developed an additional 26 subwatersheds (see Table 4-1) that drain into the estuary that were not already accounted for in the USGS gaged river inflows. Flows from each of these areas were applied to the model at point sources located at the downstream intersection with the model domain. Flow magnitudes were computed based on relative drainage area, such that a measured flow for a particular gaged drainage area was multiplied by the ratio of subwatershed vs. gaged watershed areas. Figure 4-36 shows the gaged watersheds (shaded polygons) where flow is fully accounted for by the USGS stations, as well as the ungaged drainage areas draining to the estuary and model point sources (Figure 4-37) where derived freshwater inflows are applied.

While scaling the subwatershed freshwater inflow from measured discharge at one of the major river boundaries, such as the Cape Fear River, would be the most straightforward, rainfall patterns and resulting local hydrology for the particular period in late summer 2017 dictated an alternative approach. The strong freshening trend observed in the measured salinity during the calibration period required the early, gradual input of large freshwater flows. Measured discharges for all three river inputs do show sharp increases in flow during this period; however, the increases occur several days too late to match the measured freshening in the estuary. Measured flows in the adjacent Waccamaw River (see Figure 4-36) show a more gradual increase that occurs earlier in the calibration period and more closely aligns with the timing of the measured freshet. This discrepancy in the timing of flow increase is partially explained by rainfall patterns. While rainfall gage coverage of the area is insufficient to fully characterize spatial patterns, it seems that a large rainfall event occurred along the coast around August 8, 2017, but rainfall was limited to the coastal areas so it did not significantly increase runoff from the upstream river drainage basins. In this instance, measurements at the Waccamaw River are more indicative of the runoff into the Cape Fear estuary than the upstream boundary flow, so ungaged subwatershed freshwater input was scaled from the Waccamaw River USGS discharge measurements.

All runoff inflow sources were assumed to be completely fresh with salinities of 0 PSU and were set to discharge into the surface vertical layer. Similarly, three open boundaries for the upstream river discharges were also assumed completely fresh with salinities of 0 PSU.

Table 4-1: Subwatersheds used to derive freshwater inflows into the model domain

Watershed Name	Drainage Point Latitude	Drainage Point Longitude	Area [1000 acres]
Walden Creek	33.9521°	-77.9728°	8.1
Jump and Run Creek - Gully Creek	33.9206°	-78.0681°	16.4
Town of Southport - Cape Fear River	33.9323°	-77.9895°	25.0
Barnards Creek-Cape Fear River	34.1426°	-77.9575°	14.3
Indian Creek-Cape Fear River	34.2907°	-78.0156°	18.2
Town of Woodburn - Sturgeon Creek	34.2446°	-77.9907°	10.1
Barnards Creek-Cape Fear River	34.1815°	-77.9602°	18.3
Grist Mill Branch-Cape Fear River	34.3663°	-78.1333°	10.5
Hood Creek	34.3395°	-78.0784°	27.0
Liliput Creek	34.0703°	-77.9395°	16.0
Mott Creek-Cape Fear River	34.0998°	-77.9274°	12.9
Orton Creek	34.0472°	-77.9436°	13.3
Town of Kure Beach - Cape Fear River	34.0275°	-77.9225°	14.9
Cross Way Creek - Black River	34.3713°	-78.0702°	13.6
Lyon Creek	34.3685°	-78.1223°	27.7
Prince George Creek-Northeast Cape Fear River	34.3611°	-77.9293°	20.4
Turkey Creek	34.3775°	-77.9590°	9.4
Smith Creek	34.2581°	-77.9482°	21.2
Ness Creek - Northeast Cape Fear River	34.2877°	-77.9592°	17.6
Black River (Ungaged Portion)	34.4217°	-78.1314°	532.0
Northeast Cape Fear River (Ungaged Portion)	34.5448°	-77.8212°	453.8
Long Creek	34.3792°	-77.9692°	89.9
Harrisons Creek	34.4035°	-77.8122°	60.7
Pike Creek - Northeast Cape Fear River	34.4650°	-77.8412°	54.6
Livingston Creek	34.3523°	-78.1981°	81.1
Town Creek	34.1287°	-77.9540°	80.4

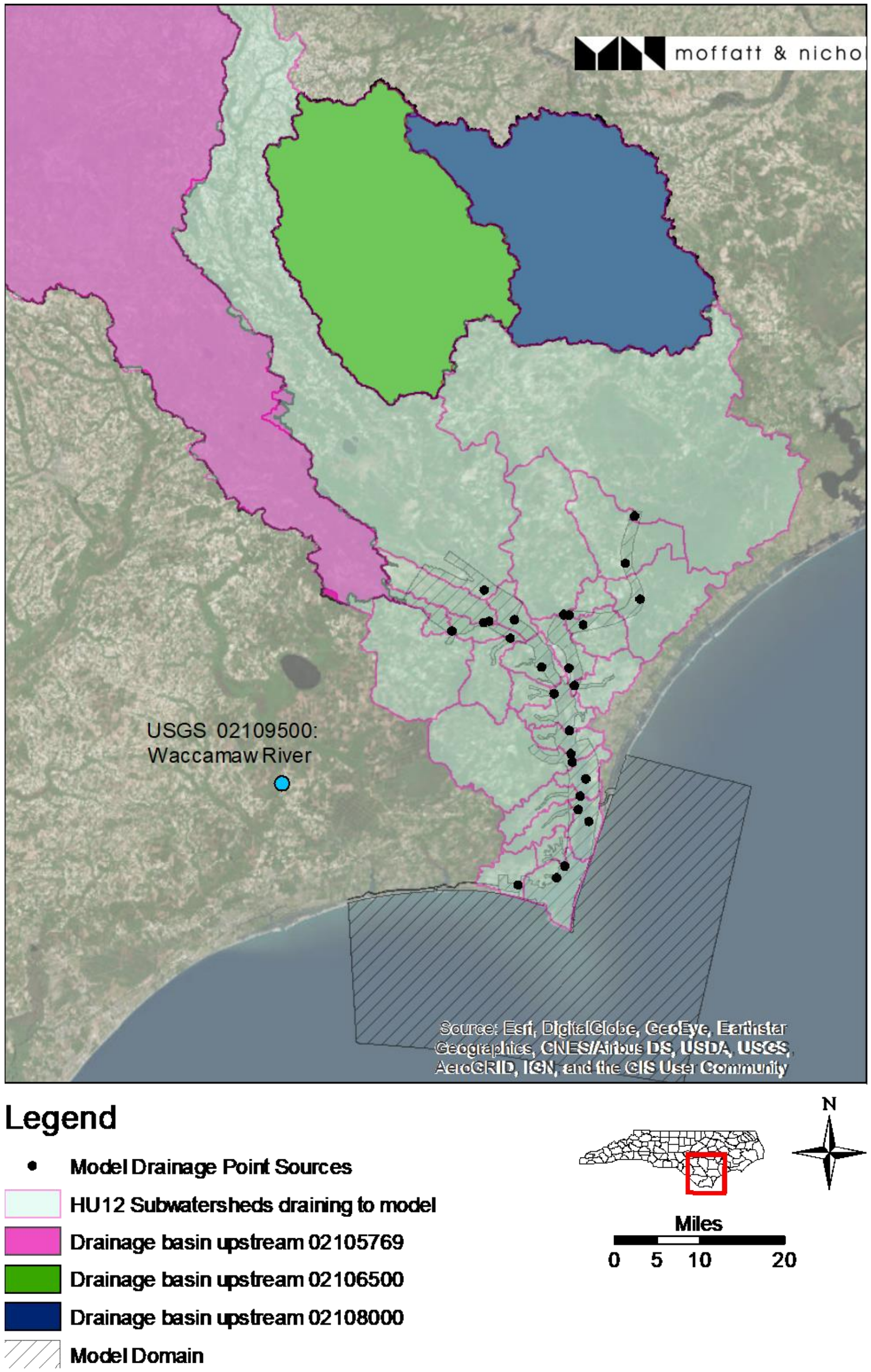

Figure 4-36: Gaged drainage areas for upstream discharge boundaries, ungaged subwatersheds draining to the estuary, and locations of modeled point sources where ungaged subwatershed freshwater inflows are applied in the model.

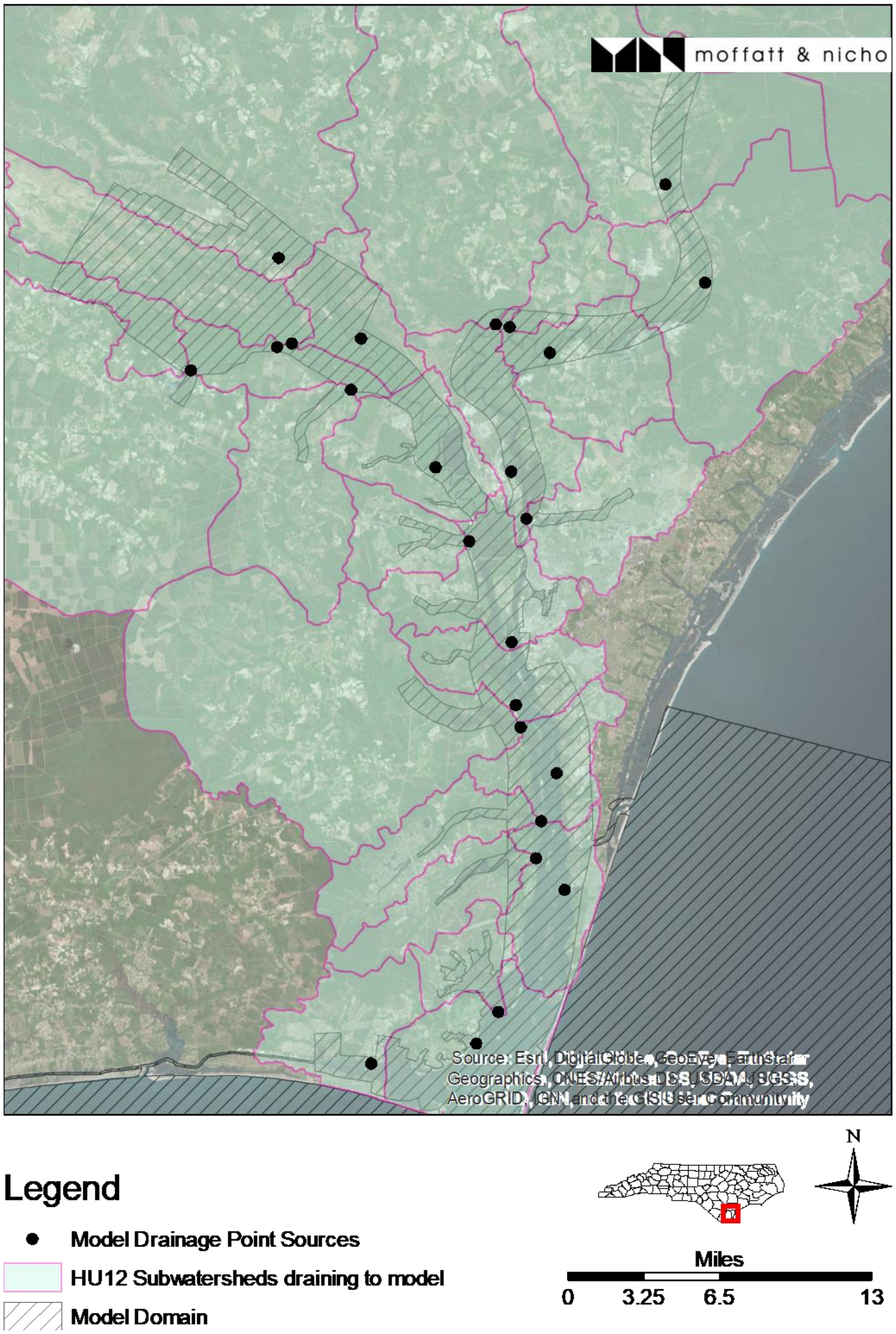

Figure 4-37: Zoom view of subwatersheds draining to the estuary and locations of modeled point sources where ungaged subwatershed freshwater inflows are applied in the model.

4.3.2.3. Precipitation and Evaporation

Precipitation rates were calculated from the data available at the weather station at Wilmington International Airport (METAR Station KILM). The closest measurements of evaporation rates to the project site were available from Aurora, North Carolina along the Pamlico River (NOAA, 2017). The precipitation and unadjusted pan evaporation rate was applied uniformly over the model domain. While pan evaporation rates can overpredict the corresponding evaporation from an open water body, the measured pan evaporation rate was not corrected since model results indicated that evaporation had negligible impacts to simulated salinities.

4.3.3. Initial Conditions

The effect of initial conditions on modeled salinities can persist for months in a simulation. Therefore, initial values must be chosen to closely replicate salinity distribution in the beginning of the simulated period and to allow a shorter spin-up period. For both the calibration and validation simulations, salinity initial conditions were manually generated, based on spatial interpolation between the initial values at each available measurement station. A weakly-stratified initial condition was imposed with linear variation between surface and bottom values that approximated the observed initial stratification in the measurements. The initial conditions were imposed several days before the start of measurements to allow for spin-up time for the hydrodynamics. Figure 4-38 shows the surface and bottom salinity initial conditions for the calibration period.

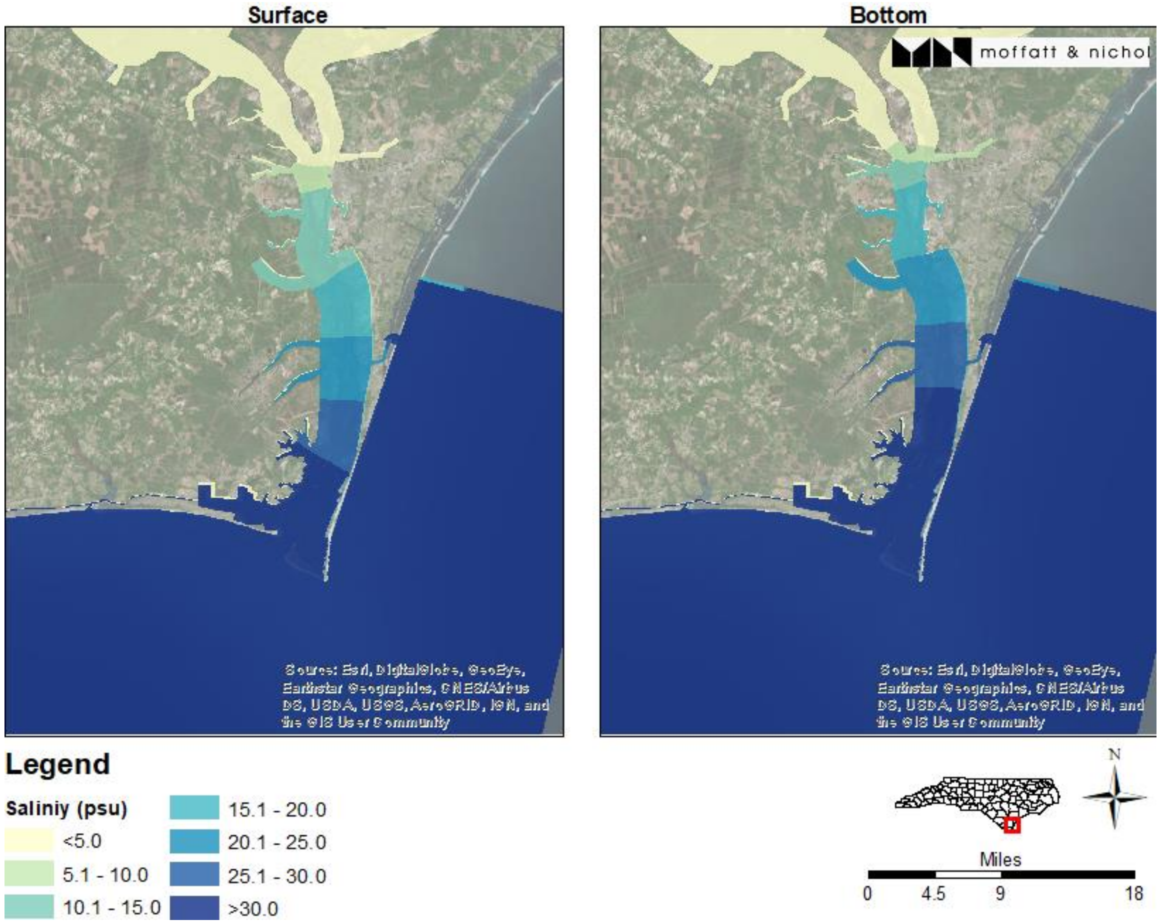

Figure 4-38: Surface (left) and bottom (right) initial salinity conditions for the late summer 2017 calibration period.

4.3.4. Model Calibration

4.3.4.1. Calibration Period

The model was calibrated for the late summer period of available measurements between August 9, 2017 and August 21, 2017 and then validated for the spring period between March 27, 2017 and April 2, 2017.

4.3.4.2. Calibration Parameters

Once the treatment of open boundary conditions and freshwater inflows was established in the model, salinity calibration was achieved by adjusting the horizontal and vertical eddy viscosity and diffusivity coefficients. Vertical turbulence parameters were chosen to discourage vertical mixing and enable the development of persistent vertical gradients. Calibration simulations employed background vertical eddy viscosities ranging from 0.001 to 0.0001 m^2/s.

Table 4-2 provides the modeling calibration parameter settings which resulted in the best agreement between measured and modeled salinity data.

Table 4-2: Salinity Calibration Parameters

Horizontal		Vertical		Turbulence Closure Model
Background Eddy Viscosity (m^2/s)	Background Eddy Diffusivity (m^2/s)	Background Eddy Viscosity (m^2/s)	Background Eddy Diffusivity (m^2/s)	
0.01	0.1	0.0005	0.0	K-Epsilon

The background horizontal eddy viscosity was set to the value given in Table 4-2 (0.01 m^2/s) over almost all of the model domain; however, a band of higher viscosity (up to 1.0 m^2/s) was imposed along the model offshore boundary to aid in stability, with no effect on hydrodynamics and transport within the estuary.

4.3.4.3. Calibration Metrics

Several statistical parameters were used to assess model calibration and validation results. These include the mean error (*ME*), root mean square (*RMS*) error, normalized *RMS* error, mean absolute error (*MAE*), correlation coefficient (*R*), index of agreement (*d*), and time delay or lag (ΔT). These parameters are briefly described here.

If x and y are the measured and calculated data respectively, then the following statistics can be calculated:

Mean error (*ME*):

$$ME = \bar{y} - \bar{x} \tag{7}$$

Where "bar" denotes the sample mean. *ME* is a measure of model bias error with positive values indicating over-prediction and negative values under-prediction.

Root mean square (*RMS*) error:

$$\varepsilon_{RMS} = \sqrt{\overline{(x-y)^2}} \tag{8}$$

To reduce the effect of measurement errors and possible outliers, a one-hour low-pass filter was applied to the measured data to compute the trend x_f. Then the normalized error is calculated as:

$$\varepsilon_{norm} = \frac{\varepsilon_{RMS}}{x_{f,\max} - x_{f,\min}} \cdot 100\% \tag{9}$$

Where $x_{f,\max}$ and $x_{f,\min}$ are the maximum and minimum values of the trend x_f. The residual in the denominator defines the range of measured data.

The root mean square error of measured data was estimated as:

$$\varepsilon_{meas} = \sqrt{\overline{\left(x - x_f\right)^2}} \tag{10}$$

Mean absolute error (*MAE*):

$$MAE = \overline{\left|x - y\right|} \tag{11}$$

The correlation coefficient *R* was calculated using standard method and represents a non-squared value. The model prediction capability was estimated with an index of agreement between measured and calculated data (after Willmott, 1982 and Willmott et al., 1985):

$$d = 1 - \frac{\overline{(x-y)^2}}{\overline{\left(\left|x-\bar{x}\right| - \left|y-\bar{x}\right|\right)^2}}, 0 \le d \le 1 \tag{12}$$

The time delay ΔT shows expected time difference between corresponding events in measured and calculated data. To estimate the delay, the cross-correlation function between measured and calculated data is computed and the smallest time lag at which a maximum occurs is found. Because the cross-correlation function is calculated from discrete data, the resulting time resolution may not be sufficient to accurately define the maximum. Therefore, computed values of the cross-correlation function were interpolated with a piecewise polynomial of 5^{th} order, which was then used to determine the maximum.

4.3.5. Calibration and Validation Results

The following sections present plots of model results compared with measured values as a demonstration of the model's ability to simulate key estuarine processes. For each measurement station, salinity data were available at near-surface and near-bottom gages so that both the surface and bottom salinities as well as the difference in salinity over the vertical water column were known. For the calibration, simulated salinity concentrations were extracted at a model grid point corresponding to the station location at surface and bottom vertical layers for comparisons to the measured surface salinity, bottom salinity, and vertical salinity difference. Results are first presented for the August 2017 calibration period then the Late March 2017 validation period.

4.3.5.1. August 2017 Calibration Period

Figure 4-39 to Figure 4-43 show comparisons of the measured and modeled (calculated) salinities at the long-term, fixed station locations of the August 2017 calibration period. A summary of the calibration metrics for this period is given in Table 4-3.

Full Timeseries Results

The model simulates both the tidal variation and subtidal trends of the salinity fairly well at the stations distributed along the length of the estuary. Near the Cape Fear River mouth at station ADM, salinities, especially those at the bottom, match measurements quite well with an RMS error of approximately 2 PSU. Surface salinities show a similar good agreement during the first week of calibration period, though calculated surface salinities are slightly lower in the later week.

Moving up the estuary, the model is just as successful in simulating the tidal variation in surface and bottom salinities at the UBI and KM stations, as well as the magnitudes and trends in salinity differences. RMS errors for surface and bottom salinities are between 2 and 3 PSU for these stations. It is at these gages that the measurements show a pronounced subtidal freshening trend, where the lowest salinities are reached around August 14. The model performs best in simulating the subtidal salinity trend before and after the freshet, though it is simulated to occur less gradually than in the measurements.

The freshening trend is driven by freshwater inflow from the upstream river boundaries as well as runoff from adjacent watersheds. Measurements of these flows are incomplete and representing them in the model required assumptions and approximations. While further adjustment of freshwater inflows could improve the modeled timing of the subtidal trends, simulating this process is not considered a part of the model calibration since similar adjustments cannot be replicated for another arbitrary period for which salinity measurements are not available. For the model calibration, it was important to select a set of model parameters which allow the model to accurately compute horizontal and vertical distribution of salinity under accurate forcing (such as boundary conditions, fresh water inflows, etc.). It also can be noted, that high fresh water inflow conditions are short in duration and, therefore, less important to the goals of the modeling effort, since the potential impacts of the deepening alternatives would be most critical during drought conditions.

Results at the two stations in the upstream river channels (NECF and CFBW) show good agreement with measured values (RMS errors of 1.2 to 1.4 PSU), especially early in the simulation before the freshet occurs. Freshwater input is sufficient during the freshet to reduce salinities to 0 PSU at peak discharge, which is also simulated in the model. Salinities during peak ebb-tides in the recovery period after the freshet are somewhat underpredicted, which is likely due to discrepancies in the timing and magnitude of freshwater inputs but could also indicate a reduced ability of the model to propagate salinity to the uppermost estuary reaches after large inflows.

Table 4-3: Summary of Calibration Metric Results for the August 2017 Calibration Period

Station	RMS Error ε_{rms} [PSU]	Normalized Error ε_{norm} [%]	Correlation Coefficient	Mean Error [PSU]	Mean Absolute Error [PSU]	Index of Agreement d
ADM: Surface	3.6	25%	0.88	-2.8	3.0	0.84
ADM: Bottom	2.0	15%	0.91	-1.4	1.6	0.92
ADM: Difference	2.6	31%	0.51	1.4	2.0	0.64
UBI: Surface	2.9	18%	0.88	-1.2	2.5	0.89
UBI: Bottom	2.4	15%	0.87	0.0	2.0	0.91
UBI: Difference	2.1	23%	0.54	1.2	1.7	0.68
KM_SB: Surface	2.4	19%	0.85	0.1	2.0	0.89
KM_SB: Bottom	2.7	18%	0.87	0.5	2.3	0.91
KM_SB: Difference	1.6	19%	0.63	0.4	1.2	0.78
NECF_SB: Surface	1.2	12%	0.82	-0.1	0.8	0.88
NECF_SB: Bottom	1.4	11%	0.81	-0.1	0.9	0.88
NECF_SB: Difference	0.4	18%	0.41	0.0	0.2	0.60
CFBW: Surface	-	-	-	-	-	-
CFBW: Bottom	1.1	13%	0.80	0.1	0.6	0.86
CFBW: Difference	-	-	-	-	-	-

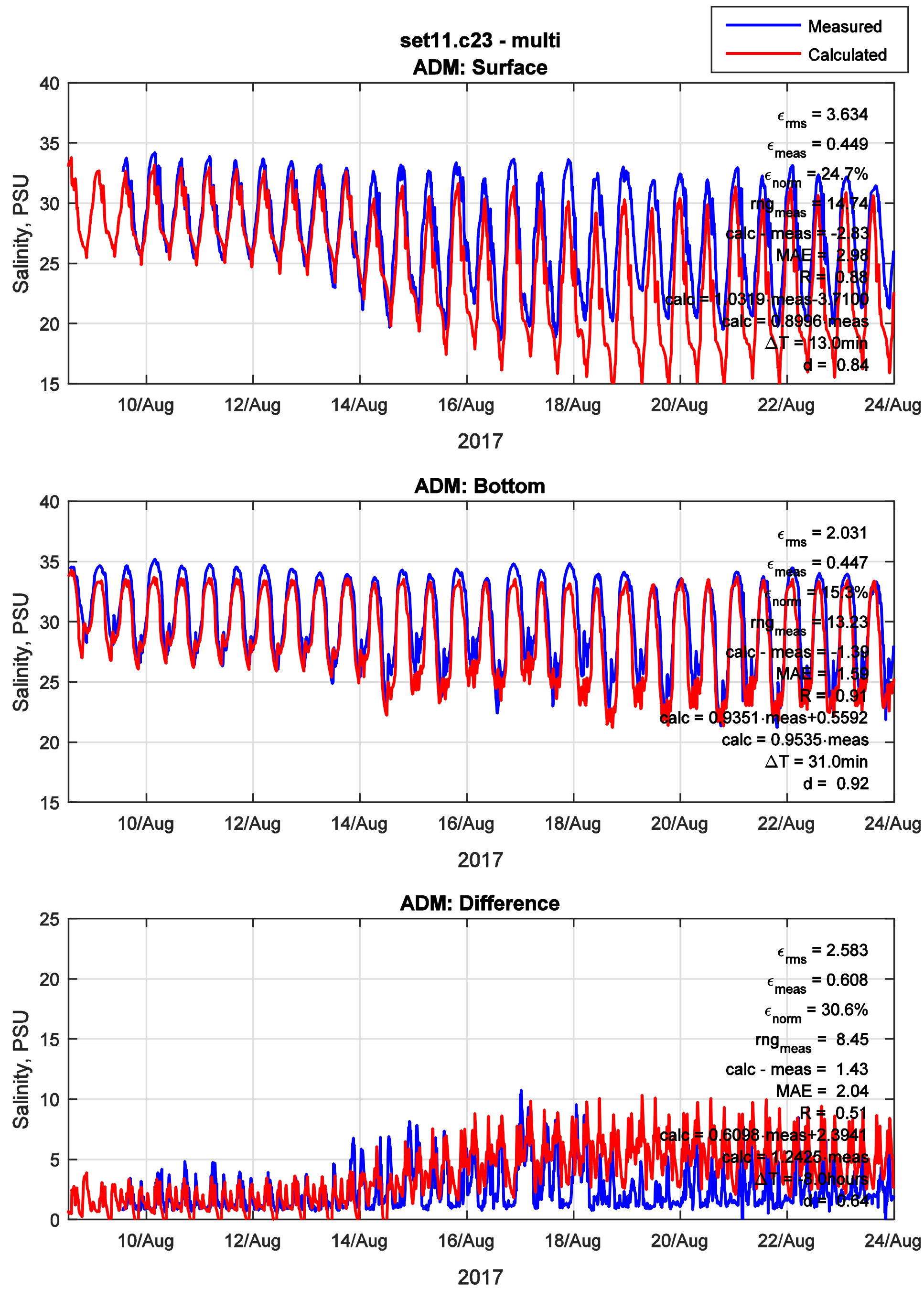

Figure 4-39: Comparison of measured and calculated surface salinity, bottom salinity, and vertical gradient at the ADM station for August 2017

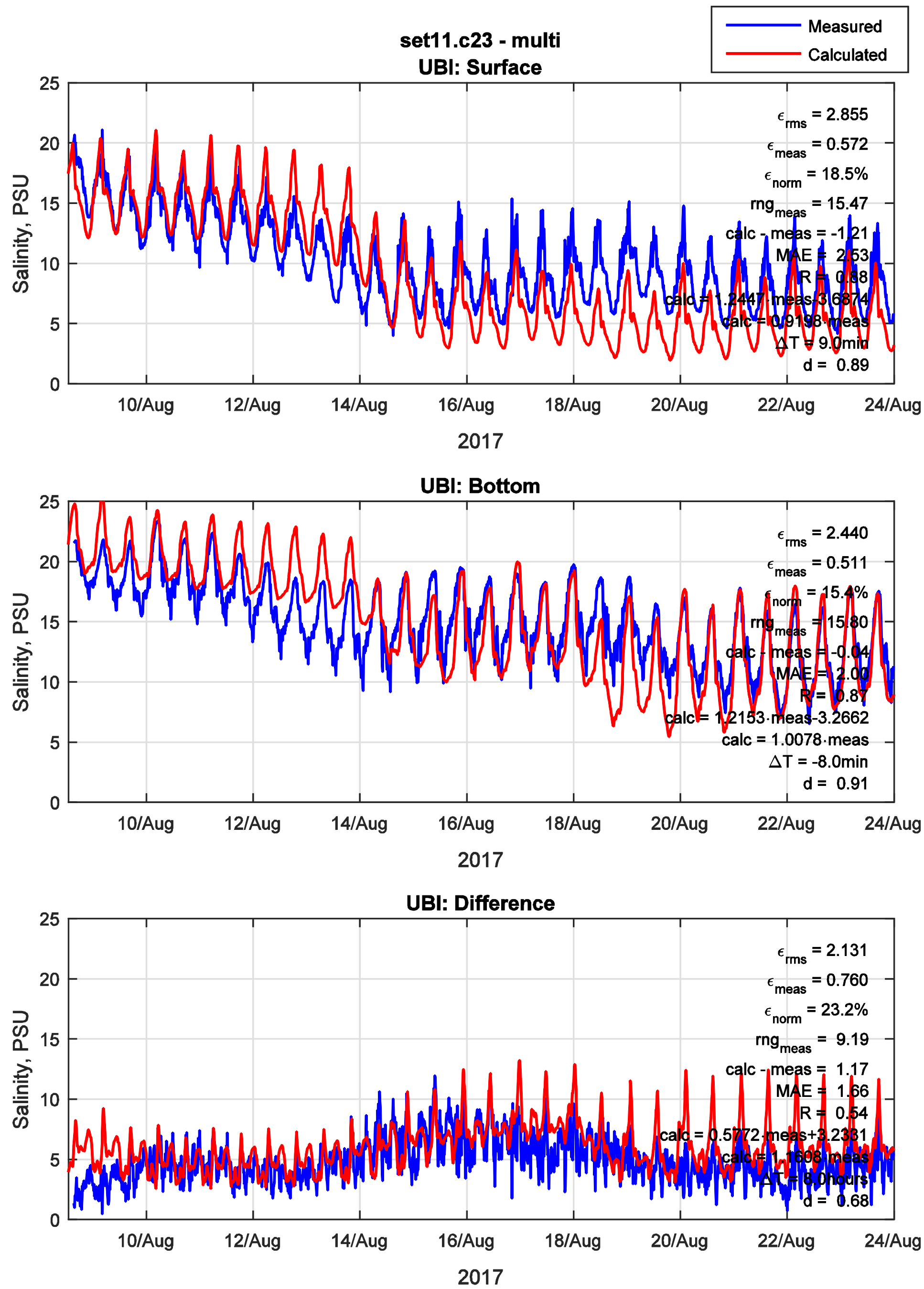

Figure 4-40: Comparison of measured and calculated surface salinity, bottom salinity, and vertical gradient at the UBI station for August 2017

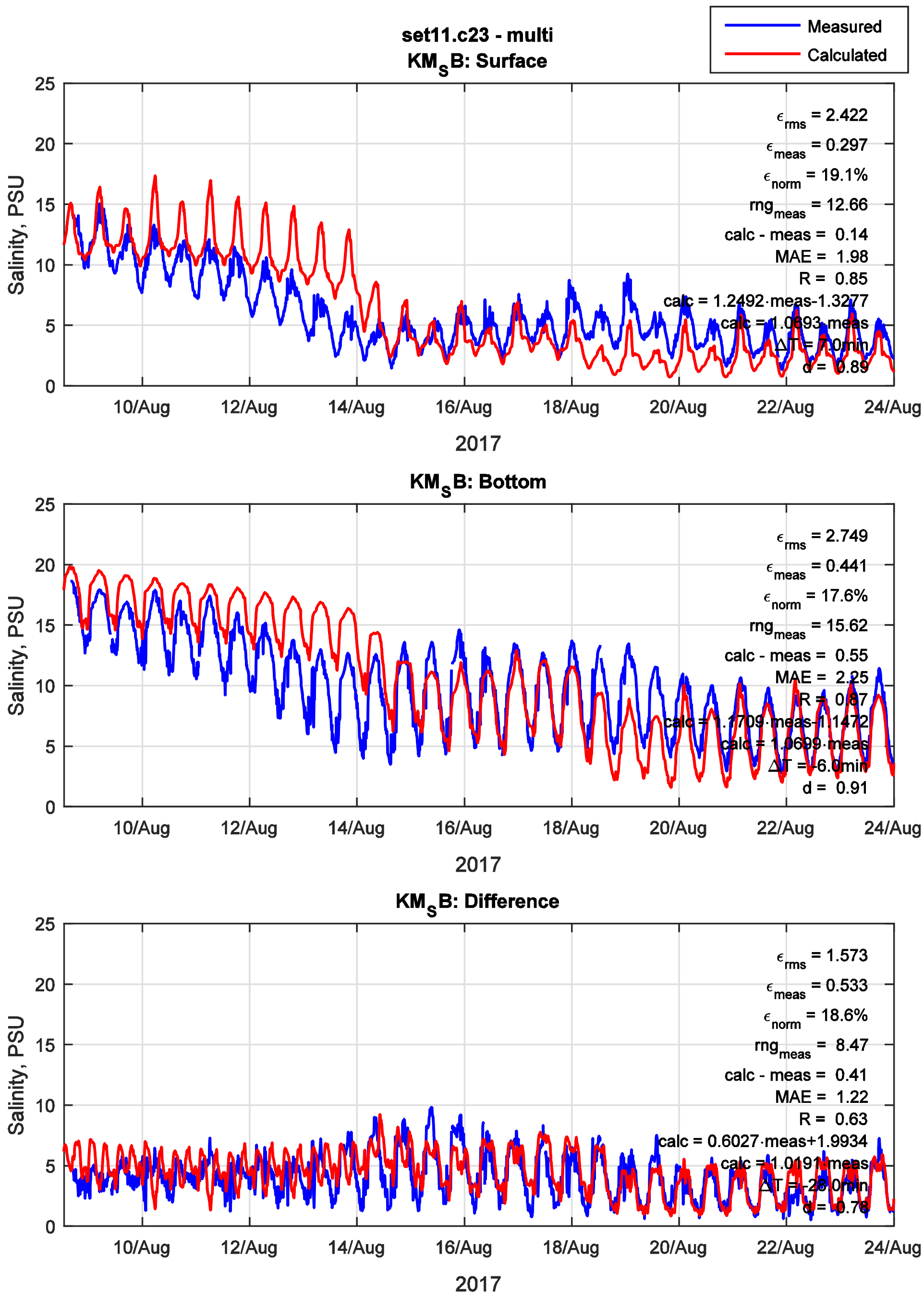

Figure 4-41: Comparison of measured and calculated surface salinity, bottom salinity, and vertical gradient at the KM station for August 2017

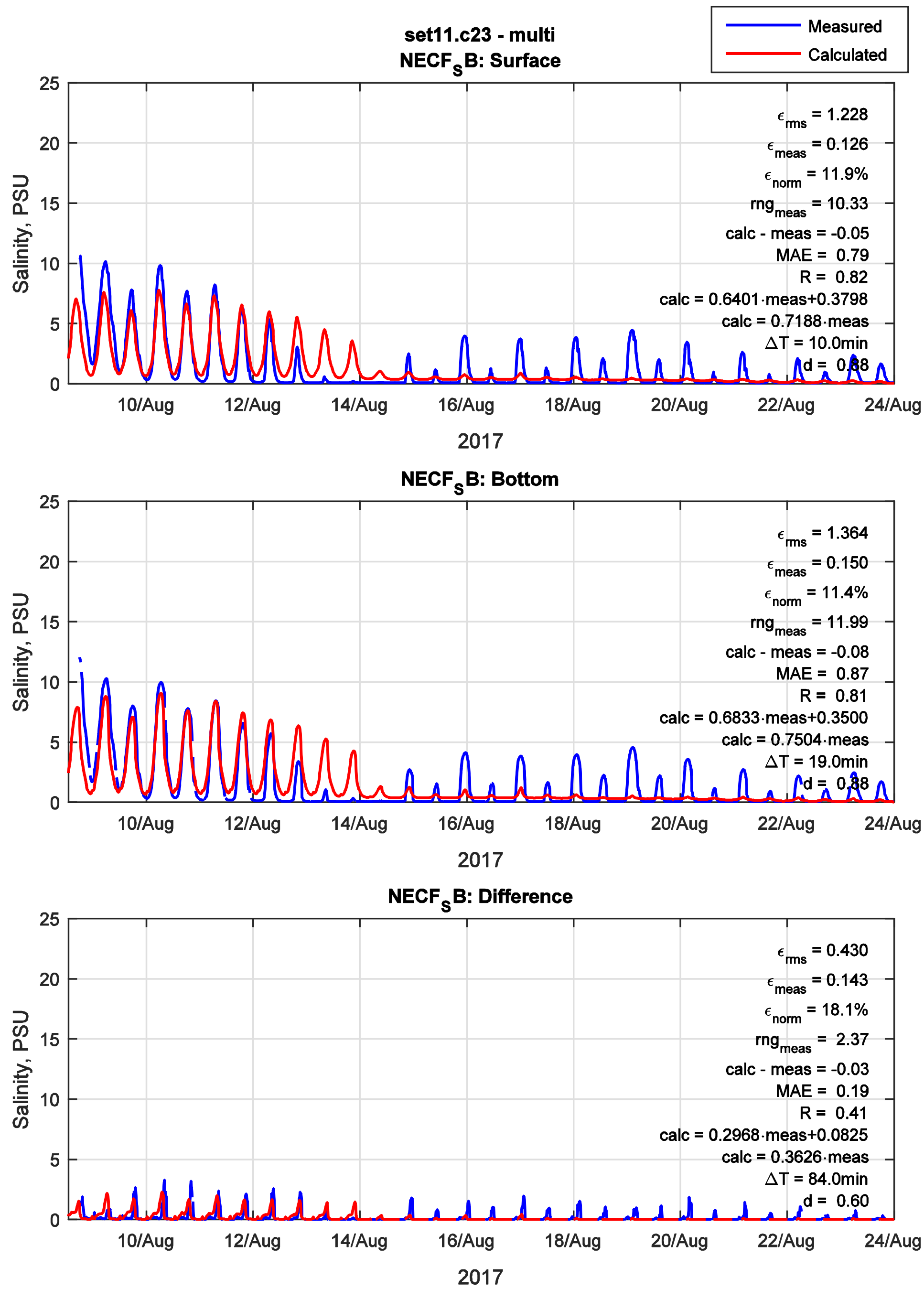

Figure 4-42: Comparison of measured and calculated surface salinity, bottom salinity, and vertical gradient at the NECF station for August 2017

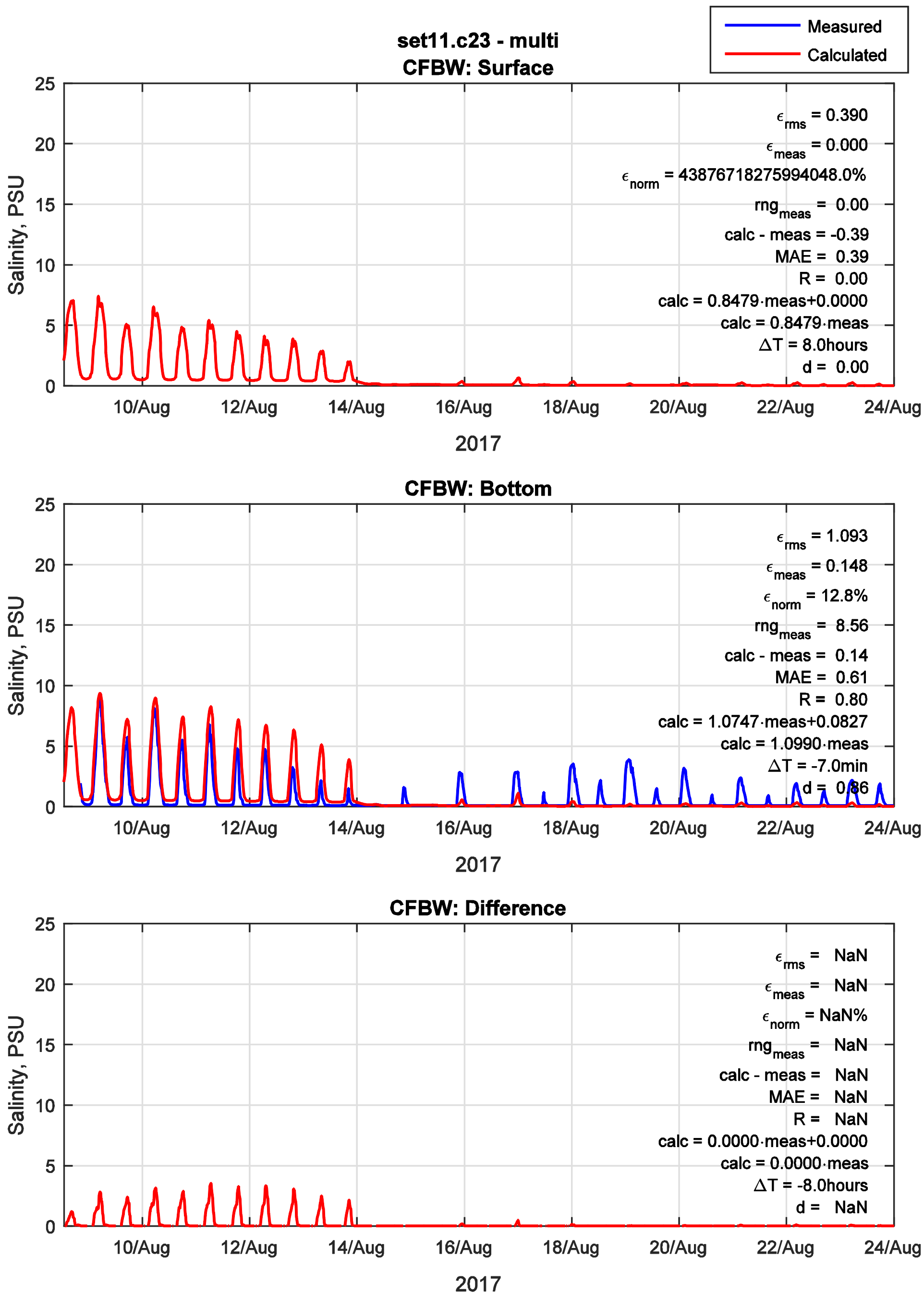

Figure 4-43: Comparison of measured and calculated bottom salinity at the CFBW station for August 2017. Surface salinity measurements were unavailable for this station.

Detrended Timeseries Results

Figure 4-44 to Figure 4-48 show comparisons between measured and modeled results for the same stations and time period, though with the subtidal trend removed. In this case, the figures are plotting the deviation of salinity concentrations from the subtidal value. The subtidal trend is calculated using a running mean filter with a window length equal to the duration of approximately four semi-diurnal tidal cycles (about 50 hours). With the subtidal trend removed, these results focus on the model's ability to simulate the tidal fluctuations and vertical differences in salinity independent of initial conditions and freshwater input. With normalized errors of approximately 10% at all stations, the model is successful in simulating the tidal advection, dispersion, and salt wedge intrusion characteristics of the Cape Fear River estuary.

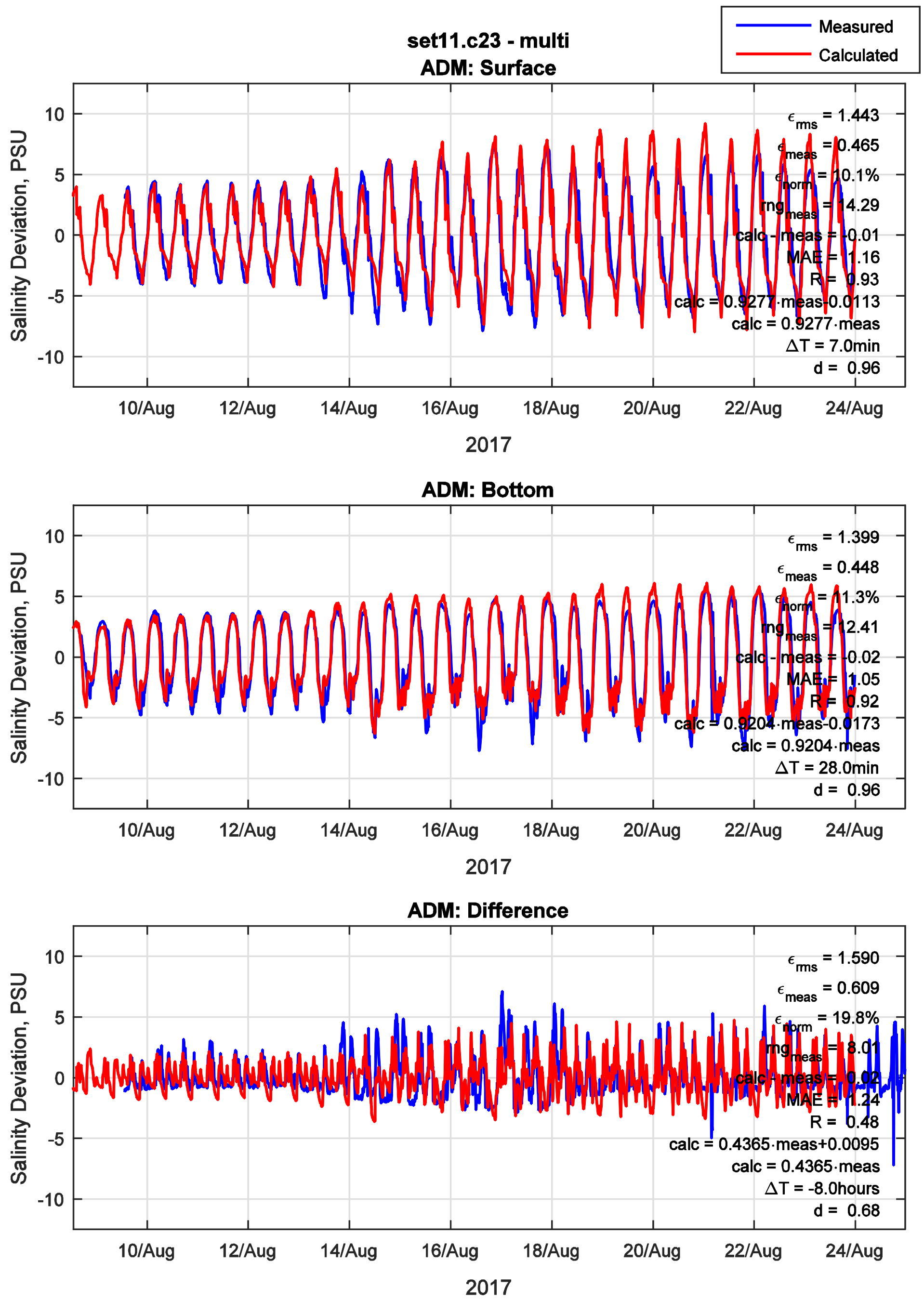

Figure 4-44: Comparison of measured and calculated surface salinity, bottom salinity, and vertical gradient at the ADM station for August 2017 with subtidal trends removed

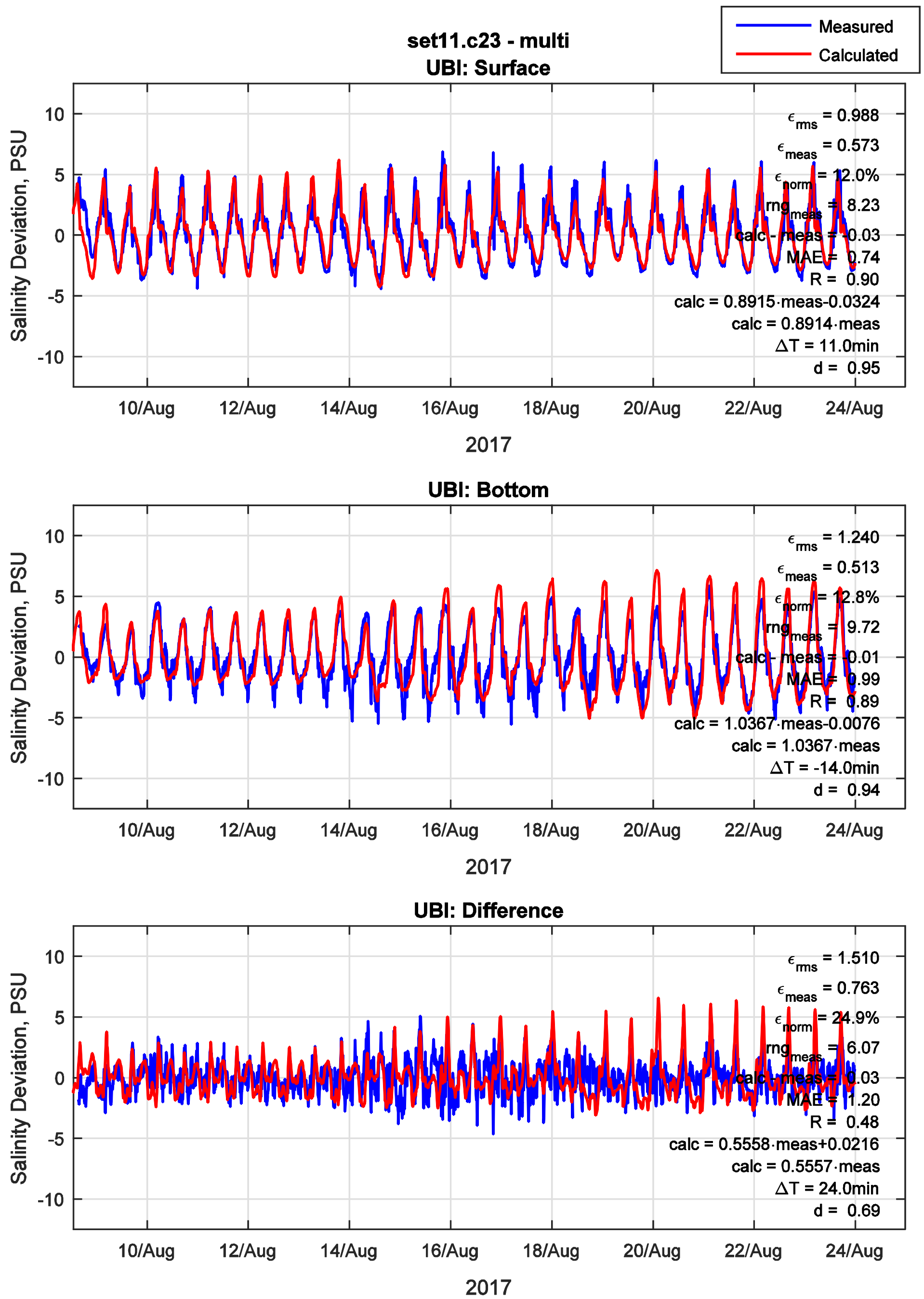

Figure 4-45: Comparison of measured and calculated surface salinity, bottom salinity, and vertical gradient at the UBI station for August 2017 with subtidal trends removed

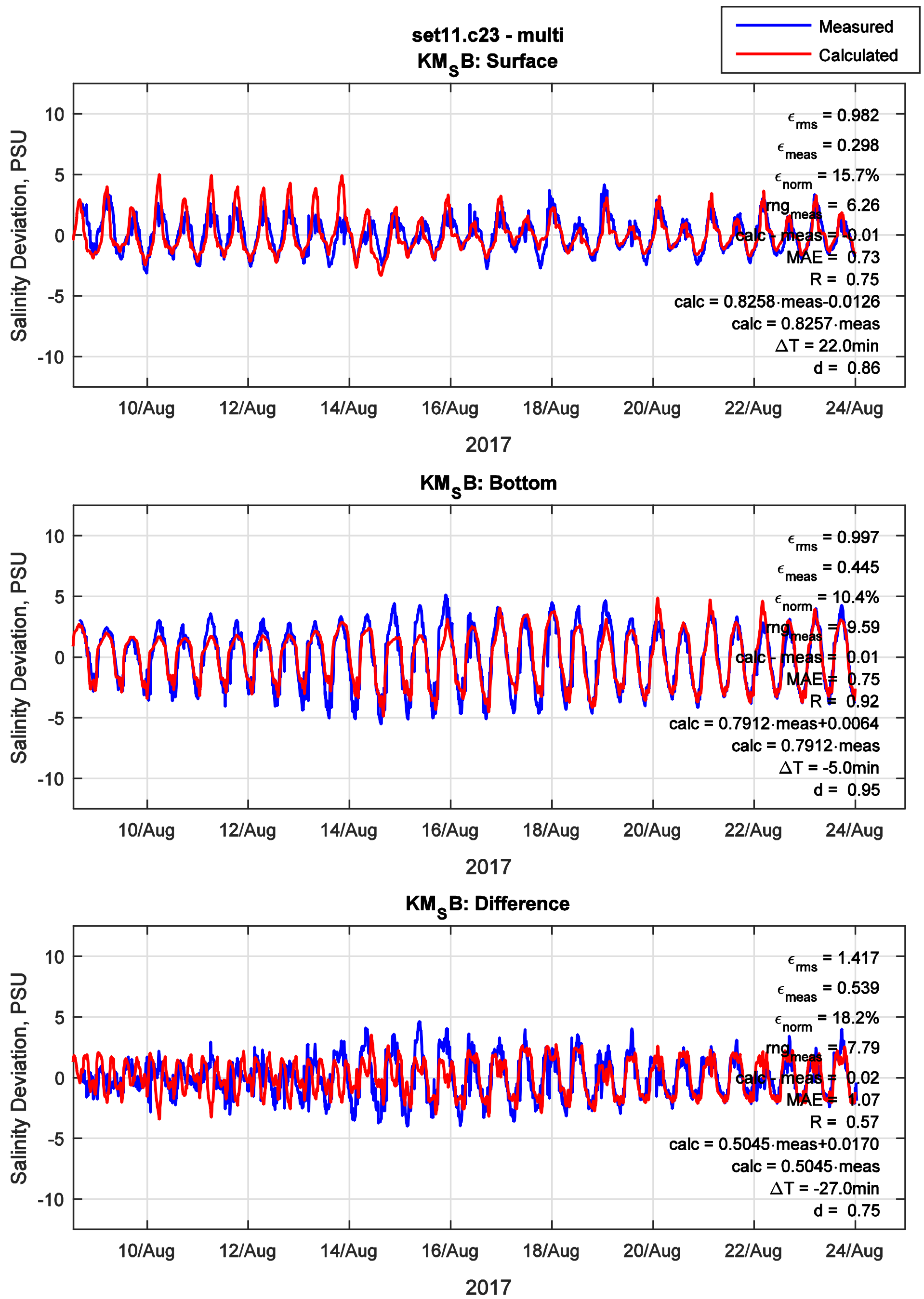

Figure 4-46: Comparison of measured and calculated surface salinity, bottom salinity, and vertical gradient at the KM station for August 2017 with subtidal trends removed

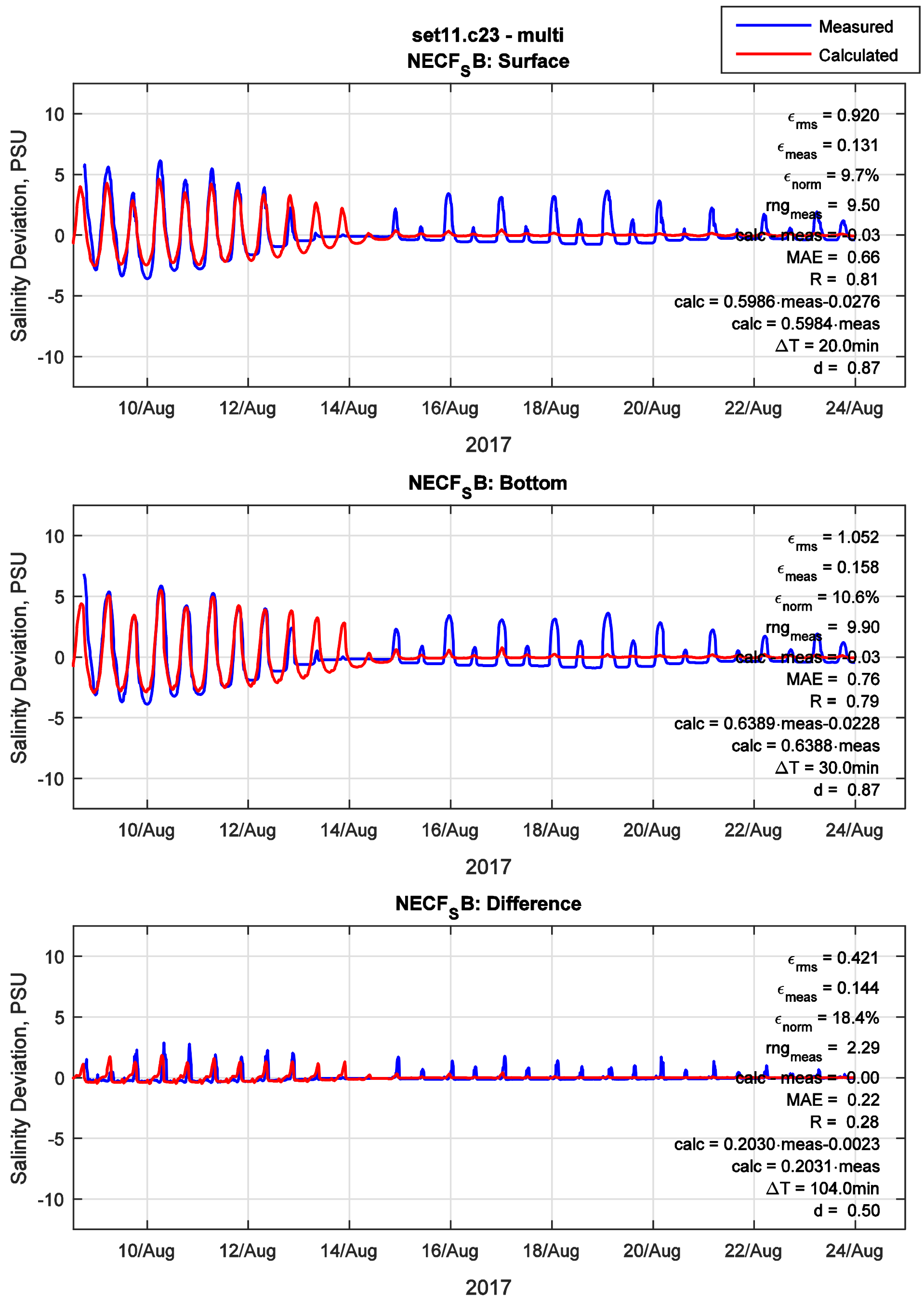

Figure 4-47: Comparison of measured and calculated surface salinity, bottom salinity, and vertical gradient at the NECF station for August 2017 with subtidal trends removed

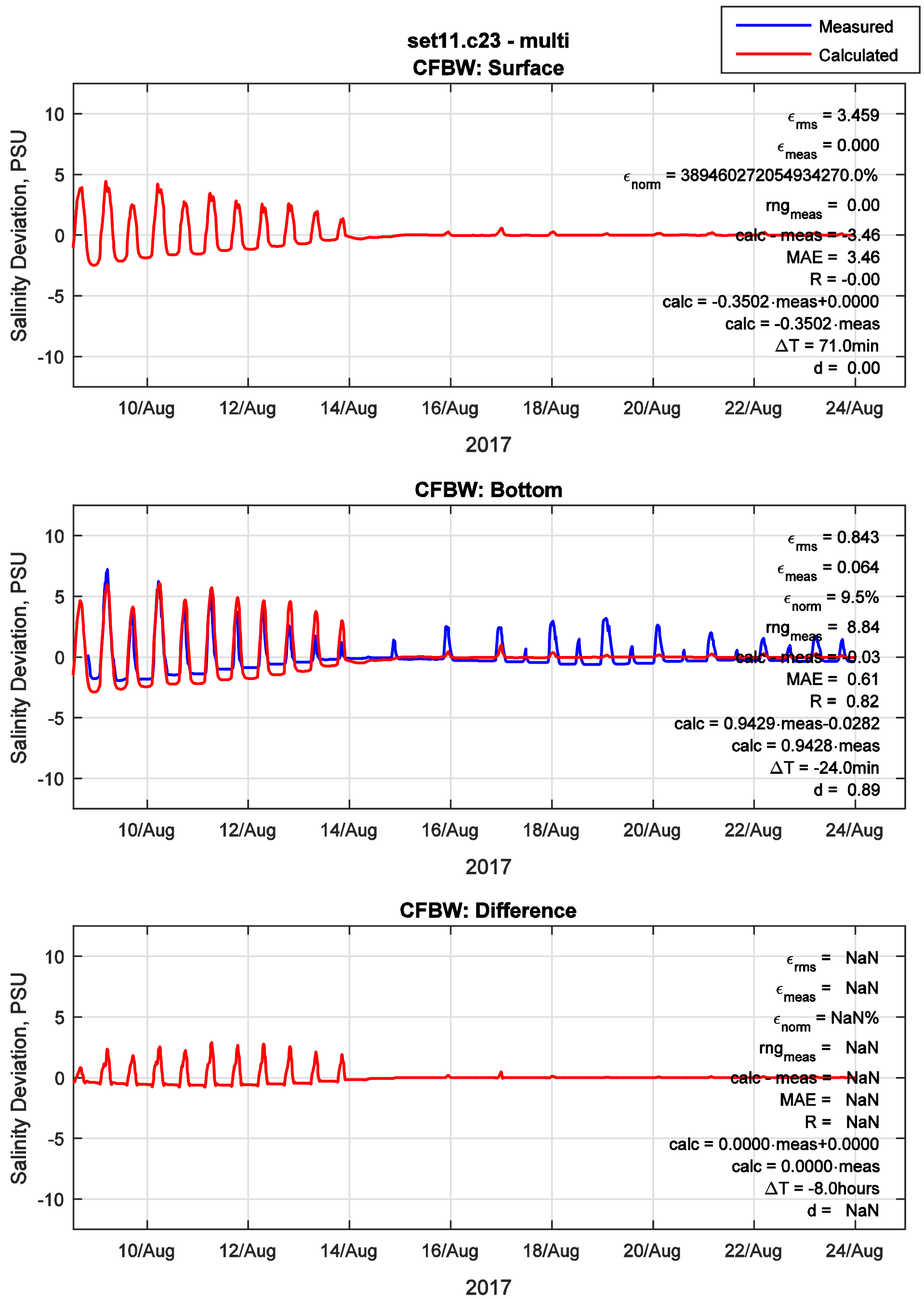

Figure 4-48: Comparison of measured and calculated bottom salinity at the CFBW station for August 2017 with subtidal trends removed. Surface salinity measurements were unavailable at this station.

3D Profile Results

Figure 4-49 to Figure 4-52 show comparisons between measured and modeled vertical salinity profiles for the CTD casts taken at various times on August 10, 2017 in the upper estuary. Each figure organizes the comparisons for casts at the same location in rows with subsequent times in columns. The locations for each cast (CTD_01 through CTD_16) are shown in Figure 2-15.

The model shows good agreement with the measured salinities in the upstream river tributaries (CTD_01 – CTD_03, CTD_15, and CTD_16), where vertical profiles are generally uniform and near zero. Within the estuary at and downstream of Wilmington (CTD_06 – CTD_10), the modeled profiles also show good agreement with measurements at most times, though in general the salinity is slightly overpredicted due to the discrepancies in measured and calculated subtidal trends. Results at cast locations in the downstream portion of the Northeast Cape Fear River (CTD_11 – CTD_14) generally overpredict bottom salinities and stratification by 2 to 5 PSU, likely a result of slight discrepancies in the timing of wedge propagation with each flood tide. Overall, the simulated profiles match the shape of the measured profiles at most locations and times, indicating that the model adequately simulates salinity stratification within the estuary.

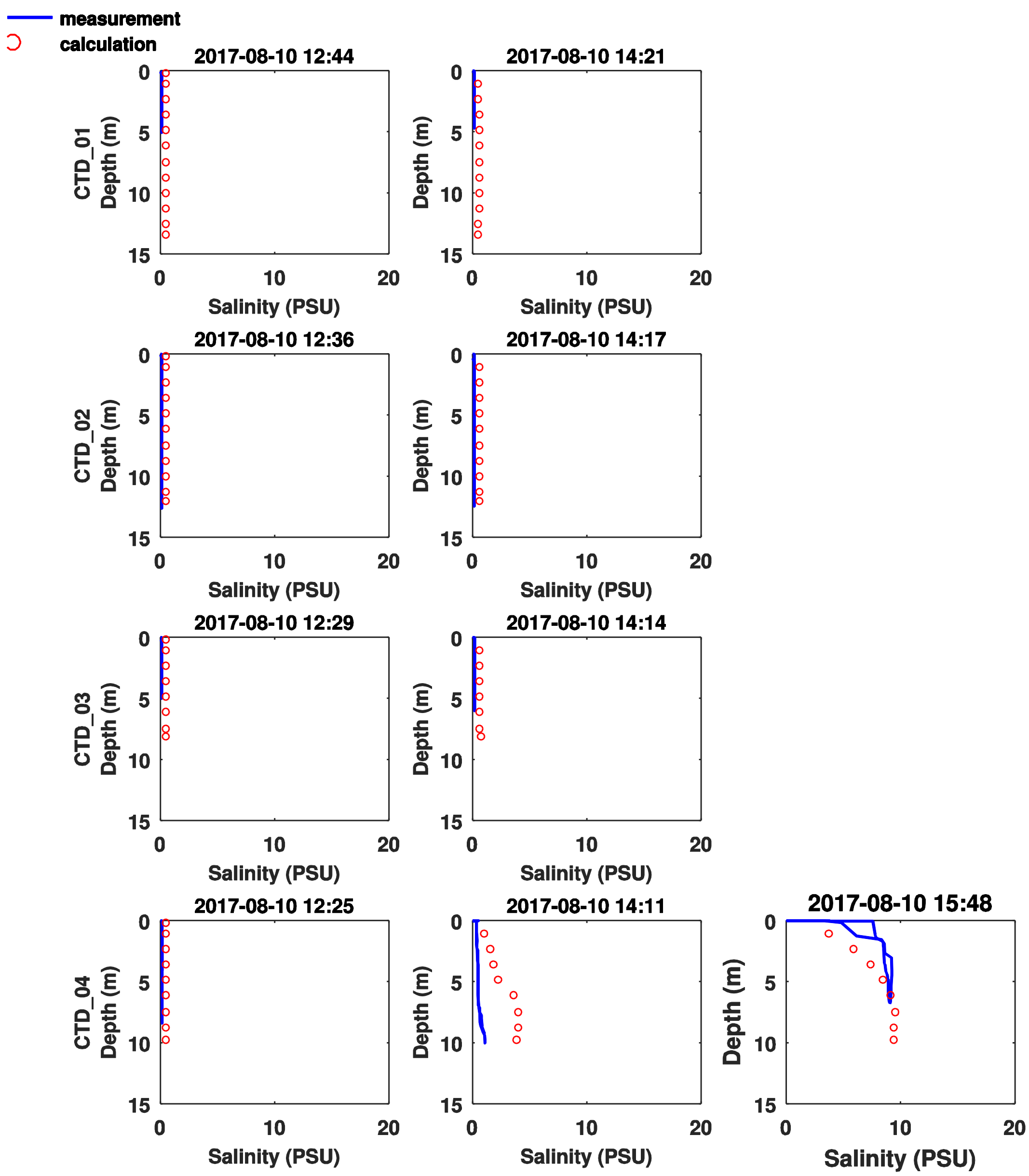

Figure 4-49: Comparison of measured and calculated salinity profiles at CTD cast locations 1 through 4

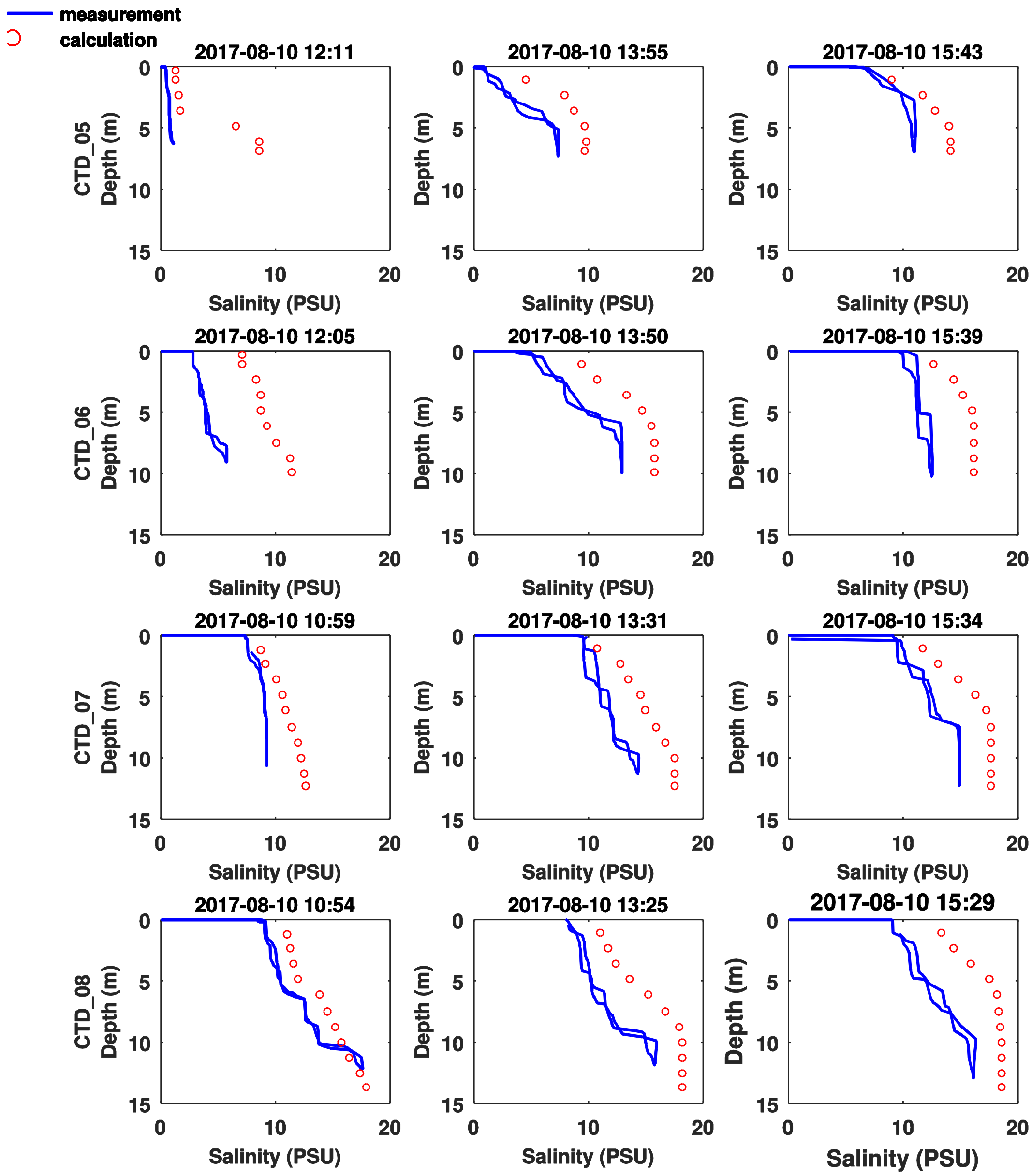

Figure 4-50: Comparison of measured and calculated salinity profiles at CTD cast locations 5 through 8

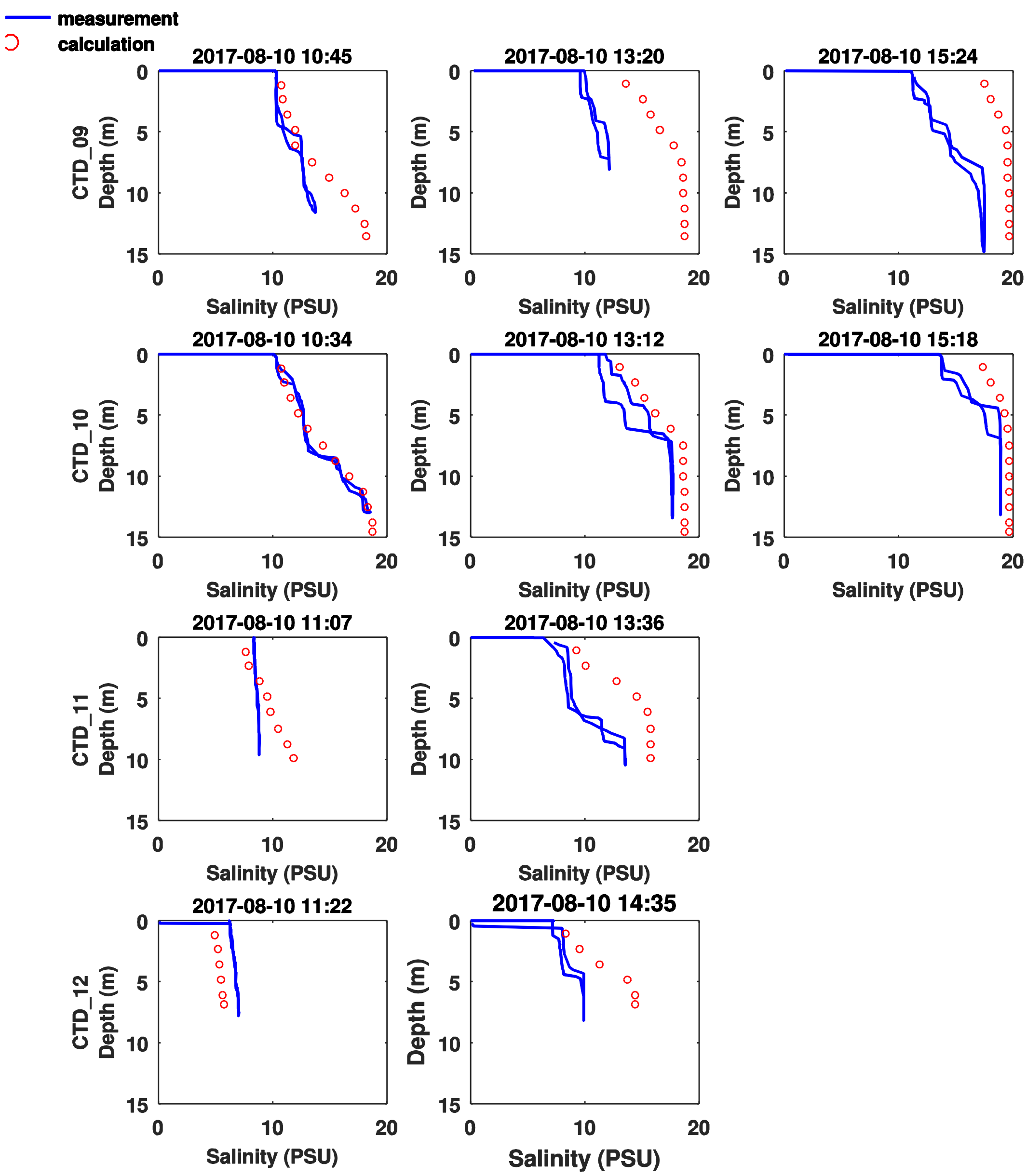

Figure 4-51: Comparison of measured and calculated salinity profiles at CTD cast locations 9 through 12

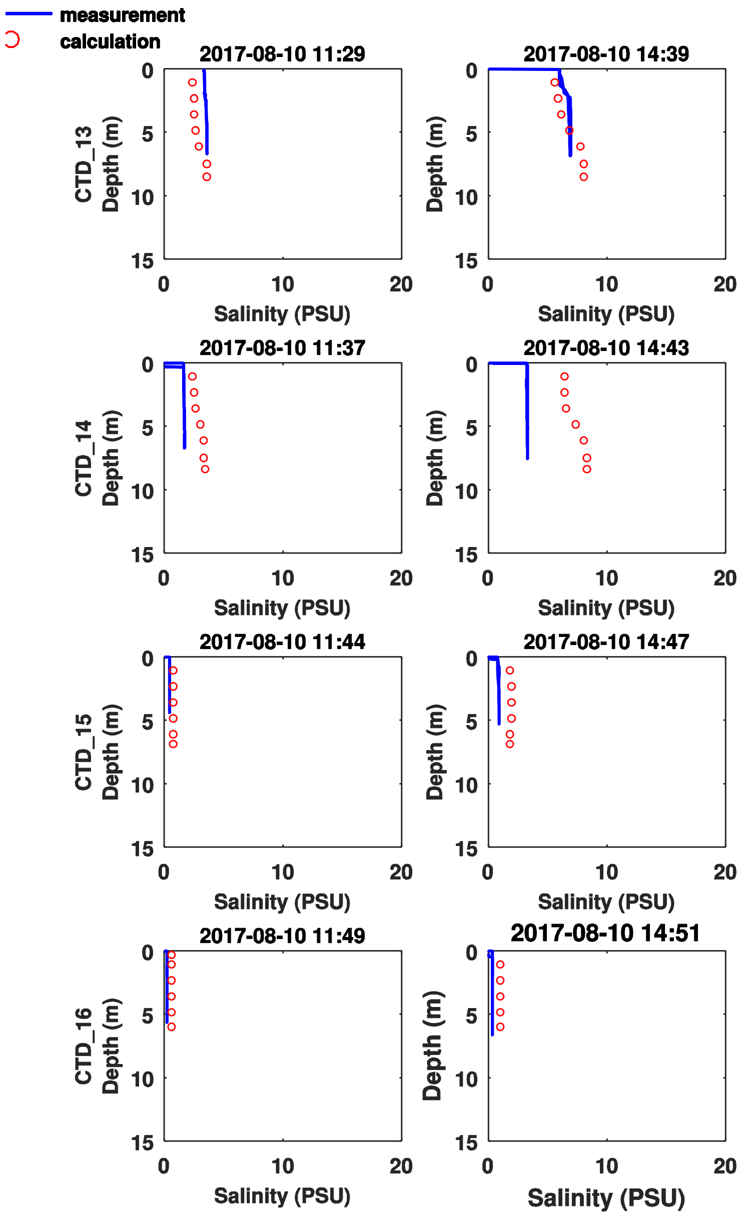

Figure 4-52: Comparison of measured and calculated salinity profiles at CTD cast locations 13 through 16

4.3.5.2. March 2017 Validation Period

Figure 4-53 and Figure 4-54 show comparisons of the measured and modeled (calculated) salinities at the two long-term, fixed station locations of the late March 2017 validation period. During this period, measurements show that subtidal trends are minor, with a nearly-constant tidally-averaged salinity at each location. The model salinities closely match both the surface and bottom salinities at the South station, with RMS errors of approximately 1 PSU. Measured vertical differences are small, varying between 0 to less than 3 PSU over the tidal cycle. Simulated differences are similarly minor, though slightly under predicted at the peaks. A summary of the calibration metrics for this period is given in Table 4-4.

At the North station, only surface salinity measurements were available for comparison. Again, the calculated tidal variation matches very well with the measured concentration values, though a relatively constant bias of 1 to 2 PSU slightly overestimates salinities. While subtidal trends are minor, it is possible that the bias is due to errors in the estimation of a relatively constant freshwater inflow from unaged areas.

Validation results show that the model is successful in propagation of salinity upstream in the estuary and closely matching measured surface and bottom salinities over the tidal cycle in both the upper and lower estuary, especially during periods when the influence of freshwater inflows is minor.

Table 4-4: Summary of Calibration Metric Results for the March 2017 Validation Period

Station	RMS Error ε_{rms} [PSU]	Normalized Error ε_{norm} [%]	Correlation Coefficient	Mean Error [PSU]	Mean Absolute Error [PSU]	Index of Agreement d
South: Surface	1.0	13%	0.95	-0.7	0.8	0.95
South: Bottom	0.5	8%	0.97	0.0	0.4	0.99
South: Difference	1.0	57%	0.26	0.7	0.8	0.44
North: Surface	2.6	39%	0.89	2.5	2.5	0.60

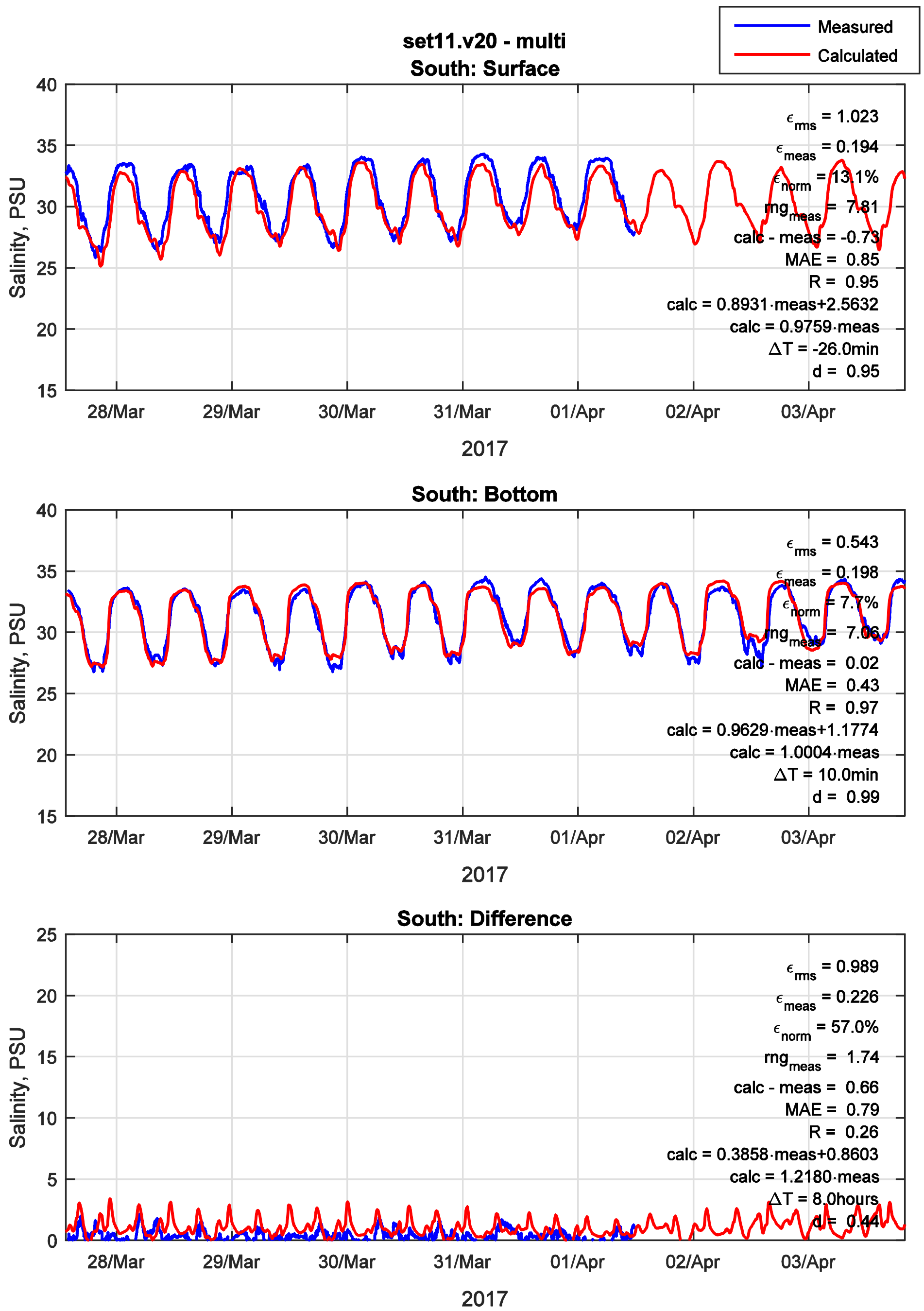

Figure 4-53: Comparison of measured and calculated surface salinity, bottom salinity, and vertical gradient at the South station for Late March 2017

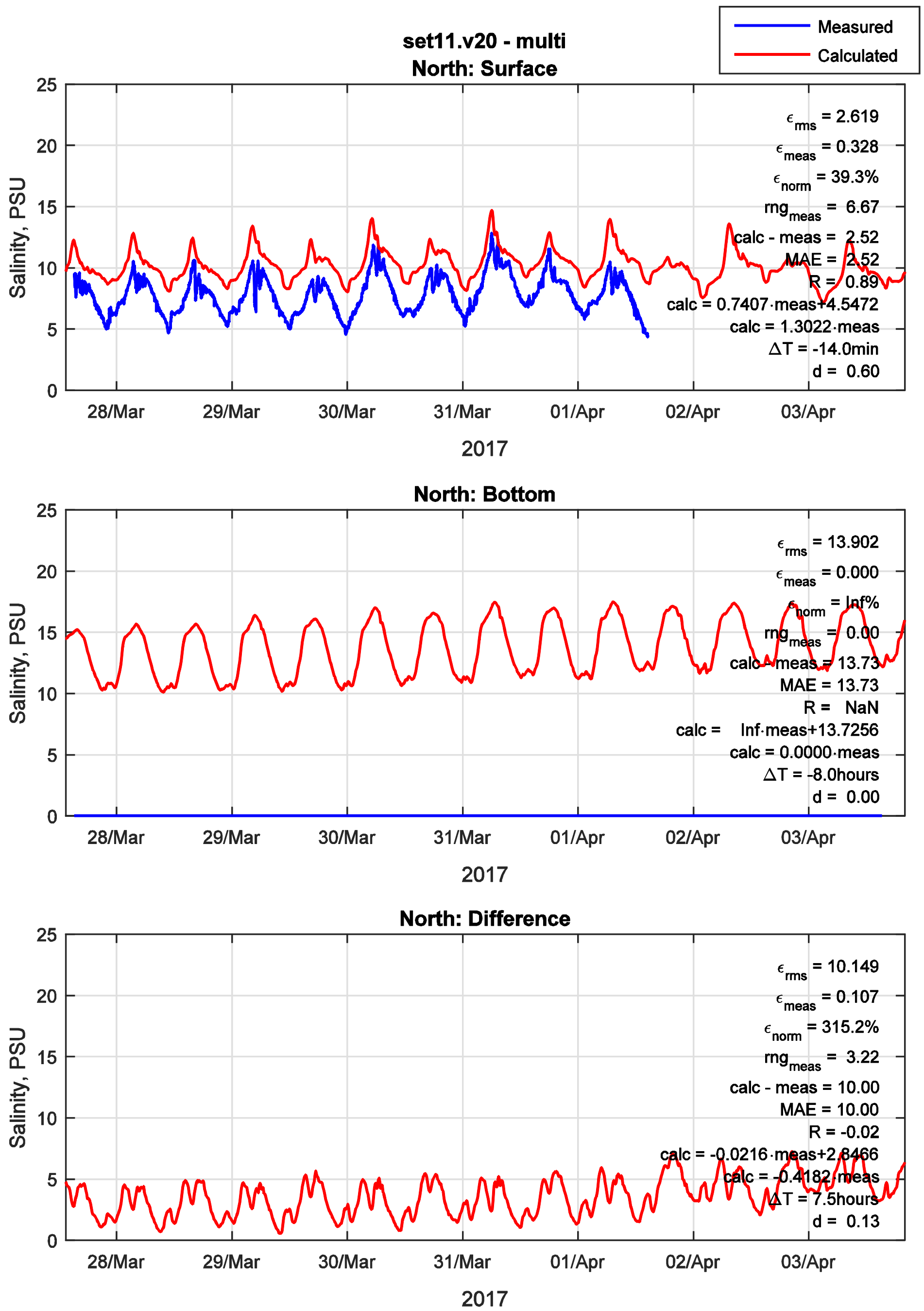

Figure 4-54: Comparison of measured and calculated surface salinity at the North station for Late March 2017. Bottom salinity measurements were unavailable, so only calculated bottom and gradient values are shown

4.3.6. Conclusions

The extension of the Delft3D three-dimensional hydrodynamic model of the Cape Fear River estuary to include salinity has enabled the simulation of tidal advection of salinities and development of vertical salinity gradients with a reasonable degree of accuracy. During model calibration, it was determined that subtidal trends are not limited to the effects of the major inflows from the Cape Fear River and Black River, but significantly affected by the fresh water inflows from smaller watersheds along the estuary. The adjustments applied to the fresh water inflows during calibration period were selected based on available salinity measurements so cannot be replicated for an arbitrary period. Therefore, the ability of the model to accurately propagate salinity along the estuary was evaluated using comparisons with salinity measurements and with salinity measurements with removed subtidal trends. In comparing model predictions with detrended measurements during a freshet (calibration period of August 2017) and with measurements without detrending during periods with little to no subtidal variations (validation period of March 2017), the model results showed that the variations of surface and bottom salinities from ebb- to flood-tide and over the fortnightly neap to spring cycle are reproduced accurately at locations ranging from near the Cape Fear River mouth to the upstream river channels.

The model is able to simulate the range of salinity changes under tidal flows, the development of vertical salinity gradients, the propagation of salinity into the upper reaches of the estuary, and the subtidal salinity trends resulting from episodes of high freshwater input. Estimates of measurement RMS errors are approximately equal to 0.5 PSU at all stations, while RMS errors between detrended calculations and measurements range from less than 1 to 1.5 PSU. Based on the model skill level, the model is considered suitable for evaluation of the impacts of channel deepening alternatives on estuarine salinity processes. Remaining uncertainties and sources of error could be attributed to the specification of spatially-varying, three-dimensional initial salinity conditions which can continue to affect results for months of simulation, salinity boundary conditions based on results of a global model with its own uncertainty, errors in the model bathymetry especially in the most upstream reaches, and the specification of unmeasured freshwater inflows.

4.4. Suspended Sediments

The sediment transport model was developed based on the calibrated Delft3D three-dimensional hydrodynamic model (HD model) coupled with salinity in order to capture the density effect on the sediment transport. The purpose of selecting the 3-D model is due to the stratification caused by the interaction of fresh and salt water in the estuary. In the Cape Fear Estuary especially near the Wilmington Harbor where relatively fine sediment and strong flow conditions exist, the stratification effect can be very significant on the sediment concentration throughout the water column. As a result, the 3D model (both HD and sediment transport) coupled with salinity will capture the stratification caused by the water density variation throughout the water column. However, the salinity effect on sediment flocculation was not implemented in this model, due to lack of in-situ settling velocity measurements.

The model was used to evaluate suspended sediment transport in the Cape Fear River estuary. The model grid, bathymetry, and boundary conditions were the same as the HD model. The horizontal grid is curvilinear with 5 m × 100 m inside the navigation channel and the vertical grid uses 25 uniform Z-layers with 1.3 m thickness for each layer. As an example, the horizontal and vertical gird in Anchorage Basin are shown in Figure 4-55 and Figure 4-56. Although the aspect ratio (length/width) in the horizontal grid is high, the flow direction in the channel generally follows the longitudinal direction of the grid and will not introduce any significant errors numerically. Additional sediment properties and TSS at the boundaries were added and are discussed in the following sections.

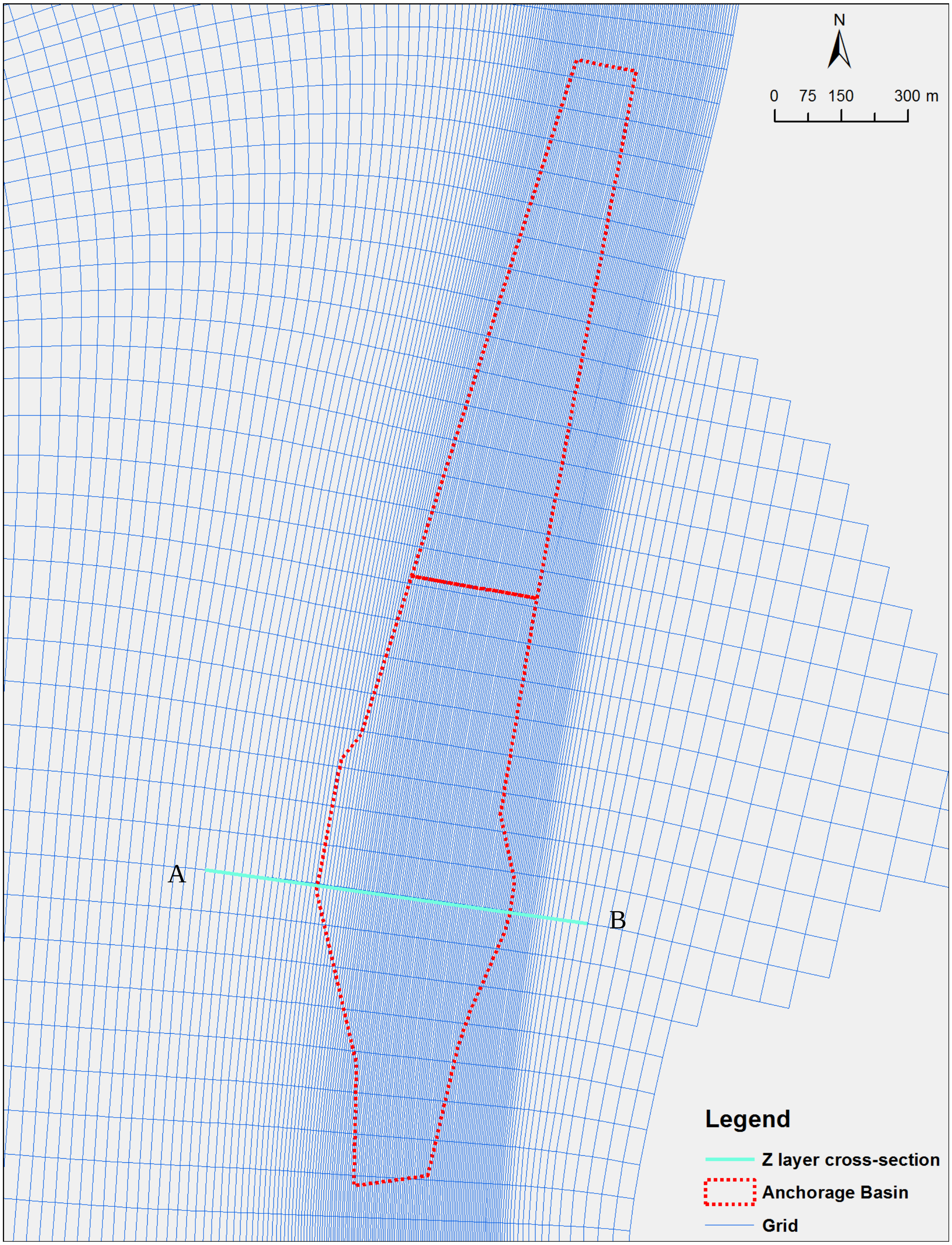

Figure 4-55: Horizontal grid in Anchorage Basin

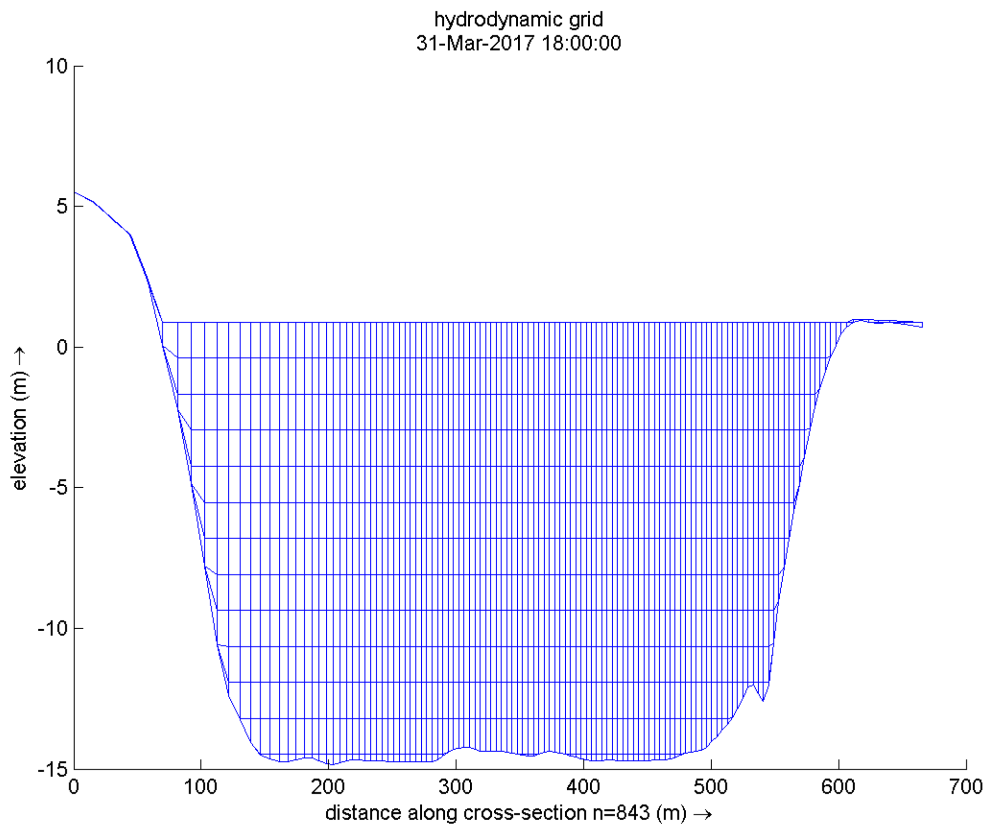

Figure 4-56: Vertical grid of cross-section AB

4.4.1. Sediment Properties

Only one fraction of cohesive sediment (mud) was included in the model, with the governing model parameters listed in Table 4-5. Among those parameters in Table 4-5, settling velocity, critical bed shear stress for sedimentation, critical bed shear stress for erosion and erosion parameter were used as calibration parameters.

Table 4-5: Model sediment transport parameters

Parameter	Value
Sediment type	mud
Specific density	2,650 (kg/m3)
Settling velocity	0.0005 (m/s)
Critical bed shear stress for sedimentation	0.9 (N/m2)
Critical bed shear stress for erosion	0.50 (N/m2)
Erosion parameter	0.0002 (kg/m2/s)
Dry bed density	500 (kg/m3)

4.4.2. Boundary Conditions

Two sets of boundary conditions were developed to allow the model to reproduce 1) measured sediment concentration profiles during the March 2017 field measurement campaign; and 2) annual shoaling rates in the Anchorage Basin in the two calibration simulations.

4.4.2.1. Initial Conditions

The initial depth of the Anchorage Basin was generated based on the post-dredge survey on 02/06/2017 (USACE Surv & Map). The initial conditions of salinity were obtained from the validation run of the salinity simulation. The model was then run for a week to obtain the initial TSS concentrations before outputting the results.

According to the survey data by USACE (USACE 2014) and the historical geotechnical data by Fugro (see Geotechnical Appendix), bed sediments in the channel reaches upstream of Reaves Point are predominantly silt and clay. Bed sediments downstream of Reaves Point are predominantly sand. In the model, the initial sediment thickness was set to 16.4 ft (5 m) upstream of Reaves Point providing enough sediment to avoid bed sediment shortage during the model simulation, and 0 ft downstream of Reaves Point (Figure 4-57).

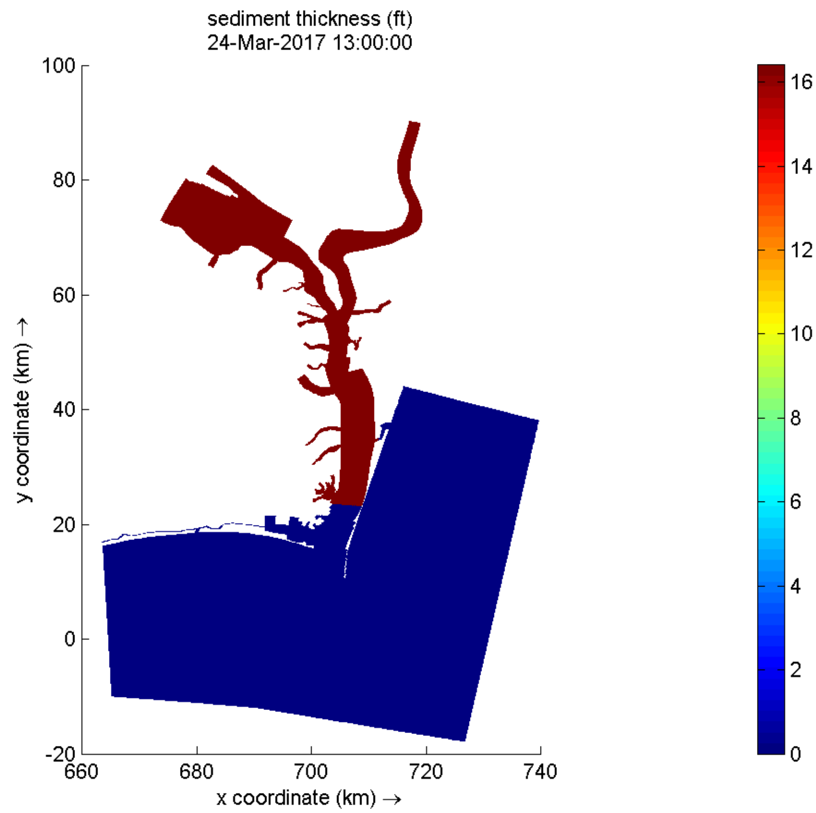

Figure 4-57: Initial sediment thickness (cohesive only)

4.4.3. Model Calibration

4.4.3.1. Calibration to March 2017 Measurements

The calibration was performed to reproduce vertical variation in the total sediment concentrations during a period when measurements were available. The model simulation period was from March 24, 2017 to April 1, 2017 which contains the period of measurements between March 27, 2017 and April 1, 2017. For the calibration, TSS casts were available at TR03, TR06, TR09 and TR11 (Figure 2-18 - Figure 2-21). For the TSS concentration profile calibration, real-time water discharges (Q) derived from USGS measurements were used at the three upstream river boundaries (Table 4-6 and Figure 4-58) and the method to calculate Q from USGS stations to the upstream boundaries is described in the HD calibration section. TSS values at the Cape Fear River (CFR), NE Cape Fear River (NECFR) and Black River (BR) were obtained from Simmons (1993) which were 27 mg/L, 9 mg/L and 8 mg/L respectively. TSS values at the offshore boundaries were all set to zero, because the offshore boundaries are far away from the Wilmington Harbor and majority of the sediment in the downstream part of the estuary and offshore area is sand (USACE 2014). The model parameters including settling velocity, critical shear stress for erosion and sedimentation and erosion parameters were adjusted to match the measured TSS concentration in the water column and their values are shown in Table 4-5.

Results of calibration are shown from Figure 4-59 to Figure 4-78. These TSS casts are typical TSS vertical profile during measurements, and the cast locations include the center, left side and right side of the transect line (Figure 2-19, Figure 2-20 and Figure 2-21) except along TR03 where the cast was taken only at the center (Figure 2-18). It can be seen that the measurement data have some “noisy data” especially at the bottom. For example, in Figure 4-59 there are various TSS values of the similar depth at the bottom. As a result, a 3-order polynomial line were plotted to fit the measurement data and were used to calculate the statistics later.

The model results match the measurements well at TR06, TR09 and TR11 but not at TR03. At TR03 (Figure 4-59 and Figure 4-60), the model results are lower than the measurements especially in the lower portion of the water column. At TR06 (Figure 4-62 to Figure 4-66), TSS in the water column varies largely from bottom to top. On the surface, TSS is about 10 mg/L while TSS can reach around 150 mg/L at the bottom. TSS at TR09 (Figure 4-67 to Figure 4-72) shows similar vertical variance as TR06. The only difference is that TSS at the bottom is around 100 mg/L, which is lower than that at TR06. At TR11 (Figure 4-73 to Figure 4-78), TSS is more uniform from 10mg/L – 40 mg/L throughout the water column.

Maps of bed shear stress and depth-averaged current velocity in the estuary are shown from Figure 4-79 to Figure 4-82 including flood and ebb phase in both neap and spring tides. At the Anchorage Basin, the bed shear stress and current velocity are much smaller than other sections of the channel. It is because the Anchorage Basin is wider and deeper than the surrounding areas, and the lower bed shear stress will cause large amount of sedimentation which will be discussed later. It also can be observed from those four tide conditions that bed shear stress and depth-averaged current velocity have similar values at all the transects except at TR11 which is located near the river mouth. Although bed shear stress and depth-averaged current velocity are high at TR11, the TSS values are smaller comparing to other transects. This validates the initial condition set-up with no cohesive sediment downstream to Reaves Point. There are no significant differences between TR03 and TR06/TR09 in bed shear stress and depth-averaged current velocity. From the hydrodynamic perspective, similar TSS results should be expected at TR03, TR06 and TR09. As discussed above, the model results and measurements fit very well at TR06 and TR09 and capture the TSS gradient through the water column, but not at TR03 especially at the bottom. This is mainly due to the local effects at TR03 such as excess available sediments at the bottom and re-suspension for which there was not enough information and was not resolved in the model. Additionally, the high bottom TSS values at TR03 may be partly due to disruption by a ship passage prior to the measurement according to the surveyor.

Table 4-6: USGS river gage station information

Station	Period of Observations (15 min)	Period of Observations (1 day)
0210800 Northeast Cape Fear River near Chinquapin	2007-2017	1940-2017
02106500 Black River near Tomahawk	2007-2017	1951-2017
02105769 Cape Fear River at Lock 1 near Kelly	2007-2017	1969-2017

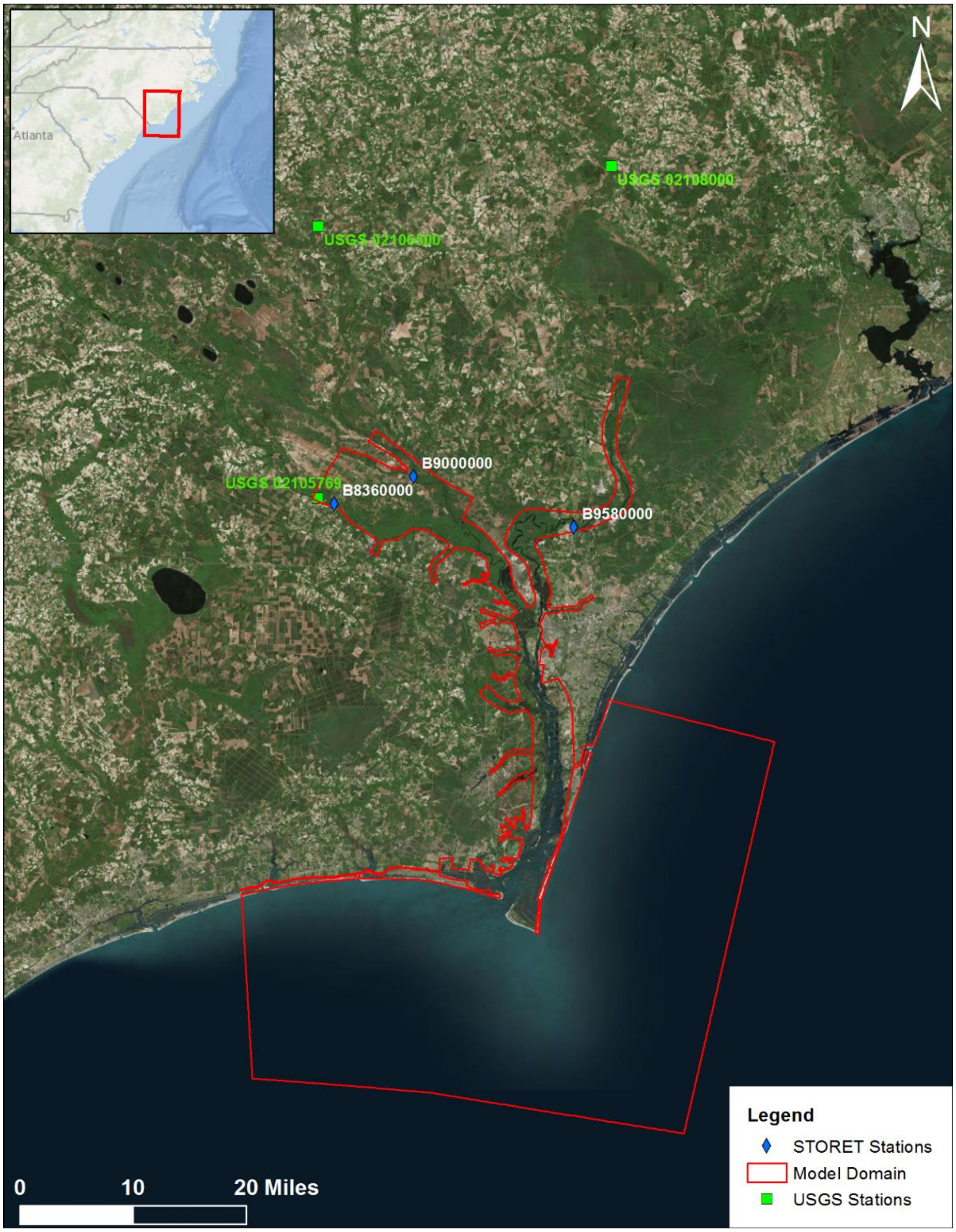

Figure 4-58: USGS and STORET stations used for Q and TSS boundary conditions

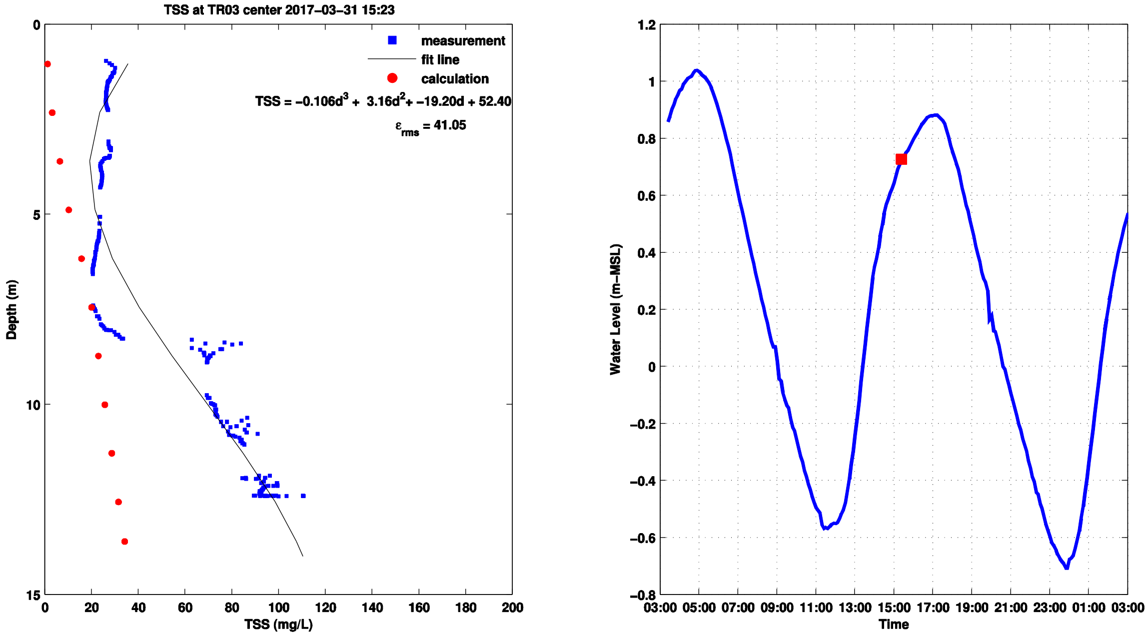

Figure 4-59: TSS cast at center of TR03 during the end of flood tide

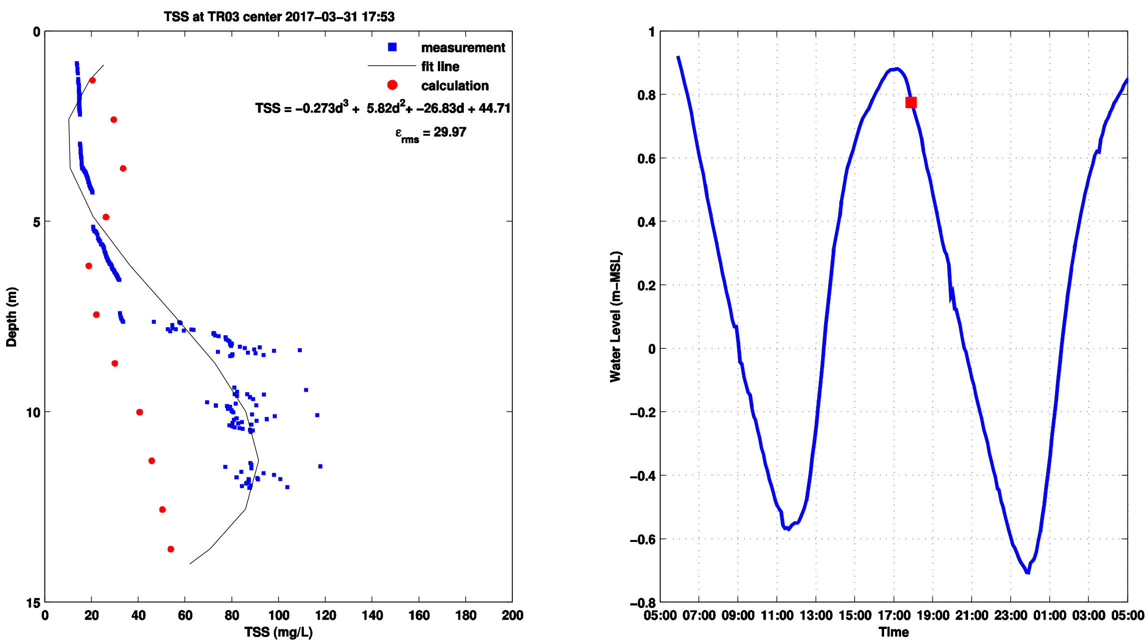

Figure 4-60: TSS cast at center of TR03 during the beginning of ebb tide

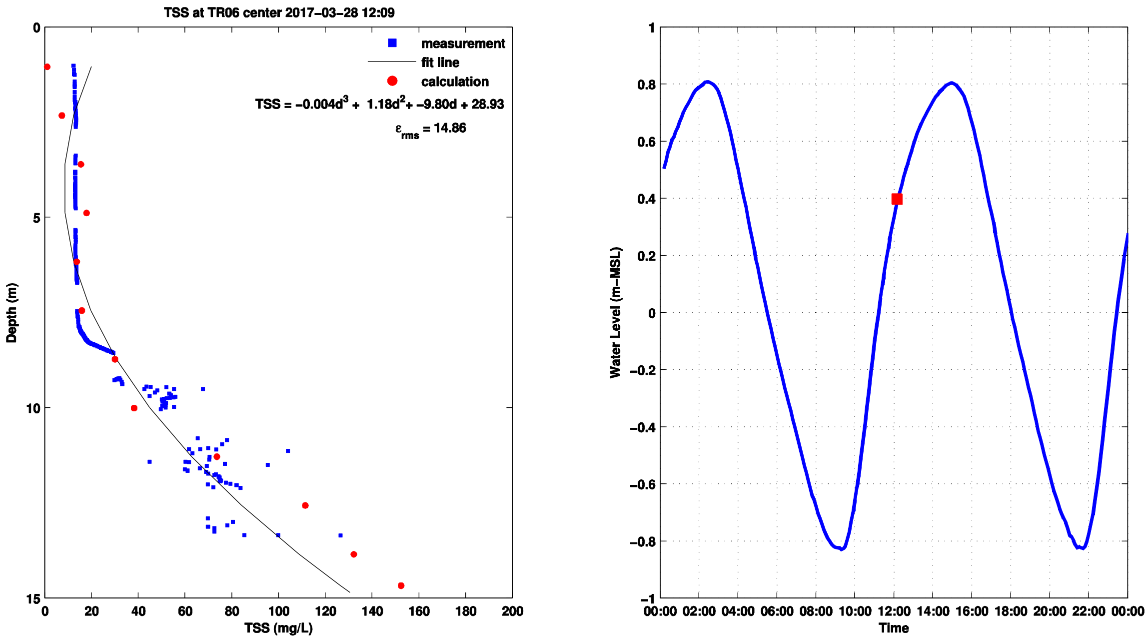

Figure 4-61: TSS cast at center of TR06 during flood tide

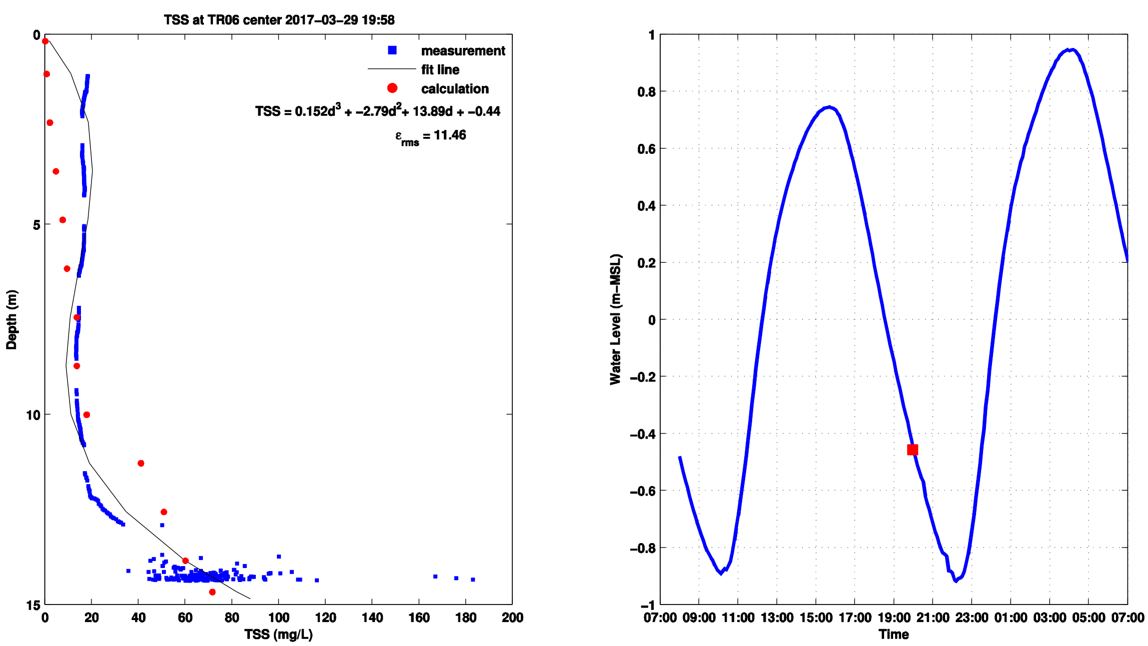

Figure 4-62: TSS cast at center of TR06 during ebb tide

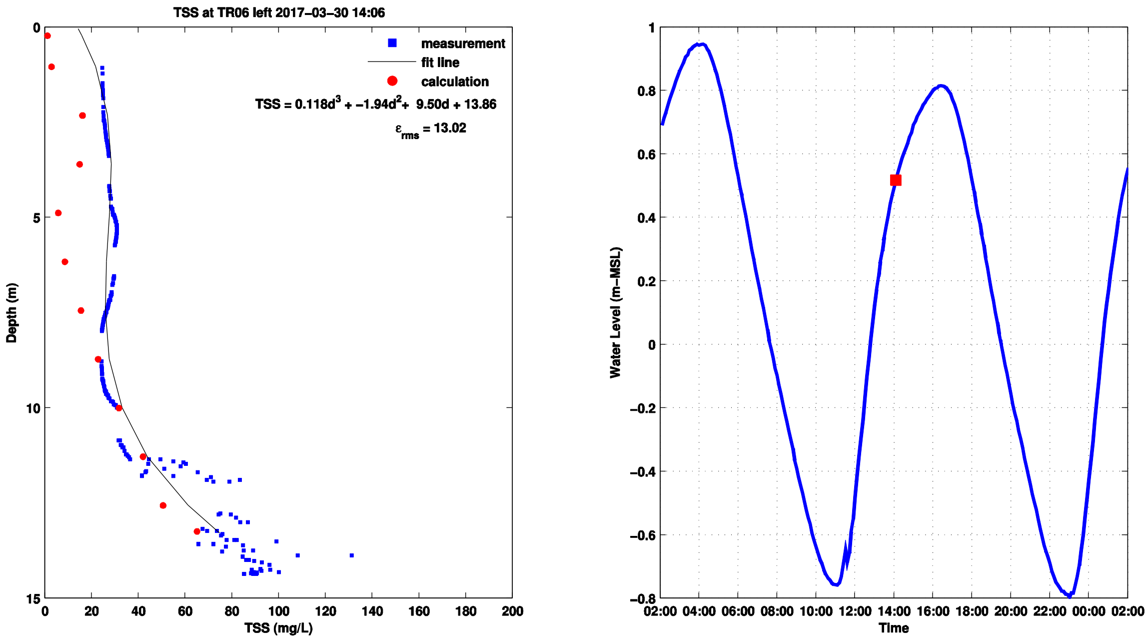

Figure 4-63: TSS cast at left side of TR06 during flood tide

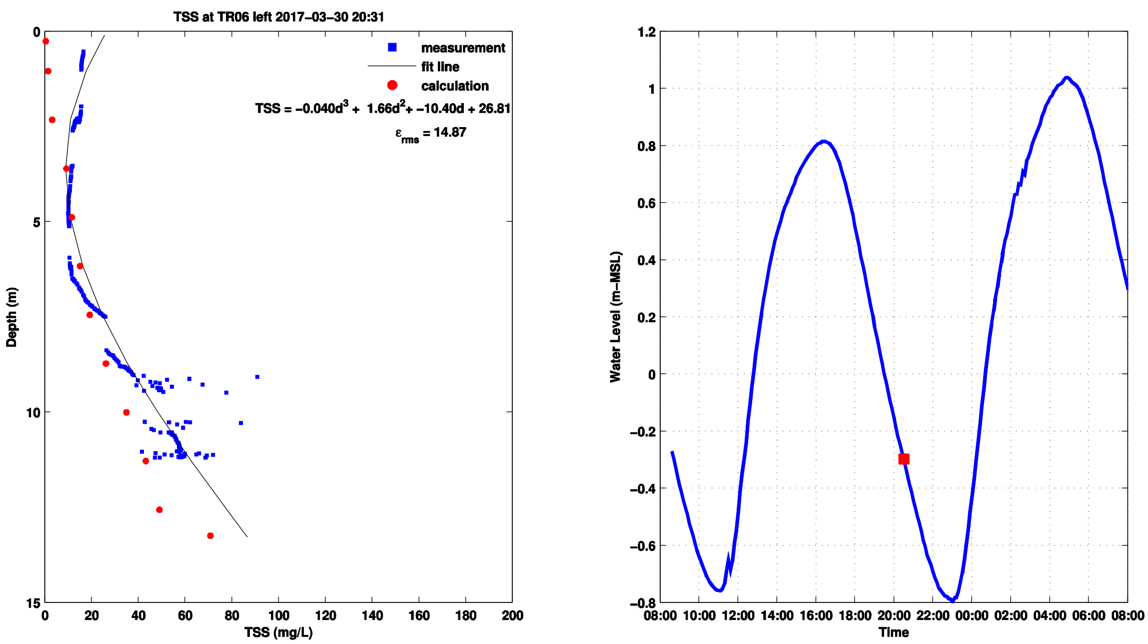

Figure 4-64: TSS cast at left side of TR06 during ebb tide

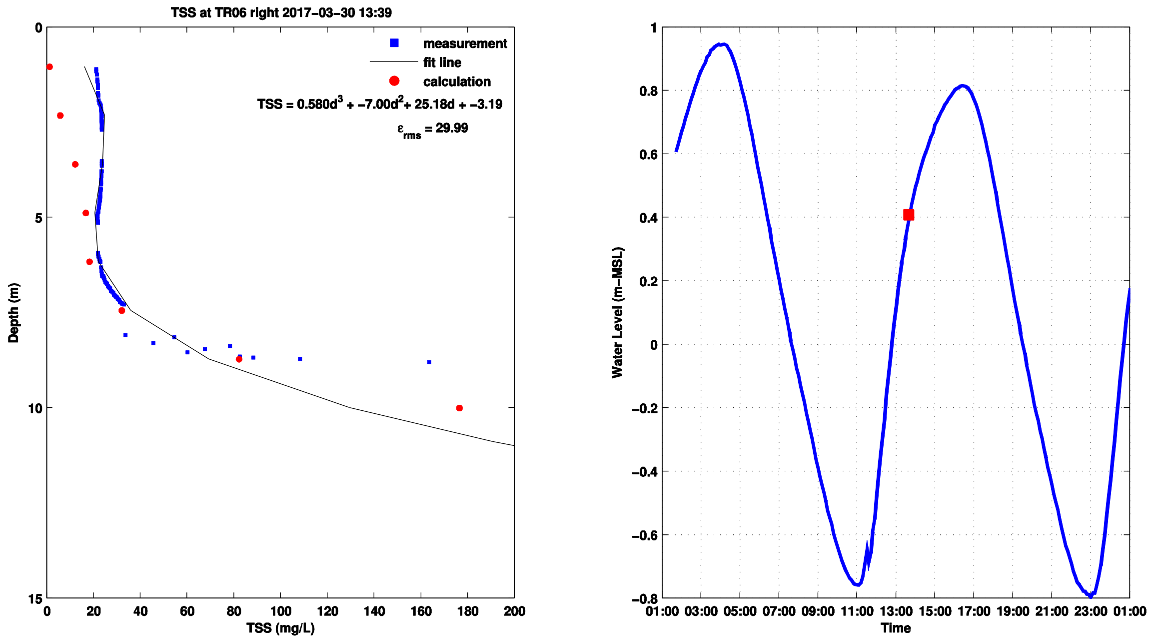

Figure 4-65: TSS cast at right side of TR06 during flood tide

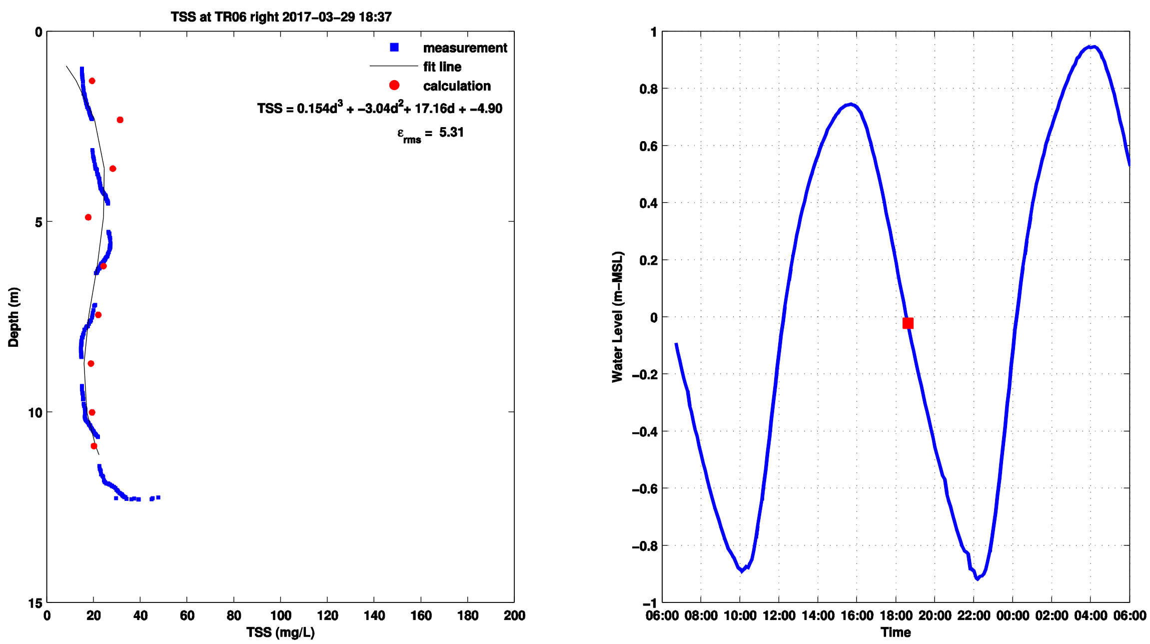

Figure 4-66: TSS cast at right side of TR06 during ebb tide

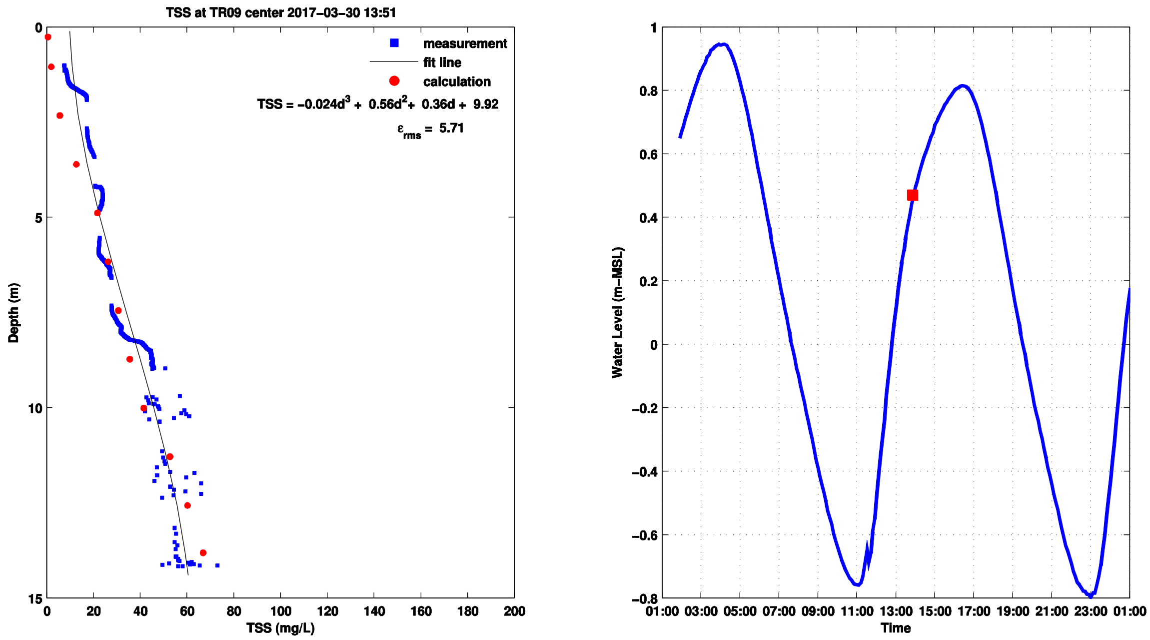

Figure 4-67: TSS cast at center of TR09 during flood tide

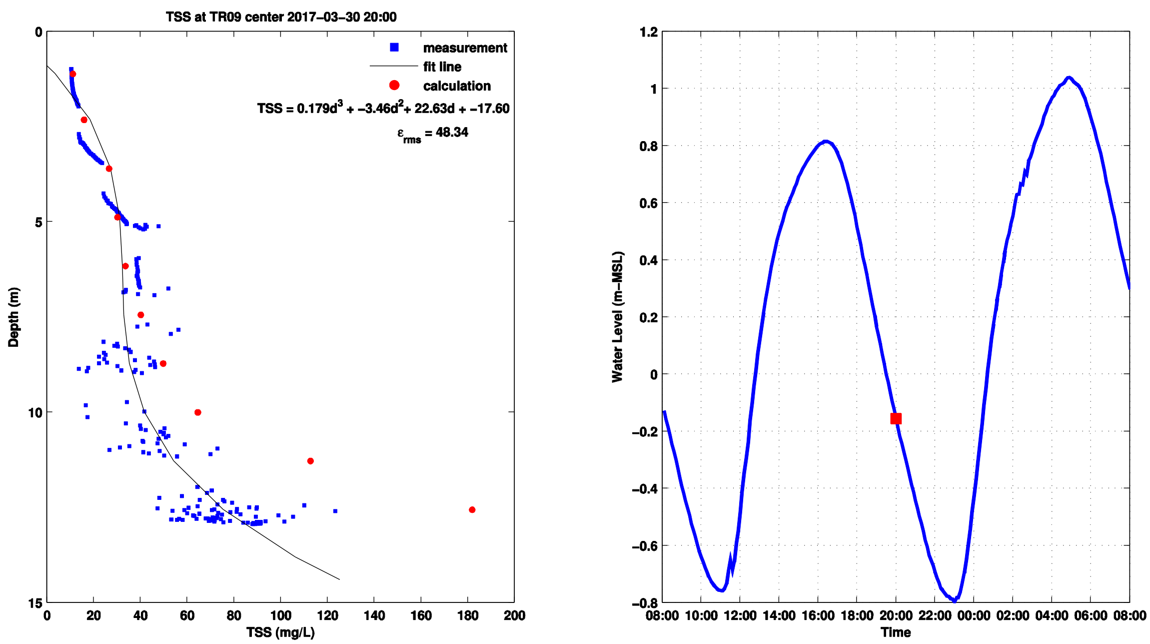

Figure 4-68: TSS cast at center of TR09 during ebb tide

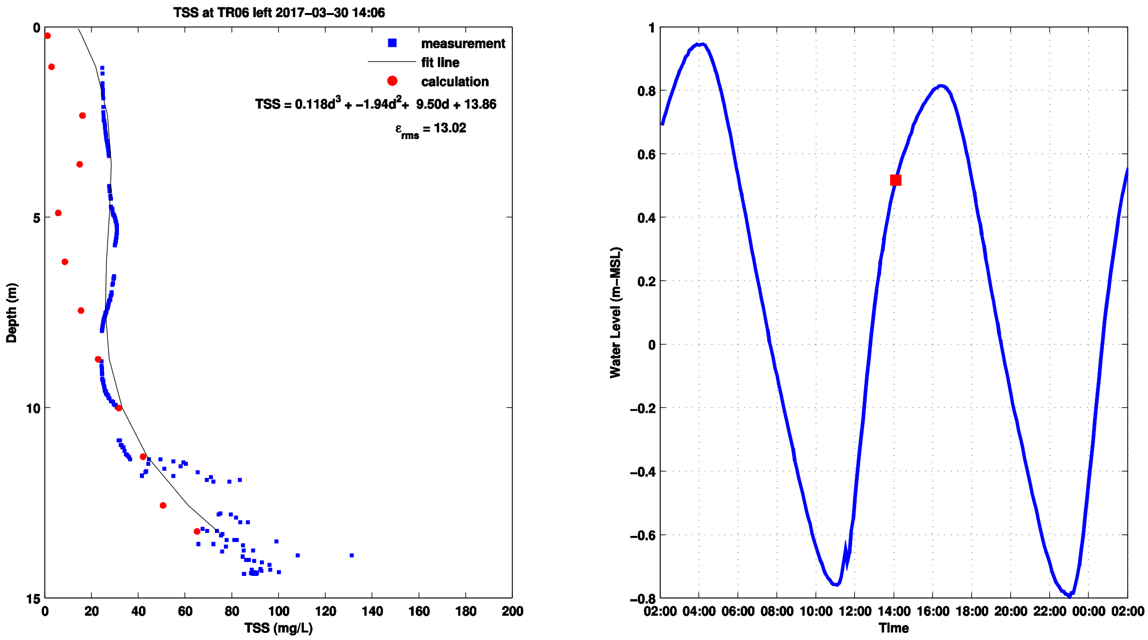

Figure 4-69: TSS cast at left side of TR09 during flood tide

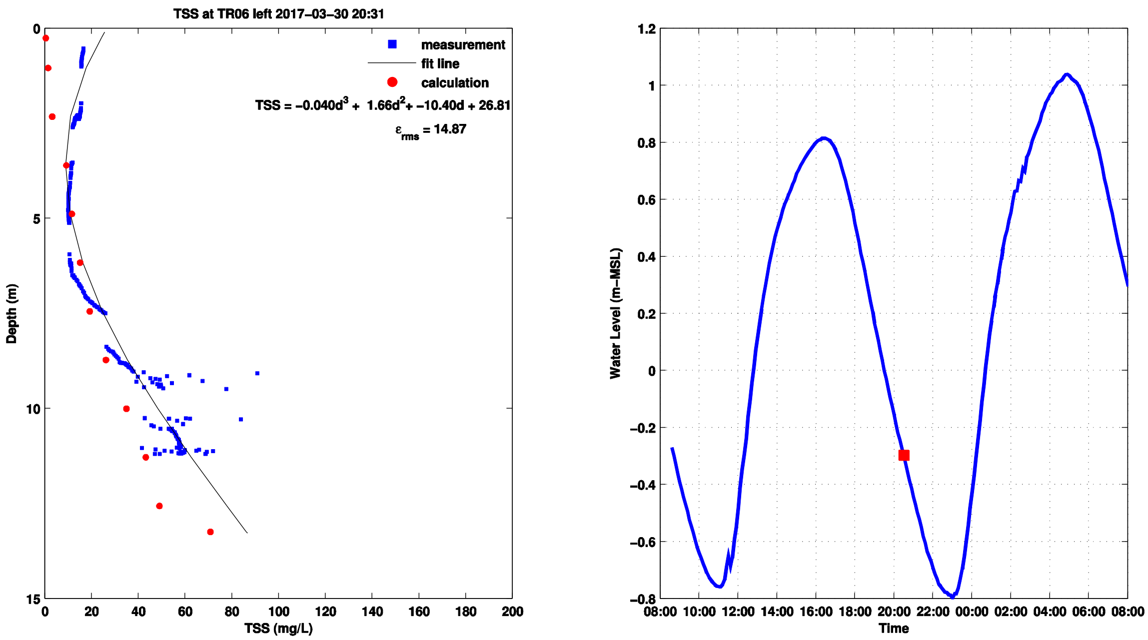

Figure 4-70: TSS cast at left side of TR09 during ebb tide

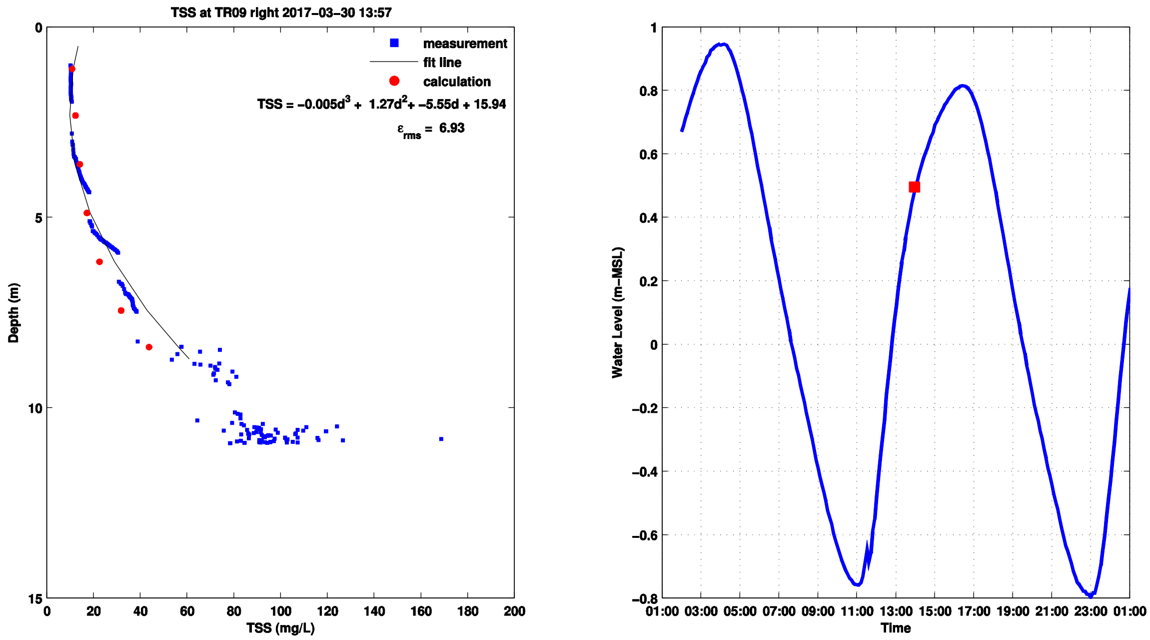

Figure 4-71: TSS cast at right side of TR09 during flood tide

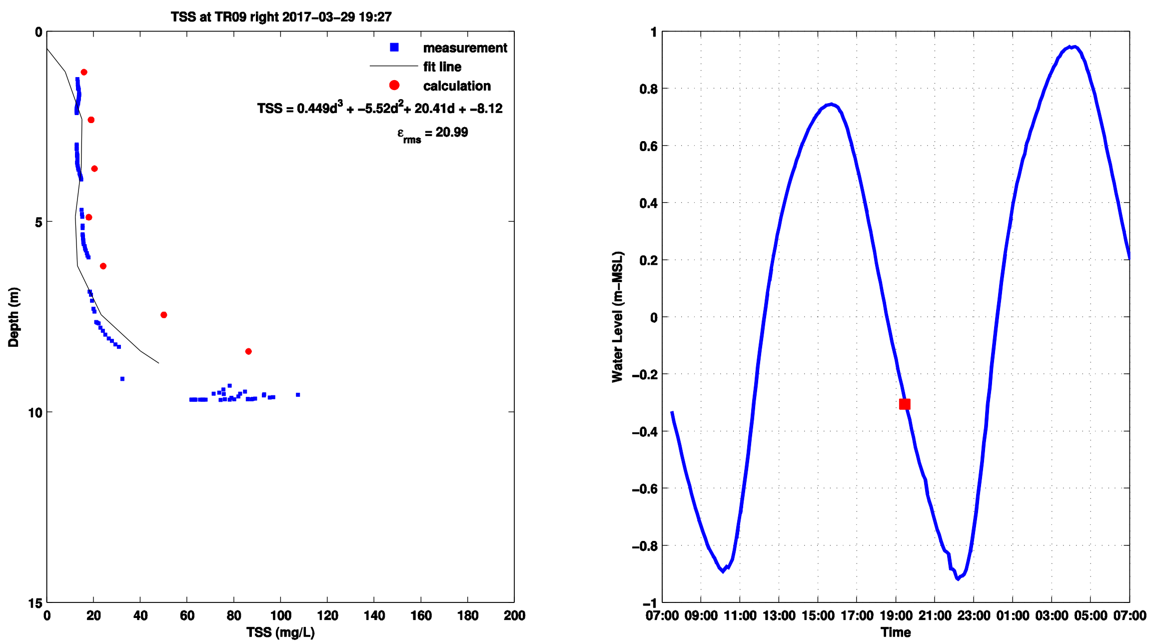

Figure 4-72: TSS cast at right side of TR09 during ebb tide

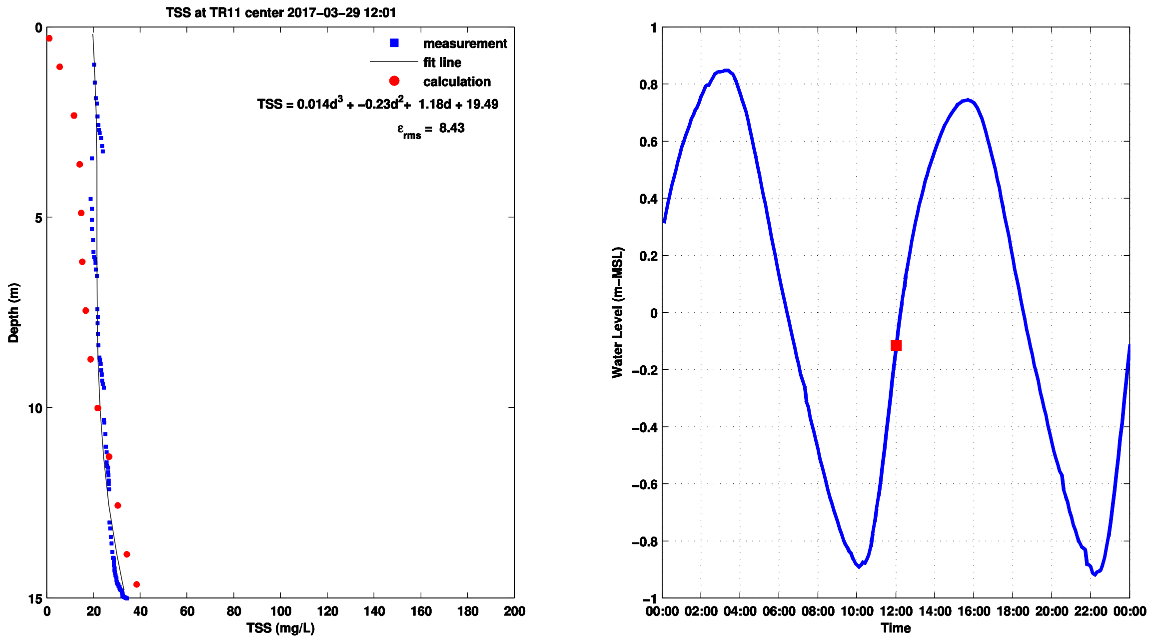

Figure 4-73: TSS cast at center of TR11 during flood tide

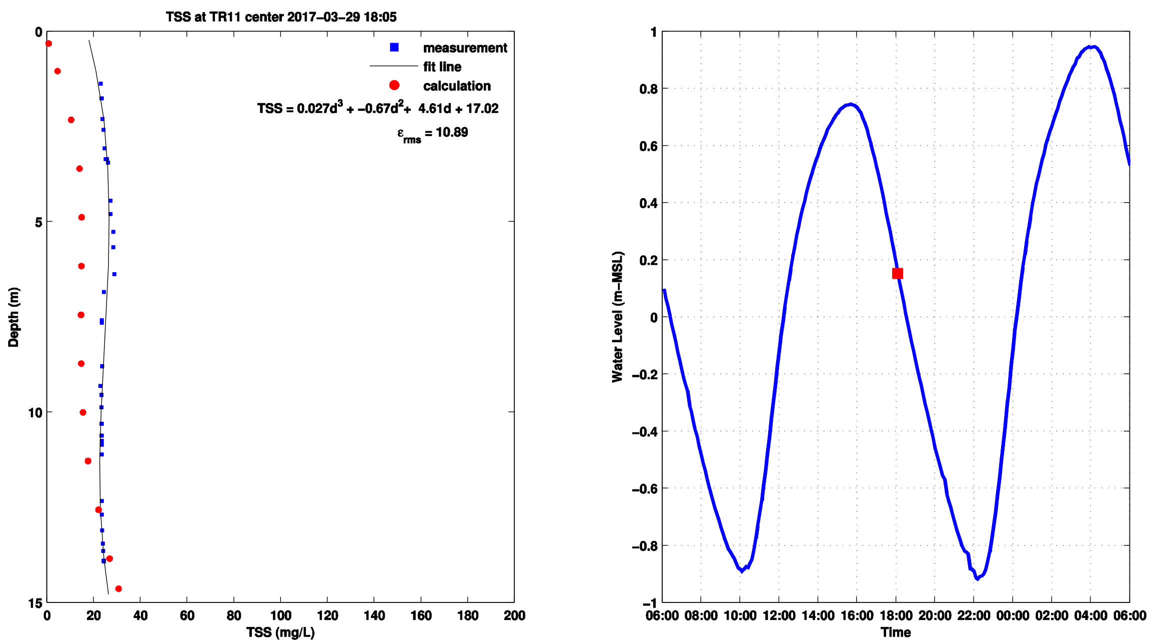

Figure 4-74: TSS cast at center of TR11 during ebb tide

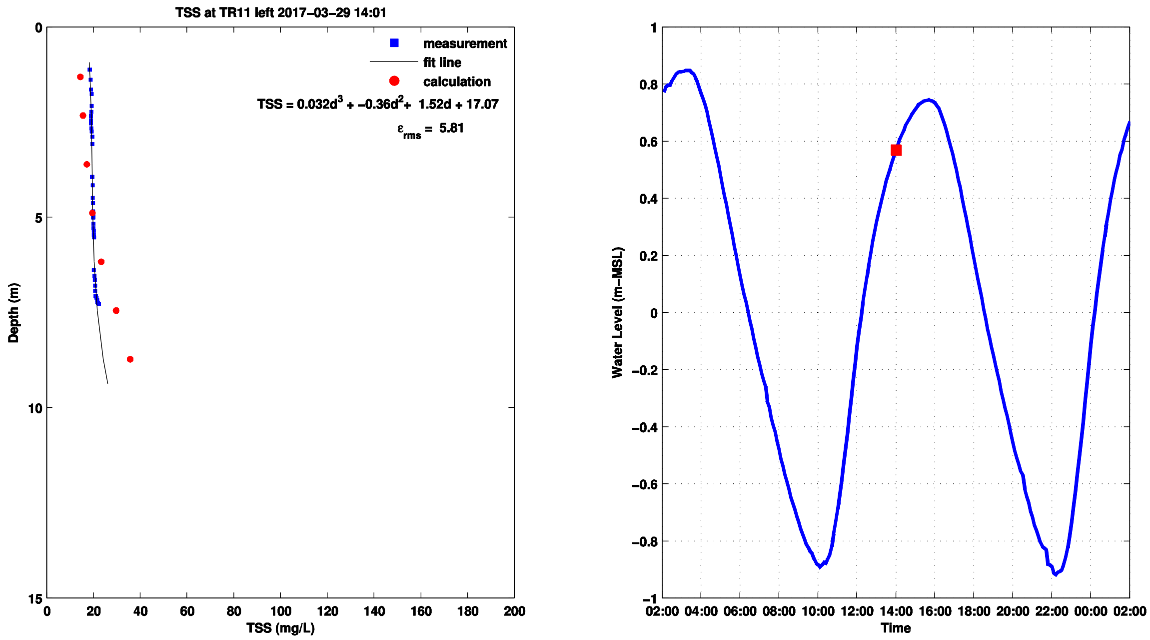

Figure 4-75: TSS cast at left side of TR11 during end of flood tide

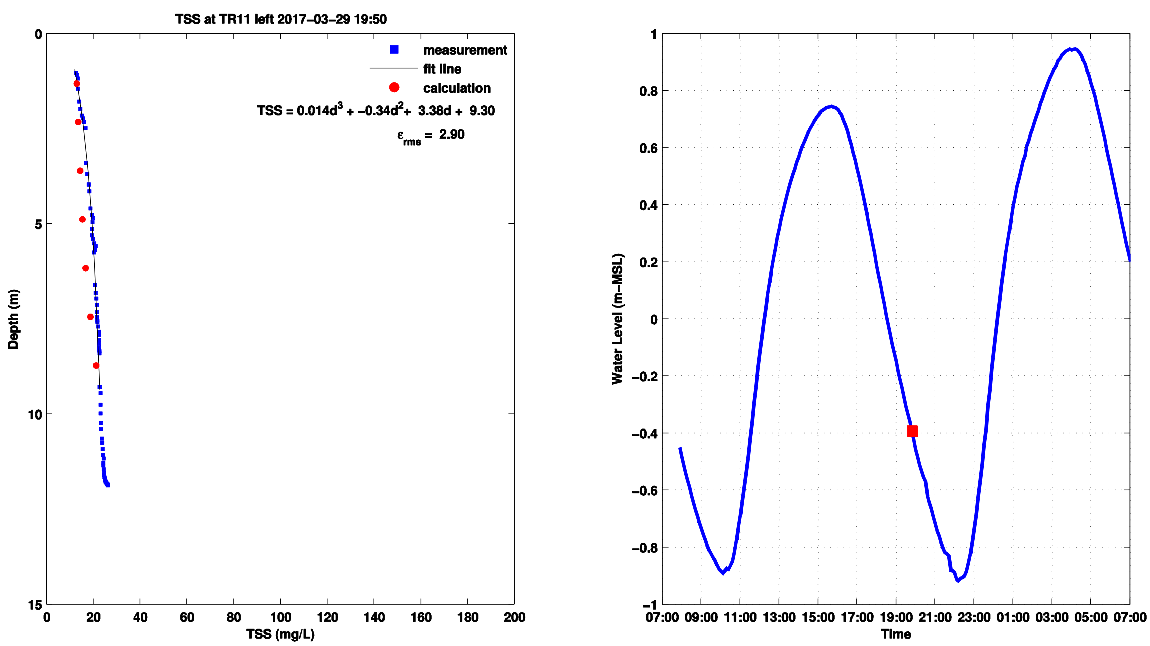

Figure 4-76: TSS cast at left side of TR11 during ebb tide

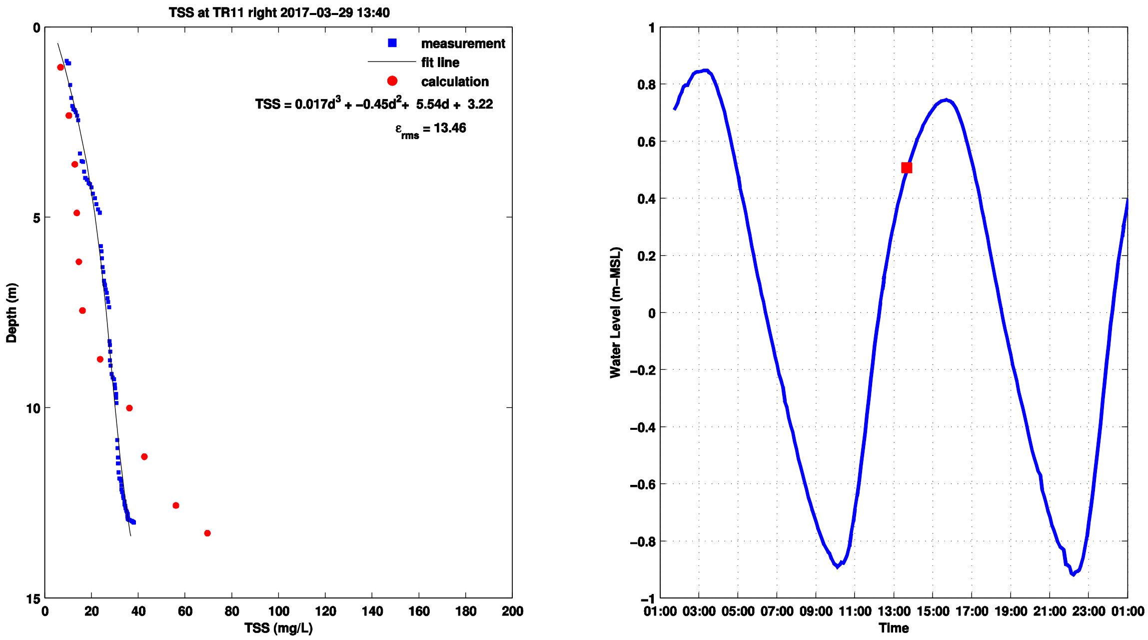

Figure 4-77: TSS cast at right side of TR11 during end of flood tide

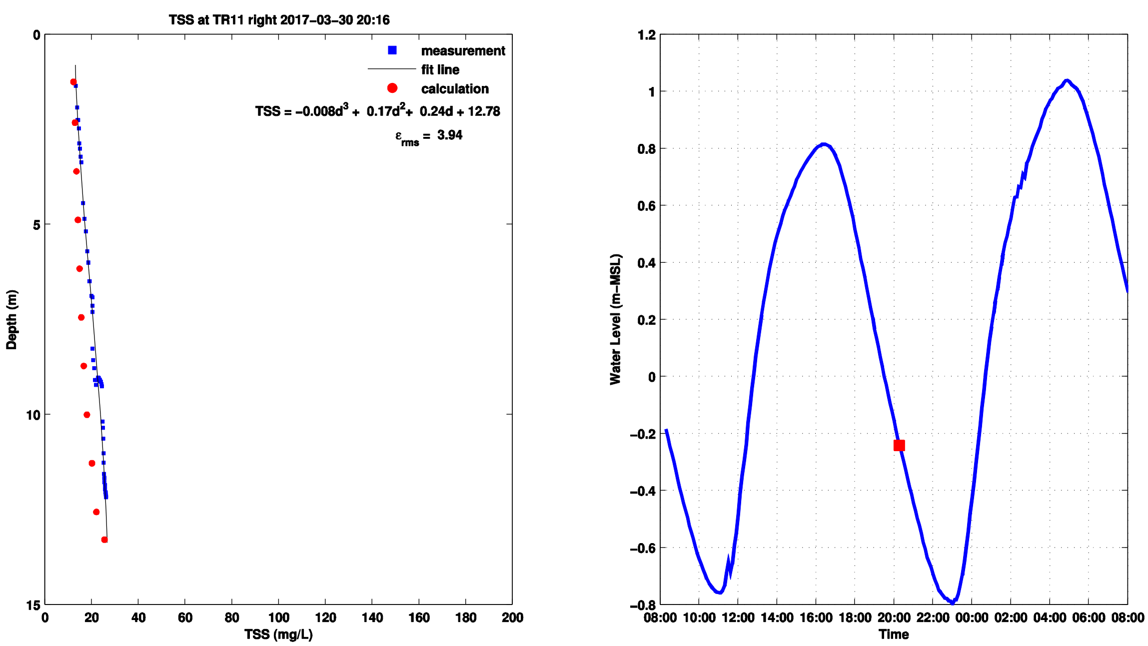

Figure 4-78: TSS cast at right side of TR11 during ebb tide

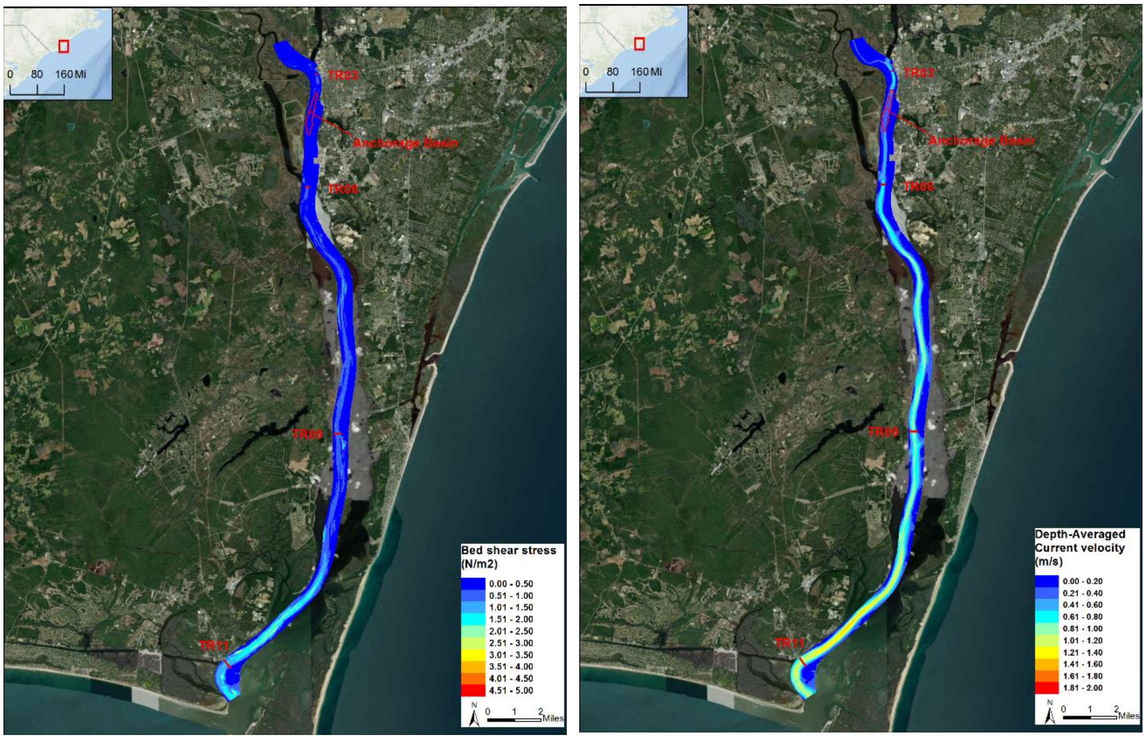

Figure 4-79: Bed shear stress and depth-averaged velocity during neap tide — flood

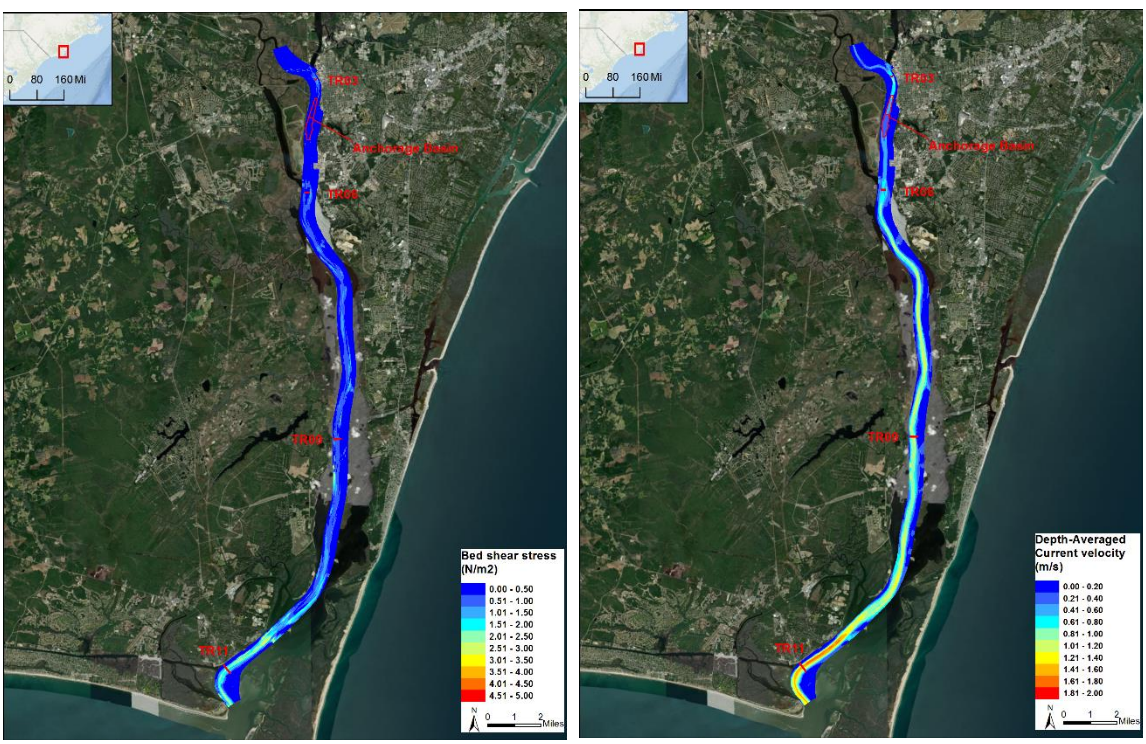

Figure 4-80: Bed shear stress and depth-averaged velocity during neap tide — ebb

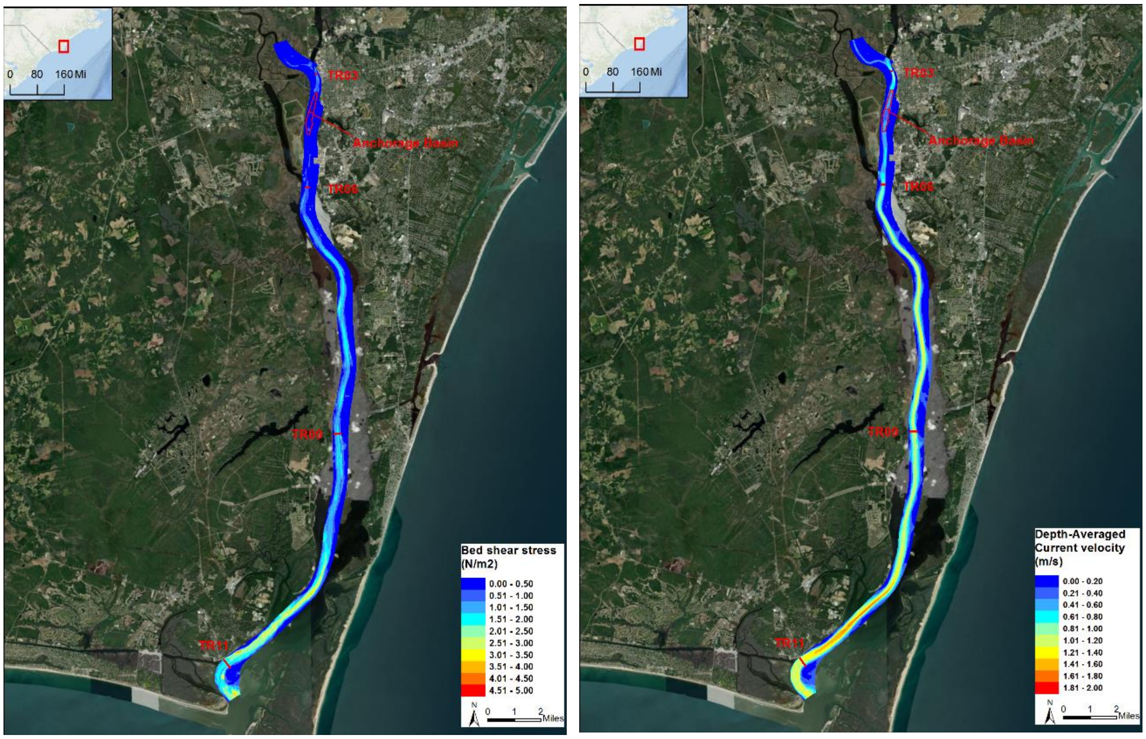

Figure 4-81: Bed shear stress and depth-averaged velocity during spring tide — flood

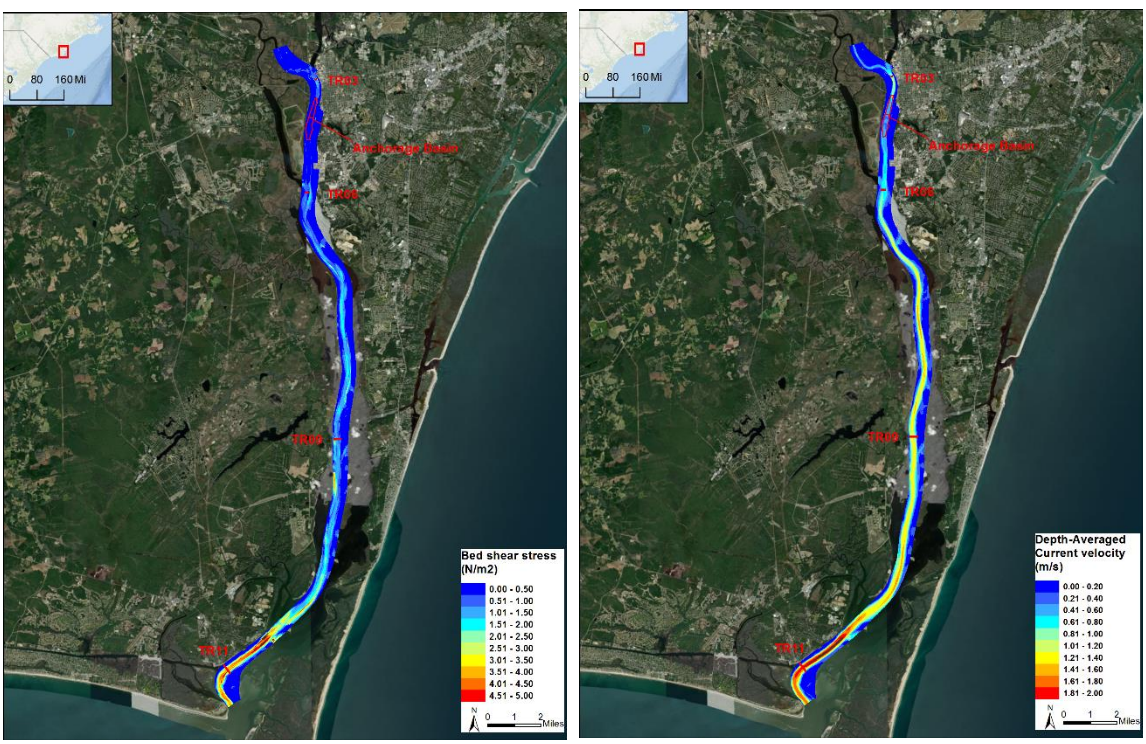

Figure 4-82: Bed shear stress and depth-averaged velocity during spring tide — ebb

4.4.3.2. Calibration of Shoaling at the Anchorage Basin

The time frame of the shoaling rate calibration is from March 24, 2017 13:00:00 to April 9, 2017 01:00:00. The total time frame includes 0.5 days spin-up interval before morphological changes and 15 days of morphological changes. Water levels during the simulation time frame are shown in Figure 4-83. This simulation period is selected to represent the typical spring-neap tide and the reason for using just half of the spring-neap tide cycle (15 days) is to save the simulation time.

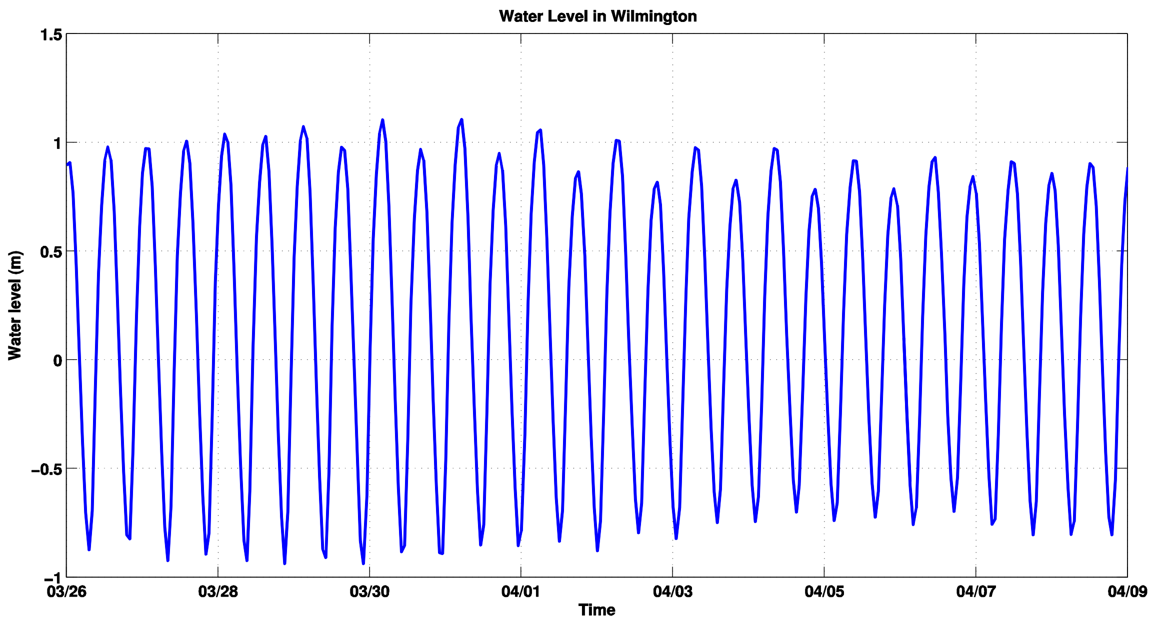

Figure 4-83: Water level in Wilmington during shoaling rate calibration

In order to simulate the annual shoaling rate in the Anchorage Basin, four flow scenarios (Table 4-8) were used to represent the upstream flow conditions during a year and assuming the half spring-neap tide cycle is representative of the overall tides in a year. Based on the percent of exceedance at the USGS stations, upstream discharges (Q) were divided into four categories — Low Flow, Medium Flow, High Flow and Extremely High Flow (Figure 4-84, Figure 4-85 and Figure 4-86). Correlations between discharge and TSS were analyzed by using discharge data from USGS stations (Table 4-6) and TSS data from STORET stations (Table 4-7), and the location map of these stations is shown in Figure 4-58. The measurement frequency of TSS data from the three STORET stations is about once per month from 2004 to 2014, and the corresponding Q was found for each TSS measurement to analyze the correlations. From Figure 4-87, Figure 4-88 and Figure 4-89, it can be seen that in BR and NECFR, there are no obvious correlations between Q and for TSS in CFR there is a linear correlation between Q and TSS to some extent. As a result, the regression equation for calculating TSS values from Q values was used only at CFR. In BR and NECFR, an estimation was made for different flow conditions (Table 4-8).

Table 4-7: STORET station information

Station	Period of Observations	Frequency of Observations
B8360000	2004-2014	Once per Month
B9000000	2004-2014	Once per Month
B9580000	2004-2014	Once per Month

Table 4-8: Upstream boundary conditions for annual shoaling rate calibration

Exceedance	CFR BC Q (m^3/s)	TSS (mg/L)	BR BC Q (m3/s)	TSS (mg/L)	NECFR BC Q (m^3/s)	TSS (mg/L)
85%	28	6	7	2	5	2
55%	54	9	20	2	20	2
25%	151	19	47	3	45	4
5%	436	48	111	4	144	6

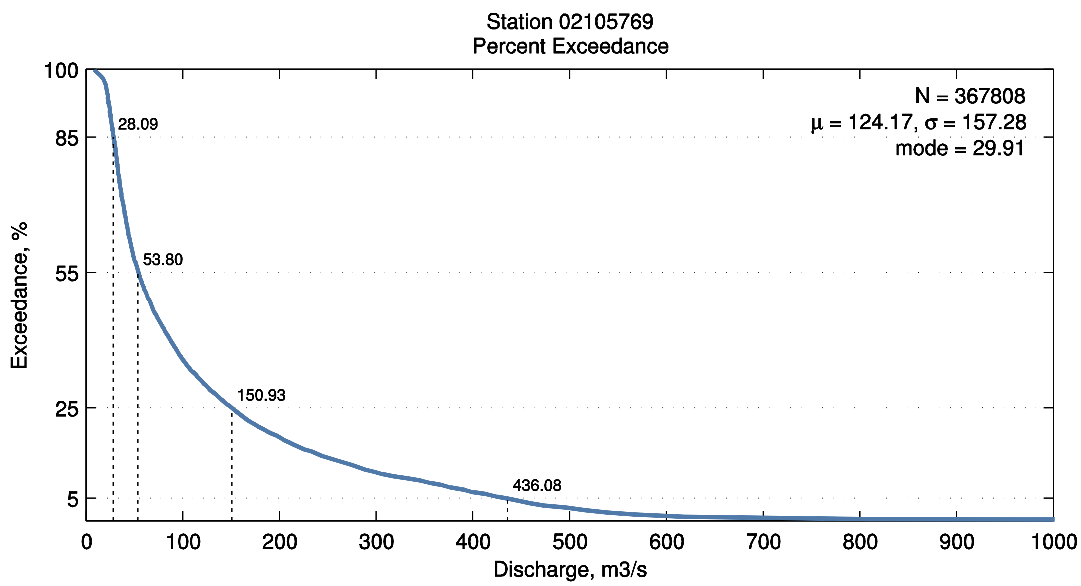

Figure 4-84: Percent exceedance of river discharge data at Station 0210579 in CFR

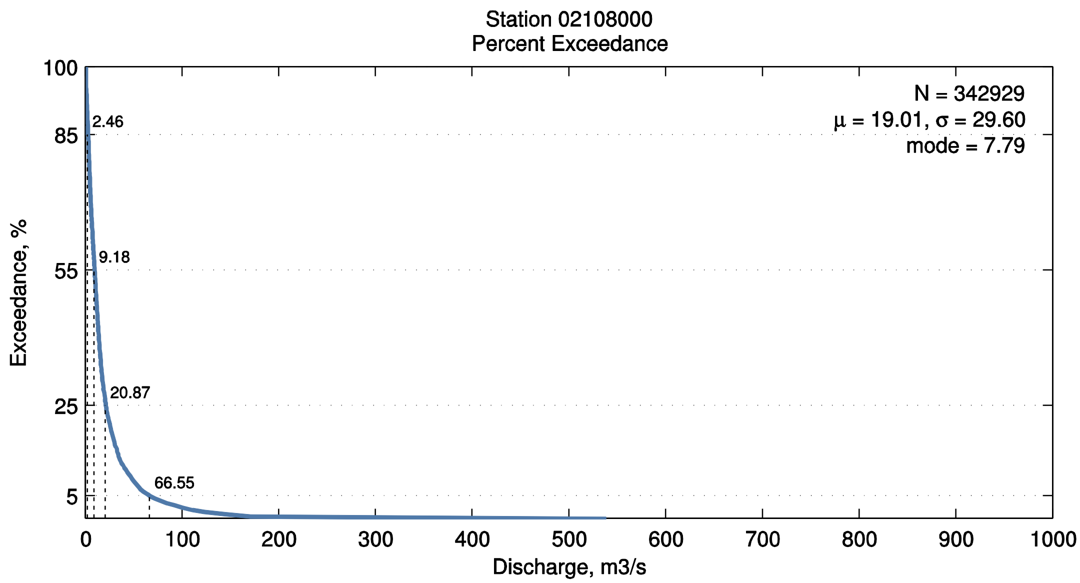

Figure 4-85: Percent exceedance of river discharge data at Station 02108000 in BR

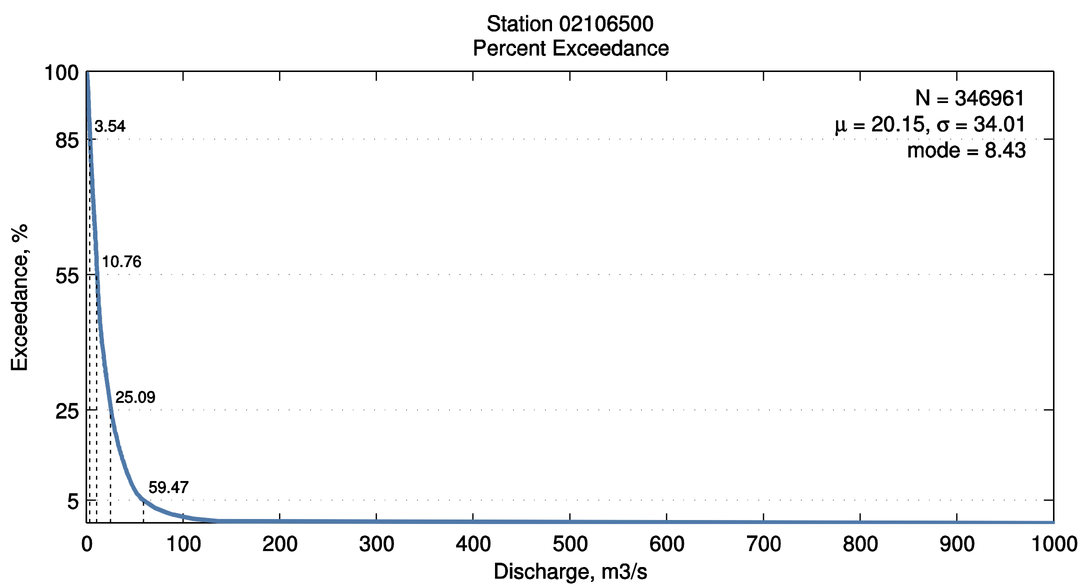

Figure 4-86: Percent exceedance of river discharge data at Station 02106500 in NECFR

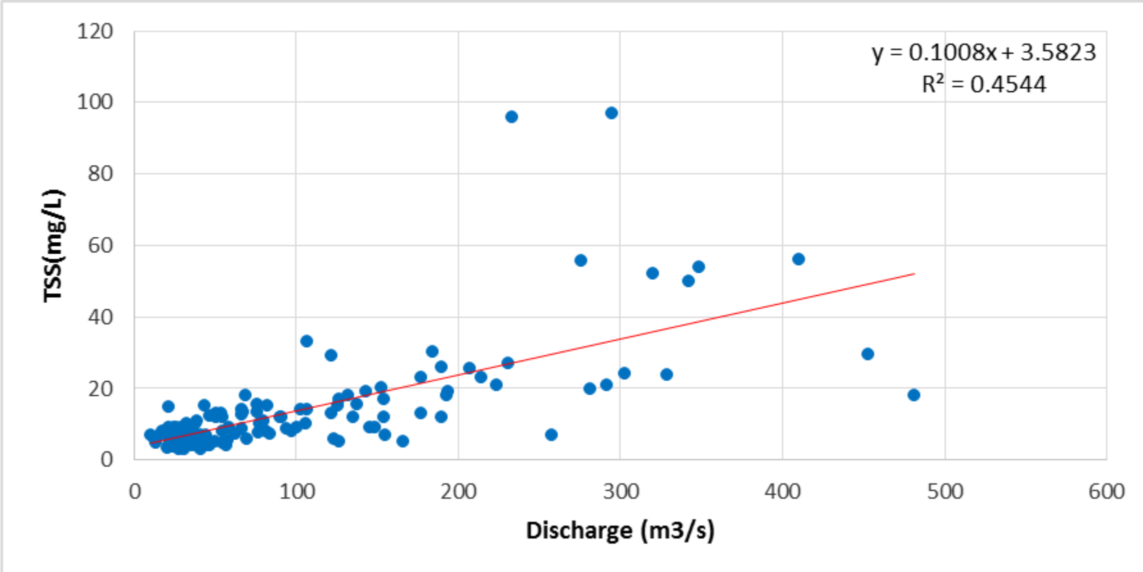

Figure 4-87: Q-TSS relationship at CFR (Station B8360000)

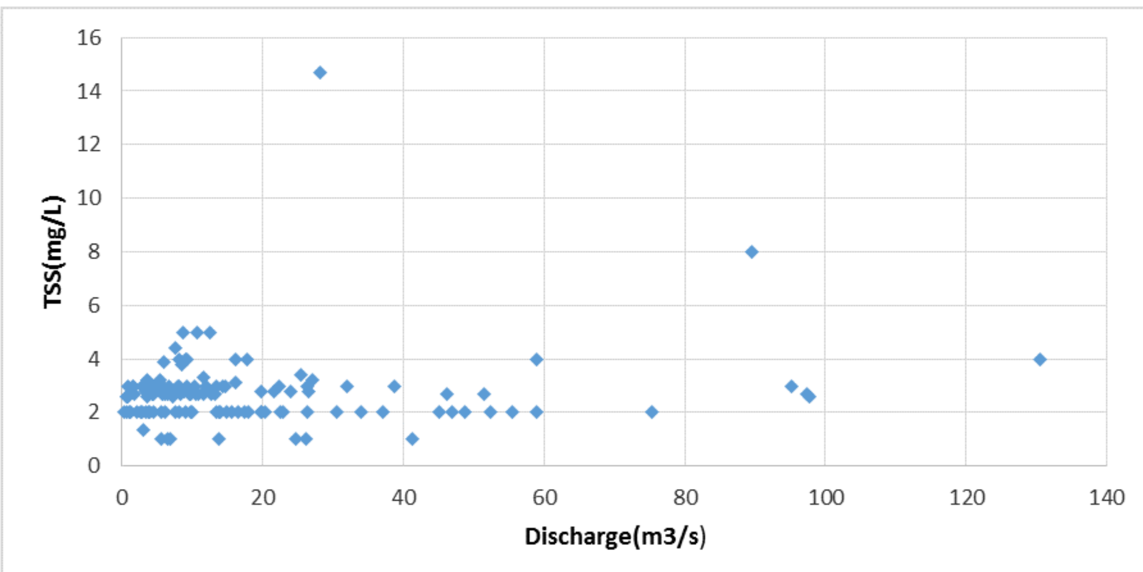

Figure 4-88: Q-TSS relationship at BR (Station B9000000)

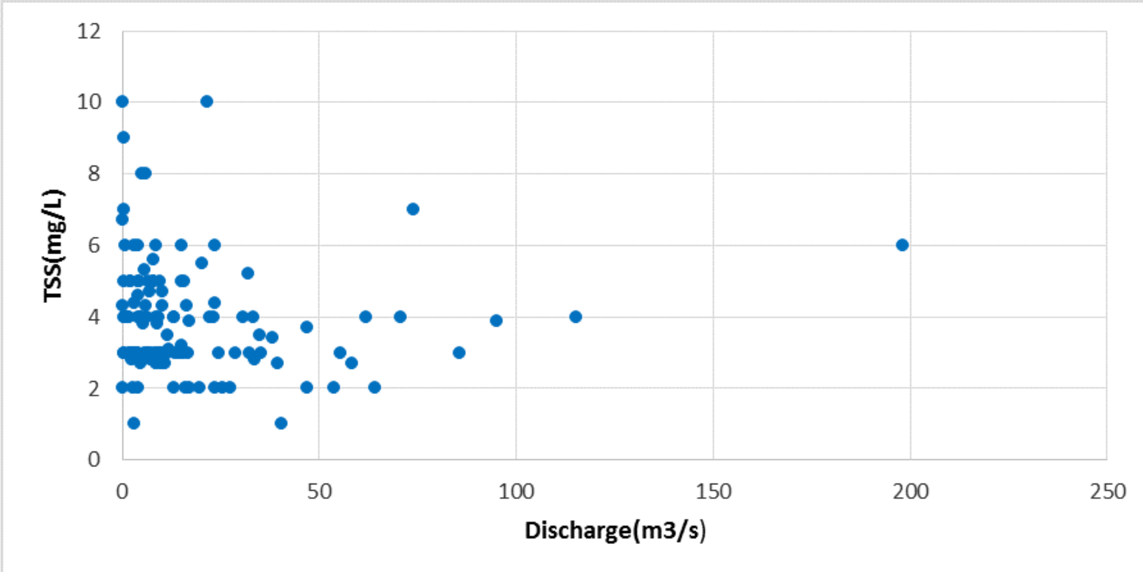

Figure 4-89: Q-TSS relationship at NECFR (Station B9580000)

The four simulation cases developed in this study are listed in Table 4-9. For example, the flows at 85% exceedance flow at each upstream boundary was used as the Low Flow case and represents the flow between 100% exceedance and 70% exceedance. The same approach was applied to Medium Flow (55% represents flow between 70% exceedance and 40% exceedance), High Flow (25% represents flow between 40% exceedance and 10% exceedance) and Extremely High Flow (5% represents flow between 10% exceedance and 0% exceedance). Among those four cases, Low, Medium and High Flow occur for 30% of the time per year, and Extremely High Flow occurs for 10% of the time per year. When calculating the morphological change, a Morphological Factor (MorFac) was introduced to scale the sedimentation/erosion amounts based on the probability of occurrence per year. The implementation of the MorFac is achieved by simply multiplying the erosion and deposition fluxes from the bed to the flow and vice-versa by the MorFac, at each computational time-step. This allows accelerated bed-level changes to be incorporated dynamically into the hydrodynamic flow calculations (WL | Delft Hydraulics, 2014). For example, the Low Flow case has a 0.3 probability per year. MorFac then equals 365×0.3/15 = 7.30, where 365 are the total days per year; 0.3 is the probability of occurrence and 15 is the number of days of morphological change in the actual simulation.

Table 4-9: Four cases simulated for annual shoaling rate calibration

Cases	Flow Exceedance	Probability/year	MorFac
Low Flow	85%	0.3	7.30
Medium Flow	55%	0.3	7.30
High Flow	25%	0.3	7.30
Extremely High Flow	5%	0.1	2.43

The annual shoaling rate is calculated based on the four flow cases inside the Anchorage Basin (Figure 4-90 dash line). As shown in Figure 4-90, the initial bed level inside the basin is about 40-50 ft deep relative to NAVD88, with shallower areas in the upstream part and deeper areas inside the downstream turning basin.

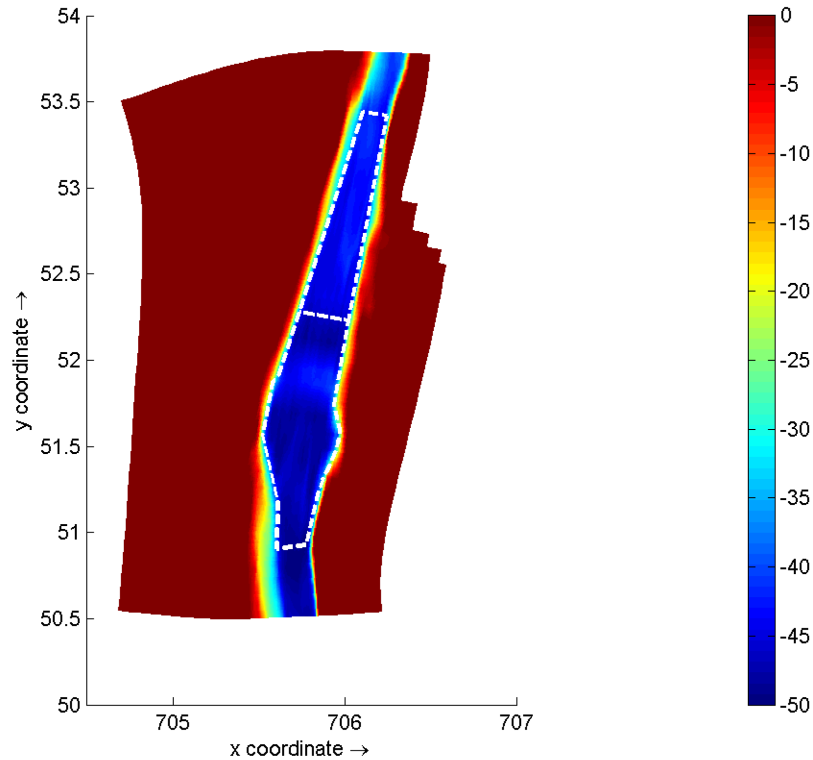

Figure 4-90: Initial bed level inside Anchorage Basin (ft-NAVD88)

A cumulative erosion and sedimentation map for the Anchorage Basin for Low Flow is shown in Figure 4-91. It can be seen from Figure 4-91 that deposition occurred inside the upper Anchorage Basin with a maximum value of 2 ft/yr while deeper areas such as the turning basin had greater amounts of sedimentation. Because the erosion and sedimentation patterns between different flow conditions are very small, except for the Extremely High Flow condition, only the differences in erosion and sedimentation as compared to the Low Flow condition are shown in Figure 4-92 and Figure 4-93 for the Medium Flow and the High Flow conditions respectively. Comparing the Low Flow to the Medium Flow, the morphological change is almost the same with about 0.2 ft more sedimentation along the banks for Medium Flow. Due to the greater discharge and sediment load during High Flow, the morphological change between Low Flow and High Flow shows 0.4 – 0.6 ft more sedimentation along the banks for High Flow.

The Extremely High Flow condition only has a 10% probability of occurrence compared to 30% for the other three flow conditions, so in order to make a graphic comparison, the erosion/sedimentation values for the Extremely High Flow condition are multiplied by three for illustration purposes as shown in Figure 4-94. While there is more sedimentation inside the turning basin, the upstream part of the Anchorage Basin experiences some erosion. This is because the Extremely High Flow has a discharge of 436 m^3/s at CFR upstream boundary (Table 4-8), which is comparable to the total discharge in the order of 1,000 m^3/s near the Anchorage Basin, while the other three flow conditions have relatively small discharges at CFR upstream boundary compared to the tidal flow. Thus, during ebb tide, the combined effect of a very high fresh water discharge (Extremely High Flow) and the discharge during ebb tide will re-suspend more sediment at the bottom and cause more erosion at the upstream part of the Anchorage Basin. This phenomena can be seen from the velocity time series shown in Figure 4-95, where the current velocity in the channel within the Anchorage Basin for the Extremely High Flow is more than 1 m/s, which is greater than the other three flow conditions.

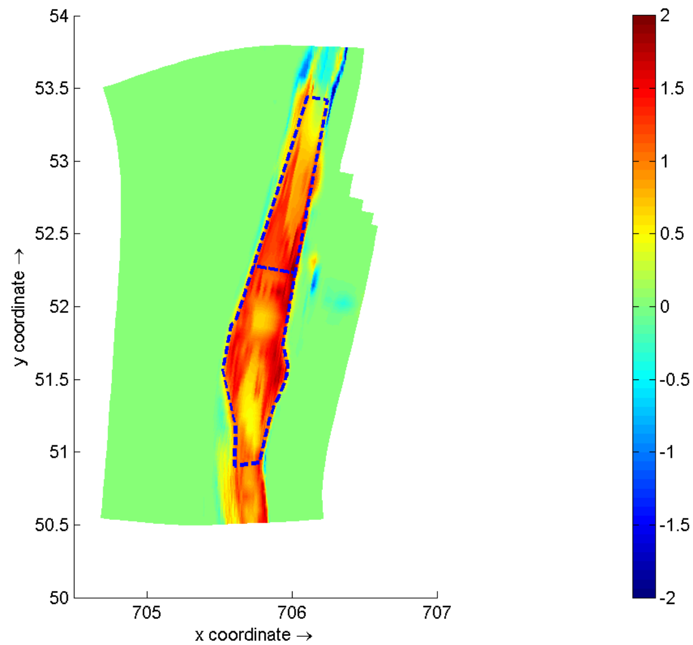

Figure 4-91: Cumulative erosion/sedimentation for Low Flow (ft/yr)

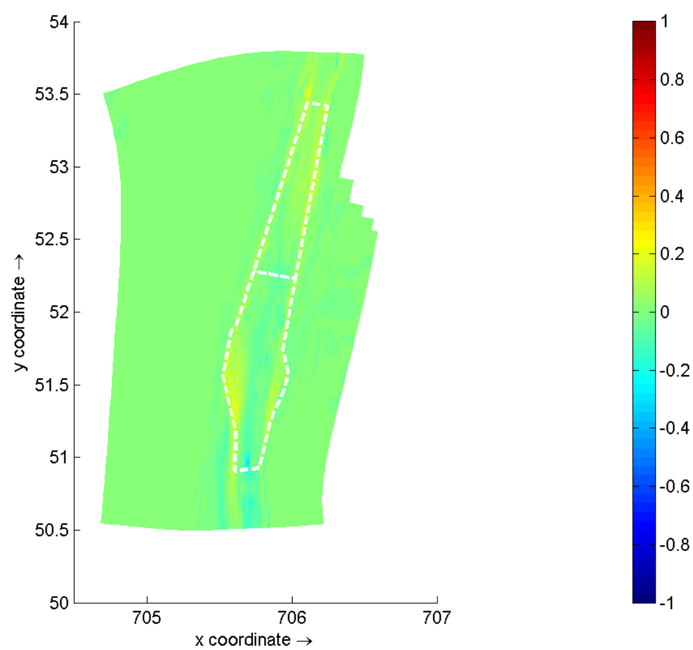

Figure 4-92: Erosion/sedimentation differences between Medium Flow and Low Flow (Medium minus Low) (ft/yr)

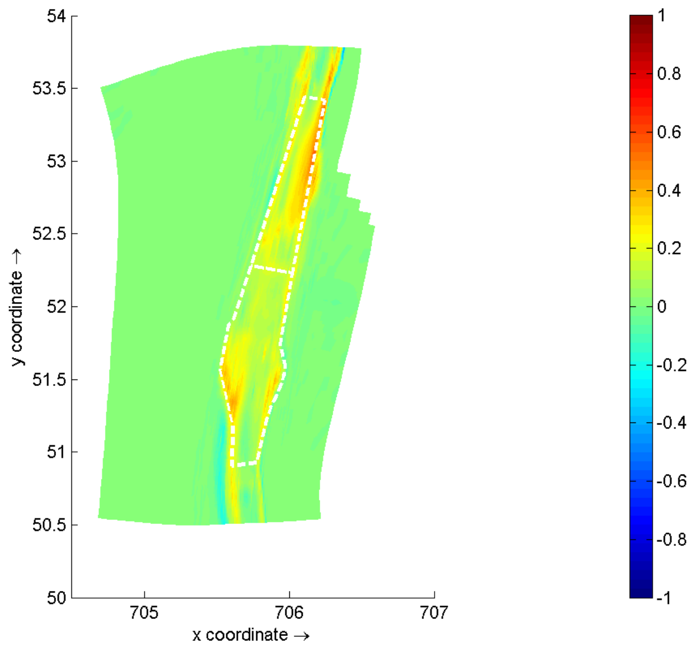

Figure 4-93: Erosion/sedimentation differences between High Flow and Low Flow (High minus Low) (ft/yr)

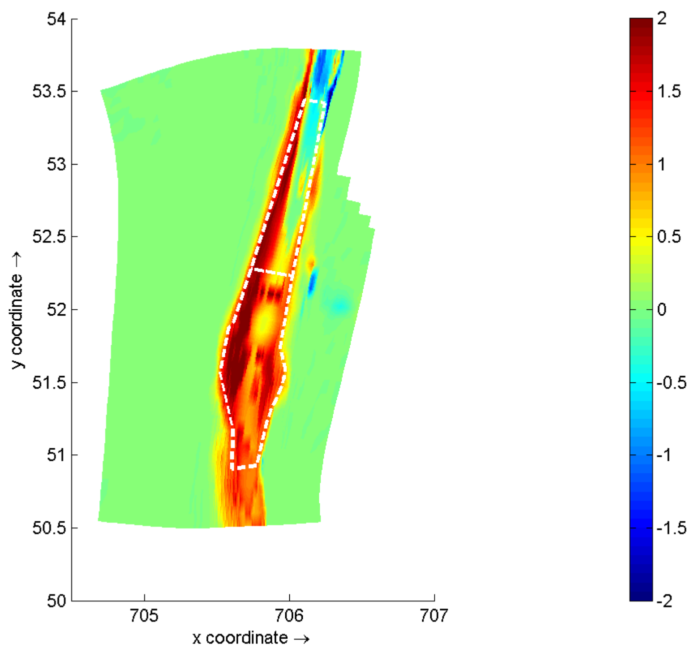

Figure 4-94: Cumulative erosion/sedimentation (ft/yr) for Extremely High Flow (Extremely High × 3)

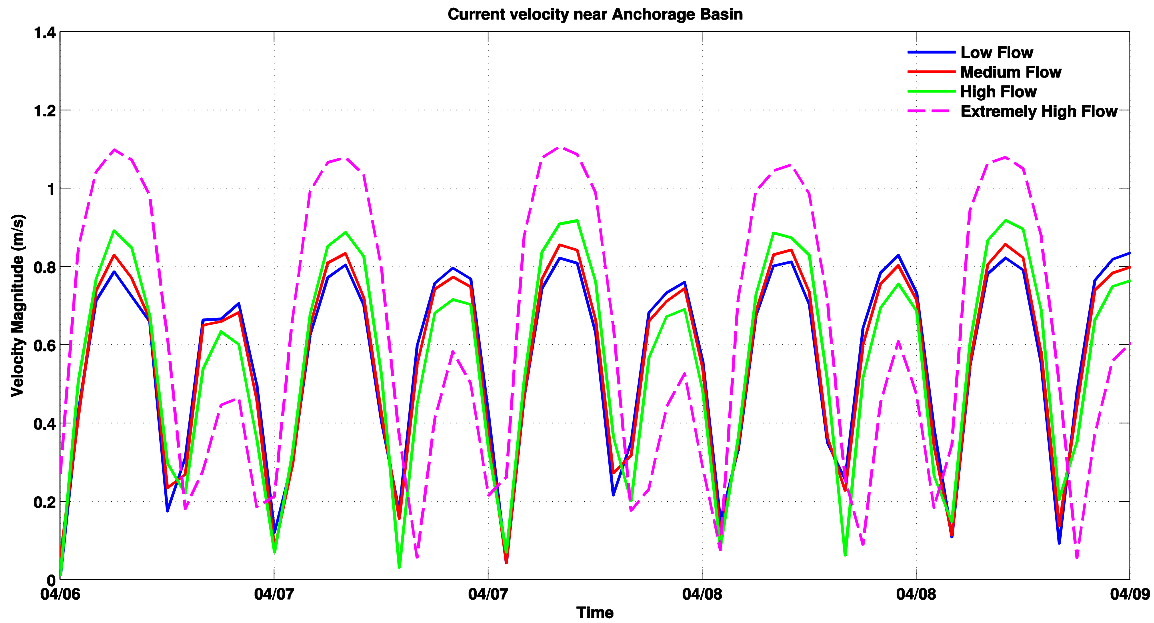

Figure 4-95: Current Velocity comparison in the Channel inside Anchorage Basin

The shoaling volume for each flow case were calculated inside the area outlined with the dash line shown in Figure 4-90, and the results are listed in Table 4-10. Due to increased discharges and sediment loads from the upstream rivers, the shoaling volumes increase except for the Extremely High Flow condition where the shoaling volume, times three for comparison to account for its duration, is close to that of the Medium Flow condition. This total predicted annual shoaling volume is a little more than 1 million cy which closely approximates the annual dredging volume of 1,156,694 cy/yr (USACE 2014).

Table 4-10: Shoaling volume for four flow cases

Cases	Volume (cy/yr)
Low Flow	291,000
Medium Flow	295,000
High Flow	337,000
Extremely High Flow	100,000
Total	**1,023,000**

4.4.4. Conclusion

The developed 3-D sediment transport model of cohesive sediments is well calibrated to reproduce variation of vertical concentration of the total suspended solids at selected locations and the annual shoaling rates in the Anchorage Basin. The computed TSS vertical profiles matched well with the measurements in different reaches of the channel for the majority of available locations with slightly under prediction at the bottom of the water column. The average root mean square (*RMS*) errors at TR06, TR09 and TR11 are 15 mg/L, 18 mg/L and 8 mg/L respectively. The model under predicted TSS at TR03 (upstream to Wilmington) due to local effects such as re-suspension and ship passages prior to measurements which were not resolved in the model and the average *RMS* error is 35 mg/L. The model accurately predicts the annual sedimentation in the Anchorage Basin with the estimated shoaling volume within 12% of the measured volume which also validates the model independent from the TSS calibration efforts. Thus, the cohesive sediment transport developed in this study has the capacity to predict the morphological changes in Wilmington Harbor.

4.5. Water Quality

The module, DELWAQ, was selected to address water quality (Deltares, 2016; Deltares, 2018) and is discussed further in this section. Nineteen state variables are simulated in the water quality model including water temperature, TSS, various forms of nitrogen and phosphorus, carbon, BOD, Chl *a*, and DO. The performance of all of the state variables is important since they interact in a variety of ways. However, temperature and DO in the navigation channel are the most important for the purposes of the project.

4.5.1. Water Quality Modeling Framework

A previous water quality model of the lower Cape Fear River developed by Bowen et al. (2009) is based on the Environmental Fluid Dynamics Code (EFDC) model using the CE-QUAL-ICM option for water quality algorithms. The EFDC model's generalized framework showing 22 state variables and their relationships using the CE-QUAL-ICM option are shown in Figure 4-96. It is noted that under this option the sinks on dissolved oxygen (DO) are nitrification, algal respiration, mineralization of dissolved organic carbon (DOC), sediment oxygen demand (SOD), and oxidation of chemical oxygen demand (COD) that has been released from the benthic sediments. A benthic sediment diagenesis sub-model is available that accounts for accumulation of settled organic matter and its subsequent mineralization and burial and associated processes including SOD and fluxes of inorganic substances between the water column and benthic sediment pore water. It is also noted that the EFDC model tracks labile and refractory particulate organic carbon (C), nitrogen (N), and phosphorus (P), which hydrolyze into their dissolved organic forms, which are considered labile. The dissolved organic forms mineralize into the inorganic forms, with the exception of C since inorganic C is not included in this model. Total phosphate (PO4t) and available silica (SA) are partitioned into dissolved and particulate forms via equilibrium partitioning, thus, requiring only total concentrations for each of those state variables.

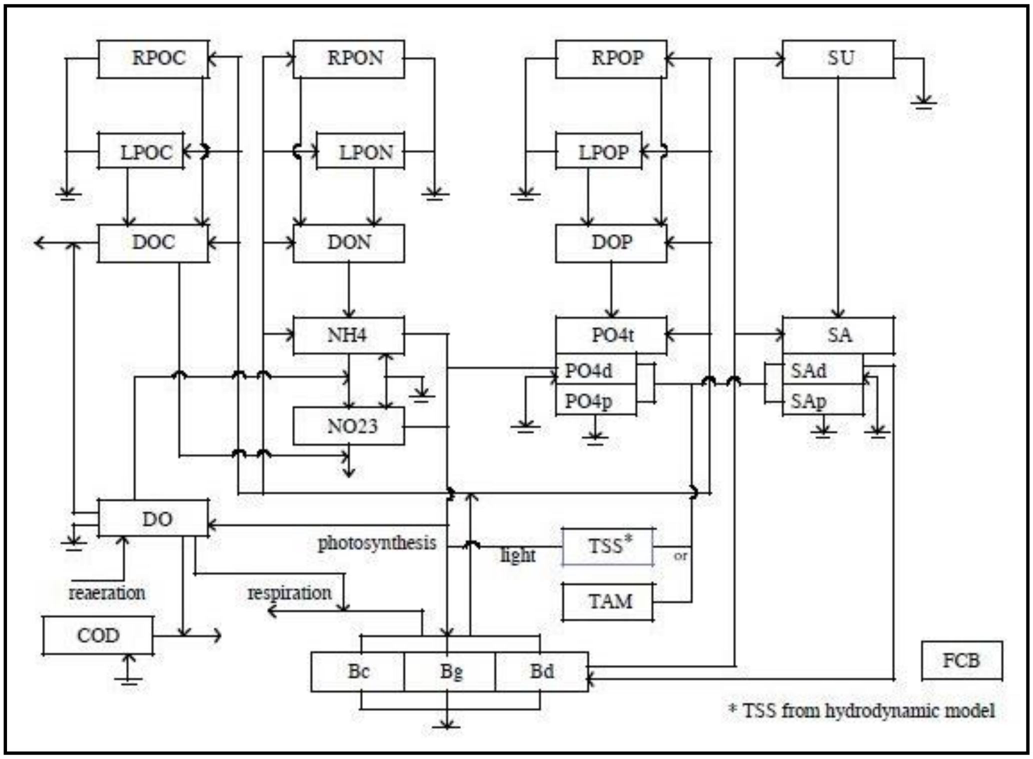

Figure 4-96: Water quality model state variables and their relationships for CE-QUAL-ICM option in the EFDC model (from Bowen et al., 2009)

The approach by Bowen et al. (2009) differed from the generalized EFDC framework shown in Figure 4-96 in a few areas. The benthic sediment diagenesis sub-model was not used, rather benthic sediment fluxes and SOD were prescribed. Thus, the state variable COD was not included. Temperature was modeled within the EFDC hydrodynamic model. The other 21 state variables shown were included in the EFDC water quality model. However, the refractory particulate organic variables, RPOC (refractory particulate organic carbon), RPON (refractory particulate organic N), and RPOP (refractory particulate organic phosphorus) were assumed to represent refractory dissolved organic matter by assigning zero settling rates for RPOC, RPON, and RPOP. Thus, only labile particulate organic matter was included, whereas two forms (labile and refractory) of dissolved organic matter were included. It appears that refractory dissolved organic matter in the Bowen et al. (2009) model mineralizes into labile dissolved organic matter including dissolved organic carbon (DOC), dissolved organic nitrogen (DON), and dissolved organic phosphorus (DOP) without any uptake of DO. The primary reason for using refractory particulate organic matter to represent refractory dissolved organic matter was due to the need to represent labile and refractory organic loadings from wastewater dischargers. These discharges included biochemical oxygen demand (BOD) data, some of which were studied in detail to define labile and refractory fractions and associated decay rates. BOD was not included in the Bowen et al. (2009) model, rather it was converted to the labile and refractory dissolved organic matter components noted above.

The Delft3D water quality model, DELWAQ, was selected for the present modeling of the lower Cape Fear River and Estuary. The primary period of interest for calibration of the model is late summer, when DO is lowest. A spring validation period is also implemented, as well as a year-long validation. The present model maintains much of the Bowen et al. (2009) water quality process framework but with some modifications to facilitate the application while maintaining a robust capability to accurately predict DO. Model specifications are described below.

As with Bowen et al. (2009), the benthic diagenesis sub-model of DELWAQ was not employed. Additionally, the DYNAMO option for modeling primary producers (i.e., phytoplankton or algae) was used, and only one algal group was included for late summer conditions. This algal group is referred as non-diatoms or also as green algae by the manual and the model user interface. Green algae can be considered a broad group of summer algae that differ substantially from diatoms and blue green algae, the other two algal groups available in the model. However, the green algal group does not represent any specific algae in the present application since this single group is applied throughout the annual seasons. The DYNAMO option is easier to apply than the BLOOM option requiring far fewer input parameters that must be calibrated.

Several state variables of the previous model by Bowen were not incorporated in the present model, which included unavailable and available silica, total active metal (TAM), and fecal coliform bacteria. Silica was not required since diatom algae were not included. TAM is used for P partitioning which can be adequately handled via portioning to total suspended solids (TSS). Also, without benthic diagenesis, COD was not required as with the previous model.

The DELWAQ model has many options, and it is possible to model organic matter and BOD at the same time with options for how these substances interact. This is a highly useful feature of DELWAQ since it allows modeling the point-source, wastewater discharges using BOD while modeling the freshwater tributary inflows using organic matter, which is a better approach than having to use either BOD or organic matter alone for these different types of discharges. Thus, labile and refractory carbonaceous BOD, or CBOD1 and CBOD2, respectively, were included as state variables, as well as organic C. Detrital C is a source for the particulate organic C variable. Various options and parameter values were selected such that CBOD and organic C are independent of each other, and they both affect DO independently in the present model application. Temperature was included in the water quality model rather than in the HD model. Due to the various options for handling phosphate sorption in DELWAQ, two variables are required for modeling dissolved and particulate (adsorbed) orthophosphate, PO4 and AAP (algal uptake and adsorption forming particulate orthophosphate), respectively. This brings the total number of DELWAQ states variables to 19 for the present model; these variables are listed in Table 4-11.

Table 4-11: Applicable DELWAQ state variables

Physical	Nutrients	Carbon	BOD	Response Variables
Temperature	PON1 (labile PON)	POC1 (labile POC)	CBOD1, as ultimate and labile	DO
ISS (inorganic suspended solids)	PON2 (refractory PON)	POC2 (refractory POC)	CBOD2, as ultimate and refractory	ALG (non-diatom or green algae as C)
	DON	DOC		
	NH4 (ammonium N)			
	NO3 (nitrite + nitrate N)			
	POP1 (labile POP)			
	POP2 (refractory POP)			
	DOP			
	PO4 (dissolved orthophosphate P)			
	AAP (PO4 adsorbed to TSS)			

Similar to Bowen et al. (2009), SOD was specified as a constant benthic boundary condition. Fluxes of nitrite + nitrate nitrogen (NO3) into sediment due to benthic denitrification was also handled via a constant benthic mass transfer rate. Benthic fluxes of ammonium nitrogen (NH_4) and PO_4 into the overlying water column did not require specification since the bottom of the water column does not typically become anoxic in the lower Cape Fear River.

Unlike the CE-QUAL-ICM modeling option in EFDC, the DELWAQ model allows DO utilization during decay of POC, as well as during mineralization of DOC. It also allows the user to specify the fractions of POC1 that transfer to POC2 and DOC and the fraction of POC2 that transfers to DOC during POC decay. Dissolved oxygen can be consumed by POC decay for the fractions of POC1 and POC2 that are not transferred during decay. Values for these fractions, as well as decay rates and other parameters used in the model are discussed in the Model Calibration section. The next section describes the processes used in this DELWAQ application.

4.5.1.1. DELWAQ Processes

The DELWAQ Processes Library Configuration Tool (PLCT) was used to select model state variables, processes, and parameter values. There are numerous options and inputs available within the PLCT, and most are made operable by checking a box next to the input that indicates the value can be edited, or changed, from the default value. A default value is imposed if the editable box is not checked. Thus, the terminology "made editable" is often used in the discussion below to indicate that values other than default could be imposed in the inputs.

Temperature

The absolute temperature option, rather than reference temperature option, was selected, thus, observed air temperature and wind speed data were provided as input. The option to impose special processes for modeling temperatures of intertidal sand and mud flats was not used.

Dissolved Oxygen

Processes implemented for DO included reaeration, primary production and respiration, nitrification, oxidation of CBOD, mineralization of organic carbon (POC1, POC2, and DOC), and SOD. CBOD was modeled as ultimate CBOD, and the decay rates of CBOD1 and CBOD2 were made editable and set to 0.15 and 0.03 per day, respectively, to be consistent with the values used by Bowen et al. (2009). The fraction of algae contributing to CBOD and the fraction of POC contributing to CBOD were made editable and set to zero. The ratio of oxygen to C utilization during mineralization was made editable and set to the default value of 2.67 g O_2/g C. The processes affecting DO and the relationships to other state variables are shown in Figure 4-97.

ISS

The settling rate and the critical shear stress for sedimentation of inorganic suspended solids (ISS) was made editable and varied during model calibration of ISS. The composition (Compos) option was activated so that TSS output included all forms of suspended solids (organic and inorganic) to facilitate comparison of model results with measured TSS data.

Nitrogen

Processes affecting NH_4 included losses due to nitrification and algal uptake and contributions due to mineralization of DON and algal autolysis associated with respiration. The fraction of algal autolysis was made editable for model calibration. Nitrate is generated by nitrification and lost by algal uptake and sediment denitrification flux. The first order sediment denitrification rate as well as the nitrification rate and associated half saturation constants for DO and NH_4 were set as editable for model calibration. PON1 and PON2 are gained by algal mortality and lost by settling and hydrolysis to DON. The processes affecting N and the relationship to other state variables are shown in Figure 4-98.

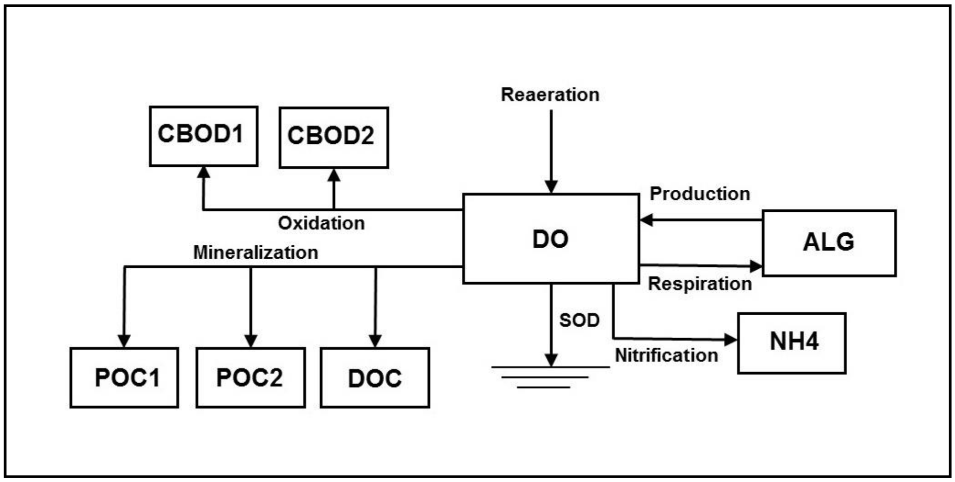

Figure 4-97: Processes affecting DO

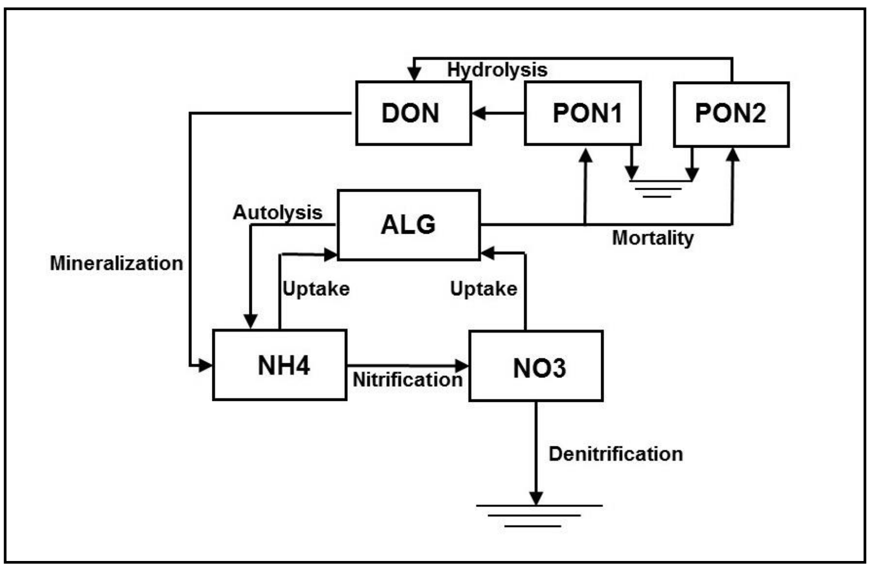

Figure 4-98: Processes affecting N

Phosphorus

Dissolved orthophosphate (PO4) is lost by algal uptake and adsorption forming particulate orthophosphate (AAP) and is gained by mineralization of DOP, algal autolysis associated with respiration and desorption from AAP. The linear, equilibrium partitioning option was selected for sorption, and the sorption distribution coefficient (K_d) was made editable and varied during model calibration. The settling rate of adsorbed PO4 (AAP) was made editable and varied during model calibration. POP1 and POP2 are gained by algal mortality and lost by settling and hydrolysis to DOP. The processes affecting P and the relationships to other state variables are shown in Figure 4-99.

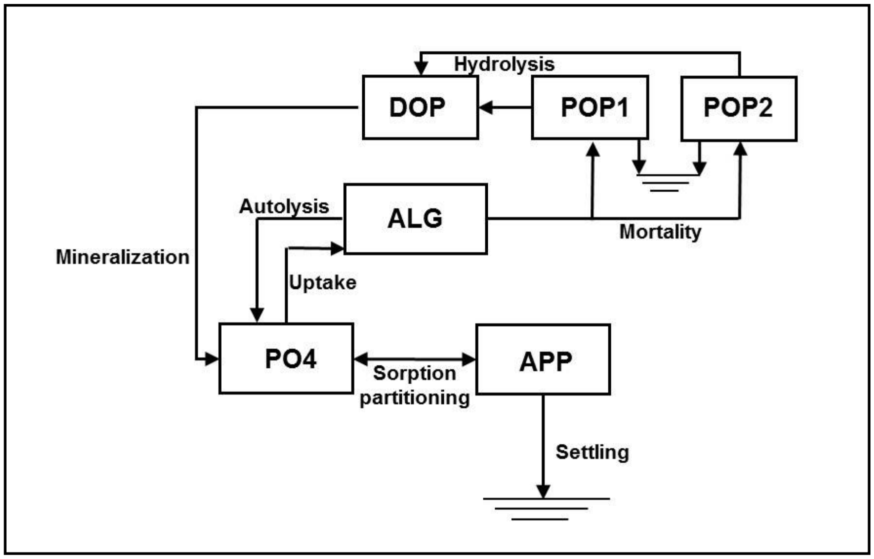

Figure 4-99: Processes affecting P

Organic Carbon

Particulate organic matter (POC1, POC2, PON2, PON2, POP1, and POP2) is generated by algal detritus associated with mortality and is lost by settling and transfer to other forms of organic matter and/or mineralization during decay. The upper and lower limits of labile and refractory hydrolysis/mineralization transfer rates were made editable, so they could be varied during model calibration. The transfer fractions (POC1 to POC2, POC1 to DOC, and POC2 to DOC) and settling rate of POC were made editable. The fraction of POC1 transferred to POC2 was set to zero, and the fractions of POC1 and POC2 transferred to DOC were set to 1 throughout the model application and were not changed. Transfer fractions and settling rates for PON and POP mirror those set for POC in the model code.

Dissolved organic C, as well as DON and DOP, is generated by hydrolysis from POC and is lost by mineralization. The mineralization rate for DOC was made editable for calibration. The processes affecting organic C and the relationships to algae are shown in Figure 4-100.

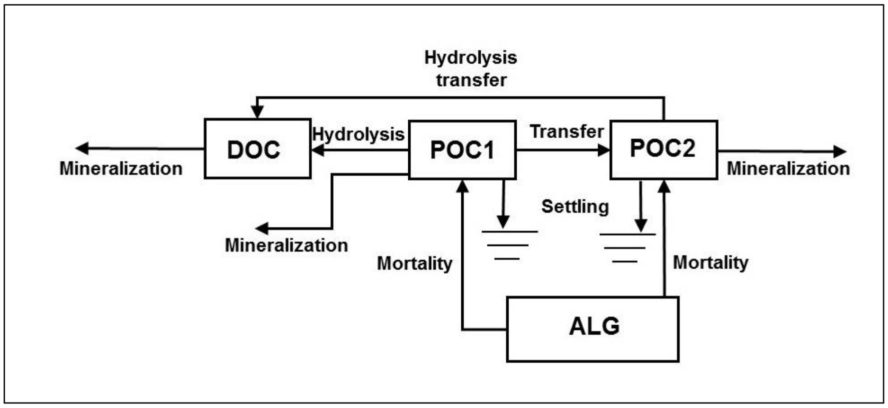

Figure 4-100: Processes affecting organic carbon

Algal production and mortality were activated. The growth limitation functions for nutrients, light, and temperature were activated. Mortality as affected by temperature and salinity was activated. Rates for maximum production, growth and maintenance respiration, and mortality were made editable for calibration. The upper and lower salinity limits for salinity mortality and the algae settling rate were also made editable for calibration.

The values of model parameters used in the application and resulting from model calibration are discussed in the section on Model Calibration.

4.5.2. Water Quality Model Development

The water quality model for the Cape Fear River estuary builds on the development, calibration, and validation for hydrodynamics and salinity in Delft3D. The following section focuses on the additional model development tasks necessary to extend the model to simulate water quality.

4.5.2.1. Model Grid

The model grid developed for the HD model was aggregated both horizontally and vertically for use in the water quality model in order to reduce model computation time. D-Waq DIDO module as part of the Delft3D Suite (Deltares, 2017) was used to facilitate the grid aggregation.

D-Waq DIDO is an interactive grid editor for coupling hydrodynamic models with the DELWAQ model. It uses a rectilinear, curvilinear or finite element hydrodynamic grid layout as input. It produces the administration file needed by the Delft3D water quality model, DELWAQ, to condense the fine HD grid to a coarser water quality grid.

The HD model was vertically aggregated from 25 Z-layers to 14 Z-layers. The top six HD model layers (from land elevation of 6 m-NAVD88 to water depth of 1.7 m-NAVD88) were aggregated to form one DELWAQ model layer which includes the normally dry overland area and the tidally wetting and drying surface water layer. The bottom seven hydrodynamic layers (from water depth of 18.3 m-NAVD88 to 26 m-NAVD88) were aggregated to form one DELWAQ model layer which only applies to the modeled offshore region and has no influence on the river channel layers. In between these two vertically aggregated layers, the hydrodynamic layers were kept the same thicknesses in the DELWAQ model as the HD model.

Figure 4-101 presents the horizontal grid aggregation applied in the DELWAQ model. Figure 4-102 shows the detailed aggregation for the model domain adjacent to the Wilmington Port and the Cape Fear River entrance.

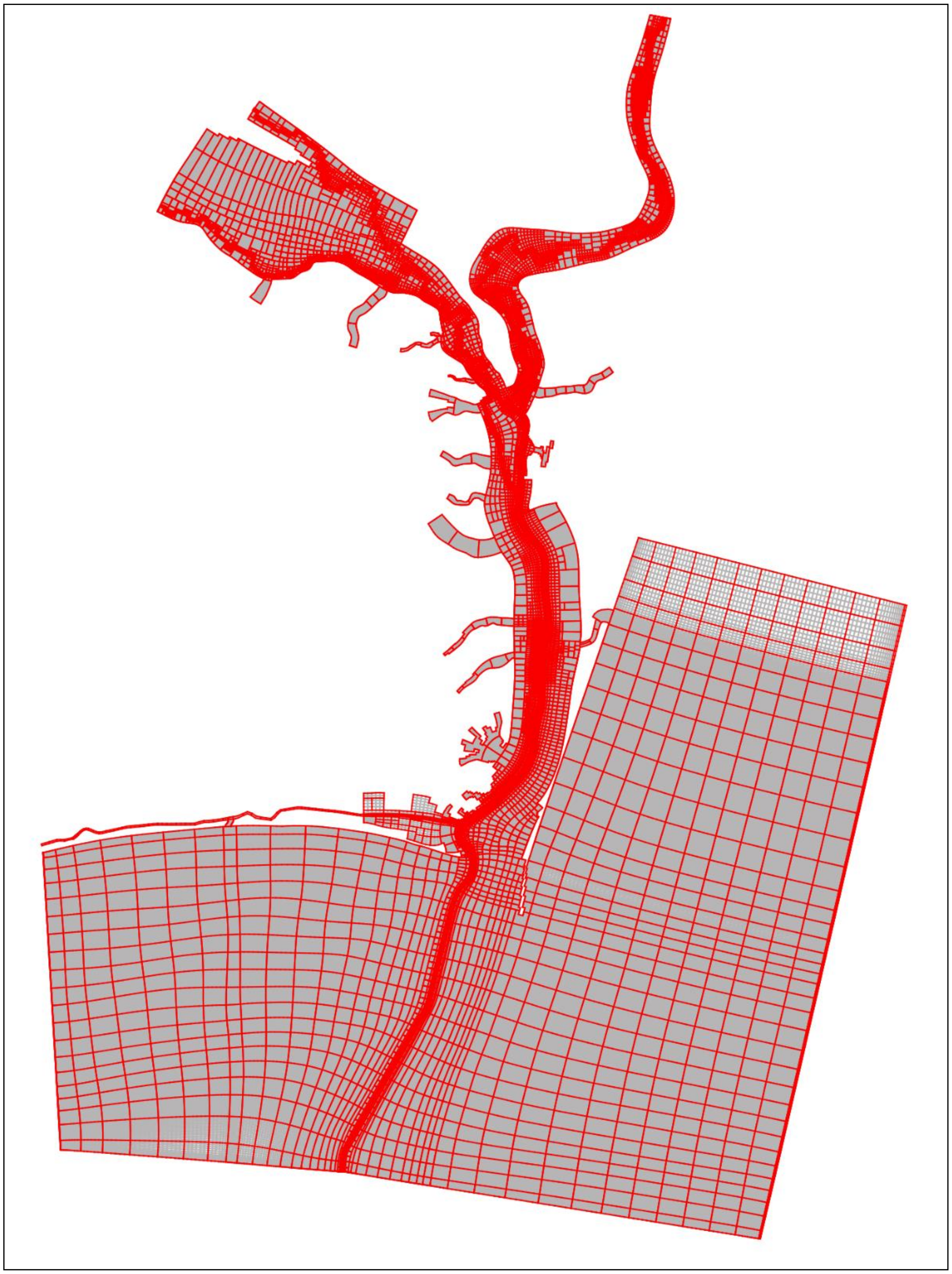

Figure 4-101: DELWAQ model horizontal grid aggregation (red – aggregated DELWAQ grid; gray – hydrodynamic model grid)

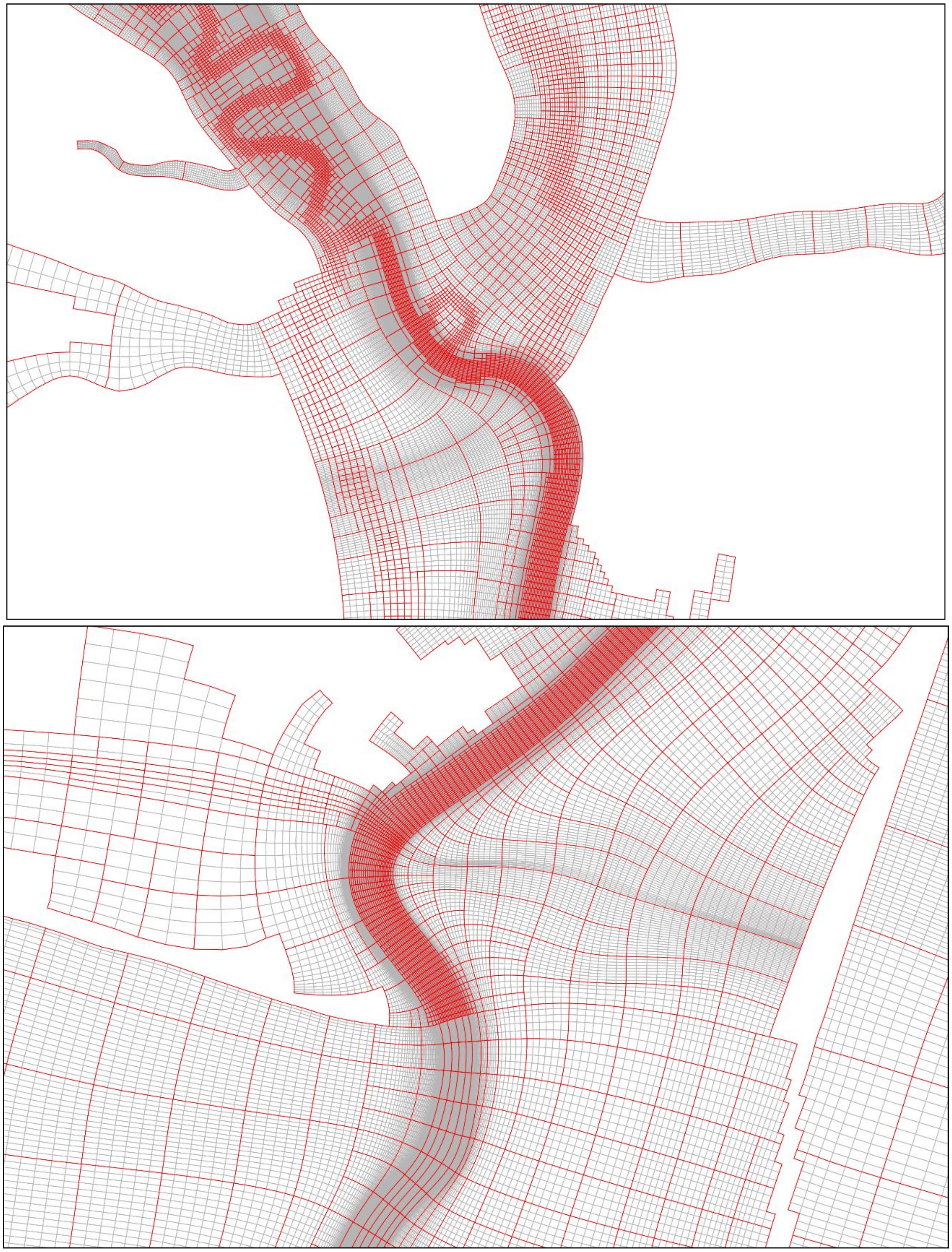

Figure 4-102: DELWAQ model horizontal grid aggregation adjacent to the Wilmington Port and the Cape Fear River entrance (red – aggregated DELWAQ grid; gray – hydrodynamic model grid)

4.5.2.2. Boundary Conditions

Permitted Point Source Loading

Loadings were developed for fourteen permitted wastewater discharges within the model domain. These are shown in Table 4-12 and Figure 4-103 along with descriptive information for each. There are some additional minor industrial discharges that were not included, which is consistent with Bowen et al. (2009). Duke Energy Progress Sutton Steam Electric Plant (permit no. NC0001422) was not included since the plant now uses a cooling pond minimizing river discharges.

Measured and reported discharge flow rates and concentrations (as well as loads in some cases, i.e., mass/time) were obtained from the NPDES records for the year 2017 from the USEPA's Enforcement and Compliance History Online (ECHO) datasets. Constituents that were available in this data and that were consistent with developing loadings for this model included flow rate, five-day biochemical oxygen demand (BOD_5), DO, temperature, TN, TKN, NH_4, TP, and TSS.

Table 4-12: Permitted, point-source, wastewater discharges in the model

NPDES Permit No.	Name	Facility	Type	Max Permitted Flow (MGD)[1]
NC0001112	Invista S A R L	Invista S A R L	Industrial Process & Commercial (Major)	1.25
NC0003298	International Paper Company	Riegelwood Mill WWTP	Industrial Process & Commercial (Major)	50
NC0086819	Brunswick County	Northeast Brunswick Regional WWTP	Municipal, Large (Major)	3.8
NC0082295	Fortron Industries	Fortron Industries WWTP	Industrial Process & Commercial (Major)	0.834
NC0023965	Cape Fear Public Utility Authority	James A. Loughlin (Northside) WWTP	Municipal, Large (Major)	16
NC0023973	Cape Fear Public Utility Authority	Southside WWTP	Municipal, Large (Major)	24
NC0001228	Global Nuclear Fuel - Americas LLC	GNF-A Wilmington Plant	Municipal, Large (Major)	1.875
NC0023256	Town of Carolina Beach	Carolina Beach WWTP	Municipal, Large (Major)	3
NC0057703	Aqua North Carolina, Inc.	The Cape WWTP	100% Domestic < 1MGD	0.75
NC0065480	Aqua North Carolina, Inc.	Beau Rivage Plantation WWTP	100% Domestic < 1MGD	0.5
NC0025763	Town of Kure Beach	Kure Beach WWTP	Municipal, < 1MGD	0.285
NC0003875	Elementis Chromium L P	Castle Hayne Manufacturing Facility WWTP	Industrial Process & Commercial (Minor)	1.361
NC0027065	Archer Daniels Midland Company	Southport Manufacturing Facility WWTP	Industrial Process & Commercial (Major)	3.51
NC0075540	Brunswick Regional Water & Sewer H2GO	Belville WWTP	Municipal, < 1MGD	0.8

[1]*MGD = million gallons per day*

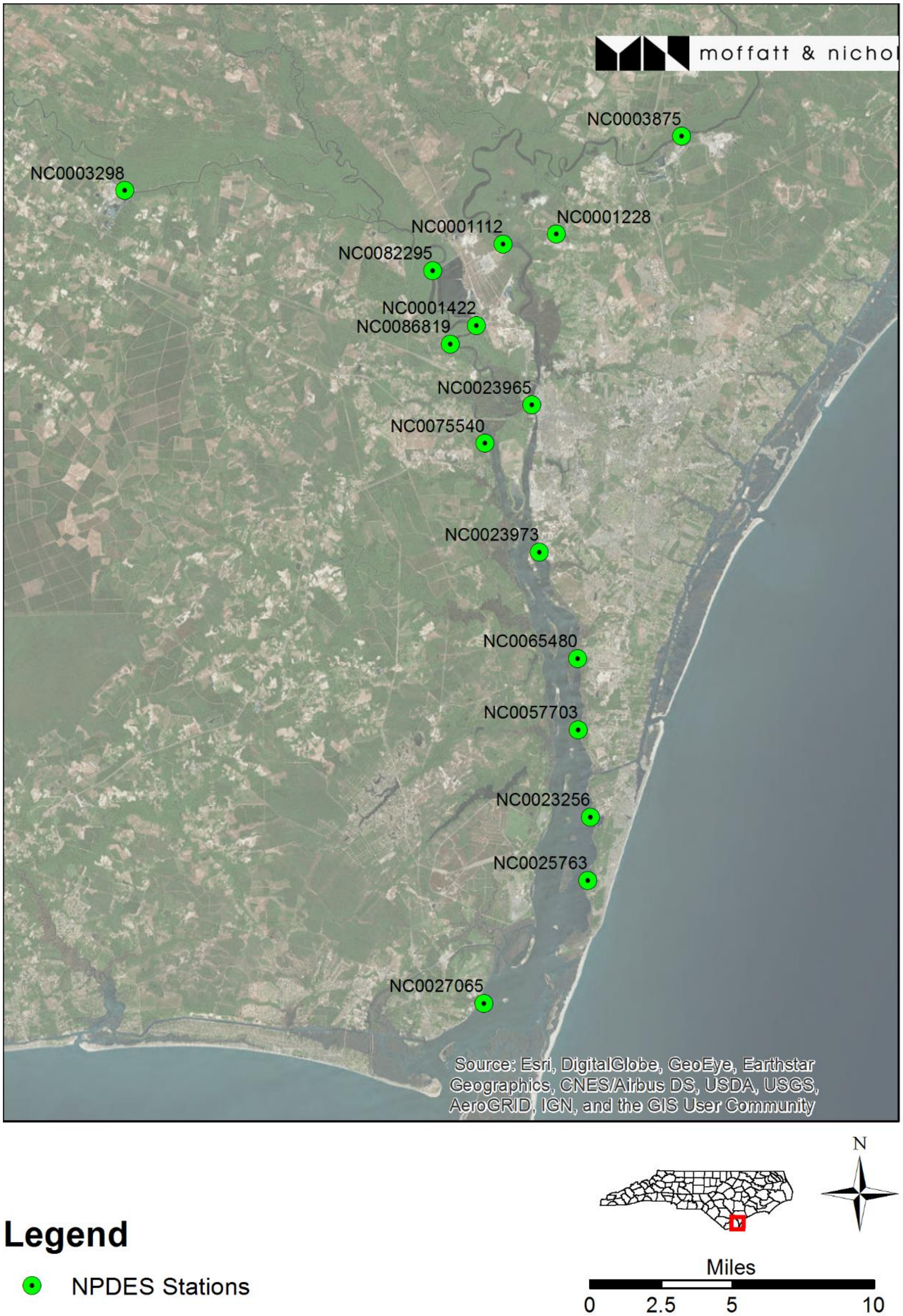

Figure 4-103: NPDES Point Sources included in the model

Of the 19 water quality state variables in the model, point-source loadings were required for the following eight state variables: TSS, carbonaceous ultimate labile BOD (CBODu1), carbonaceous ultimate refractory BOD (CBODu2), DON, NH_4, NO_3, DOP, and PO_4.

Two of the above constituents (TSS and NH_4) were part of the available reported data, although values were not available for every discharge. The other six constituents in the above list had to be derived from the reported constituent data. Nine other water quality state variables in the model were assumed to have zero loading. These constituents included labile and refractory particulate organic matter (C, N, and P), DOC, algal C (ALG), and particulate (adsorbed) orthophosphate (i.e., AAP). Having zero loadings for these constituents is consistent with the assumptions and methods used by Bowen et al. (2009) for these waste loads, with the exception of DOC which is discussed further below.

Temperature and DO values were available from the available wastewater discharge data, although all of the temperature values were daily maximum values, and all of the DO values were either daily maximum or daily minimum values. The use of maximum and minimum values for T and DO at the wastewater discharge locations was satisfactory considering the small discharge flow rates involved.

The permitted waste loading observational data were reported once each month. These data for calendar year 2017 were used to determine the constituent loading concentrations for all months of 2017. The product of loading concentration and discharge flow rate produced mass loading rates (mass/time) that were input to the model. The methods used to compute the loading concentrations are described below.

The available reported data consisted of 30-day average (3C), 7-day average (7A), daily maximum (DD), and daily minimum (DC) values, with varying levels of reporting, i.e., from none to all four of these metrics included for the discharge. The order of priority (from highest to lowest) of use consisted of 3C, 7A, DD, and DC. In some cases, loadings rather than concentrations were reported. In such cases, the loadings were divided by the reported flow rates to obtain concentrations so that non-reported, but required, constituents could be derived.

Only one discharge (NC0001228) included data for TKN, and there was no NH_4 data for that discharge. TKN is the sum of total organic N and NH_4. Additionally, the TKN values were all DD values and were greater than the 3C values reported for TN. Therefore, it was assumed that DON and NH_4 were zero, and all of the TN was NO_3 for the discharge NC0001228. For all of the other discharges, the nitrogen methodology of Bowen et al. (2009) was used, which is that 25 % of the remaining N (i.e., TN minus NH_4) is DON, and 75 % is NO_3. There was no N data for two discharges, so for those cases, all N components were set to zero.

For discharge NC0027065, half of the TP was set to DOP as per Bowen et al. (2009). For the other discharges, Redfield stoichiometry (106:16:1 for C:N:P) was used to compute DOP from DON (DOP = 0.1384 DON) as per Bowen et al. (2009). With values for DOP, PO4 can be computed (PO4 = TP – DOP). For discharges without TP data, both P components (PO4 and DOP) were set to zero.

It is noted that in the present model, particulate organic matter is split between labile and refractory, while dissolved organic matter is not split and is treated with a single set of mineralization rates that can be considered as labile. In the Bowen et al. (2009) model, all particulate organic matter was assumed to be labile, and dissolved organic matter was split between labile and refractory. The present model is in keeping with the original water quality model formulations built into the EFDC model when using the CE-QUAL-ICM option, where labile and refractory particulate organic matter hydrolyze into dissolved organic matter, which mineralizes. There are no loadings of organic C for the wastewater discharges in the present model since BOD, not organic C, is reported and is used in the model (rather than organic C) for utilizing DO during mineralization of permitted wastewater discharges. Organic C is used rather than BOD for the non-point source loading concentrations discussed in the next section. Both organic C and BOD are modeled independently in the present model to cause oxygen demand.

The BOD_5 data had to be converted to ultimate BOD (BOD_u). The scale-up factors reported by Bowen et al. (2009) were used (i.e., BOD_u = factor x BOD_5). In all but three cases, the scale-up factor was 1.9, which is based on a labile (L) and refractory (R) BOD split of 100:0 percent and a labile BOD decay rate of 0.15 per day. Two discharges, Northside and Southside Cape Fear Public Utility Authority wastewater treatment plants (WWTP) (NC0023965 and NC0023973), had a scale-up factor of 3.51, which is based on L:R BOD split of 70:30 percent with L and R BOD decay rates of 0.15 and 0.03 per day, respectively. International Paper (NC0003298) had L:R BOD split of 25:75 percent with the same L and R BOD decay rates, resulting in a scale-up factor of 6.11. Scale-up factors and L:R splits were available for all but two discharges, NC0057703 and NC0065480. Both of these discharges are small (< 1 MGD) domestic WWTPs, similar to NC0075540, which had L:R split of 100:0 percent and a scale-up factor of 1.9; thus, this split and scale-up factor were used for these two discharges.

Ultimate CBOD ($CBOD_u$) was determined by subtracting ultimate nitrogenous BOD ($NBOD_u$) from BOD_u as long as $CBOD_u$ remained a positive number. If $CBOD_u$ was determined to be negative, $NBOD_u$ was not subtracted from BOD_u, and it was assumed that $CBOD_u = BOD_u$. $NBOD_u$ resulting from nitrification was computed from $NBOD_u = 4.57 \times (DON + NH_4)$. The L:R split was used to compute labile and refractory $CBOD_u$. In summary, BOD_u was computed from BOD_5; $BOD\underline{u}$ was converted to $CBOD_u$ if availability of TKN data permitted; and $CBOD_u$ was split between L and R, yielding CBODu1 and CBODu2.

<u>Mainstem River Loading</u>

There were three major river inputs in the model: Cape Fear River, Black River, and the Northeast Cape Fear River. Flows were derived during HD model development. Pollutant concentrations for these boundaries were developed from LCFRP data as described in the next section.

<u>Non-Point Source Loading</u>

An approach similar to that of Bowen et al. (2009) was used to model flows and loadings associated with non-point source (NPS), freshwater inflows to the river. Whereas 17 freshwater loadings were included in the Bowen et al. (2009) model, 29 freshwater inflows were included in the present model as discussed in the HD model development to represent the three major rivers and 26 local watershed NPS inflows (Figure 4-104). With water discharge rates specified for inflows, there is the option of using either water quality constituent concentrations or loadings as model input. To facilitate simulations of various management scenarios that could involve changes in freshwater inflows, concentrations of freshwater inflows were specified. In such cases, the implicit assumption is made that freshwater constituent concentrations do not change as flow rate changes, which is consistent with the Bowen et al. (2009) model and portions of other models (Cerco and Noel, 2017). Regardless, an extensive database and analysis would be required to develop flow-dependent concentration relationships for the Cape Fear River. Thus, the approach here was to specify constituent concentrations independent of flow rate based on observed concentrations at locations deemed to be representative of the freshwater flow sources.

Bowen et al. (2009) used three observation stations of the Lower Cape Fear River Program (LCFRP) to characterize their 17 freshwater inflow concentrations. These three stations were: NC11 (Cape Fear River), NCF117 (Northeast Cape Fear River), and B210 (Black River) as shown Figure 1-22. The same approach was used for the present model to characterize inflow concentrations for the 26 local watershed NPS freshwater inflows. The assignments of observation stations to freshwater sources are shown in Table 4-13. The three stations were also used to set inflow concentrations for the respective three major river inflows.

The assumption as made by Bowen et al. (2009) was made in this study, which is that atmospheric loadings of nutrients are included in the freshwater NPS loadings. This assumption is quite adequate considering the large size of the Cape Fear River system watershed relative to the surface area of the river.

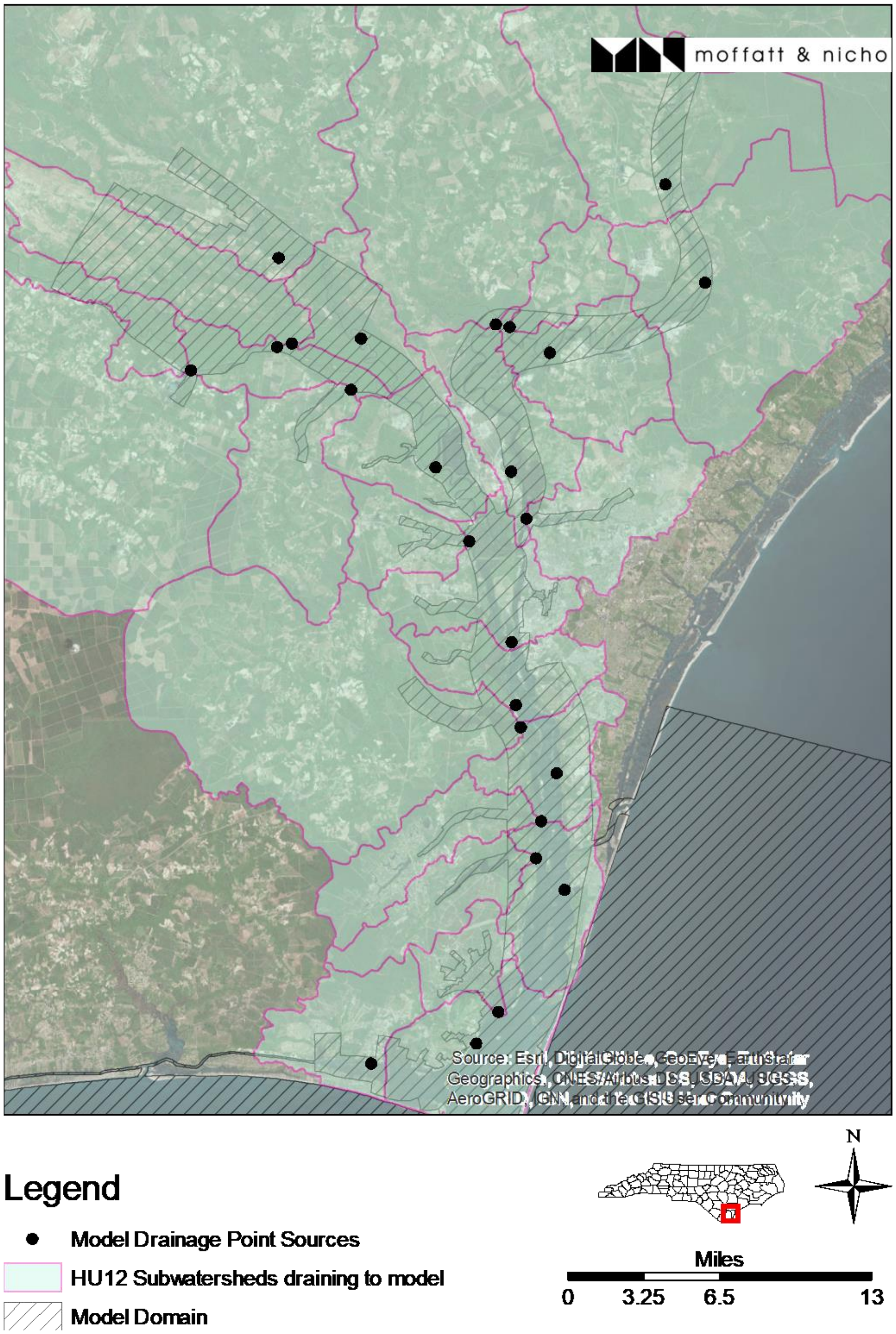

Figure 4-104: Subwatersheds draining to the estuary and locations of modeled point sources where ungaged subwatershed freshwater inflows are applied in the model

Table 4-13: Watershed freshwater NPS discharge locations, watershed areas, and assigned LCFRP stations

Longitude	Latitude	Watershed Name	Source ID in model	Area (km^2)	LCFRP station assignment
-78.1981	34.3523	Livingston Creek	discharge_1	328.38	NCF117
-78.1314	34.4217	Black River (Ungaged Portion)	discharge_2	2,152.91	B210
-78.1223	34.3685	Lyon Creek	discharge_3	112.15	NCF117
-78.0702	34.3713	Cross Way Creek - Black River	discharge_4	54.95	B210
-78.0784	34.3395	Hood Creek	discharge_5	109.09	NCF117
-77.9692	34.3792	Long Creek	discharge_6	363.96	NCF117
-77.9590	34.3775	Turkey Creek	discharge_7	37.87	NCF117
-77.9293	34.3611	Prince George Creek-Northeast Cape Fear River	discharge_8	82.60	NCF117
-77.8122	34.4035	Harrisons Creek	discharge_9	245.52	NCF117
-77.8412	34.4650	Pike Creek - Northeast Cape Fear River	discharge_10	220.93	NCF117
-77.8212	34.5448	Northeast Cape Fear River (Ungaged Portion)	discharge_11	1,836.41	NCF117
-78.0156	34.2907	Indian Creek-Cape Fear River	discharge_12	73.51	NCF117
-77.9592	34.2877	Ness Creek - Northeast Cape Fear River	discharge_13	71.36	NCF117
-77.9482	34.2581	Smith Creek	discharge_14	85.87	NCF117
-77.9907	34.2446	Town of Woodburn - Sturgeon Creek	discharge_15	41.05	NCF117
-77.9602	34.1815	Barnards Creek-Cape Fear River	discharge_16	73.88	NCF117
-77.9575	34.1426	Barnards Creek-Cape Fear River	discharge_17	57.96	NCF117
-77.9540	34.1287	Town Creek	discharge_18	325.55	NCF117
-77.9274	34.0998	Mott Creek-Cape Fear River	discharge_19	52.27	NCF117
-77.9395	34.0703	Liliput Creek	discharge_20	64.59	NCF117
-77.9436	34.0472	Orton Creek	discharge_21	53.96	NCF117
-78.0681	33.9206	Jump and Run Creek – Gully Creek	discharge_22	66.57	NCF117
-77.9895	33.9323	Town of Southport – Cape Fear River	discharge_23	101.03	NCF117
-77.9728	33.9521	Walden Creek	discharge_24	32.85	NCF117
-77.9225	34.0275	Town of Kure Beach - Cape Fear River	discharge_25	60.23	NCF117
-78.1333	34.3663	Grist Mill Branch-Cape Fear River	discharge_26	42.48	NCF117

Water quality observational data for calendar year 2017 were obtained from LCFRP and loaded into an Excel workbook for filtering and analysis. The data were filtered to use the three river stations noted above plus station M18, which was used for the seaward boundary conditions. All sampling dates within 2017 were processed for these four stations. The filtered data of interest were copied to other sheets in the workbook. These observational data included the following constituents:

- temperature
- DO
- TSS
- Chl *a*
- TN
- TKN
- NH_4
- NO_3 + NO_2 (or simply NO_3)
- TP
- PO_4

Freshwater NPS inflow concentrations are required for 16 constituents, which include:

- temperature
- DO
- TSS
- ALG (mg C/L)
- NH_4
- NO_3 (including NO_2)
- PO_4
- DOC
- DON
- DOP
- POC1
- POC2
- PON1
- PON2
- POP1
- POP2

Six of the above concentrations (T, DO, TSS, NH_4, NO_3, PO_4) were in the observed data. Thus, concentrations had to be derived for the following 10 constituents:

- ALG
- DOC
- DON

- DOP
- POC1
- POC2
- PON1
- PON2
- POP1
- POP2

Concentrations for CBODu1, CBODu2, and AAP were not required since organic C rather than CBOD is used to represent oxygen utilization during organic C mineralization for NPS loads. The observed PO4 was not filtered when measured, so observed PO_4 represent total PO_4. Inputs of total PO4 should instantly re-partition between model PO_4 (dissolved PO_4) and AAP upon entry into the model domain. The concentrations for the above 10 derived constituents were obtained as described below.

A C to Chl *a* ratio of 60 (Bowen et al., 2009) was used to convert Chl *a* (µg/L) to ALG (mg C/L); thus, the Chl *a* concentrations were multiplied by 0.06 to obtain ALG, which takes into account the division by 1000 for conversion of µg to mg. Total organic nitrogen (TON) was obtained from mass balance, TON = TKN – NH4. Total organic phosphorus (TOP) was obtained from mass balance, TOP = TP – PO4. There was not any organic C or BOD data; thus, total organic carbon (TOC) was initially obtained from TON assuming Redfield stoichiometry, or TOC = 5.68 TON. However, during model calibration, measured DO and some limited DOC data indicated that organic C loadings were too low. Thus, a ratio of 8 was used rather than 5.68 to obtain TOC from TON for the river loadings. This ratio was found to be appropriate for all but one of the major tributaries entering Chesapeake Bay (Cerco and Noel, 2017).

Bowen et al. (2009) did not specify any freshwater inflow loadings for particulate organic matter (C, N, and P). Their organic loadings consisted of labile and refractory DOC (C), N, and P. The present model is different in that regard, i.e., loadings of labile and refractory particulate organic C, N, and P, as well as dissolved organic C, N, and P, were included. Thus, it was necessary to find a way to split total organic C, N, and P into particulate and dissolved forms. In the present model, all dissolved organic C, N, and P are assumed to be labile.

Splits of total organic C and N into particulate and dissolved organic C and N were performed using the average of such splits used for the eight major freshwater inflows to the Chesapeake Bay eutrophication model (Cerco and Noel, 2017). The averages of these splits, i.e., the fraction of particulate to total concentration, for C and N was 0.29. Ignoring inorganic C, POC = 0.29 TOC. Likewise, PON = 0.29 TON was used. It cannot be assumed that particulate P is mostly POP since considerable amounts of AAP can exist, as well as other forms of inorganic P. To derive POP it was assumed that the ratios of POP/TOP and PON/TON are equal, thus, POP = PON/TON x TOP, which also results in POP = 0.29 TOP.

The Bowen et al. (2009) splits for refractory and labile (R:L) organic matter were used to determine the L and R concentrations of POC, PON, and POP (i.e., POC1, POC2, PON1, PON2, POP1, POP2). The R:L splits for NC11, B210, and NCF117 were respectively, 0.645:0.355, 0.69:0.31, and 0.786:0.214. Concentrations for DOC, DON, and DOP were determined from mass balance, i.e., DOC = TOC – POC, DON = TON – PON, DOP = TOP – POP. This completed the calculation of the 10 derived constituents.

There were observational data that were reported below detection (i.e., non-detect, or ND). On one date (6/12/2017) at NC11, TKN < ND, so TKN was determined from TKN = TN – NO_3. Also, NH_4 < ND for multiple dates at all four stations (NC11, NCF117, B210, and M18). NH_4 was assumed to equal half of ND, or NH_4 = 0.5 ND for those dates and stations with one exception. For NC11 and 6/12/2017, NH_4 was set to zero since using half of ND resulted in zero TON as well as zero TOC. For multiple dates at all four stations, there were recordings of NO3 < ND. For those cases, NO_3 was determined from NO3 = TN – TKN. However, in every case, this calculation resulted in NO_3 = 0.0. For two dates at Station M18, TP < ND. For one of those dates (4/10/2017), TP was set to half of ND. For the other date (3/9/2017), TP was set to 0.012 mg/L, which was the value recorded for PO_4, thus, TP = PO_4 on that date.

Seaward Boundary Condition

LCFRP station M18 was used to represent the seaward boundary condition except a ratio of 5.68 was used to obtain TOC from TON for the offshore concentrations.

Air Temperature and Wind

The hourly inputs for air temperature and wind speed were taken from the Wilmington International Airport (Meteorological Aviation Report or METAR station, KILM).

Light Extinction

Observed Secchi depth measurements obtained during August and September 2017 by the LCRFP at their monitoring stations varied between 0.5 m at NCF 6 and 1.7 m at M23 and M18. In general, Secchi depth was lower upstream and higher downstream indicating light extinction decreases in the downstream direction. Light extinction is generally higher in the upstream reaches, most probably due to highly dispersed, fine suspended solids. Although TSS concentrations tend to be higher in the mid to lower river, possibly due to navigation traffic causing bottom resuspension, it is believed that higher salinity of the mid and lower river reduces the particle dispersion resulting in particle aggregation with larger particles, which can result in greater light penetration (lower light extinction). Algal Chl *a* concentrations also increase moving towards the ocean, probably due to increasing light availability. Thus, the goal was to create a light climate that has lower water column penetration upstream and higher penetration downstream. In model terms, the total light extinction coefficient needed to vary from roughly 0.9 m^{-1} upstream to 1.5 m^{-1} downstream based on conversion of observed Secchi depths to light extinction coefficients.

In the model, the total light extinction coefficient is computed as the sum of the base light extinction coefficient and the partial light extinction coefficients associated with the model state variables IM1 (i.e., ISS), POC1, POC2, DOC, and ALG. The partial light extinction coefficient for each state variable is the product of the specific light extinction parameter (m^2/g) for that state variable and the variable concentration (g/m3). The base light extinction coefficient was set to 0.3, and the specific light extinction parameters for POC1, POC2, DOC, and ALG were set to 0.05 m^2/g. Suspended solids had a much stronger influence on light extinction than the other state variables, thus, its specific light extinction parameter was varied to provide total light extinction (and estimated Secchi depth) that was consistent with observed Secchi depth. Thus, the specific light extinction parameter for IM1 was set to linearly vary between 0.15 at the far upstream reaches and 0.04 at station M23 and to 0.026 below station M23.

Sediment Oxygen Demand

In the WAQ module, the relevant process parameters are as follows:

- fSOD, user-specified SOD [$gO_2\ m^{-2}\ d^{-1}$]
- TcSOD, temperature coefficient for SOD decay [-]

The NC Division of Water Quality measured SOD at five sites during the Summer and Fall of 2003. These data (Table 4-14) were used to support development of the Bowen model.

Table 4-14: Sediment oxygen demand for the Cape Fear River

Date	Location	Water Temperature (degrees C)	SOD at ambient temp ($g/m^2/d$)	SOD corrected to 20 degrees C ($g/m^2/d$)
8/6/2003	Prince George Creek, tributary to Northeast Cape Fear River	26.3	0.5189	0.3490
11/20/2003	Northeast Cape Fear River upstream from Wilmington near channel marker 4	15.9	0.1900	0.2460
10/29/2003	Cape Fear River downstream from Wilmington near channel marker 61	19.3	0.4440	0.4640
7/17/2003	Cape Fear River downstream from Wilmington near channel marker 55	27.6	0.4679	0.2899
10/2/2003	Town Creek, tributary to Cape Fear River	20.7	0.6951	0.6651

For the current effort, an SOD value for 20 degrees C was inserted, and then corrected for the actual, computed local cell temperature using the following equation.

$$SOD(t) = SOD(20) \times \Theta^{T-20} \tag{13}$$

where Θ is TcSOD. A rate multiplier coefficient of 1.058 was applied based on Bowen et al. (2009) and an initial SOD value at 20 degrees C of 0.5 g/m^2/d constant was used across the domain. SOD was varied during model calibration.

4.5.2.3. Initial Conditions

For the initial conditions of each state variable, the available August and March 2017 measured LCFRP data were spatially interpolated to generate the assumed vertically constant initial conditions for model calibration and validation, respectively.

Figure 4-105 presents an example of the initial DO condition for the model calibration.

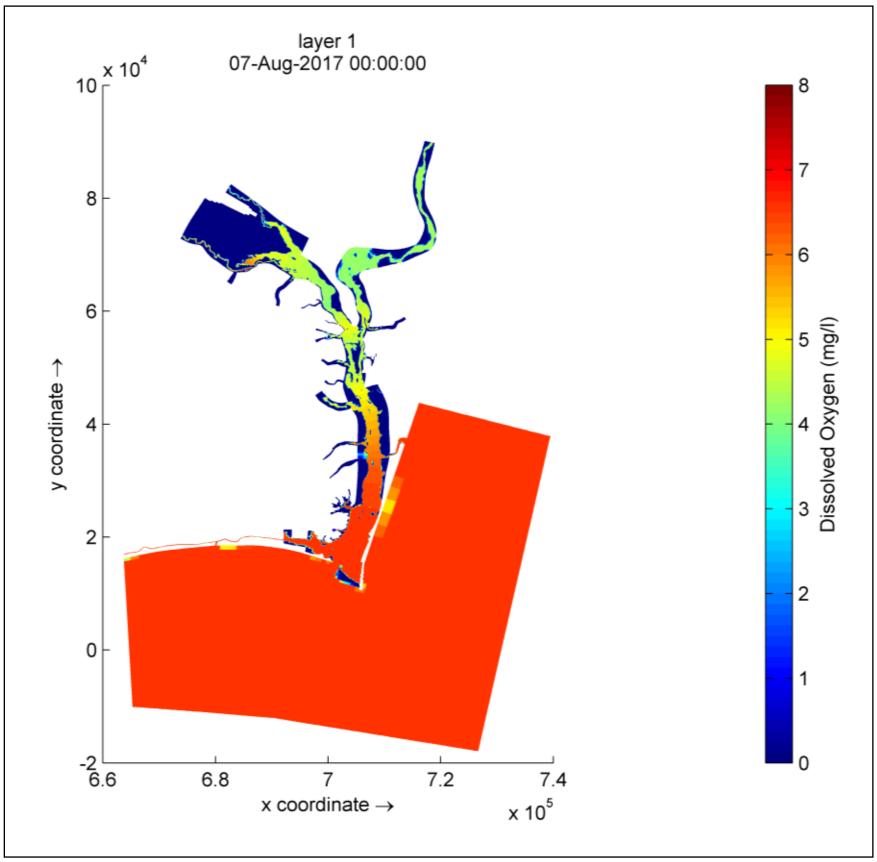

Figure 4-105: Initial DO condition for model calibration

4.5.3. Model Calibration and Validation Process

The water quality model calibration and validation process is described in this section. Calibration was performed first, and the final model parameters determined through calibration were used in validation for a different time period.

4.5.3.1. Calibration and Validation Periods

The model was calibrated for the late summer period, August 7 through September 15, 2017, and then validated for the spring period, March 27, 2017 through April 2, 2017. An additional, year-long validation test was constructed based on typical (or average) flow conditions.

4.5.3.2. Calibration Parameters

Once the treatment of boundary and initial conditions were established in the model, water quality calibration was achieved by adjusting various parameters within the model. Model parameters include all input options, stoichiometric values, kinetic reaction rates, temperature rate coefficients, half-saturation values and other coefficients and inputs related to water quality processes and reactions. All the model input parameters for the processes within the model framework described previously are listed in Section 4.5.4.1. The initial (at the beginning of the calibration process) and final (after achieving calibration) parameter values are also shown in Table 4-15. The initial values were based on a combination of past experience, judgement, information reported by Bowen et al. (2009), and/or recommended model default values. The model was run numerous times for the calibration period in an attempt to bring model water quality concentrations into agreement with observed data, thus, eventually resulting in the final calibration parameters. The final calibration parameters were then applied for the validation period. Calibration and validation results are presented in Section 4.5.4.

4.5.3.3. Calibration and Validation Metrics

In addition to graphical comparisons of model-computed and observed (measured) results, several statistical metrics were used to assess model calibration and validation results. These include the mean error (*ME*), root mean square (*RMS*) error, mean absolute error (*MAE*), relative error (*RE*), correlation coefficient (*R*), and index of agreement (*d*). These metrics are briefly described here.

If x and y are the measured and calculated data respectively, then the following statistics can be calculated:

Mean error (*ME*):

$$ME = \bar{y} - \bar{x} \qquad (14)$$

Where "bar" denotes the sample mean.

Root mean square (*RMS*) error:

$$\varepsilon_{RMS} = \sqrt{\overline{(x-y)^2}} \tag{15}$$

Mean absolute error (*MAE*):

$$MAE = \overline{|x-y|} \tag{16}$$

Relative Error (RE):

$$RE = MAE \big/ \overline{x} \tag{17}$$

The correlation coefficient, *R*, was calculated using the standard method and represents a non-squared value. The model prediction capability was estimated with an index of agreement between measured and calculated data (after Willmott, 1982 and Willmott et al., 1985):

$$d = 1 - \frac{\overline{(x-y)^2}}{\overline{\left(|x-\bar{x}| - |y-\bar{x}|\right)^2}}, 0 \le d \le 1 \tag{18}$$

4.5.4. Calibration and Validation Results

The following sections present graphical plots and statistical metrics of model results compared with measured values for the calibration and validation. These comparisons serve as a demonstration of the model's ability to simulate key estuarine water quality processes.

4.5.4.1. Summer 2017 Calibration

The water quality model was calibrated for the period August 7 – September 15, 2017, in three stages, starting with only temperature, then only total ISS, and then full water quality simulation (i.e., all 19 state variables). The first two stages could be executed with the single state variable (temperature or ISS) without having to include the other 18 variables since their processes are independent of the other 18 variables. However, 16 of the other 17 state variables depend on temperature and several variables depend on ISS. Each stage is presented in the following sections. The model parameters that had to be set and that could be varied during calibration are shown in Table 4-15 along with the initial values and the final values of each.

Table 4-15: Initial and final calibration parameters for water quality

Parameter	Units	Description	Initial Value	Final Value
FactRCHeat	none	Factor on rate constant for surplus temperature exchange	1.0	1.0
ZHeatExch	ºC/day	Zeroth order temperature exchange flux	0.0	0.5
Vertdisper	m^2/sec	Vertical dispersion	from HD model	from HD model
NH4KRIT	gN/m^3	Critical concentration of NH4 for uptake by algae	0.01	0.01
RcNit20	gN/m^3/day	Michaelis-Menten nitrification reaction rate at 20 ºC	0.0	0.0
TcNit	none	Temperature coefficient for nitrification	1.085	1.085
KsAmNit	gN/m^3	Half saturation constant for NH4 limitation in Michaelis-Menten nitrification	0.1	0.1
KsOxNit	g/m^3	Half saturation constant for oxygen limitation in Michaelis-Menten nitrification	0.5	0.5
RcNit	1/day	First-order nitrification reaction rate at 20 ºC	0.1	0.15 below M54 and 0.5 above M54
SWRear	none	Switch for selection of options in transfer rate for oxygen reaeration	7	7
KLRear	none	Scaling factor for wind speed in the wind function of the reaeration equation	1.0	0.0 above M42 and 1.0 below M42
TCRear	none	Temperature coefficient for reaeration	1.016	1.016
RcBOD	1/day	CBOD1 decay rate	0.15	0.15
RcBOD_2	1/day	CBOD2 decay rate	0.03	0.03
TcBOD	none	Temperature coefficient for CBOD decay	1.04	1.04
AlgFrBOD	none	Fraction of ALG contributing to CBOD	0.0	0.0
OXCCF	gO2/gC	O2:C ratio on mineralization	2.67	2.67
POCFrBOD	none	Fraction of POC contributing to CBOD	0.0	0.0
AMCCF	gO2/gC	Amount of oxygen used for nitrogen in mineralization	0.0	0.55

Parameter	Units	Description	Initial Value	Final Value
fSOD	$gO2/m^2/day$	Zero order sediment oxygen demand	0.5	0.20 downstream of M35, 1.5 for all marsh cells, 1.0 elsewhere
TcSOD	none	Temperature coefficient for SOD	1.04	1.058
PPMaxGreen	1/day	Maximum production rate of green algae at 20 ^oC	1.8	1.5
MRespGreen	1/day	Maintenance respiration rate of green algae at 20 ^oC	0.05	0.075
GRespGreen	none	Growth respiration factor of green algae	0.15	0.15
Mort0Green	1/day	Minimum mortality rate of green algae as affected by salinity at 20 ^oC	0.05	0.05
MortSGreen	1/day	Maximum mortality rate of green algae as affected by salinity at 20 ^oC	0.05	0.05
SalM1Green	g/kg	Minimum salinity value for mortality of green algae	25	33
SalM2Green	g/kg	Maximum salinity value for mortality of green algae	35	35
DayL	day	Day length	0.58	0.58
KsOxCon	g/m^3	Half saturation constant for oxygen limitation in decomposition of organic matter	1.0	1.0
TcOxCon	none	Temperature coefficient for oxygen consumption in decomposition of organic matter	1.07	1.07
TaucSIM1	N/m^2	Critical shear stress for settling of inorganic sediment	0.1	0.1
ku_dFdcC20	1/day	Upper limit on fast mineralization rate on organic C at 20 ^oC	0.1	0.1
kl_dFdcC20	1/day	Lower limit on fast mineralization rate on organic C at 20 ^oC	0.1	0.1
ku_dFdcN20	1/day	Upper limit on fast mineralization rate on organic N at 20 ^oC	0.1	0.05
kl_dFdcN20	1/day	Lower limit on fast mineralization rate on organic N at 20 ^oC	0.1	0.05
ku_dFdcP20	1/day	Upper limit on fast mineralization rate on organic P at 20 ^oC	0.1	0.05

Parameter	Units	Description	Initial Value	Final Value
kl_dFdcP20	1/day	Lower limit on fast mineralization rate on organic P at 20 ºC	0.1	0.05
kT_dec	none	Temperature coefficient for mineralization of organic matter	1.04	1.04
b_poc1poc2	none	Fraction of POC1 converted to POC2	0	0
b_poc1doc	none	Fraction of POC1 converted to DOC	1	1
SWOMDec	none	Option for nutrient stripping	1	1
ku_dMdcC20	1/day	Upper limit on medium mineralization rate on organic C at 20 ºC	0.015	0.03
kl_dMdcC20	1/day	Lower limit on medium mineralization rate on organic C at 20 ºC	0.015	0.03
ku_dMdcN20	1/day	Upper limit on medium mineralization rate on organic N at 20 ºC	0.015	0.01
kl_dMdcN20	1/day	Lower limit on medium mineralization rate on organic N at 20 ºC	0.015	0.01
ku_dMdcP20	1/day	Upper limit on medium mineralization rate on organic P at 20 ºC	0.015	0.01
kl_dMdcP20	1/day	Lower limit on medium mineralization rate on organic P at 20 ºC	0.015	0.01
b_poc2doc	none	Fraction of POC2 converted to DOC	1	1
k_DOCdcC20	1/day	Mineralization rate for DOC at 20 ºC	0.1	0.15
FrAutGreen	none	Fraction autolysis for green algae during mortality	0.3	0.4
FrDetGreen	none	Fraction detritus for green algae during mortality	0.7	0.6
RcDenSed	m/day	First order mass transfer rate for sediment denitrification	0.1	0.2
SWAdsP	non	Switch for PO4 – AAP sorption formulation	0	N/A*
KdPO4AAP	m^3/g	Linear sorption distribution coefficient, K_d	0.01	N/A*
VSedAAP	m/day	Settling rate for AAP	0.2	N/A*

Parameter	Units	Description	Initial Value	Final Value
V0SetlM1	m/day	Settling rate of inorganic sediment	0.1	0.1
VSedPOC1	m/day	Settling rate for POC1	0.1	0.05
VSedPOC2	m/day	Settling rate for POC2	0.1	0.05
VSedGreen	m/day	Settling rate for green algae	0.05	0.01
OptDLGreen	day	Optimal day length for algal growth	0.58	0.58
PrfNH4Gree	none	NH4 over NO3 preference factor for green algae	1	1
KMDINgreen	gN/m^3	N half saturation constant for nutrient limitation of green algae	0.005	0.05
KMPgreen	gP/m^3	P half saturation constant for nutrient limitation of green algae	0.001	0.005
RadSatGree	W/m^2	Optimal light intensity at 20 ºC for green algae	100	80
RadSurf	W/m^2	Irradiation at the water surface	190	106
ExtVIIM1	m^2/g	Specific light extinction coefficient for inorganic solids	0.05	linearly interpolate between 0.15 at river inflow and 0.04 at M23; 0.026 below M23
ExtVIPOC1	m^2/gC	Specific light extinction coefficient for POC1	0.05	0.05
ExtVIPOC2	m^2/gC	Specific light extinction coefficient for POC2	0.05	0.05
ExtVIDOC	m^2/gC	Specific light extinction coefficient for DOC	0.05	0.05
ExtVlGreen	m2/gC	VL specific extinction coefficient Greens	0.15	0.05
ExtVIBak	1/m	Background light extinction coefficient	0.3	0.3
EnhSedIM1	-	Salinity enhanced settling factor for IM1	5	5
SWTauVeloc	-	Switch Tauveloc	2	2

Parameter	Units	Description	Initial Value	Final Value
TauFlow	N/m2	Bottom shear stress by FLOW	from HD model	from HD model
ZResDM	gDM/m2/d	Zeroth-order resuspension flux	100	100
TaucRS1DM	N/m2	Critical shear stress for resuspension	0.5	0.5
NCRatGreen	gN/gC	N:C ratio Greens	0.16	0.176
PCRatGreen	gP/gC	P:C ratio Greens	0.02	0.024
TaucSGreen	N/m2	Critical shear stress for sedimentation Greens	0.1	0.1
Grtochl	mg Chlfa/g C	Chlorophyll-a:C ratio in Greens	50	60
Latitude	deg	Latitude of study area	52.1	34
RefDay	day	Daynumber of reference day simulation	0	219
SWSatOXY		Saturation DO option switch	1	2

* N/A = not used after removing AAP from the model due to instabilities.

Temperature

Water temperature determines the rate at which water quality processes take place. As such, it is important that the water temperature simulation is as accurate as possible. Thus, the first stage of the water quality model calibration was concentrated on water temperature. In DELWAQ, the water temperature is calculated as a function of the ambient air temperature, and the heat gain from or loss to the atmosphere takes into account the wind speed. A more elaborate temperature modeling approach using solar radiation, cloudiness, scattering and evaporation is not currently implemented in DELWAQ.

The parameters that were adjusted for the water temperature calibration were a factor on the rate constant for surplus temperature exchange (FactRCHeat) and zeroth order temperature exchange flux (ZheatExch). Their final values are listed in Table 4-15. The calibration results for temperature are discussed in section 0.

Inorganic Suspended Solids

The second stage of the calibration was to roughly calibrate the ISS comparing to the measured TSS without accounting for the organic matter. In this study, only the fine-grained suspended matter (silt and clay) was considered for the water quality model given its role in determining the underwater light climate affecting algae growth and its pollutant absorption capacities. It should be noted that although suspended fine sediment was included in the HD model, the results could not be imported into the water quality model directly, similar to salinity, because this functionality has not yet been implemented in Delft3D. In addition to transport by advection and turbulent motion, the fate of the fine-grained suspended sediments is determined by settling and deposition, as well as by bed processes such as consolidation, bioturbation and resuspension. The two layered approach in the DELWAQ was adopted for the suspended sediment modeling. The parameters that were adjusted during the calibration process were the critical shear stresses for erosion (TaucRS1DM) and deposition (TaucSIM1), settling velocity (V0SetlM1), and first order erosion rate (ZResDM). Their final values are listed in Table 4-15 .

Full Water Quality

Numerous model runs were executed for the calibration period (August 7 – September 15, 2017) with various adjustment in model parameters with the goal of bringing model results as close to measured data as possible for all water quality constituents with the exception of temperature and ISS, which were calibrated separately as discussed above. Measured data were available from two data sets, LCFRP and RPS EH (or simply RPS for short).

Initially, calibration efforts focused on nutrients, then Chl *a*, and progressing to DO. With so many interactions among constituents, calibration eventually focused on all constituents simultaneously until Chl *a* and nutrients had converged towards calibration. Final calibration efforts centered mostly on NH_4 and DO. The final recommended calibration parameters are listed in the last column of Table 4-15. Model calibration results are discussed below along with some of the rationale for final parameters values. Model final calibration results are plotted versus time with measured data at multiple stations for both the LCFRP and RPS data sets. These plots are provided in Appendix C-1. It is noted that measured values preceding and following the calibration period are also included in the LCFRP data plots so that general longer-term trends can be observed.

A discussion of model accuracy focuses on the model versus measured data plots and model relative error (*RE*) for each water quality constituent. The statistic, *RE,* is commonly used during calibration as a quick and reliable assessment criterion. The *RE* values discussed below are the mean values for all LCFRP data or across all RPS stations and are presented in Table 4-16. Additional model statistics are provided but not discussed in detail (Table 4-17 through Table 4-20).

Chl a: Model-computed Chl *a* generally compares fairly well with measured values at most stations for the LCFRP data. Model Chl *a* values are lower than the measured RPS values for the most part. Additionally, the RPS values are greater than the LCFRP values at most stations with the same proximity. Preference was given to the LCFRP data since the collection of LCFRP data has been a long-term, continuing effort with university, state, and numerous municipal and industry partners. The *RE* for Chl *a* is 0.40 which is considered satisfactory and is lower than the phytoplankton median *RE* value of 0.44 based on an assessment of 153 water quality model studies by Arhonditsis and Brett (2004). The algal maximum specific growth rate (PPMaxGreen) was lowered some from 1.8 to 1.5 per day and algal maintenance respiration rate (MRespGreen) was increased from 0.05 to 0.075 per day to bring closer agreement of model Chl *a* with measured LCFRP values.

Table 4-16: Calibration *RE* values for LCFRP and RPS data

Constituent	*RE* for LCFRP calibration data	*RE* for RPS calibration data
Chl *a*	0.40	0.58
PO_4	0.94	NA
TP	0.23	0.46
NH_4	0.34	NA
NO_3	0.65	0.43
TKN	0.46	0.51
TN	0.26	0.47
DO	0.12	0.15*
TSS	0.51	NA
Wtemp	0.03	0.02*

* Average of individual station statistics

Table 4-17: Calibration statistics for LCFRP data

Constituent	ME	RMS	MAE	RE	R	d
Chl *a*	0.27	1.19	0.87	0.40	0.75	0.85
PO_4	0.05	0.07	0.06	0.94	0.40	0.48
TP	0.02	0.03	0.03	0.23	0.92	0.91
NH_4	0.00	0.02	0.02	0.34	0.46	0.67
NO_3	0.07	0.15	0.13	0.65	0.91	0.92
TKN	-0.29	0.35	0.29	0.46	0.33	0.46
TN	-0.22	0.31	0.22	0.26	0.83	0.85
DO	-0.30	0.89	0.61	0.12	0.43	0.67
TSS	3.68	5.82	4.92	0.51	0.60	0.68
Wtemp	-0.36	0.88	0.73	0.03	0.88	0.87

Table 4-18: Calibration statistics for RPS data

Constituent	ME	RMS	MAE	RE	R	d
Chl *a*	-3.82	5.15	4.25	0.58	-0.57	0.25
PO_4	NA	NA	NA	NA	NA	NA
TP	-0.01	0.11	0.07	0.46	0.26	0.36
NH_4	NA	NA	NA	NA	NA	NA
NO_3	-0.10	0.14	0.12	0.43	0.38	0.52
TKN	-0.37	0.47	0.37	0.51	-0.90	0.28
TN	-0.47	0.52	0.47	0.47	-0.46	0.26
DO*	0.38	0.73	0.63	0.15	-0.11	0.35
TSS	NA	NA	NA	NA	NA	NA
Wtemp*	-0.23	0.58	0.48	0.02	0.94	0.89

*Average of individual station statistics

Table 4-19: Calibration statistics by station for RPS continuous DO data

	CFBW_B	NECF_S	NECF_B	KM_S	KM_B	UBI_S	UBI_B	ADM_S	ADM_B
RMS	0.43	1.32	1.43	0.67	0.73	0.54	0.56	0.43	0.49
ME	-0.24	0.89	1.13	0.43	0.54	0.21	0.42	0.01	0.06
MAE	0.36	1.19	1.31	0.55	0.59	0.46	0.49	0.33	0.38
RE	0.08	0.3	0.35	0.14	0.16	0.1	0.12	0.06	0.07
R	0.3	-0.81	-0.74	-0.31	-0.26	0.15	0.39	0.35	-0.09
d	0.49	0.11	0.13	0.26	0.27	0.46	0.53	0.56	0.33

Table 4-20: Calibration statistics by station for RPS continuous temperature data

	CFBW_B	NECF_S	NECF_B	KM_S	KM_B	UBI_S	UBI_B	ADM_S	ADM_B
RMS	0.55	0.58	0.57	0.32	0.42	0.49	0.58	0.87	0.88
ME	-0.19	0.43	0.35	-0.19	-0.36	-0.38	-0.49	-0.61	-0.62
MAE	0.44	0.47	0.45	0.26	0.36	0.42	0.5	0.72	0.74
RE	0.02	0.02	0.02	0.01	0.01	0.01	0.02	0.03	0.03
R	0.87	0.94	0.91	0.96	0.98	0.95	0.98	0.95	0.95
d	0.91	0.92	0.92	0.97	0.94	0.91	0.87	0.82	0.79

Nutrients: Overall, model PO_4 values are higher than measured. The reason for this is due to the inability to include PO_4 losses via sorption partitioning with AAP with settling of AAP. The original intent was to include PO_4, which represented dissolved orthophosphate, and AAP, which represented adsorbed particulate orthophosphate, and to compare the model total PO_4 (PO_4 plus AAP) with measured PO_4, which as not filtered, thus, is total orthophosphate. However, there were problems with maintaining model numerical stability when trying to include both PO_4 and AAP with sorption. This instability is believed to be caused by the model formulation rather than model time step issues. Thus, transfers between PO_4 and AAP were turned off, and all computed AAP was zero with no sorption/settling losses of PO_4, resulting in over-prediction of PO_4. Model PO_4 is assumed to be dissolved and available for algal uptake. With an over-abundance of PO_4, it would have been difficult to cause any phosphorous limitation for algal growth, which is not a severe problem considering that the Cape Fear Estuary and indeed most estuarine systems are predominately N and light limited, though there can be some occasional P limitation and co-limitation (i.e., N+P) in the Cape Fear, particularly in the spring (Mallin et al. 1999). Light, N, and temperature were the limiting factors for algal growth in this model. The observed algal-available N and P data indicate that N is the limiting nutrient according to the Redfield ratio for P/N = 0.14, particularly for the lower estuary where P/N for observed nutrients is about ten times greater than the Redfield ratio during the calibration period. Nitrogen limitation is much less in the upper estuary where P/N for observed nutrients is between about 0.2 to 0.4 for the calibration period.

Without the ability to remove PO_4 via settling, an exceedingly high *RE* value of 0.94 resulted for PO_4. Fortunately, the poor model performance for PO_4 is not a problem for model reliability for DO predictions since the predicted algal concentrations are reasonably accurate, and PO_4 only affects DO through its effect on algal growth.

Model-computed TP compared quite well with measured TP as exhibited by plots for both the LCFRP and RPS stations/data. The *RE* for TP of 0.23 is considered very good.

Model-computed NH_4 agrees fairly close with measured values at all stations. The first order nitrification option was used, and the first order nitrification rate (RcNit) was increased from 0.1 per day to 0.15 below station M54 and 0.5 above station M54 to bring good agreement. The *RE* for NH_4 of 0.34 is considered good. The median *RE* for NH_4 is 0.48 based on the study by Arhonditsis and Brett (2004).

The measured $NO_3 + NO_2$ (or simply NO_3 for short) values in the LCFRP data are near or at zero for a number of dates and stations particularly in the lower Cape Fear River, whereas non-zero NO_3 values are reported for all of the RPS data. The primary loss mechanism for NO_3 is sediment denitrification. The first order mass transfer rate for sediment denitrification (RcDenSed) was increased from 0.1 to 0.2 to cause more NO_3 loss. However, emphasis was placed on matching the measured RPS data rather than the LCFRP data since the many zero NO_3 values of the LCFRP data were considered suspicious. The model NO_3 results agree fairly well with the RPS values while they are higher than the zero/near zero LCFRP values. As a result, the NO_3 *RE* is higher for the LCFRP data than for the RPS data with values of 0.65 and 0.43, respectively. Ideally, a lower *RE* for nitrate is desired and can be achieved for the LCFRP data by using a higher value of RcDenSed, but nitrate only affects DO in this model though its effect on algal growth, so further adjustment is not warranted. The median *RE* for NO_3 is 0.36 based on the study by Arhonditsis and Brett (2004).

Total organic N is included in TKN, and model TKN agrees fairly well with measured TKN at most stations; however, overall model TKN is lower than measured, particularly in the Northeast Cape Fear River (NECFR) arm. It is believed that the organic matter loadings (particularly for N and C) are too low in the NECFR. As stated in section 0, measured data from station NCF117 were used to characterize all fresh-water NPS loadings along the NECFR. There was an unusually high flow period for an un-gaged watershed of the NECFR during the calibration period that could have contributed higher loadings than specified in the inputs based on NCF117 concentrations. As shown by Figure 4-106, un-gaged watersheds 2 and 11 are larger than the gaged watersheds for the Black River and the NECFR, where watershed 2 drains into the Black River, and watershed 11 drains into the NECFR. Drainage streams within watershed 11 include Angola Swamp, Cypress Creek, and Rockfish Creek. During the latter part of August 2017, the estimated water flow rates for these two un-gaged watersheds are greater than the gaged flow rates for all three rivers during that period (see Figure 4-107). Although NPS freshwater discharges 2 and 11 are represented in the model, the organic matter loadings for these sources could be misestimated if the runoff concentrations from the watersheds differ from those measured at B210 and NCF117. Even long-term data tend to support the idea that loadings along the NECFR could be under-estimated. However, without additional supportive data, there is not adequate information for arbitrarily adjusting the estimated loading concentrations. It is not possible to increase model TKN without increasing loading concentrations in the NECFR. The TKN *RE* values are 0.46 and 0.51 for the LCFRP and RPS data, respectively.

Model TN agrees fairly well with measured TN, but the computed TN is lower than measured in the NECFR due to under-prediction of TKN in that arm. The TN *RE* values are 0.26 and 0.47 for the LCFRP and RPS data, respectively.

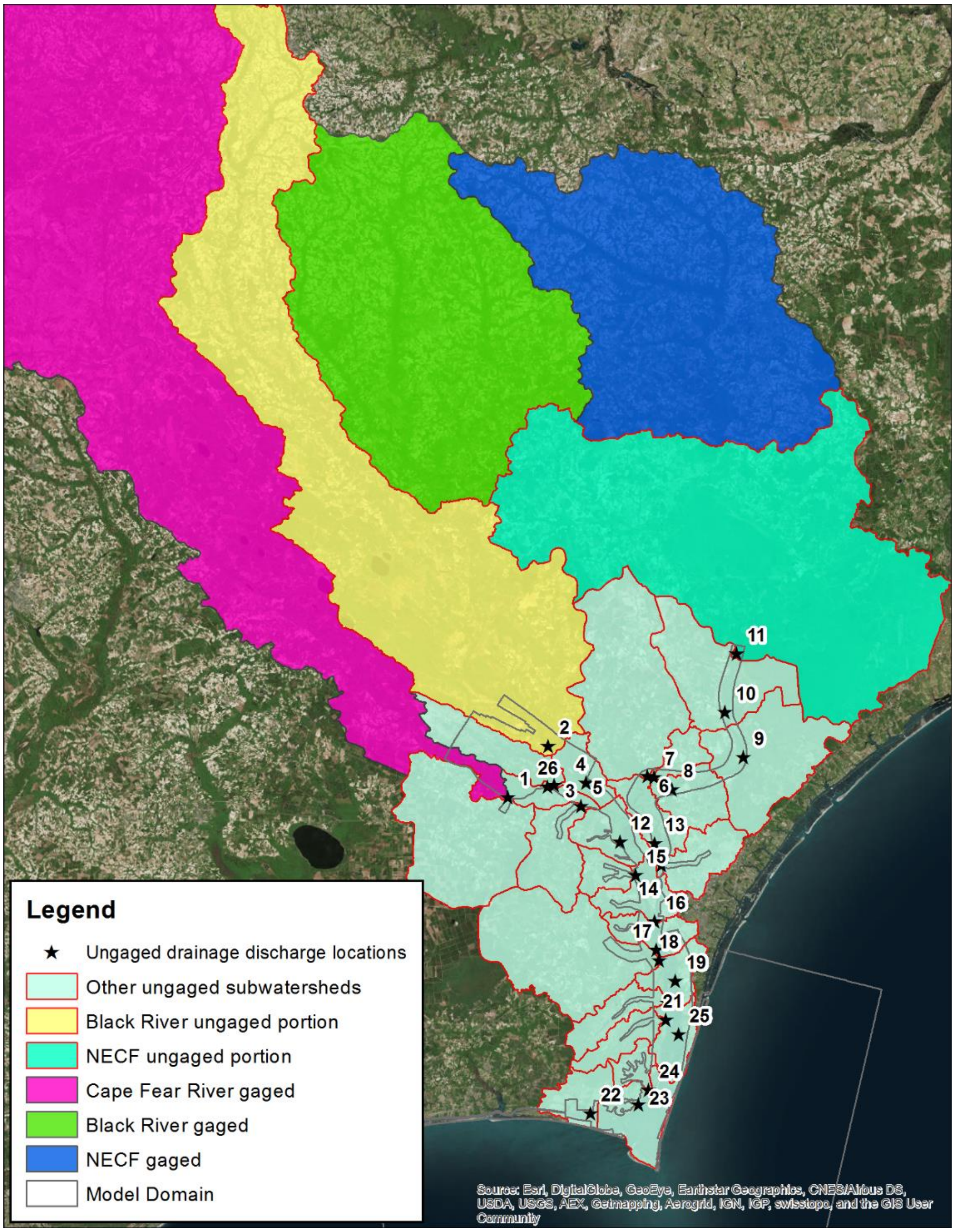

Figure 4-106: Gaged and un-gaged watershed of the Cape Fear River system

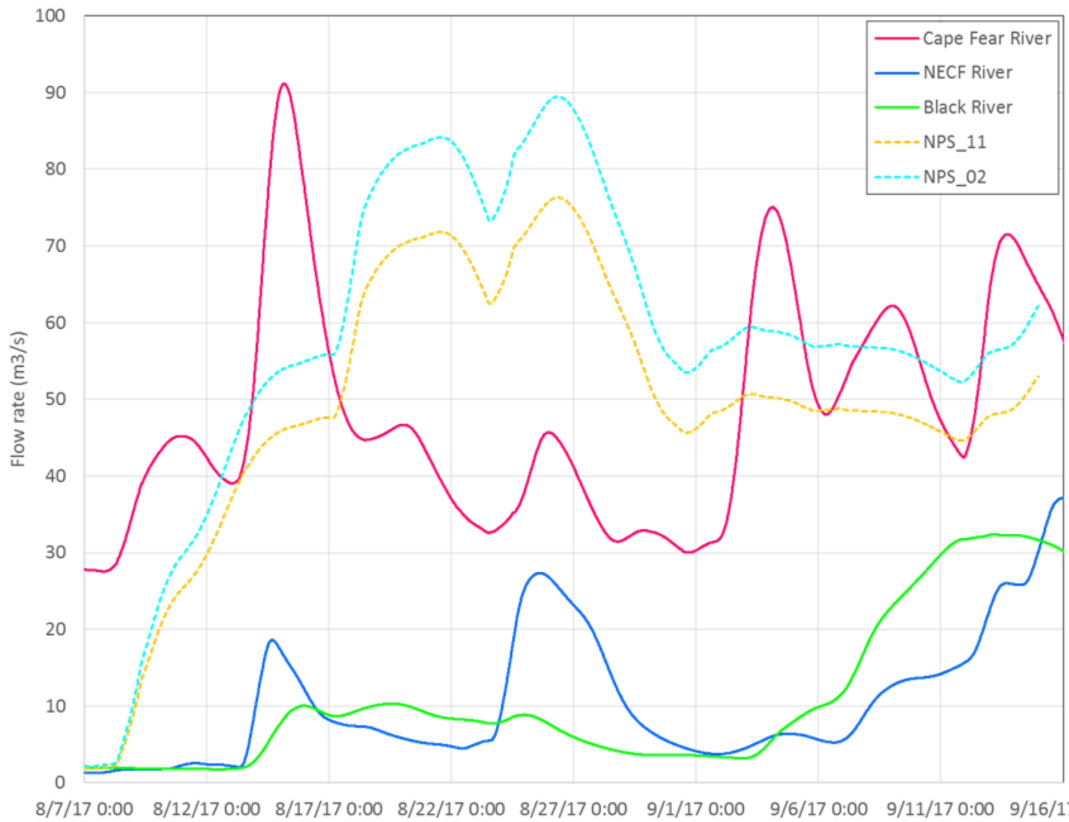

Figure 4-107: Water flow hydrographs for the three gaged rivers and un-gaged watersheds 2 and 11 for the calibration period

Dissolved Oxygen: Comparisons plots of model-computed DO with LCFRP measured DO indicates fairly good agreement for all stations except station AC, which is located on the upper Cape Fear River. There is some anomaly at this location that could not be resolved. As for the RPS data, good agreement between model and measured DO is evident for stations CFBW and ADM, which are on the upper and lower Cape Fear River, respectively. Poor agreement is exhibited for stations NECF and KM, which are on the NECFR. Moderately good agreement is apparent for station UBI, which is below the confluence of the upper Cape Fear River and NECFR. Agreement at UBI is good until the latter half of August when there are high inflows along the NECFR. As stated previously, it is believed that organic matter loadings are under-estimated for the NECFR, which explains why DO is over-predicted along the NECFR and immediately below its confluence with the upper Cape Fear River. The DO *RE* values are 0.12 and 0.15 for the LCFRP and RPS data, respectively. Even with the error along the NECFR, these *RE* values are fairly consistent with the median *RE* of 0.12 from the study by Arhonditsis and Brett (2004).

Calibration of DO was more difficult than normal. The DO seemed particularly more sensitive to algal growth and respiration and reaeration than usual, and it was not very sensitive to SOD. This sensitivity could be related to under-estimation of organic loading concentrations for freshwater non-point sources. Some of the parameters affecting DO have already been discussed, such as algal growth and respiration rates, nitrification rates, and CBOD decay rates. To increase the rates of DO utilization, the medium decay rate for particulate organic C was increased from 0.015 to 0.03 per day, and the decay rate for DOC was increased from 0.1 to 0.15 per day, the same value used for CBOD1. SOD was adjusted from 0.5 g O_2/m^2/day to 1.0 g O_2/m^2/day except below station M35 where it was set to 0.2 and for the marsh cells where it was set to 1.5 g O_2/m^2/day. Option 7 was used for reaeration, which is the O' Connor and Dobbins formula for stream reaeration plus the Banks and Herrera formula for wind reaeration. The wind scaling factor KLRear was set to zero for no wind reaeration above station M42 and to 1.0 below station M42. Winds from Wilmington were used, so a factor of 1.0 has the effect of using the full Wilmington winds.

A smoothing effect is observed in the DO results. Both the observed surface and bottom DO show roughly diurnal variations as expected, but these are smoothed out in the model. This smoothing effect is attributed to excessive diffusion (same for temperature). The fluctuations in observed temperature and DO are semidiurnal and related to tides, but these semidiurnal fluctuations are dampened in the model.

TSS and Temperature: Model output of TSS includes ISS plus all forms of organic solids. No other adjustments were performed to obtain TSS, rather the parameters affecting organic solids were set to impact primarily algae and DO without regard to the effect on TSS. Organic solids provide a relatively small contribution to TSS since most of TSS is ISS. Model-computed TSS compares fairly well with measured TSS, which was only available from the LCFRP data, although overall TSS is over-predicted. The *RE* for TSS is 0.51.

Model-computed water temperature (Wtemp) agrees very closely with measured values for both data sets with *RE* values of 0.03 and 0.02 for the LCFRP and RPS data, respectively. The median *RE* for Wtemp is 0.07 based on the study by Arhonditsis and Brett (2004).

4.5.4.2. Spring 2017 Validation

Validation did not involve the three stages for calibration, rather the final calibration parameters were applied to the validation period with the associated model boundary inputs and initial conditions, and a run was made using all 19 state variables. Thus, no adjustments were made to model parameters for validation except for one exception. Model-computed DO for validation was consistently lower than measured for the RPS data, where RPS DO values were near saturation. Thus, the wind scaling factor KLRear was adjusted during validation to increase DO values towards saturation. An analysis of winds indicated that winds at a nearby off-shore buoy (NOAA National Data Buoy Center, buoy number 41013) are about four times greater than winds at Wilmington during winter and early spring months. These buoy winds are considered to be more representative of effective winds in the lower Cape Fear River during late fall through early spring when leaves are off trees. Thus, KLRear was set to 4.0 below station M42 and to 1.0 above station M42 for the validation run, as well as for the year-long runs during late fall to early spring. For the remainder of the year, KLRear was set to zero above station M42 and 1.0 below station M42.

Time series plots of model-computed and measured water quality constituents are provided in Appendix C-2 for all observation stations. Multiple constituents are available in the LCFRP data for the validation period, but only water temperature and DO are available from the RPS data, and recordings of both were continuous. The *RE* values for the validation period are shown in Table 4-21, and additional summary statistics for the validation period are shown in Table 4-22 through Table 4-24.

Note that statistics for the LCFRP validation data were developed with only four data pairs.

Table 4-21: Validation *RE* values for LCFRP and RPS data

Constituent	*RE* for LCFRP validation data	*RE* for RPS validation data
Chl *a*	0.08	NA
PO4	0.59	NA
TP	0.12	NA
NH4	0.42	NA
NO3	0.23	NA
TKN	0.37	NA
TN	0.15	NA
DO	0.09	0.07*
TSS	0.93	NA
Wtemp	0.02	0.04*

* Average of individual station statistics

Table 4-22: Validation statistics for LCFRP data

Constituent	ME	RMS	MAE	RE	R	d
Chl *a*	-0.06	0.55	0.50	0.08	0.97	0.98
PO_4	0.03	0.04	0.03	0.59	-0.02	0.38
TP	0.02	0.02	0.02	0.12	0.98	0.92
NH_4	-0.04	0.08	0.05	0.42	0.79	0.52
NO_3	0.07	0.17	0.12	0.23	0.92	0.70
TKN	-0.22	0.28	0.25	0.37	-0.03	0.34
TN	-0.15	0.25	0.18	0.15	0.75	0.72
DO	0.45	0.80	0.66	0.09	-1.00	0.37
TSS	11.34	14.24	11.34	0.93	0.67	0.22
Wtemp	0.47	0.66	0.47	0.02	0.71	0.46

Table 4-23: Validation statistics by station for RPS continuous DO data

	North_S	South_S	South_B
RMS	0.55	0.88	0.65
ME	-0.50	-0.78	-0.59
MAE	0.5	0.79	0.59
RE	0.06	0.09	0.07
R	0.51	0.41	0.52
d	0.42	0.43	0.44

Table 4-24: Validation statistics by station for RPS continuous temperature data

	North_S	South_S	South_B
RMS	0.49	1.05	0.74
ME	-0.41	-0.88	-0.65
MAE	0.41	0.88	0.66
RE	0.02	0.05	0.04
R	0.96	0.77	0.93
d	0.92	0.66	0.79

Chl a: Although there are only four measured values for Chl *a* during the validation period, the model agreement with those values is excellent (*RE* = 0.08, see Table 4-21). The model also shows a tendency to follow the measured trends for those data that fall outside the validation period. Such good model agreement is encouraging since only one algal group is included, and this group was calibrated for summer algal concentrations, whereas the spring algae are most likely diatoms, which are quite different from summer algae.

Nutrients: Similar to the calibration, PO_4 is mostly over-predicted for the validation due to the inability to create adsorption to AAP with settling. However, the error for PO_4 in the validation is less than in the calibration with *RE* of 0.59. The agreement of model TP with measured TP is excellent, although there are only four measured values during the validation period. However, the model trend for TP is quite similar to the measured trend for the data outside the validation period. The *RE* for TP validation is 0.12, which is very good.

Model-computed NH_4 tends to agree fairly well with the measured trends in NH_4 and is quite close to three of the four measured values available during the validation period. There is an outlier for the computed versus measured NH_4 at station AC, which is the same station that exhibited an anomaly for DO calibration. The *RE* for NH_4 validation is 0.42. Model-computed NO_3 agrees quite closely with three of the four measured values available during the validation period and the computed trend in NO_3 tends to agree with the measured trend for those data outside the validation period. The *RE* for NO_3 validation is 0.23.

Overall, model TKN for validation is low compared with measured, same as for calibration, which is probably due to the under-estimated loadings of organic matter along the NECFR. However, model accuracy for TKN validation is better than for calibration, with *RE* = 0.37. Likewise, model accuracy for TN validation is better than for calibration, with *RE* = 0.15, which is quite good although measured data are sparse.

Dissolved Oxygen: There are only two measured DO values in the LCFRP data set during the validation period, but the model DO agrees closely with those two values. There are continuous DO recordings at two stations from the RPS data. These stations are denoted as North and South stations. The North Station is near LCFRP station M61, and the South station is near LCFRP station M18. Model DO is lower than measured at both RPS stations throughout the validation period, with an under-predicted mean error between 0.50 and 0.78 mg/L. The measured RPS DO is close to saturation, whereas the model DO is under-saturated. As discussed previously, model DO was fairly sensitive to reaeration, but such adjustments did not increase DO to saturation. Evidently the model DO uptake mechanisms were slightly too strong for the validation period. It is possible that the temperature coefficients that affect kinetic mineralization rates could be too low for temperatures below 20 degrees C. It is also possible that adjusting these temperature coefficients could reduce DO uptake in cool seasons, but such adjustments also impact DO uptake in warm seasons. Thus, the default temperature coefficients were used. Even with the model under-predicting DO, the *RE* values of 0.09 and 0.07 for the LCFRP and RPS data, respectively, are quite good.

TSS and Temperature: Although model TSS is over-predicted, the model trends in TSS are similar to those measured. The TSS *RE* for validation is 0.93, which is higher than for calibration. The only constituent affected by TSS is algae due to the effect of TSS on light.

Model-computed water temperature agrees very closely with measured values for both data sets. The validation *RE* values for water temperature are 0.02 and 0.04 for the LCFRP and RPS data, respectively, which are quite good. Except for PO_4, the validation confirms that the calibration is acceptable to excellent based on the LCFRP data; however, most of the RPS does not exist due to instrument failure. The temperature that was available at RPS showed that this part of the model was well validated. In some cases, the validation statistics are better than the calibration statistics. The water is much colder with less biological activity for the validation period, and these conditions may contribute substantially to better model performance statistics.

4.5.4.3. Year-Long Validation

The calibrated model was tested further through a full year, validation using a typical (or average) flow year. Development of this validation and the results are described below.

Model Setup

Wind and Air Temperature: For the full model domain, long-term hourly average wind speed and air temperature were obtained from METAR KILM (Wilmington airport). The time period obtained was 1943-2017 and the data were at a typical frequency of hourly.

Offshore Boundary Condition: The offshore water level boundary conditions are the same as those used in the HD calibration process. The constituent loadings were varied monthly using measured concentrations averaged for each month over the years 2004 through 2017 at LCFRP station M18. The same approach described previously was employed to derive concentrations for unmeasured constituents. Water temperature for the offshore boundary was based on the long-term hourly average from NDBC 41031 for the period 2004 through 2017. Finally, salinities were set using the same methods as in the salinity calibration and validation: salinity data along the model offshore boundaries were extracted from the Global Hybrid Coordinate Ocean Model (HYCOM) hindcast simulations from April/May 2017 and vertically uniform salinity boundary conditions were imposed.

Upstream Flow Boundary Conditions: The upstream, flow boundary conditions were based on an analysis of discharge data from three USGS stations as shown in Figure 4-108 and Table 4-25. They are USGS Station 02105769 (Cape Fear River), USGS Station 02106500 (Black River), and USGS Station 02108000 (Northeast Cape Fear River). For computational efficiencies given long run times for the HD model, the long term, daily measured flows for each of these stations was averaged for twenty-six, two week periods over periods of record to determine three typical flow regimes for each two week period categorized as high, medium and low as shown in Table 4-26, Table 4-27, and Table 4-28. The total average flow for these three regimes distributed over a full year is equivalent to the average annual mean flow at each gage. Model runs were developed for the high/medium/low flow periods and assembled together to create a year-long, typical (or average) flow for the model for an entire year.

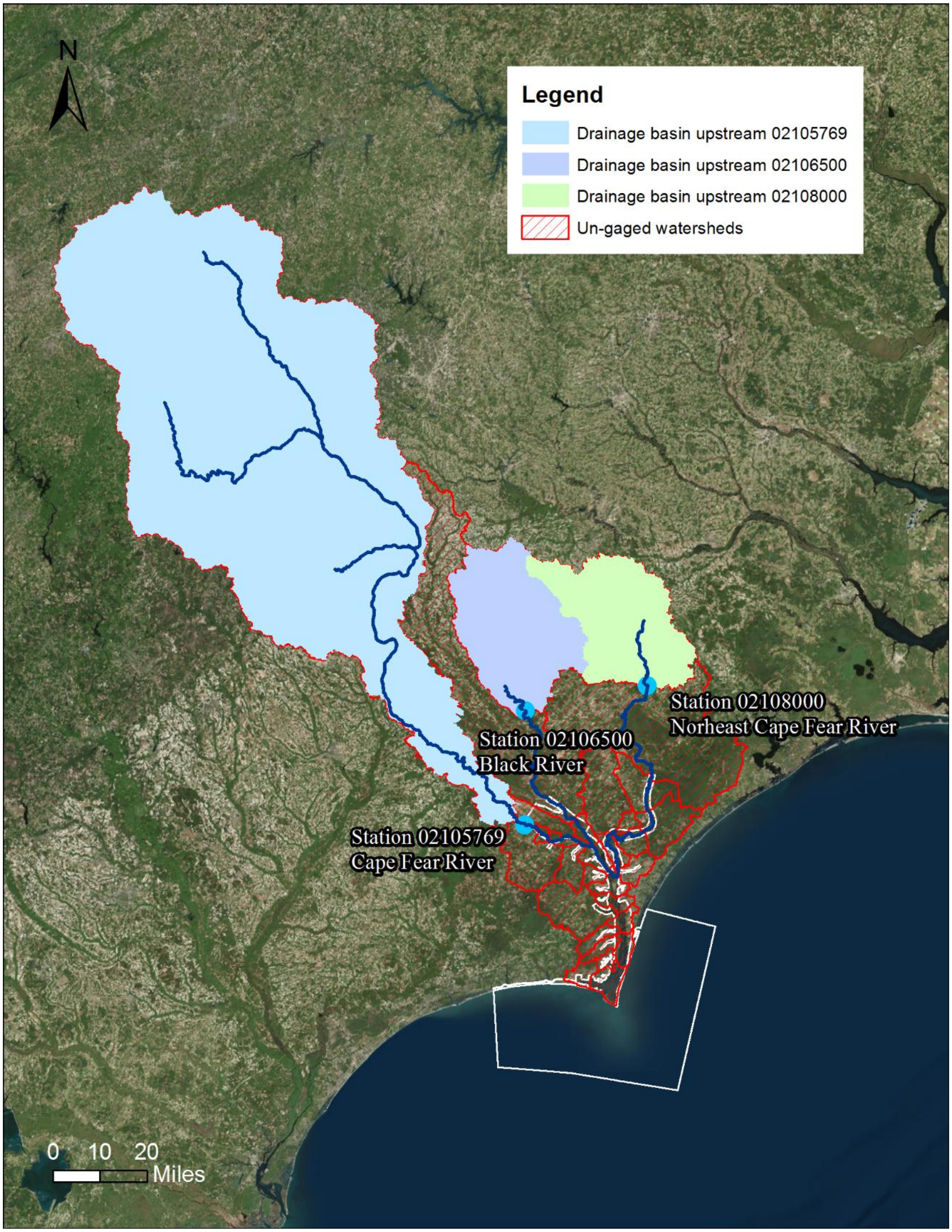

Figure 4-108: Gaged and un-gaged drainage areas

Table 4-25: USGS river gage station information

Station	Period of Observations (1 day)
0210800 Northeast Cape Fear River near Chinquapin	1940-present
02106500 Black River near Tomahawk	1951-present
02105769 Cape Fear River at Lock 1 near Kelly	1969-present

Table 4-26: Typical year flows – Cape Fear River

Statistics	Mean Flow at CFR (m^3/s)	Modeled flow at CFR (m^3/s)	Flow Condition
Bi-week01	195.53	160	Medium
Bi-week02	249.02	260	High
Bi-week03	247.89	260	High
Bi-week04	246.11	260	High
Bi-week05	289.89	260	High
Bi-week06	267.26	260	High
Bi-week07	257.02	260	High
Bi-week08	191.31	160	Medium
Bi-week09	159.95	160	Medium
Bi-week10	123.93	160	Medium
Bi-week11	106.93	95	Low
Bi-week12	101.93	95	Low
Bi-week13	100.16	95	Low
Bi-week14	84.96	95	Low
Bi-week15	92.27	95	Low
Bi-week16	84.81	95	Low
Bi-week17	83.85	95	Low
Bi-week18	80.55	95	Low
Bi-week19	103.37	95	Low
Bi-week20	99.92	95	Low
Bi-week21	99.82	95	Low
Bi-week22	84.3	95	Low
Bi-week23	94.85	95	Low
Bi-week24	115.84	95	Low
Bi-week25	129.09	160	Medium
Bi-week26	157.48	160	Medium
Total Year	148	148	-

Table 4-27: Typical year flows – Black River

Statistics	Mean Flow at BR (m^3/s)	Modeled flow at BR (m^3/s)	Flow Condition
Bi-week01	28.21	22	Medium
Bi-week02	33.20	36	High
Bi-week03	35.82	36	High
Bi-week04	35.94	36	High
Bi-week05	39.77	36	High
Bi-week06	36.31	36	High
Bi-week07	33.49	36	High
Bi-week08	29.19	22	Medium
Bi-week09	19.97	22	Medium
Bi-week10	15.35	22	Medium
Bi-week11	12.87	16	Low
Bi-week12	12.79	16	Low
Bi-week13	13.43	16	Low
Bi-week14	12.87	16	Low
Bi-week15	15.37	16	Low
Bi-week16	16.52	16	Low
Bi-week17	19.65	16	Low
Bi-week18	17.27	16	Low
Bi-week19	23.06	16	Low
Bi-week20	17.48	16	Low
Bi-week21	18.86	16	Low
Bi-week22	11.85	16	Low
Bi-week23	14.20	16	Low
Bi-week24	17.24	16	Low
Bi-week25	18.89	22	Medium
Bi-week26	23.20	22	Medium
Total Year	22	22	-

Table 4-28: Typical year flows – Northeast Cape Fear River

Statistics	Mean Flow at NECFR (m^3/s)	Modeled flow at NECFR (m^3/s)	Flow Condition
Bi-week01	38.35	21	Medium
Bi-week02	31.98	33	High
Bi-week03	35.74	33	High
Bi-week04	34.49	33	High
Bi-week05	34.61	33	High
Bi-week06	30.89	33	High
Bi-week07	29.95	33	High
Bi-week08	24.1	21	Medium
Bi-week09	18.13	21	Medium
Bi-week10	13.23	21	Medium
Bi-week11	12	15	Low
Bi-week12	11.35	15	Low
Bi-week13	10.75	15	Low
Bi-week14	11.84	15	Low
Bi-week15	12.69	15	Low
Bi-week16	13.44	15	Low
Bi-week17	19.66	15	Low
Bi-week18	19.84	15	Low
Bi-week19	23.39	15	Low
Bi-week20	16.85	15	Low
Bi-week21	16.51	15	Low
Bi-week22	10.58	15	Low
Bi-week23	12.04	15	Low
Bi-week24	16.28	15	Low
Bi-week25	18.71	21	Medium
Bi-week26	22.73	21	Medium
Total Year	21	21	-

In a similar manner, discharges for the un-gaged drainage areas (red polygons in Figure 4-108) were included as point discharges in the model (Figure 4-106), and their total combined discharges are listed in Table 4-29 for the three flow conditions. These are treated the same as the gaged areas with 2-week variations stitched together to form a year-long run.

Table 4-29: Total discharge for un-gaged watersheds (typical year)

Flow	Q (m^3/s)
High Flow	129
Medium Flow	79
Low Flow	47

Additional Boundaries and Model Inputs: The permitted point source loadings were based on monthly data for each month from 2017 using the approach developed for model calibration.

The freshwater NPS loadings were varied monthly as well using measured concentrations averaged for each month over the years 2004 through 2017 at the three river inflow stations. The same approach described previously was employed to derive concentrations for unmeasured constituents.

Water temperatures at the three upstream river boundaries and non-point sources (un-gaged watershed) were based on the long-term daily average from USGS station 02105500 located at Lock and Dam 2 (time period: 06/2000-04/2004, frequency: daily).

Simulation Time Period: For the typical year, the HD model was initially simulated for a five-week period to allow for spin-up and to capture a complete month-long spring-neap tidal cycle for each of the high, medium and low flow conditions. The latter two weeks of each run were then used to develop the year-long water quality model run by stitching them together for the 26 bi-weekly periods. Simulating the full year with daily varying flow would have been computationally prohibitive.

Year-Long Validation Results

The year-long model output is plotted versus time for multiple constituents and multiple stations. These plots are provided in Appendix C-3. The plots compare model output to the boxplots of measured LCFRP station data for 2004-2017 for the typical flow year.

For the boxplots, the horizontal line in the box is the median value, the vertical extent of the box is the upper and lower quartile (i.e., 25 % of the data are above or below the quartile), and the whiskers (vertical lines with end bars) represent the upper and lower 1 percentile (i.e., 1 % of the data are above or below this value). The asterisks are the measured data that are outliers, i.e., they are above or below the whiskers or 1 percentile. The solid red and blue lines are the model results for the surface and bottom layers of the water column at the station. In most cases the two lines coincide indicating no differences in surface and bottom model values. The observed LCFRP data are based on surface measurements.

In comparing the results, it should be noted that although the model is compared in Appendix C-3 with long term, measured data obtained, the model results are influenced by 2017 point source loading concentrations, period-average flow rates from the HD model, and the overall parameters calibrated to summer of 2017. The measured data are affected by the actual loading concentrations and flow rates that occurred for each year. Therefore, model comparisons with observed data should be viewed in a general sense rather than specific metrics. Typical flow year results are discussed next.

There are many months and stations where model *Chl a* passes through the measured boxes, however, overall model *Chl a* values are over-predicted compared with measured data. The measured data indicates that *Chl a* peaks in the summer. The model *Chl a* also peaks in the summer for most stations, with the exceptions that it peaks in May at four stations in the lower estuary near the ocean and May – June for one station in the NECFR (station NCF6). The reason for the earlier model peak at station NCF6 could be due to lower computed TSS at that station during spring compared with the other stations. The reason for the earlier computed *Chl a* shift at the lower four stations is not known since TSS and TP concentrations at those stations appear similar in the late spring compared with other months. However, TN is higher during winter and spring than in summer and fall at almost all stations, but model TN is lower than measured overall. PO_4 is over-predicted overall with the highest over-predictions around September, so it is doubtful that abundance of PO_4 is the reason for the spring blooms in the model. It is possible that there are some algal limitation shifts between N and light during late spring for the lower four stations that promote earlier peak blooms. Overall, the model follows the measured *Chl a* trends fairly well with some over-prediction during peak blooms in the upper estuary, some under-prediction during peak blooms in the mid-estuary, and over-prediction during peak blooms (in the spring) at the two lower most stations.

Model PO_4 agrees fairly well with measured PO_4 in the upper estuary, although PO_4 is over-predicted at some of those stations for summer and fall. Model PO_4 is over-predicted throughout the year in the lower estuary. Over-prediction of PO_4 is due to the inability to remove PO4 via partitioning to and settling of AAP as explained previously in the calibration discussion. Some over-prediction of TP is evident in the comparison plots, particularly in the lower estuary, but model TP agrees better with measured TP than does PO_4 probably due to more accurate model representation of organic P.

Overall model NH_4 agrees fairly well with measured values for most stations throughout the year. Interestingly, model NH_4 is higher than all measured values at station B210 in July, where B210 is a model boundary station for the Black River, and NH_4 was measured at this station and used for model inputs. Reasonably good agreement for NH_4 is important since it affects DO.

Model NO_3 agrees quite well with measured values with the only exception in the lower estuary during winter when NO_3 is over-predicted. This over-prediction may be related to specification of the seaward boundary condition for NO_3 which used measured concentrations at station M18.

Model TKN agrees quite well with measured values in the upper Cape Fear River. Model TKN is generally lower than measured values in the NECFR and downstream of the confluence of the NECFR with the upper Cape Fear River. This result is due to NPS organic N loadings along the NECFR that are higher than specified in the model. As explained previously, model NPS organic N loadings were based only on measured TKN at station NCF117. Evidently, there are higher NPS loadings along the NECFR that could not be substantiated with the available measured data. Model TN agreement with measured values tends to follow the same trends as TKN, where TN is under-predicted along the NECFR and downstream of its confluence. This result is due to the under-specification of organic N along the NECFR.

Model DO follows the annual trend in measured DO extremely well, capturing the summer lows and winter highs. Overall, the model summer DO is slightly lower than measured values, which places model predictions on the conservative side for evaluating environmental impacts. Only at one station (NCF6) is model DO higher than measured values in the summer. This result is probably related to under-estimation of organic matter loadings along the NECFR as discussed previously.

Overall, model TSS appears to tend towards over-prediction compared with measured values. However, model TSS falls with bounds of measured data most of the time for all stations. Only *Chl a* is directly affected in the model by TSS via light attenuation. Of course, DO is indirectly affected by TSS due to TSS effect on algae.

Model water temperature follows the seasonal trend in measured water temperature quite well for all stations. There are some months where model and period measured data are different, which could be due to unusual meteorological conditions for that month in 2017. This potential reason is somewhat substantiated by the fact that the calibration/validation statistics for water temperature were excellent. Additionally, the rather simplified temperature modeling approach within DELWAQ does not include the effects of solar radiation on temperature. Considering this model simplification, the model-computed water temperatures are still quite accurate.

4.5.5. Model Sensitivity Test

To test the model's sensitivity to an alternative flow condition, a year-long simulation for dry year conditions was conducted to assess the effects on temperature, salinity, and DO relative to a typical year with normal flow conditions. The setup for this model test followed the general approach provided previously with a few differences explained below.

4.5.5.1. Model Setup

Data for meteorology and NPS concentrations were from 2011 rather than based on long term averages. In addition, flows for the dry year were developed to match the seasonal pattern and annual flow of 2011, a relatively low flow year, historically. The year-long run was developed in same manner as the typical year (e.g., stitching together 2-week periods of high, medium, and low flows). The assembled flow regimes are shown in Table 4-30 through Table 4-32. Un-gaged flows were based on information provided in Table 4-33.

Table 4-30: Dry year flows – Cape Fear River

Statistics	Mean Flow at CFR (m^3/s)	Modeled flow at CFR (m^3/s)	Flow Condition
Bi-week01	45.25	40	Medium
Bi-week02	41.53	40	Medium
Bi-week03	104.28	95	High
Bi-week04	63.22	95	High
Bi-week05	79.85	95	High
Bi-week06	100.98	95	High
Bi-week07	138.41	95	High
Bi-week08	125.76	95	High
Bi-week09	57.07	96	High
Bi-week10	50.54	40	Medium
Bi-week11	37.37	40	Medium
Bi-week12	24.11	25	Low
Bi-week13	34.39	40	Medium
Bi-week14	27.7	25	Low
Bi-week15	25.6	25	Low
Bi-week16	23.38	25	Low
Bi-week17	35.14	40	Medium
Bi-week18	35.51	40	Medium
Bi-week19	28.56	25	Low
Bi-week20	51.52	40	Medium
Bi-week21	24.46	25	Low
Bi-week22	27.31	25	Low
Bi-week23	36.3	40	Medium
Bi-week24	104.62	96	High
Bi-week25	93.58	96	High
Bi-week26	51.16	40	Medium
Total Year	56	56	-

Table 4-31: Dry year flows – Black River

Statistics	Mean Flow at BR (m^3/s)	Modeled flow at BR (m^3/s)	Flow Condition
Bi-week01	12.05	8	Medium
Bi-week02	12.21	8	Medium
Bi-week03	26.61	16	High
Bi-week04	17.36	16	High
Bi-week05	14.97	16	High
Bi-week06	12.87	16	High
Bi-week07	21.71	16	High
Bi-week08	13.81	16	High
Bi-week09	13.15	16	High
Bi-week10	8.04	8	Medium
Bi-week11	4.66	8	Medium
Bi-week12	0.81	3	Low
Bi-week13	1.31	8	Medium
Bi-week14	1.27	3	Low
Bi-week15	0.72	3	Low
Bi-week16	2.06	3	Low
Bi-week17	3.79	8	Medium
Bi-week18	17.49	8	Medium
Bi-week19	6.61	3	Low
Bi-week20	8.48	8	Medium
Bi-week21	4.09	3	Low
Bi-week22	4.33	3	Low
Bi-week23	8.08	8	Medium
Bi-week24	7.42	16	High
Bi-week25	7.91	16	High
Bi-week26	5.93	8	Medium
Total Year	9	9	-

Table 4-32: Dry year flows – Northeast Cape Fear River

Statistics	Mean Flow at NECFR (m^3/s)	Modeled flow at NECFR (m^3/s)	Flow Condition
Bi-week01	10.82	12	Medium
Bi-week02	13.41	12	Medium
Bi-week03	36.57	15	High
Bi-week04	18.61	15	High
Bi-week05	12.96	15	High
Bi-week06	8.75	15	High
Bi-week07	15.9	15	High
Bi-week08	10.4	15	High
Bi-week09	11.36	15	High
Bi-week10	4.18	12	Medium
Bi-week11	1.67	12	Medium
Bi-week12	0.34	4	Low
Bi-week13	0.26	12	Medium
Bi-week14	0.2	4	Low
Bi-week15	0.2	4	Low
Bi-week16	2.34	4	Low
Bi-week17	3.03	12	Medium
Bi-week18	58.84	12	Medium
Bi-week19	12.16	4	Low
Bi-week20	8.75	12	Medium
Bi-week21	10.69	4	Low
Bi-week22	5.28	4	Low
Bi-week23	10.41	12	Medium
Bi-week24	7.15	15	High
Bi-week25	7.64	15	High
Bi-week26	4.67	12	Medium
Total Year	11	11	-

Table 4-33: Total discharge for un-gaged watersheds (dry year)

Flow	Q (m^3/s)
High Flow	47
Medium Flow	20
Low Flow	12

4.5.5.2. Model Sensitivity Results

Time series plots of DO, water temperature, and salinity at the LCFRP stations are provided in Appendix C-4 for the year-long, dry year model results with comparison to the typical year model results. The boxplots of measured data for years 2004 – 2017 are included in the plots to provide reference conditions. Model surface and bottom constituent concentrations are also included in the plots. As explained previously, the comparisons are provided as a sensitivity analysis to assess how a dry year affects the three constituents relative to a typical year with normal flow conditions.

Comparison of DO for the dry year relative to the typical year shows that both years follow the same seasonal trend, but overall, the warm season DO of the dry year is higher than that of the typical year primarily for the mid-estuary. This result seems counter-intuitive to experience with rivers, where low summer water flow rate, or discharge, often results in lower DO compared with higher summer flow rate. However, estuaries can respond quite differently to discharge rate than rivers. For example, it is well known that the summer hypoxia (or dead zone) of Chesapeake Bay is usually greater for high flow years (https://www.chesapeakebay.net/state/dead_zone). This result is attributed to greater vertical stratification associated with higher freshwater flow and greater mass loadings of nutrients (and organic matter) that create oxygen demand and fuel algal blooms, which settle as detritus that exerts higher oxygen depletion below the pycnocline. Given the weaker stratification in the Cape Fear River, much of the cause of higher summer DO for the dry year could be attributed to lower loadings of organic matter, particularly nitrogen. Organic nitrogen not only contributes to DO depletion directly via mineralization to NH_4 followed by nitrification, but it also relates to loading of organic carbon, which also directly contributes to DO depletion via mineralization. The annual total mass loading of total nitrogen into the Cape Fear River system model is 9,700 and 4,000 metric tons N for the typical and dry years, respectively. Thus, it is concluded that much of the cause of higher DO for the dry year compared with the typical year is most likely due to about half as much nitrogen (or organic matter) loading for the dry year. It is possible that a high flow year will cause lower summer DO than the typical year. It is noted that DO values in the lower estuary are very similar for the dry and typical years, mostly likely due to coastal influence, which is more related to ocean conditions than freshwater flows. Very little DO vertical stratification is evident for both years.

Comparison of water temperature for the dry and typical years reveals much similarity over the year. However, the dry year summer temperatures are a little warmer overall, particularly in the upper estuary which is influenced more by water flow rate and local meteorological conditions. The higher summer water temperatures of the dry year could be attributed to the warmer conditions that usually coincide with low flow years. In fact, the summer average (June 1 – August 31) air temperature at Wilmington for the dry and typical years was 27.1 and 25.8 degrees C, respectively. Very little water temperature vertical stratification is evident for both years.

Comparison of salinity for the dry and typical years shows that the salinity is higher overall throughout the year for the dry year. Furthermore, surface and bottom salinity for the dry year is greater than the respective surface and bottom salinity for the typical year. However, vertical salinity stratification is greater for the typical year due to the higher freshwater flow rates. The differences in salinity for the two years are greater in the mid-estuary than in the upper and lower estuary.

4.5.6. Conclusion

To support a Feasibility Study and Environmental Impact Statement for the potential deepening of the navigation channel at the Port of Wilmington, a dynamic, water quality model was developed to represent the lower Cape Fear River and Estuary, using the Delft3D platform for water quality, DELWAQ.

The DELWAQ model was developed based on the best, available data from a variety of sources. In addition, a number of inputs and approaches are informed by a previous modeling effort of the waterbody by Bowen et al. (2009). Calibration focused on late summer of 2017, while validation was performed using two methods: a spring validation period from 2017 as well as a year-long validation representing long term, average conditions.

Nineteen state variables are simulated in the water quality model including water temperature, TSS, various forms of nitrogen and phosphorus, carbon, BOD, Chl *a*, and DO. The performance of all of the state variables is important since they interact in a variety of ways. However, temperature and DO in the navigation channel are the most important for the purposes of the project. To that end, *RE* values for DO ranged from 0.07 to 0.15 spanning the summer calibration, spring validation, and all observed data sets. These are in line with Arhonditsis and Brett (2004) suggesting a model of sufficient fit for its intended purpose. Indeed, DO follows the long-term, annual trends well and captures seasonal variations as demonstrated by the long-term, annual validation runs for typical and dry conditions.

Although model DO calibration and validation results are quite satisfactory along the Cape Fear River as well as where navigation channel deepening is proposed, the model DO is not satisfactory in the Northeast Cape Fear River (NECFR). Model DO is over-predicted in the NECFR with the reason attributed to under-estimation of NPS organic matter loadings, particularly organic nitrogen, which was used to estimate organic carbon. There are relatively large un-gaged NPS freshwater flows along the NECFR, especially during the calibration period. These flows were estimated based on scaling of watershed areas with the gaged watershed area and flows on the NECFR and were included in the model. However, due to lack of data, it was necessary to use monitoring data at station NCF117 for specifying inflow concentrations for both gaged and un-gaged freshwater flows. Although NPS organic matter loadings set in the model are believed to be too low, there were no available measured data that could be used to justify increasing these loads. As a result, model DO is under-predicted in the NECFR. Although the accuracy of the NECFR loadings and DO are less than desired, the effects of these inadequacies have a minimal impact on the relatively accurate DO predictions farther downstream along the navigation channel project. However it is recommended that future monitoring studies expend efforts to better quantify NPS loadings along the NECFR.

In addition to DO, model water temperature follows the seasonal trend in measured data quite well. Calibration and validation statistics for water temperature were excellent, with *RE* values ranging from 0.02 to 0.04.

Overall, the water quality model performs acceptably for various seasons throughout the year and can be used to predict the impacts of project alternatives on water quality relative to existing conditions with a high degree of confidence for proposed project alternatives.

5. Estuarine Numerical Modeling Results

The calibrated Delft 3-D models for hydrodynamics, salinity, cohesive sediments and water quality were utilized to calculate the changes in water levels, currents, salinity, water temperature, dissolved oxygen (DO), and anchorage basin shoaling rates due to the proposed project under various sea level rise scenarios.

5.1. Tentatively Selected Plan (TSP)

5.1.1. Project Configuration

The economic analyses determined that the only feasible channel deepening alternative is that for an authorized depth of -47 ft-MLLW in the river and -49 ft-MLLW beginning at the Battery Island Reach and extending offshore. Additionally, the vessel simulations determined that some widenings of the channel were necessary as well as a re-configuration of the turn near Battery Island. These modifications comprise the Tentatively Selected Plan and are summarized in Table 5-1.

In order to determine the potential impacts of the project, the models were run for two cases.

- Future without project (FwoP): -44 ft-MLLW (42 ft authorized depth + 2 ft over-dredge) in the river channel sections and -46 ft-MLLW (44 ft authorized depth + 2 ft over-dredge) from the Battery Island reach and extending offshore.

- Future with project (FwP): -49 ft-MLLW (47 ft authorized depth + 2 ft over-dredge) in the river channel sections and -51 ft-MLLW (49 ft authorized depth + 2 ft over-dredge) from the Battery Island reach and extending offshore.

The river bathymetry for these two configurations near Wilmington, the Lilliput Reach and Battery Island are shown in Figure 5-1, Figure 5-2 and Figure 5-3 respectively.

Table 5-1: Summary of Existing and Proposed Channel Widths

ID	Range Name	Channel Widths [Ft]		Widening Details
		Existing Channel	Proposed	
0	Entrance	N/A	600	New
1	Bald Head Shoal Reach 3	500 - 900	600 - 900	Symmetric
2	Bald Head Shoal Reach 2	900	900	No Change
3	Bald Head Shoal Reach 1	700	900	Green Side Only
4	Smith Island	650	900	Red Side Only
5	Bald Head - Caswell	500	800	Red Side Only
6	Southport	500	800	Re-orientation Red Side then Green Side
7	Battery	500	800 - 1300	Replaced with 4000-ft Radius Curve And Green Side at Apex
8	Lower Swash	400	800 - 500	Green Side to Symmetric
9	Snows Marsh	400	500	Symmetric
10	Horseshoe Shoal	400	500	Symmetric
11	Reaves Point	400	500	Symmetric
12	Lower Midnight	600	600	No Change
13	Upper Midnight	600	600	No Change
14	Lower Lilliput	600	600	No Change
15	Upper Lilliput	400	500	Symmetric
16	Keg Island	400	500	Symmetric
17	Lower Big Island	400	500	Symmetric
18	Upper Big Island	660	660	No Change
19	Lower Brunswick	400	500	Symmetric
20	Upper Brunswick	400	500	Symmetric
21	Fourth East Jetty	500	550	Green Side Only
22	Between Channel	550	625	Green Side Only
22	Anchorage Basin	625	625 - 1509	No Change

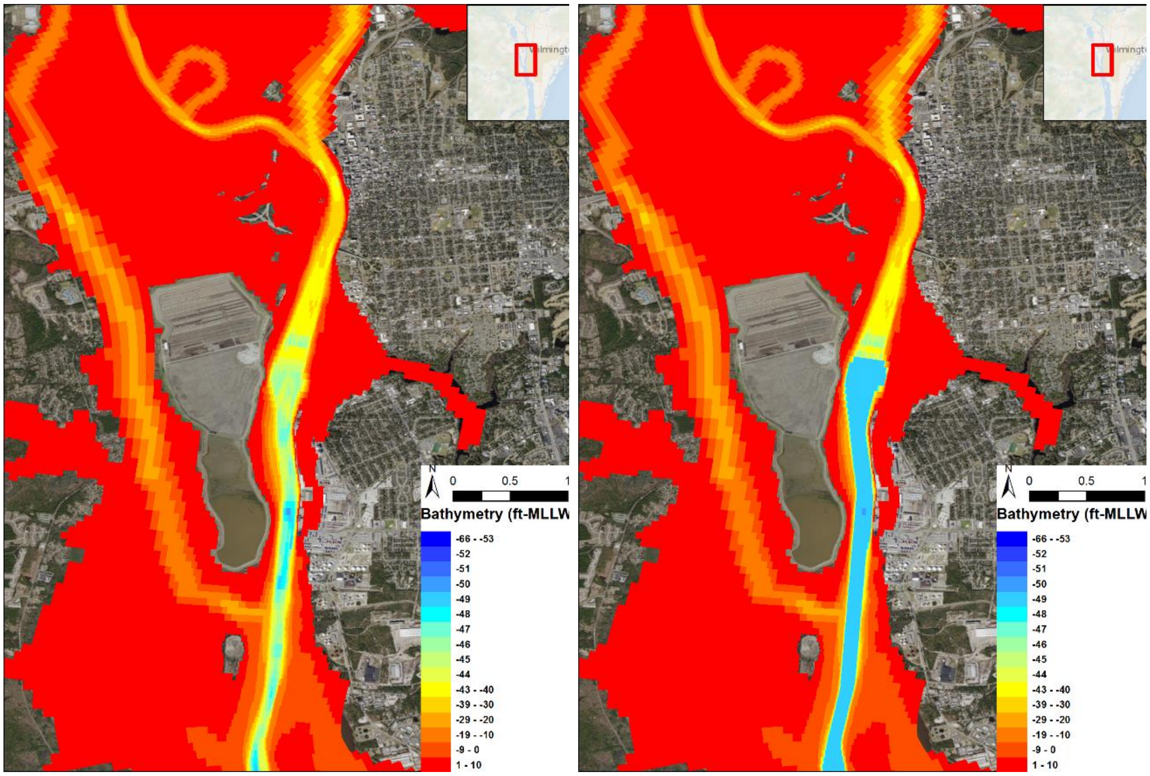

Figure 5-1: Bathymetry map near Wilmington (left: FwoP, right: FwP)

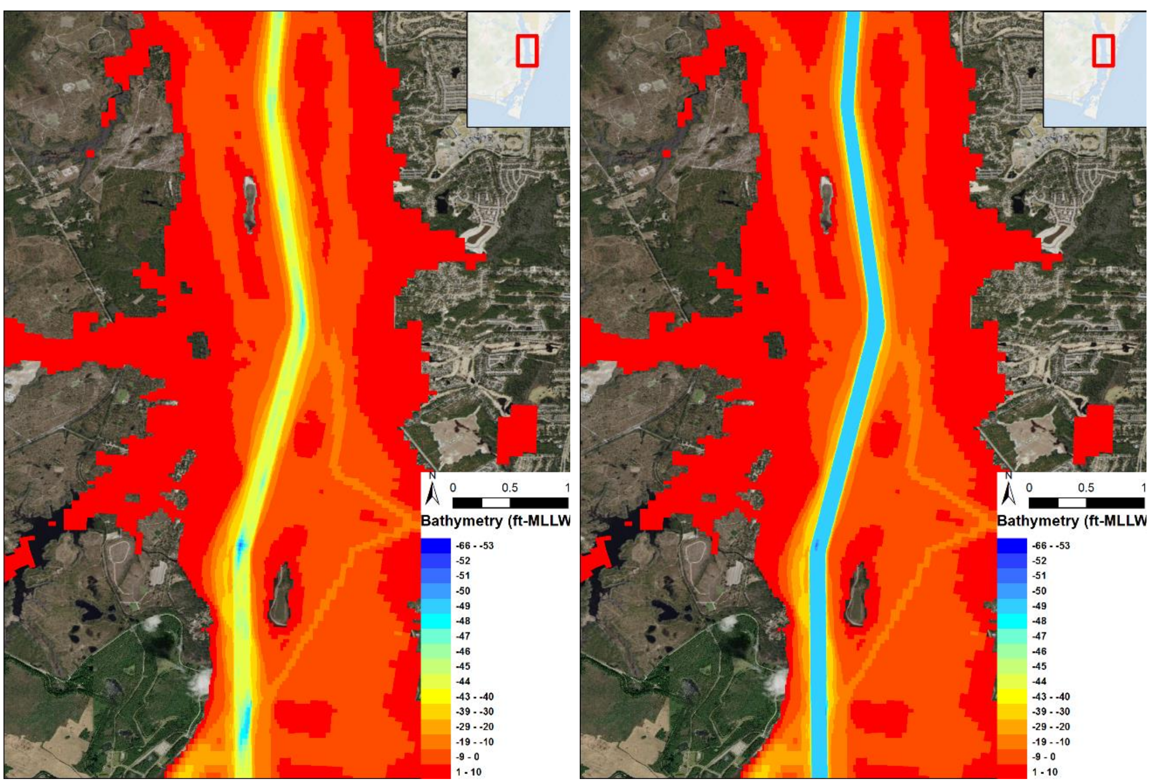

Figure 5-2: Bathymetry map near Lilliput Reach (left: FwoP, right: FwP)

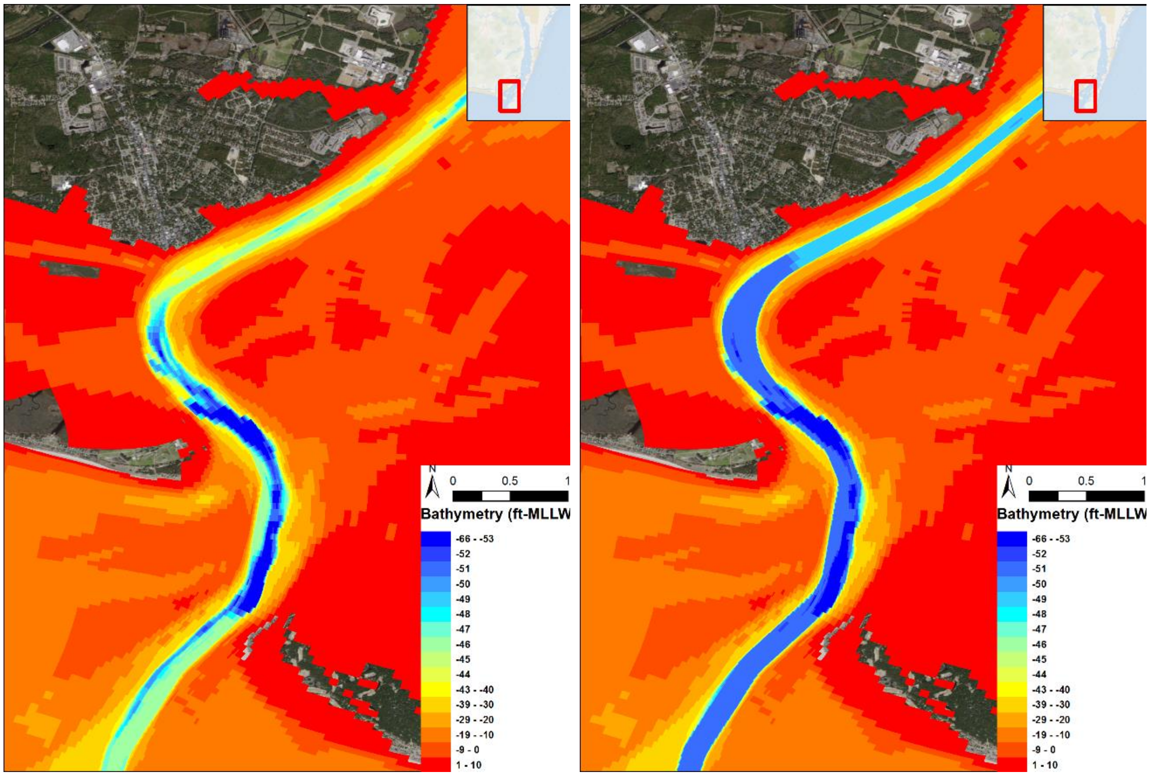

Figure 5-3: Bathymetry map near Battery Island (left: FwoP, right: FwP)

5.2. Boundary Condition

5.2.1. Offshore Boundary Condition

For the analysis of potential impacts of the project, the offshore boundary conditions for the model are the same as those used in the HD calibration process: an astronomical tide boundary for the Typical and Dry Year cases, and a time series of measured water levels from Wrightsville Beach with wind velocities from the KILM weather station corresponding to Hurricane Matthew for the Hurricane case. The offshore hydrograph with the RSLR low scenario for Hurricane Matthew is shown in Figure 5-4.

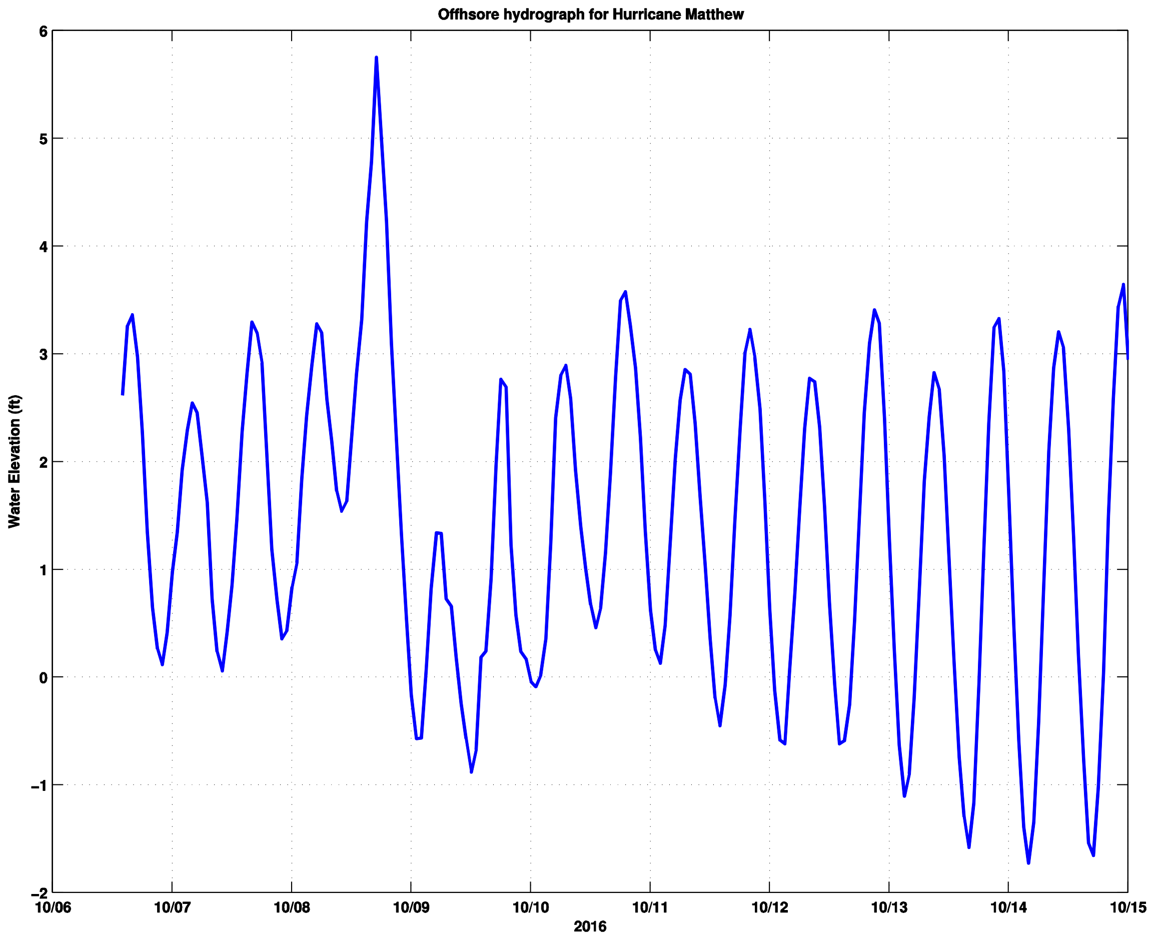

Figure 5-4: Offshore hydrograph for Hurricane Matthew

5.2.2. Upstream Boundary Condition

The upstream, flow boundary conditions were based on an analysis of discharge data from three USGS stations. They are USGS Station 02105769 (Cape Fear River), USGS Station 02106500 (Black River), and USGS Station 02108000 (Northeast Cape Fear River). For computational efficiencies given long run times for the HD model, the long term, daily measured flows for each of these stations were averaged for twenty-six, two week periods over the period of record to determine three typical flow regimes for each two week period categorized as high, medium and low as shown in Table 5-2 through Table 5-4. The total average flow for these three regimes distributed over a full year is equivalent to the average annual mean flow at each gage. Model runs were developed for the high/medium/low flow periods and assembled together to create a year-long, Typical (or average) flow for the model for an entire year.

To test the model's sensitivity to an alternative flow condition, a year-long simulation for Dry year conditions was conducted to assess the effects on temperature, salinity, and DO relative to a typical year with normal flow conditions. Flows for the Dry year were developed to match the seasonal pattern and annual flow of 2011, a relatively dry / low flow year, historically. In addition, data for meteorology and NPS concentrations were from 2011 rather than based on long term averages. The year-long run was developed in the same manner as the Typical year (e.g., stitching together 2-week periods of high, medium, and low flows). The assembled flow regimes are shown in Table 5-5 through Table 5-7. For the hurricane event simulation, the upstream flow condition was based on the Typical Low Flow to capture the largest tidal prism in the estuary.

Table 5-2: Typical year flows - Cape Fear River

Statistics	Mean Flow at CFR (m^3/s)	Modeled flow at CFR (m^3/s)	Flow Condition
Bi-week01	195.53	160	Medium
Bi-week02	249.02	260	High
Bi-week03	247.89	260	High
Bi-week04	246.11	260	High
Bi-week05	289.89	260	High
Bi-week06	267.26	260	High
Bi-week07	257.02	260	High
Bi-week08	191.31	160	Medium
Bi-week09	159.95	160	Medium
Bi-week10	123.93	160	Medium
Bi-week11	106.93	95	Low
Bi-week12	101.93	95	Low
Bi-week13	100.16	95	Low
Bi-week14	84.96	95	Low
Bi-week15	92.27	95	Low
Bi-week16	84.81	95	Low
Bi-week17	83.85	95	Low
Bi-week18	80.55	95	Low
Bi-week19	103.37	95	Low
Bi-week20	99.92	95	Low
Bi-week21	99.82	95	Low
Bi-week22	84.3	95	Low
Bi-week23	94.85	95	Low
Bi-week24	115.84	95	Low
Bi-week25	129.09	160	Medium
Bi-week26	157.48	160	Medium
Total Year	148	148	-

Table 5-3: Typical year flows - Black River

Statistics	Mean Flow at BR (m^3/s)	Modeled flow at BR (m^3/s)	Flow Condition
Bi-week01	28.21	22	Medium
Bi-week02	33.20	36	High
Bi-week03	35.82	36	High
Bi-week04	35.94	36	High
Bi-week05	39.77	36	High
Bi-week06	36.31	36	High
Bi-week07	33.49	36	High
Bi-week08	29.19	22	Medium
Bi-week09	19.97	22	Medium
Bi-week10	15.35	22	Medium
Bi-week11	12.87	16	Low
Bi-week12	12.79	16	Low
Bi-week13	13.43	16	Low
Bi-week14	12.87	16	Low
Bi-week15	15.37	16	Low
Bi-week16	16.52	16	Low
Bi-week17	19.65	16	Low
Bi-week18	17.27	16	Low
Bi-week19	23.06	16	Low
Bi-week20	17.48	16	Low
Bi-week21	18.86	16	Low
Bi-week22	11.85	16	Low
Bi-week23	14.20	16	Low
Bi-week24	17.24	16	Low
Bi-week25	18.89	22	Medium
Bi-week26	23.20	22	Medium
Total Year	22	22	-

Table 5-4: Typical year flows - Northeast Cape Fear River

Statistics	Mean Flow at NECFR (m^3/s)	Modeled flow at NECFR (m^3/s)	Flow Condition
Bi-week01	28.35	21	Medium
Bi-week02	31.98	33	High
Bi-week03	35.74	33	High
Bi-week04	34.49	33	High
Bi-week05	34.61	33	High
Bi-week06	30.89	33	High
Bi-week07	29.95	33	High
Bi-week08	24.1	21	Medium
Bi-week09	18.13	21	Medium
Bi-week10	13.23	21	Medium
Bi-week11	12	15	Low
Bi-week12	11.35	15	Low
Bi-week13	10.75	15	Low
Bi-week14	11.84	15	Low
Bi-week15	12.69	15	Low
Bi-week16	13.44	15	Low
Bi-week17	19.66	15	Low
Bi-week18	19.84	15	Low
Bi-week19	23.39	15	Low
Bi-week20	16.85	15	Low
Bi-week21	16.51	15	Low
Bi-week22	10.58	15	Low
Bi-week23	12.04	15	Low
Bi-week24	16.28	15	Low
Bi-week25	18.71	21	Medium
Bi-week26	22.73	21	Medium
Total Year	21	21	-

Table 5-5: Dry year flows – Cape Fear River

Statistics	Mean Flow at CFR (m^3/s)	Modeled flow at CFR (m^3/s)	Flow Condition
Bi-week01	45.25	40	Medium
Bi-week02	41.53	40	Medium
Bi-week03	104.28	95	High
Bi-week04	63.22	95	High
Bi-week05	79.85	95	High
Bi-week06	100.98	95	High
Bi-week07	138.41	95	High
Bi-week08	125.76	95	High
Bi-week09	57.07	95	High
Bi-week10	50.54	40	Medium
Bi-week11	37.37	40	Medium
Bi-week12	24.11	25	Low
Bi-week13	34.39	40	Medium
Bi-week14	27.7	25	Low
Bi-week15	25.6	25	Low
Bi-week16	23.38	25	Low
Bi-week17	35.14	40	Medium
Bi-week18	35.51	40	Medium
Bi-week19	28.56	25	Low
Bi-week20	51.52	40	Medium
Bi-week21	24.46	25	Low
Bi-week22	27.31	25	Low
Bi-week23	36.3	40	Medium
Bi-week24	104.62	95	High
Bi-week25	93.58	95	High
Bi-week26	51.16	40	Medium
Total Year	56	55	-

Table 5-6: Dry year flows – Black River

Statistics	Mean Flow at BR (m^3/s)	Modeled flow at BR (m^3/s)	Flow Condition
Bi-week01	12.05	8	Medium
Bi-week02	12.21	8	Medium
Bi-week03	26.61	16	High
Bi-week04	17.36	16	High
Bi-week05	14.97	16	High
Bi-week06	12.87	16	High
Bi-week07	21.71	16	High
Bi-week08	13.81	16	High
Bi-week09	13.15	16	High
Bi-week10	8.04	8	Medium
Bi-week11	4.66	8	Medium
Bi-week12	0.81	3	Low
Bi-week13	1.31	8	Medium
Bi-week14	1.27	3	Low
Bi-week15	0.72	3	Low
Bi-week16	2.06	3	Low
Bi-week17	3.79	8	Medium
Bi-week18	17.49	8	Medium
Bi-week19	6.61	3	Low
Bi-week20	8.48	8	Medium
Bi-week21	4.09	3	Low
Bi-week22	4.33	3	Low
Bi-week23	8.08	8	Medium
Bi-week24	7.42	16	High
Bi-week25	7.91	16	High
Bi-week26	5.93	8	Medium
Total Year	9	9	-

Table 5-7: Dry year flows – Northeast Cape Fear River

Statistics	Mean Flow at NECFR (m^3/s)	Modeled flow at NECFR (m^3/s)	Flow Condition
Bi-week01	10.82	12	Medium
Bi-week02	13.41	12	Medium
Bi-week03	36.57	15	High
Bi-week04	18.61	15	High
Bi-week05	12.96	15	High
Bi-week06	8.75	15	High
Bi-week07	15.9	15	High
Bi-week08	10.4	15	High
Bi-week09	11.36	15	High
Bi-week10	4.18	12	Medium
Bi-week11	1.67	12	Medium
Bi-week12	0.34	4	Low
Bi-week13	0.26	12	Medium
Bi-week14	0.2	4	Low
Bi-week15	0.2	4	Low
Bi-week16	2.34	4	Low
Bi-week17	3.03	12	Medium
Bi-week18	58.84	12	Medium
Bi-week19	12.16	4	Low
Bi-week20	8.75	12	Medium
Bi-week21	10.69	4	Low
Bi-week22	5.28	4	Low
Bi-week23	10.41	12	Medium
Bi-week24	7.15	15	High
Bi-week25	7.64	15	High
Bi-week26	4.67	12	Medium
Total Year	11	11	-

Discharges for the un-gaged drainage areas were estimated as point discharges in the model as discussed previously and their total combined discharges are listed in Table 5-8.

Table 5-8: Total discharge for un-gaged watersheds

Year	Flow	Q (m^3/s)
Typical	High	129
Typical	Medium	79
Typical	Low	47
Dry	High	47
Dry	Medium	20
Dry	Low	12

TSS data were calculated using the same method as discussed previously and are presented in Table 5-9.

Table 5-9: Upstream TSS boundary conditions

Year	Flow	CFR TSS (mg/L)	BR TSS (mg/L)	NECFR TSS (mg/L)	Ungaged TSS (mg/L)
Typical	High	30	3	4	4
Typical	Medium	20	2	2	2
Typical	Low	13	2	2	2
Dry	High	13	2	2	2
Dry	Medium	8	2	2	2
Dry	Low	6	2	2	2

5.3. Simulation Time Period

For the typical year, the HD model was initially simulated for a five-week period to allow for spin-up and to capture a complete month-long spring-neap tidal cycle for each of the high, medium and low flow conditions. The latter two weeks of each run were then used to develop the year-long water quality model run by stitching them together for the 26 bi-weekly periods as previously discussed since simulating the full year with daily varying flow would have been computationally prohibitive.

In addition, at the end of the five week model run for the Typical year low flow and low RSLR scenario, Hurricane Matthew conditions for offshore water levels and wind velocities were added for both FwoP and FwP to determine the potential project impacts in the context of an extreme event.

5.4. Results

5.4.1. Hydrodynamic Results

The HD model results were analyzed for the Typical Year low, medium and high flow cases. The hydrodynamic results including water levels and current velocities were extracted at the locations shown in Figure 5-5 in order to compare the differences between the FwoP and FwP alternatives. For these hydrodynamic results, four weeks (28 days) of data from each flow condition were extracted and analyzed, so that a full spring-neap tide cycle was taken into account for the statistical analyses.

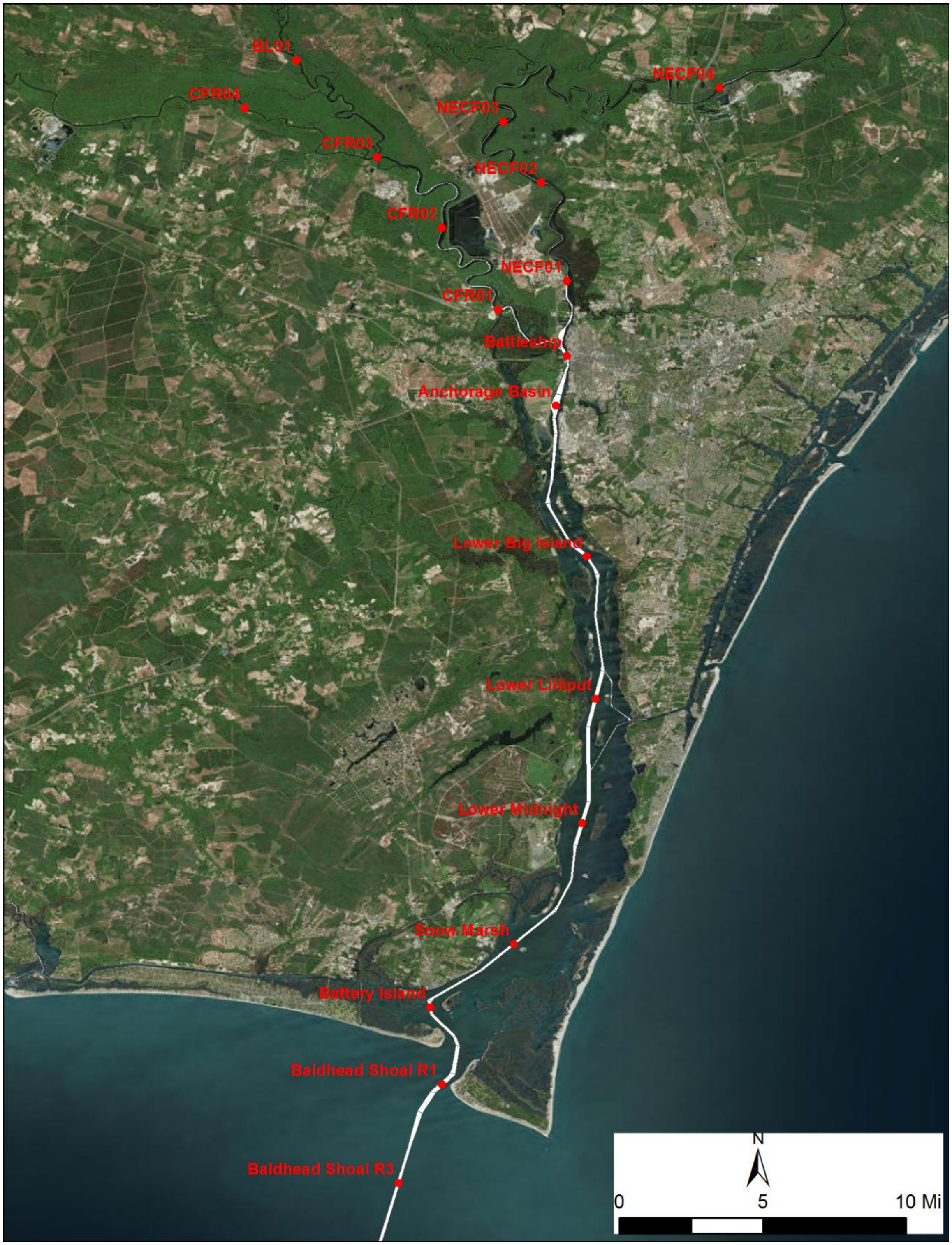

Figure 5-5: Extraction locations of HD and WAQ model results

5.4.1.1. Water level – Typical Conditions

To evaluate the proposed project's potential impacts on water levels under Typical river flow conditions, time series of water levels were extracted from the model results at the locations shown in Figure 5-5 and tidal parameters were calculated including Mean High Water (MHW), Mean Low Water (MLW) and Mean Tide Range (MTR) for the 28-day simulation period. Additionally, the differences between the *with project* and *without project* conditions (Δ = FwP - FwoP) were calculated for each of these parameters. The FwoP and FwP results for MTR, MHW and MLW are shown in Figure 5-6 to Figure 5-14, and detailed statistics are presented in Appendix D-1.

In general, FwP will slightly increase the overall tidal prism in the estuary (i.e., MHW increases, MLW decreases and MTR increases) compared to FwoP. For the Low and Intermediate sea level rise scenarios, the largest increase of MTR occurs at the Anchorage Basin (~0.3 ft). The change in tide range, though, is disproportional as MHW increases up to 0.12 ft while MLW decreases up to 0.18 ft at this location. For the High SLR scenarios, these values are minimally greater by approximately 0.01 ft for MHW and MLW, and by approximately 0.02 ft for MTR. The smallest changes occurred at the upstream riverine sites and downstream at the mouth of the Cape Fear Estuary (i.e., Baldhead Shoal).

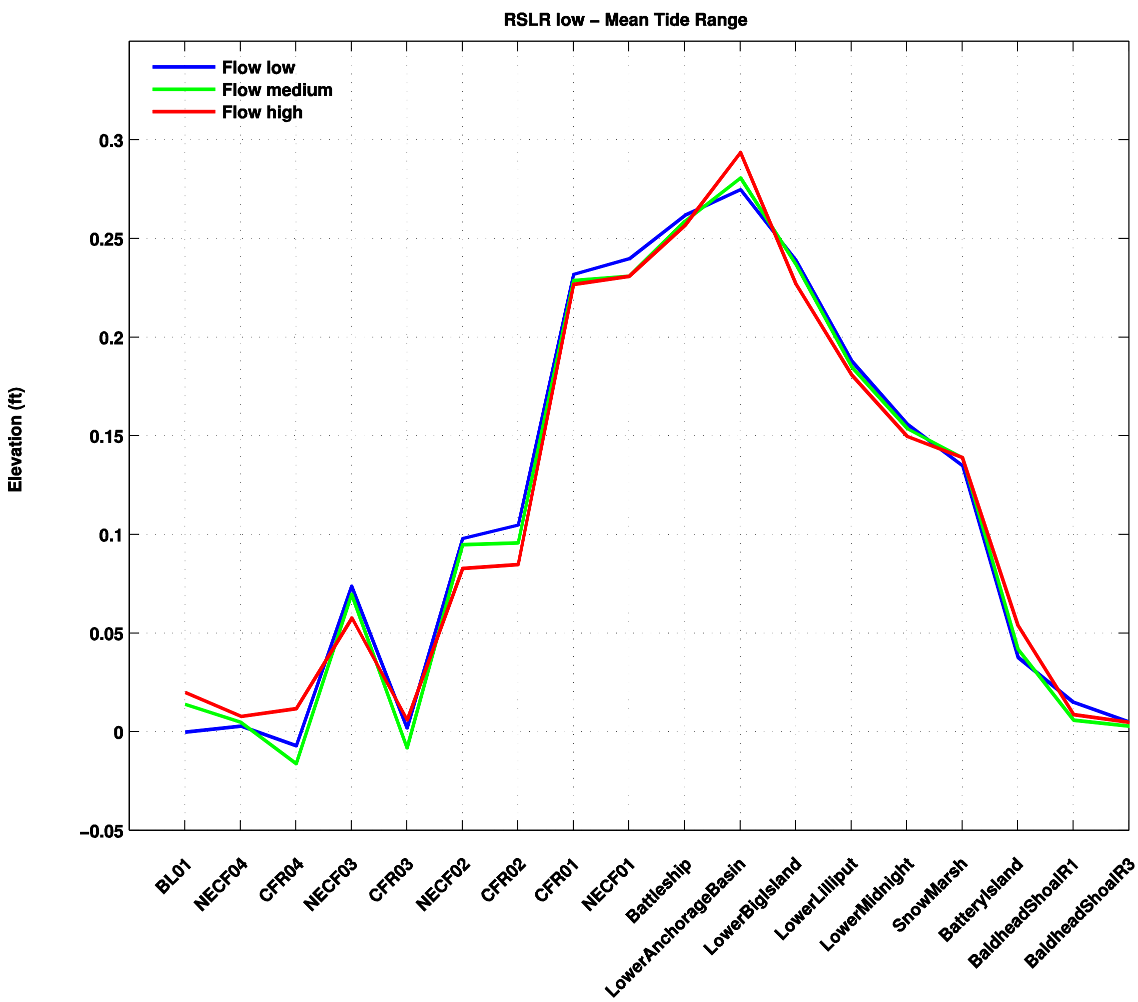

Figure 5-6: Differences between FwoP and FwP of Mean Tide Range (MTR) throughout the channel for RSLR low projection

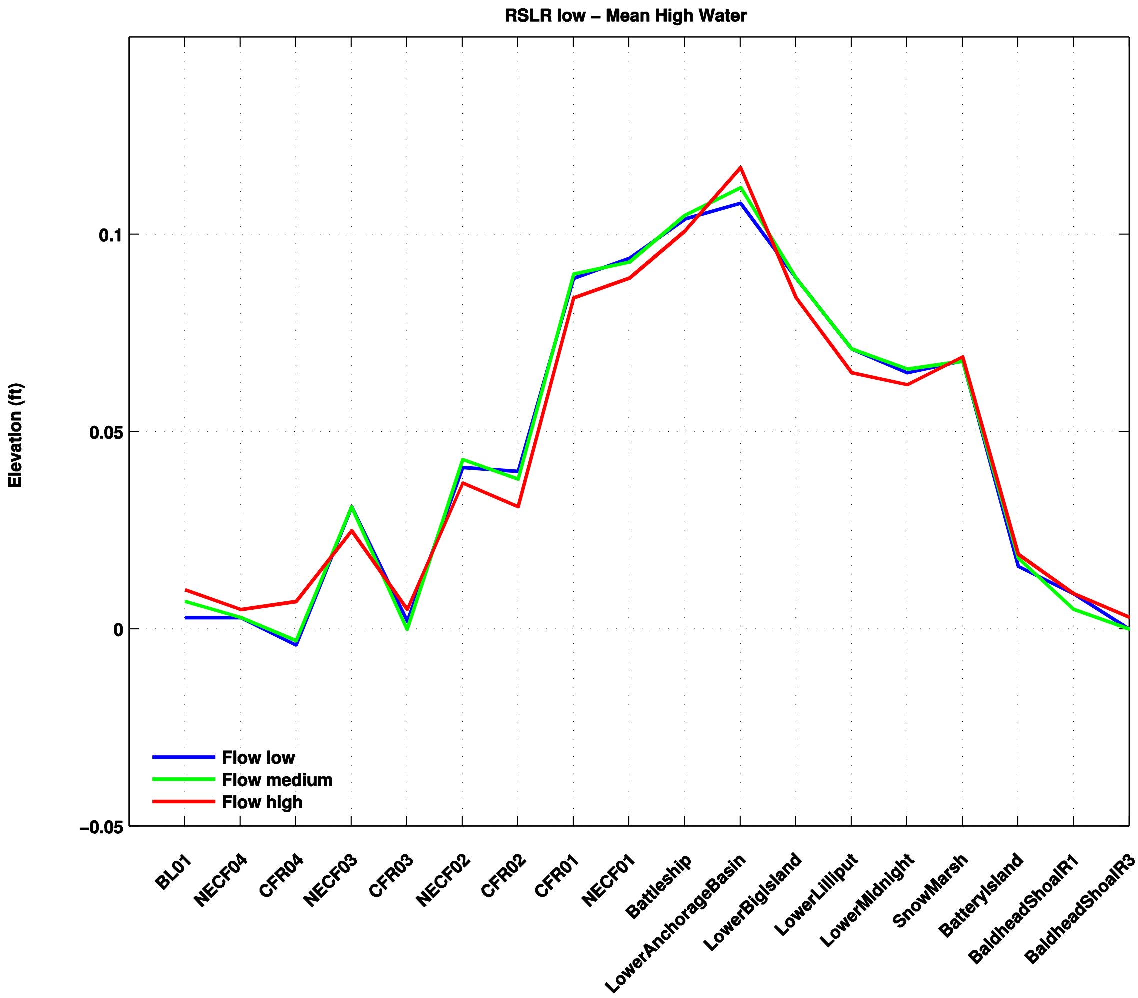

Figure 5-7: Differences between FwoP and FwP of Mean High Water (MHW) throughout the channel for RSLR low projection

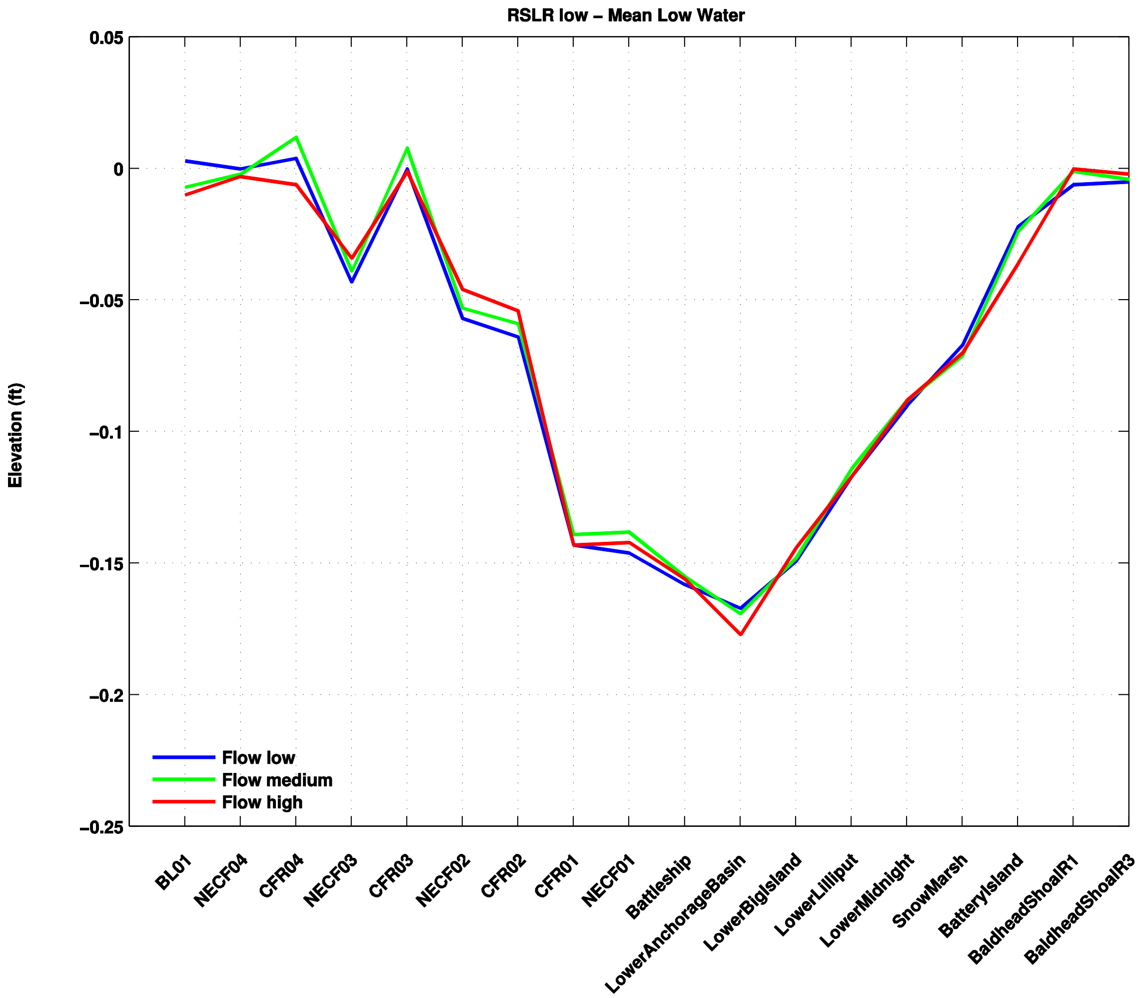

Figure 5-8: Differences between FwoP and FwP of Mean Low Water (MLW) throughout the channel for RSLR low projection

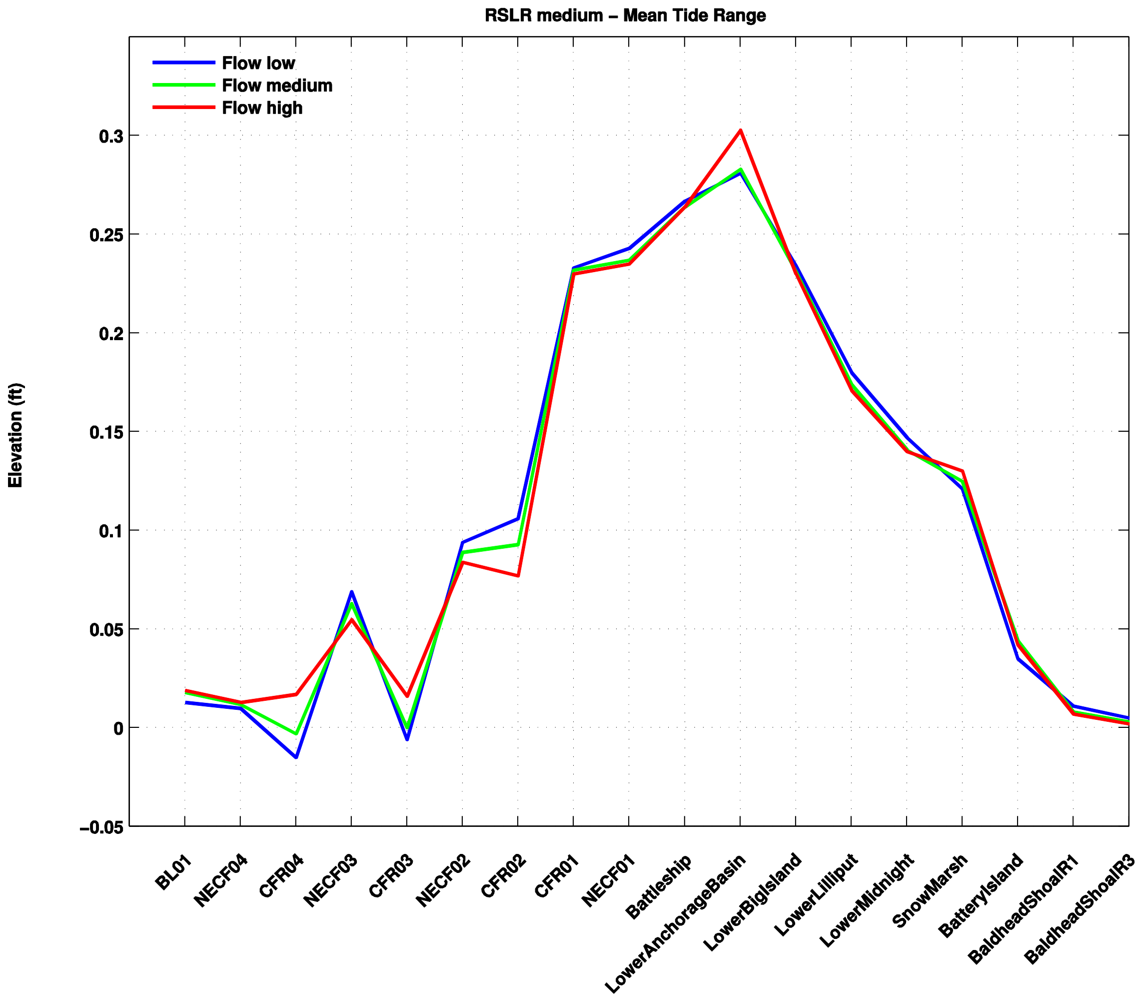

Figure 5-9: Differences between FwoP and FwP of Mean Tide Range (MTR) throughout the channel for RSLR Intermediate projection

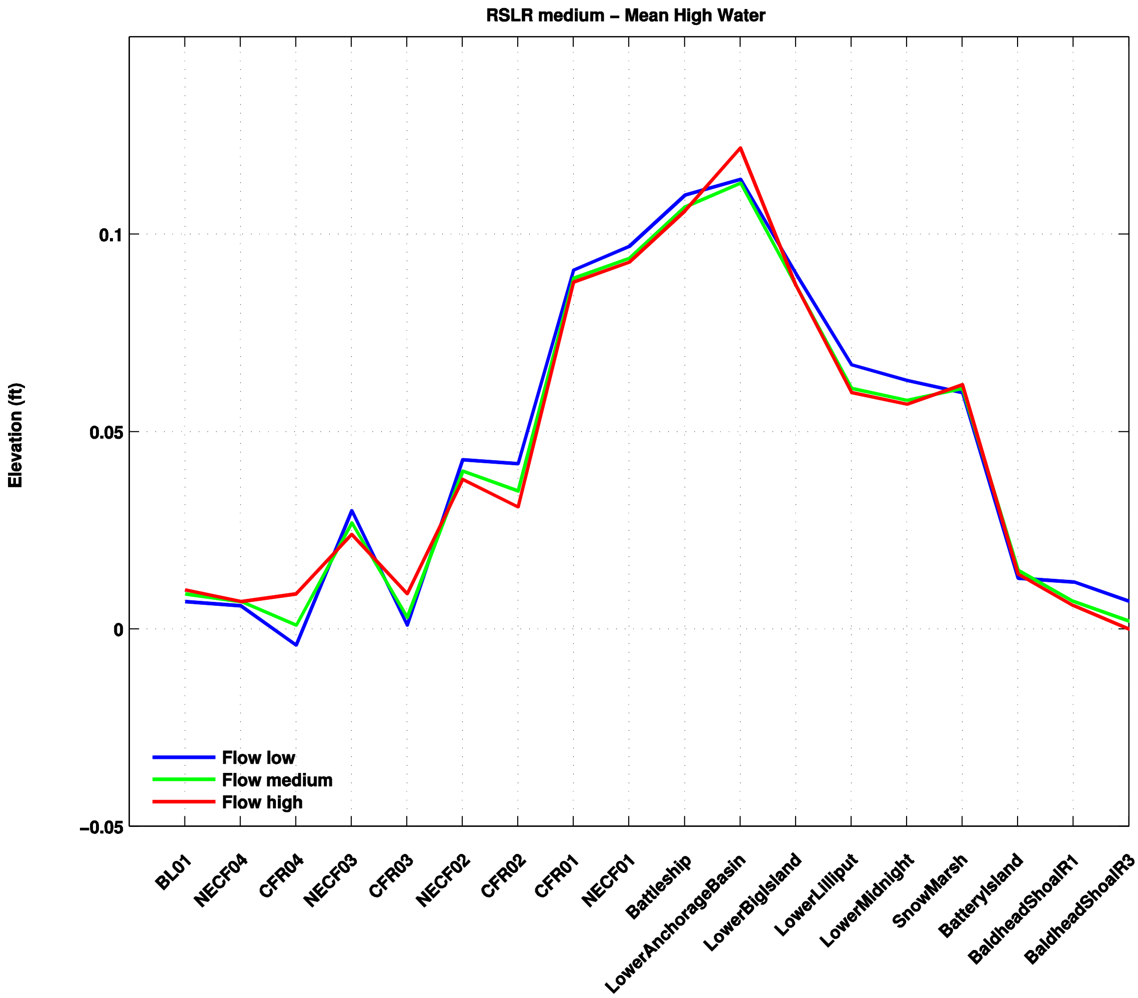

Figure 5-10: Differences between FwoP and FwP of Mean High Water (MHW) throughout the channel for RSLR Intermediate projection

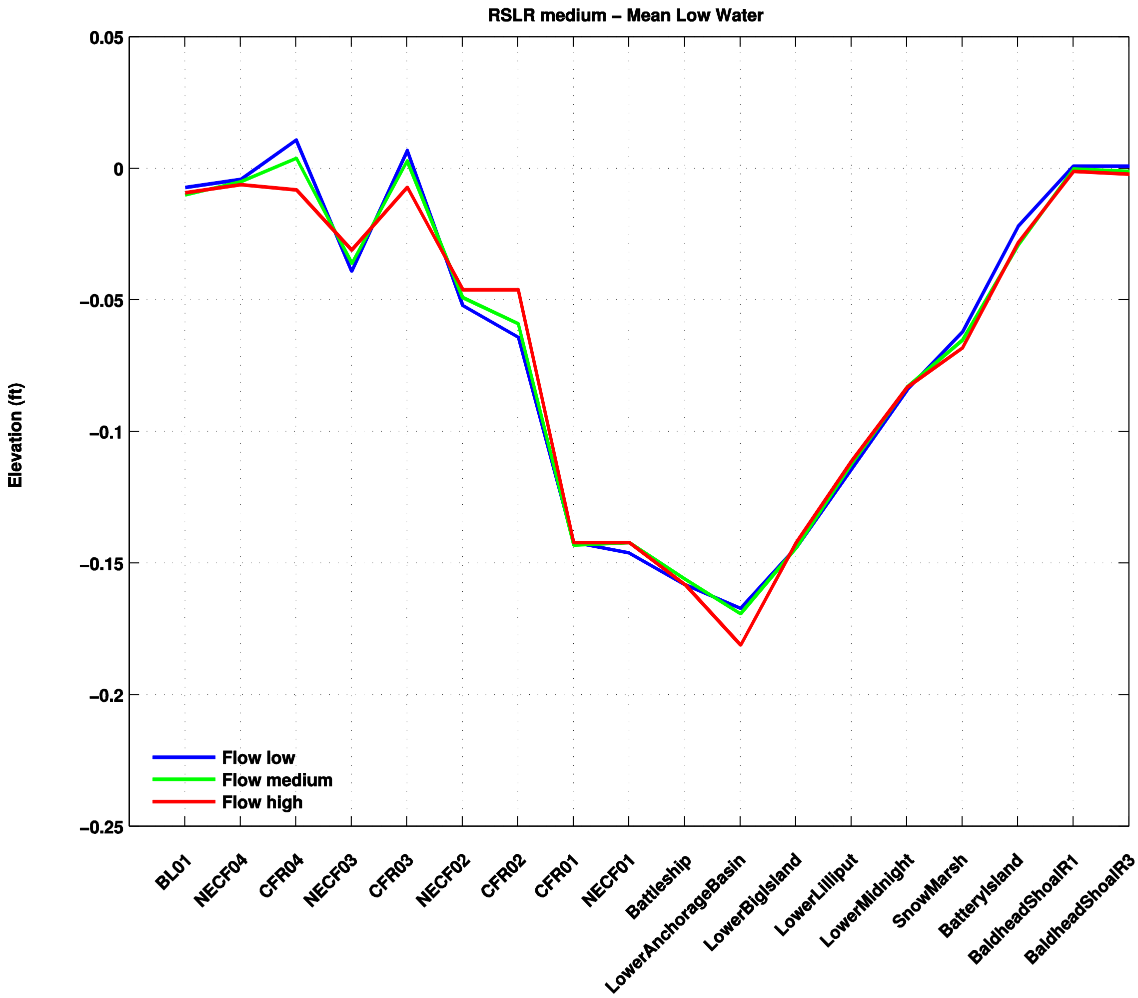

Figure 5-11: Differences between FwoP and FwP of Mean Low Water (MLW) throughout the channel for RSLR Intermediate projection

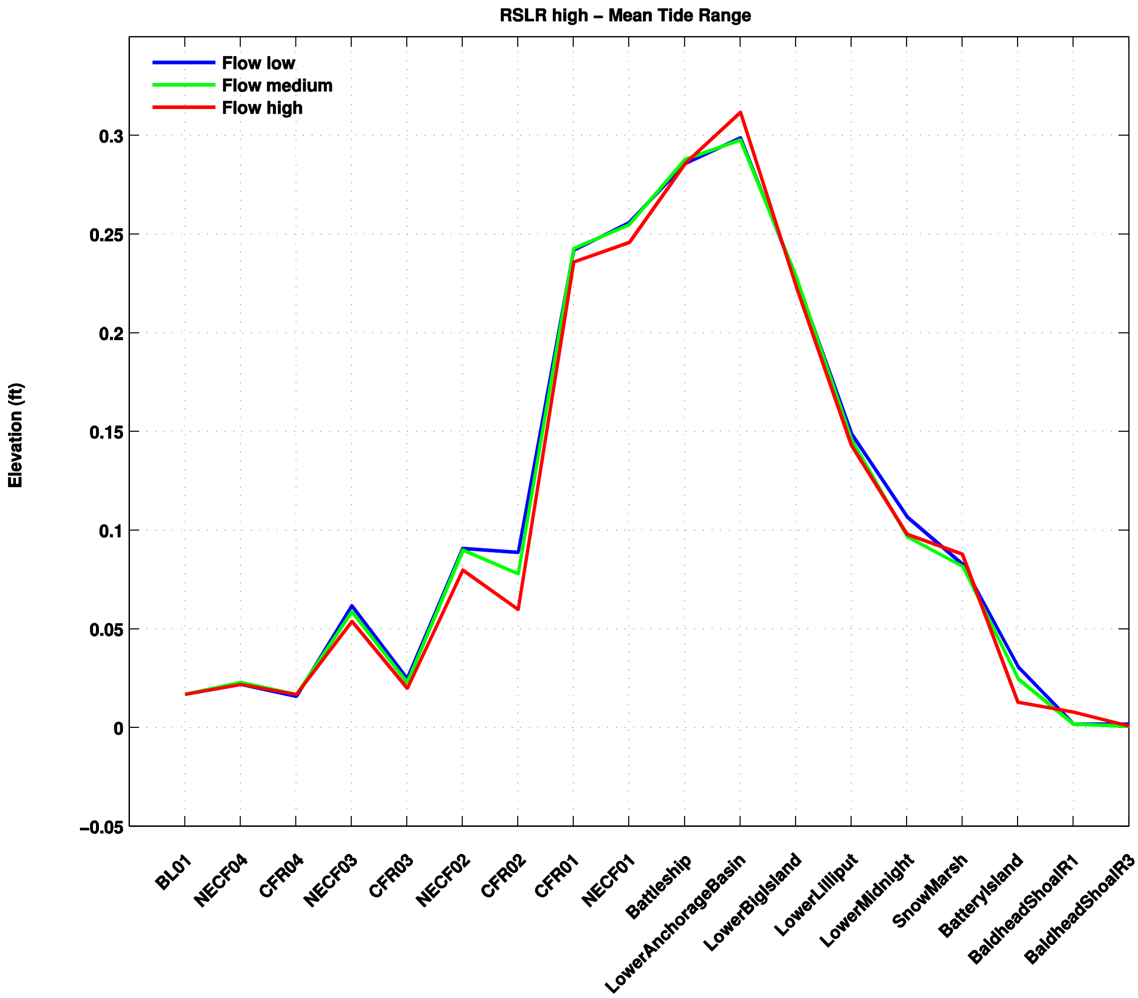

Figure 5-12: Differences between FwoP and FwP of Mean Tide Range (MTR) throughout the channel for RSLR high projection

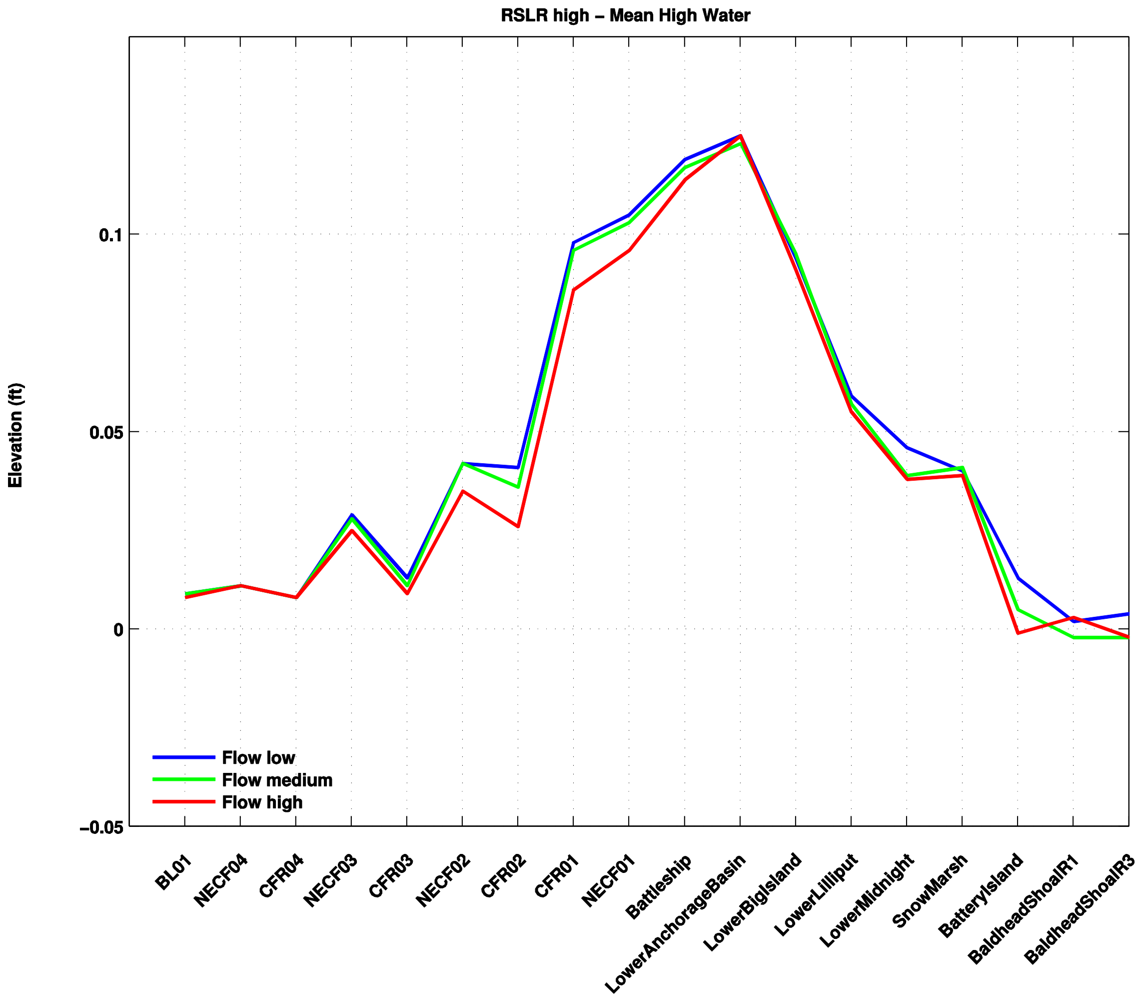

Figure 5-13: Differences between FwoP and FwP of Mean High Water (MHW) throughout the channel for RSLR high projection

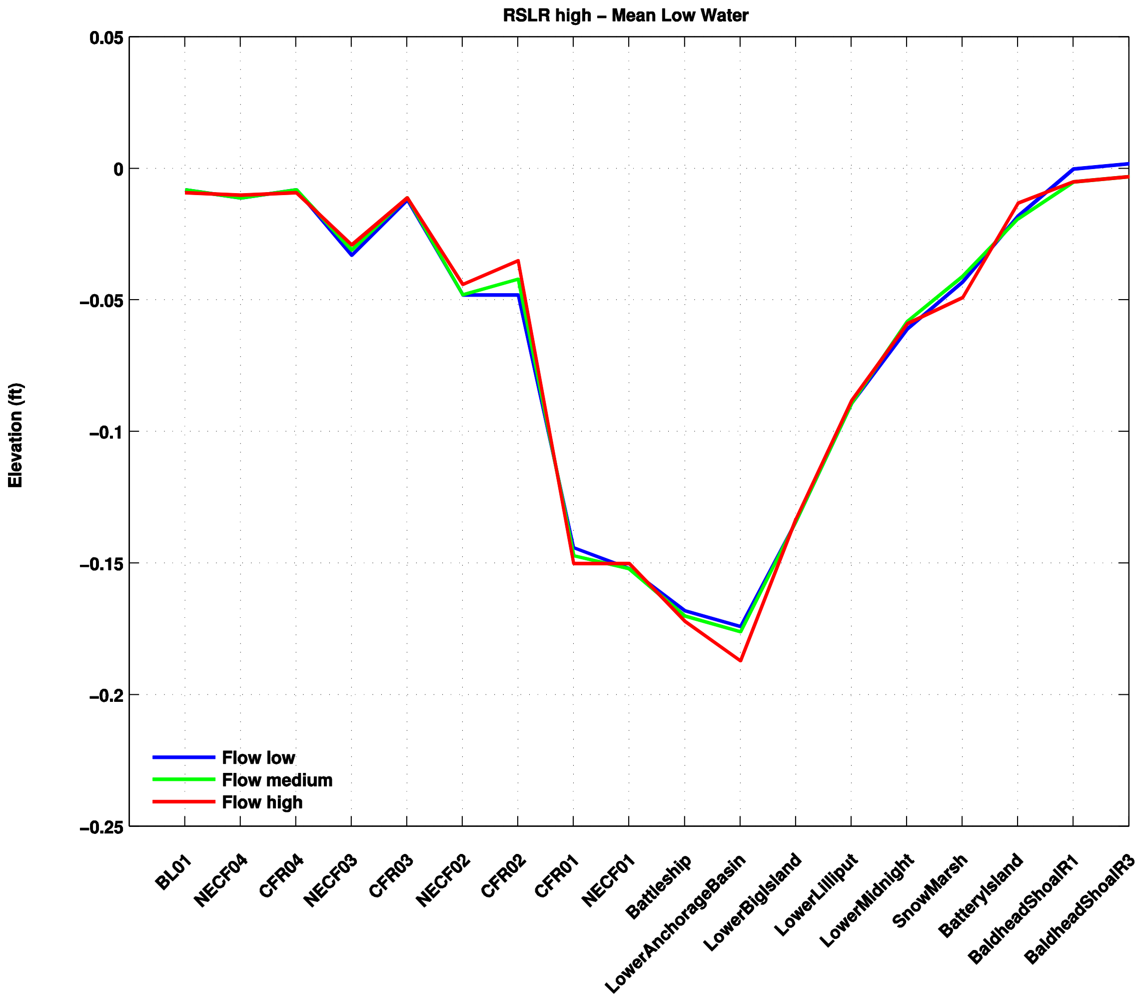

Figure 5-14: Differences between FwoP and FwP of Mean Low Water (MLW) throughout the channel for RSLR high projection

5.4.1.2. Water level – Hurricane Conditions

For the hurricane case, the maximum water level during the simulation time period was calculated (see Table 5-10), with the maximum difference occurring at lower Big Island with an increase of 0.13 ft. At the Battleship, the difference was an increase of only 0.08 ft.

Table 5-10: Water level Comparison (ft) during Hurricane for RSLR low scenario with low flow

	FwoP	FwP	Δ
BL01	4.18	4.21	0.04
NECF04	4.08	4.11	0.02
CFR04	4.32	4.35	0.03
NECF03	4.42	4.48	0.06
CFR03	4.32	4.36	0.04
NECF02	4.69	4.74	0.05
CFR02	4.89	4.93	0.05
CFR01	5.77	5.86	0.09
NECF01	5.65	5.73	0.08
Battleship	5.68	5.76	0.08
LowerAnchorageBasin	5.71	5.75	0.04
LowerBigIsland	5.76	5.89	0.13
LowerLilliput	5.78	5.84	0.06
LowerMidnight	5.58	5.63	0.04
SnowMarsh	5.87	5.91	0.04
BatteryIsland	6.05	6.06	0.01
BaldheadShoalR1	5.96	5.96	0.00
BaldheadShoalR3	5.69	5.69	0.00

5.4.1.3. Current

Percentiles of current speed based on the four-week time period results for surface, middle and bottom layers at each location shown in Figure 5-5 were analyzed. The depths for the surface, middle and bottom layers at each location are provided in Table 5-11 . Current statistics for the three layers are presented in Appendix D-2.

The results show maximum surface layer increases of 0.13 fps at the 50th percentile and 0.55 fps at the 90th percentile for Snows Marsh (RSLR Low scenario, Medium Flow) and the Anchorage Basin (RSLR Low scenario, High Flow), respectively.

The results show maximum bottom layer increases of 0.43 fps at the 50th percentile and 0.62 fps at the 90th percentile for Snows Marsh (RSLR Low scenario, Medium Flow) and Snows Marsh (RSLR High scenario, Medium Flow), respectively.

Greatest decreases in the surface layer were 0.42 and 0.43 fps for the 50th and 90th percentiles, respectively, at Battery Island under the RSLR Low scenario, High Flow (primarily due to the significant increase in channel width through this turn).

Greatest decreases in the bottom layer were 0.11 and 0.14 fps for the 50th and 90th percentiles, respectively, at the Anchorage Basin under multiple scenarios.

Table 5-11: Depth of surface, middle and bottom layer at each location (ft-MLLW)

	Surface	Middle	Bottom
BL01	-1.19	-1.19	-5.39
NECF04	-1.19	-5.39	-9.59
CFR04	-1.19	-5.39	-9.59
NECF03	-1.19	-9.59	-17.99
CFR03	-1.19	-13.79	-26.39
NECF02	-1.19	-9.59	-17.99
CFR02	-1.19	-9.59	-22.19
CFR01	-1.19	-9.59	-22.19
NECF01	-1.19	-13.79	-26.39
Battleship	-1.11	-17.91	-38.91
LowerAnchorageBasin	-1.04	-22.04	-43.04
LowerBigIsland	-0.95	-21.95	-42.95
LowerLilliput	-0.85	-21.85	-42.85
LowerMidnight	-0.78	-21.78	-42.78
SnowMarsh	-0.68	-21.68	-42.68
BatteryIsland	-0.58	-21.58	-42.58
BaldheadShoalR1	-0.41	-21.41	-42.41
BaldheadShoalR3	-0.44	-21.44	-42.44

5.4.2. Water Quality Results

Water quality results from the production runs were extracted including salinity, water temperature and DO in the surface, middle and bottom layers. The depths for the surface, middle and bottom layers at each location shown in Figure 5-5 are provided in Table 5-11.

5.4.2.1. Salinity

The monthly averaged salinities for the surface, middle and bottom layers at each location shown in Figure 5-5 were extracted and the results for the typical year for all three RSLR scenarios and for the Dry year conditions for the Low RSLR scenario are presented in Appendix D-3.

Salinity intrusion increases from FwoP to FwP, with the bottom layer having larger salinity increases relative to the surface layer at each location. Locations near Wilmington such as Battleship and Lower Anchorage Basin have the highest salinity increases compared to other locations: about 0.6 – 1.4 ppt at the surface layer, 2.0 – 5.0 ppt at the middle layer, and 2.3 – 6.1 ppt at the bottom layer across low, intermediate, and high RSLR conditions. The salinity differences decrease downstream and upstream from these two stations with the last noticeable change upstream occurring at NECF02 (with increases of about 0.1 ppt in the surface layer and 0.2 ppt in the bottom layer for the low RSLR scenario and increases of about 0.4 ppt in the surface layer and 0.6 ppt in the bottom layer for the high RSLR scenario) and at CFR01 (with increases of about 0.2 ppt in the surface layer and 1.2 ppt in the bottom layer for the low RSLR scenario and increases of about 0.5 ppt in the surface layer and 1.2 ppt in the bottom layer for the high RSLR scenario).

Figure 5-15 and Figure 5-16 present the results for February of a typical year / low SLR scenario for the surface and bottom layers, respectively, while Figure 5-17 and Figure 5-18 present the results for August for a typical year / low SLR for the surface and bottom layers, respectively. Near Wilmington where the greatest changes occur, the high RSLR scenario reduces the relative impact (i.e., smaller salinity increases) of the proposed project. It should be noted, though, that although the differences in salinity due to the proposed project are lower for the high RSLR scenario, the absolute salinity values are higher for the high RSLR scenario

For the Dry year flow condition, the salinity differences are more uniformly distributed throughout the water column. Differences remain the largest at Battleship and Lower Anchorage Basin, with increases of about 1.1 – 1.4 ppt at the surface layer, 1.6 – 3.3 ppt at the middle layer and 1.5 – 3.3 ppt at the bottom layer. As with the Typical conditions, the salinity differences decrease going both downstream and upstream from these two stations, although the last noticeable change does occur slightly further upstream at NECF03 (with an increase of about 0.3 ppt) and at CFR02 (with an increase of about 0.1 ppt).

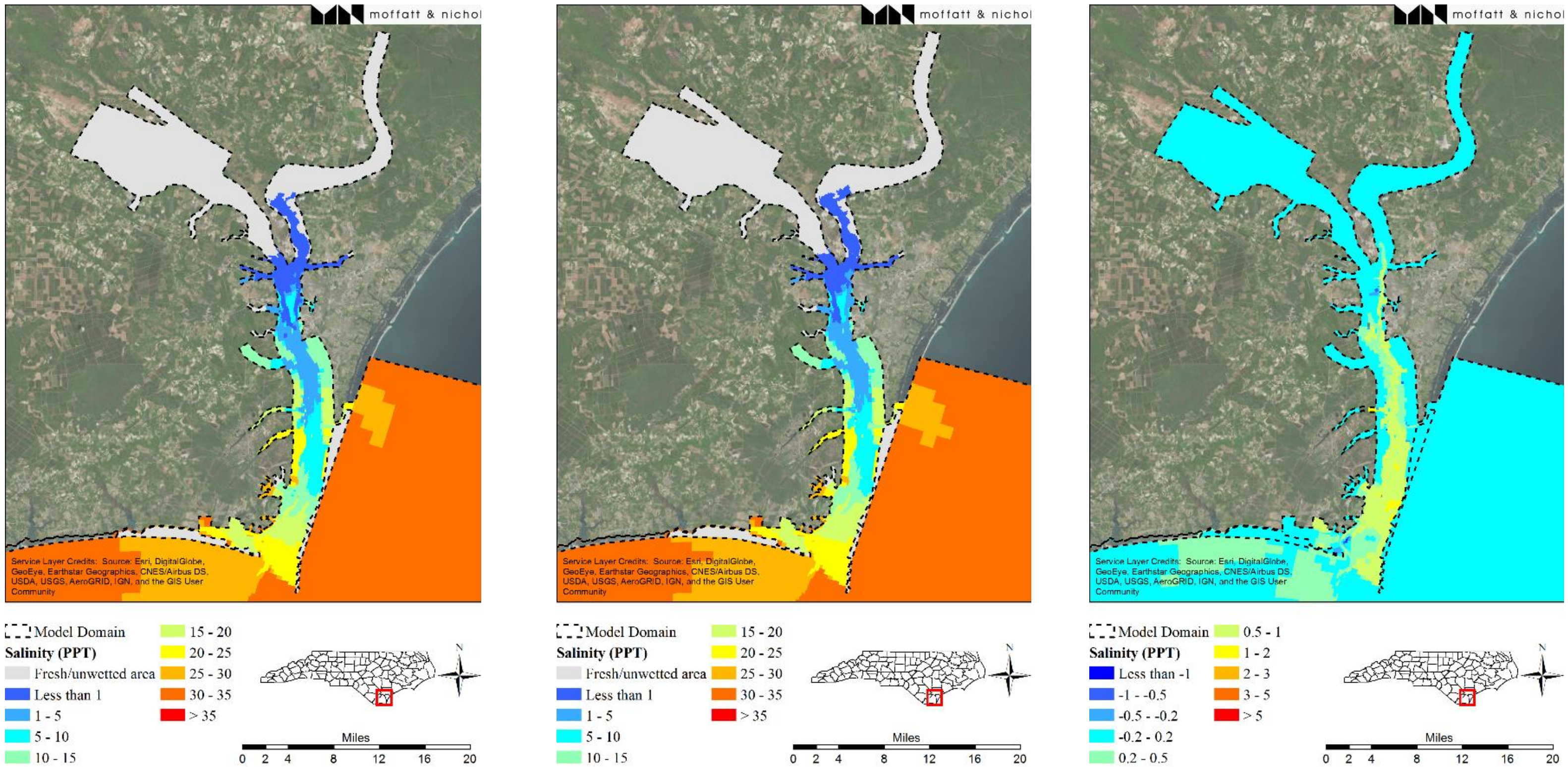

Figure 5-15: Averaged salinity in February for surface layer (left: FwoP, middle: FwP, right: Δ)

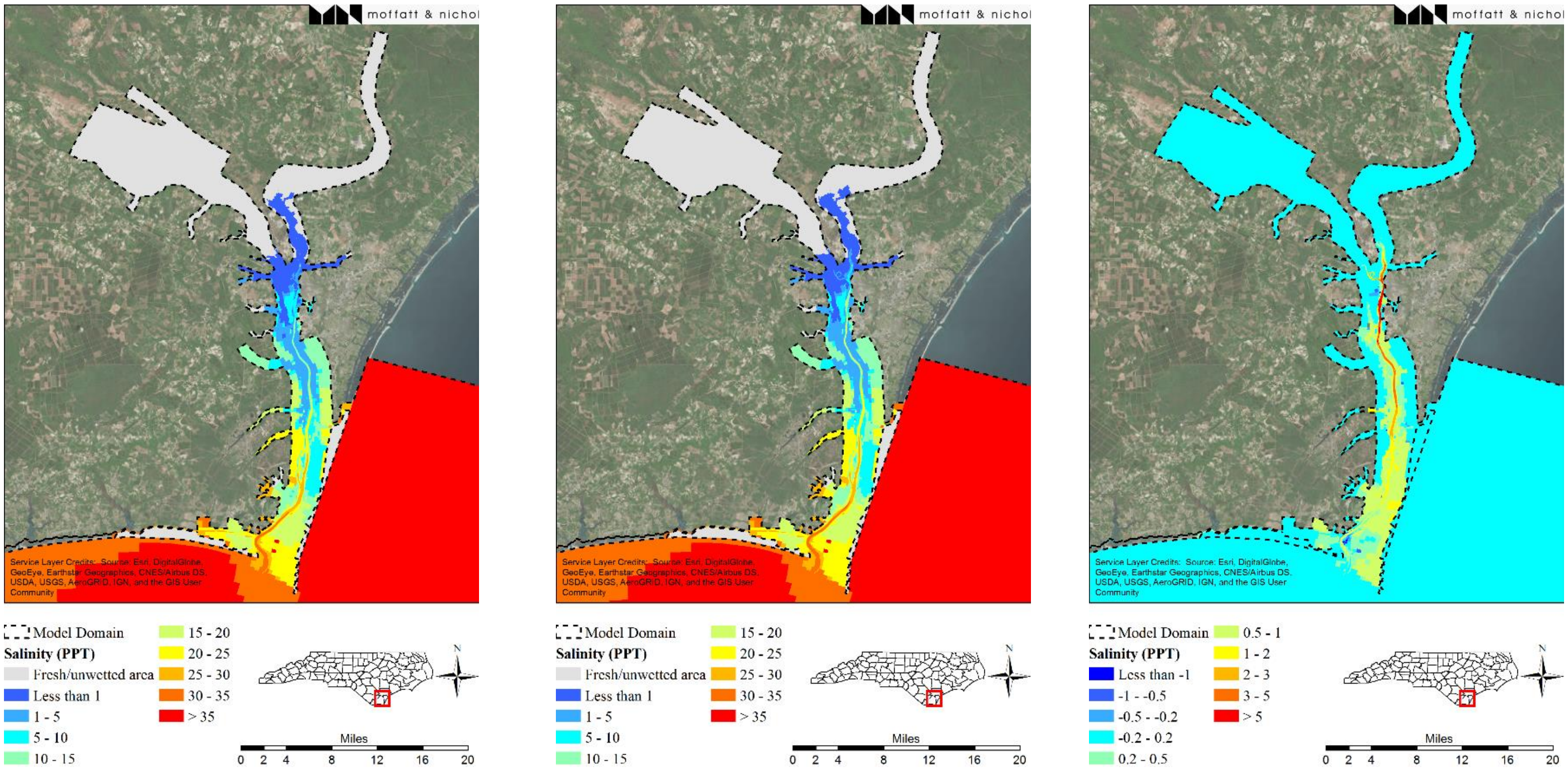

Figure 5-16: Averaged salinity in February for bottom layer (left: FwoP, middle: FwP, right: Δ)

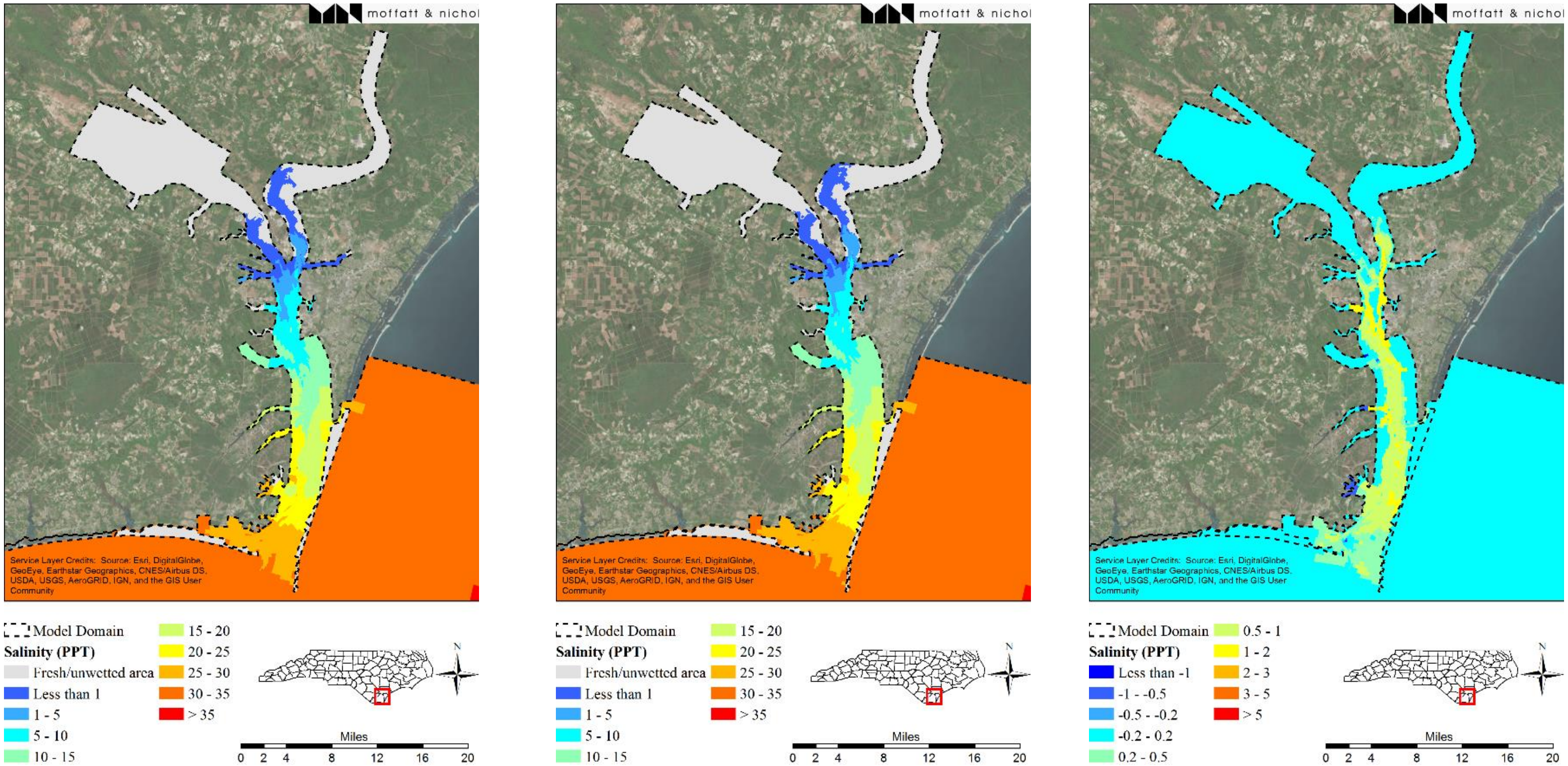

Figure 5-17: Averaged salinity in August for surface layer (left: FwoP, middle: FwP, right: Δ)

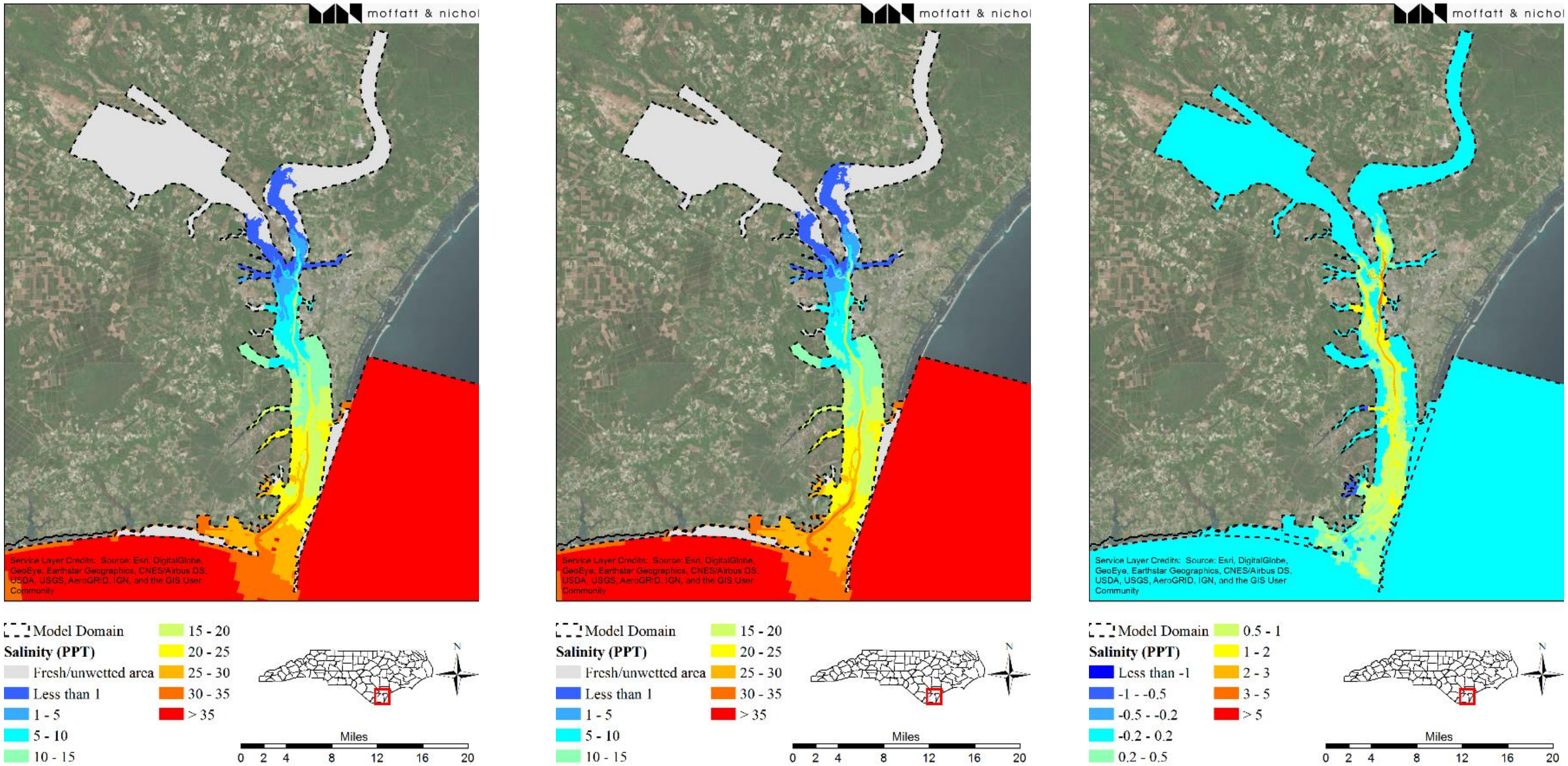

Figure 5-18: Averaged salinity in August for bottom layer (left: FwoP, middle: FwP, right: Δ)

5.4.2.2. Water temperature

The monthly averaged water temperatures for the surface, middle and bottom layers at each location shown in Figure 5-5 were extracted and the results for the typical year for all three RSLR scenarios and for the Dry year conditions for the Low RSLR scenario are presented in Appendix D-4.

Overall, the water temperature changes are within 0.2 °C, except for some locations near Wilmington (Lower Anchorage Basin) where the maximum water temperature increase can reach 0.4 °C in the bottom layer during the winter season due to the relative differences between the amounts of colder freshwater moving downstream from the rivers and the warmer salt water moving further upstream. Figure 5-19 and Figure 5-20 present the results for February of a typical year / low RSLR scenario for the surface and bottom sections, respectively, while Figure 5-21 and Figure 5-22 present the results for August for a typical year / low RSLR for the surface and bottom sections, respectively. The proposed project's relative impact on temperature decreases slightly with the larger sea level rise scenarios.

For the Dry year condition, the water temperature changes are smaller than those during Typical conditions, and near Wilmington the maximum water temperature only increases 0.2 °C in the bottom layer during the winter season.

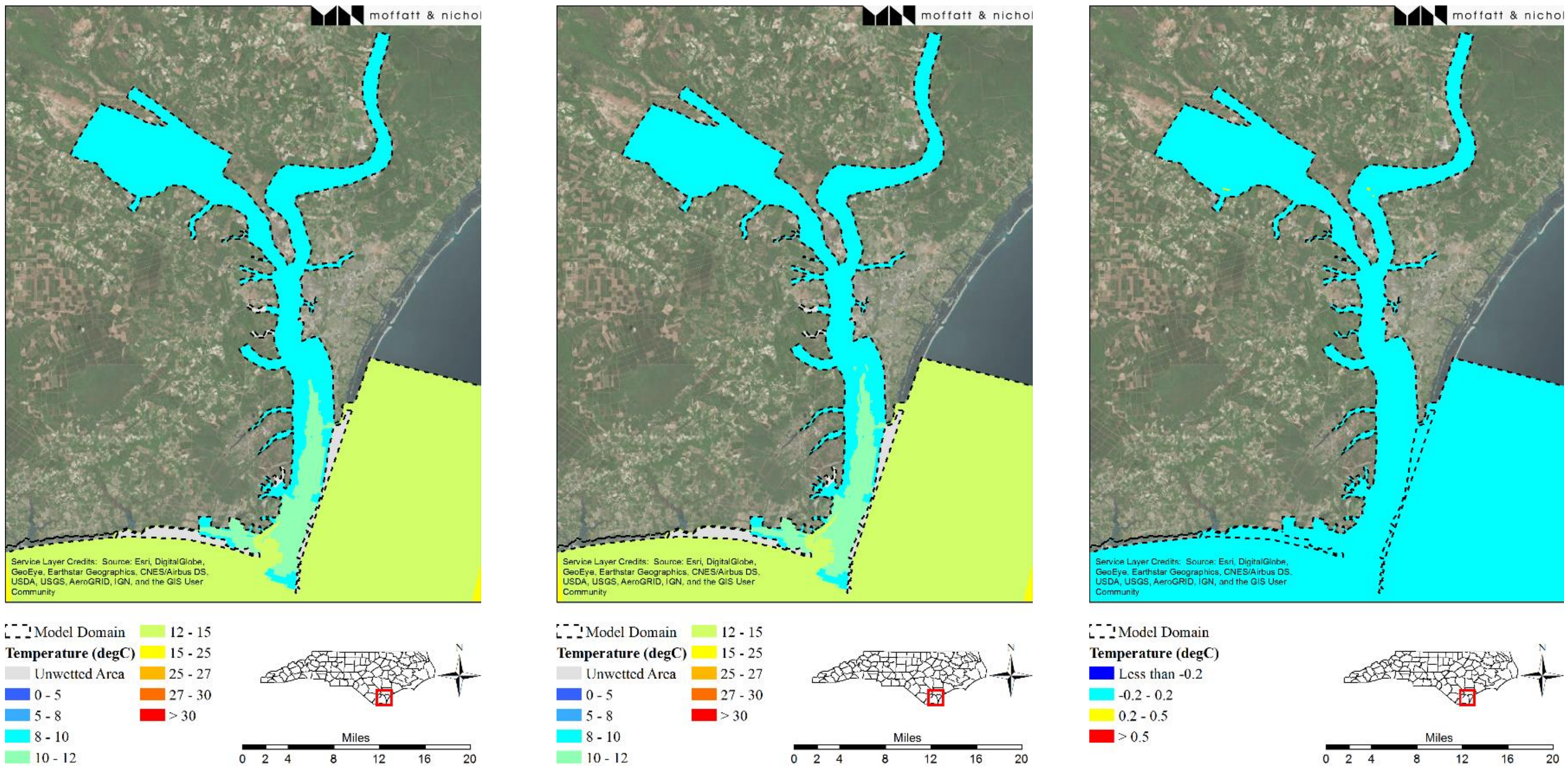

Figure 5-19: Averaged water temperature in February for surface layer (left: FwoP, middle: FwP, right: Δ)

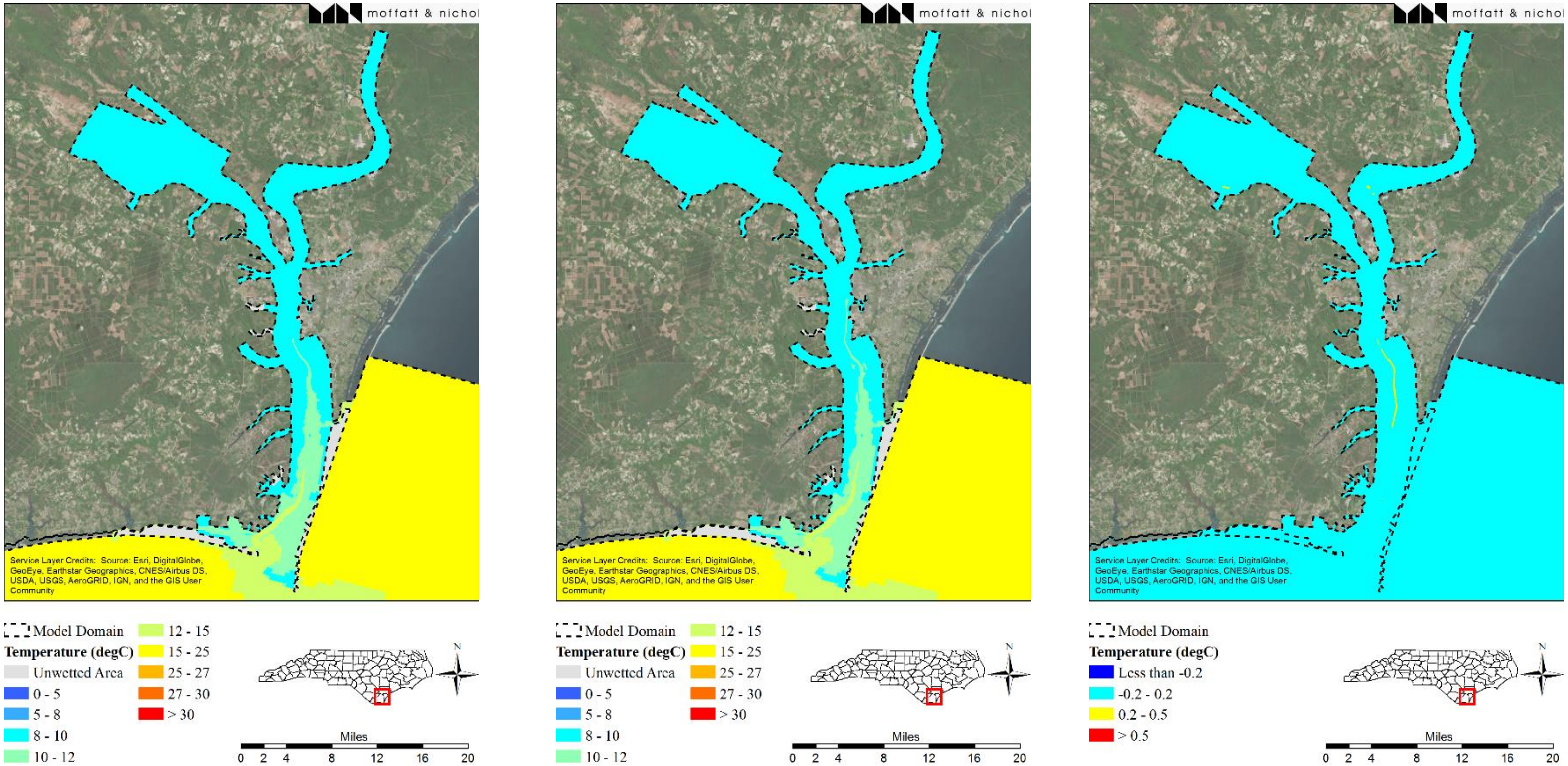

Figure 5-20: Averaged water temperature in February for bottom layer (left: FwoP, middle: FwP, right: Δ)

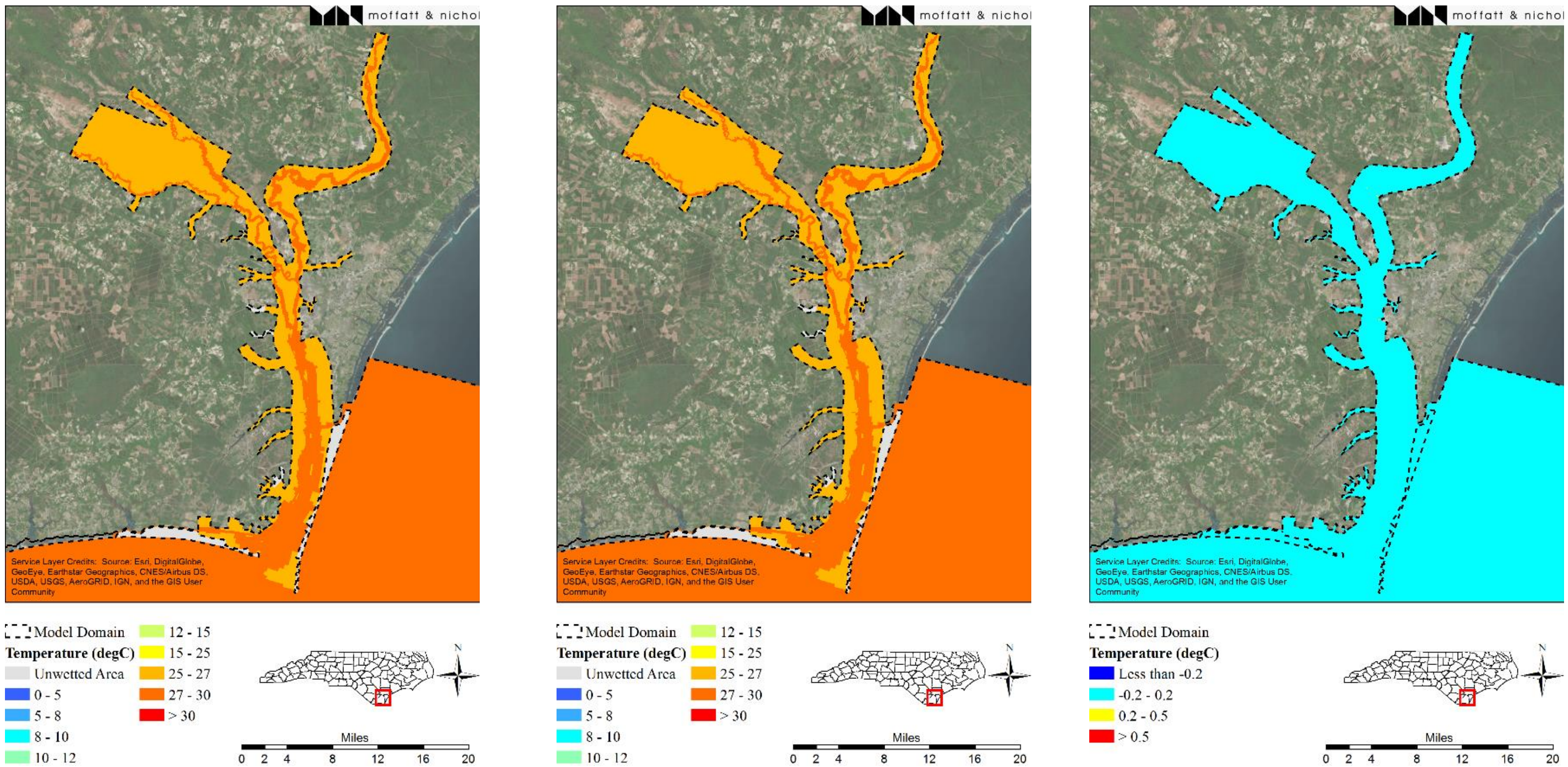

Figure 5-21: Averaged water temperature in August for surface layer (left: FwoP, middle: FwP, right: Δ)

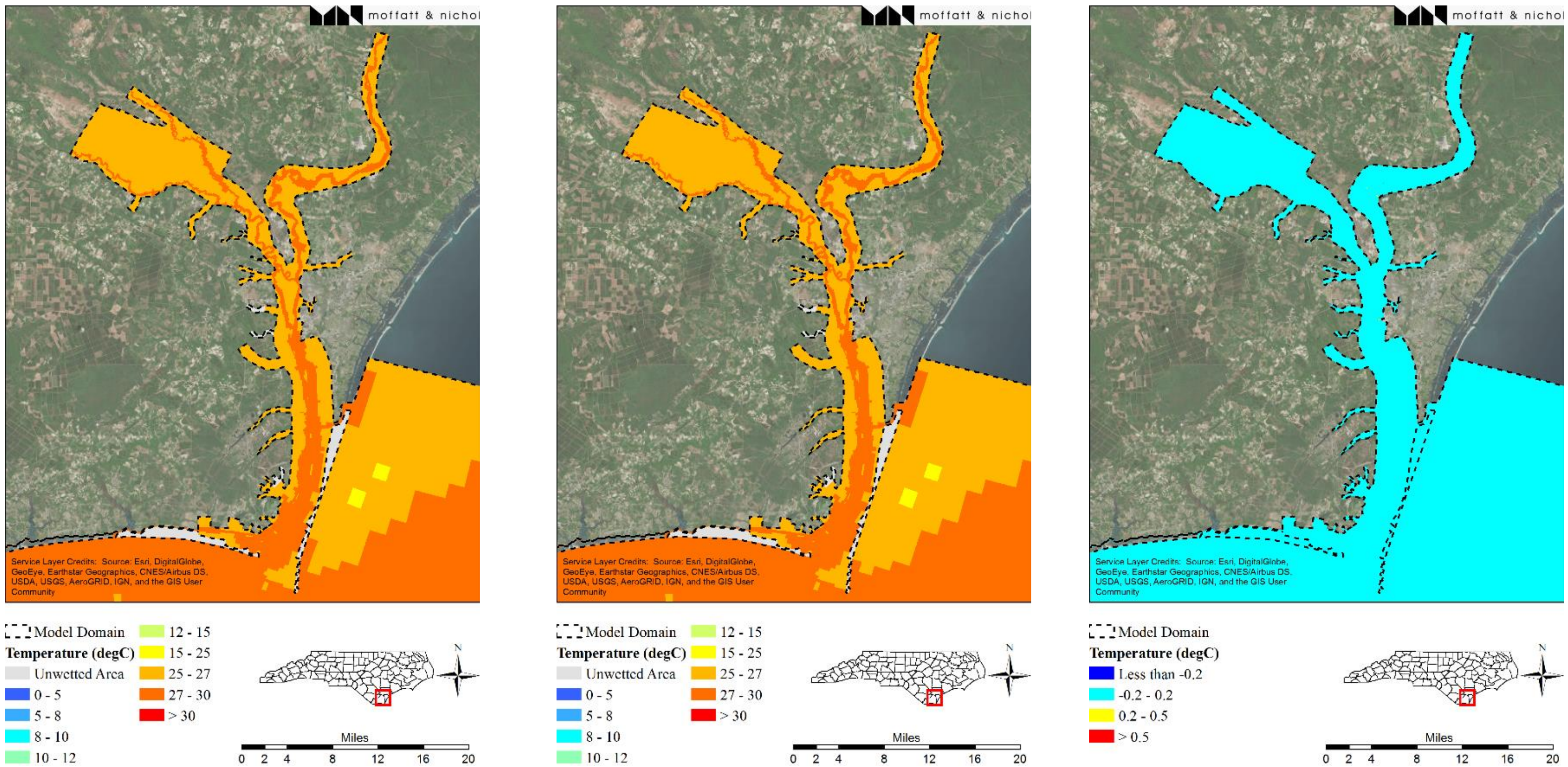

Figure 5-22: Averaged water temperature in August for bottom layer (left: FwoP, middle: FwP, right: Δ)

5.4.2.3. Dissolved Oxygen

The monthly averaged DO for the surface, middle and bottom layers at each location shown in Figure 5-5 were extracted and the results for the typical year for all three RSLR scenarios and for the dry year flow conditions for the Low RSLR scenario are presented in Appendix D-5.

Overall, the DO decreases from FwoP to FwP. The changes are less than 0.3 mg/L in the bottom layer of the middle sections of the river (Battleship to Lower Big Island) and only about 0.1 mg/L in the other sections of the river. The largest decreases, though, occur during the winter months when absolute DO levels are at their highest. Figure 5-23 and Figure 5-24 present the results for February of a typical year / low RSLR scenario for the surface and bottom sections, respectively, while Figure 5-25 and Figure 5-26 present the results for August for a typical year / low RSLR for the surface and bottom sections, respectively. The proposed project's relative impact on DO decreases slightly with the larger sea level rise scenarios.

For the Dry year condition, the results indicate that the DO changes are slightly smaller than those during Typical flow conditions.

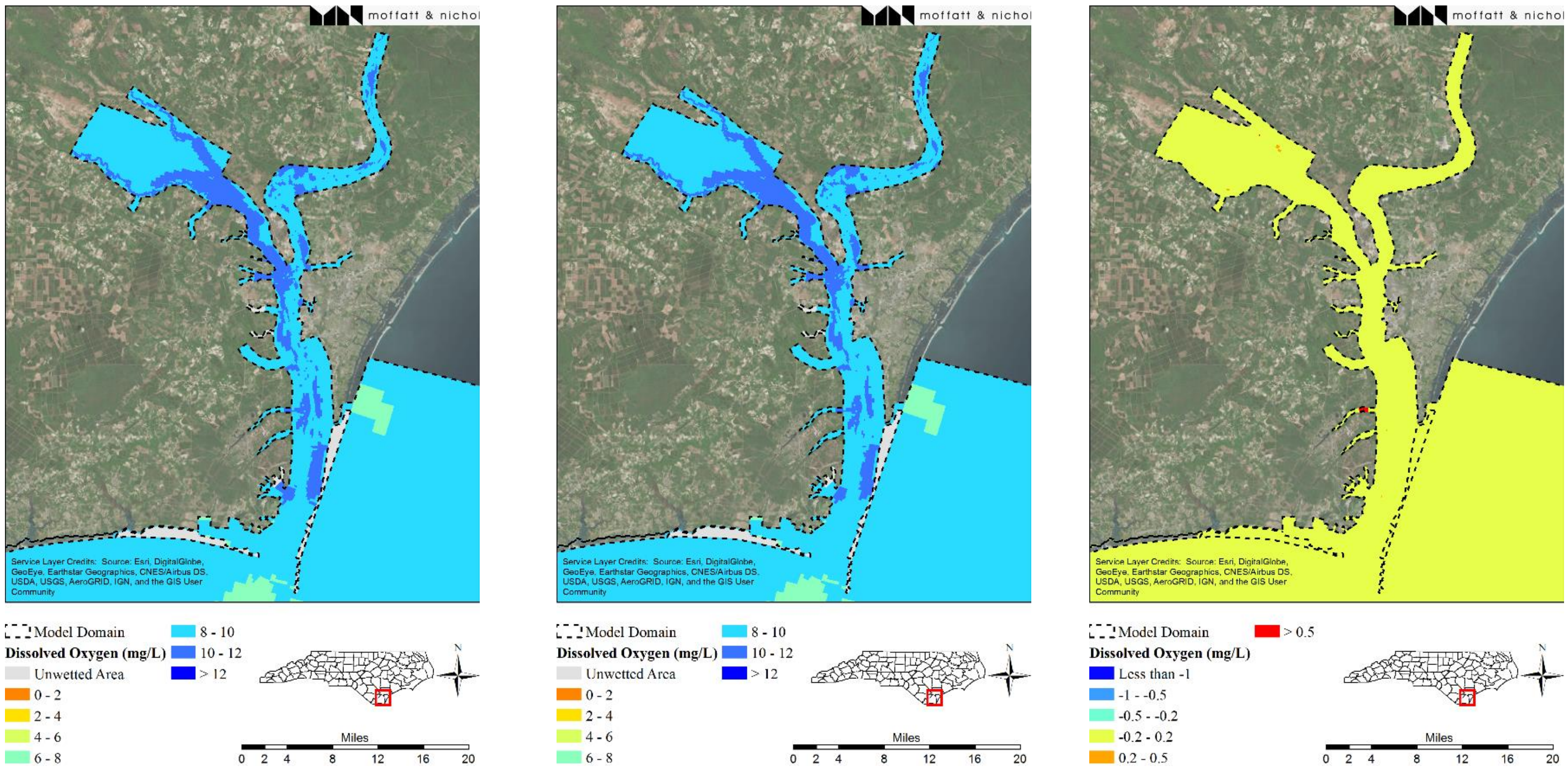

Figure 5-23: Averaged DO in February for surface layer (left: FwoP, middle: FwP, right: Δ)

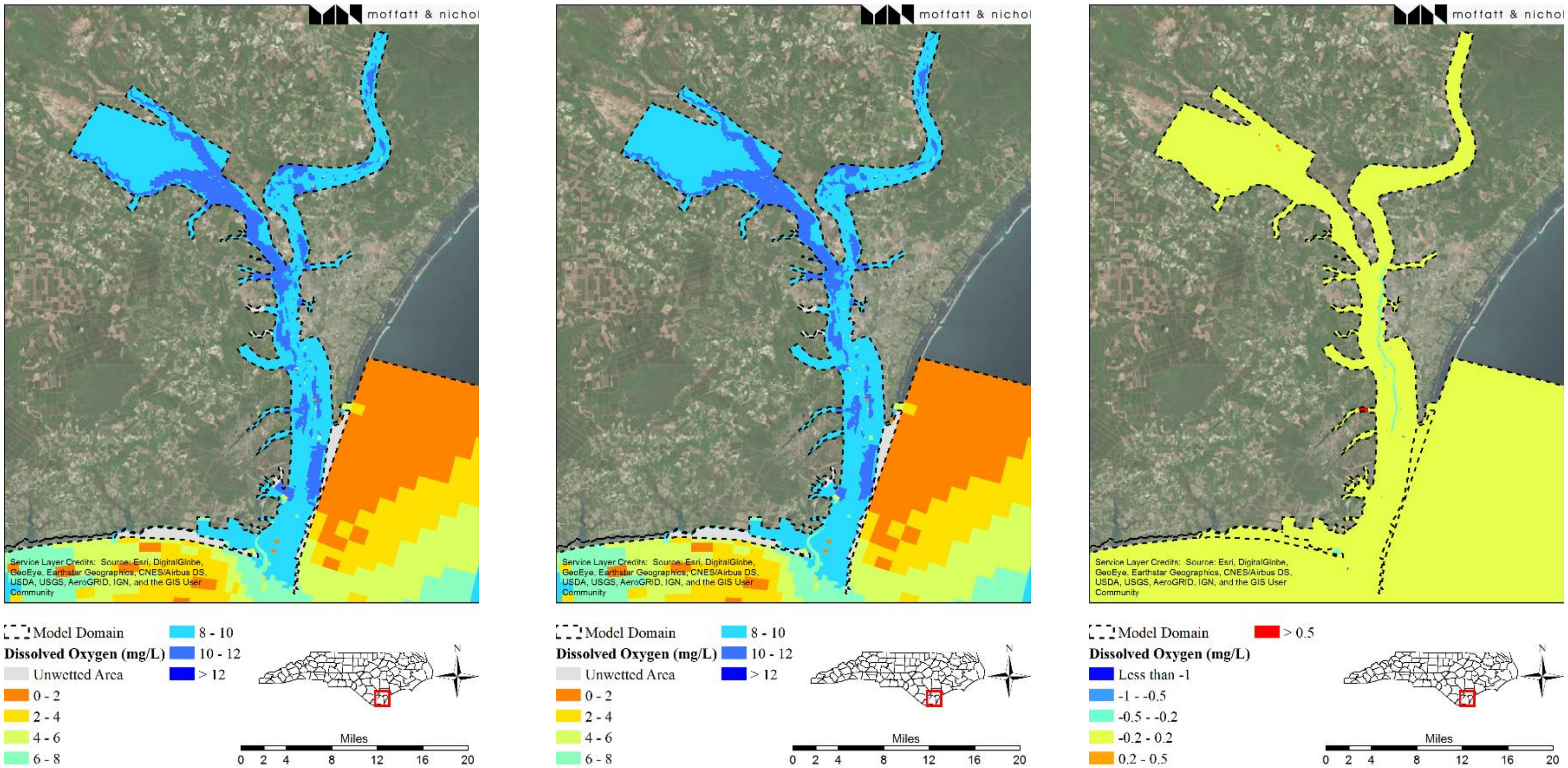

Figure 5-24: Averaged DO in February for bottom layer (left: FwoP, middle: FwP, right: Δ)

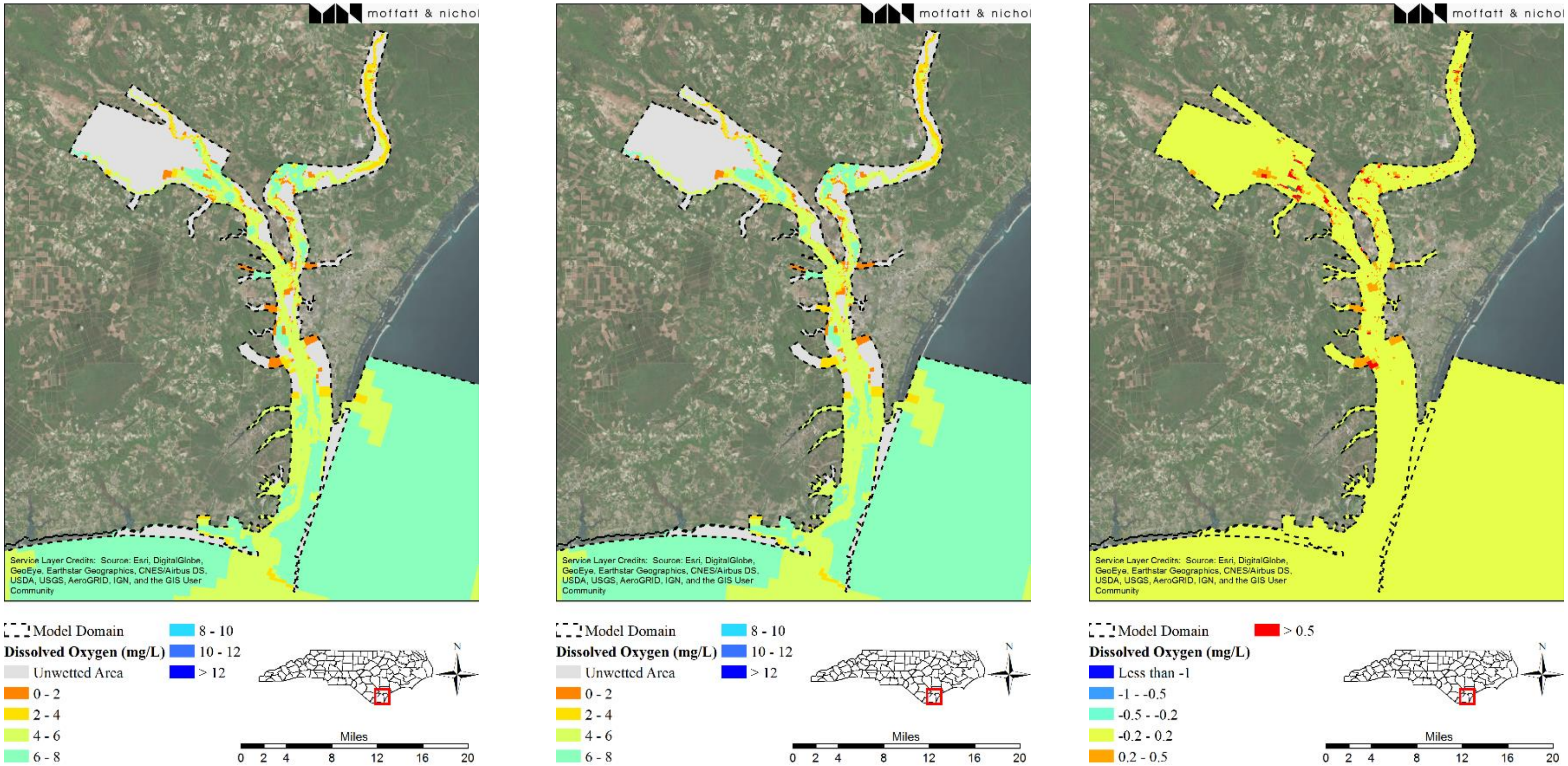

Figure 5-25: Averaged DO in August for surface layer (left: FwoP, middle: FwP, right: Δ)

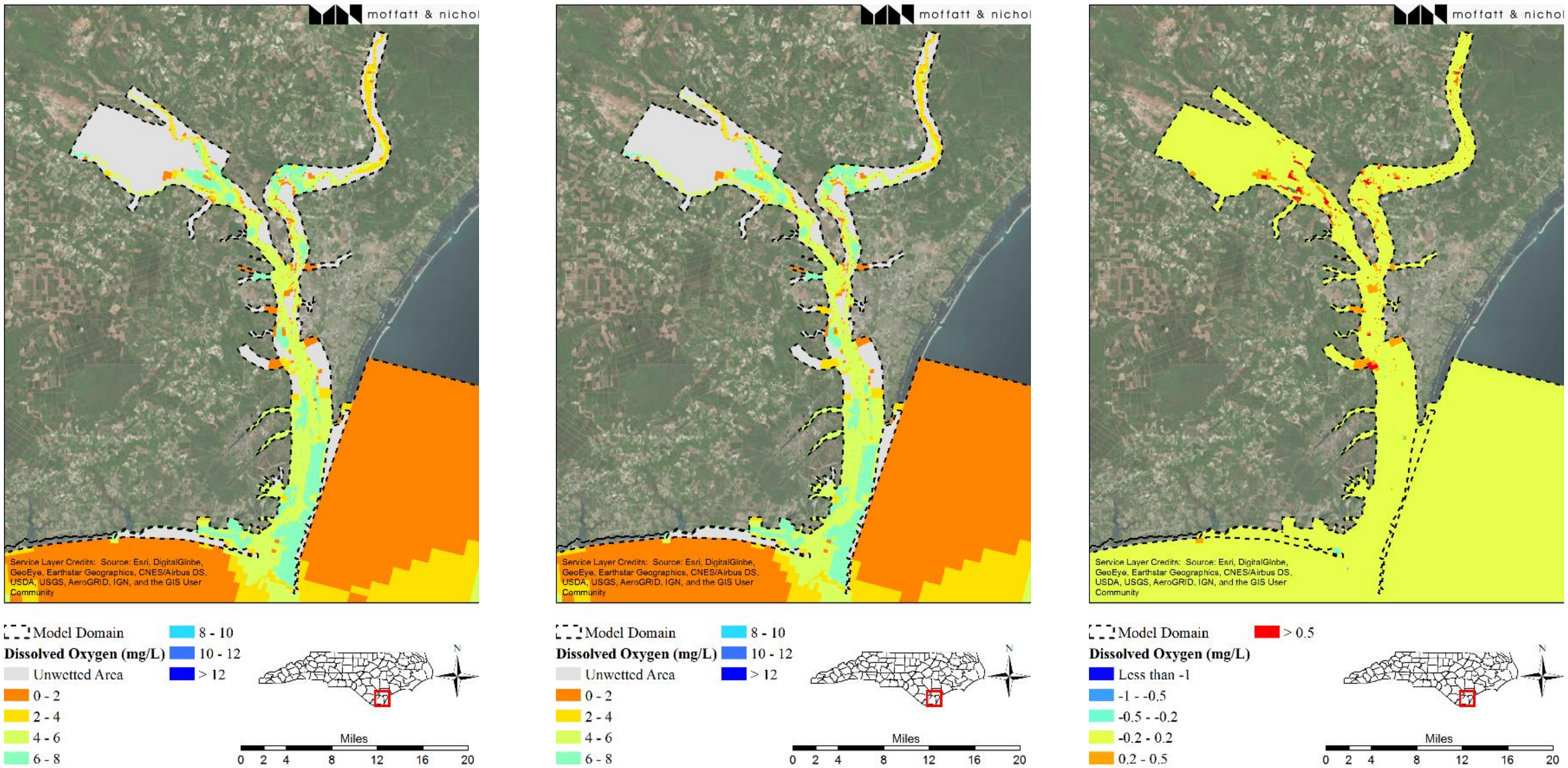

Figure 5-26: Averaged DO in August for bottom layer (left: FwoP, middle: FwP, right: Δ)

5.4.3. Annual Shoaling Rate in Anchorage Basin

The annual shoaling volumes for FwoP and FwP for a typical year under the three RSLR scenarios were calculated inside the Anchorage Basin as estimations for future annual dredging volumes (Figure 5-27), and the results are listed in Table 5-12. For the same RSLR projection, the annual shoaling volumes increase about 11% from FwoP to FwP due to the increased depth in the Anchorage Basin. It is also evident that increasing RSLR will increase the sedimentation amounts in the Anchorage Basin due to greater water and sediment fluxes but decreases the potential impact of the proposed project.

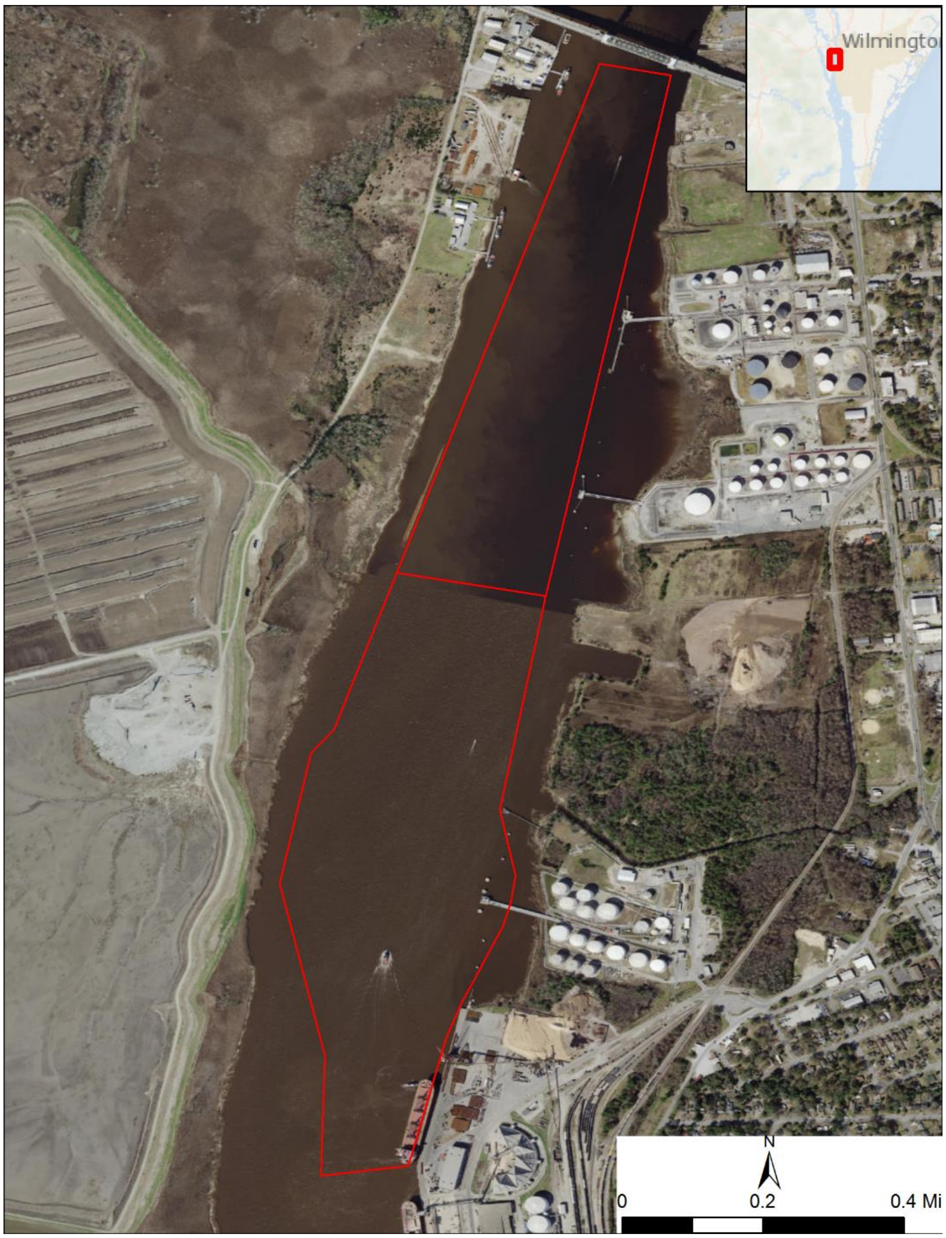

Figure 5-27: Anchorage Basin where annual shoaling rate were calculated

Table 5-12: Annual shoaling rate (cy) at Anchorage Basin

	FwoP	FwP	Change
RSLR Low projection			
Shoaling Rate	999,308	1,108,736	+11%
RSLR Intermediate projection			
Shoaling Rate	1,133,169	1,254,673	+11%
RSLR High projection			
Shoaling Rate	1,746,966	1,810,932	+4%

Additional analyses were later performed for the turning basin expansion project which determined a minimal increase (<1%) in sedimentation within the new turning basin limits. Thus, the changes presented here are representative for the channel deepening as the widening will already be completed and is assumed part of the FWoP conditions.

5.5. Conclusion

The impact of deepening the channel for the Tentatively Selected Plan has been evaluated through the use of a suite of Delft3D models. A summary of the results follows:

Normal Water Level: The Mean Tide Range will increase slightly with maximum increases near 0.3 ft at the Lower Anchorage Basin consisting of an increase in MHW of just over 0.1 ft and a decrease in MLW of just under 0.2 ft.

Extreme Water Level: The maximum increase in water level during the simulated hurricane event is 0.13 ft at Lower Big Island and 0.08 ft at the Battleship.

Current Speed: There are no uniform changes in the estuary but increased current speeds to about 0.4 ft/s and 0.6 ft/s are predicted in the bottom layer near Snows Marsh at the 50^{th} and 90^{th} percentiles, respectively, and decreased current speeds of just over 0.4 ft/s for the 50^{th} and 90^{th} percentiles are predicted in the surface layer near Battery Island.

Salinity: There will be increased salinity intrusion with the most impacted areas located near Wilmington (Battleship and Lower Anchorage Basin) with a 0.6 – 1.4 ppt increase at the surface layer and a 2.3 – 6.1 ppt increase at the bottom layer under Typical conditions with the last noticeable upstream changes occurring at NECF02 and CFR01.

Water Temperature: There will be a slight increase, below 0.2 °C, for most of the year in the estuary, except for a maximum increase of 0.4 °C in the bottom layer at the Lower Anchorage Basin during the winter season.

Dissolved Oxygen: The DO changes are less than 0.3 mg/L in the middle sections of the river (Battleship to Lower Big Island) and about 0.1 mg/L in the other sections of the river. The largest decreases occur during the winter months when absolute DO levels are at their highest. For the dry year flow condition the DO changes are slightly smaller than those during typical flow conditions.

Shoaling Rate at the Anchorage Basin: The sedimentation volume will increase by about 11% for the Low and Intermediate sea level rise scenarios and about 4% for the High sea level rise scenario.

6. Tidal Creek Salinity Numerical Model Results

A localized, more detailed Delft3D model was developed to investigate the salinity level changes in the tidal creeks caused by the Project which may potentially affect tidal wetland community composition and mitigation requirements in the tidal creeks and is discussed herein. This localized model was necessary to better define the bathymetry within the tidal creeks while keeping model runtimes to a reasonable duration.

6.1. Model Development

6.1.1. Model Grid

The local detailed model grid was developed based on the full Delft3D model as discussed previously. The local model extent is shown in Figure 6-1 with the area-of-interest tidal creeks such as Lilliput Creek, Town Creek, Sturgeon Creek, and Smith Creek. Figure 6-2 presents the local model grid with more detailed tributary coverages than in the full HD model, especially along Town Creek. The majority of the local model grid resolution was kept the same as in the full model in the river but more detailed resolution was used in the tidal creeks.

The local model grid used the same vertical Z-layer positions as in the full HD model. However, there were only 18 vertical layers available in the local model compared to 25 layers in the full model because the bottom 7 layers in the full model were in the offshore region and thus excluded in the local model. Thus, the first Z-layer in the local model is corresponding to the 8th Z-layer in the full model, and so on.

Figure 6-1: Local model extent

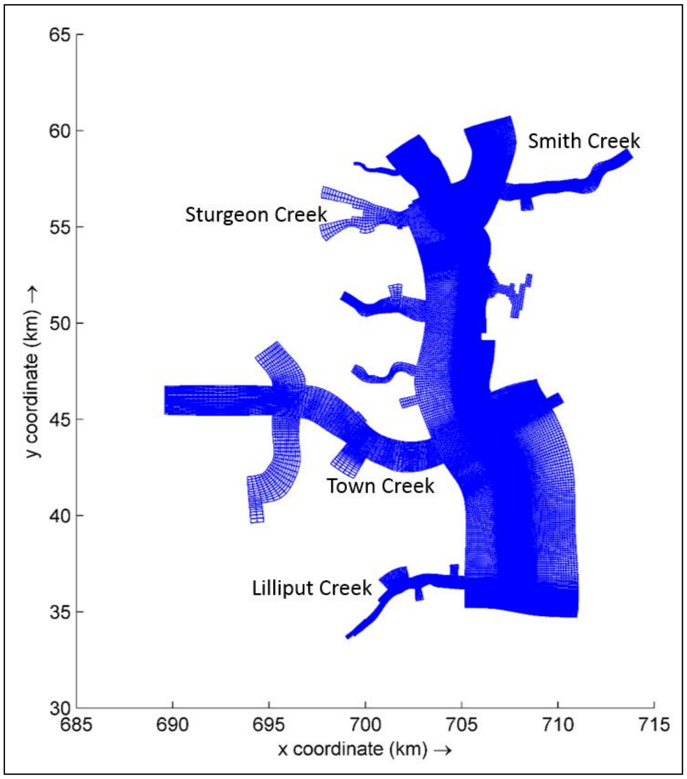

Figure 6-2: Local model grid

6.1.2. Model Bathymetry

The local model bathymetry was copied from the full model bathymetry except for the depths of the main small channels and adjacent wetlands in the tributaries. The channel depths were determined based on NOAA nautical charts wherever available, LIDAR and local knowledge of the tidal creeks based on past studies. Figure 6-3 presents the final local model bathymetry for the existing condition. The model bathymetry for the with Project conditions was modified only along the main Cape Fear River channels according to the Tentatively Selected Plan configuration.

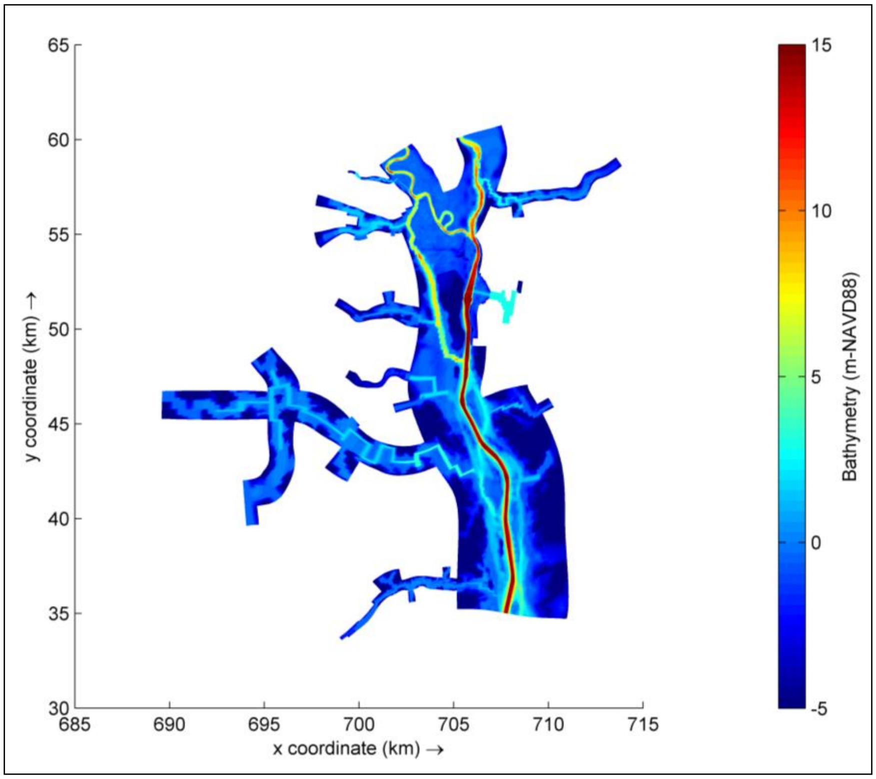

Figure 6-3: Local model bathymetry for the existing condition

6.1.3. Model Boundary Conditions

The local model boundary conditions were developed based on the model results from the full model runs. The local model is considered to be "nested" within the full model.

6.1.3.1. Downstream Boundary

At the downstream boundary, horizontal spatial varying water level and salinity boundary conditions were prescribed. Salinity values were also varied vertically along the boundary (a 3D profile in Delft3D). As shown in Figure 6-4, 8 downstream boundary segments were used in the model. Partially wetting and drying sections of the downstream boundary between tidal cycles were excluded. A reflection coefficient alpha=1000 was chosen to make the boundary weakly reflective to damp the spurious oscillations originating from the initial conditions.

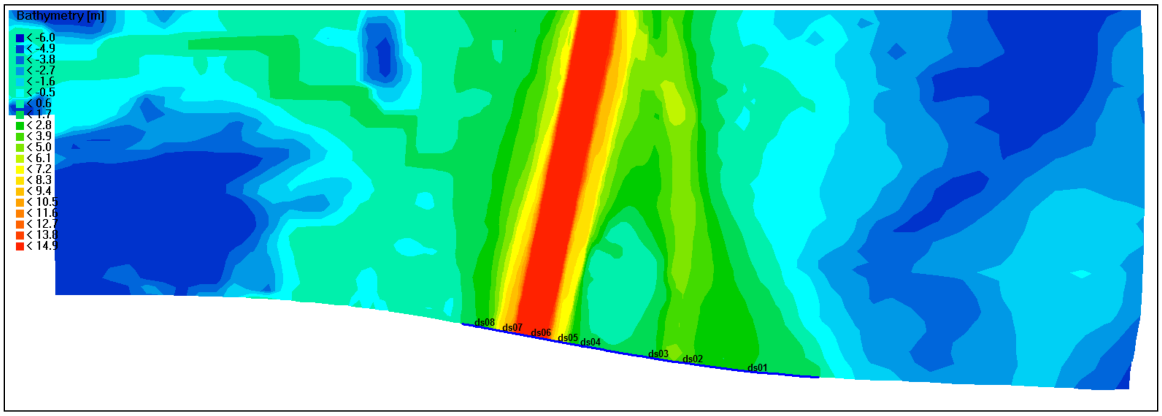

Figure 6-4: Local model downstream boundary segments

6.1.3.2. Upstream Boundaries

There are two upstream boundaries in the local model as shown in Figure 6-5: one at the Cape Fear River (CFR); and the other at the Northeast Cape Fear River (NECF). The total discharges and spatially averaged salinities were applied at the upstream boundaries. The total discharges were calculated from velocity and water depth at hourly interval from the full model HD results. The associated salinity values from the full model results were averaged both horizontally and vertically at the same time step. The vertical profiles for hydrodynamics and salinity were chosen to be logarithmic and uniform, respectively at both upstream boundaries.

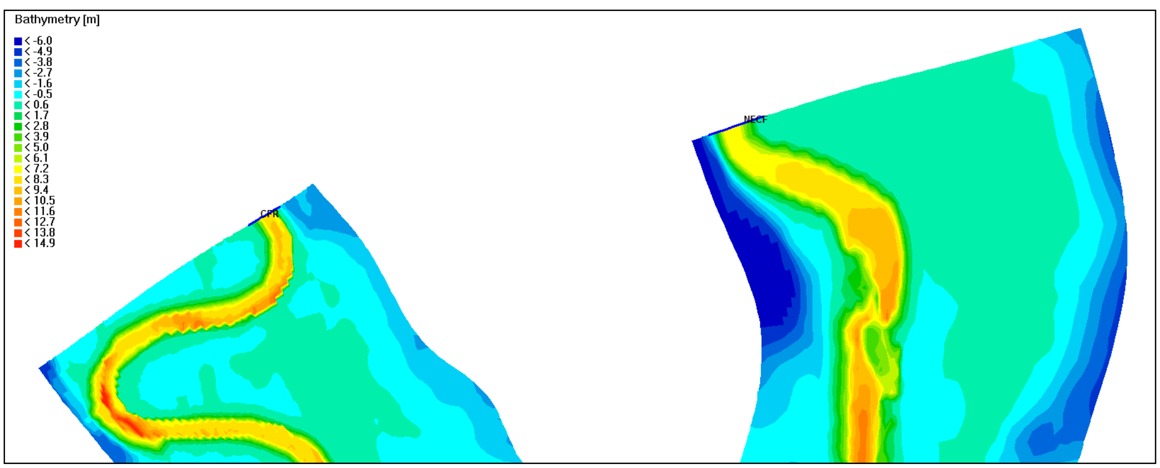

Figure 6-5: Local model upstream boundaries

6.1.3.3. Freshwater Discharges

For the freshwater flows from ungaged drainage areas developed for the full model, most of them were discharged directly into the main Cape Fear River channels in the full model as shown in Figure 6-6.

For the local model, the freshwater flows were redistributed within each subwatershed based on sub-drainage surface areas and their discharge locations were assigned to the most upstream locations as shown in Figure 6-6.

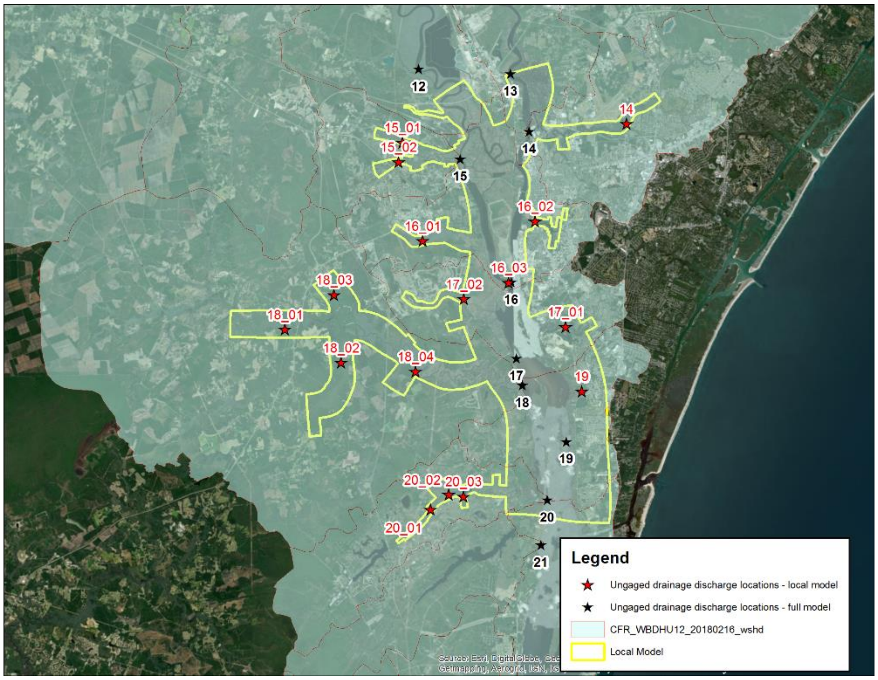

Figure 6-6: Local model freshwater discharge locations

6.1.4. Model Initial Conditions

In order to reduce the spin-up time, the local model runs were started with initial conditions derived from the corresponding full model results. The constructed initial conditions included water levels and salinities at each Z-layer interpolated from the full model results, but with a value of zero for both the horizontal velocity components.

6.1.5. Model Parameters

All other model parameters such as bottom roughness, horizontal eddy viscosity and eddy diffusivity, background vertical viscosity and diffusivity, and 3D turbulence, etc., were kept the same in the local model as in the full model to ensure consistency.

6.1.6. Model Calibration

The focus of this effort was to determine potential changes in the tidal wetland community composition and mitigation requirements in the tidal creeks, and thus additional calibration of salinity within the tidal creeks was performed based on matching existing vegetation patterns therein. Since wetland community composition change is influenced by average salinities over seasonal timescales, this calibration method has more relevance to the wetland community impacts than one based on short-term, synoptic salinity measurements. As discussed in Appendices F & I, surface salinity data were extracted from the year-long model simulation results and averaged for each grid cell to produce average annual surface salinity layers. Based on the grid cell average salinity values, salinity isopleths were developed to define the boundaries or thresholds between the polyhaline, mesohaline, oligohaline and tidal freshwater salinity zones in the tidal creek channels. Minor adjustments in the tidal creek widths and / or depths were then performed, if necessary, such that these isopleths had general agreement with the baseline wetland classifications. This approach thus allowed for a more accurate assessment of the potential with project changes in the tidal wetland community composition due to accurately matching the existing wetland conditions.

6.1.7. Project Configuration

In order to determine the potential impacts of the Project, the local model was run for two cases:

- Future without project (FwoP): -44 ft-MLLW (42 ft authorized depth + 2 ft over-dredge) in the river channel sections.
- Future with project (FwP): -49 ft-MLLW (47 ft authorized depth + 2 ft over-dredge) in the river channel sections.

6.1.8. Sea Level Rise Scenarios

Similar to the full model as listed in Table 6-1, three different future sea level rise scenarios were considered for the local model.

Table 6-1: Relative Sea Level Rise (RSLR) in 2077 at Wilmington, NC

RSLR Scenario	RSLR (ft)
Low	0.34
Intermediate	0.88
High	2.57

6.1.9. Flow Conditions

As discussed previously for the full model production runs, upstream low/medium/high river flow conditions in both “Typical” and “Dry” years were simulated for the local model. Model runs for the Dry year flow conditions were only conducted under the low sea level rise scenario; whereas model runs under all three sea level rise scenarios were performed for the Typical year flow conditions. Table 6-2 lists the local model production run conditions. The Dry year high flow condition is the same as the Typical year low flow condition.

Table 6-2: Local model production runs

Flow Conditions	Existing	Low RSLR	Intermediate RSLR	High RSLR
Typical High	×	×	×	×
Typical Medium	×	×	×	×
Typical Low (Dry High)	×	×	×	×

Flow Conditions	Existing	Low RSLR	Intermediate RSLR	High RSLR
Dry Medium	×	×		
Dry Low	×	×		

6.1.10. Simulation Time Period

The boundary and initial conditions for the local model runs were extracted from the corresponding full model run results. Then each local model run was simulated for a five-week period to allow for spin-up and to capture a complete month-long spring-neap tidal cycle under each flow condition.

6.2. Model Results

Salinity results from the local model production runs were extracted at selected locations along pertinent tidal creeks as shown in Figure 6-7 to investigate the potential Project impacts on salinity level changes. The tidal wetland salinity zones under current existing conditions are also presented for reference. The vegetation-based salinity zone boundaries are: freshwater < 0.5 ppt; brackish 0.5 – 18 ppt; and saltwater > 18 ppt.

The model runs are considered reaching a dynamic steady state after the first three weeks, so the model results from the last two-week period were assumed as representative salinity levels under each flow condition. They are presented and discussed at each tidal creek separately in the following subsections. The average salinities are also computed. The results are presented in the following order based on river flow conditions: Typical High flow, Typical Medium flow, Typical Low flow (Dry High flow), Dry Medium flow, and Dry Low flow. The salinity level under the Existing condition is included as the basis for determining the Project impacts under different future sea level rise scenarios.

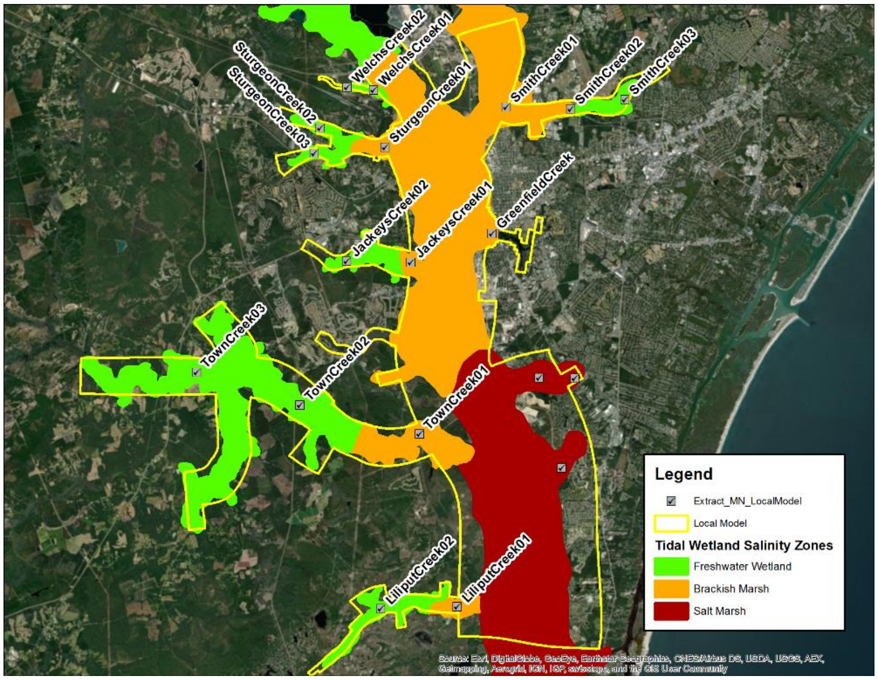

Figure 6-7: Extraction locations of local model salinity results

6.2.1. Lilliput Creek

Figure 6-8 to Figure 6-12 present the surface salinity results along Lilliput Creek under each flow condition. Table 6-3 summarizes the average salinity results at these two locations (where Δ = FwP – FwoP). The salinity level increases caused by the Project are no more than 1.2 ppt under Typical year flow conditions.

Table 6-3: Average surface salinities at Lilliput Creek

	Flow Conditions	Existing	Low RSLR			Intermediate RSLR			High RSLR		
			FwoP	FwP	Δ	FwoP	FwP	Δ	FwoP	FwP	Δ
LilliputCreek01	Typical High	3.1	3.9	4.6	0.7	4.7	5.4	0.7	6.3	7.1	0.8
	Typical Medium	6.2	7.5	8.4	0.9	8.7	9.7	1.0	10.3	11.3	1.0
	Typical Low/ Dry High	10.1	11.8	13.0	1.2	13.2	14.3	1.1	14.7	15.8	1.1
	Dry Medium	17.3	18.5	19.6	1.1						
	Dry Low	22.0	22.8	24.0	1.2						
LilliputCreek02	Typical High	0.0	0.0	0.1	0.1	0.2	0.3	0.1	2.3	2.8	0.5
	Typical Medium	0.0	0.2	0.3	0.1	0.9	1.2	0.3	5.1	6.0	0.9
	Typical Low/ Dry High	0.1	0.7	1.1	0.4	2.7	3.5	0.8	9.1	10.2	1.1
	Dry Medium	1.1	3.5	4.8	1.3						
	Dry Low	2.8	5.7	7.9	2.2						

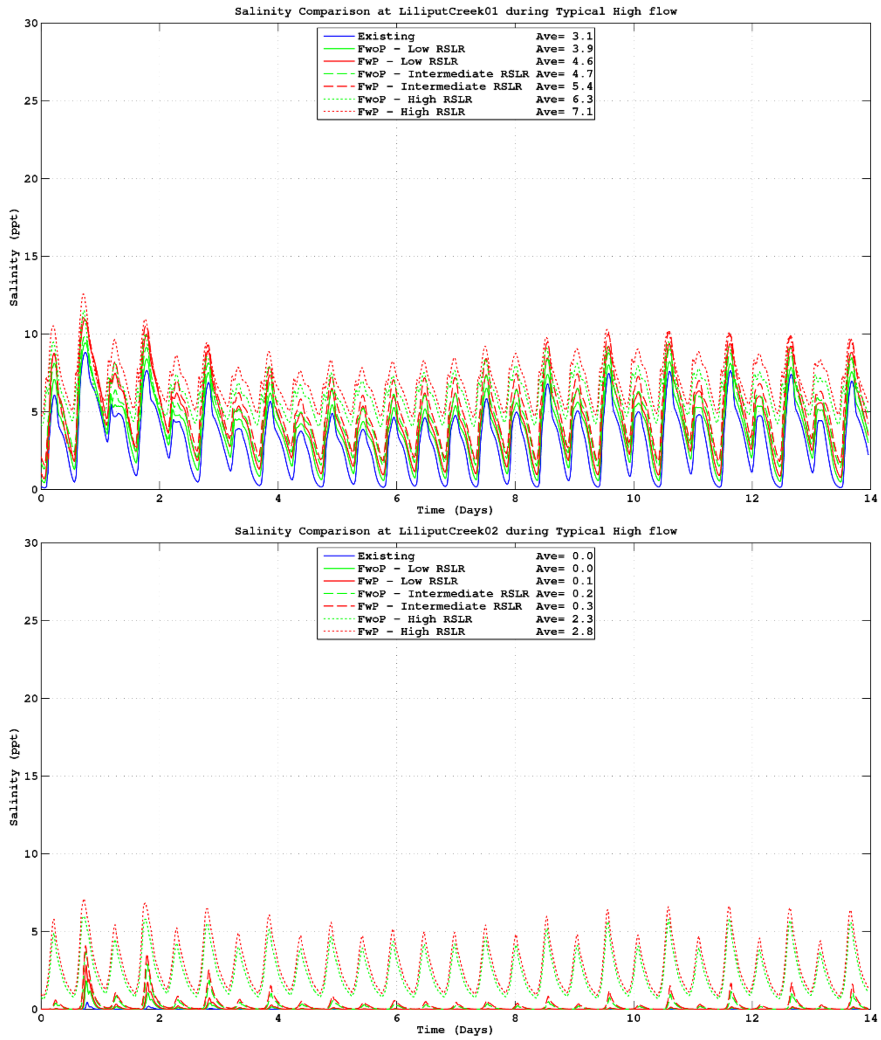

Figure 6-8: Surface salinity along Lilliput Creek during Typical High flow

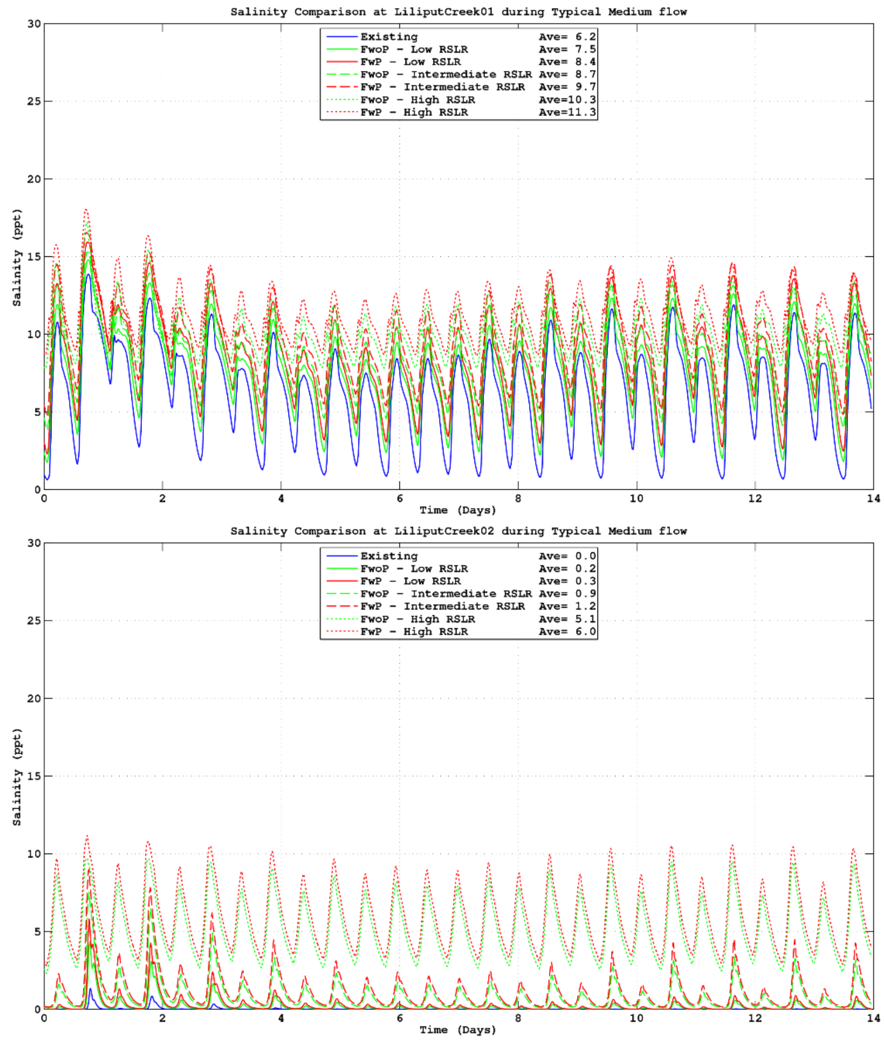

Figure 6-9: Surface salinity along Lilliput Creek during Typical Medium flow

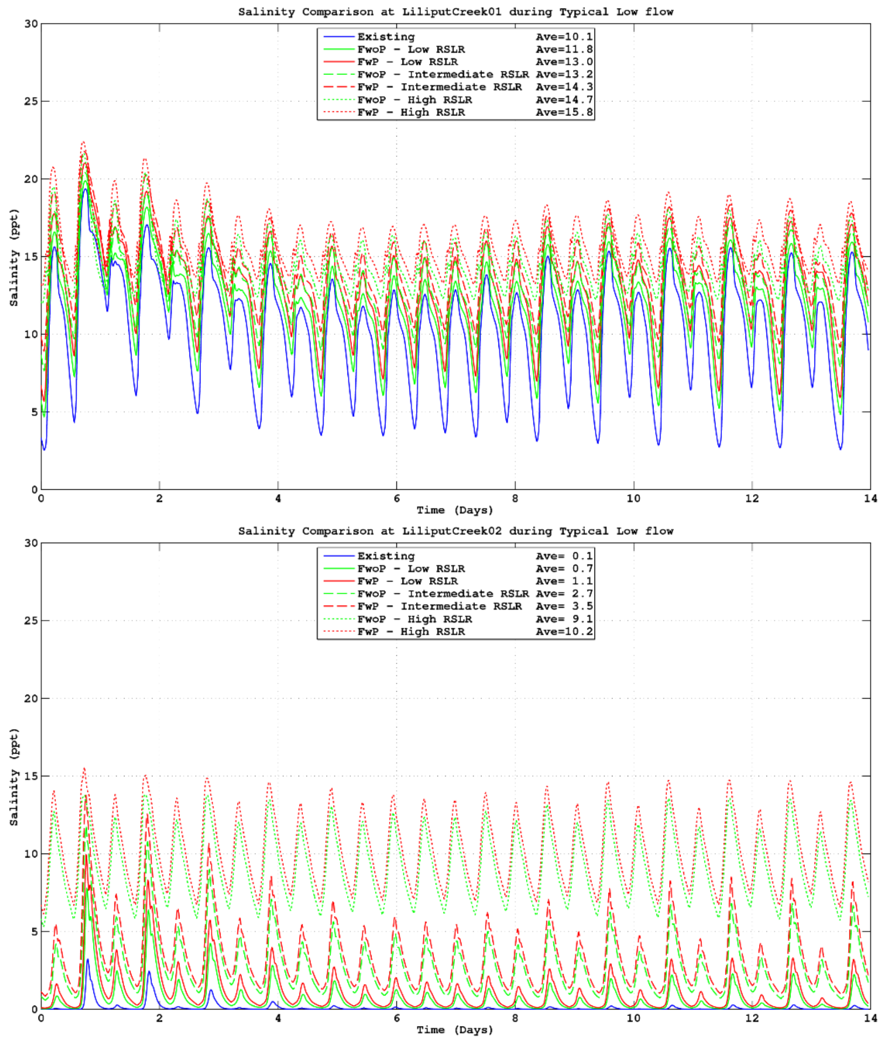

Figure 6-10: Surface salinity along Lilliput Creek during Typical Low (Dry High) flow

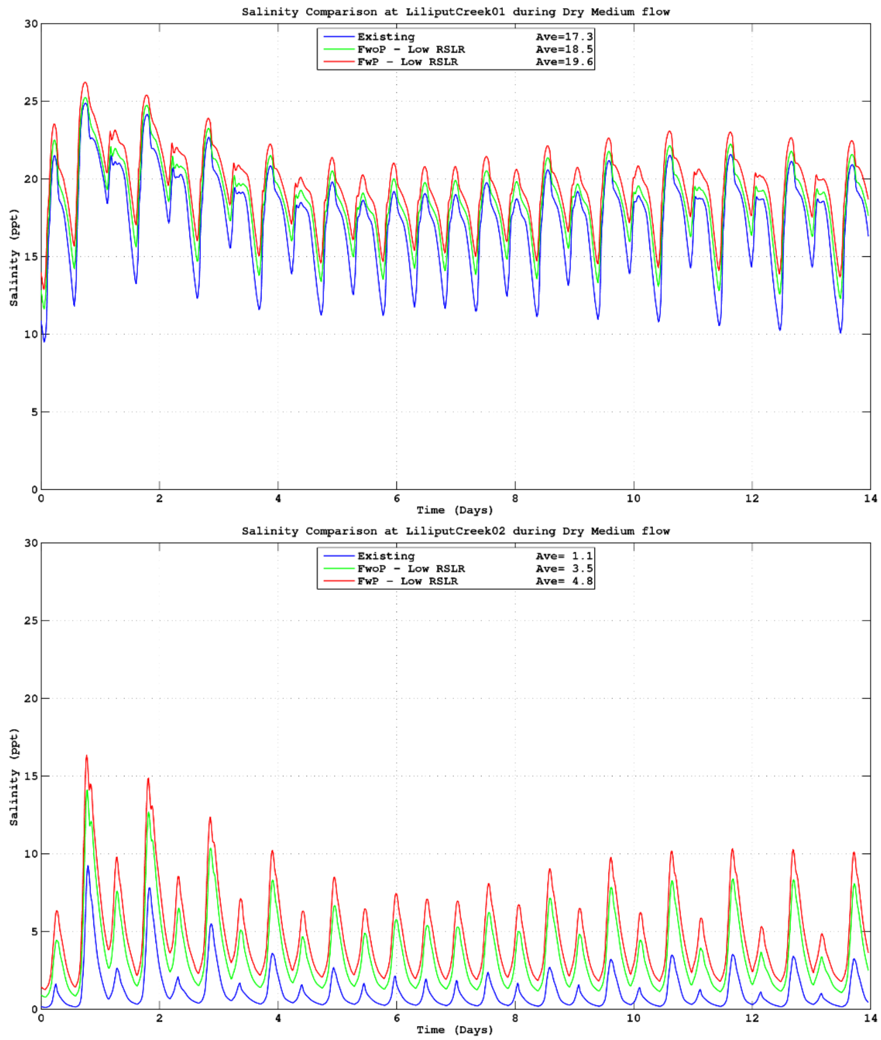

Figure 6-11: Surface salinity along Lilliput Creek during Dry Medium flow

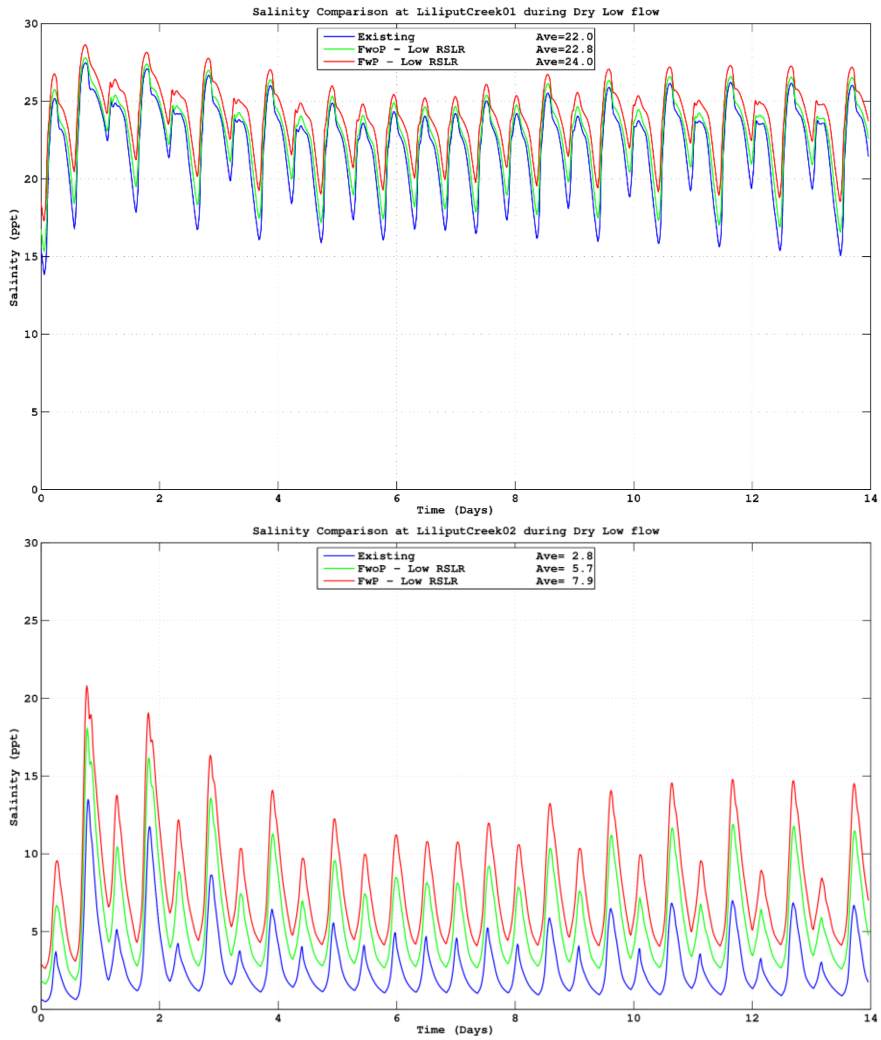

Figure 6-12: Surface salinity along Lilliput Creek during Dry Low flow

6.2.2. Town Creek

Figure 6-13 to Figure 6-17 present the surface salinity results along Town Creek under each flow condition. The average salinity results at Town Creek are summarized in Table 6-4. At the downstream location TownCreek01, the salinity increases caused by the Project are less than 1.0 ppt. The Project's impacts on salinity levels at the upstream location, TownCreek03, are 0.2 ppt or less.

Table 6-4: Average surface salinities at Town Creek

	Flow Conditions	**Existing**	**Low RSLR**			**Intermediate RSLR**			**High RSLR**		
			FwoP	FwP	Δ	FwoP	FwP	Δ	FwoP	FwP	Δ
TownCreek01	Typical High	1.7	2.0	2.6	0.6	2.5	3.3	0.8	3.9	4.7	0.8
	Typical Medium	4.4	4.8	5.6	0.8	5.4	6.2	0.8	7.0	7.9	0.9
	Typical Low /Dry High	8.0	8.5	9.3	0.8	9.1	9.9	0.8	10.7	11.6	0.9
	Dry Medium	14.3	14.9	15.3	0.4						
	Dry Low	19.0	19.6	19.8	0.2						
TownCreek02	Typical High	0.0	0.1	0.1	0.0	0.1	0.2	0.1	0.6	0.8	0.2
	Typical Medium	0.3	0.5	0.7	0.2	0.7	1.0	0.3	1.8	2.3	0.5
	Typical Low /Dry High	1.3	1.7	2.1	0.4	2.2	2.6	0.4	3.7	4.5	0.8
	Dry Medium	4.1	4.7	5.3	0.6						
	Dry Low	6.2	6.8	7.5	0.7						
TownCreek03	Typical High	0.0	0.0	0.0	0.0	0.0	0.0	0.0	0.0	0.0	0.0
	Typical Medium	0.0	0.0	0.0	0.0	0.0	0.0	0.0	0.1	0.2	0.1
	Typical Low /Dry High	0.0	0.0	0.1	0.1	0.1	0.1	0.0	0.4	0.6	0.2
	Dry Medium	0.2	0.3	0.5	0.2						
	Dry Low	0.5	0.7	0.9	0.2						

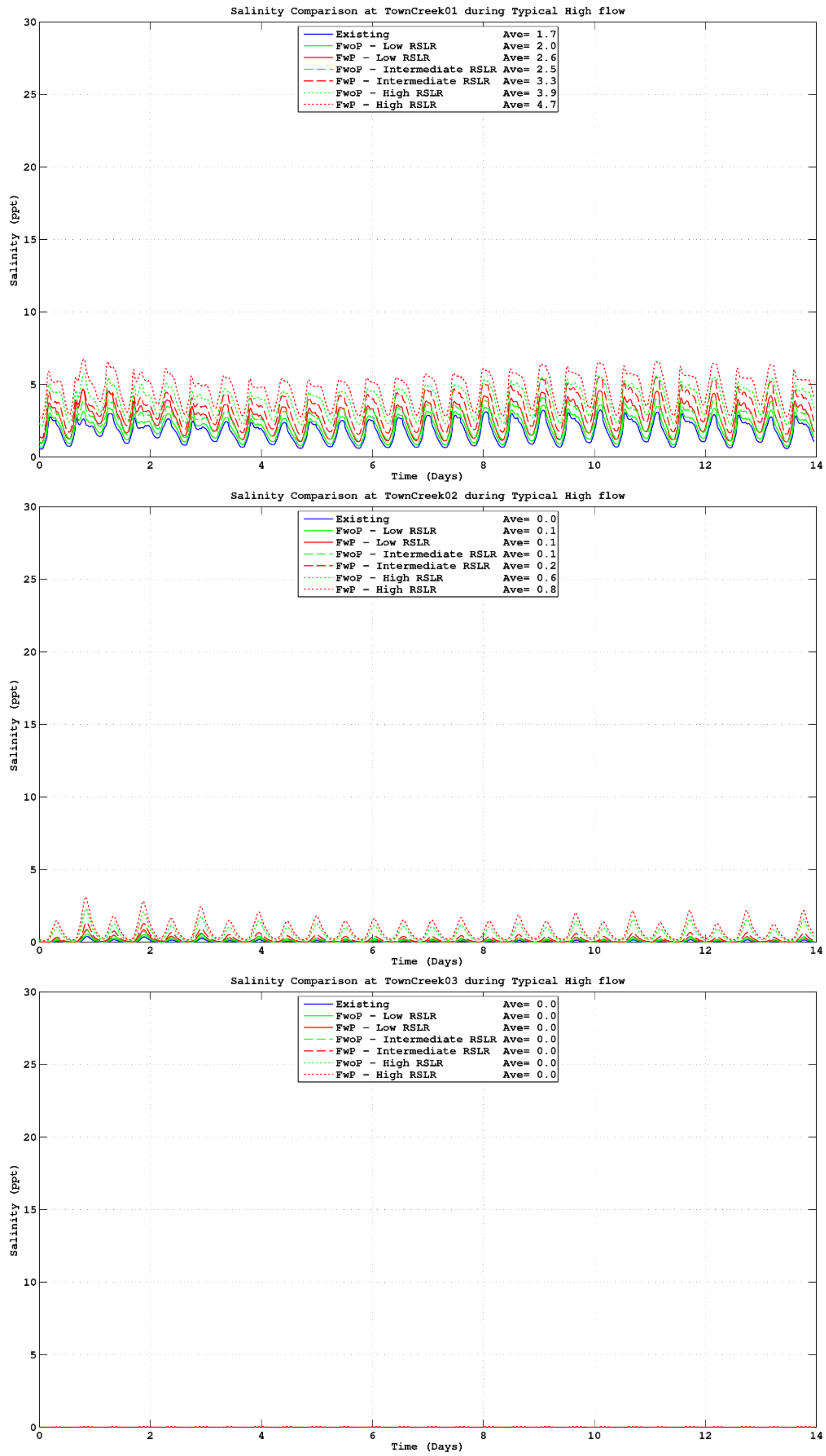

Figure 6-13: Surface salinity along Town Creek during Typical High flow

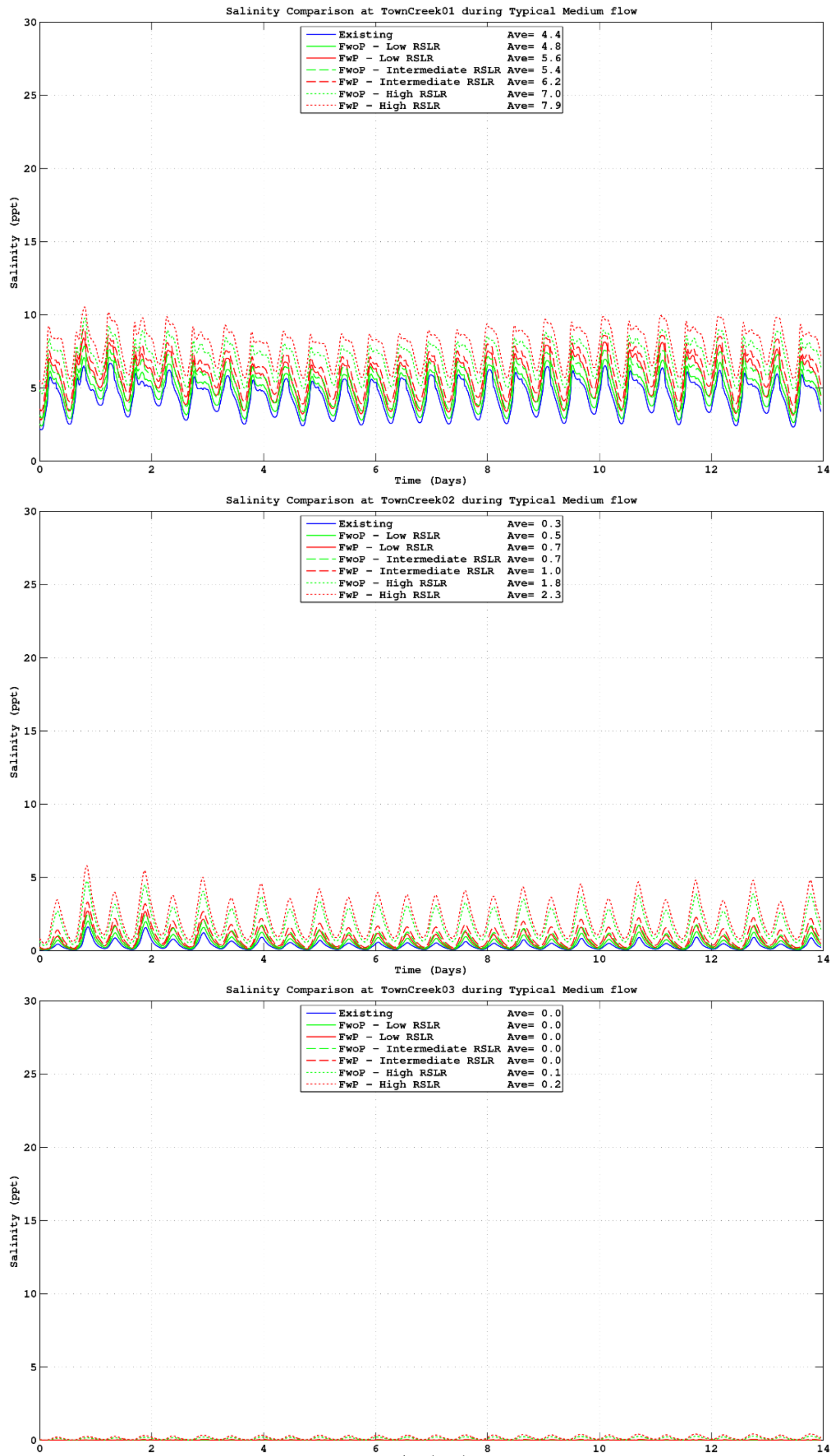

Figure 6-14: Surface salinity along Town Creek during Typical Medium flow

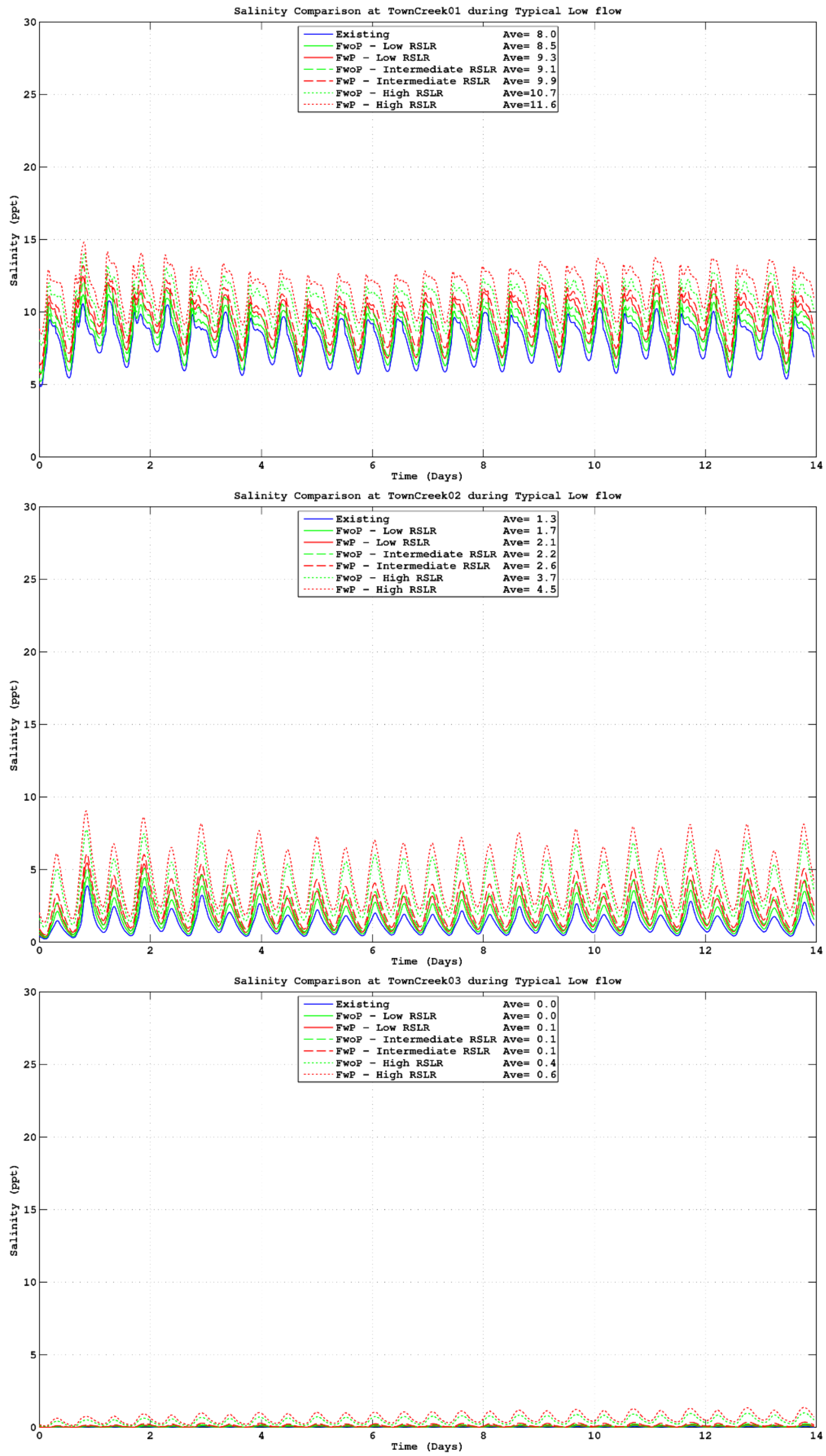

Figure 6-15: Surface salinity along Town Creek during Typical Low (Dry High) flow

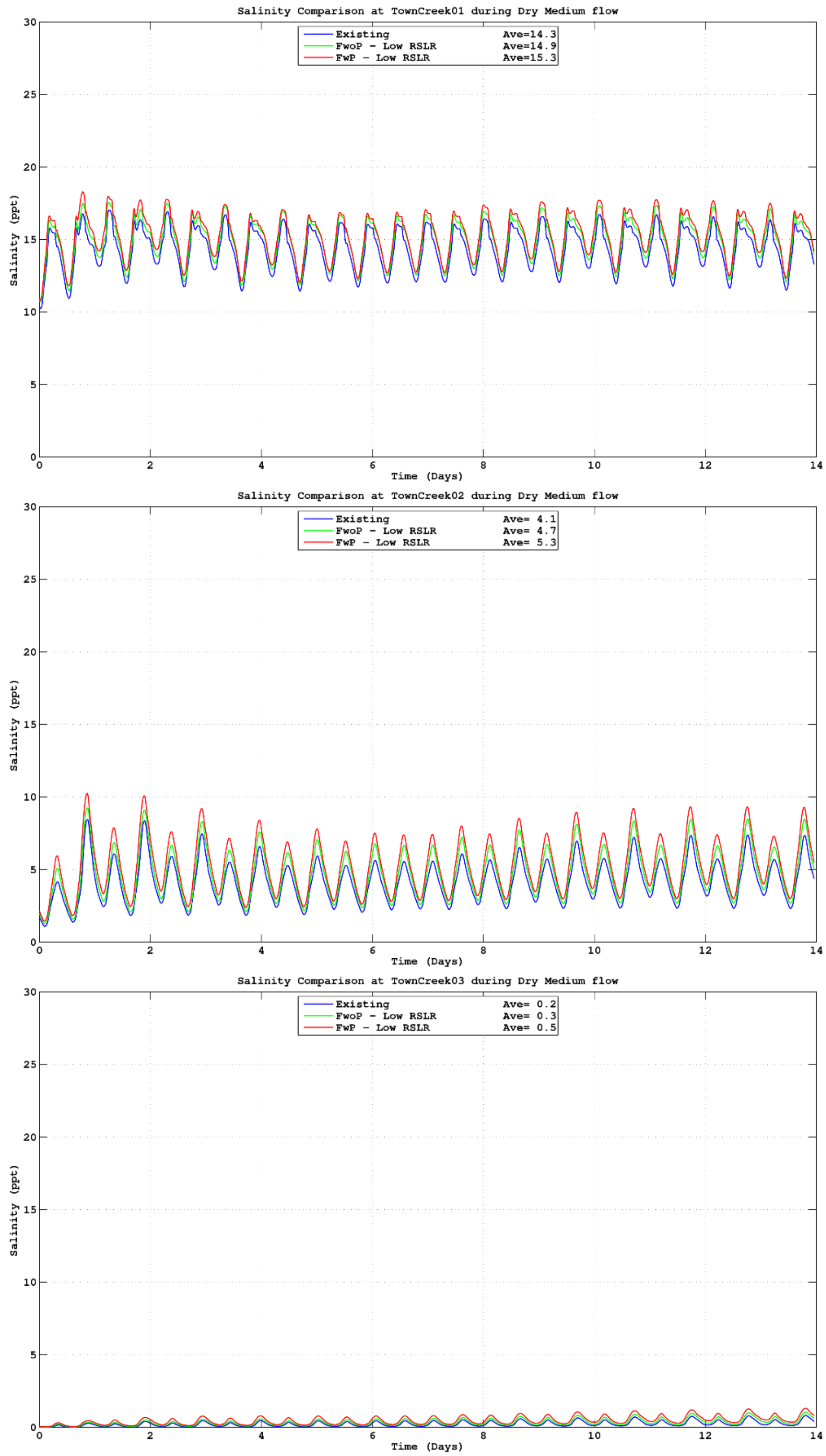

Figure 6-16: Surface salinity along Town Creek during Dry Medium flow

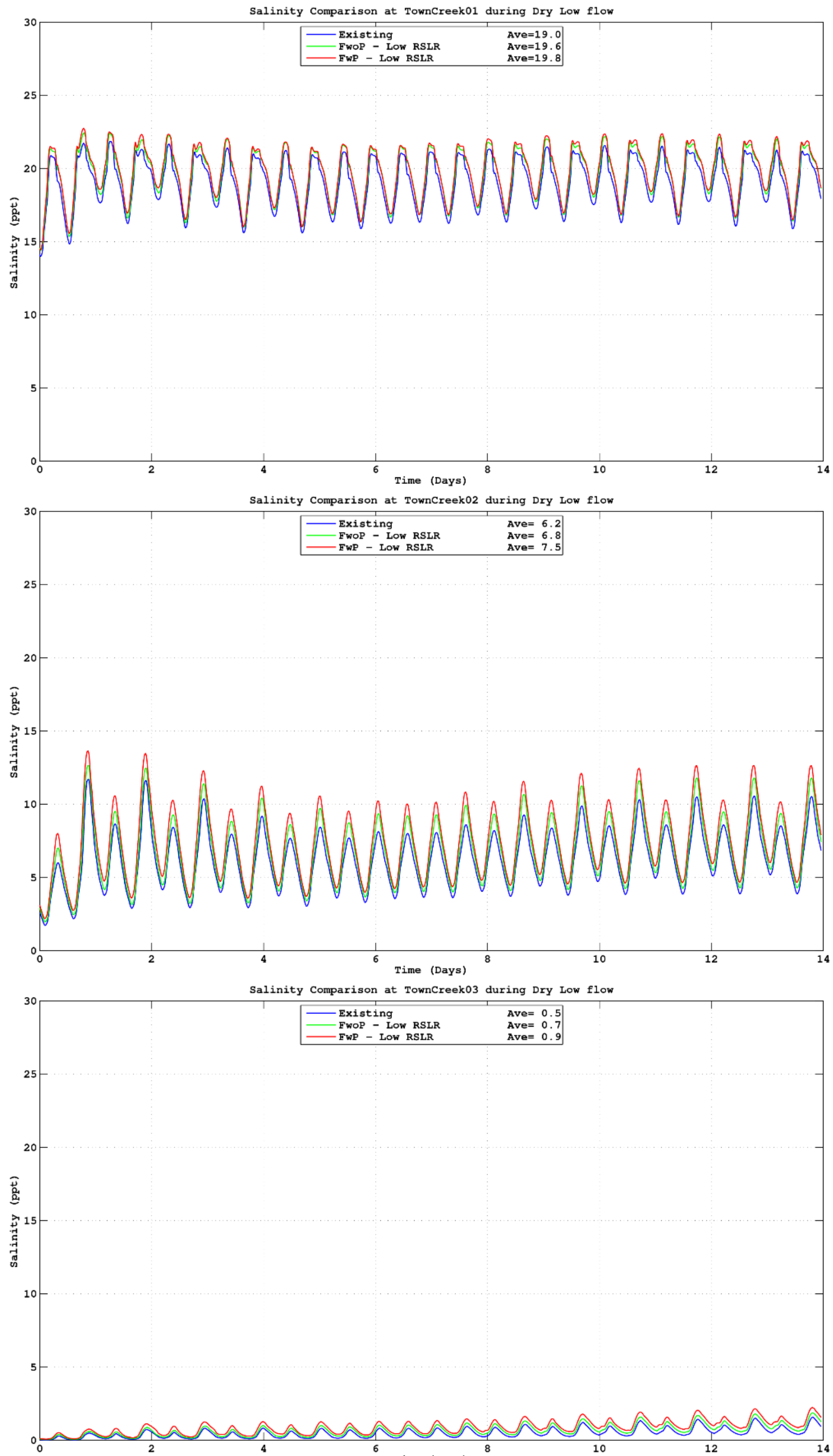

Figure 6-17: Surface salinity along Town Creek during Dry Low flow

6.2.3. Jackeys Creek

Figure 6-18 to Figure 6-22 present the surface salinity results along Jackeys Creek under each flow condition. Table 6-5 summarizes the average salinity results at Jackeys Creek. The salinity level increases caused by the Project are less than 1.5 ppt under Typical year flow conditions.

Table 6-5: Average surface salinities at Jackeys Creek

	Flow Conditions	Existing	Low RSLR			Intermediate RSLR			High RSLR		
			FwoP	FwP	Δ	FwoP	FwP	Δ	FwoP	FwP	Δ
JackeysCreek01	Typical High	0.2	0.2	0.6	0.4	0.3	0.8	0.5	0.5	1.0	0.5
	Typical Medium	1.2	1.4	2.3	0.9	1.6	2.6	1.0	2.0	3.0	1.0
	Typical Low /Dry High	3.9	4.2	5.5	1.3	4.4	5.7	1.3	4.9	6.2	1.3
	Dry Medium	9.8	10.2	11.6	1.4						
	Dry Low	15.3	15.7	16.8	1.1						
JackeysCreek02	Typical High	0.0	0.0	0.0	0.0	0.0	0.1	0.1	0.1	0.2	0.1
	Typical Medium	0.1	0.1	0.3	0.2	0.2	0.5	0.3	0.6	1.1	0.5
	Typical Low /Dry High	0.7	1.0	1.7	0.7	1.5	2.2	0.7	2.4	3.4	1.0
	Dry Medium	4.1	5.1	6.4	1.3						
	Dry Low	8.2	9.6	11.2	1.6						

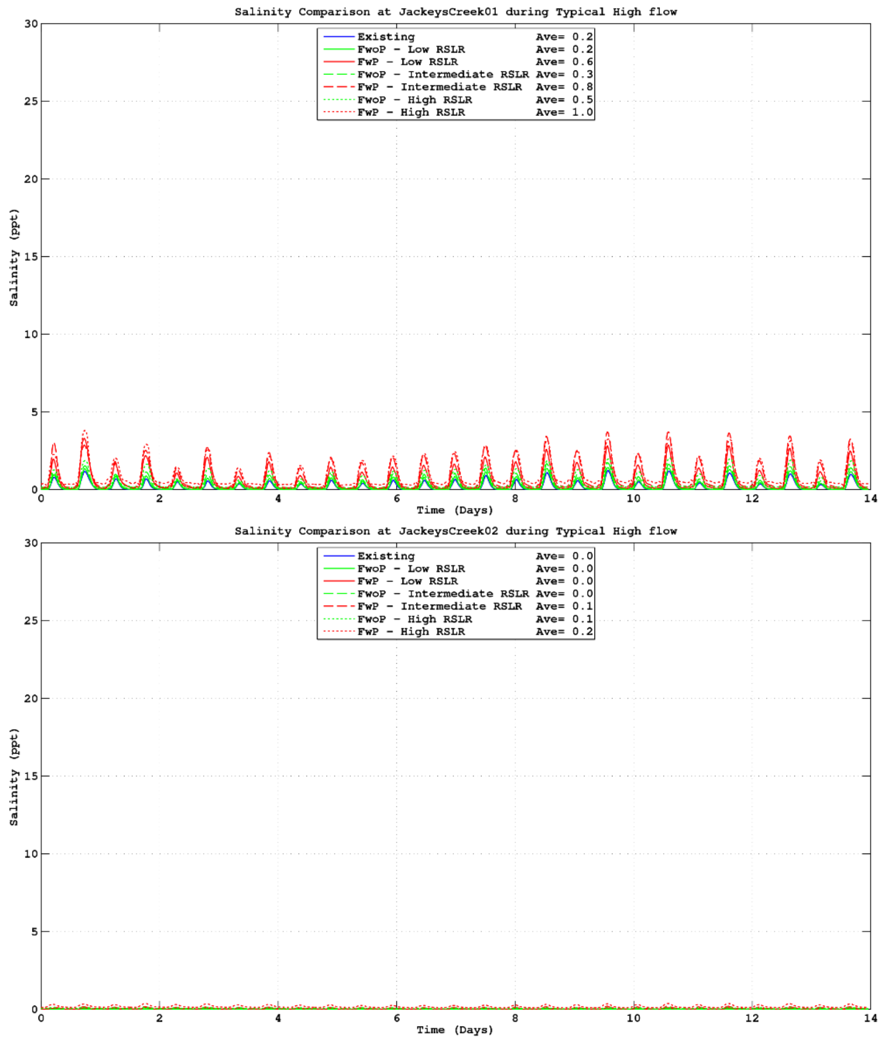

Figure 6-18: Surface salinity along Jackeys Creek during Typical High flow

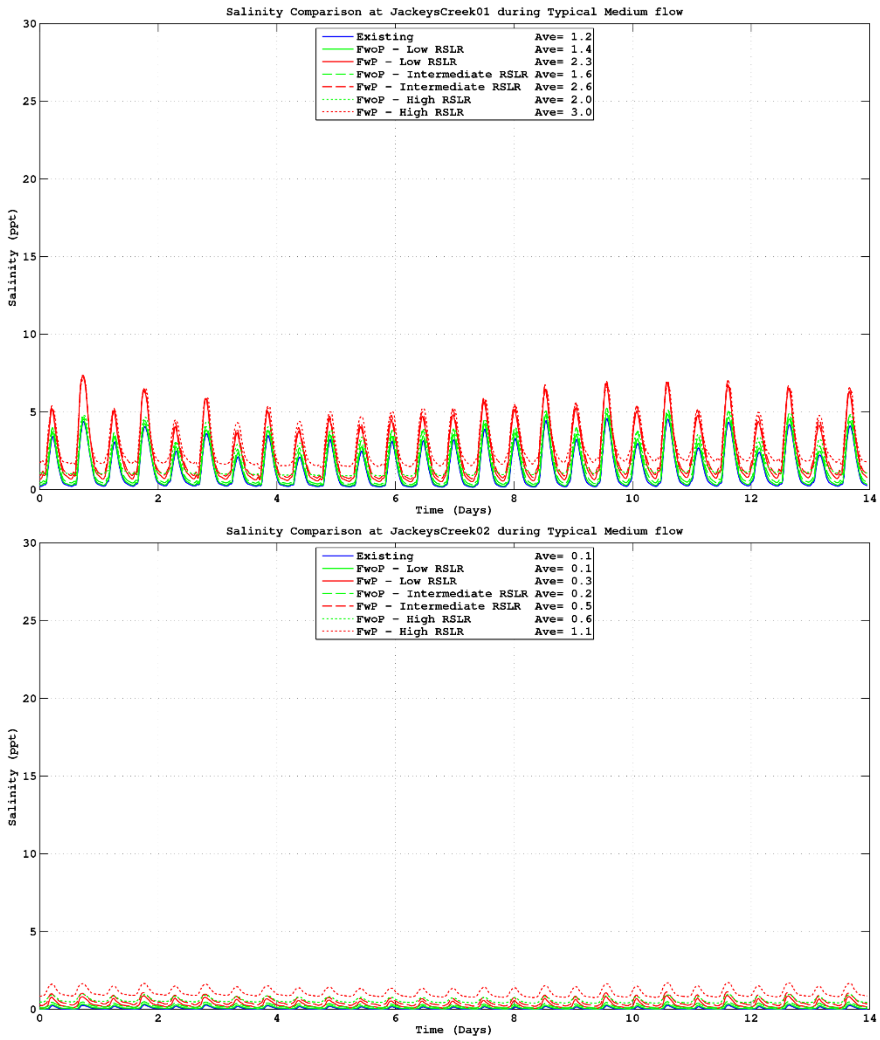

Figure 6-19: Surface salinity along Jackeys Creek during Typical Medium flow

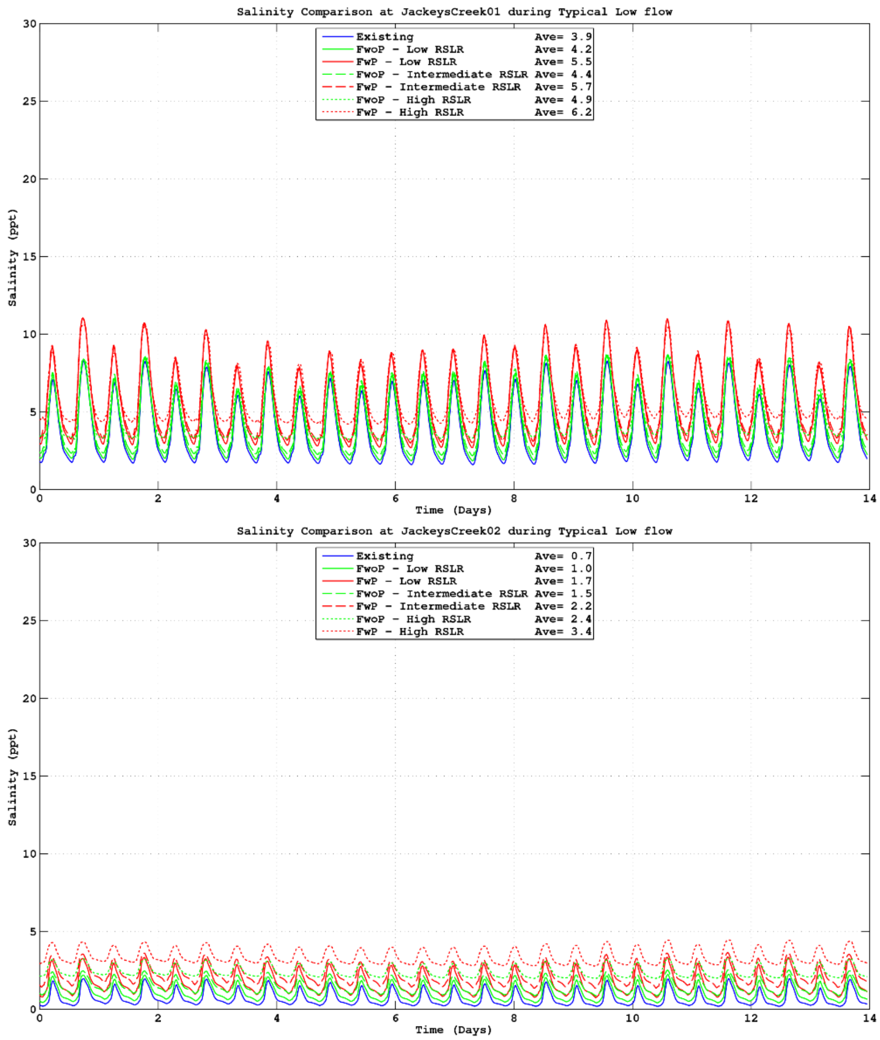

Figure 6-20: Surface salinity along Jackeys Creek during Typical Low (Dry High) flow

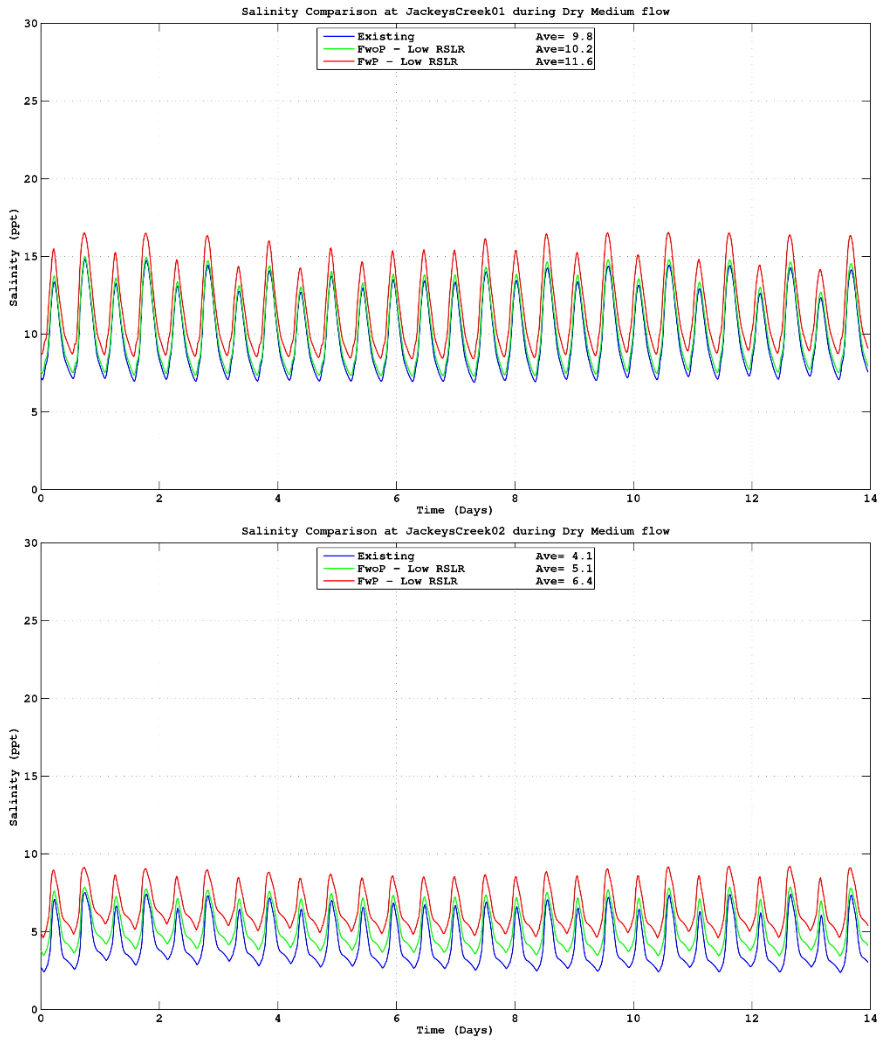

Figure 6-21: Surface salinity along Jackeys Creek during Dry Medium flow

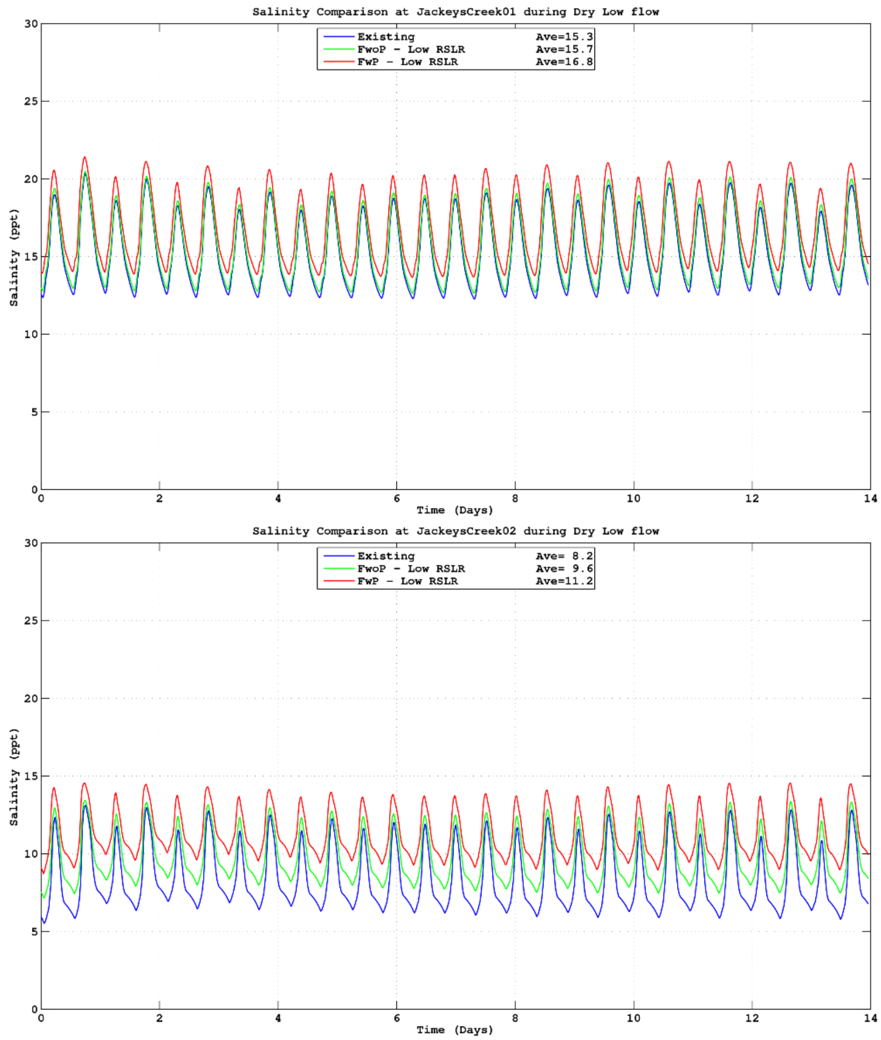

Figure 6-22: Surface salinity along Jackeys Creek during Dry Low flow

6.2.4. Sturgeon Creek

Figure 6-23 to Figure 6-27 present the surface salinity results along Sturgeon Creek under each flow condition. The average salinity results at Sturgeon Creek are summarized in Table 6-6. The Project's impacts on the salinity levels are 0.6 ppt or less near the river and no more than 0.3 ppt in the upper parts of the creek under Typical year flow conditions.

Table 6-6: Average surface salinities at Sturgeon Creek

	Flow Conditions	**Existing**	**Low RSLR**			**Intermediate RSLR**			**High RSLR**		
			FwoP	FwP	Δ	FwoP	FwP	Δ	FwoP	FwP	Δ
SturgeonCreek01	Typical High	0.0	0.0	0.0	0.0	0.0	0.0	0.0	0.0	0.0	0.0
	Typical Medium	0.1	0.1	0.2	0.1	0.1	0.3	0.2	0.3	0.6	0.3
	Typical Low /Dry High	1.1	1.2	1.8	0.6	1.2	1.8	0.6	1.8	2.4	0.6
	Dry Medium	6.0	6.1	7.0	0.9						
	Dry Low	11.4	11.5	12.2	0.7						
SturgeonCreek02	Typical High	0.0	0.0	0.0	0.0	0.0	0.0	0.0	0.0	0.0	0.0
	Typical Medium	0.0	0.0	0.0	0.0	0.0	0.0	0.0	0.0	0.0	0.0
	Typical Low /Dry High	0.3	0.3	0.6	0.3	0.3	0.5	0.2	0.6	0.9	0.3
	Dry Medium	3.9	4.0	4.6	0.6						
	Dry Low	8.9	8.9	9.5	0.6						
SturgeonCreek03	Typical High	0.0	0.0	0.0	0.0	0.0	0.0	0.0	0.0	0.0	0.0
	Typical Medium	0.0	0.0	0.0	0.0	0.0	0.0	0.0	0.0	0.0	0.0
	Typical Low /Dry High	0.3	0.3	0.6	0.3	0.3	0.5	0.2	0.6	0.9	0.3
	Dry Medium	4.0	4.0	4.6	0.6						
	Dry Low	9.0	9.0	9.6	0.6						

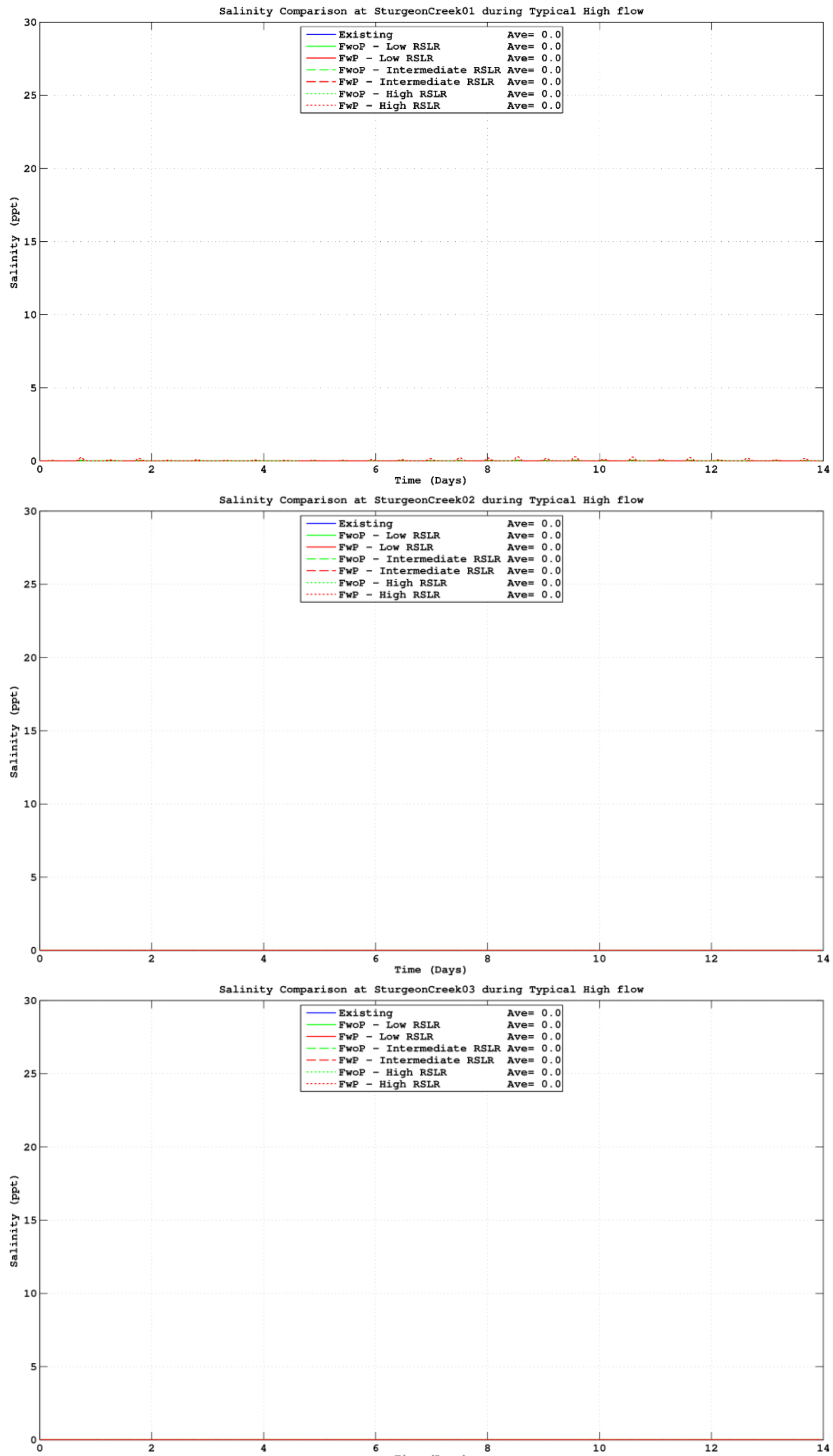

Figure 6-23: Surface salinity along Sturgeon Creek during Typical High flow

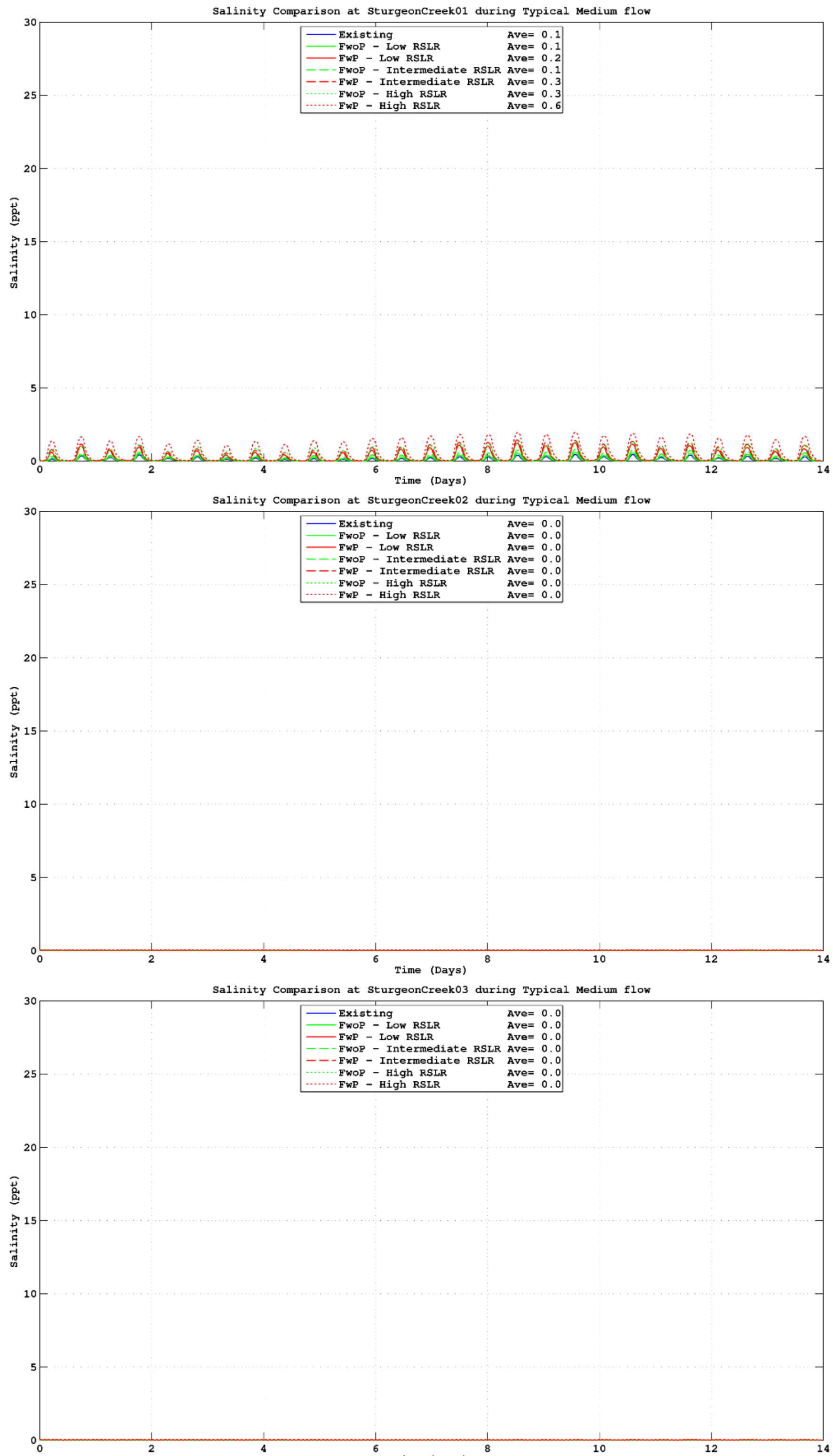

Figure 6-24: Surface salinity along Sturgeon Creek during Typical Medium flow

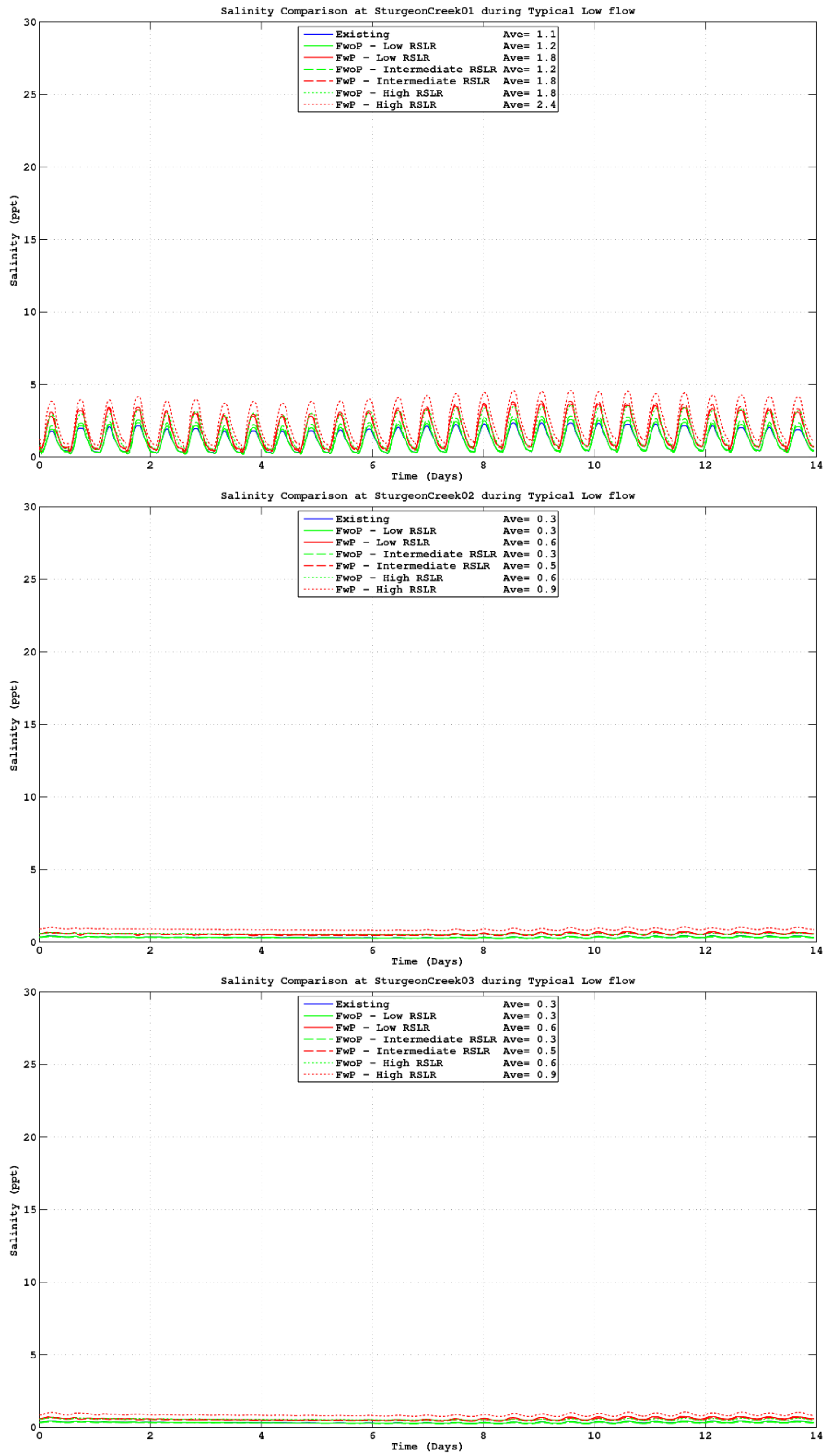

Figure 6-25: Surface salinity along Sturgeon Creek during Typical Low (Dry High) flow

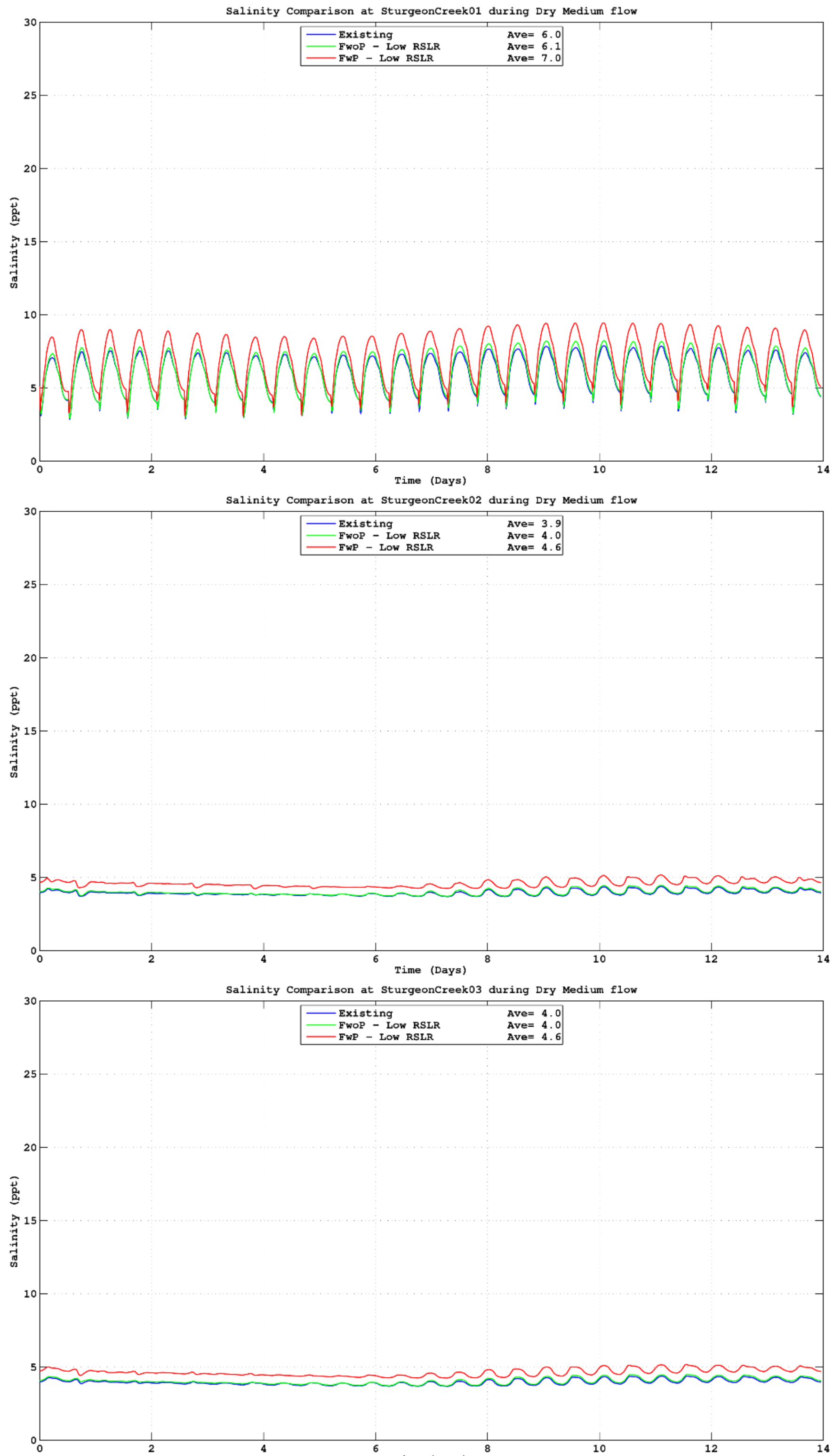

Figure 6-26: Surface salinity along Sturgeon Creek during Dry Medium flow

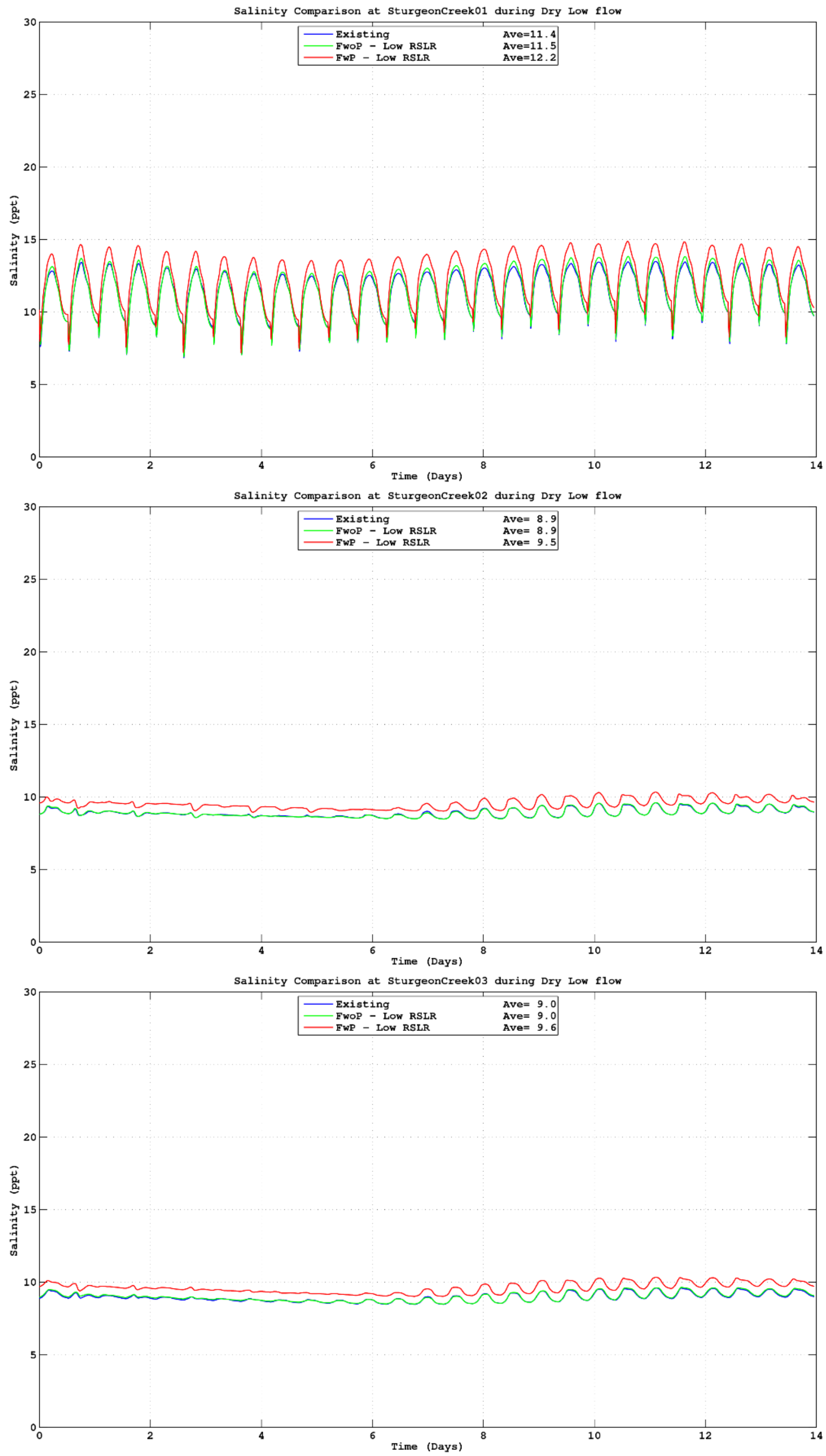

Figure 6-27: Surface salinity along Sturgeon Creek during Dry Low flow

6.2.5. Welchs Creek (Cartwheel Branch)

Figure 6-28 to Figure 6-32 present the surface salinity results along Welchs Creek under each flow condition. The average salinity results at Welchs Creek are summarized in Table 6-7. The absolute FwP salinity levels under Typical year flow conditions are no more than 0.5 ppt even for the High RSLR scenario.

Table 6-7: Average surface salinities at Welchs Creek

	Flow Conditions	Existing	Low RSLR			Intermediate RSLR			High RSLR		
			FwoP	FwP	Δ	FwoP	FwP	Δ	FwoP	FwP	Δ
WelchsCreek01	Typical High	0.0	0.0	0.0	0.0	0.0	0.0	0.0	0.0	0.0	0.0
	Typical Medium	0.0	0.0	0.0	0.0	0.0	0.0	0.0	0.0	0.0	0.0
	Typical Low /Dry High	0.1	0.1	0.3	0.2	0.1	0.3	0.2	0.3	0.5	0.2
	Dry Medium	1.6	1.7	2.2	0.5						
	Dry Low	4.4	4.5	5.3	0.8						
WelchsCreek02	Typical High	0.0	0.0	0.0	0.0	0.0	0.0	0.0	0.0	0.0	0.0
	Typical Medium	0.0	0.0	0.0	0.0	0.0	0.0	0.0	0.0	0.0	0.0
	Typical Low /Dry High	0.0	0.0	0.0	0.0	0.0	0.0	0.0	0.1	0.1	0.0
	Dry Medium	0.1	0.1	0.2	0.1						
	Dry Low	1.2	1.2	1.5	0.3						

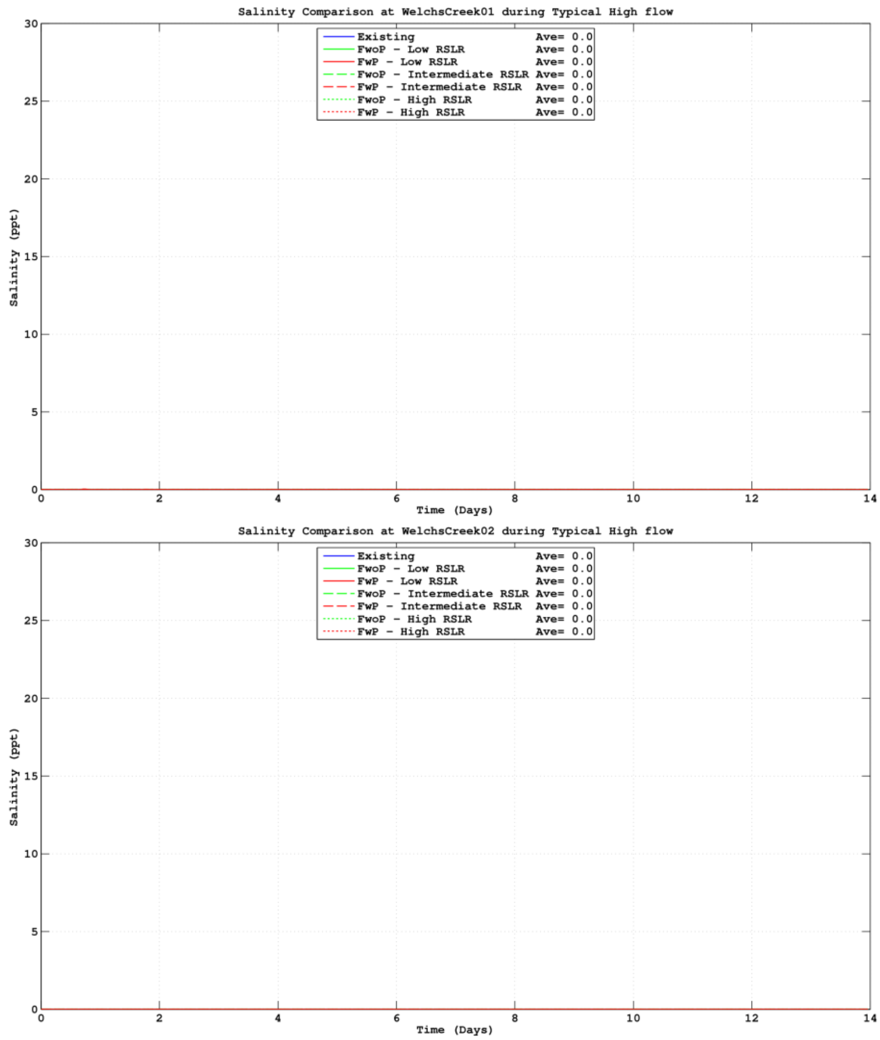

Figure 6-28: Surface salinity along Welchs Creek during Typical High flow

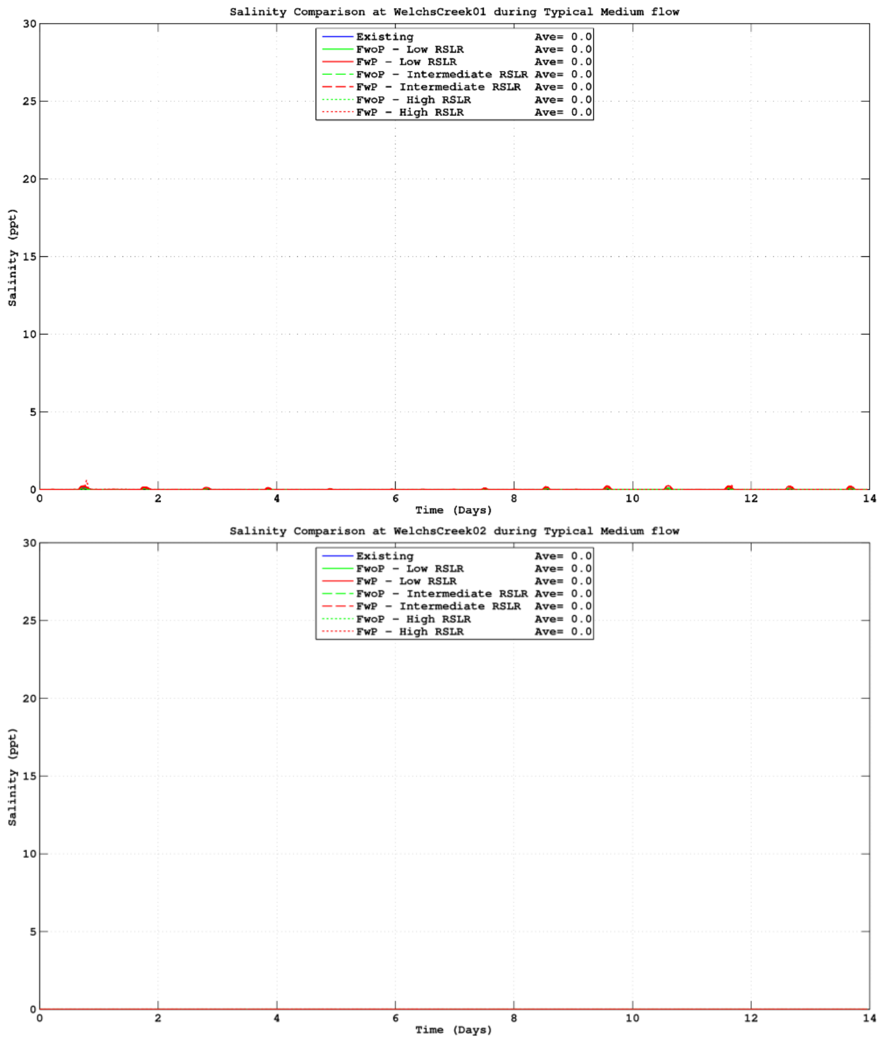

Figure 6-29: Surface salinity along Welchs Creek during Typical Medium flow

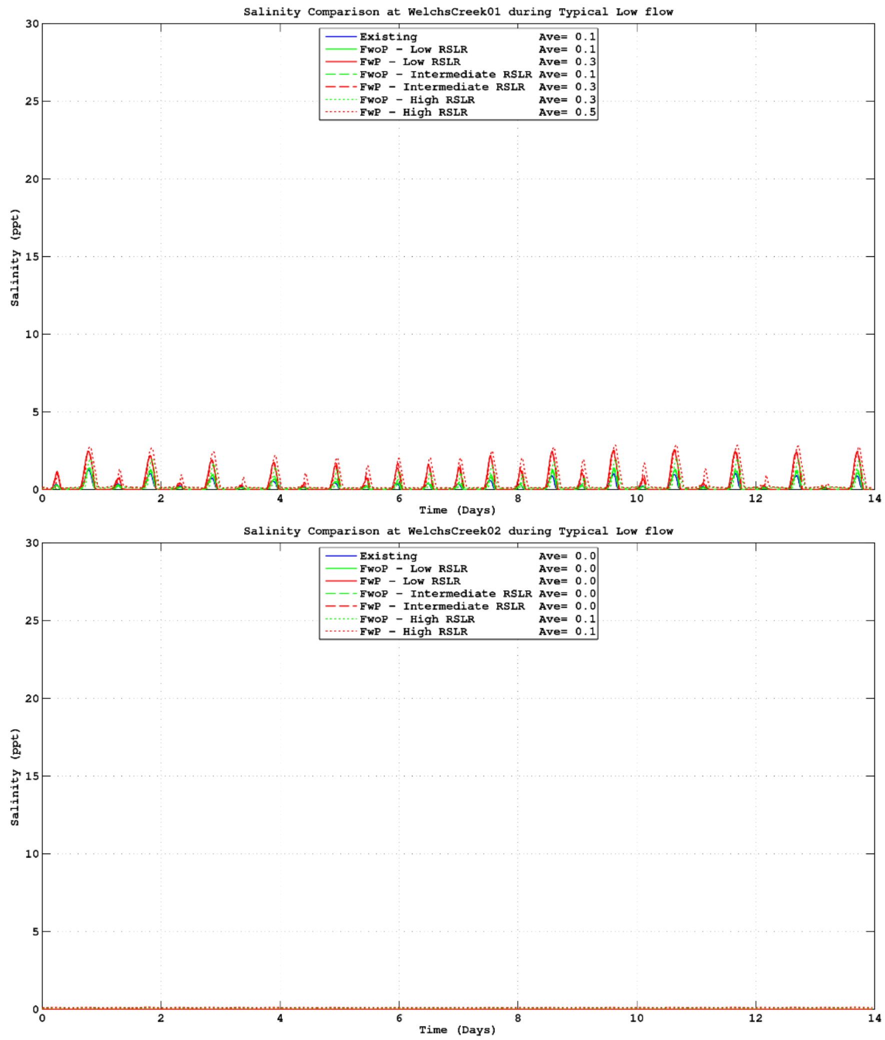

Figure 6-30: Surface salinity along Welchs Creek during Typical Low (Dry High) flow

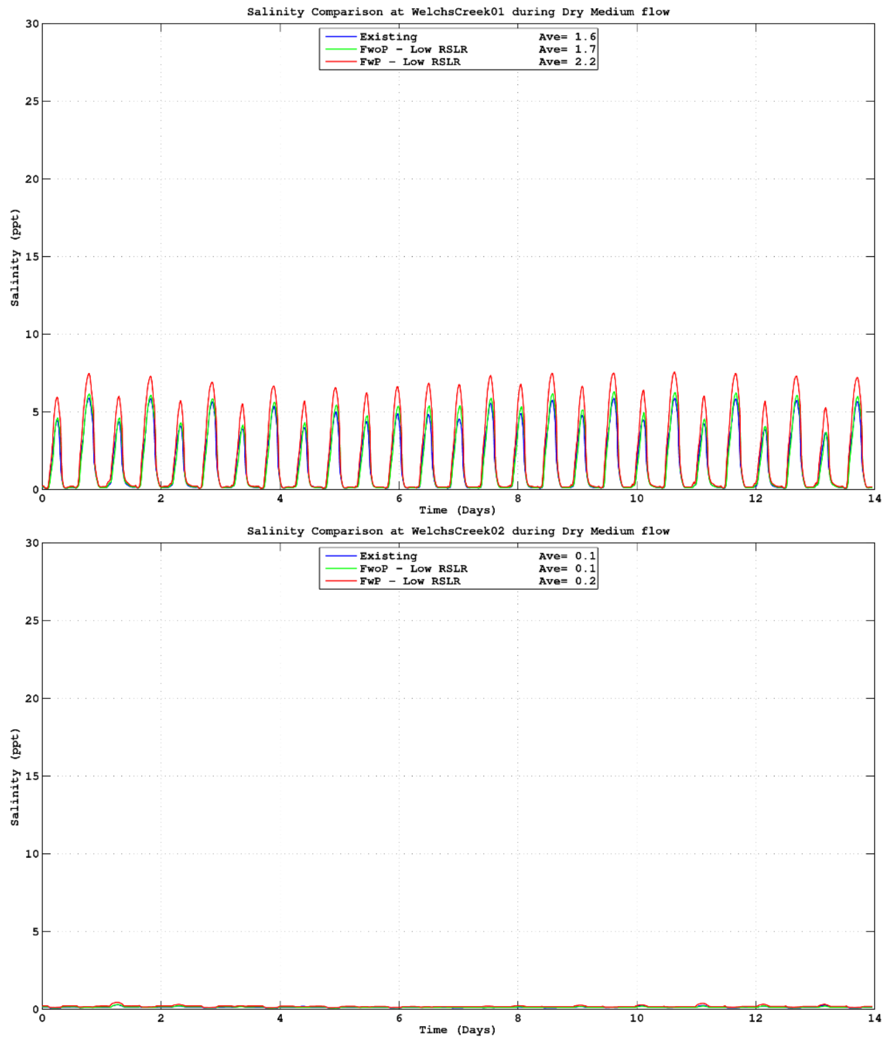

Figure 6-31: Surface salinity along Welchs Creek during Dry Medium flow

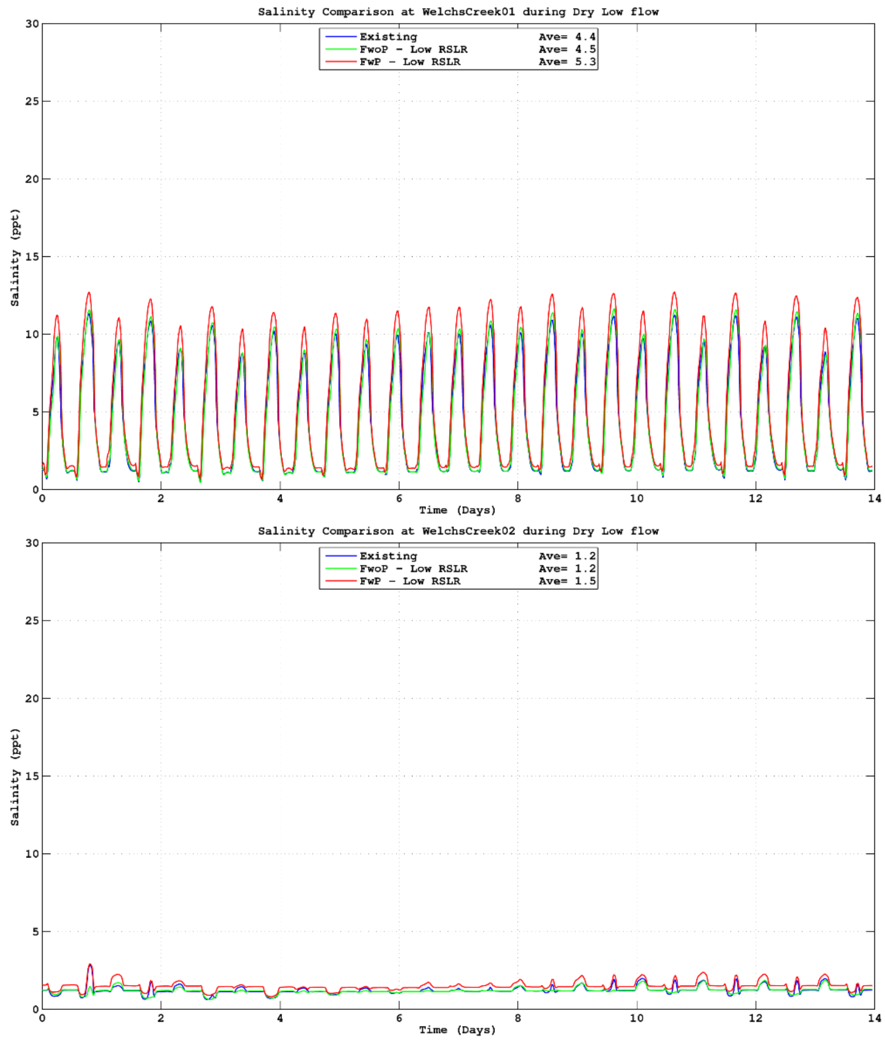

Figure 6-32: Surface salinity along Welchs Creek during Dry Low flow

6.2.6. Smith Creek

Figure 6-33 to Figure 6-37 present the surface salinity results along Smith Creek under each flow condition. Table 6-8 summarizes the average salinity results along Smith Creek. Under Typical year flows, the salinity level increases caused by the Project are less than 1 ppt in the middle and upper portions of the creek.

Table 6-8: Average surface salinities at Smith Creek

	Flow Conditions	Existing	Low RSLR			Intermediate RSLR			High RSLR		
			FwoP	FwP	Δ	FwoP	FwP	Δ	FwoP	FwP	Δ
SmithCreek01	Typical High	0.0	0.0	0.2	0.2	0.1	0.4	0.3	0.3	0.7	0.4
	Typical Medium	0.6	0.7	1.5	0.8	0.9	1.7	0.8	1.8	2.7	0.9
	Typical Low /Dry High	2.6	2.8	4.0	1.2	3.1	4.3	1.2	4.7	5.8	1.1
	Dry Medium	7.3	7.7	8.9	1.2						
	Dry Low	13.0	13.4	14.4	1.0						
SmithCreek02	Typical High	0.0	0.0	0.0	0.0	0.0	0.1	0.1	0.1	0.2	0.1
	Typical Medium	0.2	0.2	0.5	0.3	0.3	0.6	0.3	0.9	1.3	0.4
	Typical Low /Dry High	1.2	1.4	2.0	0.6	1.6	2.3	0.7	3.0	3.8	0.8
	Dry Medium	4.6	5.1	6.0	0.9						
	Dry Low	10.1	10.6	11.7	1.1						
SmithCreek03	Typical High	0.0	0.0	0.0	0.0	0.0	0.0	0.0	0.0	0.0	0.0
	Typical Medium	0.0	0.0	0.1	0.1	0.1	0.2	0.1	0.3	0.5	0.2
	Typical Low /Dry High	0.3	0.5	0.8	0.3	0.7	1.1	0.4	1.7	2.4	0.7
	Dry Medium	2.5	3.1	3.9	0.8						
	Dry Low	6.6	7.4	8.6	1.2						

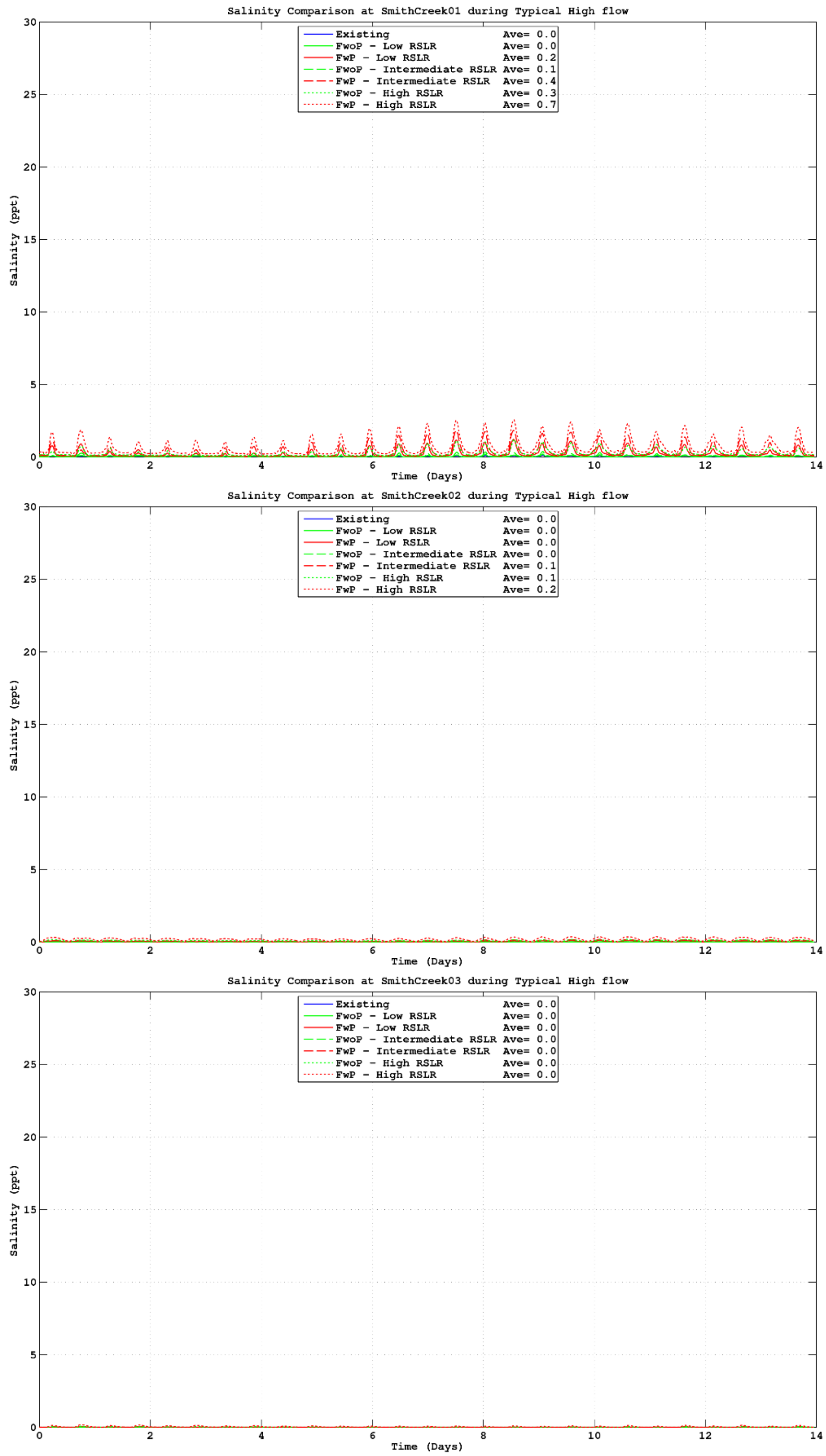

Figure 6-33: Surface salinity along Smith Creek during Typical High flow

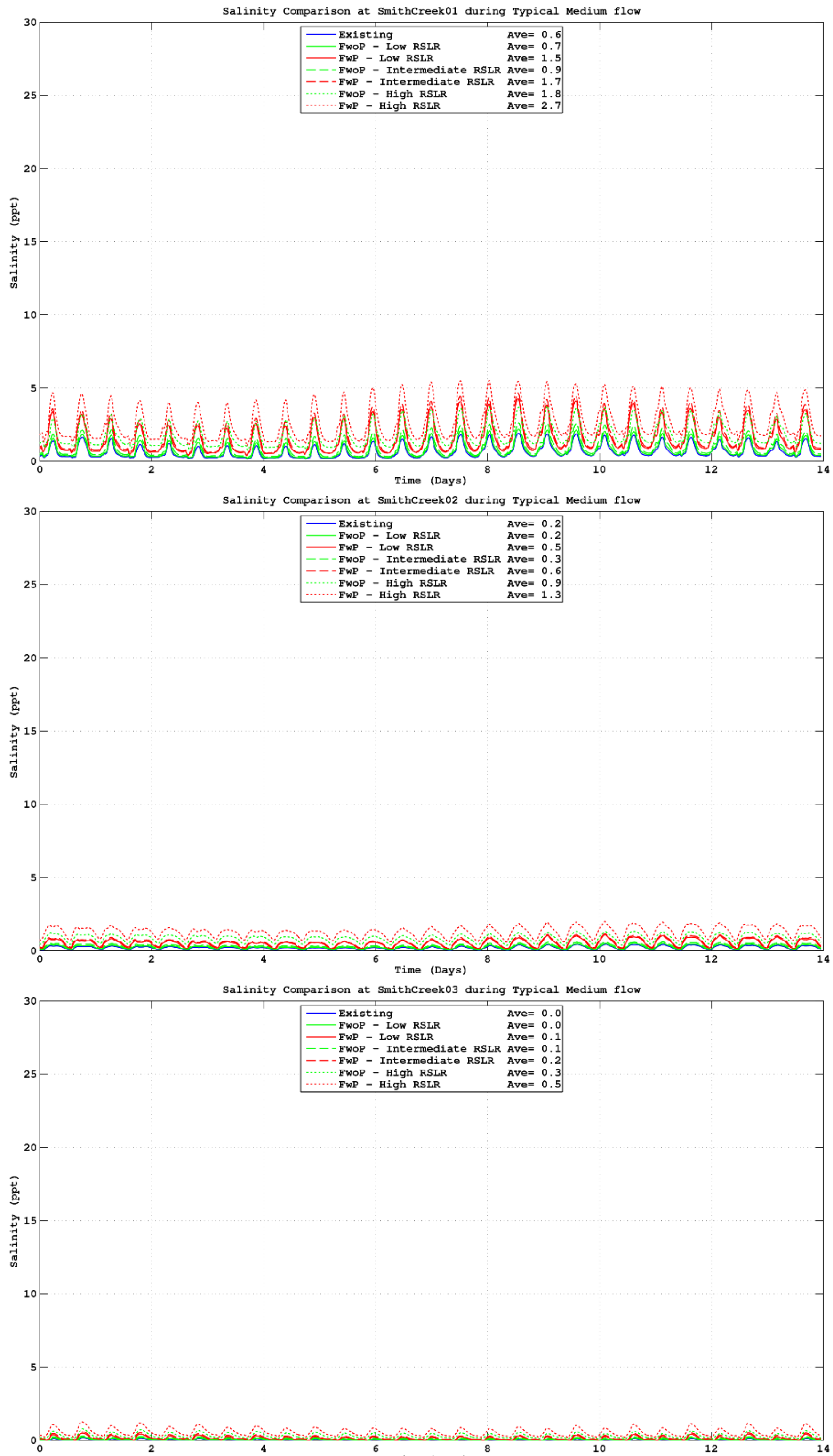

Figure 6-34: Surface salinity along Smith Creek during Typical Medium flow

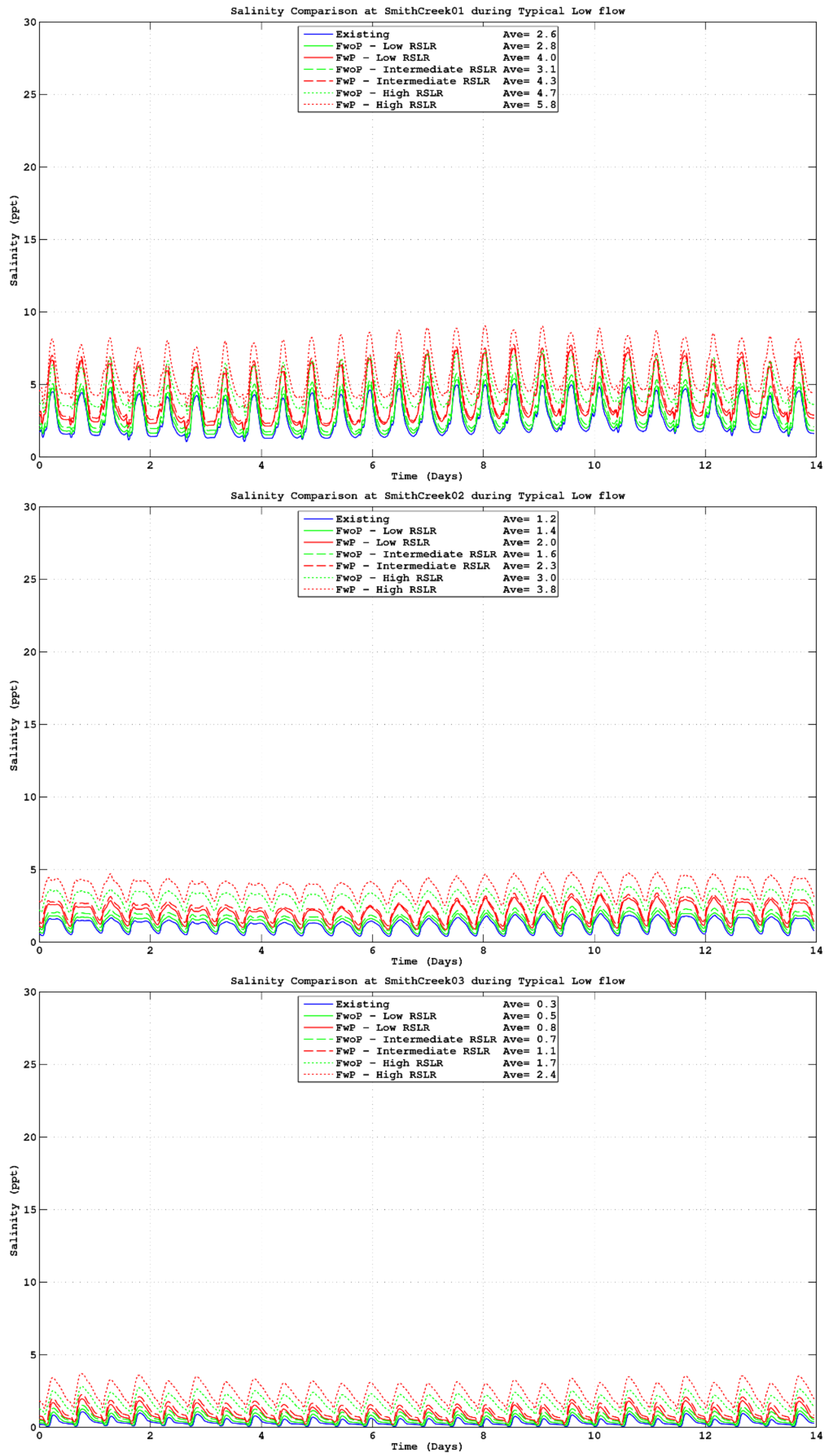

Figure 6-35: Surface salinity along Smith Creek during Typical Low (Dry High) flow

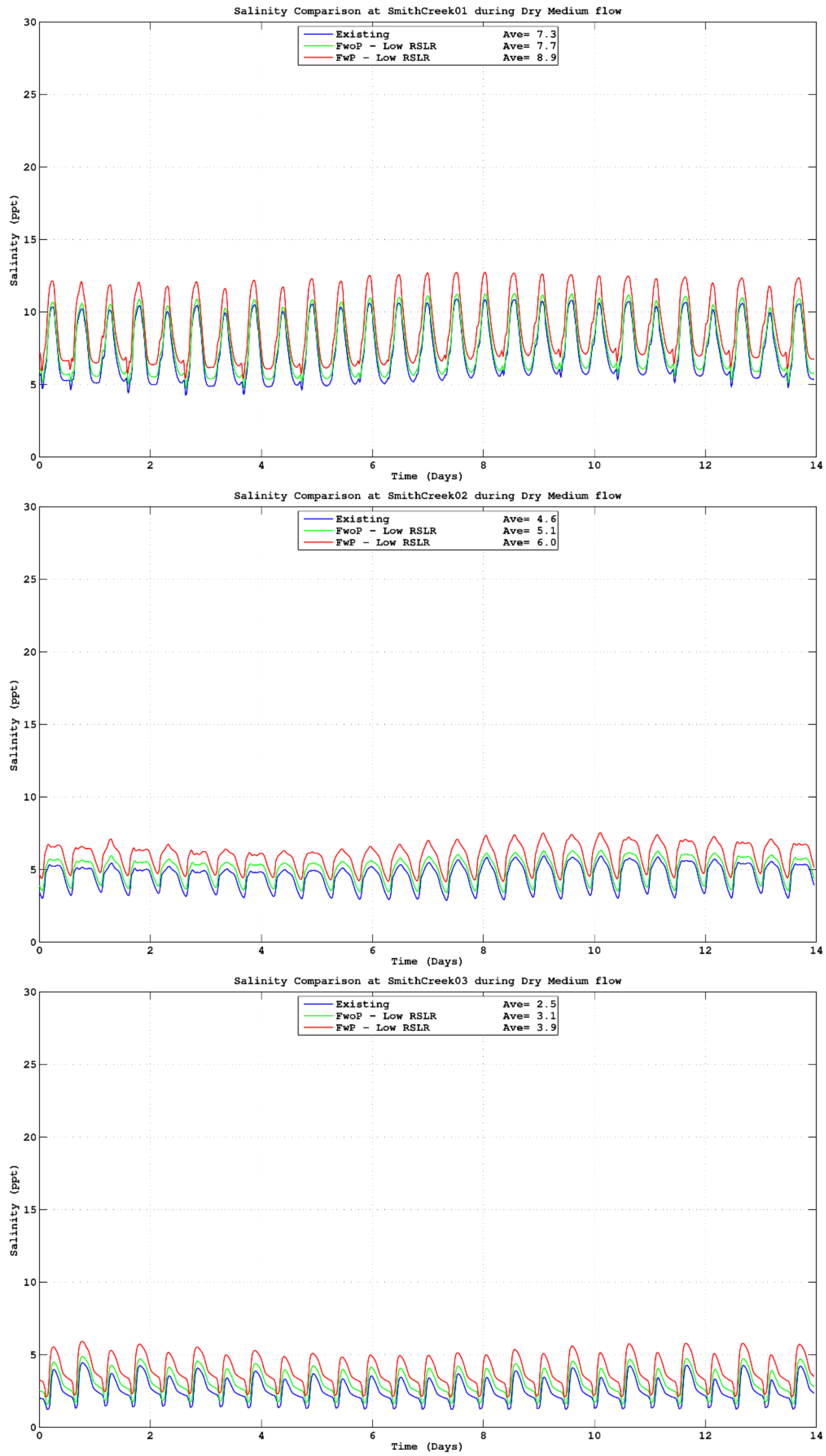

Figure 6-36: Surface salinity along Smith Creek during Dry Medium flow

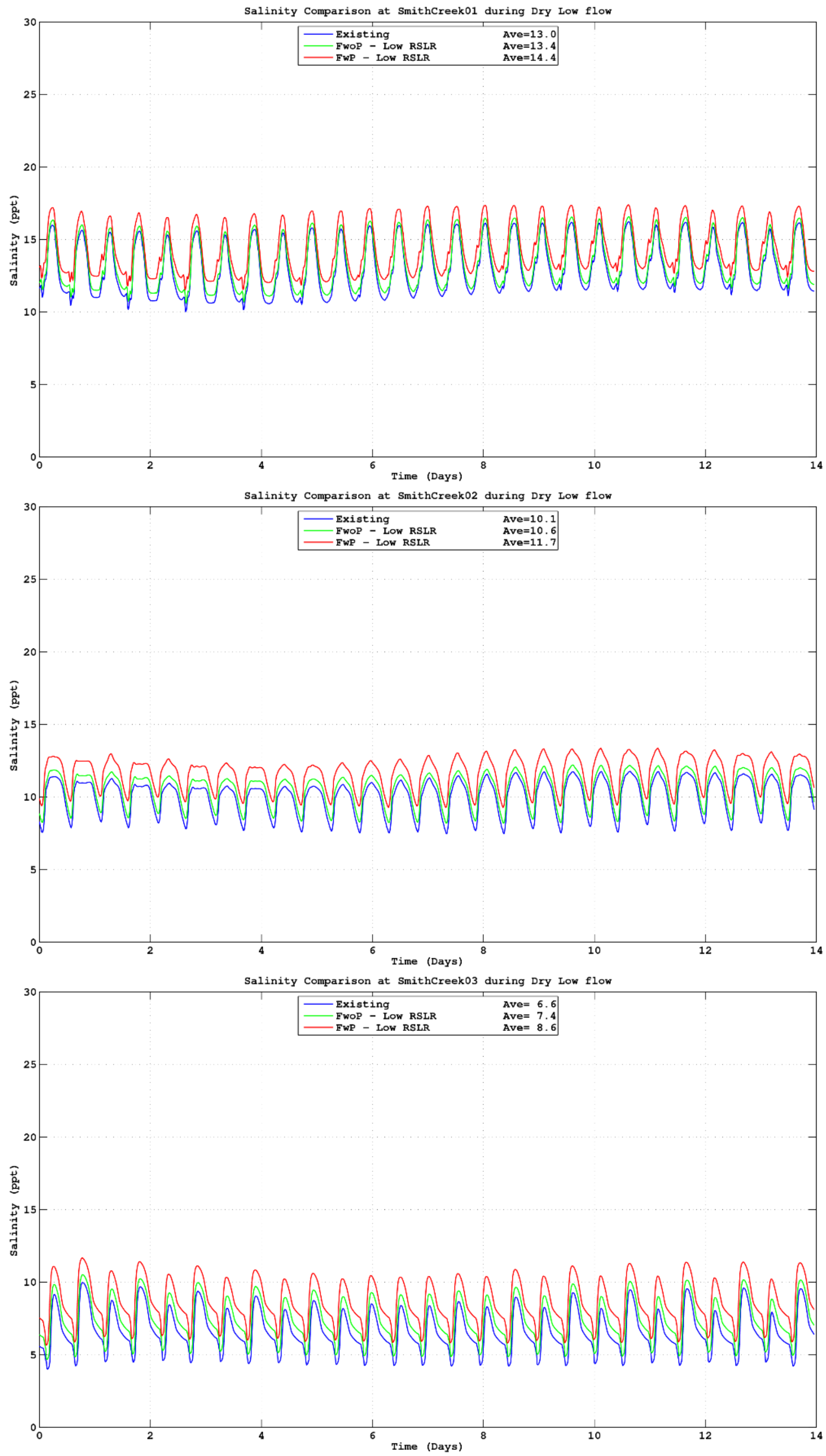

Figure 6-37: Surface salinity along Smith Creek during Dry Low flow

6.2.7. Greenfield Creek

Figure 6-38 to Figure 6-42 present the surface salinity results at Greenfield Creek under each flow condition. Table 6-9 summarizes the average salinity results at Greenfield Creek. Salinity level increases caused by the Project are less than 1.5 ppt.

Table 6-9: Average surface salinities at Greenfield Creek

Flow Conditions	Existing	Low RSLR			Intermediate RSLR			High RSLR		
		FwoP	FwP	Δ	FwoP	FwP	Δ	FwoP	FwP	Δ
Typical High	0.1	0.1	0.5	0.4	0.2	0.8	0.6	1.1	2.1	1.0
Typical Medium	1.1	1.3	2.2	0.9	1.7	2.7	1.0	3.8	4.9	1.1
Typical Low/Dry High	3.6	4.0	5.2	1.2	4.6	5.8	1.2	7.2	8.5	1.3
Dry Medium	9.6	10.0	11.0	1.0						
Dry Low	15.1	15.5	16.2	0.7						

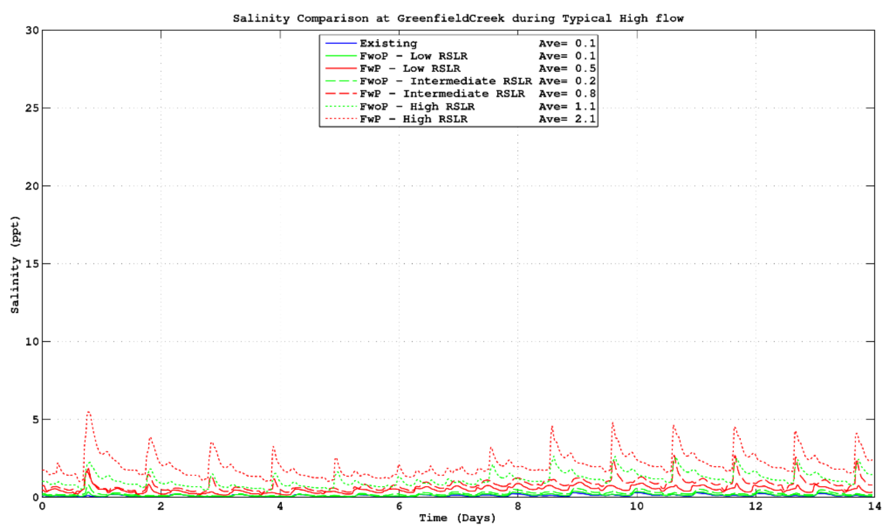

Figure 6-38: Surface salinity at Greenfield Creek during Typical High flow

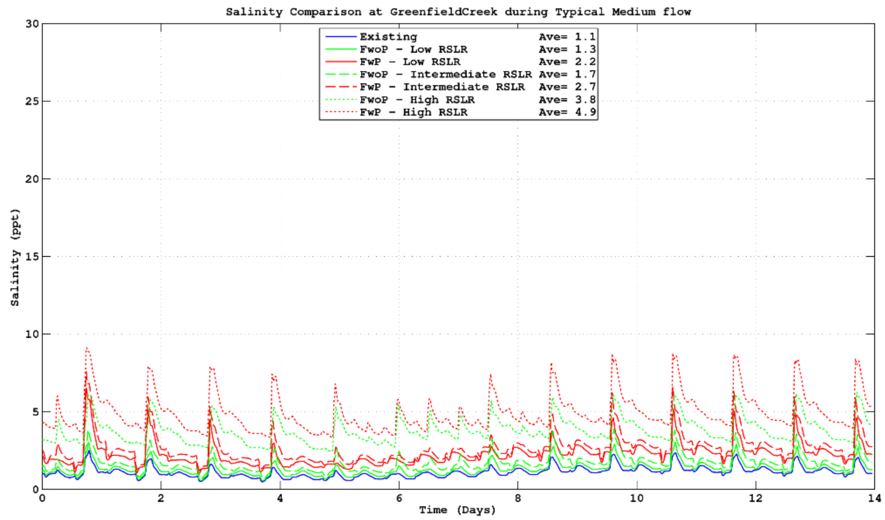

Figure 6-39: Surface salinity at Greenfield Creek during Typical Medium flow

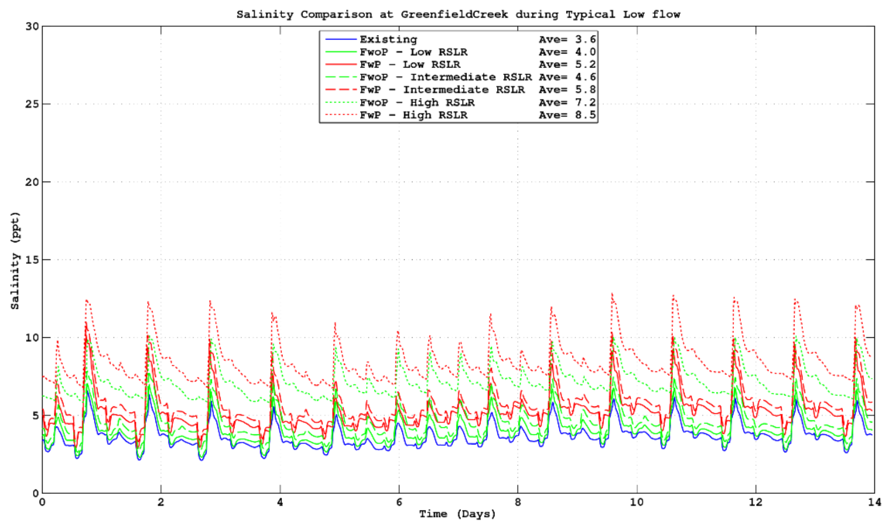

Figure 6-40: Surface salinity at Greenfield Creek during Typical Low (Dry High) flow

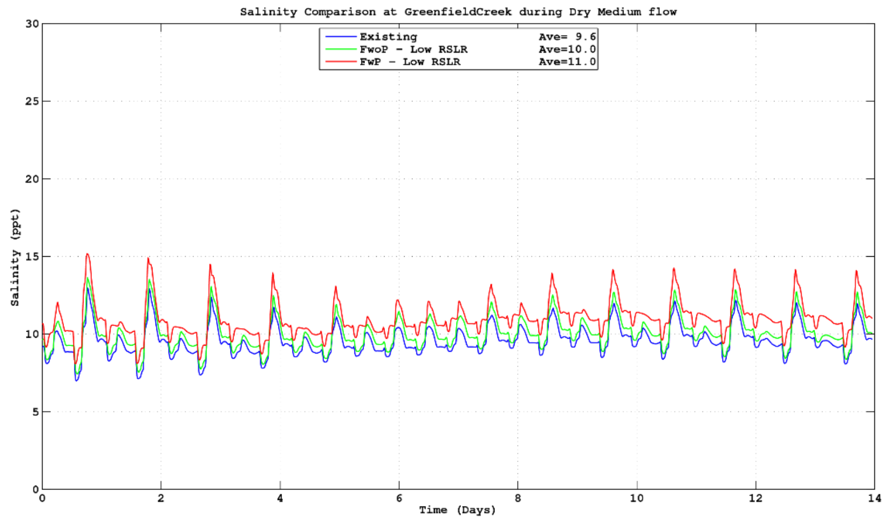

Figure 6-41: Surface salinity at Greenfield Creek during Dry Medium flow

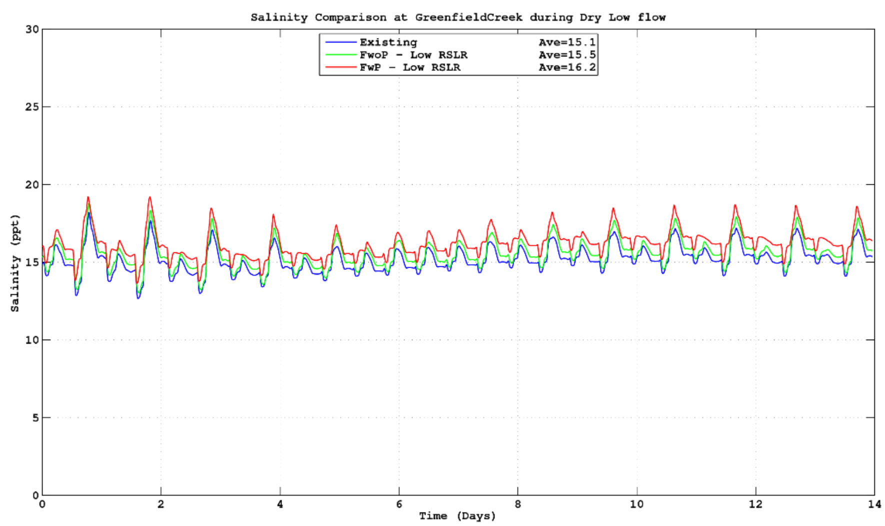

Figure 6-42: Surface salinity at Greenfield Creek during Dry Low flow

6.3. Conclusion

The impact of deepening the channel on salinity level changes in tidal creeks has been evaluated through the use of a local Delft3D model. The boundary and initial conditions for the local model runs were derived from the model results from the full model runs.

The salinity levels in the tidal creeks in many cases are highly sensitive to decreased freshwater flow inputs and higher future sea level rise. However, the potential impacts due to the proposed Project are generally less than 1.5 ppt in the tidal creeks under both Typical year and Dry year flow conditions except for a couple of Dry year Low flow conditions.

Depending on the potential sea level rise magnitude, the absolute change in salinity could be significant for both FWOP and FWP. Thus a shift in the vegetation type could occur irrespective of the project.

7. Shoreline and Inlet Numerical Modeling Development

7.1. Offshore Waves

Nearshore wave data are essential for the study of any potential impacts of the Cape Fear River Deepening Project on inlet morphology and adjacent beach shoreline changes. Although there are some measured wave data available in the nearshore region of the project area (Figure 7-1), they are not sufficient for the study's purpose. A numerical wave model was thus developed to simulate the wave transformation from deep water offshore to the shoreline. The WAVE module from the state-of-art numerical modeling suite Delft3D, is applied in this study. The model development and calibration/validation are described in detail in the following sections.

7.1.1. Model Development

7.1.1.1. Model Domains

Wave transformation from deep water to the shoreline was accomplished by nesting three increasingly resolved model domains within the WAVE model. The computational grids are shown in Figure 7-1.

The coarsest grid (gray) is comprised of 40,660 cells with size ranging from 500 m to 1000 m alongshore and 500 m cross shore. The offshore limits of the coarse grid correspond with the location of NOAA wave buoy 41013 from which offshore wave conditions were derived and the grid is extended 46 and 60 nautical miles east and west of the Cape Fear River entrance. The intention of the east and west grid extension is to eliminate the lateral boundary shadowing effects of the wave model.

The medium-resolved wave domain (blue) is comprised of 37,400 cells with resolution ranging from 125 m to 250 m alongshore and 250 m cross-shore.

The fine wave grid (red) is comprised of 110,773 cells with resolution of 50 m both alongshore and cross-shore. The fine wave grid is designed to be approximately parallel to the general shoreline orientation of Oak Island and Bald Head Island in the alongshore direction.

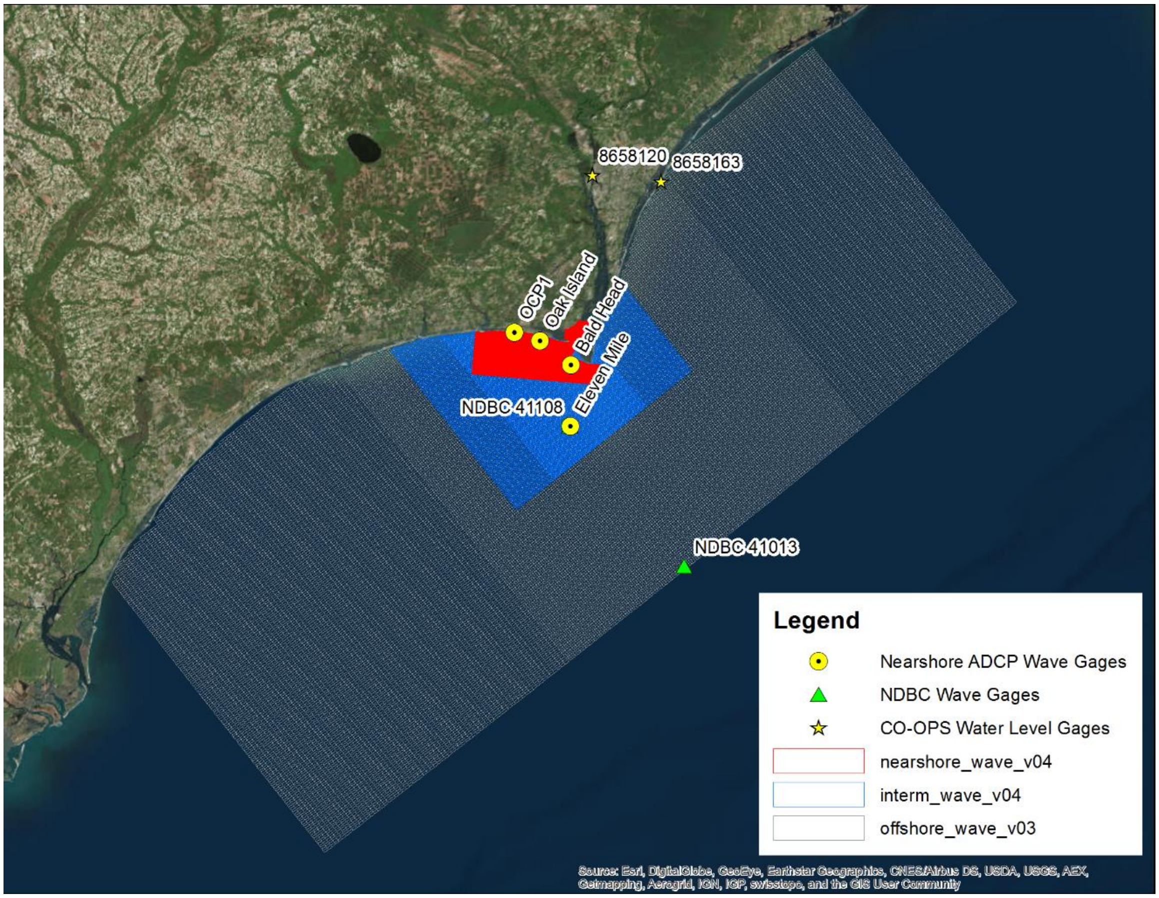

Figure 7-1: Wave model grids and wave gage locations

7.1.1.2. Model Bathymetry

Bathymetric data from different sources were compiled and processed to cover the entire computational domain. All bathymetric datasets were adjusted to the North American Vertical Datum of 1988 (NAVD88). The data sources used for the wave model bathymetry developments are listed in Table 7-1 from high priority to low priority. Most recent bathymetry data were selected where available to construct the model bathymetry. Figure 7-2 presents the input bathymetry used in the coarse model domain; while the same bathymetry is reflected at higher resolution in the fine wave grid as shown in Figure 7-3.

Table 7-1: Wave model bathymetry data sources

Data Set	Source
Wilmington Harbor hydrographic surveys	USACE 2016 – 2017
Fugro channel bank surveys	Fugro 2016 – 2017
Oak Island post Matthew beach profile surveys (STA 210+00 – 700+00)	TI Coastal 2016
Bald Head Island beach profile surveys (STA 000+00 – 238+00)	USACE 2013
Oak Island beach profile surveys (STA 005+00 – 210+00)	USACE 2012
Cape Fear River 2010 surveys	USACE 2010
NOAA hydrographic surveys	NOAA 1973 – 2007
NOAA Navigation Charts	MIKE C-MAP
ADCIRC bathymetry	NCDPS 2011
NC LiDAR	NOAA 2014 – 2016

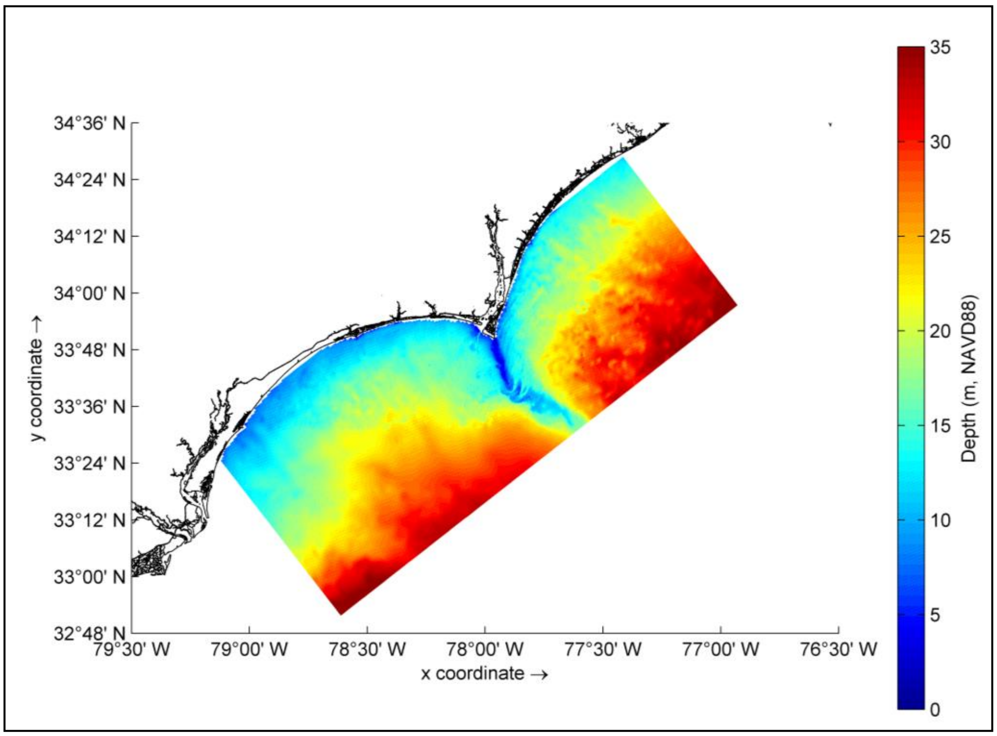

Figure 7-2: Coarse wave grid bathymetry

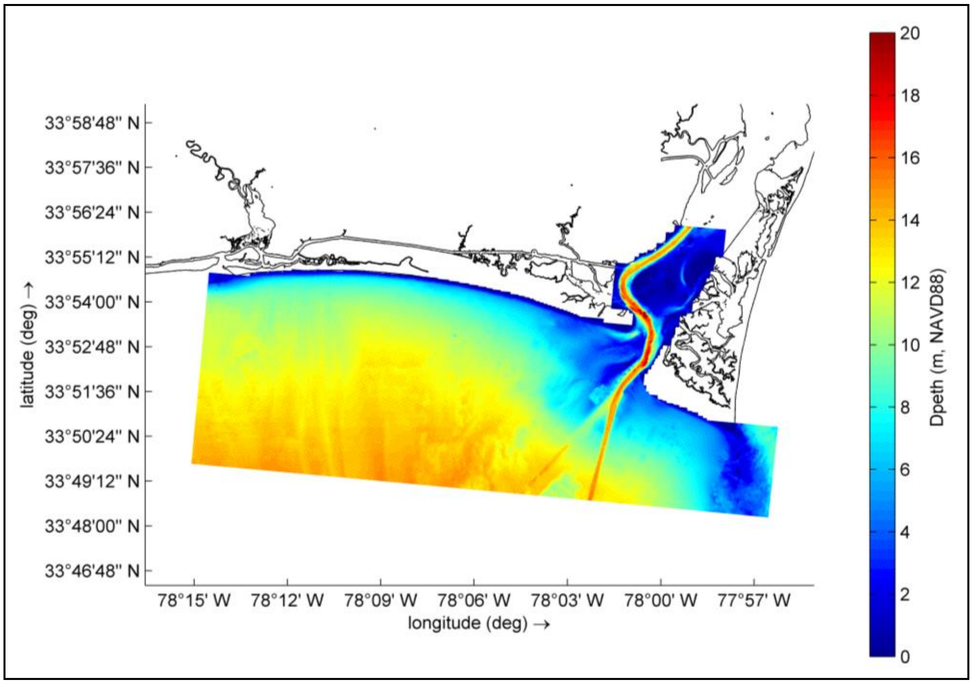

Figure 7-3: Fine wave grid bathymetry

7.1.2. Model Calibration

7.1.2.1. Wave Data

There are five stations (as shown in Figure 7-1) with measured wave data available inside the wave model domains: one NOAA NDBC buoy – 41108; three USACE Acoustic Doppler Current Profiler (ADCP) gages – Eleven Mile, Bald Head and Oak Island; and one Coastal Ocean Research and Monitoring Program (CORMP) ADCP gage – OCP1 (Ocean Crest Pier, NC). Table 7-2 presents general information about these stations. The NOAA buoy 41108 is at the same location as the USACE Eleven Mile ADCP. The following bulk wave parameters are reported at both the NOAA buoys and the USACE ADCPs: significant wave height, peak and average wave periods, and peak wave direction. At the CORMP ADCP, the same bulk wave parameters except average wave period are reported. In addition, the directional wave spectra are also reported at the USACE ADCPs and NOAA buoy 41013.

Table 7-2: Information of offshore and nearshore wave measuring stations

Source	Station	Start Date	End Date	Frequency
NDBC	41108	02/2013	07/2017 (active)	30 min
NDBC	41013	11/2003	07/2017 (active)	1 hr
USACE	Eleven Mile	09/2000	05/2010	3 hr
USACE	Oak Island	09/2000	05/2010	1 hr
USACE	Bald Head	09/2000	01/2010	3 hr
CORMP	OCP1	05/2006	06/2013	1 hr

7.1.2.2. Model Calibration Setup

For the wave transformation modeling, in addition to the offshore wave data as the boundary conditions, wind and water level inputs are also important especially during storm events. Based on the contiguous data available at all wave stations along with overlapping wind and water level data, the period of August 1st, 2008 to October 1st, 2008 was selected for the wave model calibration purpose. Large waves generated by Hurricane Hanna were included in this period; thus, the wave model's ability to replicate both large and normal waves can be verified.

7.1.2.3. Offshore wave boundary conditions

There are three open boundaries for the coarse wave model. The directional wave spectra from NOAA buoy 41013 were applied as spatially uniform wave conditions at all three boundaries. The wave spectra were calculated based on the spectral wave density, alpha1, alpha2, r1 and r2 data using the extended maximum likelihood method. The description of variables can be found in the NDBC website www.ndbc.noaa.gov/measdes.shtml, with the conversion method following Earle et al. (1999) and Benoit et al. (1997). Figure 7-4 shows the offshore bulk wave parameters for the calibration period. The maximum wave height of 8.4 m was observed on September 6th, 2008 during Hurricane Hanna.

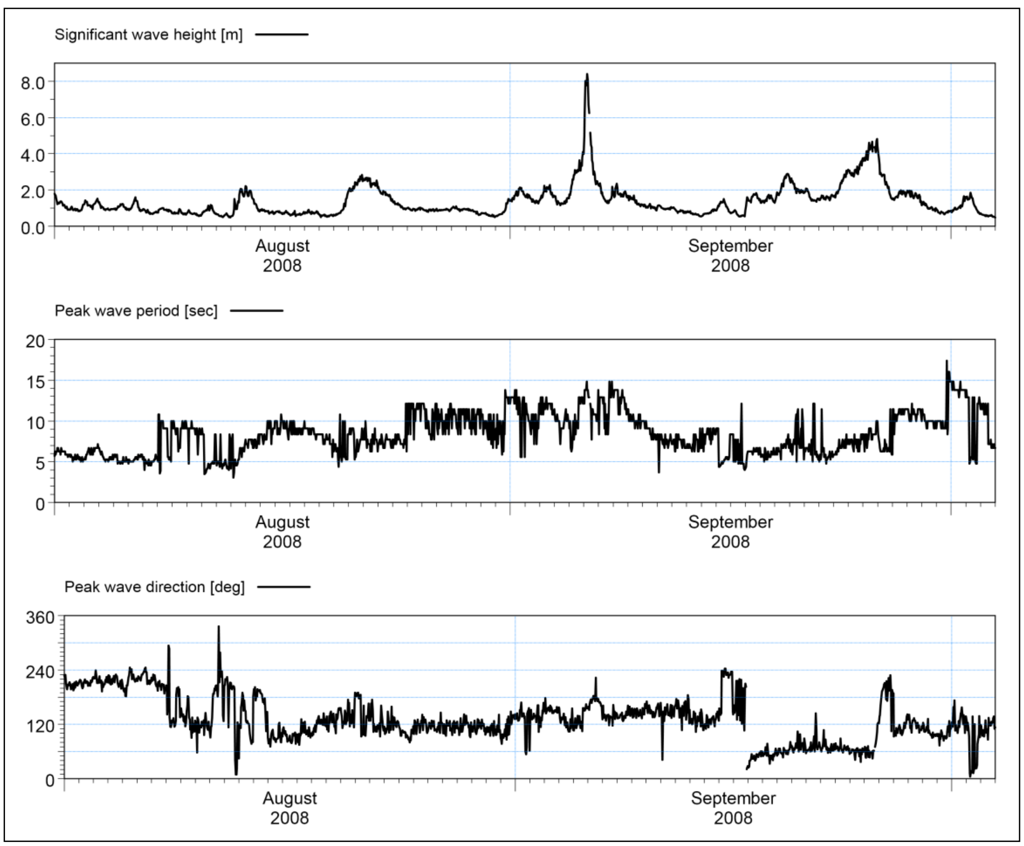

Figure 7-4: Wave data from NOAA Buoy 41013 during model calibration period

7.1.2.4. Winds

The spatially varying wind data from the National Centers for Environmental Prediction (NCEP) Climate Forecast System Reanalysis (CFSR) were applied for the model calibration period. The CFSR wind data interval is 3 hours. Figure 7-5 shows wind data comparison between NDBC and CFSR at buoy 41013.

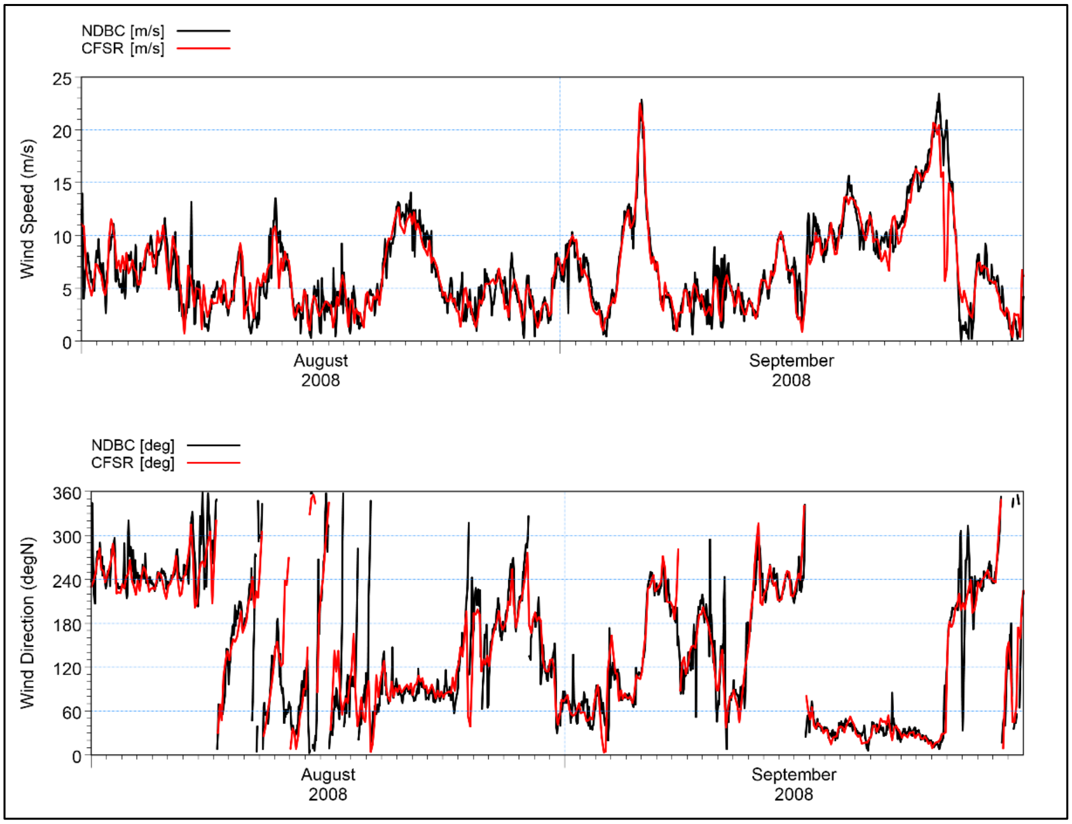

Figure 7-5: Wind data at NDBC buoy 41013 and from CFSR

7.1.2.5. Water Levels

A spatially uniform water level field was used for the model calibration. Due to the lack of available measured water level data within the model domain, the data from nearby NOAA Station 8658163 at Wrightsville Beach, NC (as shown in Figure 7-1) were used for the model calibration. Figure 7-6 presents the water level data. However, it is important to point out that Hurricane Hanna made landfall at the NC/SC border, so the surge was much greater on Oak Island/Bald Head than at Wrightsville Beach. The reported storm surge was about 5 ft at Wilmington, NC, and about 4 ft at Myrtle Beach, SC, the back side of the storm. Thus, using the measured water level data at Wrightsville Beach could adversely affect the modeled waves during Hanna. Nonetheless, it’s the closest available open coast water level station for the study area and thus used for the wave model calibration without any adjustment.

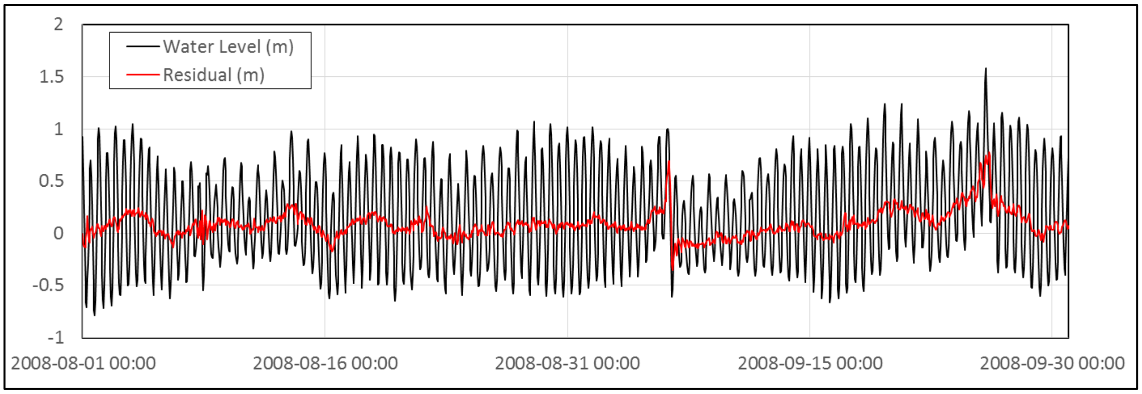

Figure 7-6: Water level data from NOAA station 8658163 for model calibration

7.1.2.6. Model parameters

Calibration of the wave model was an iterative process whereby model parameters were changed following each run until the best possible agreement between measured and predicted waves was achieved. Table 7-3 shows the parameters applied to the WAVE model.

Table 7-3: Parameters of Delft3D-WAVE

Parameter	Value	Description
GenModePhys	3	third-generation physics
Breaking	true	include wave breaking
BreakAlpha	1	alpha coefficient for wave breaking
BreakGamma	0.73	gamma coefficient for wave breaking
Triads	false	include triads
WaveSetup	false	include wave setup
BedFriction	jonswap	bed friction type
BedFricCoef	0.067	bed friction coefficient
Diffraction	false	include diffraction
WindGrowth	true	include wind growth
WhiteCapping	Komen	white capping method
Quadruplets	true	include quadruplets
Refraction	true	include refraction
FreqShift	true	include frequency shifting
WaveForces	dissipation 3d	method of wave force computation

7.1.3. Model Calibration Results

Figure 7-7 to Figure 7-9 present the direct comparison between the computed and measured time series of significant wave height, peak wave period and peak wave direction, respectively, at the gage locations of Eleven Mile ADCP, Bald Head ADCP, Oak Island ADCP and OCP1. Figure 7-10 shows the scatter plots of the measured and computed significant wave heights and includes a linear trend line fit through the data at each of the four calibration stations. Based on the model bathymetry, the OCP1 ADCP location is at a water depth of 5 m which is close to the wave breaking zone. Because the wave heights during the peak of the storms were greatly under predicted, it is suspected that the depth at the ADCP location was not correct (possibly due to the surge being higher) and therefore the model output point for the OCP1 ADCP was moved offshore to a deeper area of 7 m water depth.

Several goodness-of-fit statistics were used to help assess the model calibration and validation results. These include mean absolute error (*MAE*), root mean square (*RMS*) error, normalized *RMS* error, correlation coefficient (*R*), and index of agreement (*d*). These parameters are briefly described here and can also be found on the USACE's Coastal Inlets Research Program (CIRP) wiki page https://cirpwiki.info/wiki/Statistics.

Let x and y represent the measured and calculated data respectively. Then the following statistics can be calculated:

Mean absolute error (*MAE*):

$$MAE = \overline{|x - y|} \tag{19}$$

where "bar" denotes the sample mean.

Root-mean-squared (*RMS*) error:

$$\varepsilon_{RMS} = \sqrt{\overline{(x - y)^2}} \tag{20}$$

To reduce an effect of measurement error and possible outliers, a one hour low-pass filter is applied to the measured data and a trend x_f is determined. Then a normalized error (*RMSN*) is calculated as:

$$\varepsilon_{norm} = \frac{\varepsilon_{RMS}}{x_{f,\max} - x_{f,\min}} \cdot 100\% \tag{21}$$

where $x_{f,\max}$ and $x_{f,\min}$ are the maximum and minimum values of the trend x_f.

Correlation coefficient R is calculated using the standard method and represents a non-squared value.

Model prediction capability is estimated with an index of agreement between measured and calculated data as (Willmott et al., 1985):

$$d = 1 - \frac{\overline{(x-y)^2}}{\overline{\left(|x-\bar{x}| - |y-\bar{x}|\right)^2}}, \ 0 \le d \le 1 \tag{22}$$

The calculated goodness-of-fit parameters for the wave calibration results are listed in Table 7-4 to Table 7-6 for the significant wave height, peak wave period and peak wave direction, respectively.

Table 7-4: Goodness-of-fit parameters for significant wave height calibration

Station	***MAE* (m)**	***RMS* (m)**	***RMSN* (%)**	***R***	***d***
Eleven Mile ADCP	0.14	0.19	4.3	0.96	0.97
Bald Head Island ADCP	0.11	0.15	5.3	0.91	0.95
Oak Island ADCP	0.10	0.13	4.6	0.92	0.96
OCP1 ADCP	0.08	0.11	3.5	0.94	0.97

Table 7-5: Goodness-of-fit parameters for peak wave period calibration

Station	***MAE* (s)**	***RMS* (s)**	***R***	***d***
Eleven Mile ADCP	1.3	2.0	0.74	0.86
Bald Head Island ADCP	1.4	2.4	0.65	0.81
Oak Island ADCP	1.4	2.3	0.64	0.81
OCP1 ADCP	1.4	2.2	0.71	0.85

Table 7-6: Goodness-of-fit parameters for peak wave direction calibration

Station	***MAE* (deg)**	***RMS* (deg)**
Eleven Mile ADCP	33	46
Bald Head Island ADCP	32	56
Oak Island ADCP	15	23
OCP1 ADCP	15	22

The results suggest that:

- For the significant wave heights, the model predictions agree very well with the measured data at all four ADCP locations, with *MAE* and *RMS* errors less than 0.2 m, and *R* and *d* values greater than 0.9.

- For the peak wave periods, the *MAE* and *RMS* errors are less than 2.5 s, and *R* and *d* values around 0.7 and 0.8, respectively. The data indicates there are periods when at least two wave systems exist—long period waves from offshore and locally generated waves from onshore. In the presence of the two systems, determination of peak period may not be consistent and may alternate between two values. This negatively affects the statistics.

- For the peak wave directions, the model predictions have large deviations from the measured values. It is more pronounced at the Bald Head Island ADCP during period of September 17–26, when the reported ADCP peak wave directions are from between 90 and 180°N, whereas most of the modeled values are from between 330 and 360°N. The model predicted and measured directional wave spectra were checked for further investigation. Figure 7-11 presents the measured Bald Head ADCP wave energy spectrum at 1:00 am EST on September 24, 2008. Figure 7-12 shows the modeled wave action density spectrum at the same time. Two wave systems are evident from both the measured and the model predicted spectra: waves coming from SSE–SSW (offshore) with the frequency of around 0.1 Hz; and waves coming from NNW–N (locally wind-generated) with the frequency of around 0.4 Hz. The measured spectrum has some noise at higher frequencies beyond 0.8 Hz. It appears that the peak wave direction from the measured spectrum was calculated to be from offshore; whereas the peak wave direction from the modeled spectrum was calculated to be from onshore. This supports the fact that two or more wave systems can exist at the same time and one can dominate the wave field. The result is the large peak wave direction differences between the measurement and the model prediction. Per communication with USACE personnel[2] who is familiar with the handling of ADCP data, an upper cutoff frequency was used when post-processing the raw ADCP data to the bulk wave parameters. The cutoff frequency was the lesser of the two: when the wavelength is less than two times of the beam separation; or when the pressure response correction for amplitude is 0.1.

[2] Personal communication with Kent Hathaway from the USACE.

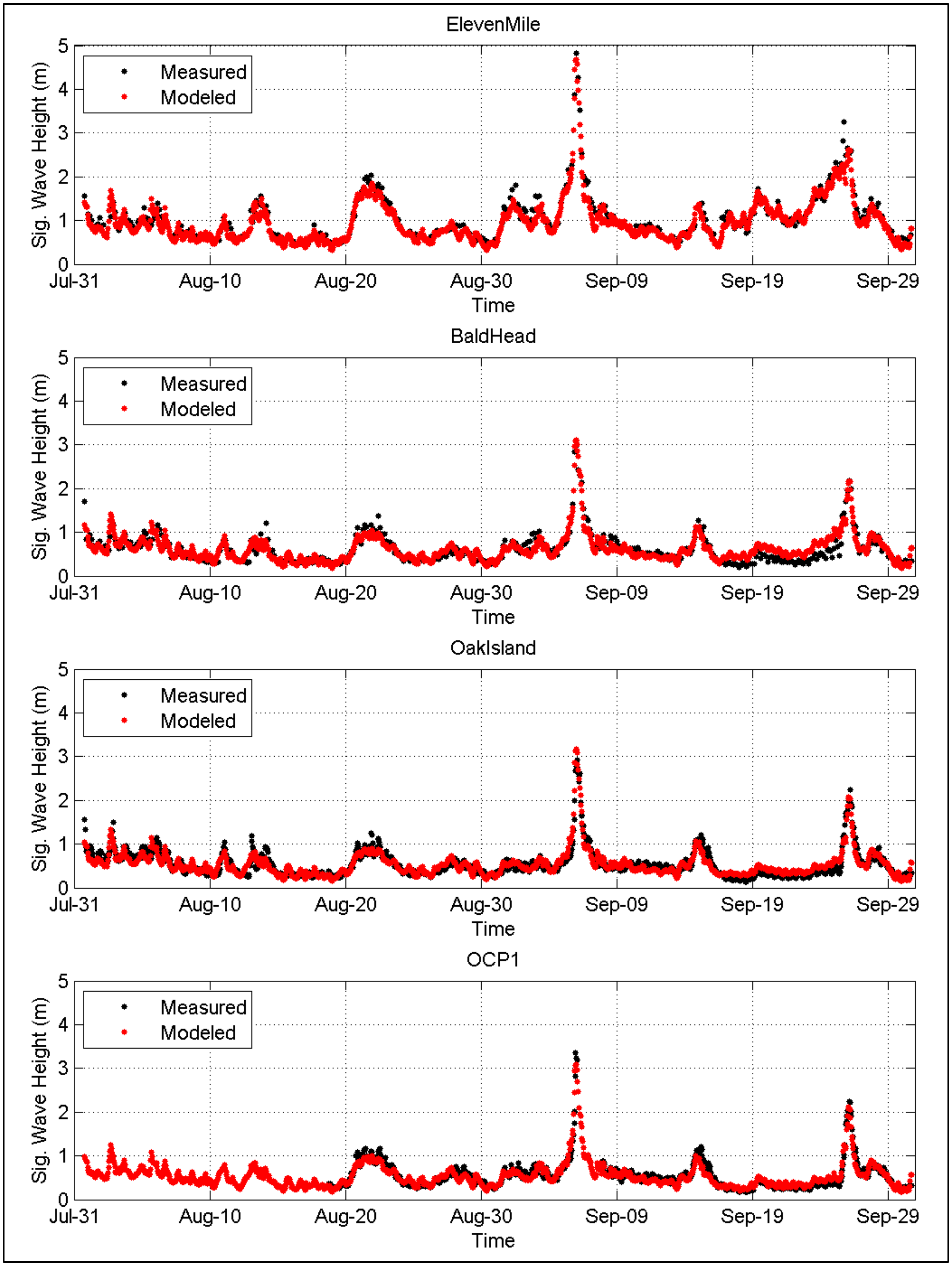

Figure 7-7: Comparison of measured and computed significant wave heights from offshore to nearshore for the calibration period

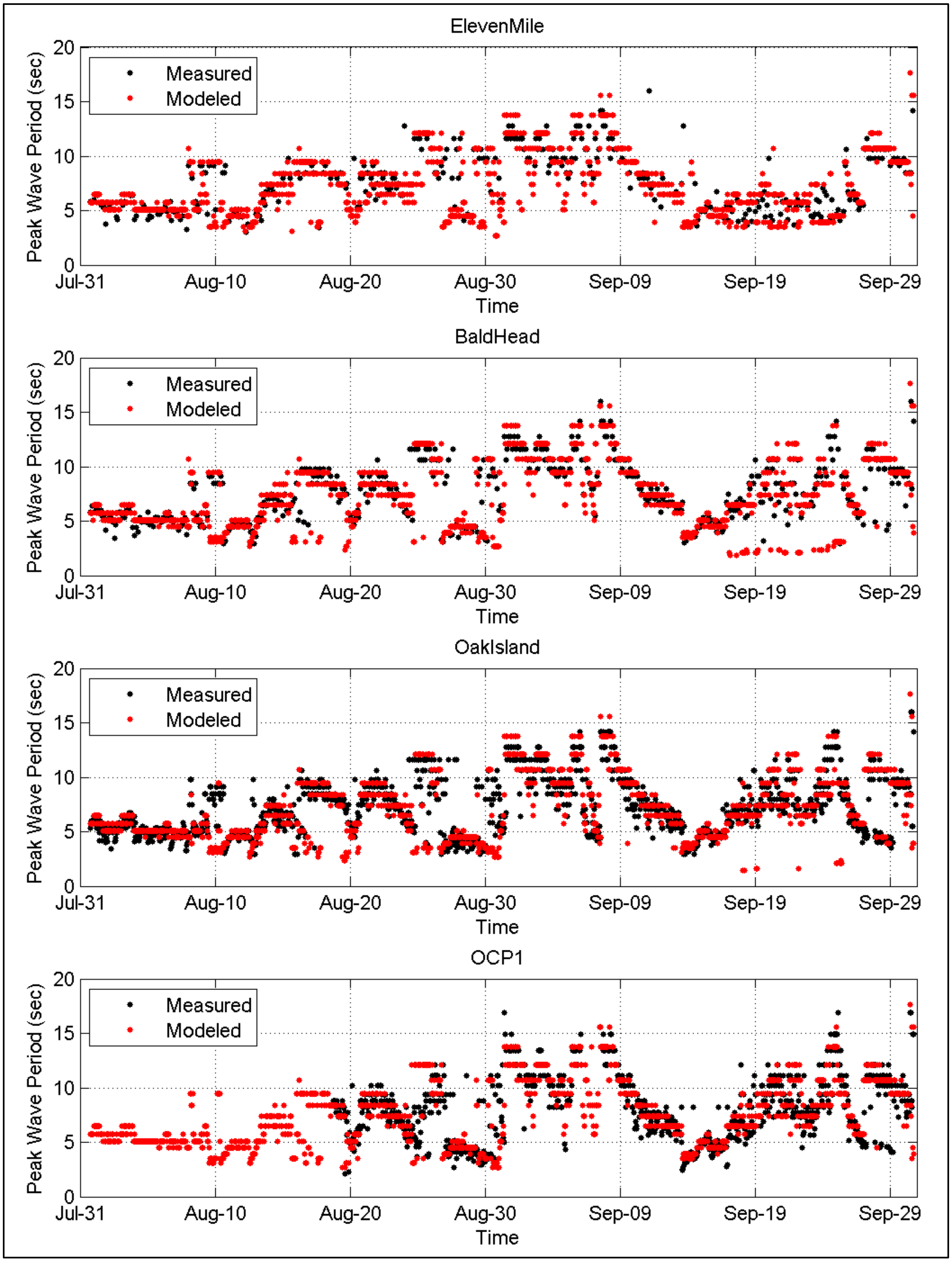

Figure 7-8: Comparison of measured and computed peak wave periods from offshore to nearshore for the calibration period

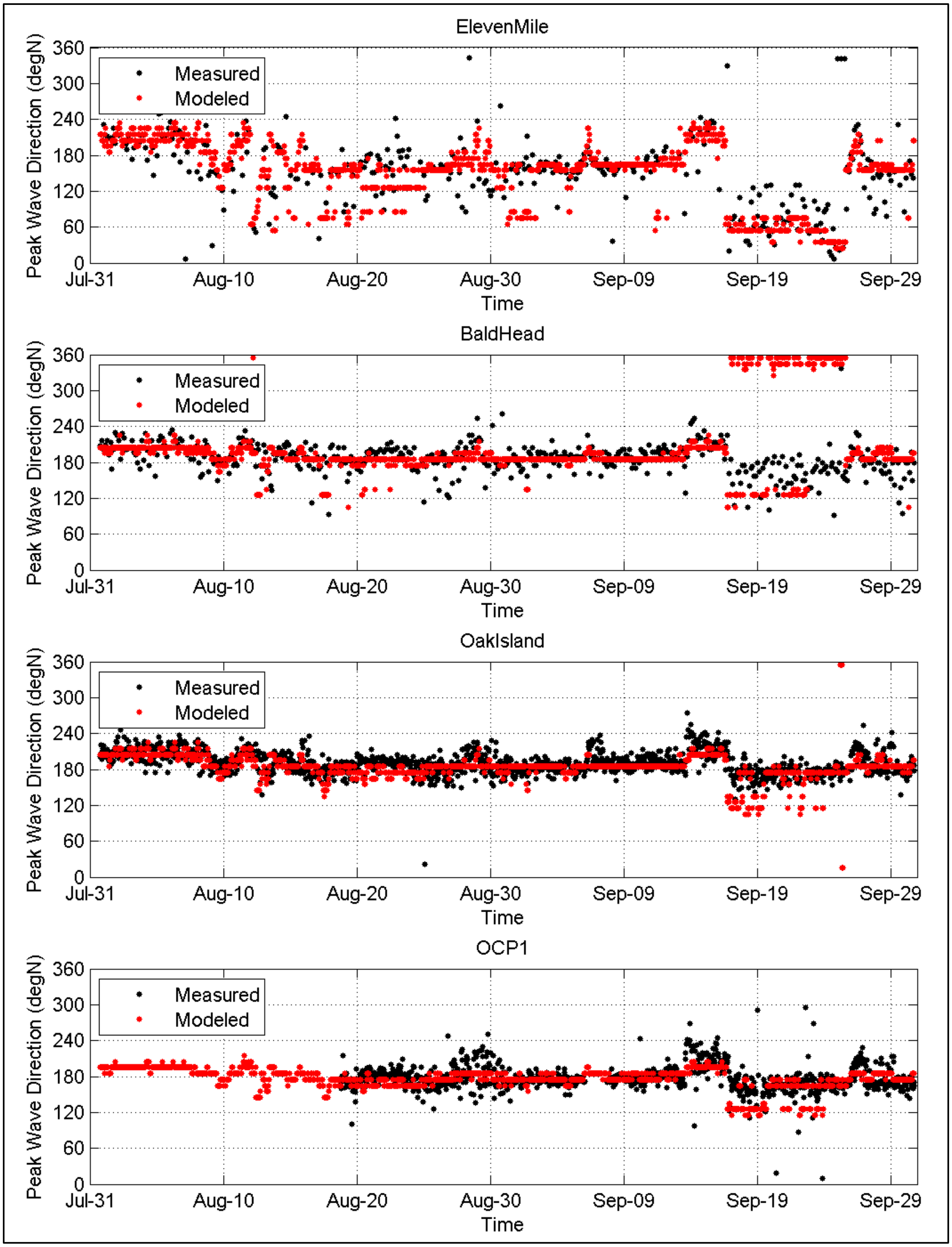

Figure 7-9: Comparison of measured and computed peak wave directions from offshore to nearshore for the calibration period

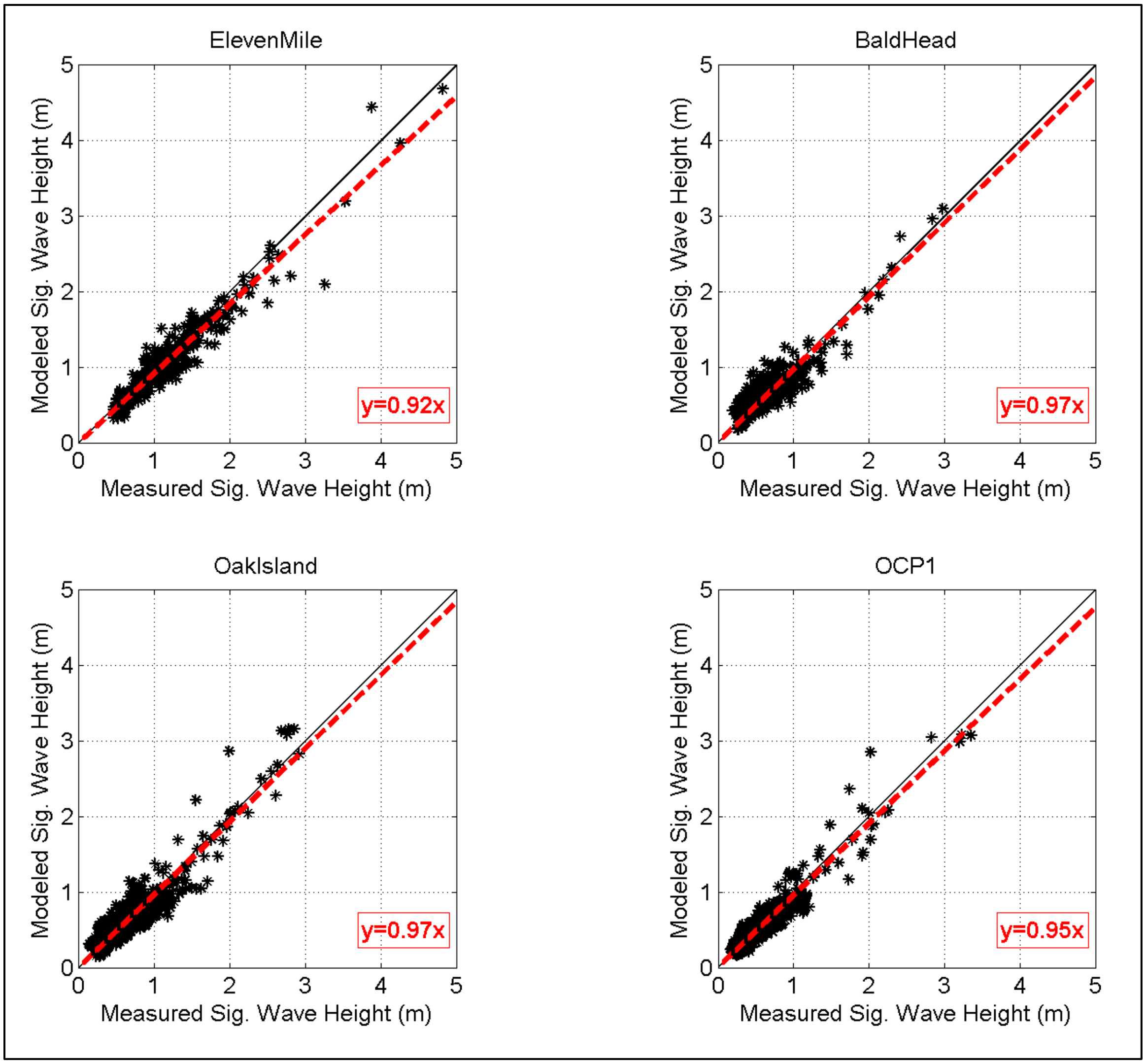

Figure 7-10: Scatter plot of computed and measured significant wave heights from offshore to nearshore for the calibration period

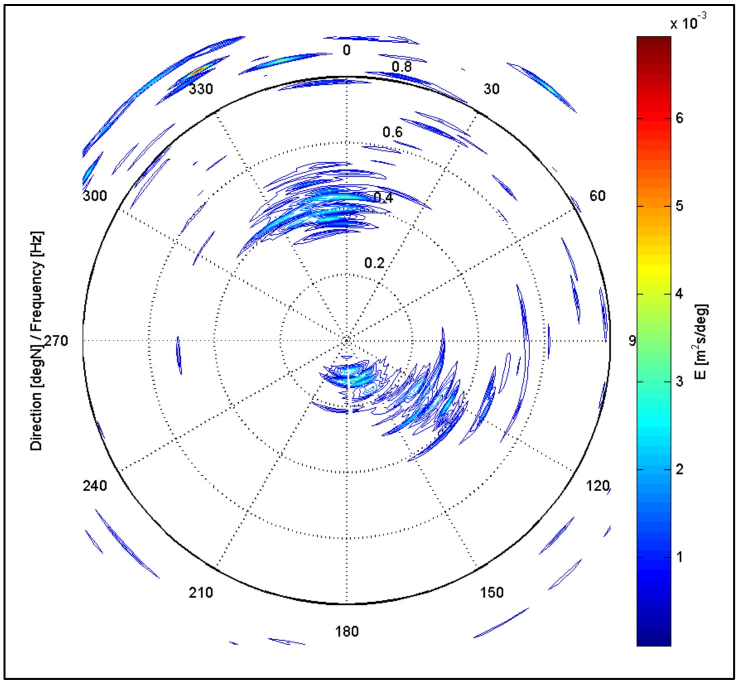

Figure 7-11: Bald Head ADCP measured wave energy spectrum at 1:00 am EST on September 24, 2008

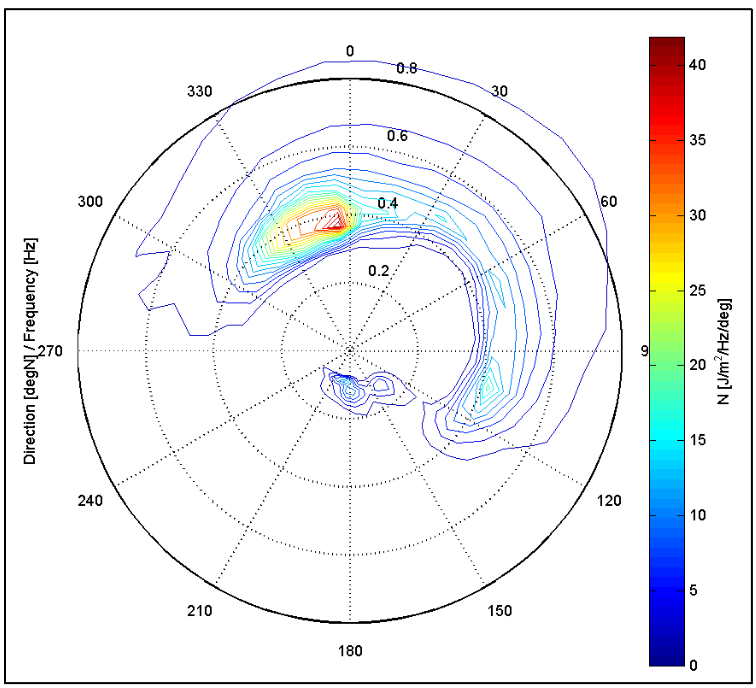

Figure 7-12: Bald Head ADCP modeled wave action density spectrum at 1:00 am EST on September 24, 2008

The main purpose of the wave modeling is to provide nearshore wave conditions for investigating potential project effects on longshore sediment transports and shoreline changes. Locally generated waves due to northerly winds do not affect the shoreline and are not important to the project. Therefore, comparisons of just waves from the offshore direction between 110 and 270 degN are further discussed here. The goodness-of-fit parameters are presented in Table 7-7 to Table 7-9 for the significant wave height, peak wave period and peak wave direction, respectively. The statistics for significant wave height and peak wave period are similar to the values in Table 7-4 and Table 7-5. The MAE and RMS errors for peak wave direction are smaller than values in Table 7-6, especially at the Eleven Mile ADCP and Bald Head Island ADCP locations. Figure 7-13 to Figure 7-15 show the time series plots.

Table 7-7: Goodness-of-fit parameters for significant wave height calibration for waves coming from 110 – 270 degN

Station	*MAE* (m)	*RMS* (m)	*RMSN* (%)	*R*	*d*
Eleven Mile ADCP	0.15	0.20	4.6	0.96	0.97
Bald Head Island ADCP	0.10	0.13	4.7	0.94	0.96
Oak Island ADCP	0.10	0.13	4.5	0.92	0.96
OCP1 ADCP	0.08	0.11	3.6	0.94	0.97

Table 7-8: Goodness-of-fit parameters for peak wave period calibration for waves coming from 110 – 270 degN

Station	*MAE* (s)	*RMS* (s)	*R*	*d*
Eleven Mile ADCP	1.3	2.1	0.72	0.85
Bald Head Island ADCP	1.2	2.1	0.72	0.85
Oak Island ADCP	1.4	2.3	0.65	0.81
OCP1 ADCP	1.5	2.3	0.69	0.84

Table 7-9: Goodness-of-fit parameters for peak wave direction calibration for waves coming from 110 – 270 degN

Station	*MAE* (deg)	*RMS* (deg)
Eleven Mile ADCP	23	32
Bald Head Island ADCP	17	23
Oak Island ADCP	14	19
OCP1 ADCP	15	20

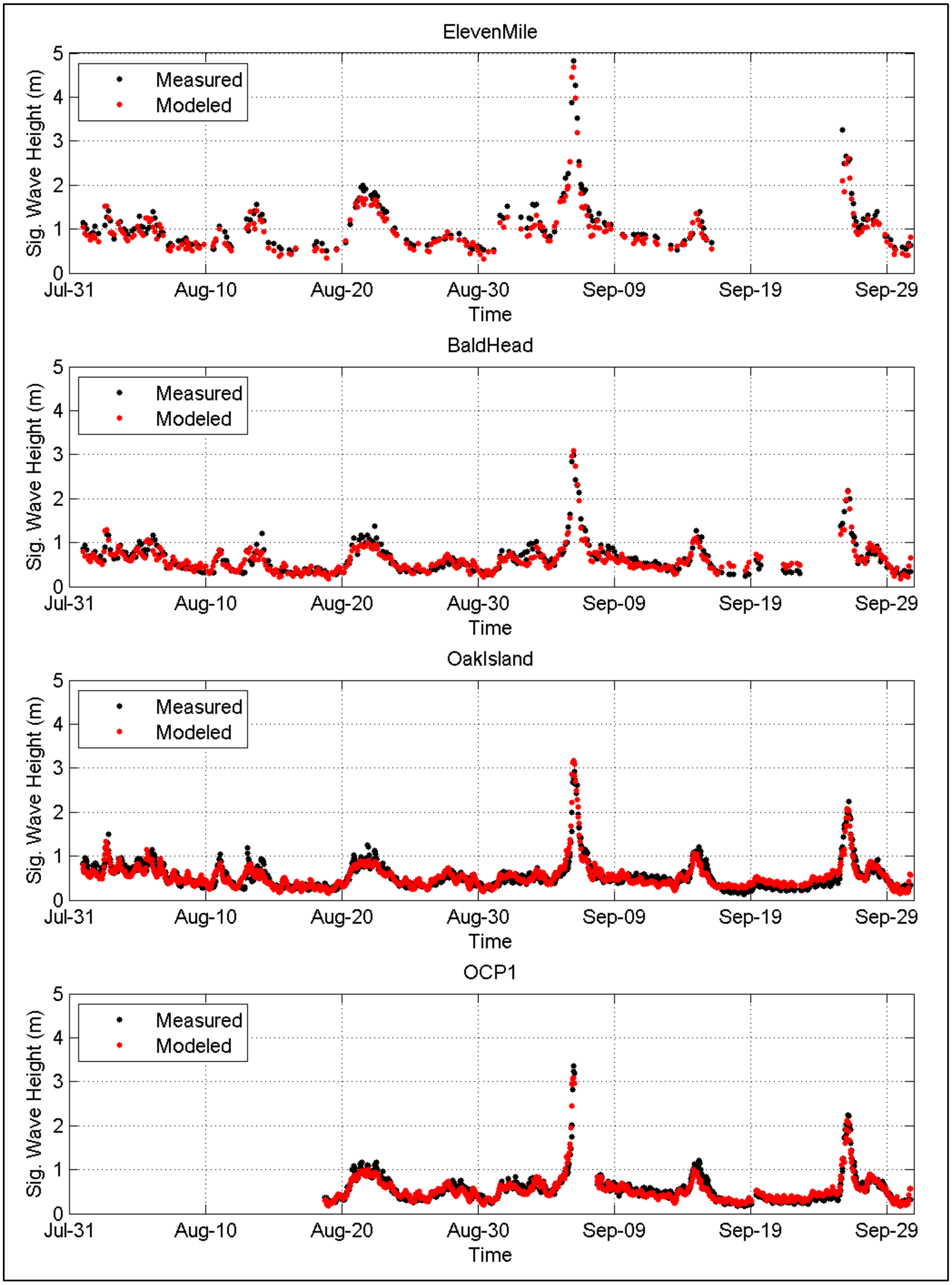

Figure 7-13: Comparison of measured and computed significant wave heights from offshore to nearshore during the calibration period for waves coming from 110 -270 degN

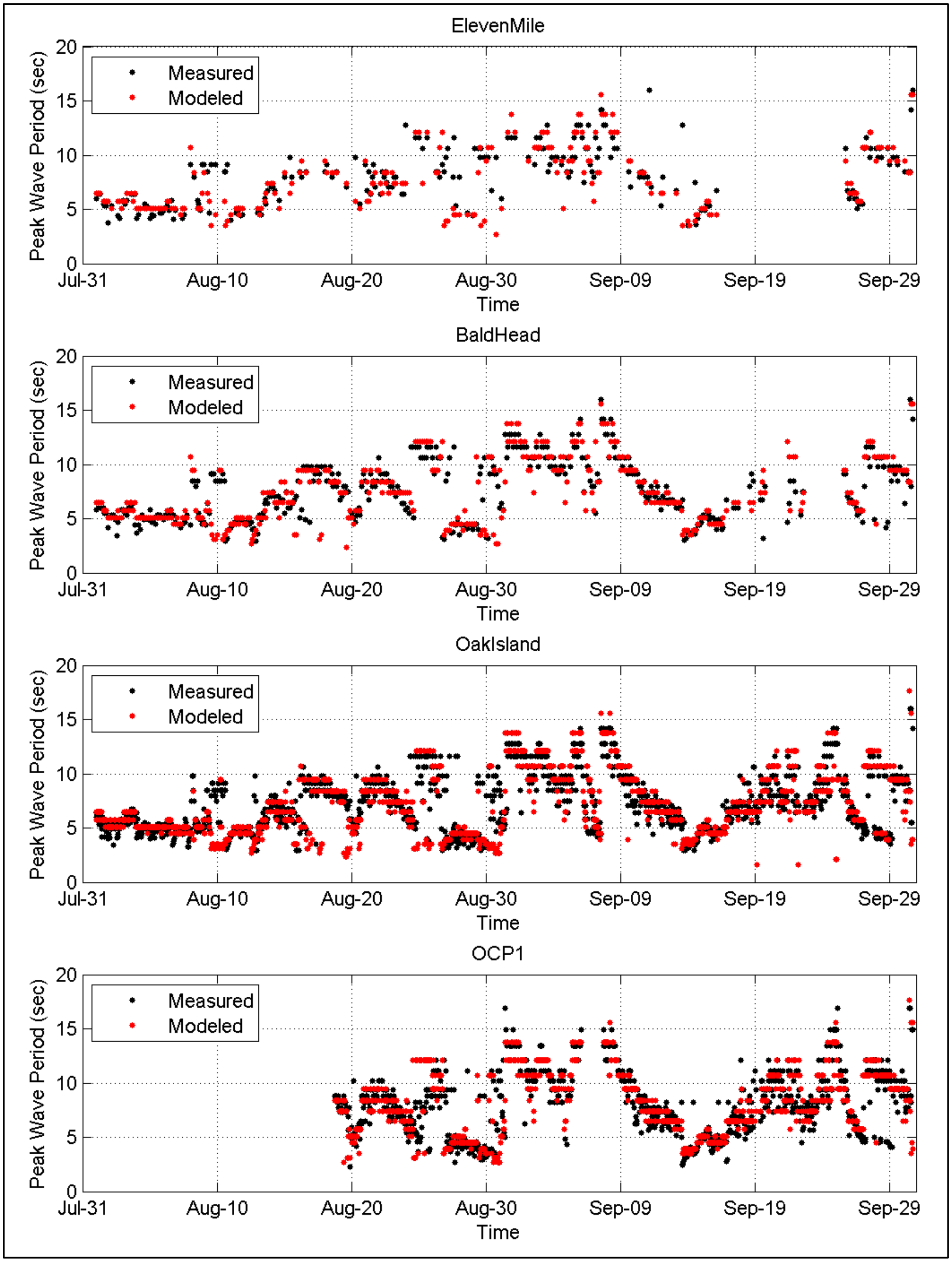

Figure 7-14: Comparison of measured and computed peak wave periods from offshore to nearshore during the calibration period for waves coming from 110 -270 degN

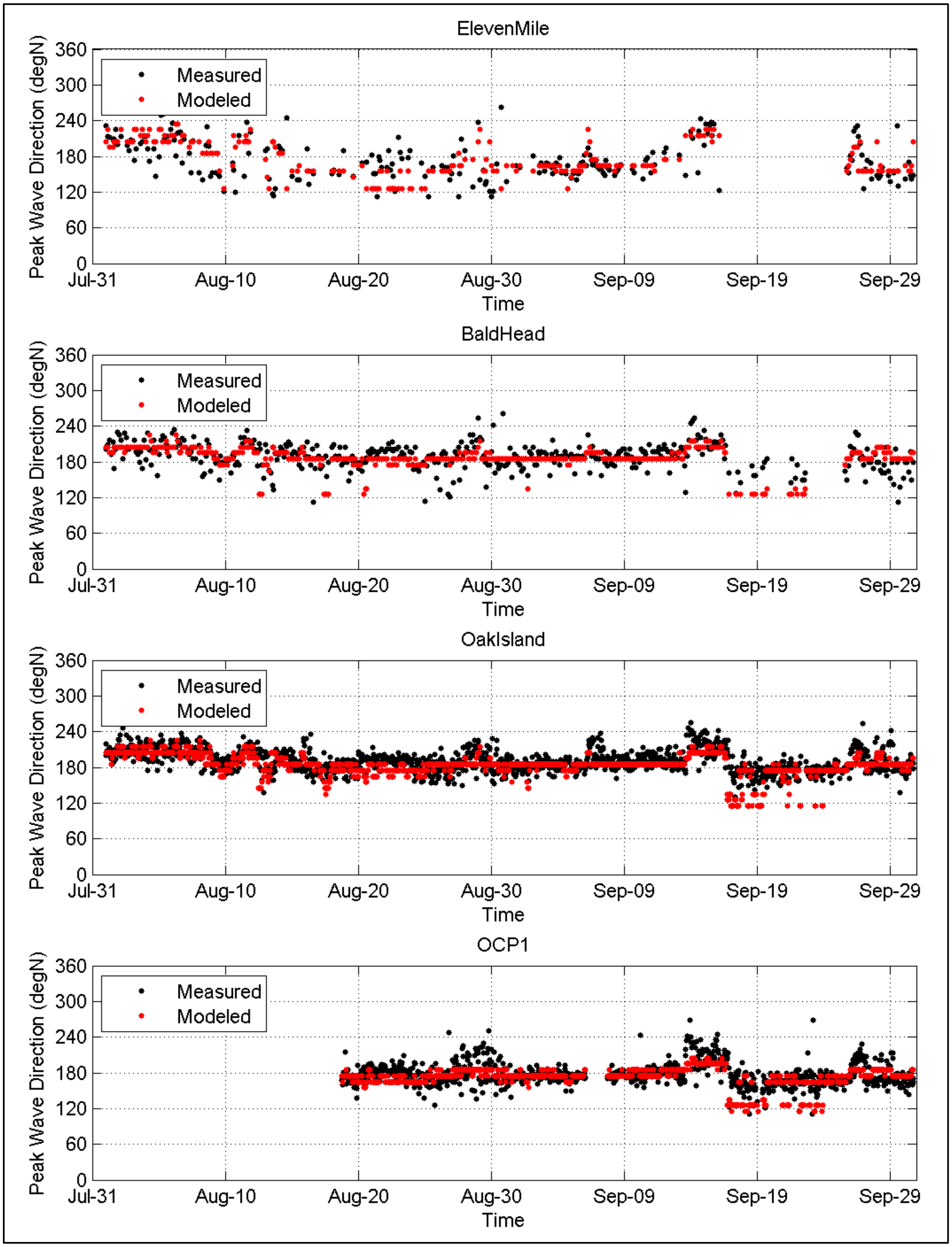

Figure 7-15: Comparison of measured and computed peak wave periods from offshore to nearshore during the calibration period for waves coming from 110 -270 degN

7.1.4. Model Validation

To validate the model parameters used in the wave calibration, another model run was conducted from a different period.

7.1.4.1. Model Validation Setup

Based on the contiguous data availability at all wave stations along with overlapping wind and water level data, the period of July 1, 2009 to December 1, 2009 was selected for the wave model validation purpose.

7.1.4.2. Offshore wave boundary conditions

The directional wave spectra from NOAA buoy 41013 were applied as spatially uniform wave conditions at all three wave boundaries. The wave spectra were calculated based on the spectral wave density, alpha1, alpha2, r1, and r2 data using the extended maximum likelihood method following methodology by Earle et al. (1999) and Benoit et al. (1997). Figure 7-16 shows the offshore bulk wave parameters for the validation period.

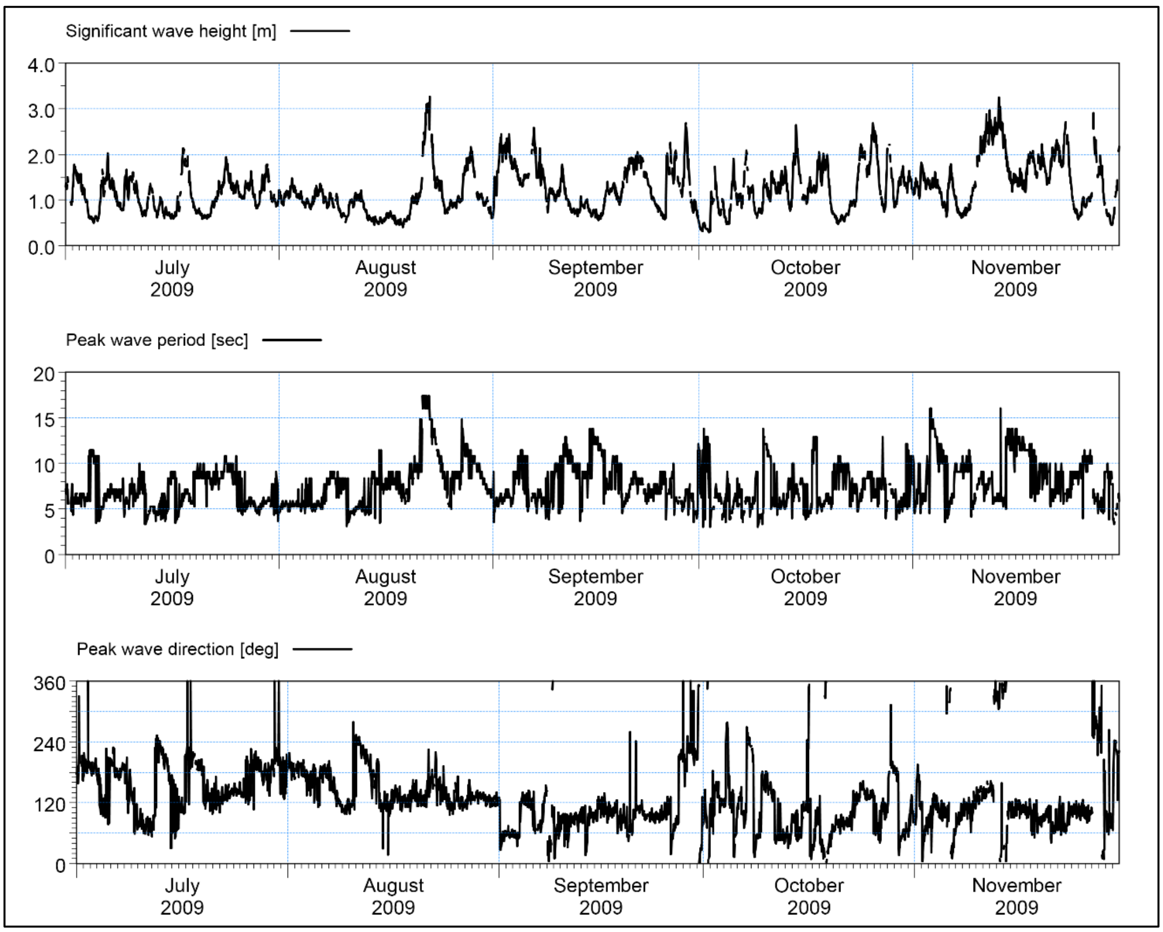

Figure 7-16: Bulk wave parameters from NOAA Buoy 41013 in the model validation period

7.1.4.3. Winds

Similar to the model calibration, spatially varying wind fields from CFSR were used for the model validation.

7.1.4.4. Water Levels

A spatially uniform water level field was used for the model validation. Due to lack of available measured water level data within the model domain, the data from nearby NOAA station 8658163 - Wrightsville Beach, NC, were used. Figure 7-17 presents the water level data.

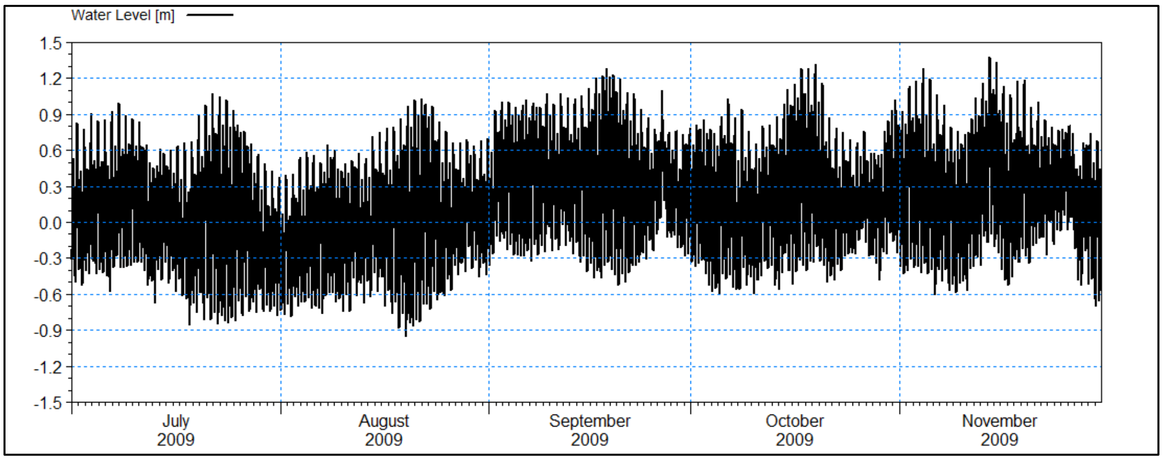

Figure 7-17: Water level data from NOAA station 8658163 for model validation

7.1.5. Model Validation Results

Figure 7-18 to Figure 7-20 present the direct comparison between the computed and measured time series of significant wave height, peak wave period and peak wave direction, respectively, at the gage locations of Eleven Mile ADCP, Bald Head ADCP, Oak Island ADCP and OCP1. Figure 7-21 shows the scatter plots of the measured and computed significant wave heights and includes a linear trend line fit through the data at each of the four stations. The goodness-of-fit parameters for the wave validation results are listed in Table 7-10 to Table 7-12 for the significant wave height, peak wave period and peak wave direction, respectively.

Table 7-10: Goodness-of-fit parameters for significant wave height validation

Station	*MAE* (m)	*RMS* (m)	*RMSN* (%)	*R*	*d*
Eleven Mile ADCP	0.14	0.18	8.7	0.88	0.93
Bald Head Island ADCP	0.12	0.15	8.6	0.87	0.92
Oak Island ADCP	0.19	0.22	20.3	0.88	0.77
OCP1 ADCP	0.09	0.13	8.2	0.90	0.94

Table 7-11: Goodness-of-fit parameters for peak wave period validation

Station	*MAE* (s)	*RMS* (s)	*R*	*d*
Eleven Mile ADCP	1.3	2.1	0.66	0.82
Bald Head Island ADCP	1.5	2.5	0.60	0.78
Oak Island ADCP	1.6	2.6	0.57	0.76
OCP1 ADCP	1.4	2.3	0.68	0.82

Table 7-12: Goodness-of-fit parameters for peak wave direction validation

Station	*MAE* (deg)	*RMS* (deg)
Eleven Mile ADCP	40	56
Bald Head Island ADCP	35	55
Oak Island ADCP	22	35
OCP1 ADCP	18	27

The results suggest that:

- For the significant wave heights, the model predictions agree very well with the measured data at all four ADCP locations except Oak Island ADCP, with *MAE* and *RMS* errors less than 0.2 m. The wave heights were consistently over-predicted at the Oak Island ADCP. The measured wave heights at Oak Island were lower than OCP1 ADCP; whereas the predicted wave heights were similar. It is possible that the deployment of the Oak Island ADCP during the validation period was in a different depth than previous deployment periods.

- For the peak wave periods, the *MAE* and *RMS* errors are less than 2.6 s, and *R* and *d* values around 0.6 and 0.8, respectively.

- For the peak wave directions, the model predictions have large deviations from the measured values. After checking the measured and model predicted directional wave spectra, the presence of a double peaked spectrum is what caused the issue.

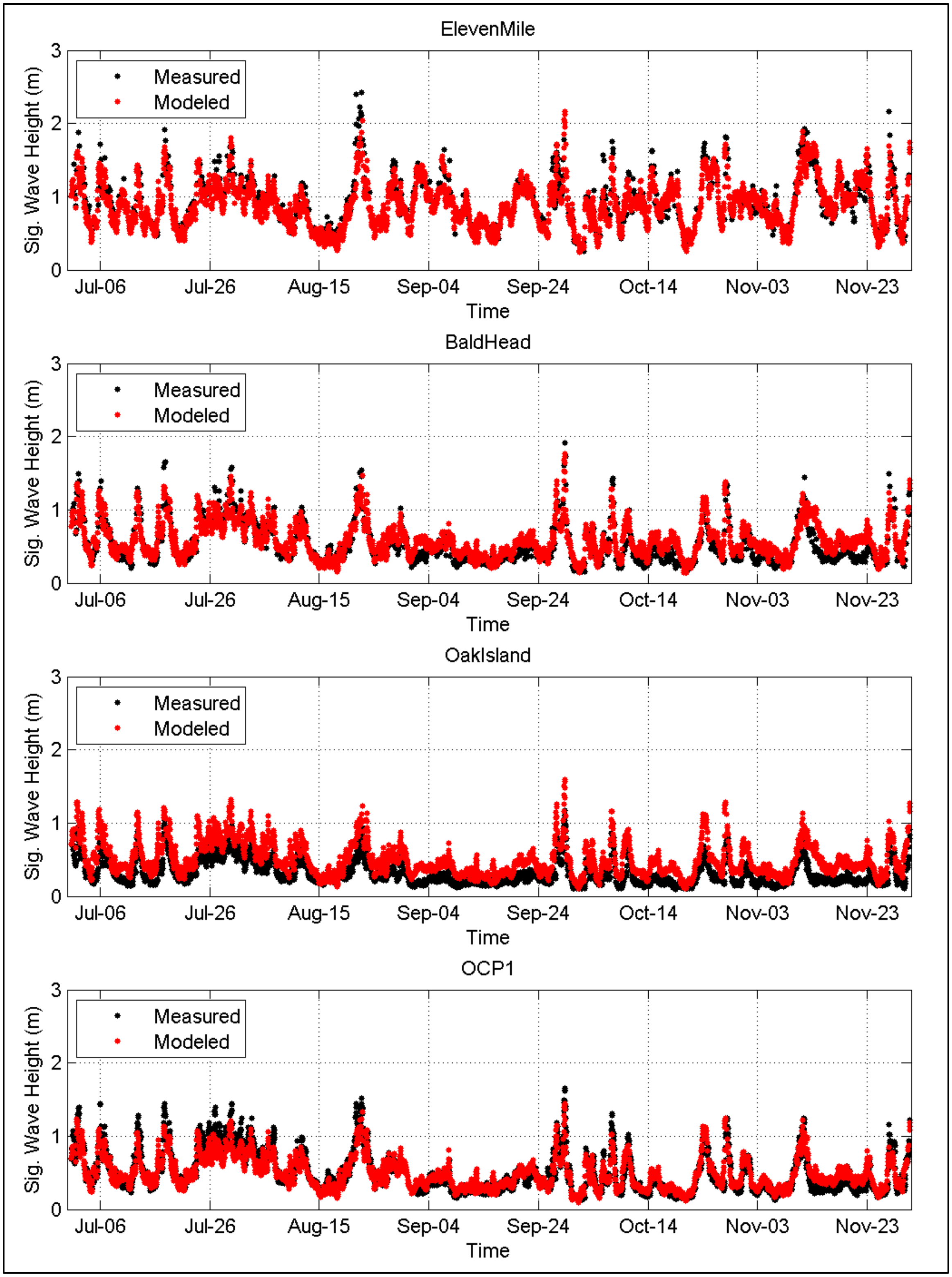

Figure 7-18: Comparison of measured and computed significant wave heights from offshore to nearshore for the validation period

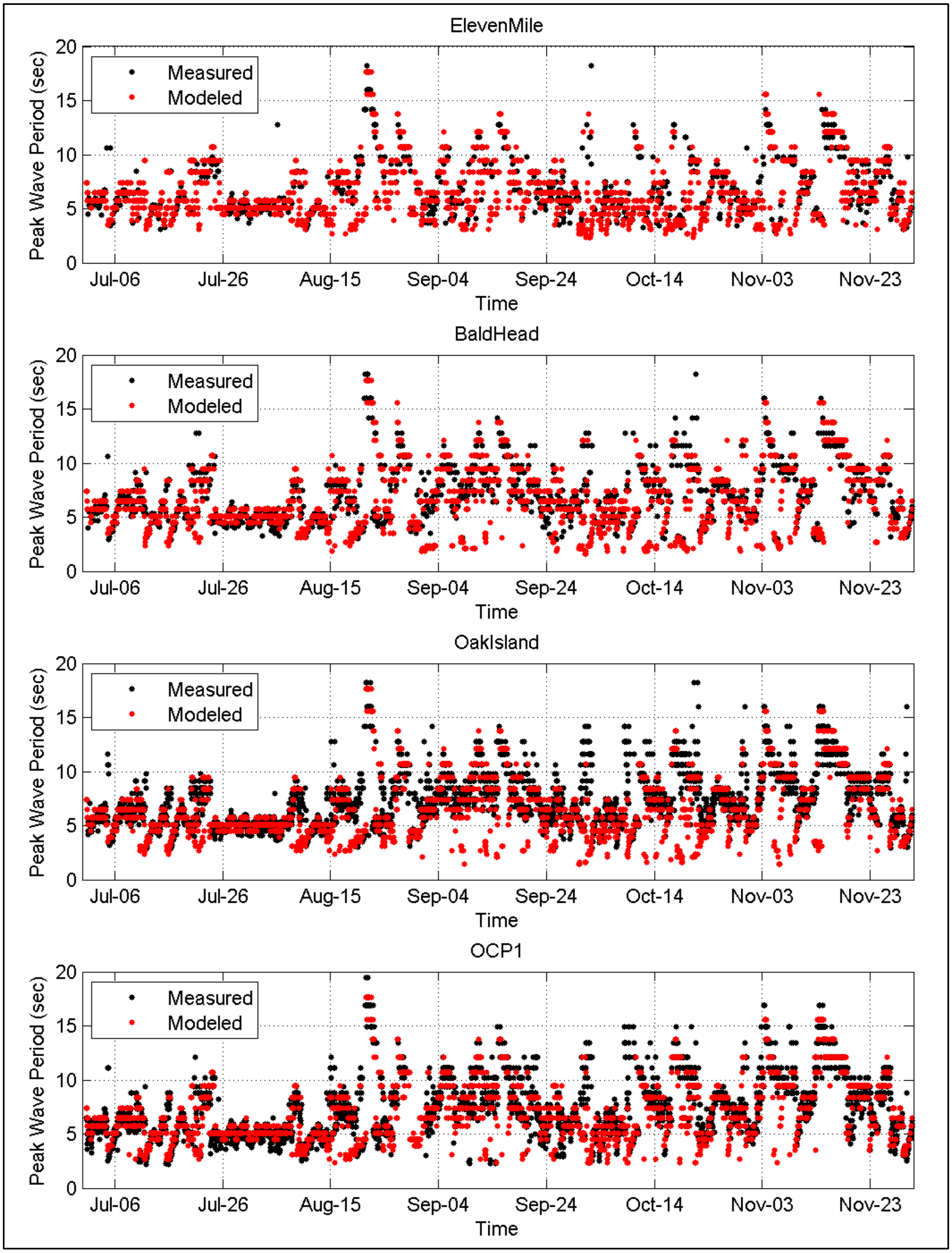

Figure 7-19: Comparison of measured and computed peak wave periods from offshore to nearshore for the validation period

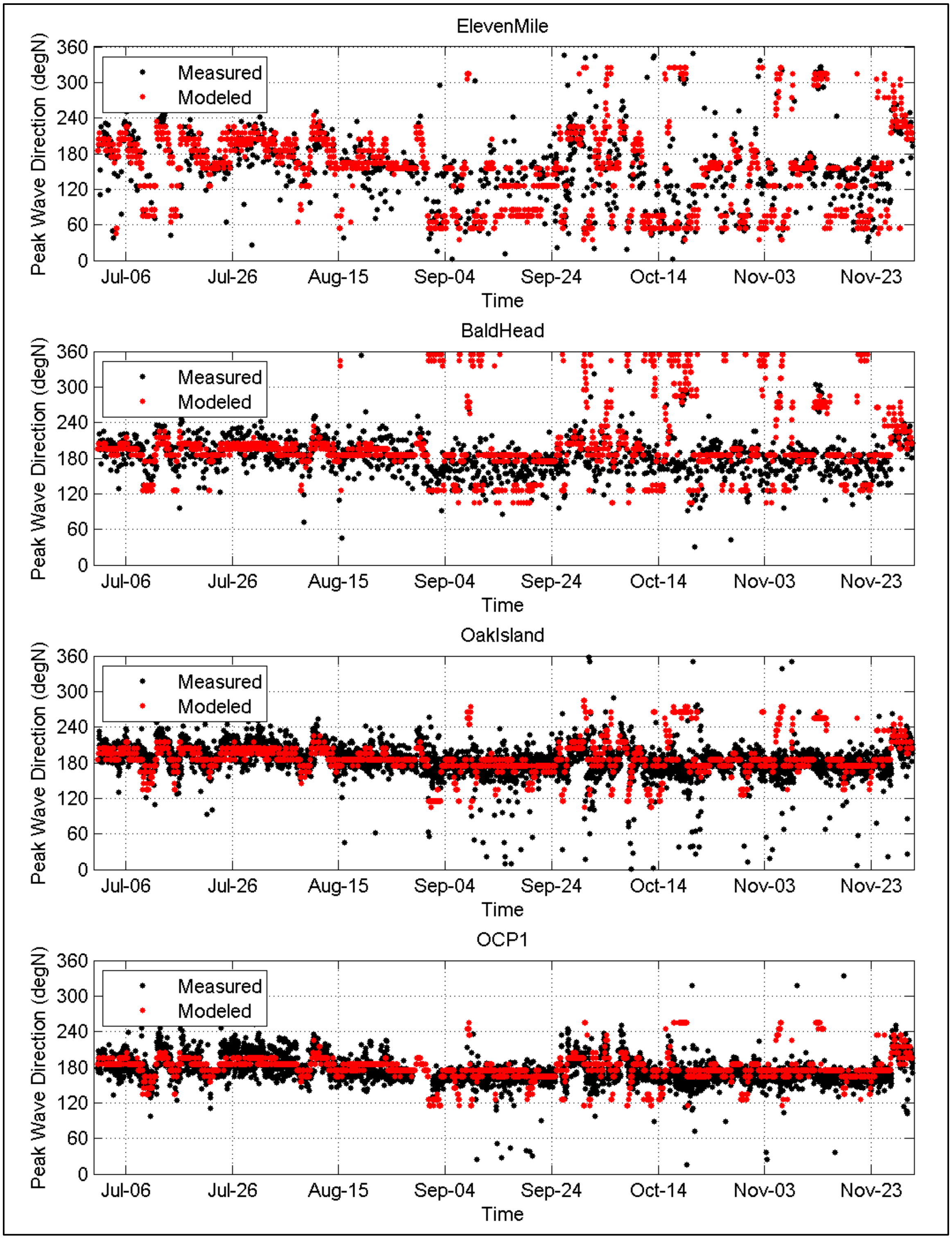

Figure 7-20: Comparison of measured and computed peak wave directions from offshore to nearshore for the validation period

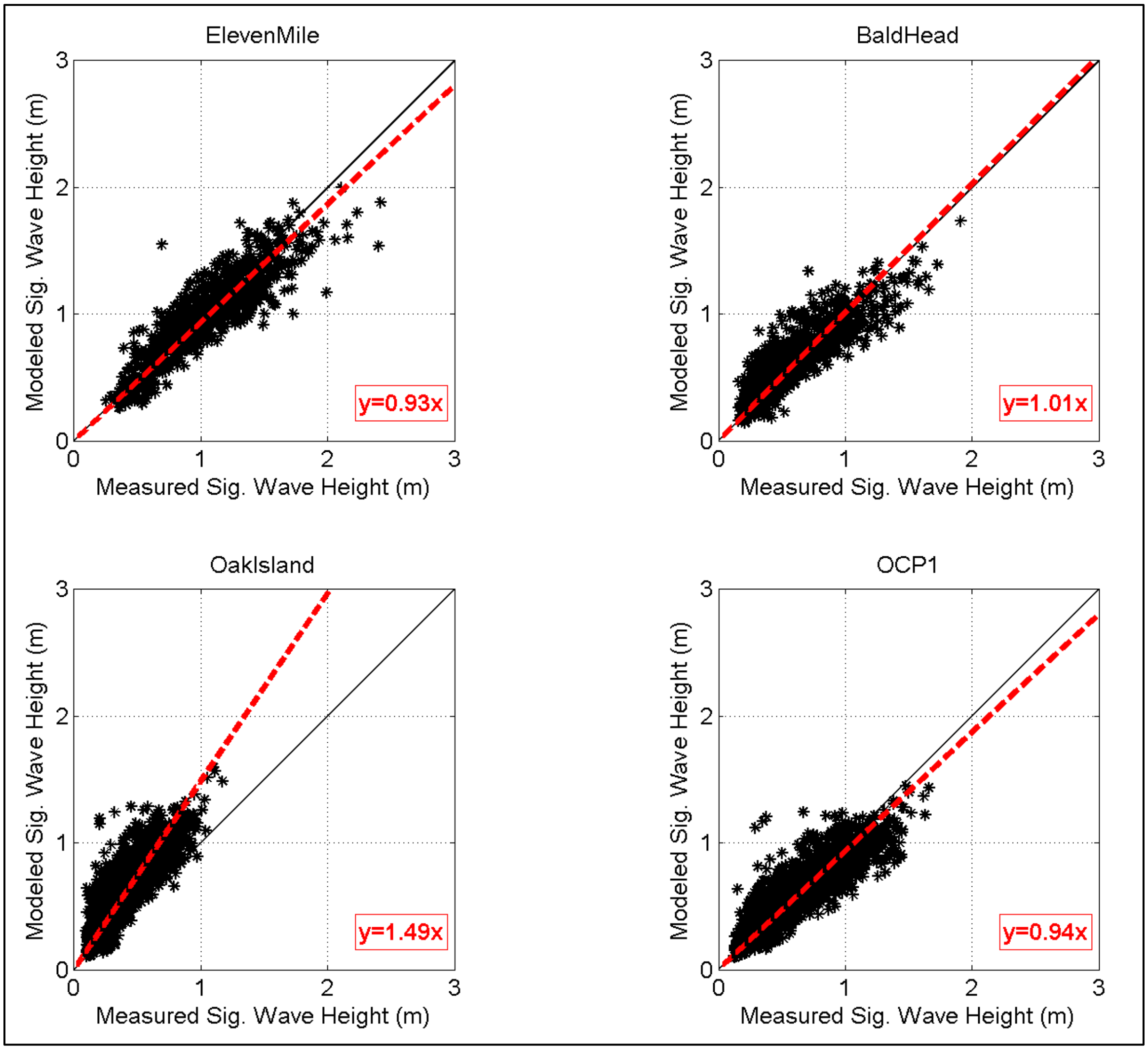

Figure 7-21: Scatter plot of computed and measured significant wave heights from offshore to nearshore for the validation period

Similar to the calibration period, comparisons of waves from the offshore direction between 110 and 270 degN are further discussed here for the validation period. The goodness-of-fit parameters are presented in Table 7-13 to Table 7-15 for the significant wave height, peak wave period and peak wave direction, respectively. The statistics for significant wave height and peak wave period are similar to the values in Table 7-10 and Table 7-11. The MAE and RMS errors for peak wave direction are smaller than values in Table 7-12 especially at the Eleven Mile ADCP and Bald Head Island ADCP locations. Figure 7-22 to Figure 7-24 show the time series plots.

Table 7-13: Goodness-of-fit parameters for significant wave height validation for waves coming from 110 – 270 degN

Station	*MAE* (m)	*RMS* (m)	*RMSN* (%)	*R*	*d*
Eleven Mile ADCP	0.14	0.18	8.5	0.89	0.93
Bald Head Island ADCP	0.11	0.14	8.0	0.88	0.93
Oak Island ADCP	0.19	0.22	20.5	0.87	0.76
OCP1 ADCP	0.09	0.12	8.1	0.89	0.94

Table 7-14: Goodness-of-fit parameters for peak wave period validation for waves coming from 110 – 270 degN

Station	*MAE* (s)	*RMS* (s)	*R*	*d*
Eleven Mile ADCP	1.0	1.8	0.76	0.87
Bald Head Island ADCP	1.3	2.1	0.69	0.83
Oak Island ADCP	1.5	2.5	0.59	0.76
OCP1 ADCP	1.4	2.4	0.67	0.82

Table 7-15: Goodness-of-fit parameters for peak wave direction validation for waves coming from 110 – 270 degN

Station	*MAE* (deg)	*RMS* (deg)
Eleven Mile ADCP	24	33
Bald Head Island ADCP	22	29
Oak Island ADCP	20	30
OCP1 ADCP	17	25

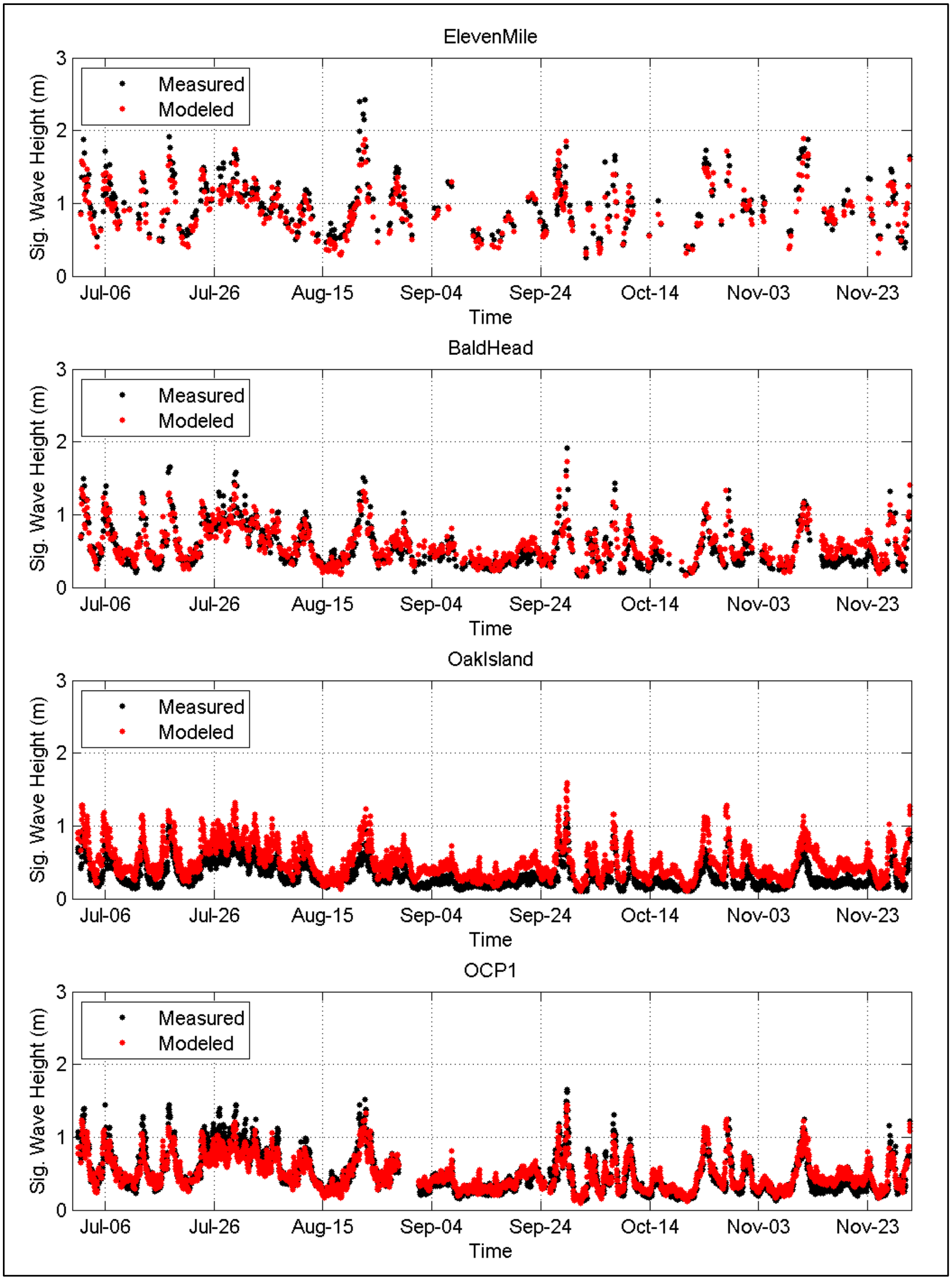

Figure 7-22: Comparison of measured and computed significant wave heights from offshore to nearshore during the validation period for waves coming from 110 -270 degN

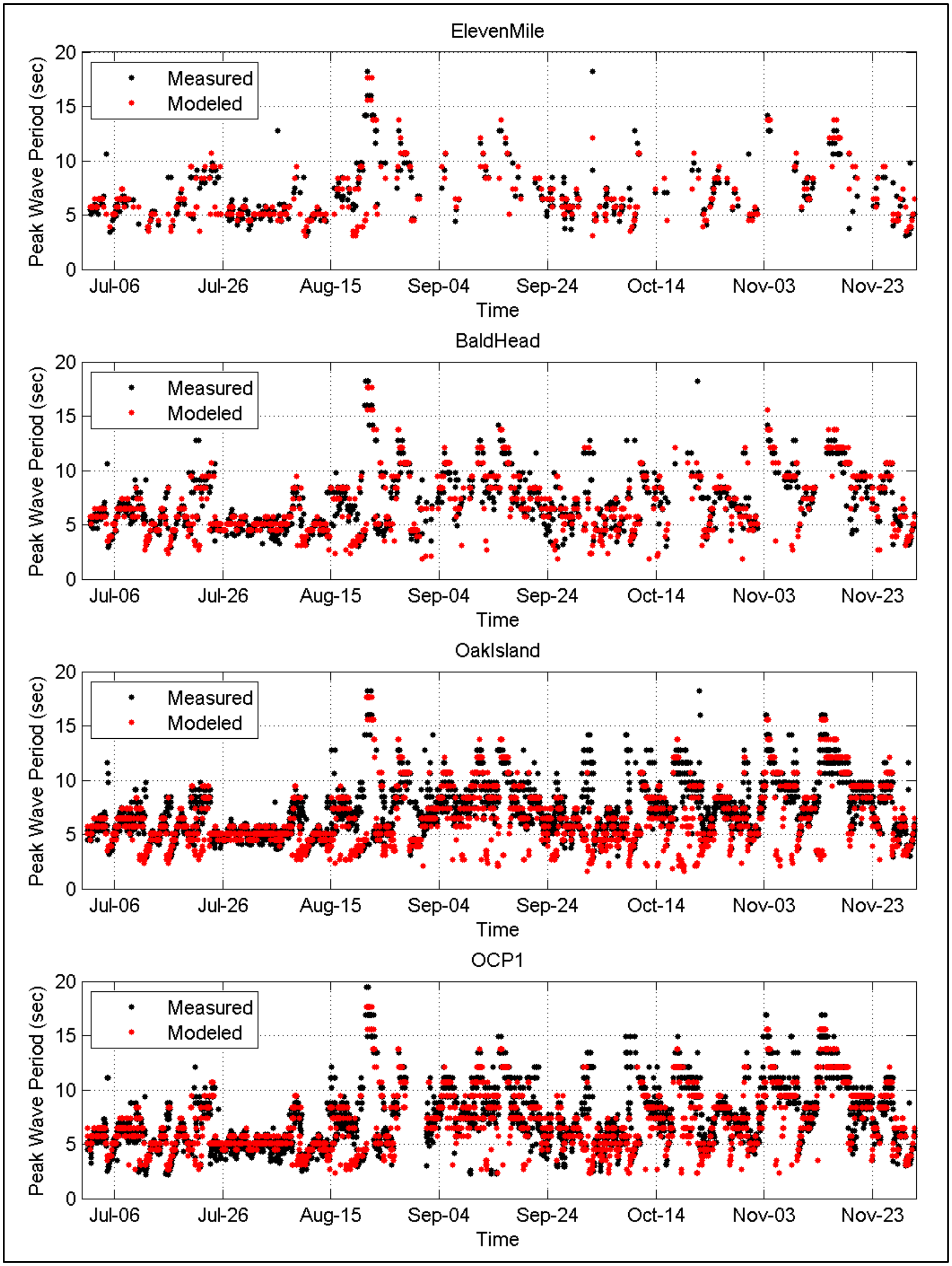

Figure 7-23: Comparison of measured and computed peak wave periods from offshore to nearshore during the validation period for waves coming from 110 -270 degN

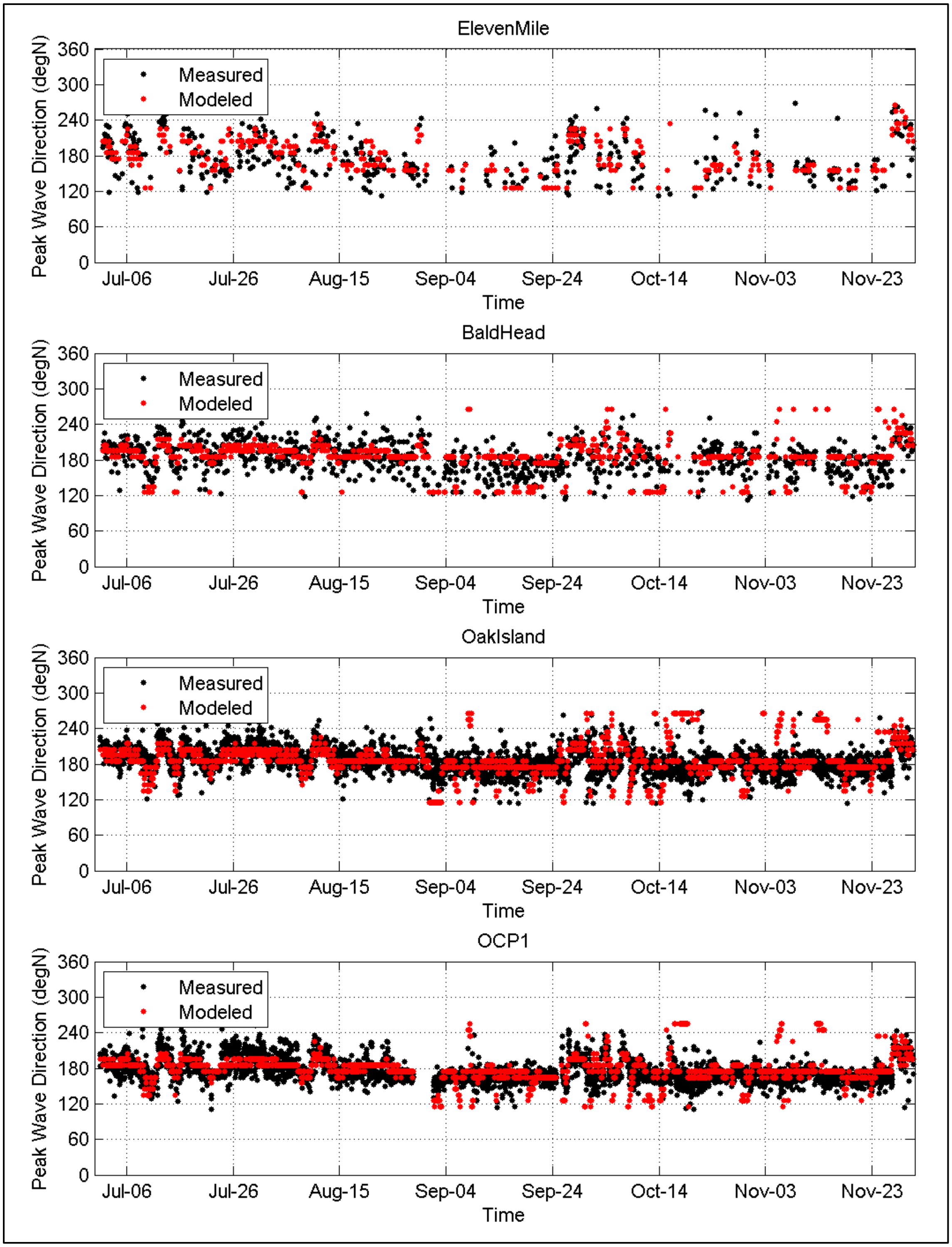

Figure 7-24: Comparison of measured and computed peak wave periods from offshore to nearshore during the validation period for waves coming from 110 -270 degN

A quantile-quantile (Q-Q) plot is a plot of the quantiles of the first data set against the quantiles of the second data set. A quantile in a Q-Q plot means the fraction (or percent) of points below the given value. A 45-degree reference line is also plotted in a Q-Q plot. If the two sets come from a population with the same distribution, the points should fall approximately along this reference line. The greater the departure from this reference line, the greater the evidence for the conclusion that the two data sets have come from populations with different distributions. The Q-Q plot between the measured and predicted significant wave heights including both the calibration and validation periods is presented in Figure 7-25 for all 4 ADCP locations. Linear best-fit regression lines (in red) are also included in the Q-Q plots. Statistically, the model consistently underpredicted the wave heights at the offshore Eleven Mile ADCP location; the model results were in good agreement with the measurement at the nearshore Bald Head ADCP; at the nearshore Oak Island ADCP, waves higher than 1.5 m were in good agreement between measurements and model results, but the model over predicted the waves below 1.5 m mostly due to the mismatches during the 2009 validation period; At OCP1 ADCP location, good agreement was achieved for waves below 2 m but the model over predicted the waves higher than 2 m.

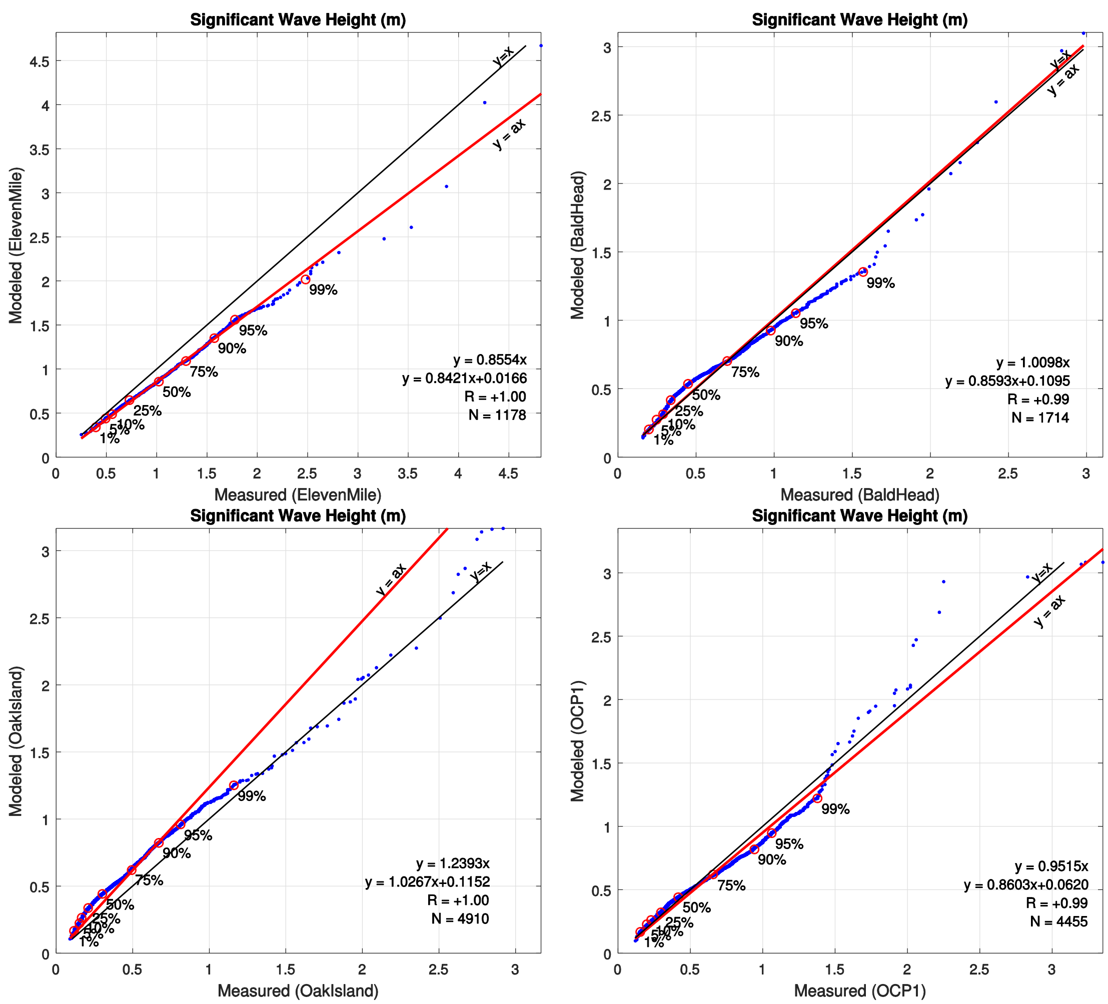

Figure 7-25: Q-Q plots between measured and modeled significant wave heights

7.1.6. Summary and Conclusions

In order to provide nearshore wave data for further detailed studies of the potential impacts of the Cape Fear River Deepening Project, a wave transformation model was developed. The model was calibrated and validated through comparison with measured offshore and nearshore wave data for both normal and storm wave conditions.

In general, the developed wave model is capable of transforming waves from deep water offshore to the shoreline of the study area particularly with respect to significant wave height and peak wave period. The differences between predicted and measured peak wave direction were significant in some instances. This is likely due to the presence of a double peaked spectrum. An upper cutoff frequency was used when post-processing the raw ADCP data to the bulk wave parameters, which could skew the peak wave direction determination if some portion of the locally wind-generated wave energy were discarded.

The purpose of the offshore wave modeling study is to provide nearshore wave conditions for investigating potential project effects on longshore sediment transports and shoreline changes along the adjacent beaches. Locally wind-generated waves propagating toward offshore do not affect the shoreline and are not important to the project. Therefore, comparisons of offshore waves coming from directions between 110 and 270 degN were further analyzed, and the agreements between the modeled and measured peak wave directions were improved.

Other possible sources of discrepancy between the model results and measurements include the model input assumptions (such as spatially uniform wave boundary conditions and water levels), ADCP location shifts between deployment intervals, and changes in the bathymetry between the calibration/validation periods and the available survey data; although, deficiencies in the measured data themselves and/or unforeseen inaccuracies in the numerical model may contribute as well.

7.2. Shoreline Evolution

This section summarizes the shoreline change model development, and calibration and validation results.

7.2.1. Numerical Modeling: GenCade

GenCade is a 1-D numerical model that combines the capabilities of GENESIS and Cascade, allowing for engineering design level calculations with the ability to span long, regional segments of shoreline that may contain inlets. GenCade is designed to simulate long-term shoreline change based on spatial and temporal differences in longshore sediment transport induced primarily by wave action. The GenCade modeling system allows for a number of user-specified inputs including wave inputs, initial shoreline positions, coastal structures and their characteristics, beach fills; and inlet system shoal volumes, all of which aid in the calculation of sediment transport and shoreline change. This model was developed at the U.S. Army Corps of Engineers (USACE), Engineer Research and Development Center (ERDC), Coastal Inlets Research Program (CIRP). For a more detailed description of the GenCade model, the reader is referred to the GenCade Version 1 Model Theory and User's Guide (Frey, et al., 2012a). GenCade operates within the Surface-water Modeling System (SMS), a suite of tools developed by Aquaveo. The software version used is GenCade 1.6 updated July 2015, obtained from CIRP's website (http://cirp.usace.army.mil/products/gencade.php).

The GenCade model has the potential for many applications in the coastal environment, including evaluation of longshore sediment transport, analysis of beach fill performance, or the analysis of the impact of coastal structures on shoreline change.

The main inputs to the GenCade model include:

- Shoreline Position Data – one-dimensional description of the shoreline position relative to a straight baseline position,
- Wave Data – long-term time dependent description of wave heights, periods, and directions applicable to the Study Area,
- Coastal Structures – position and characteristics of coastal structures (breakwaters, groins, jetties, or seawalls) acting along the Study Area,
- Beach Fill – starting and ending dates and location of beach fill defined by an added berm width,
- Inlet Shoal Volumes – Ebb, Flood, Left Bypass, Left Attachment, Right Bypass, and Right Attachment
- Sediment and Beach Characteristics – effective grain size, average berm height, and closure depth for the Study Area,

- Regional Contour – an offshore contour to account for bathymetry which may affect wave direction/energy
- Boundary Conditions – seaward boundary conditions for the input wave data and lateral boundary conditions for the shoreline (left and right).
- Sediment Transport Parameters – used to characterize longshore sediment transport and calibrate the model.

7.2.2. Model Development

7.2.2.1. Modeling Scope

The GenCade model was applied to understand the historical longshore sediment transport and erosional patterns adjacent to the Cape Fear River Channel Deepening Area including both Bald Head Island and Oak Island/Caswell Beach, and to evaluate the potential impact that might occur to oceanfront shorelines after the proposed channel deepening.

To establish the appropriate model parameters, the GenCade model was calibrated and validated for the February 2008 to February 2016 time period using historical Mean High Water (MHW) shoreline positions from aerial photography and coinciding wave data transformed to nearshore from the offshore wave data. GenCade is primarily calibrated by adjusting the longshore sand transport coefficients (K_1 and K_2). Additionally, the model may be calibrated by adjusting the characteristic transmissivity or permeability of offshore breakwaters, groins, or jetties, where applicable. Furthermore, boundary condition parameters (e.g. smoothing, wave input adjustments) may be altered to achieve calibration, or to test the model sensitivity. An offshore regional contour may also be incorporated to account for any bathymetric features that may impact wave direction and energy along the shoreline.

Model parameters established during the calibration will be used to determine the resulting shoreline response to the proposed channel deepening project to help determine any potential impacts on adjacent shorelines.

7.2.2.2. Study Area

The GenCade model coverage extends from Frying Pan Shoal at the eastern end of Bald Head Island to Lockwoods Folly Inlet at the western end of Oak Island. The Cape Fear River separates Bald Head Island and Oak Island. Figure 7-26 shows the GenCade model extent.

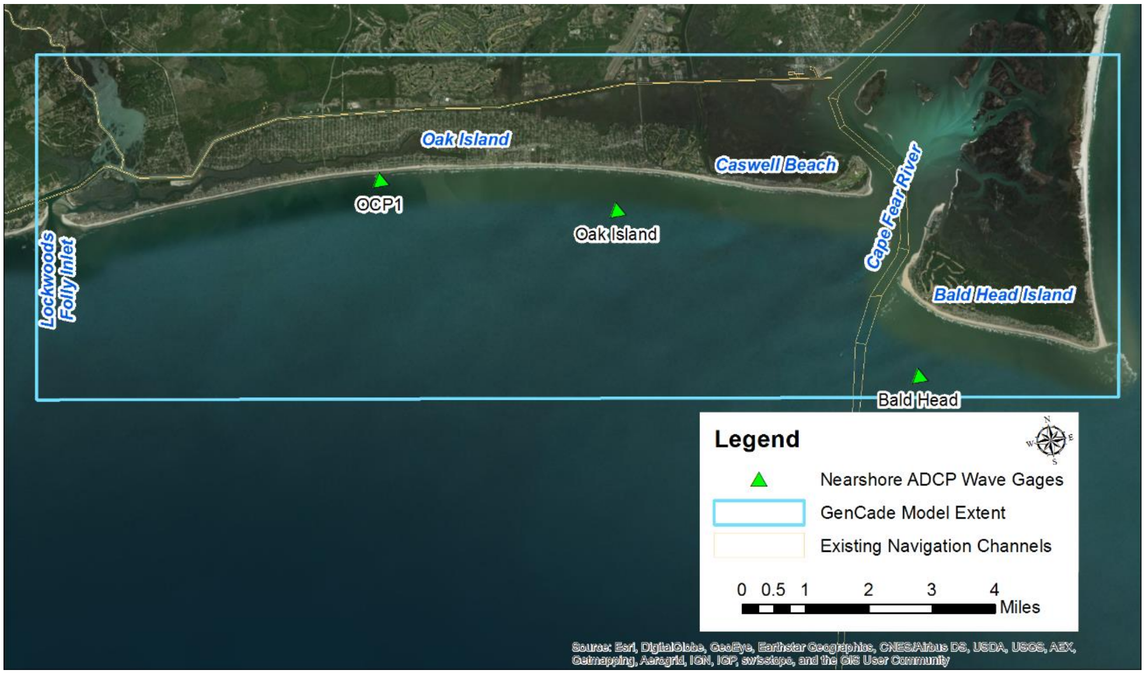

Figure 7-26: GenCade model extent

7.2.3. Model Calibration

The GenCade model was calibrated to reflect the historical trends of longshore sediment transport and the resulting shoreline change over the Study Area. The overall calibration time period was based on the availability of historical shoreline positions, wave data, and knowledge of nourishment and other engineering activities (i.e. Cape Fear River channel deepening and relocation in 2001) in the area.

For this study, the general calibration procedure involved:

- establishing known model inputs including shoreline position, waves (height, period, and direction), locations of structures, sediment and beach characteristics, inlet system shoal volumes and boundary conditions;
- establishing initial sediment transport parameters and adjusting these parameters until the relative shoreline response (erosion/accretion) matched historical trends; and
- adjusting the regional contour to account for bathymetric influences on sediment transport direction.

The final determined input data for the calibration model will be presented in the following sections, along with a discussion of the results and issues encountered during the calibration process.

7.2.3.1. Shoreline Position Data

The initial shoreline used in the GenCade model calibration was the February 2008 Wet/Dry shoreline digitized by the North Carolina Department of Coastal Management (NCDCM) based upon Brunswick County Photos. The final reference shoreline to which the model was calibrated was the February 2012 Wet/Dry shoreline digitized by NCDCM based upon 2012 NC Imagery. Figure 7-27 shows the initial and reference shoreline positions used in the GenCade calibration model.

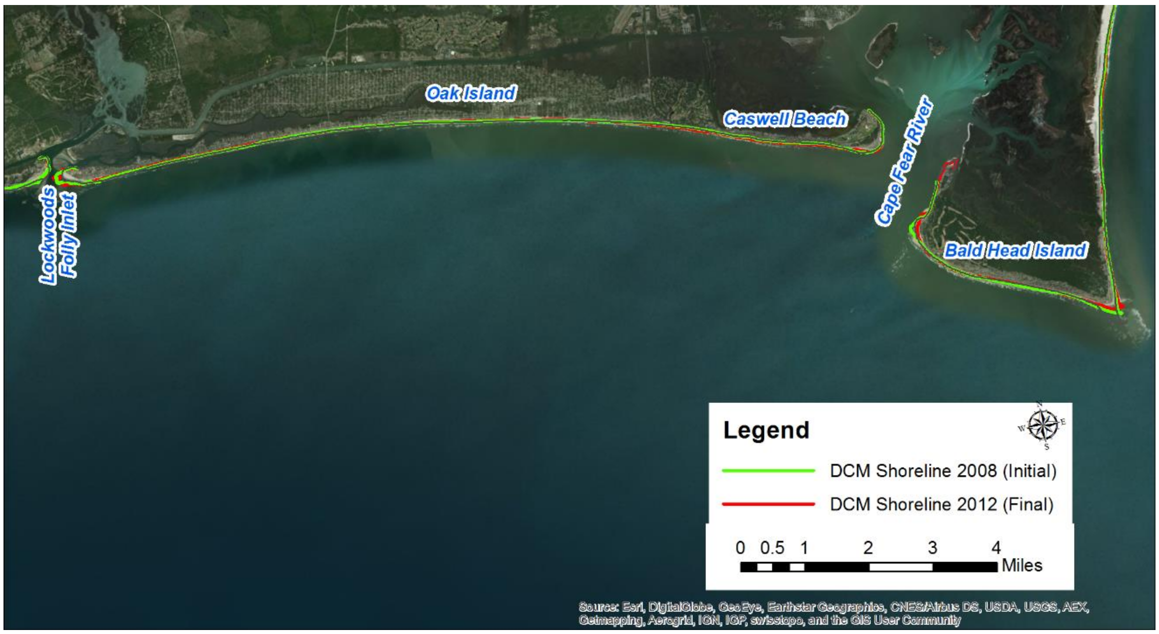

Figure 7-27: GenCade model calibration - initial and final shorelines

Based on a NCDCM study (Limber, et al., 2004) using concurrently collected Lidar and aerial photography covering the entire 516 km-long ocean coastline of North Carolina between August and September 2004, it was found that the Wet/Dry shoreline digitized from aerial photos was landward of MHW determined from Lidar by 3.5 m (11.5 ft) on average over 262 km of NC coastline, and this offset biased long-term shoreline change rates by an average of 0.06 m/yr (0.2 ft/yr). The offset was greatest on low-sloping beaches experiencing relatively high water levels at the time of surveying, but overall was small enough to suggest that the wet/dry line, under favorable conditions, can consistently approximate MHW.

7.2.3.2. Wave Data

There are three nearshore wave gages (as shown in Figure 7-26) with measured wave data available in the vicinity of the Study Area: two USACE Acoustic Doppler Current Profiler (ADCP) gages –Bald Head and Oak Island; and one Coastal Ocean Research and Monitoring Program (CORMP) ADCP gage – OCP1 (Ocean Crest Pier, NC). However, they were deemed to be insufficient for the current shoreline change study due to large gaps in the recorded data and their locations along the shoreline. The wave sheltering effects of the Jay Bird Shoals and the varying incoming wave angles relative to the shorelines are not captured in the measured data. Therefore, hindcasted nearshore wave data from the offshore wave model developed for the Project were used. The wave model discussed previously, Delft3D-WAVE, was used to transform the offshore waves at NOAA buoy 41013 to the nearshore where results were extracted at several locations along the shoreline at water depths of approximately 15 – 25 ft NAVD88 for input to the GenCade model. Hindcasted offshore waves from WAVEWATCH-III were used to fill the gaps in NOAA data. Figure 7-28 shows the nearshore wave locations for use in GenCade.

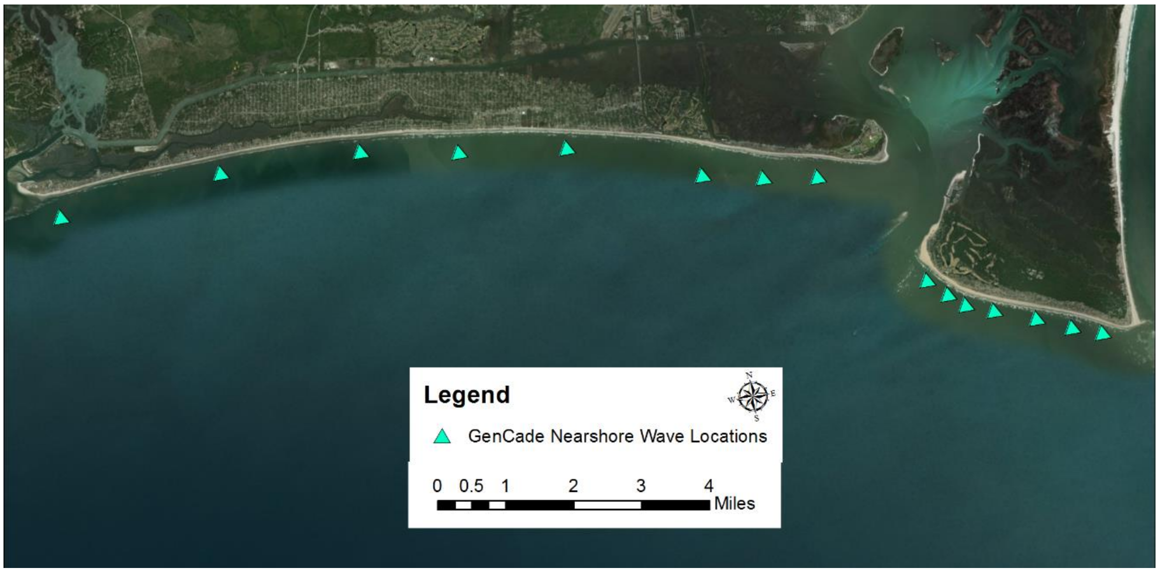

Figure 7-28: Nearshore wave data locations for GenCade Model

7.2.3.3. Coastal Structures

GenCade requires the locations and characteristics of nearshore structures as input. The coastal structures are incorporated in the GenCade model by digitizing their positions from aerial photography loaded into GenCade. Allowable structures include detached breakwaters, non-diffracting/diffracting groins, non-diffracting/diffracting jetties, and/or seawalls. Each structure is modeled uniquely with respect to longshore transport and shoreline change.

<u>Groin Field on Bald Head Island</u>

"In 1996, sixteen geo-textile groins were constructed from station 49+00 to Station 114+00 along the western end of South Beach on Bald Head Island. The groins were 9 feet in diameter and 325 feet long. The spacing between the groins was 450 feet. The groin field slowed the erosion for several years before they ceased to function in 2000. Due to apparent effectiveness of the geo-textile groins, the Village of Bald Head Island decided to rebuild the groin field following the beach fill placement in 2005. As such, a sixteen structure sand-tube groin field was reconstructed along South Beach between Stations 47+00 and 105+00. Some modifications were made to the original 1996 plan. These modifications included: (1) the spacing was reduced from 450 feet to 385 feet thereby reducing the overall extent for the groin field, (2) the tube lengths were 300 feet for 14 of the structures and 250 feet for the remaining two, (3) the individual tubes were tapered with a landward maximum diameter of 10 feet to 6 feet at the seaward end, and (4) the entire groin field was shifted westward to be more aligned with the problem area at the westernmost end of South Beach." (USACE, 2013).

The westernmost sand tube groins are subject to quickened downdrift destabilization due to navigation project related sand losses at "the Point", as well as sand starvation when the updrift portion of the groin field becomes activated to the point that net alongshore transport (toward the west) is diminished. Prior to beach fill construction by the Village in 2009/2010, several of the westernmost groins had been severely flanked and eventually destroyed by a rapidly receding dune line and downdrift shoreline (Olsen Associates, Inc. 2016). The Village of Bald Head Island obtained a renewal of the groin field permit(s) so as to be able to reconstruct all or portions of the structures subsequent to the locally funded and constructed winter 2009/10 beach renourishment project. In the spring of 2013, the westernmost five (5) sand tube groins were replaced in their entirety again. In the spring 2015, the westernmost three (3) geotube groins were removed in their entirety for the construction of a terminal groin discussed later.

Figure 7-29 shows an aerial view of the groin field from October 2008 to February 2014 Google Earth imageries. The constant state of change of the beach surrounding the groin field complicates the model calibration and validation.

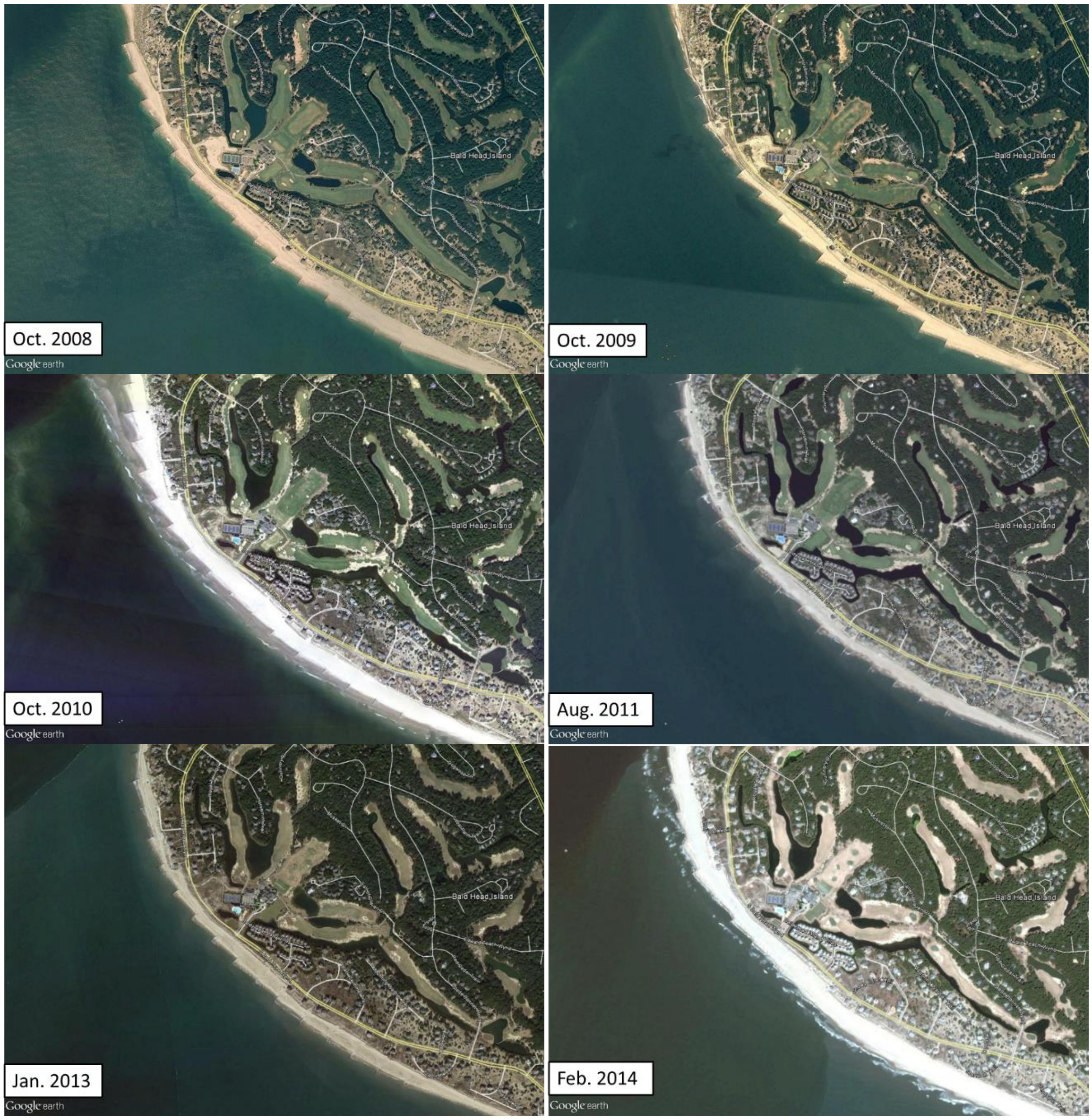

Figure 7-29: Groin field along Bald Head Island, 2008 – 2014 (Google Earth)

<u>Terminal Groin on Bald Head Island</u>

To combat the chronic rates of sediment loss at the west end of South Beach and consistent northerly recession of the Point and associated threat to public infrastructure, homes, roads, and beaches as well as wildlife habitat, the Village of Bald Head Island permitted a single 1,900 ft long terminal groin designed to complement future placement of beach fill at South Beach in 2014. The structure will be constructed in two phases. The structure is to serve as a "template" for fill material placed eastward thereof on South Beach (Olsen Associates, Inc. 2016). Phase I, a 1,300 ft long rock terminal groin constructed from June to November 2015, was designed as a "leaky" structure (i.e. semi-permeable) so as to provide for some level of sand transport to West Beach and portions of the Point (located northward of the proposed groin). Phase II will only be initiated after some period of monitoring of the groin's post-construction performance and the determination that some level of additive structure is warranted. Figure 7-30 shows the constructed terminal groin.

Figure 7-30: Terminal Groin on Bald Head Island (completed in November 2015)

A non-diffracting or diffracting groin implemented in GenCade must have a defined permeability which controls the transmission of sand over and through the structure. If the structure is diffracting, a seaward depth of structure must be defined. In this study, the geo-textile groins are treated as non-diffracting, permeable groins, and the terminal groin is included in the model validation as a diffracting and permeable structure. The permeability of the groins is a model tuning parameter. The groin field is assumed functioning continuously during GenCade simulations; thus, the structure failure impact on the shoreline changes is not captured.

7.2.3.4. Beach Fills

Table 7-16 lists the beach nourishment activities at both Bald Head Island and Oak Island since 2008. The beach fills from the third Wilmington Harbor maintenance cycle in 2009 and the Village of Bald Head Island (VBHI) 2009/2010 beach nourishment project took place during the GenCade calibration time period. The 2012 FEMA/VBHI emergency beach fill project placed sand along West Beach and the westernmost segment of South Beach. The 2012 NCDCM shoreline was dated as of February 13th, 2012. It's not clear what part of the 2012 FEMA/VBHI project was included in the 2012 NCDCM shoreline. Its impact on the majority of the Bald Head Island shoreline calibration, though, would be minimal due to its small quantity and footprint (95,000 cy placed along the westernmost of South Beach). For the model calibration, the extent of this emergency beach fill was assumed to be along the shoreline between the westernmost six groins and the added beach width was first estimated based on the equilibrium beach width for a uniform fill volume per unit beach length. To convert the total fill volume to added berm width, the volume was divided by the total alongshore distance and the active profile height (berm height plus depth of closure) (Frey, 2016). The added berm width was later adjusted based on the modeled shoreline position along the placement extent to closely match the 2012 NCDCM shoreline

GenCade requires, as input, the lateral extents of the nourishment, a start and end date, as well as an added berm width. For the 2013 beach disposal project on Bald Head Island, the added berm width was from the USACE beach fill template design drawings (USACE, 2012b). For the other nourishment projects, the added berm widths were determined from the available pre- and post-project beach profile surveys.

Table 7-16: Bald Head Island and Oak Island beach nourishments since 2008

Name	Location	Nourishment Period	Volume (cy)	Placement Area	Source	Length (ft)	Added Berm Width (ft)
Wilmington Harbor Third Maintenance	Caswell Beach	02/08/09 – 04/24/09	123,400	60+00 – 95+00	Ocean Entrance	3,500	50 – 80[a]
Wilmington Harbor Third Maintenance	Oak Island	02/08/09 – 04/24/09	941,000	120+00 – 260+00	Ocean Entrance	14,000	50 – 140[a]
Eastern Channel	Oak Island	03/09/15 – 04/30/15	221,770	660+00 – 670+00	Eastern Channel	1,000	195[a]
VBHI	Bald Head Island	11/01/09 – 03/09//10	1,594,553	40+00 – 190+00	Jay Bird Shoal	15,000	55 – 205[b]
FEMA/VBHI	Bald Head Island	01/19/12 – 02/25/12	95,000	43+48 – 65+50	Bald Head Creek	2,270	75[c]
Wilmington Harbor Fourth Maintenance	Bald Head Island	01/13 – 04/13	1,566,000	44+00 – 150+00	Ocean Entrance	10,600	130 – 180[d]
Wilmington Harbor Fifth Maintenance	Bald Head Island	01/15 – 04/15	1,330,000	41+50 – 154+00	Ocean Entrance	11,250	110 – 230[e]

a. Based on available pre- and post- project beach profile surveys
b. Based on Bald Head Island beach monitoring report No.9 (Olsen Associates, Inc., 2011)
c. Estimation based on model calibration
d. Based on USACE beach fill drawings dated on August 20th, 2012 (USACE, 2012b)
e. Based on Bald Head Island beach monitoring report No.13 (Olsen Associates, Inc., 2015)

7.2.3.5. Inlet Shoal Volumes

Inlets are defined in GenCade by shoal volumes in the inlet complex. Figure 7-31 presents a schematic of the morphological elements in an inlet as defined by GenCade. For each shoal element, initial and equilibrium volumes are required as model inputs.

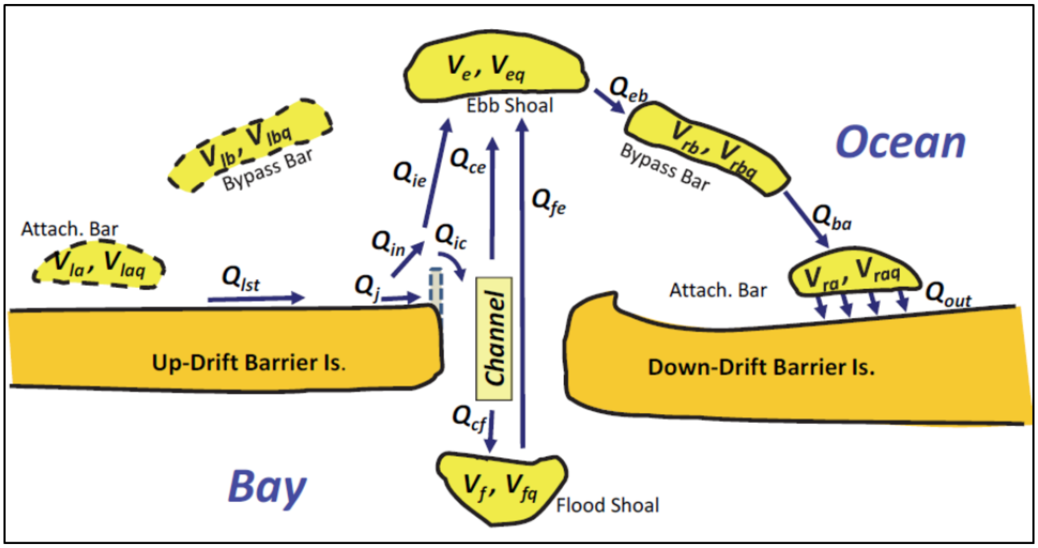

Figure 7-31: GenCade inlet schematic (Frey et al., 2012a)

The equilibrium volume of the ebb shoal complex (including ebb shoal and bypassing bars) was determined based on the tidal prism vs. ebb shoal volume relationships developed by Walton and Adams (1976):

$$V_E = C_E P^{1.23} \tag{23}$$

Where V_E is the equilibrium ebb-shoal volume in m^3, $C_E = 2.121\times10^{-2}$, and P is the tidal prism in m^3. For the Cape Fear River, the tidal prism is between (1.5 – 2.3) $\times10^8$ m^3 based on the surveys (USACE, 2011), with the average ebb tidal prism of about 1.8 $\times10^8$ m^3. The calculated equilibrium ebb-shoal volume is thus between (2.4 – 4.1) $\times10^8$ m^3 with average value of 300 million m^3 (392.4 million cubic yards).

Similar to the tidal prism and ebb-shoal volume relationship, Carr de Betts (1999) and Carr de Betts and Mehta (2001) analyzed 67 inlets in Florida and obtained correlations between flood tidal shoal volume and tidal prism, and between the flood-tidal shoal area and tidal prism.

$$V_{FT} = 2.0389 \times 10^4 P^{0.296} \tag{24}$$

Where V_{FT} is the flood shoal volume, and volume and prism are expressed in units of m^3. The average equilibrium flood shoal volume for the Cape Fear River is about 4.9 million m^3 (6.4 million cubic yards) based on the average flood tidal prism of 1.1×10^8 m^3.

For the Lockwoods Folly Inlet, with a tidal prism of about 0.135×10^8 m^3, the equilibrium ebb-shoal and flood shoal volumes are about 12.5 million m^3 (16.4 million cubic yards) and 2.6 million m^3 (3.4 million cubic yards), respectively.

Initial inlet shoal volumes were estimated based on the available bathymetry data above the 20 ft depth contour. Figure 7-32 illustrates the delineated GenCade ebb shoal system at the Cape Fear River entrance. The total equilibrium ebb shoal volumes were divided into the individual shoal volumes as required for GenCade for both inlets based on the size ratios of the estimated initial shoal volumes. Table 7-17 and Table 7-18 present the shoal volumes (initial and equilibrium) that were used as inputs for GenCade at the Cape Fear River and the Lockwoods Folly Inlet, respectively. The computed initial shoal volumes at the Cape Fear River entrance are much smaller than the equilibrium values, implying that sediments transported to the ebb shoal system from both the Bald Head Island and Oak Island shorelines in GenCade will be deposited almost entirely within the shoals and little natural sand bypassing will occur, which is the reality due to the sediment trapping in the navigation channel and continued maintenance dredging.

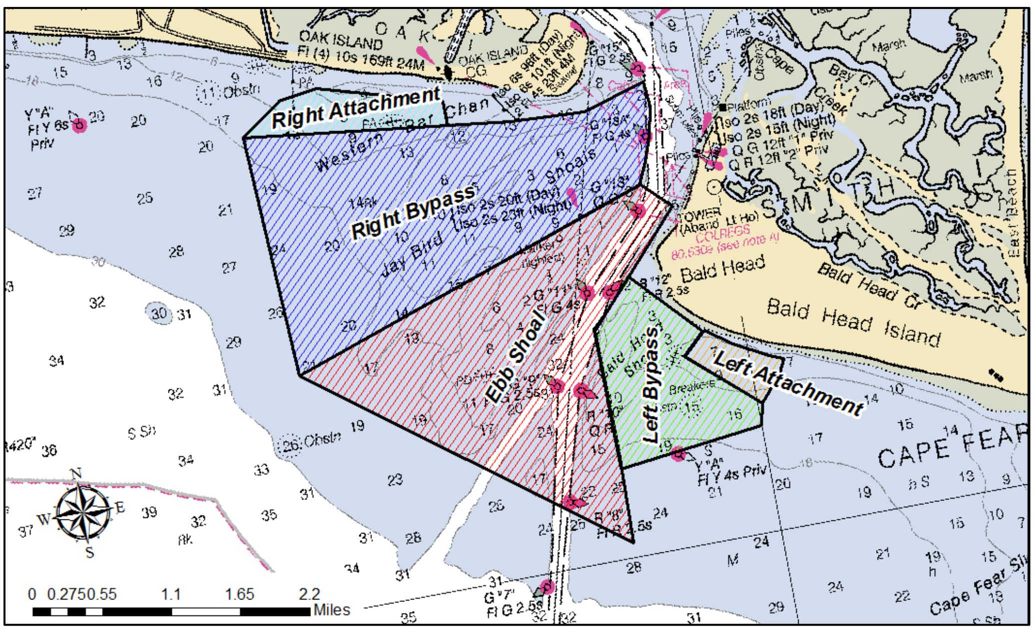

Figure 7-32: GenCade ebb shoal system at the Cape Fear River entrance

Table 7-17: Cape Fear River shoal volumes

Shoal	Initial Volume (Mcy)	Equilibrium Volume (Mcy)
Ebb Shoal	5.63	163.0
Flood Shoal	6.40	6.40
Left (East) Bypass	2.69	49.0
Left (East) Attachment	0.76	7.59
Right (West) Bypass	13.9	180.0
Right (West) Attachment	1.94	16.0

Table 7-18: Lockwoods Folly Inlet shoal volumes

Shoal	Initial Volume (Mcy)	Equilibrium Volume (Mcy)
Ebb Shoal	4.60	8.20
Flood Shoal	3.40	3.40
Left (East) Bypass	2.30	4.10
Left (East) Attachment	0.90	1.64
Right (West) Bypass	2.30	4.10
Right (West) Attachment	0.90	1.64

7.2.3.6. Sediment and Beach Characteristics

GenCade requires, as input, the effective grain size (mm), average berm height (ft), and closure depth (ft). The selected effective grain size assumed in the GenCade model was 0.25 mm. This grain size was determined based on the native beach data collected by the USACE in their Draft General Reevaluation Report and Environmental Impact Statement for the Coastal Storm Damage Reduction Projects (USACE, 2012). The draft EIS study indicated a native mean grain size ranging from 0.21 mm to 0.25 mm.

The average berm height was set to +6.0 ft-NAVD88 and the closure depth was set to -25.0 ft-NAVD88. Empirical analyses using WIS hindcast (Brutsché, et al., 2016) indicated a closure depth between 20 ft and 28 ft along this part of the US coastline. The lower value was based on Birkemeier (1985), and the higher value was from Hallermeier (1981). The actual closure depth may vary along different sections of the shoreline depending on the nearshore bathymetry. However, the current version of GenCade does not support a spatial varying closure depth. The accuracy of berm height and closure depth in GenCade can be offset by adjusting the sediment transport parameters.

7.2.3.7. Regional Contour

The regional contour is one of the many adjustment tools within GenCade that allows the model to more realistically represent the behavior of the prototype. The use of a regional contour allows the modeler to specify the underlying shoreline shape that the model will evolve towards, rather than having the model evolve toward a straight line. It is the result of all the large-scale, alongshore forcing-function non-homogeneities and underlying geology that are not accounted for in GenCade and that, in combination, cause the real-world shoreline to attain a non-straight, long-term equilibrium planform shape. A regional contour as shown in Figure 7-33 was applied in the current model study. The regional contour was initially developed based on the bathymetry contours and fine-tuned during the calibration.

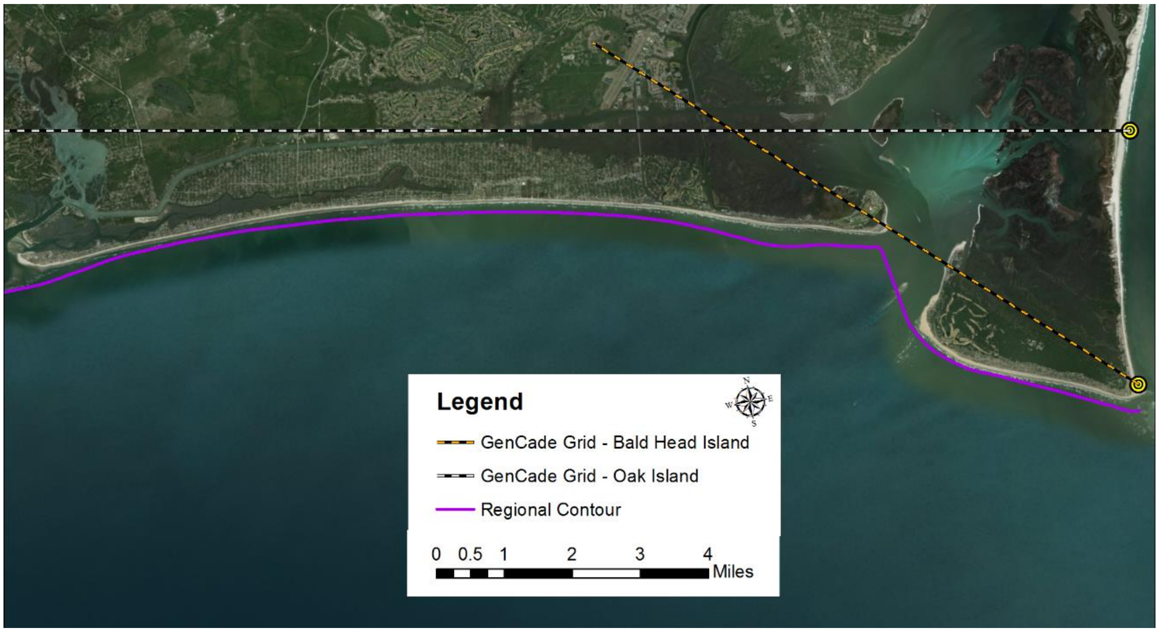

Figure 7-33: Regional Contour for GenCade

7.2.3.8. GenCade Grids

GenCade is a one-line model. It uses a grid to calculate shoreline change and longshore sediment transport. The selection of the GenCade grid orientation is an important parameter in the model setup since it affects the accuracy of calculated transport at every grid cell at every time-step. The grid axis should be oriented parallel to the shoreline as much as possible. Frey et al. (2014) recommended to orient the grid axis within +/- 25 degrees of the shoreline for most accurate results.

In this study, two separate GenCade grids are adopted as shown in Figure 7-33. One grid was used initially, but it was found impossible to calibrate both the Bald Head Island and Oak Island shoreline changes altogether using only one sediment transport parameter K_1 which cannot be varied spatially in the current version of GenCade.

7.2.3.9. Boundary Conditions

The required boundary condition inputs for GenCade include the seaward wave data boundary conditions and the lateral boundary conditions at the left and right ends of the shoreline, as described in the following sections.

<u>Seaward Boundary Conditions</u>

Within the seaward boundary conditions, the user may modify the input wave conditions (wave height and direction) by factors to analyze the impact changes in modeled wave conditions have on the resulting shoreline response. During calibration it was determined that the input wave height and wave angle derived from the Delft3D-WAVE model results were representative of nearshore conditions and were used without modification.

Lateral Boundary Conditions

The left (east) boundary of both GenCade model grids was located at the eastern end of South Beach where a moving boundary was used. The shoreline change rate based on the shoreline change between the 2008 initial shoreline and the 2012 final shoreline was applied for model calibration purpose.

The right (west) boundary of the Oak Island model grid was established on Holden Beach (3.5 miles west of the Lockwoods Folly Inlet) where a pinned boundary was used as an indication of no shoreline change at this location. For the Bald Head Island model grid, the right (west) boundary was established on Oak Island 5 miles west of Cape Fear River. A pinned boundary was also applied. These pinned right lateral boundaries are located far away from the main interest shoreline areas; thus, having no influence on the model results. Model sensitivity runs confirmed this assumption.

7.2.3.10. Sediment Transport Parameters

Based on model calibration, it was determined that the transformed wave conditions accurately represented the nearshore waves and sediment transport direction was accurately reflected as well. Therefore, attention was turned to the magnitude of the transport. Longshore sediment transport is characterized by the transport parameters K_1 and K_2 in GenCade. The transport rate coefficient, K_1, is used to control the time-scale and magnitude of the simulated shoreline change, while K_2 is used to control shoreline change and longshore sand transport in the vicinity of structures. Although the values of K_1 and K_2 have been empirically estimated, these coefficients are treated as calibration parameters in GenCade and range in value from 0 to 1.0.

The calibration models were initially run with the K_1 and K_2 coefficients of 0.6 and 0.4, respectively, which were used by the USACE in their 2012 study of Onslow Bay (Frey, et al., 2012b). The coefficients were incrementally adjusted until the desired shoreline change was achieved. The final calibration transport coefficient values were chosen to be K_1 = 0.35 and K_2 = 0.4 for the Oak Island model; whereas K_1 = 0.45 and K_2 = 0.4 were selected for the Bald Head Island model. These K values allowed for the comparable magnitude of longshore sediment transport rates along the Bald Head Island and Oak Island shorelines as compared to previous sediment transport and sediment budget studies (Thomson, et al., 1999; Offshore Coastal Technologies, Inc. (OCTI), 2008; USACE, 2012a and Olsen Associates, Inc., 2012).

Thompson et al. (1999) calculated the longshore transport rates by applying a CERC-like longshore transport equation using nearshore waves computed from a detailed STWAVE model. The offshore waves from the 1976-95 WIS hindcast were used at the STWAVE model offshore boundary. The OCTI (2008) longshore transport rates were calculated using the CEM formula with a simplified one-dimensional wave modeling approach using WIS hindcast offshore waves from 1980 to 2000. USACE (2012) applied the Corps' Cascade model for their regional sediment management study as part of the Brunswick County beach CSDR project re-evaluation. Wave characteristics for the Cascade runs were taken from WIS hindcast 1976-95. Figure 7-34 presents the longshore transport results from these studies. Cascade longshore transport rates have a general agreement in magnitude and direction with those calculated by Thompson et al. (1999). The OCTI (2008) longshore transport rates were much lower than either the Thompson et al (1999) or the Cascade model longshore transport rates.

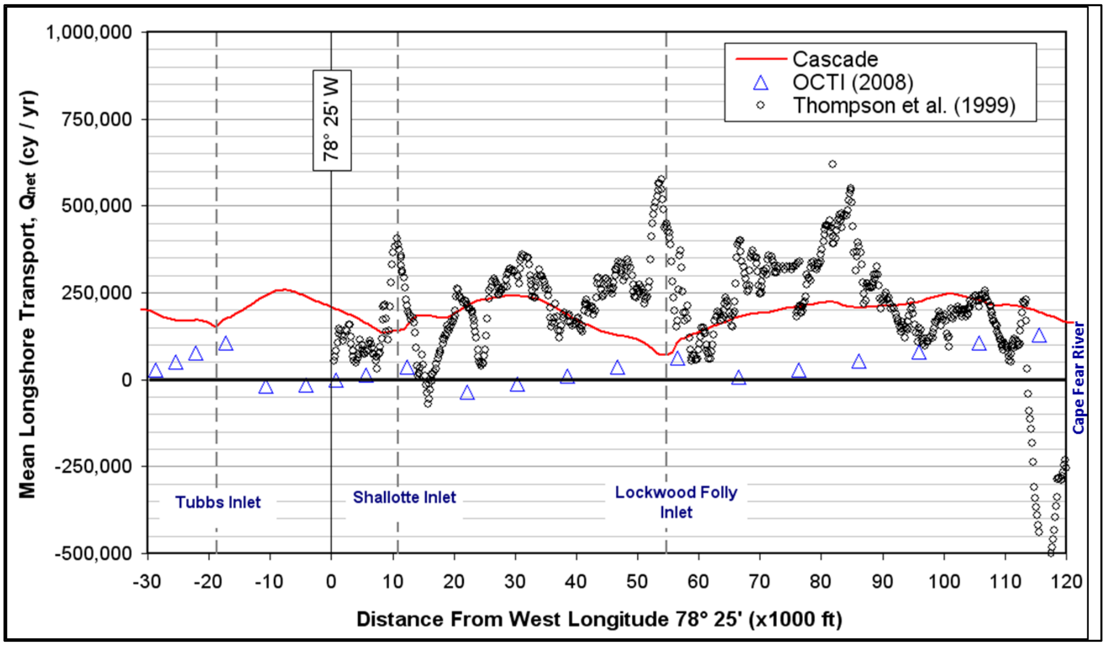

Figure 7-34: Historically calculated potential net longshore sand transport rates west of Cape Fear River (USACE, 2012a)

Olsen Associates, Inc. (2012) used the two-dimensional Delft3D model to simulate the tides, currents, waves, sediment transport, and resultant seabed changes at the Cape Fear River Entrance including the federal navigation channel and the adjacent shoals and shorelines of Oak Island and Bald Head Island. The offshore wave data for their wave modeling was from NOAA buoy 41013. Figure 7-35 presents the calculated sediment transport rates along Bald Head Island from their model.

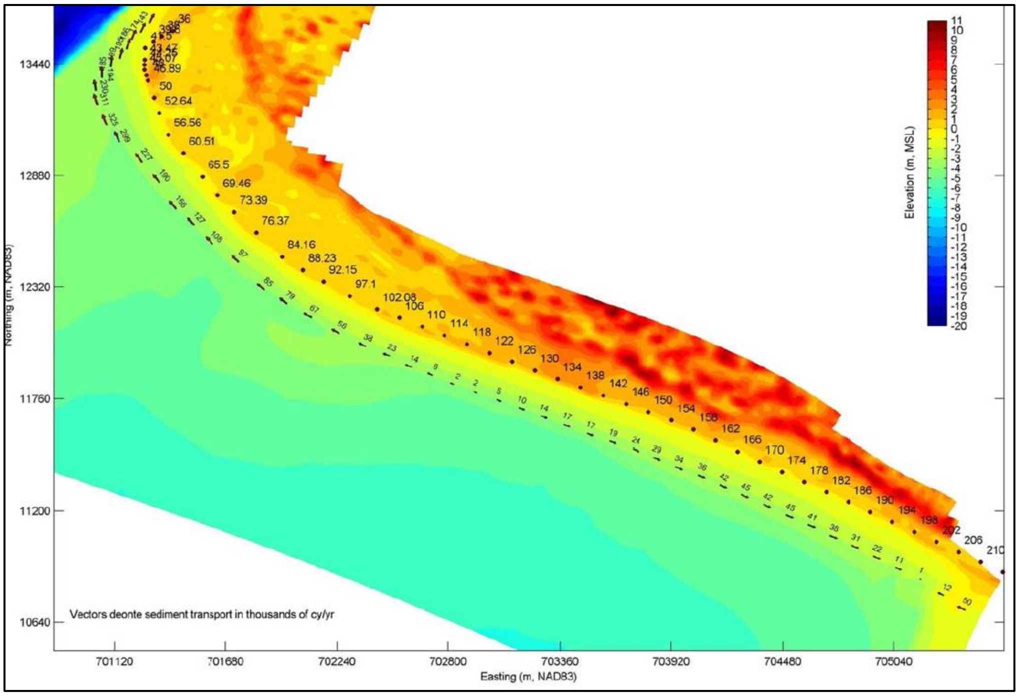

Figure 7-35: Sediment transport rates along Bald Head Island from Delft3D (Olsen Associates, Inc. 2012)

7.2.4. Model Calibration Results

7.2.4.1. Shoreline Change

Multiple GenCade model runs were completed to achieve a reasonably calibrated model. Figure 7-36 and Figure 7-37 show the final GenCade modeled shoreline changes against those measured for Bald Head Island and Oak Island, respectively. The model results matched the measured shoreline changes fairly well in most areas. The shorelines adjacent to inlets are vulnerable to tidal current induced erosion and can shift suddenly and dramatically under extreme conditions. The easternmost portion of the South Beach shoreline on Bald Head Island is highly dynamic and becomes part of Cape Fear Spit. This depositional feature is routinely subject to episodic periods of accretion and eventual detachment via tidal channel breakthrough during storms. It is highly influenced by beach fill activities and sediment added to the littoral system of South Beach as well as storm waves originating from the east or southeast. The shoreline changes adjacent to inlets and the Cape Fear spit are thus very difficult to be modeled by GenCade, a one-line model.

To determine the influence of shoreline change at the Spit on the Bald Head Island shoreline, additional runs assuming different shoreline change rates at the east lateral boundary of the Bald Head Island GenCade model were performed. The results showed that the shoreline changes west of station 170+02 were the same regardless of the Spit shoreline change rate.

Several statistical measurements are used to help assess the model shoreline change calibration results. These include the mean absolute error (*MAE*), root mean squared error (*RMSE*), correlation coefficient (*R*), and Brier Skill Score (*BSS*). These parameters are briefly described below:

$$MAE = \overline{|x - y|} \tag{25}$$

$$RMSE = \sqrt{\overline{(x - y)^2}} \tag{26}$$

$$R = \frac{\overline{xy} - \bar{x}\bar{y}}{\sqrt{\overline{x^2} - \bar{x}^2} - \sqrt{\overline{y^2} - \bar{y}^2}} \tag{27}$$

$$BSS = 1 - \frac{\overline{(x-y)^2}}{\overline{(x)^2}} \tag{28}$$

where *x* and *y* is the measured and calculated shoreline change, respectively, and "bar" denotes the sample mean.

A *BSS* (Brier Skill Score) of 1 indicates a perfect agreement between measured and calculated values; scores equal to or less than 0 indicates that the initial shoreline is as or more accurate than the calculated shoreline. Recommended qualifications for different *BSS* ranges are provided in Table 7-19 (from the Coastal Inlets Research Program (CIRP) wiki page: http://cirpwiki.info/wiki/Statistics).

Table 7-19: Brier Skill Score Qualifications

Range	Qualification
0.8<*BSS*<1.0	Excellent
0.6<*BSS*<0.8	Good
0.3<*BSS*<0.6	Reasonable
0<*BSS*<0.3	Poor
BSS<0	Bad

Table 7-20 gives the shoreline change statistics for both Bald Head Island and Oak Island shoreline calibrations. Both *R* and *BSS* values indicate very good agreements between model and observed shoreline changes.

Table 7-20: Statistics and Skill Score of Shoreline Calibrations

	Bald Head Island (52+64 – 218+02)	Oak Island (40+00 – 670+00)
MAE (ft)	11.0	13.0
RMSE (ft)	14.0	16.0
R	0.99	0.97
BSS	0.97	0.92

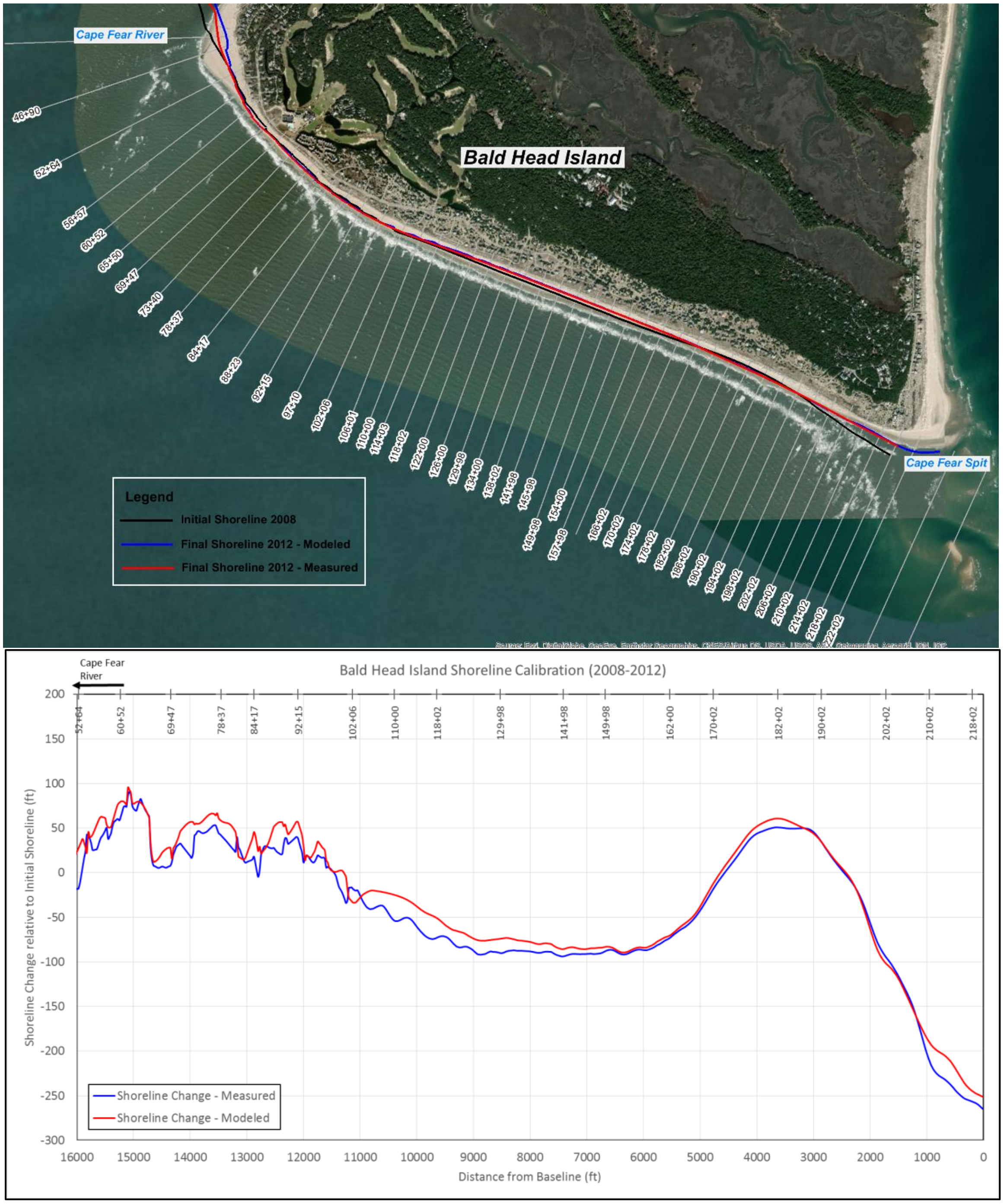

Figure 7-36: GenCade calibration – Bald Head Island shoreline changes

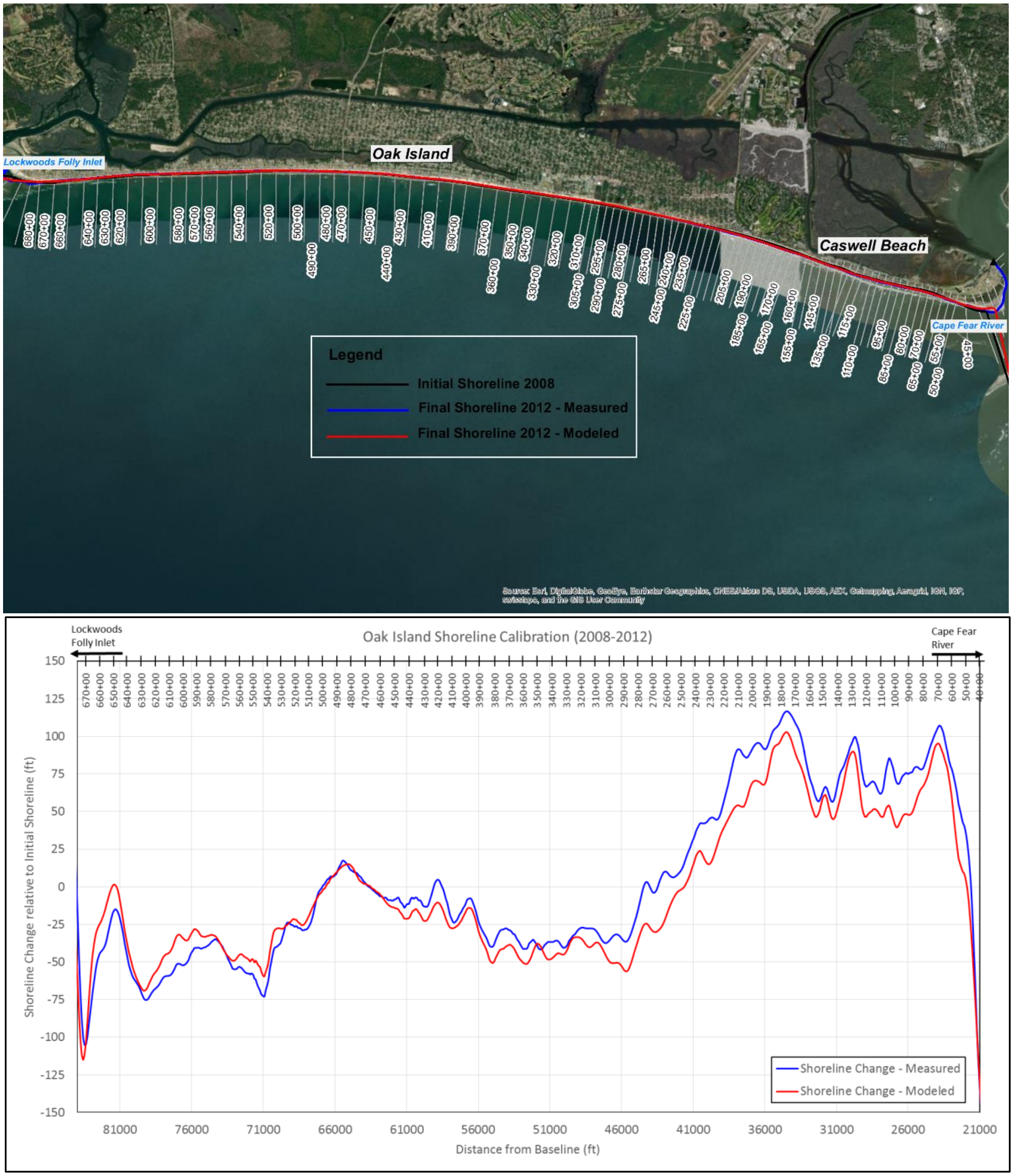

Figure 7-37: GenCade calibration – Oak Island shoreline changes

7.2.4.2. Longshore Sediment Transport

Figure 7-38 and Figure 7-39 present the calculated mean annual net longshore sediment transport rates along the Bald Head Island and Oak Island shorelines, respectively.

Along the Bald Head Island shoreline, a "nodal" point where the direction of net longshore sediment transport diverges is located near station 150 (Brown Pelican Trail) according to the GenCade model result (Figure 7-38). Olsen's 2012 Delft3D model results indicated a nodal point near station 122. The net westerly longshore sediment transport rate from GenCade is about 350,000 cy/yr directed to the Cape Fear River based on calculated value at Station 52+64, which is comparable to Olsen's model results (325,000 cy/yr) as shown in Figure 7-35.

Along the Oak Island shoreline, a nodal point is located adjacent to station 350 from the GenCade model result (Figure 7-39). The results from Thompson et al. (1999) indicated a nodal point at about 10,000 ft west of the Cape Fear River Entrance (close to station 130 at Caswell Beach). Cascade model results from USACE (2012a) did not produce a nodal point. The present study found that the net longshore sand transport rate is about 200,000 cy/yr directed to the Lockwoods Folly Inlet from Oak Island based on the calculated value at Station 650+00. The net easterly longshore transport rate from Oak Island to the Cape Fear River is about 180,000 cy/yr from the GenCade model based on the calculated value at Station 50+00.

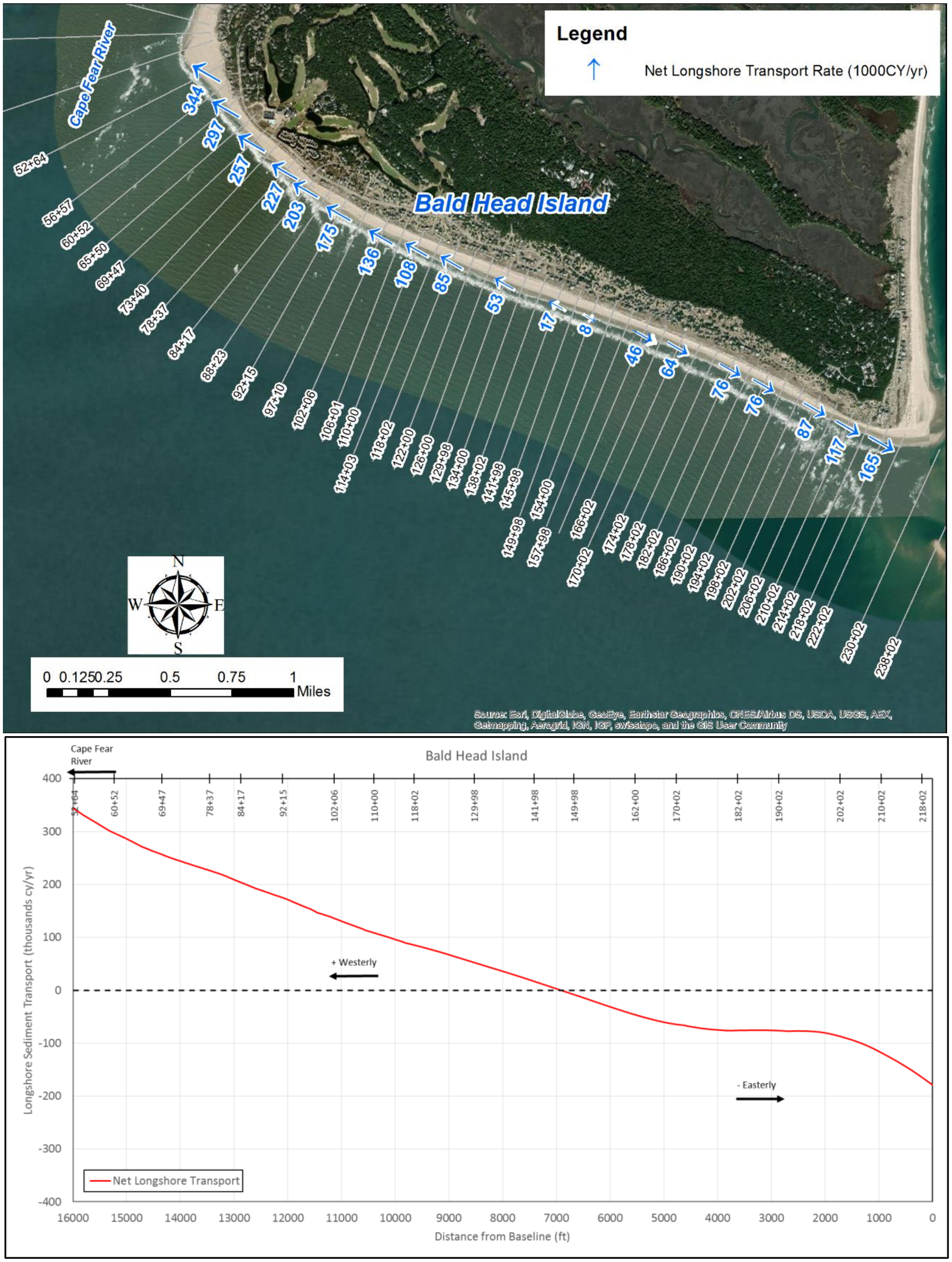

Figure 7-38: GenCade calibration – net longshore transport rate along Bald Head Island

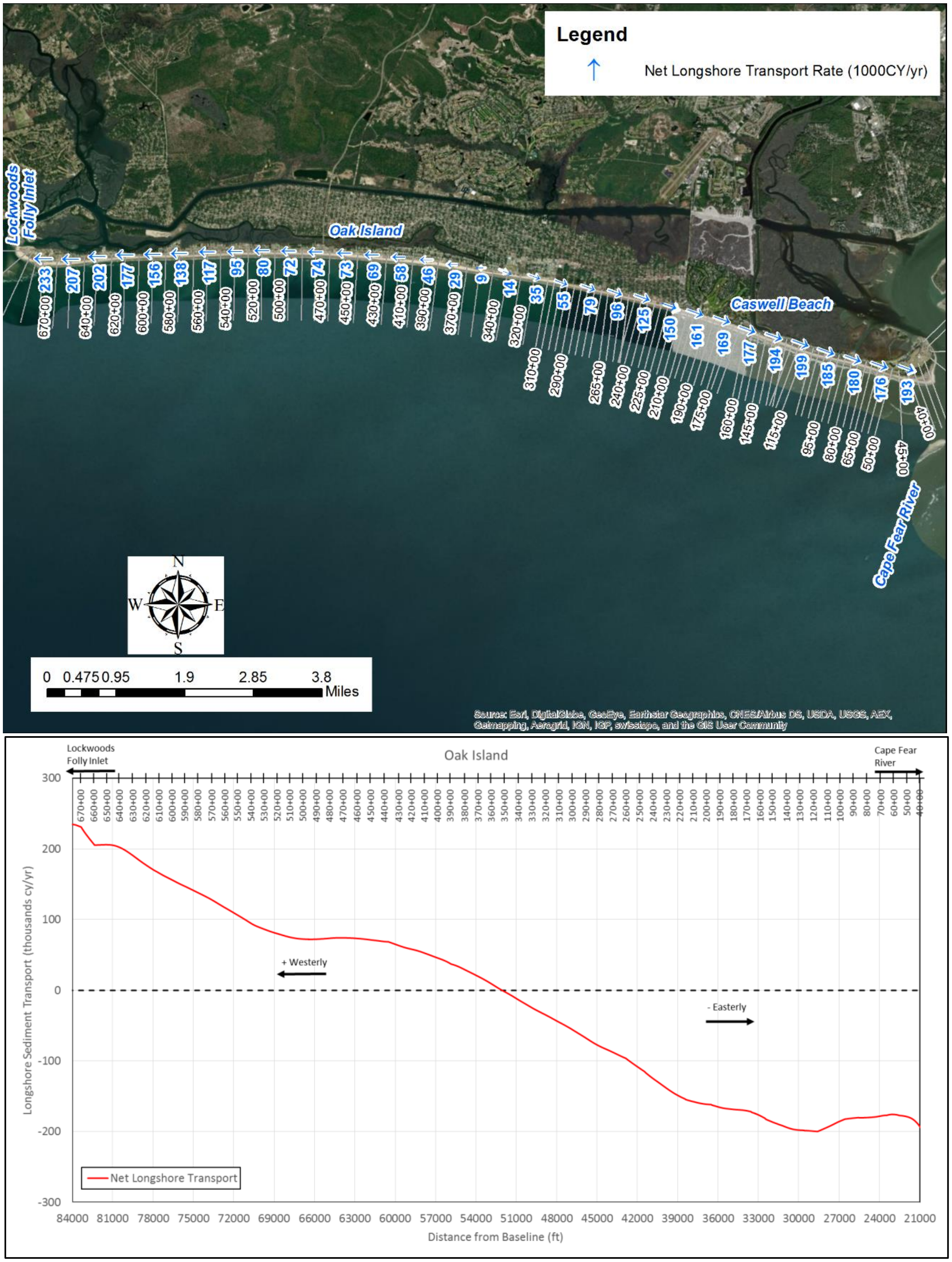

Figure 7-39: GenCade calibration – net longshore transport rate along Oak Island

7.2.5. Model Validation

The initial shoreline used in the GenCade model validation was the February 2012 Wet/Dry shoreline used as the final shoreline for model calibration. The final reference shoreline for the model validation was the February 2016 shoreline based upon 2016 NC Imagery that was digitized by NCDCM. All the GenCade model parameters were held the same as in the calibration. The groin fields on Bald Head Island were based on the 2013 aerial photo from Google Earth. To include the effect of the terminal groin, the Bald Head Island GenCade model was first run from February 2012 to November 2015 without the terminal groin, and then a hotstart run was made using the November 2015 calculated shoreline as the initial condition with the terminal groin in the GenCade setup. The last three sand tube groins were excluded during the hotstart run as well.

The Eastern Channel maintenance project in 2015 on Oak Island, and both of the 2013 and 2015 beach fill projects on Bald Head Island were included in the validation period.

Figure 7-40 presents the shoreline change validation results along Bald Head Island. Between Station 92+15 and 97+10, the model over-predicted the shoreline accretion by about 80 ft. The model predicted shoreline recession in the eastern end of shoreline adjacent to the Cape Fear Spit between Station 194+00 and 210+00; however, the digitized shoreline shows almost no change from the 2012 shoreline. Figure 7-41 depicts the variations in size and orientation of the Cape Fear Spit from aerials captured in August 2015, November 2015 and April 2016 (Olsen Associates, Inc., 2016). Between August 2015 and November 2015, the spit tip along the South Beach was turned southward due to the East Beach spit erosion and southerly extension during extreme weather conditions (Hurricane Joaquin impacted this region in October 2015). However, the April 2016 aerial shows the South Beach shoreline reverted back to the August 2015 orientation under normal wave conditions.

Figure 7-42 shows the shoreline change validation results along Oak Island. Similar to the Bald Head Island validation results, the model over-predicted shoreline change in some areas and then under-predicted shoreline changes in the immediate neighbor areas. In the western portion of Oak Island between 540+00 and 650+00, the model result shows erosion, whereas the digitized shoreline indicates accretion.

Moffatt and Nichol (2016) assessed the storm impacts of Hurricane Joaquin 2015 on the Oak Island shorelines based on July 2014 and October 2015 profile surveys. Hurricane Joaquin passed near the study area between October 4th and 5th. The impacts of Tropical Storm Ana in May 2015 along with the Eastern Channel maintenance project were also included in this survey interval. As illustrated in Figure 7-43, storm induced dune losses can cause the shoreline to either advance seaward or retreat landward. The current version of the GenCade model does not include the cross-shore sediment transport processes during storms, and thus the storm impact on the shoreline positions cannot be captured in the model results. Figure 7-44 presents the shorelines adjacent to Lockwoods Folly Inlet. The impact of extreme weather conditions on the inlet shorelines is significant.

Table 7-21 gives the shoreline change statistics for both Bald Head Island and Oak Island shoreline validations. Both *R* and *BSS* values indicate very good agreements between model and observed shoreline changes along Bald Head Island. The model performed "bad" along Oak Island when including all the shorelines, but is considered "reasonable" if the western end of the shoreline is excluded.

Table 7-21: Statistics and Skill Score of Shoreline Validations

	Bald Head Island (52+64 – 218+02)	**Bald Head Island (52+64 – 190+02)**	**Oak Island (40+00 – 670+00)**	**Oak Island (40+00 – 530+00)**
MAE (ft)	40.0	26.0	25.0	19.0
RMSE (ft)	55.0	32.0	32.0	23.0
R	0.88	0.97	-0.08	0.41
BSS	0.81	0.94	0.37	0.34

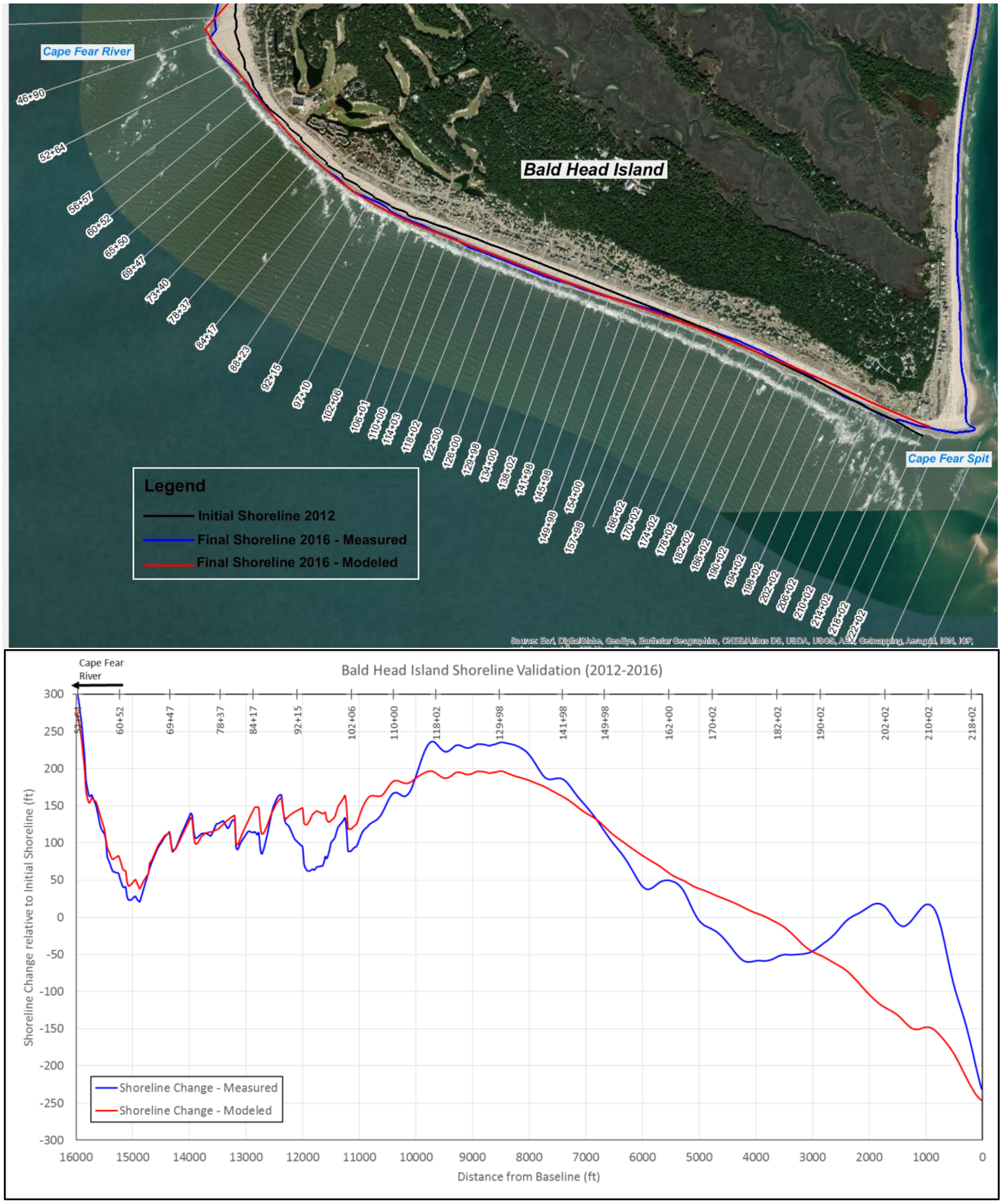

Figure 7-40: GenCade validation – shoreline change along Bald Head Island

Figure 7-41: Cape Fear Spit aerial photography (Olsen Associates, Inc., 2016)

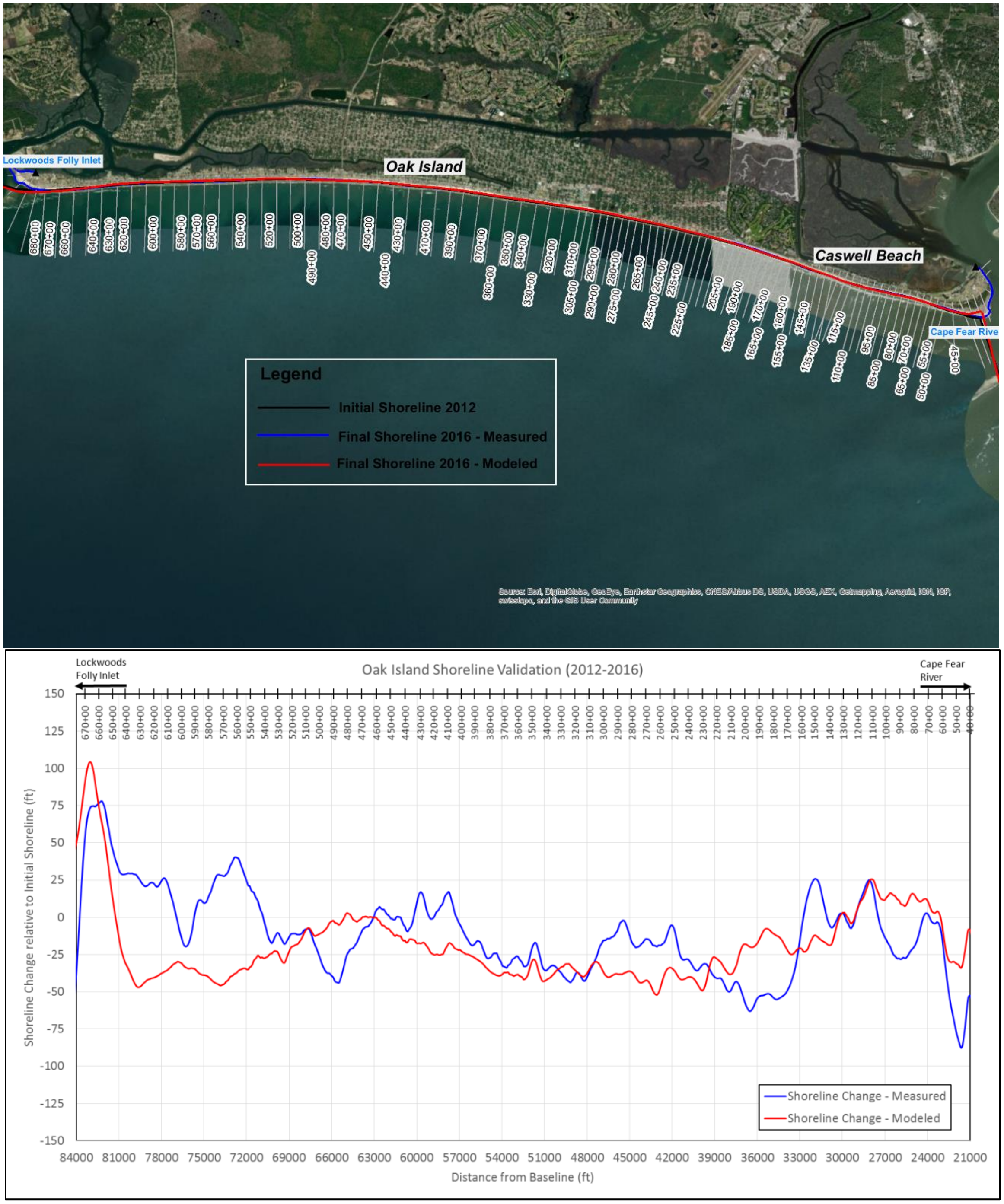

Figure 7-42: GenCade validation – shoreline change along Oak Island

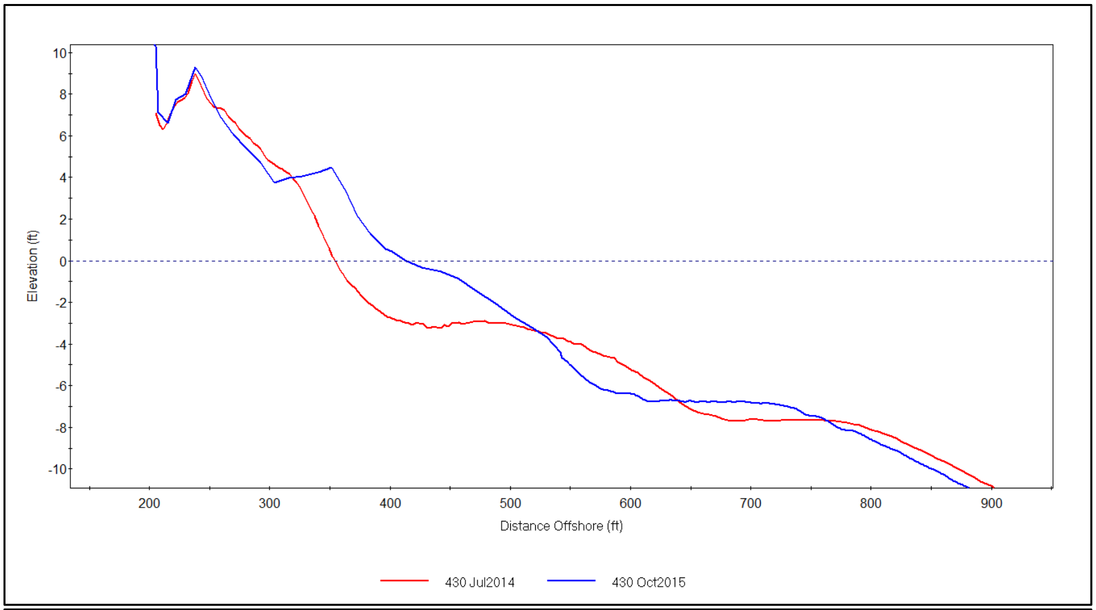

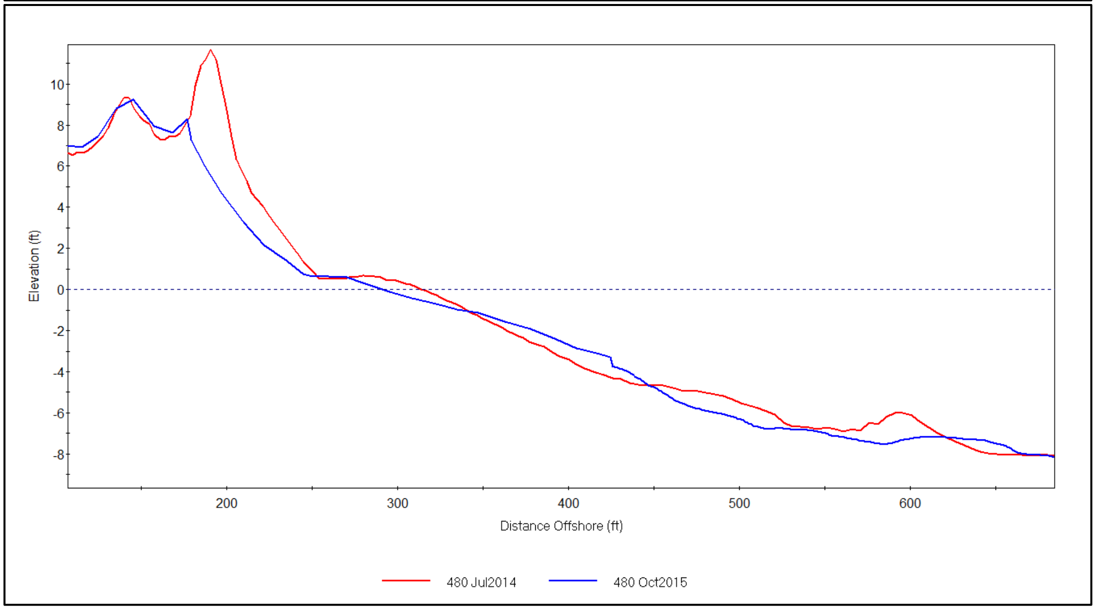

Figure 7-43: Post Hurricane Joaquin profiles surveys at Oak Island station 430 and 480

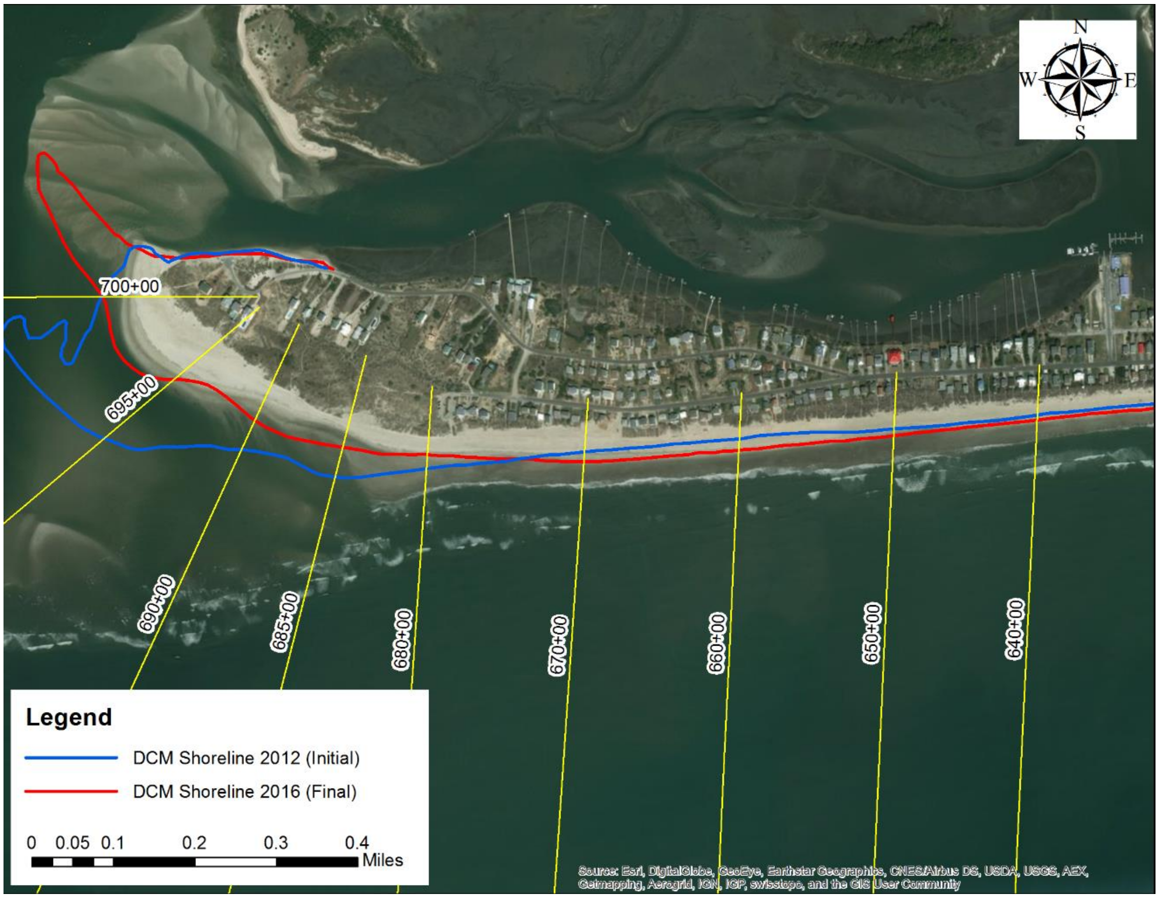

Figure 7-44: Observed shoreline changes adjacent to Lockwoods Folly Inlet from 2012 to 2016

7.2.6. Summary and Conclusions

To aid in the analysis of potential Cape Fear River navigation channel deepening impacts on the adjacent coast, shoreline change models using GenCade were developed for both the Bald Head Island and Oak Island shorelines.

The models were successfully calibrated against reference shorelines by adjusting the sediment transport parameters and regional contours.

The model calibration and validation results were affected by the exclusion of storm induced cross-shore sediment transport processes from the one-line model.

7.3. Inlet Morphology

The shoaling volumes in the entrance channel reaches (Smith Island reach, Bald Head reaches 1 and 2) and associated maintenance dredging costs are an integral part of the study of potential impacts of the Cape Fear River Deepening Project. The state-of-art numerical modeling suite Delft3D from Deltares is applied for this purpose. The model development and calibration are described in detail in the following sections.

7.3.1. Model Development

7.3.1.1. Model Grids

For the morphology modeling, sediment transport caused by both tidal flows and waves was considered. In Delft3D, this is achieved by the online coupling option between flow and waves. The modeling grids were based on the existing hydrodynamics and wave models developed for this project. The model horizontal coordinate is in North Carolina State Plane, and the vertical datum is NAVD88.

7.3.1.2. Flow Grids

The grid resolutions of the existing hydrodynamics model were not fine enough in the nearshore region of the study area to capture the sediment transport magnitudes along adjacent beaches and resulted shoaling rates in the Cape Fear River entrance channels. In order to keep a reasonable model run time, a nested flow modeling approach was adopted for the morphology modeling. The full hydrodynamics model was used to generate the model boundary conditions for a detailed local morphology model grid. In Delft3D, an "offline" nesting approach is adopted for the hydrodynamics model where the full model run is completed first and the relevant boundary data are then extracted and used in the nested model.

Figure 7-45 shows the local morphology model grid along with the full hydrodynamics model grid. The local morphology grid (red) is comprised of 575,113 cells with cross-shore resolution of ~10 m in the nearshore, covering the Bald Head Island South Beach shoreline and half of the Oak Island shoreline. Its upstream boundary is in the Upper Midnight channel range near the AIWW connection at Carolina Beach

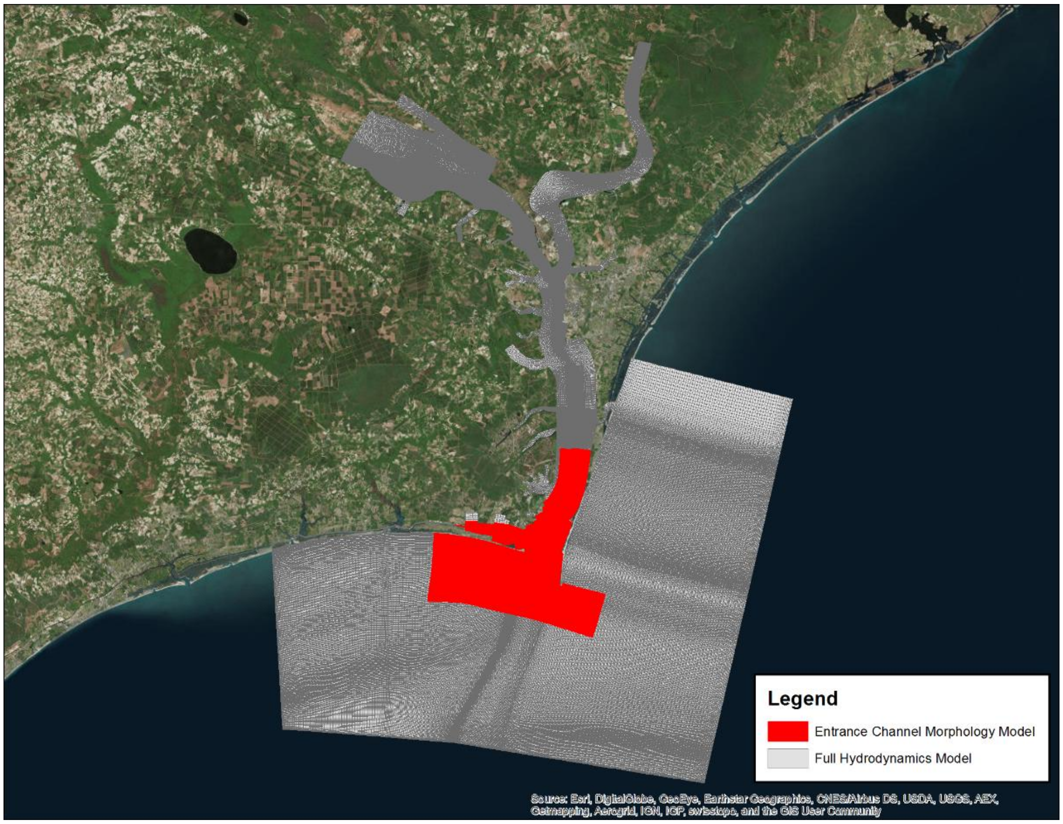

Figure 7-45: Entrance channel morphology grid

7.3.1.3. Wave Grids

Similar to the offshore wave modeling study, the nested wave modeling approach was applied to determine the wave induced currents in the nearshore. The offshore wave grid was the same as in the offshore wave study. The fine wave model grid was the same as the local morphology model grid except it was ended near Southport where wave propagation upstream ceases. Figure 7-46 shows the wave grids used for the morphology modeling.

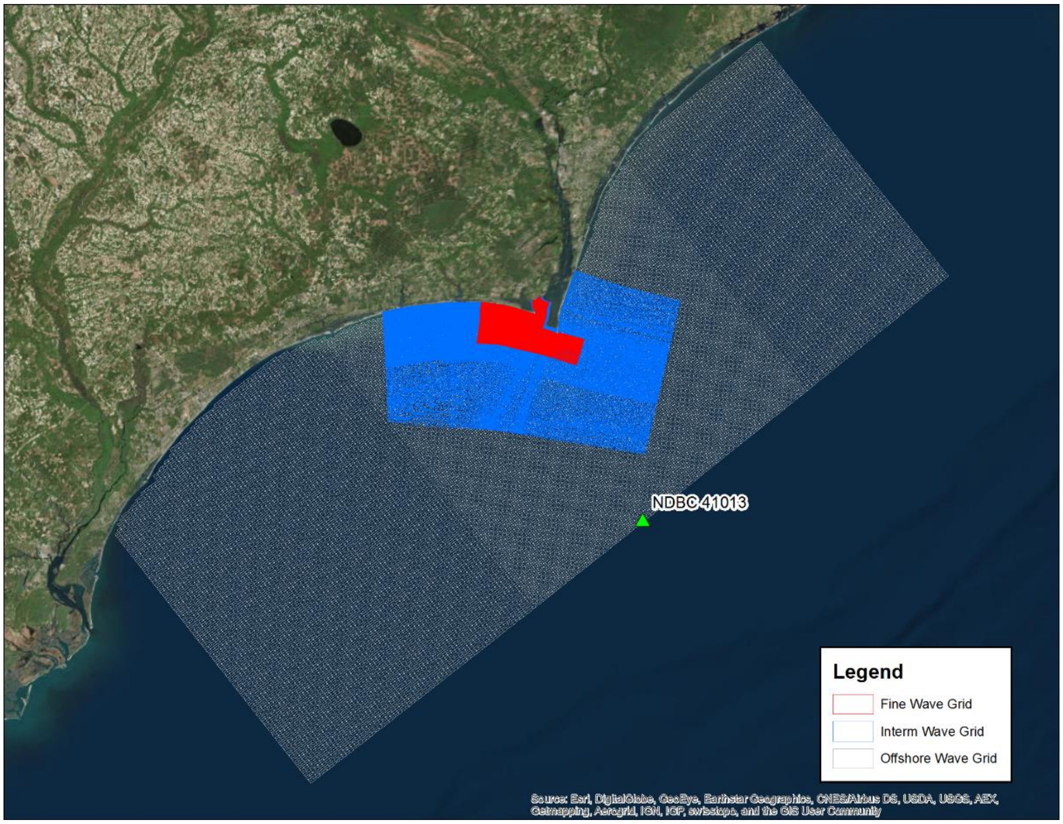

Figure 7-46: Wave grids for morphological modeling

7.3.2. Model Bathymetry

Bathymetric data from different sources were compiled and processed to cover the entire computational domains. All bathymetric datasets were adjusted to the North American Vertical Datum of 1988 (NAVD88). The data sources used for the morphology model bathymetry developments are listed in Table 7-22 from high priority to low priority. The most recent bathymetry data were selected where available to create the model bathymetry.

A terminal groin was constructed on the western tip of South Beach on Bald Head Island between June and December 2015. A fillet beach was also constructed east of the terminal groin. The November 2015 Bald Head Island beach profile surveys reported by Olsen Associates (2017) from STA 046+89 to STA 065+50 were digitized and integrated into the morphology model bathymetry in order to capture the sediment volume transported from Bald Head Island to the entrance channel bypassing the terminal groin head.

Figure 7-47 presents the full bathymetry for model calibration, whereas Figure 7-48 shows the river entrance area along with the channel range names.

Table 7-22: Morphological model bathymetry data sources

Data Set	Source
Wilmington Harbor hydrographic surveys	USACE 2016 – 2017
Fugro channel bank surveys	Fugro 2016 – 2017
Oak Island post Matthew beach profile surveys (STA 210+00 – 700+00)	TI Coastal 2016
Bald Head Island beach profile surveys (STA 000+00 – 238+00)	USACE 2013
Oak Island beach profile surveys (STA 005+00 – 210+00)	USACE 2012
Cape Fear River 2010 surveys	USACE 2010
NOAA hydrographic surveys	NOAA 1973 – 2007
NOAA Navigation Charts	MIKE C-MAP
ADCIRC bathymetry	NCDPS 2011
NC LiDAR	NOAA 2014 – 2016

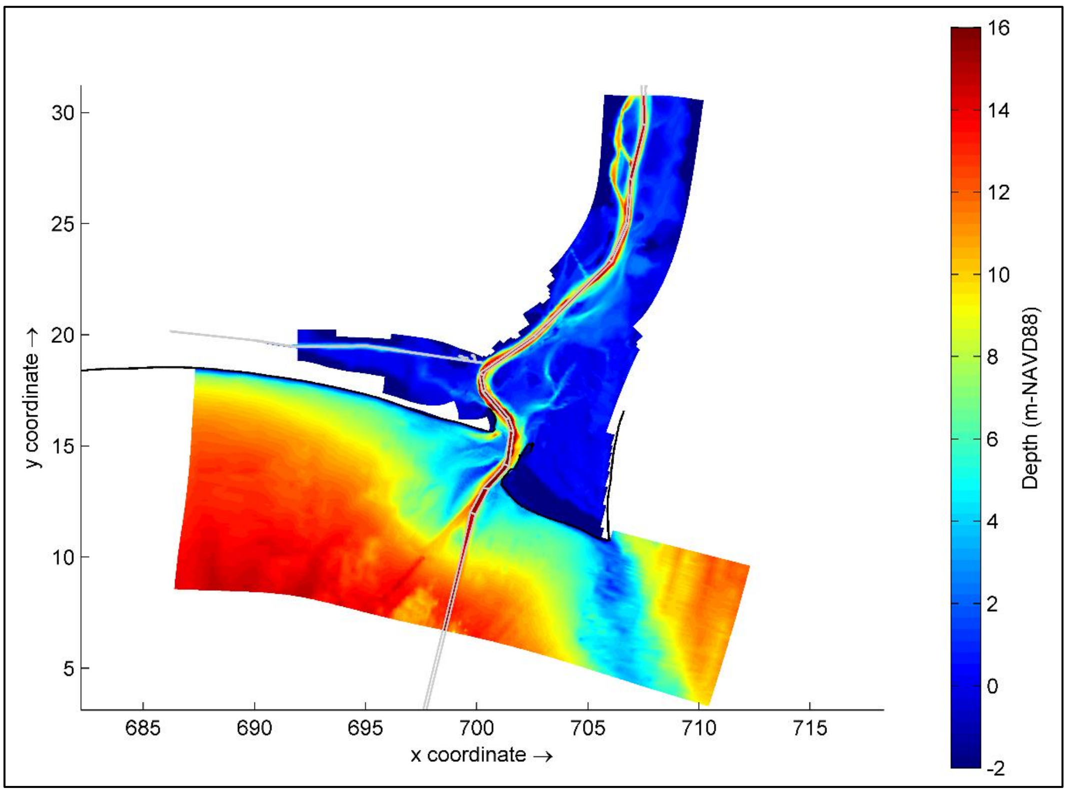

Figure 7-47: Entrance channel morphology model bathymetry

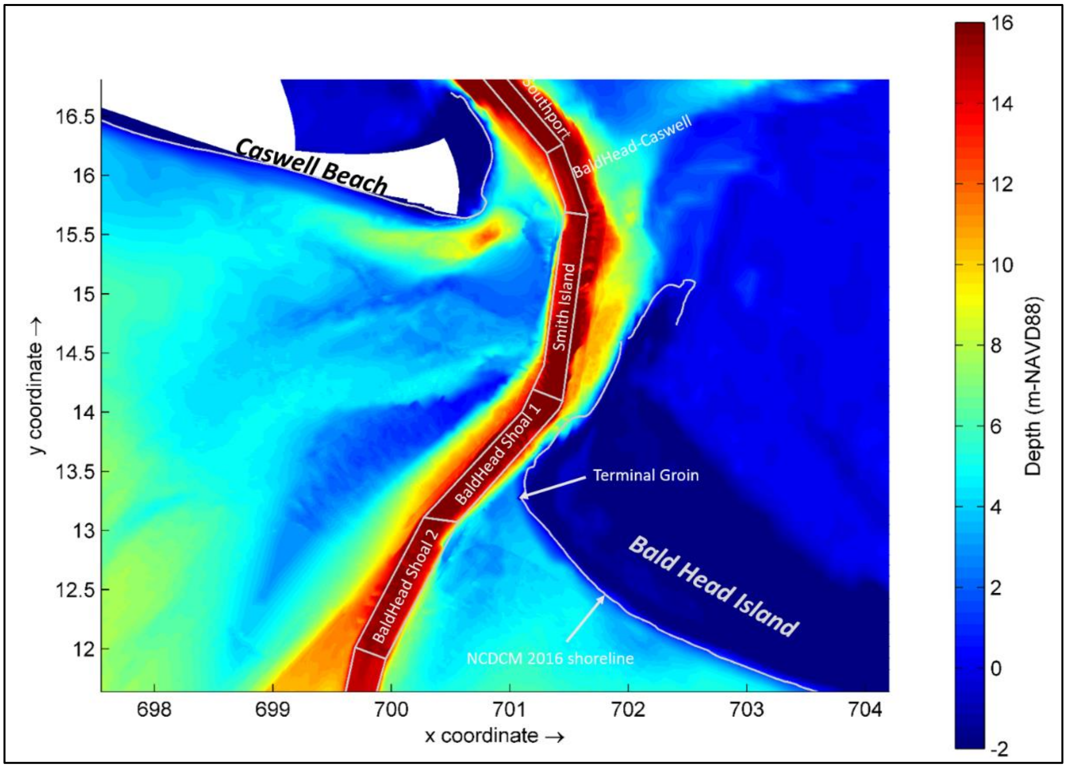

Figure 7-48: Entrance channel morphology model bathymetry near the river entrance

7.3.3. Model Inputs

7.3.3.1. Water level

Similar to the hydrodynamics model calibration (Moffatt & Nichol, 2018), tidal boundary conditions were used for this study in the offshore. The tidal constituents were extracted from the Oregon State University (OSU) tidal database based on TOPEX/Poseidon satellite altimetry data (Egbert et al., 1994).

<u>Tide Schematization</u>

Modeling long term (1 year in this study) sediment transport and the resulting coastal morphology in Delft3D using a real-time series of the astronomical tide as input would lead to unsustainably long run times. In order to avoid this problem, the real-time series is converted into a representative semi-diurnal tidal cycle, called a morphological or schematized tide. It is a proxy representation of average tidal fluctuations each month through the year. For the purposes of this investigation, the schematized tide was based on a method developed by Lesser (2009).

This method creates a representative tide fluctuation based on input values of the M2, K1 and O1 constituents, where the resulting tidal time series is based upon the following relationship:

$$\eta = Corr * M2\cos(\omega_{M2}t + \varphi_{M2}) + C1\cos(\omega_{C1}t + \varphi_{C1}) \quad (29)$$

$$C1 = \sqrt{2 * O1 * K1} \text{ and } \varphi_{C1} = 0.5(\varphi_{K1} + \varphi_{O1}) \quad (30)$$

Where, η is water surface elevation, ω denotes angular frequency of tidal constituents, φ denotes phase offset of tidal constituents, M2 is the semi-diurnal tidal constituent, C1 is the diurnal astronomical tidal constituent with amplitude and phase described as a function of O1 and K1 constituents, and Corr = correction factor for M2 tide.The tidal periods of the M2 and C1 constituents were set equal to 750 minutes (semi-diurnal) and 1500 minutes (diurnal), respectively for this study.

The purpose of the morphological tide is to represent the average currents and sediment transport that occur during a spring-neap tide cycle. This requires a morphological tide which is slightly above the mean tide given that the sediment transport attributable to the spring tide is typically larger than that attributable to the neap tide. The application of the correction factor, Corr, listed above accounts for the disproportionate spring-neap contributions to sediment transport. A typical value of 1.08 (Lesser, 2009) was adopted for this study.

A test was performed to compare morphological changes computed using the model forced with the astronomical tide and with the representative morphological tide. Figure 7-49 shows the simulated morphological change differences after one year between the morphological tide and the astronomical tide with a 0.25 mm sediment grain size. Waves were excluded during the model simulations. The result indicates that the differences occur mostly in the eastern tip of Caswell Beach and the western tip of Bald Head Island.

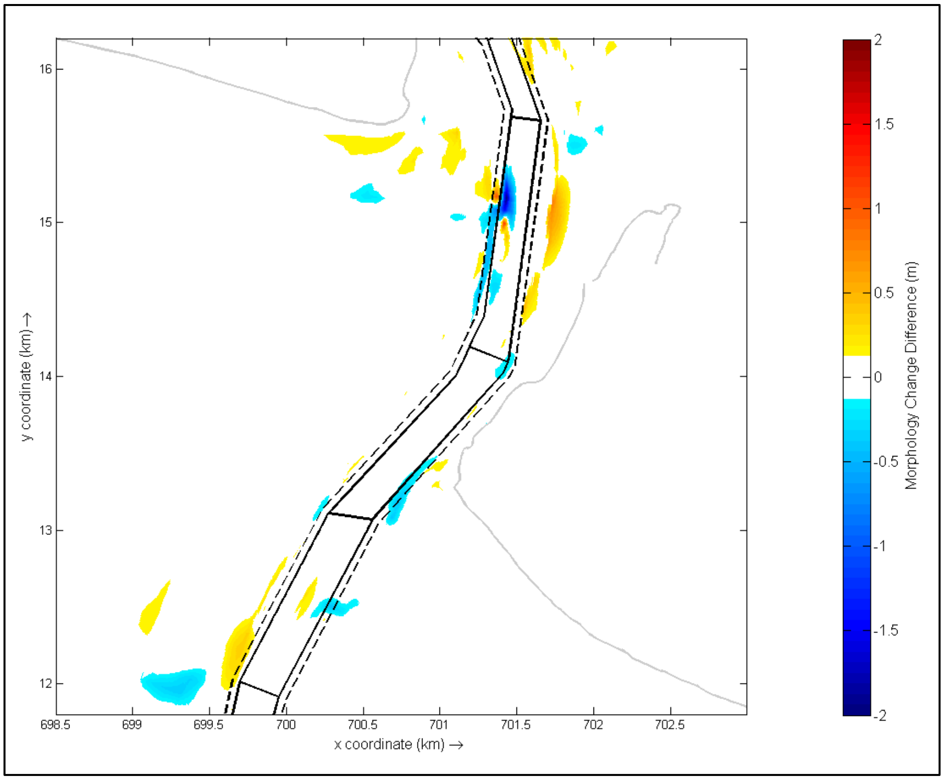

Figure 7-49: Morphological change differences between the morphological tide and the astronomical tide

7.3.3.2. Waves

The measured wave data from 2004 to 2017 at the NOAA NDBC Buoy station 41013 were the primary source of wave conditions for the morphology modeling. The data gaps in the buoy data were filled with available USACE WIS hindcast data and NOAA WW3 hindcast data at locations close to Station 41013. The WIS hindcast data were available till 2014, and WW3 data were used to fill the data gaps afterwards. The combined wave data were in an hourly time interval.

Figure 7-50 shows the wave rose of the significant wave height at the offshore boundary from the combined wave records. It indicates that the dominant wave direction in the offshore region of the project area is from the ESE. However, the largest waves are more frequently from ENE and S.

Wave Schematization

Modeling long term (1 year in this study) sediment transport and coastal morphology in Delft3D using a real-time series of waves as input would lead to unsustainably long run times. In order to avoid this problem, the wave data at the model boundary were numerically analyzed in order to derive a limited but representative set of wave conditions to be used as input into the morphology model. The goal is to reduce the wave conditions into a few classes without losing much accuracy in the morphological impact of these waves compared to the full wave time series.

To select the representative waves, two frequently used approaches exist (Van Rijn, 2012):

- The first approach is to manually determine the wave classes based on the wave height, direction and morphological impact. The morphological impact is assumed to be proportional to the wave height to some power and is derived from the CERC formula for longshore sediment transport at a uniform coastline.

- The second approach uses "target" datasets. The target datasets are usually created by short morphological simulations of all wave height-direction combinations and are weighted afterwards based on their percentage of occurrence. After the weighting, the target datasets are assumed to be representative for the morphological development of the full wave climate. The approach can be further divided into the so-called "optimum selection" (OPTI-method), or the method of correlation. The OPTI-method is more suited when several wave classes have to be determined than the method of correlation.

Olsen Associates, Inc. (2012) applied the first approach to select a set of representative waves in their Delft3D modeling of Bald Head Island beach morphology changes and later for the Bald Head Island shoreline stabilization alternative analysis (Olsen Associates, Inc., 2013) as part of the terminal groin EIS study (USACE, 2014). However, this approach does not account for the wave transformation through irregular nearshore bathymetry and uses a different method for sediment transport (the CERC formula) than what's used in the actual morphology modeling within Delft3D. This method is somewhat dependent on personal subjective judgements when selecting representative waves.

In this study, the wave class selection for the wave climate schematization with multiple classes is based on the OPTI-method (Mol, 2007). The OPTI-method is considered a more objective method, as the wave class selection will be the same regardless of whoever is using it when the same model setups are applied. It is a tool developed for Delft3D usage, so it ensures that the same sediment transport formula is used for both the representative wave class selection and the morphology modeling afterward. The overall procedure of the OPTI-method is visualized in Figure 7-51.

The combined offshore wave data at 41013 were divided into 1-m magnitudinal and 15-degree directional classes, which resulted in 95 total different combinations of wave heights and directions as shown in Table 7-23 where waves traveling toward offshore were disregarded. These waves account for 83% of the total offshore wave climate. The mean significant wave height (H_s), mean peak wave period (T_p) and mean peak wave direction (D_p) were calculated and used as the representative wave condition for each wave class. For each wave class, a coupled flow and wave model run with sediment transport but no morphology updating was conducted with a constant water level at MSL for a half day period simulation when a quasi-steady state sediment transport rate condition was achieved. In this way, only the wave induced sediment transport was considered when determining the representative waves. Two "target" datasets were used for the OPTI-method in this study: net and gross annual transport rates through 40 predefined cross-shore transects as shown in Figure 7-52. These transects match the profile monitoring transects for both the Bald Head Island and Caswell Beach periodic surveys conducted by

USACE as part of the Wilmington Harbor Sediment Management Plan (WHSMP). After conducting the OPTI analysis, the final selected 6 wave classes were chosen and are listed in Table 7-24. These wave classes were used later for the 1-year morphology model runs.

Significant Wave Height (Annual)
Station 41013_comb_NDBC_WIS_WW3
Period 01–Jan–2004 to 31–Dec–2017

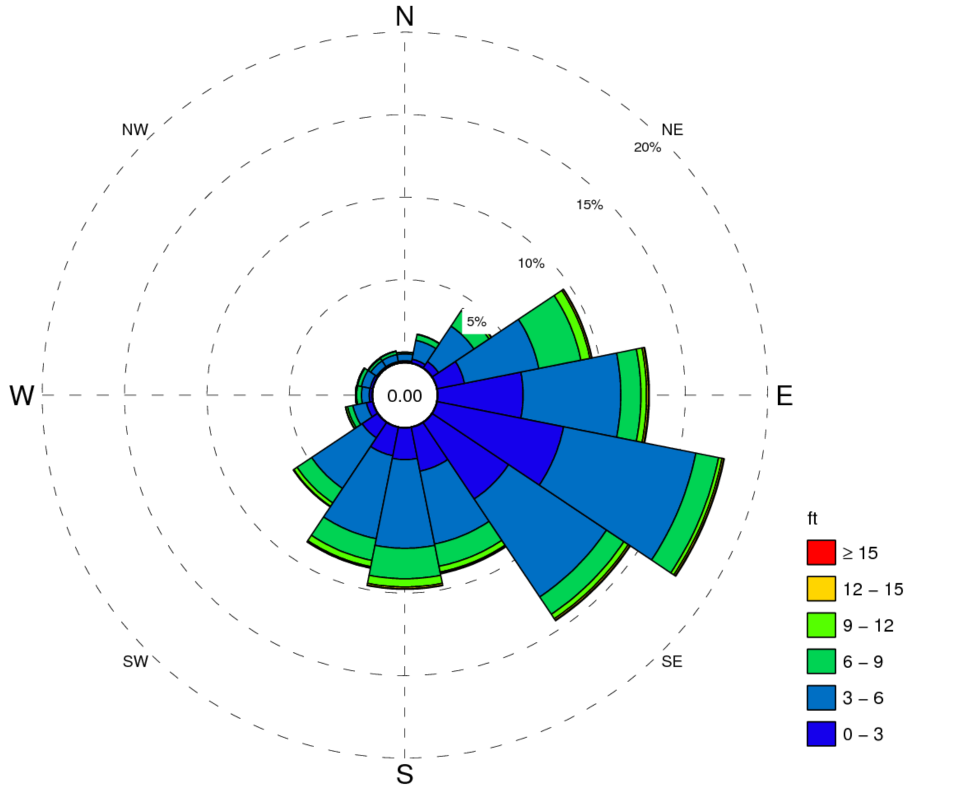

Direction FROM is shown
Center value indicates calms below 0 ft
Total observations 122736, calms 0
No missing observations

Percentage of Occurrence

Significant Wave Height, ft	N	NNE	NE	ENE	E	ESE	SE	SSE	S	SSW	SW	WSW	W	WNW	NW	NNW	Total
Total	0.61	1.77	4.31	9.56	12.83	17.75	14.45	9.04	9.76	8.69	6.14	1.67	1.00	0.97	0.71	0.73	100.00
15 –																	0.22
12 – 15				0.11	0.12	0.11	0.11		0.11								0.78
9 – 12			0.15	0.56	0.35	0.22	0.33	0.35	0.50	0.39	0.24	0.12					3.37
6 – 9	0.10	0.36	1.11	2.60	1.22	1.40	1.26	1.38	1.85	1.34	1.06	0.33	0.30	0.24	0.17	0.20	14.92
3 – 6	0.42	1.17	2.58	4.60	5.92	8.18	7.14	4.50	5.37	5.13	3.68	0.84	0.47	0.55	0.43	0.43	51.43
0 – 3		0.22	0.45	1.68	5.17	7.81	5.57	2.69	1.91	1.74	1.12	0.38	0.16	0.14			29.28

Figure 7-50: Wave rose of significant wave height at the offshore boundary (2004 – 2017)

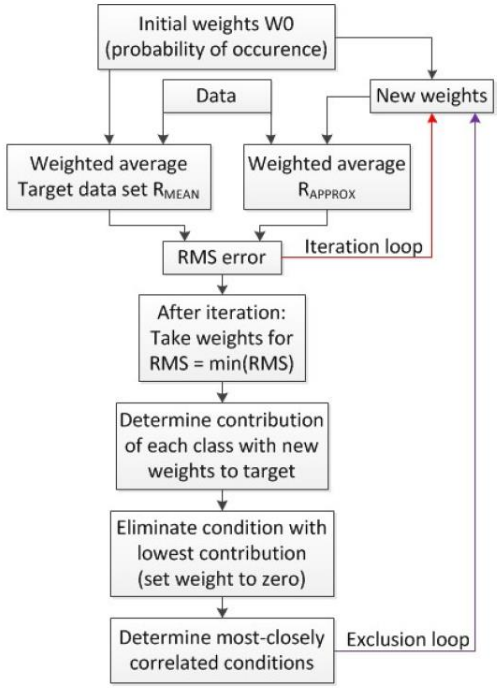

Figure 7-51: Overview of OPTI-method procedure modified from Van Rijn (2012)

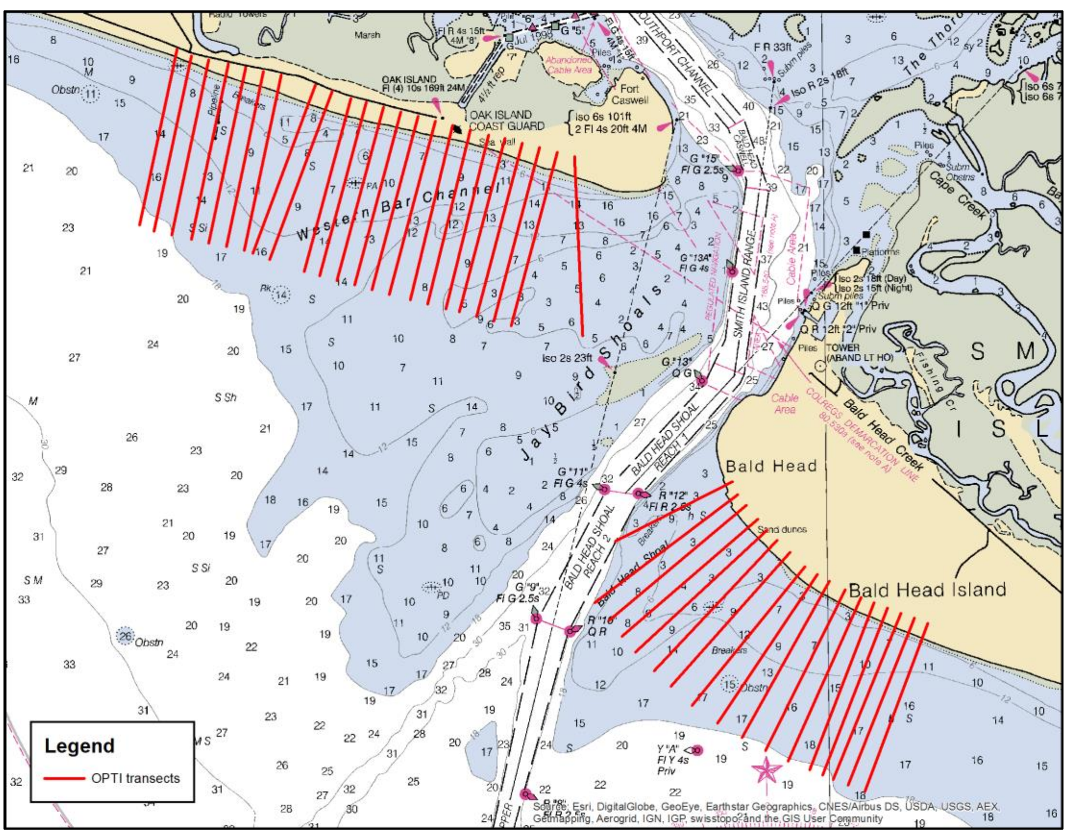

Figure 7-52: Transects for OPTI-method

Table 7-23: Wave climate classes at model offshore boundary

Wave height bin (m)	Wave direction bin (°N)	Mean H_s (m)	Mean T_p (s)	Mean D_p (°N)	Mean wind speed (m/s)	Joint probability of occurrence (%)
0 - 1	75 - 90	0.8	8.9	83.2	4.3	3.332
1 - 2	75 - 90	1.4	8.6	82.6	7.0	3.044
2 - 3	75 - 90	2.4	8.8	81.1	11.4	0.771
3 - 4	75 - 90	3.3	10.2	82.6	14.1	0.153
4 - 5	75 - 90	4.4	12.3	83.1	16.8	0.045
5 - 6	75 - 90	5.4	13.7	80.8	21.2	0.015
6 - 7	75 - 90	6.2	13.6	87.2	22.2	0.003
0 - 1	90 - 105	0.8	9.0	97.8	4.3	4.891
1 - 2	90 - 105	1.3	9.5	97.9	6.4	3.918
2 - 3	90 - 105	2.4	10.0	97.2	9.9	0.647
3 - 4	90 - 105	3.4	11.8	97.1	12.0	0.173
4 - 5	90 - 105	4.3	12.4	97.9	15.1	0.055
5 - 6	90 - 105	5.3	13.9	99.0	16.6	0.017
6 - 7	90 - 105	6.3	13.1	98.0	18.7	0.002
0 - 1	105 - 120	0.7	8.9	112.5	4.2	6.345
1 - 2	105 - 120	1.3	9.4	112.4	6.3	4.963
2 - 3	105 - 120	2.3	9.6	112.8	10.1	0.696
3 - 4	105 - 120	3.4	10.9	112.3	12.6	0.125
4 - 5	105 - 120	4.3	12.3	112.0	14.6	0.037
5 - 6	105 - 120	5.4	11.2	115.9	17.8	0.005
6 - 7	105 - 120	6.3	12.3	115.8	20.7	0.002
7 - 8	105 - 120	7.1	15.3	115.1	22.3	0.002
0 - 1	120 - 135	0.8	8.6	126.9	4.3	5.566
1 - 2	120 - 135	1.4	9.0	127.2	6.2	4.642
2 - 3	120 - 135	2.4	9.7	127.1	9.2	0.735
3 - 4	120 - 135	3.4	10.1	128.1	12.8	0.131
4 - 5	120 - 135	4.4	10.2	126.7	16.3	0.030
5 - 6	120 - 135	5.5	11.3	128.7	20.9	0.011
6 - 7	120 - 135	6.2	12.2	130.1	23.9	0.002
8 - 9	120 - 135	8.2	14.8	128.6	21.9	0.002
0 - 1	135 - 150	0.8	8.0	141.6	4.5	3.427
1 - 2	135 - 150	1.4	8.4	141.9	6.4	3.626
2 - 3	135 - 150	2.4	9.0	142.4	9.6	0.595
3 - 4	135 - 150	3.5	10.0	142.2	12.5	0.192
4 - 5	135 - 150	4.3	10.4	142.1	14.9	0.055
5 - 6	135 - 150	5.6	11.1	142.9	20.6	0.012
6 - 7	135 - 150	6.2	12.3	142.6	21.9	0.003
7 - 8	135 - 150	7.7	15.9	141.2	23.4	0.002

Wave height bin (m)	Wave direction bin (°N)	Mean H_s (m)	Mean T_p (s)	Mean D_p (°N)	Mean wind speed (m/s)	Joint probability of occurrence (%)
8 - 9	135 - 150	8.4	14.8	143.3	19.5	0.001
0 - 1	150 - 165	0.8	7.1	156.9	4.7	2.262
1 - 2	150 - 165	1.4	7.4	157.3	6.9	2.763
2 - 3	150 - 165	2.4	8.2	157.7	9.8	0.721
3 - 4	150 - 165	3.4	9.3	157.1	12.5	0.164
4 - 5	150 - 165	4.5	9.6	157.5	16.3	0.037
5 - 6	150 - 165	5.3	11.1	154.1	19.8	0.007
6 - 7	150 - 165	6.3	11.9	154.8	22.3	0.003
7 - 8	150 - 165	7.3	13.0	159.0	35.2	0.001
0 - 1	165 - 180	0.8	6.1	172.3	5.1	1.797
1 - 2	165 - 180	1.4	6.7	172.6	7.2	3.175
2 - 3	165 - 180	2.4	8.0	172.6	10.4	0.979
3 - 4	165 - 180	3.4	9.0	173.1	13.2	0.199
4 - 5	165 - 180	4.4	9.6	173.5	16.4	0.024
5 - 6	165 - 180	5.4	11.2	169.7	16.7	0.004
6 - 7	165 - 180	6.3	12.0	175.7	21.5	0.004
7 - 8	165 - 180	7.9	13.8	169.7	21.1	0.002
8 - 9	165 - 180	8.2	14.2	170.8	21.3	0.002
0 - 1	180 - 195	0.8	5.5	187.0	5.3	1.621
1 - 2	180 - 195	1.4	6.4	187.2	7.7	3.505
2 - 3	180 - 195	2.4	8.0	186.6	11.1	1.060
3 - 4	180 - 195	3.4	9.2	187.1	13.9	0.227
4 - 5	180 - 195	4.3	9.8	186.5	16.5	0.042
5 - 6	180 - 195	5.4	11.2	186.6	19.1	0.006
6 - 7	180 - 195	6.2	12.8	183.0	19.0	0.001
0 - 1	195 - 210	0.8	5.1	202.0	5.5	1.628
1 - 2	195 - 210	1.4	6.0	202.4	8.3	3.301
2 - 3	195 - 210	2.4	7.6	201.7	11.9	0.743
3 - 4	195 - 210	3.4	8.9	201.9	14.6	0.203
4 - 5	195 - 210	4.3	9.4	201.5	17.3	0.035
5 - 6	195 - 210	5.2	10.3	197.5	18.7	0.002
0 - 1	210 - 225	0.8	4.9	216.9	5.9	1.302
1 - 2	210 - 225	1.4	5.8	217.1	9.0	3.077
2 - 3	210 - 225	2.4	7.2	217.4	12.6	0.671
3 - 4	210 - 225	3.4	8.3	217.9	15.3	0.123
4 - 5	210 - 225	4.3	9.4	215.7	17.6	0.011
0 - 1	225 - 240	0.8	4.6	231.3	6.4	0.711
1 - 2	225 - 240	1.4	5.5	230.8	9.6	1.606
2 - 3	225 - 240	2.4	7.0	231.1	13.4	0.374

Wave height bin (m)	Wave direction bin (°N)	Mean H_s (m)	Mean T_p (s)	Mean D_p (°N)	Mean wind speed (m/s)	Joint probability of occurrence (%)
3 - 4	225 - 240	3.3	8.3	231.0	15.5	0.076
4 - 5	225 - 240	4.3	9.2	228.9	17.2	0.007
0 - 1	240 - 255	0.8	4.9	246.4	6.8	0.310
1 - 2	240 - 255	1.4	5.6	246.2	9.8	0.534
2 - 3	240 - 255	2.4	6.7	246.5	13.7	0.189
3 - 4	240 - 255	3.3	7.4	247.0	15.9	0.040
4 - 5	240 - 255	4.1	7.5	249.3	17.7	0.002
0 - 1	255 - 270	0.8	4.8	261.3	6.8	0.174
1 - 2	255 - 270	1.4	5.4	262.0	10.1	0.327
2 - 3	255 - 270	2.4	6.3	262.4	13.6	0.168
3 - 4	255 - 270	3.3	6.9	261.3	16.1	0.042
4 - 5	255 - 270	4.6	8.2	259.0	20.6	0.002
0 - 1	270 - 285	0.8	5.0	277.2	6.6	0.117
1 - 2	270 - 285	1.5	5.3	277.5	10.3	0.346
2 - 3	270 - 285	2.4	6.2	276.7	13.9	0.152
3 - 4	270 - 285	3.5	7.2	277.1	18.9	0.019
4 - 5	270 - 285	4.4	8.0	277.6	19.4	0.002
5 - 6	270 - 285	5.1	8.8	277.3	24.2	0.001

Table 7-24: Wave schematization results from OPTI-method and morfac

No. wave class	Significant wave height (m)	Peak wave period (s)	Peak wave direction (°N)	Wind speed (m/s)	Wind direction (°N)	Original weight (%)	OPTI calculated weight (%)	Morfac
1	2.4	8.2	157.7	9.8	157.7	0.72	3.53	12.4
2	2.4	8.0	172.6	10.4	172.6	0.98	0.14	0.5
3	3.4	9.0	173.1	13.2	173.1	0.20	2.34	8.2
4	2.4	7.6	201.7	11.9	201.7	0.74	1.48	5.2
5	1.4	5.8	217.1	9.0	217.1	3.08	16.83	16.7
6	2.4	7.0	231.1	13.4	231.1	0.37	2.12	7.4

7.3.3.3. Winds

For this study, the winds were used only in the wave model and considered spatially uniform across the model domain. Wind generated currents were thus not considered. The wind data from the offshore NOAA station 41013 were used for the morphology modeling.

Wind Schematization

The mean wind speed in each wave class was used as the representative wind condition. The wind directions were assumed to be the same as the incoming offshore wave directions. The wind schematization results are listed in Table 7-24.

7.3.3.4. Morphological Time Scale Factor (morfac)

Morphological developments take place on a time scale several times longer than typical flow changes. For example, tidal flows change significantly in a period of hours, whereas it may take weeks, months, or years for significant morphological changes of a coastline. Simulating long term morphological changes in real-time is simply not practical from a computational point of view. To address this problem, Delft3D adopted a technique called "morphological time scale factor" whereby the speed of the changes in the morphology is scaled up to a rate that it begins to have a significant impact on the hydrodynamic flows (Deltares, 2016a). The implementation of the morphological time scale factor (morfac) is achieved by simply multiplying the erosion and deposition fluxes to and from the bed by the morfac, at each computational time-step. This allows accelerated bed-level changes to be incorporated dynamically into the morphological calculations.

For the purpose of this study, the time-varying morfac method was used. During a morphological simulation, each of the selected wave conditions in Table 7-24 was simulated for the duration of one or more morphological tides (1500 minutes) in order to account for the random phasing between waves and tides that occurs in nature. Morfac was then used to increase the morphological changes occurring during this period to the changes that would occur during the entire duration of occurrence of that wave condition in one year. For each wave condition, the morfac applied was dependent on the percentage occurrence of that particular wave condition. This approach has the desirable effect that higher morfac are applied to the more common, and generally smaller, wave conditions during which the morphology is less active, and smaller acceleration factors are applied to the larger (and less common) wave conditions (when the morphology is more active and large morfac might cause a problem). The morfac applied to each wave condition is indicated in Table 7-24.

The maximum morfac applied was decided to be no more than 20. The reason for this is that changes in morphology influence the hydrodynamics. When the morphological time step is too large (as a result of a too large morfac), part of this influence on the hydrodynamics is lost. Consequently, the hydrodynamics differ from the hydrodynamics based on a smaller morphological time step (a smaller morfac). The difference in hydrodynamics could consequently result in a difference in the simulated morphological development.

For the 1-year morphological simulations, the sequence of the wave classes in the model was from 1 to 6 as numbered in Table 7-24. A different sequencing of the waves might affect the model results. However, since small morfac values were used, the assumption was that the chance for irreversible bathymetric changes to happen under each wave class was small.

7.3.3.5. River Flows

For the upstream river flows, the annual average flows were used for the entrance channel morphology modeling purpose. The flow rates were 148 m^3/s (5,227 cfs), 22 m^3/s (777 cfs), and 21 m^3/s (742 cfs) from Cape Fear River, Black River and Northeast Cape Fear River, respectively.

7.3.3.6. Sediments

Riverine sediments of the Wilmington Harbor generally consist of sands, silts and clays in various mixtures. From the Lower Midnight Channel upstream, the sediments are predominantly silts and clay, and from Reaves Point Channel downstream they are predominantly sand, except for the outer Baldhead Shoal Channel which is predominantly silts and clays (USACE, 2014).

Littoral sediments of the nearshore ocean bottom affected by wave action consist of fine to medium quartz sand, shell hash, silt and clay. The silt/clay component of the active profile ranges from about 2% to 5% to a depth of about 24 ft NGVD. Seaward of the littoral zone is predominantly mud bottom (USACE, 2014).

The purpose of this study is to investigate the shoaling volumes in the Ocean Entrance Channels consisting of the following ranges: Smith Island, and Baldhead Shoal Reaches 1 and 2. Materials dredged from these three channel reaches are normally placed on nearby beaches following the Wilmington Harbor Sand Management Plan (USACE, 2000). -

As part of an ongoing project for the Town of Oak Island, vibracore sediment data are being collected from previous geotechnical investigations in the study area. Figure 7-53 lists the available vibracores. In the Jay Bird Shoal area, the surficial median grain size ranges between 0.15 mm and 0.66 mm, whereas it ranges between 0.13 mm and 0.54 mm in the Frying Pan Shoals area. Additionally, the median grain size in the Outer Entrance Channel extension ranges mostly between 0.12 mm and 0.19 mm (Dial Cordy and Associates Inc., 2017).

Figure 7-53: Vibracores from previous geotechnical investigations

As stated in Table 6.4 of the General Reevaluation Report on Coastal Storm Damage Reduction for Brunswick County beaches (USACE, 2012), the native beach mean sediment sizes around the study area are between 0.20mm – 0.25 mm. In this study, three sediment sizes were used in the model runs separately to determine the potential shoaling volumes associated with the different sizes: 0.15, 0.20, and 0.25 mm. The approach with multiple sediment classes within one model was not considered. The current approach provides a sensitivity analysis of the channel shoaling volumes related to different sediment sizes. As indicated by the model results for the 0.25mm sediment size, the shoaling volumes in the Baldhead Shoal Reach 1 & 2 were much less than the actual values from condition surveys. Thus, coarser sediment classes than 0.25mm were not considered because they are less movable which would have resulted in even less shoaling volumes in the channels.

The initial sediment thickness of the sediment layer throughout the model domain is required by the morphological model. For this study, it was assumed that there was no sediment available in the channel bottom initially, and the sediment thickness was 10 meter in the littoral zone for each sediment size. From the model results, it was discovered that the shoaling volumes in the Smith Island range and upstream channels were mostly controlled by the available sediments in the intertidal flats inside the estuary. Thus the sediment thickness is a key parameter for the morphological model. It was determined that a thickness of 0.5 m would produce a reasonable shoaling volume in the Smith Island range. Figure 7-54 presents the final sediment thickness map used in the final model calibration.

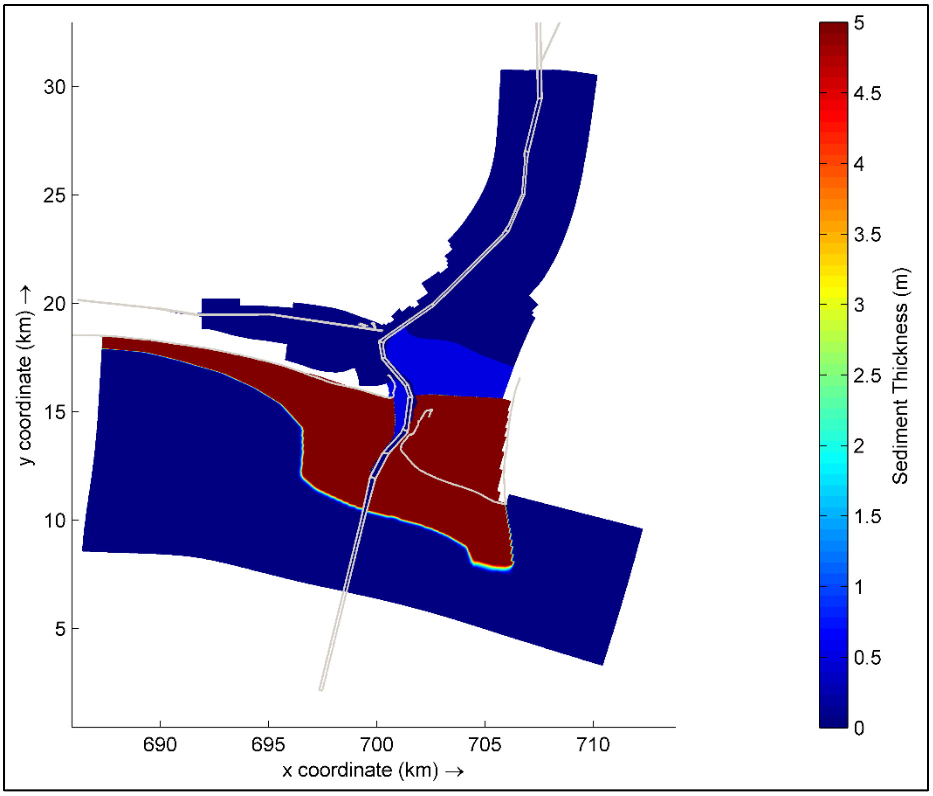

Figure 7-54: Delft3D initial sediment layer thickness

7.3.4. Model Calibration

Coincident with the initiation of the ocean entrance channel modifications as part of the Wilmington Harbor Federal Navigation Project in 2001, a companion physical monitoring program was developed to examine the response of adjacent beaches, entrance channel shoaling patterns, and the ebb tide delta. Details of the program and results are chronicled in a series of annual reports which can be found on the Wilmington District website[3] . These data and results were utilized in drawing conclusions regarding the effectiveness and potential future modifications of a Sediment Management Plan (SMP) developed to address the disposal of the dredged material associated with both the initial construction of the new channels and subsequent channel maintenance (USACE, 2000). Some of the results from the reevaluation report (USACE, 2011) are presented in this section to compare with the morphological model results for model calibration purposes.

[3] https://www.saw.usace.army.mil/Missions/Navigation/Dredging/Wilmington-Harbor/

7.3.5. Model Parameters

For this study, the default non-cohesive sediment transport formulations in Delft3D based on Van Rijn et al. (2012) were applied. The parameters for both hydrodynamics and waves were determined during their calibration processes and were kept the same for the morphological modeling. Values used for parameters not iteratively altered during the calibration process were determined from the published literature and/or recommendations from Deltares, the developers of Delft3D. The primary sediment transport parameters adjusted in the calibration of the morphology model were: Sus, Bed, SusW, BedW. SusW and BedW are related to waves and were recommended to be close to zero for the depth-average Delft3D application. Sus and Bed are parameters related to current induced sediment transport. The sediment transport magnitudes increase when Sus and Bed become larger. Table 7-25 lists the parameters related to the morphological model.

Table 7-25: Morphological model parameters

Parameter	Value [unit]	Description
IopKCW	1	Flag for determining Rc and Rw
RDC	0.01 [m]	Current related roughness height (only used if IopKCW <> 1)
RDW	0.02 [m]	Wave related roughness height (only used if IopKCW <> 1)
MorFac	variable	Morphological scale factor
MorStt	0.0 [min]	Spin-up interval from TStart till start of morphological changes
Thresh	0.05 [m]	Threshold sediment thickness for transport and erosion reduction
MorUpd	TRUE	Update bathymetry during FLOW simulation
EqmBc	TRUE	Equilibrium sand concentration profile at inflow boundaries
DensIn	FALSE	Include effect of sediment concentration on fluid density
AksFac	1.0	van Rijn's reference height = AKSFAC * KS
RWave	2.0	Wave related roughness = RWAVE * estimated ripple height. Van Rijn Recommends range 1-3
AlfaBs	1.0	Streamwise bed gradient factor for bed load transport
AlfaBn	15.0	Transverse bed gradient factor for bed load transport
WetSlope	0.2	Avalanching slope sV:1H
AvalTime	86400.0 [s]	Avalanching time in 1 day
Sus	1.0	Multiplication factor for suspended sediment reference concentration
Bed	1.0	Multiplication factor for bed-load transport vector magnitude
SusW	0.0	Wave-related suspended sed. transport factor
BedW	0.0	Wave-related bed-load sed. transport factor
SedThr	0.1 [m]	Minimum water depth for sediment computations
ThetSD	0.5	Factor for erosion of adjacent dry cells
HMaxTH	1.5 [m]	Max depth for variable THETSD. Set < SEDTHR to use global value only

7.3.6. Channel Shoaling Patterns

Figure 7-55 presents the condition surveys for the three ocean entrance channel ranges in January 2007, November 2008, and August 2010 which are near the end of the first, second, and third maintenance dredging cycles, respectively, when the channels are typically in their more shoaled condition. The SMP assumed that maintenance dredging would be required on a 2-year basis based on historical dredging activity. For all three periods, the surveys show very similar shoaling patterns for the channel areas of interest.

The following observations are stated in the USACE's reevaluation report (USACE, 2011): "*As noted on the figures, the specific shoaling areas are found along the eastern margins of Baldhead Shoal Channel-Reaches 1 & 2, and along the western margins of Smith Island Channel. For the shoaling within the Baldhead Shoal-Reach 1 portion of the channel, sediment appears to enter directly from the spit area of Bald Head Island and adjacent nearshore. The sediment is then found to migrate seaward along the margin between the channel and the western periphery of Baldhead Shoal eventually extending into Baldhead Shoal-Reach 2. Shoaling within Reach 2 also results from sediment moving directly from Baldhead Shoals. For the Smith Island Range, the shoaling results from the direct encroachment of inner edge of Jay Bird Shoals, which gradually fills along the western margin of this portion of the channel. Current patterns measured under the monitoring program suggest that sediment moving off of Oak Island is the primary feeding mechanism for Jay Bird Shoal.*"

The predicted cumulative sedimentation and erosion patterns from the 1-year morphology modeling results for a grain size of 0.15 mm is presented in Figure 7-56. The model result shows the similar shoaling patterns as observed from the condition surveys in all three channel reaches. The modeled results for the other two grain sizes indicate similar shoaling patterns as well.

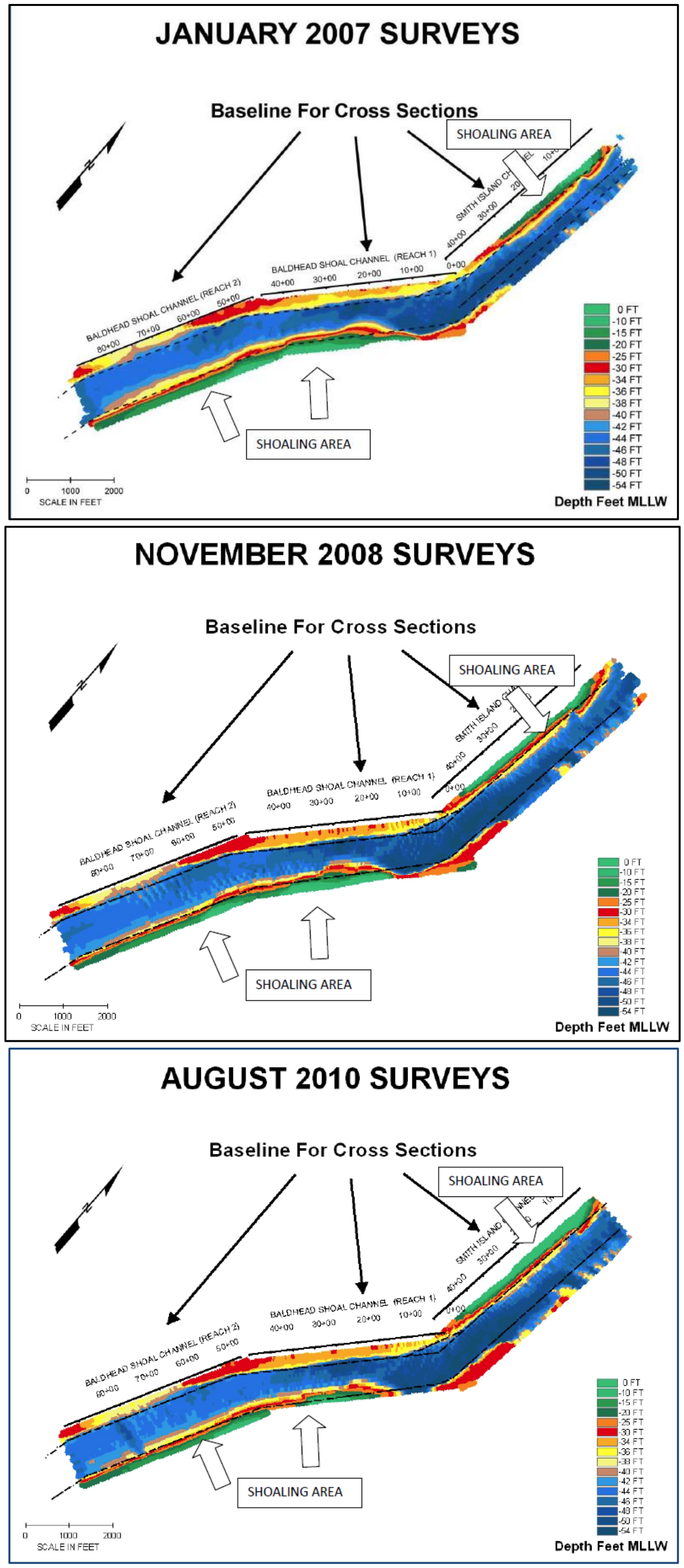

Figure 7-55: Condition surveys at the Cape Fear Entrance Inner Ocean Bar Channels (USACE, 2011)

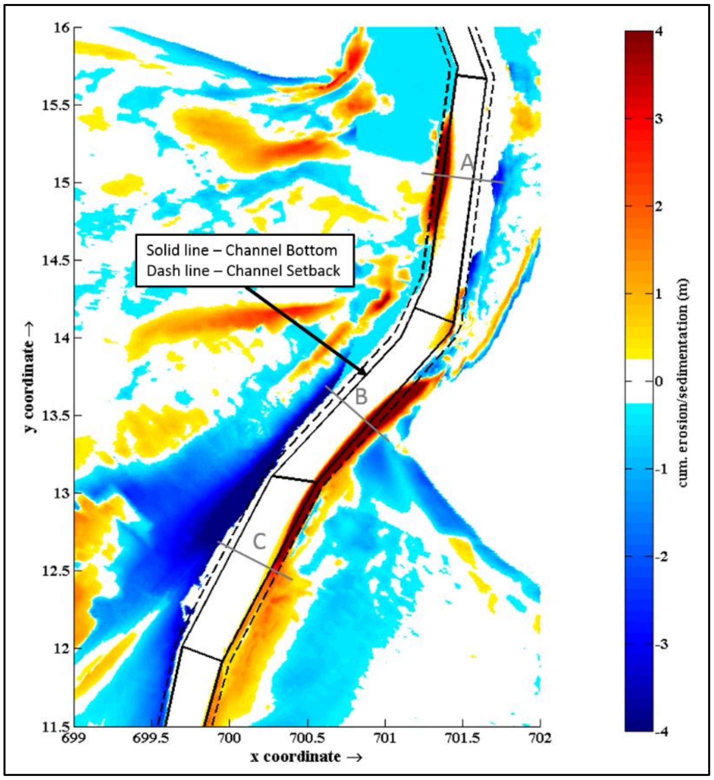

Figure 7-56: Delft3D 1-year channel shoaling patterns from the morphology model (d_{50}=0.15 mm)

7.3.7. Channel Shoaling Rates

7.3.7.1. Historical Rates from Condition Surveys

The shoaling rates were also computed based on condition surveys in the SMP reevaluation report (USACE, 2011). Figure 7-57 presents the calculated channel volumes over time above the -46 ft, mean low water (MLW) channel prism in the three Inner Bar Channel ranges over the three dredging cycles. All three channel ranges show similar patterns with the channel volumes drawn down with each dredging action followed by fairly uniform infilling over each maintenance cycle. The only exception to this pattern was noted in Baldhead Shoal Reach 1 during the third cycle. In this instance, the rate of shoaling was relatively low just before the start of the local beach nourishment project along Bald Head Island, and rather high after this project.

Shoaling rates, as given in cubic yards per day (cy/d) in Table 7-26, were then computed using the volumetric data for each of the maintenance dredging periods and each of the three channel reaches. The rates computed for the last dredging cycle excluded the post Bald Head fill period so as to not bias the data due to the influence of this locally performed project. An overall weighted average was calculated for the entire maintenance period spanning the three cycles. As shown in the table, the results show fairly similar daily rates for each of the three channel reaches. The total shoaling rate in all three channel reaches is 1,610 cy/d which results in a total of volume of 587,470 cubic yards if this rate is used to project an average annual shoaling volume. This total compares very favorably to the dredging amount as formulated in the SMP. The shoaling volume ratio between Baldhead Shoal Channel 1 & 2 and Smith Island is close to 2:1 based on these results.

Table 7-26: Shoaling Rates for the Wilmington Harbor Inner Ocean Bar Channels from surveys (USACE, 2011)

Channel	1st Cycle			2nd Cycle			3rd Cycle (Pre-BH Fill)			Weighted Ave		
	Rate	Days	Rate	Rate	Days	Rate	Rate	Days	Rate	Rate	Days	Rate
	cy/d		cy/yr	cy/d		cy/yr	cy/d		cy/yr	cy/d		cy/yr
Baldhead Shoal Reach 1	442.5	772	161,513	589.3	608	215,095	505.8	216	184,617	507.0	1596	185,055
Baldhead Shoal Reach 2	517.0	773	188,705	712.2	512	259,953	321.7	152	117,421	565.9	1437	206,554
Smith Island	431.0	811	157,315	591.2	611	215,788	878.2	153	320,543	536.6	1575	195,859
Total			507,533			690,836			622,581			587,468

Between June and December 2015, a terminal groin was built on the west tip of the South Beach on Bald Head Island. To check the impact of the terminal groin, condition surveys in November 2015, November 2016 and December 2017 by USACE were used to compute the shoaling volumes in these three channel reaches. The same approach as in USACE (2011) was applied to calculate the volume changes above -46ft MLW channel prism, and the results are presented in Table 7-27. The total shoaling volumes are 592,000 cy and 635,000 cy during the periods of November 2015 – November 2016 and November 2016 – December 2017, respectively. The magnitudes are similar to the annual average shoaling volume of 587,470 cy/yr prior to the terminal groin construction (USACE, 2011).

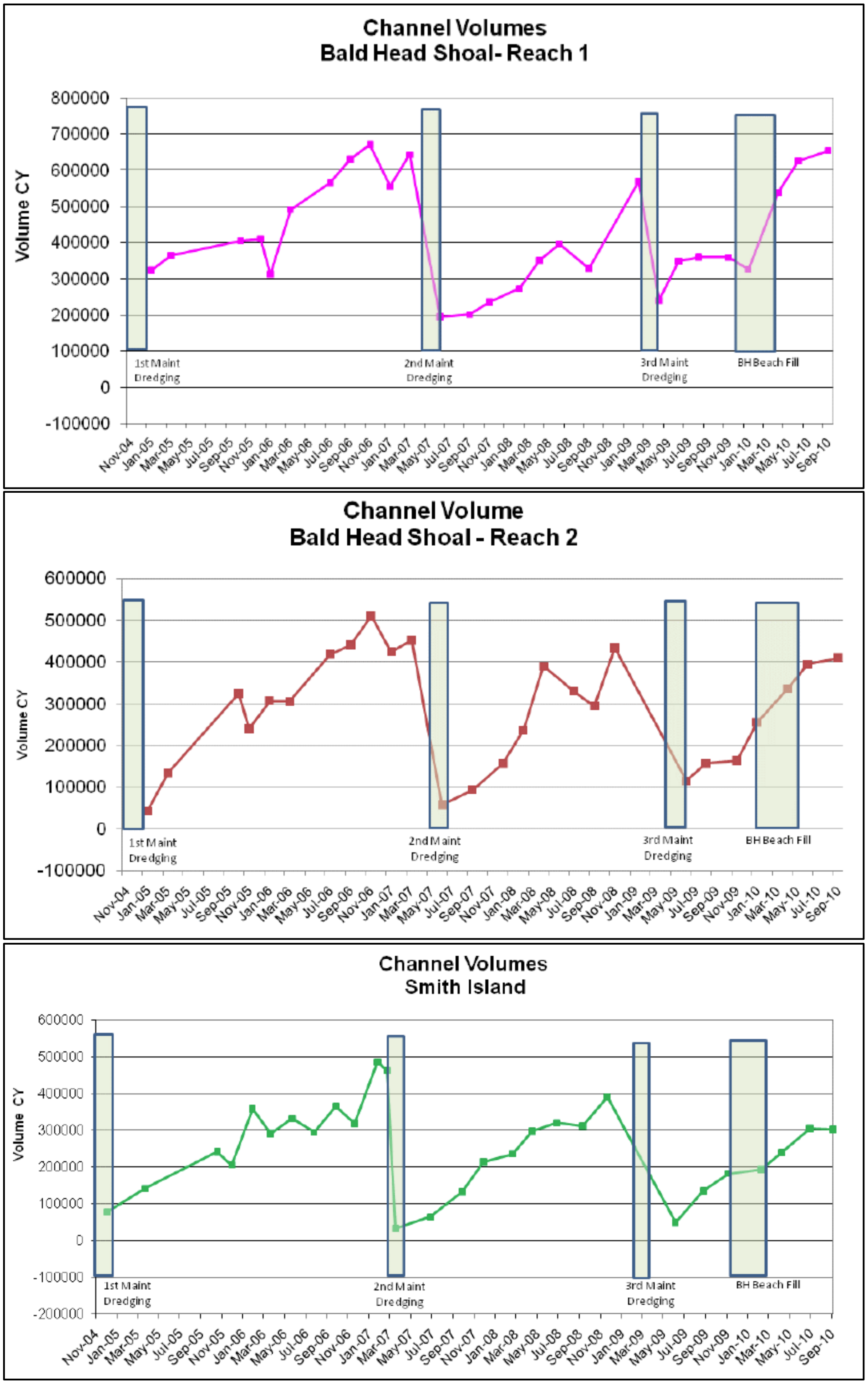

Figure 7-57: Channel shoaling volumes from condition surveys (USACE, 2011)

7.3.7.2. Model Calibration Results

The predicted shoaling volumes were calculated from the 1-year morphology model results in the same three channel reaches for the three sediment grain sizes. Figure 7-58 presents the initial and final channel bathymetry from the model along three cross sections as indicated on Figure 7-56. The 5:1 slope on Figure 7-58 is the design side slope of the dredged channel and was applied in Delft3D as the avalanche slope. To account for the sediment accumulation that would be dredged from the navigation channel, the volume confined between the channel setback lines established by USACE (about 150 ft along the Cape Fear Entrance Ocean Channels) can be seen as an adequate approximation. The setback lines are indicated by the dash line on Figure 7-56. The shoaling volumes calculated form the model results that are included in Table 7-27.

The modeled total shoaling volume of 549,150 cy within the three reaches with the grain size of 0.25mm is within the range of the historical shoaling rates from condition surveys. The predicted shoaling volume in Baldhead Shoal Reach 1 is close to that observed after construction of the terminal groin. However, the predicted shoaling volume in Baldhead Shoal Reach2 is much less than was observed, whereas more shoaling was predicted in Smith Island than observed from the surveys.

For a finer grain size of 0.20mm, modeled shoaling volumes in Baldhead Shoal Reach 1 are in line with the surveys pre-construction of the terminal groin. In Baldhead Shoal Reach 2, the predicted shoaling volume, though, is lower than observed.

For the finest grain size of 0.15mm, the predicted shoaling volumes in all three channel ranges are much larger than historical rates, which results in a total shoaling volume about 140% more than the historical rates.

A plausible explanation is the sediment size decreases from the river entrance to offshore. For sediments transported from Caswell Beach and Jay Bird Shoals to Smith Island range, the grain size might be coarser than 0.25mm. Sediments feeding into Baldhead Shoal Reach 1 are in the range of 0.25mm, mostly from Bald Head Island. Further offshore, the grain size is finer (between 0.15 and 0.20mm) in Baldhead Shoal Reach 2 where sediments mostly come from Bald Head Shoal.

Another -factor that could affect the shoaling volume calculations in Baldhead Shoal Reach 1 & 2 is periodic beach nourishments on the Bald Head Island beaches which provide extra amounts of sediment to be transported back to the adjacent channel. The beach fill placement activities at Bald Head Island since 2001 are summarized in Table 7-28. Most of the historical shoaling volumes calculated from the condition surveys are within 1 to 2 years of post- beach nourishment. Beach nourishment was not incorporated in the model bathymetry.

Other contributing factors to the model results include inherent model limitations, nearshore and shoal bathymetry which influence both wave transformation and sediment transport magnitude, and exclusion of potential storm impacts, etc.

Table 7-27: Shoaling volume rate calibration results (cy/yr)

		Baldhead Shoal Reach1	Baldhead Shoal Reach 2	Smith Island	Total
Modeled	d_{50} = 0.15mm	483,000	429,540	508,600	1,421,140
	d_{50} = 0.20mm	207,570	176,730	395,760	780,060
	d_{50} = 0.25mm	126,270	130,250	292,630	549,150
USACE (2011)		184,690	206,590	196,000	587,280
Condition survey (11/2015 – 11/2016)		106,090	324,600	161,180	591,870
Condition survey (11/2016 – 12/2017)		109,830	287,490	237,890	635,210

Table 7-28: Beach placement activities at Bald Head Island since 2001 (Olsen, 2018)

Year	Volume	Sponsor	Location
2001	1.849 ± Mcy	USACE*	South Beach (Sta. 41+60 to 205+50)
2005	1.217 ± Mcy	USACE*	South Beach (Sta. 46+00 to 126+00)
2006	47,800 cy	VBHI	West Beach (Sta. 16+00 to 34+00)
2007	0.9785 ± Mcy	USACE*	South Beach (Sta. 46+00 to 174+00)
2009/10	1.850 ± Mcy	VBHI	West Beach (Sta. 8+00 to 32+00)
2012	137,990 cy	FEMA/VBHI	West Beach & Western South Beach
2013	1.566 ± Mcy	USACE*	South Beach (Sta. 44+00 to 150+00)
	92,500 cy		West Beach (Sta. 8+00 to 27+00)
2015	1.33 ± Mcy	USACE*	South Beach (Sta. 41+50 to 154+00)
2016/17	50,000 cy	VBHI	West Beach and Row Boat Row

**Disposal pursuant to the WHSMP*

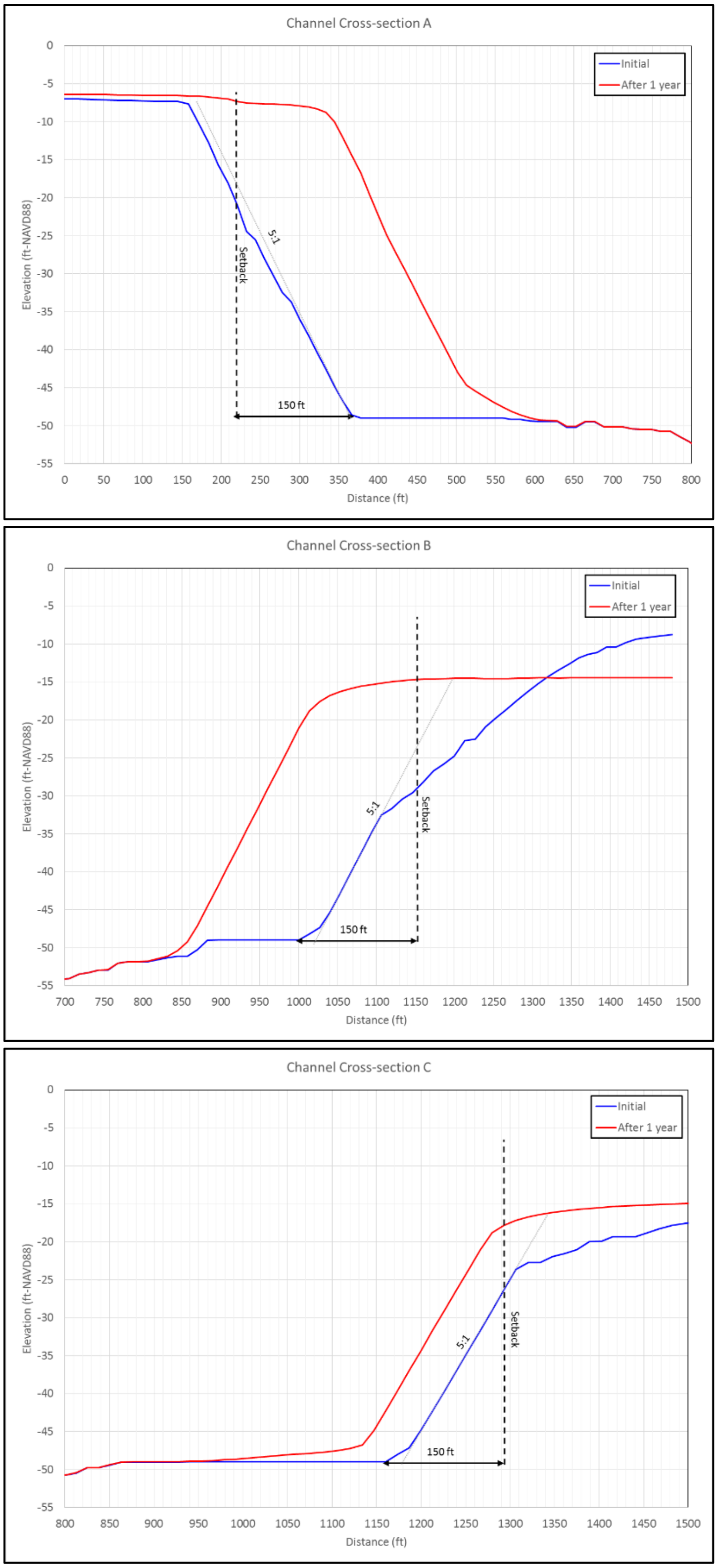

Figure 7-58: Delft3D initial and final channel bathymetry along three cross-sections (d_{50}=0.15 mm)

7.3.8. Summary and Conclusions

Based on existing hydrodynamic and wave models developed within the scope of this project, a morphology model was developed to investigate the project impact on the shoaling volumes in the Cape Fear Entrance Inner Ocean Bar channel ranges: Smith Island and Baldhead Shoal Reach 1& 2.`

The morphology model was calibrated against historical shoaling volumes computed from condition surveys by USACE. The modeled shoaling patterns in the channels are similar to the surveys. However, the shoaling volumes from the model were found to be strongly dependent on the sediment grain size within each reach.

The morphology model is capable of reproducing ongoing shoaling patterns and quantities within the entrance channel for purposes of comparing the proposed channel configuration to the existing conditions. For this comparison, it is recommended to use the results for the 0.25 mm grain size for Bald Head Reach 1; and average of the results for the 0.15mm and 0.2mm grain sizes for Bald Head Reach 2; and the results for the 0.25mm grain size for the Smith Island Reach. This implies that the grain size reduces in the channel progressing from north to south.

8. Shoreline and Inlet Numerical Modeling Results

The previously discussed models developed and calibrated for wave transformation, shoreline change, and entrance channel morphology were utilized to calculate the changes in nearshore wave climates, shoreline changes, and entrance channel shoaling rates due to the proposed project under the low sea level rise scenario.

8.1. Tentatively Selected Plan (TSP)

8.1.1. Project Configuration

The economic analyses determined that the only feasible channel deepening alternative is that for an authorized depth of -47 ft-MLLW in the river and -49 ft-MLLW beginning at the Battery Island Reach and extending offshore. Additionally, the vessel simulations determined that some widenings of the channel were necessary as well as a re-configuration of the turn near Battery Island. These modifications comprise the Tentatively Selected Plan.

In order to determine the potential impacts of the project, the models were run for two cases.

- Future without project (FwoP): -44 ft-MLLW (42 ft + 2 ft over-dredge) in the river channel sections and -46 ft-MLLW (44 ft + 2 ft over-dredge) from the Battery Island reach and extending offshore.

- Future with project (FwP): -49 ft-MLLW (47 ft + 2 ft over-dredge) in the river channel sections and -51 ft-MLLW (49 ft + 2 ft over-dredge) from the Battery Island reach and extending offshore.

The river bathymetry for these two configurations near Battery Island and offshore are shown in Figure 8-1 and Figure 8-2, respectively.

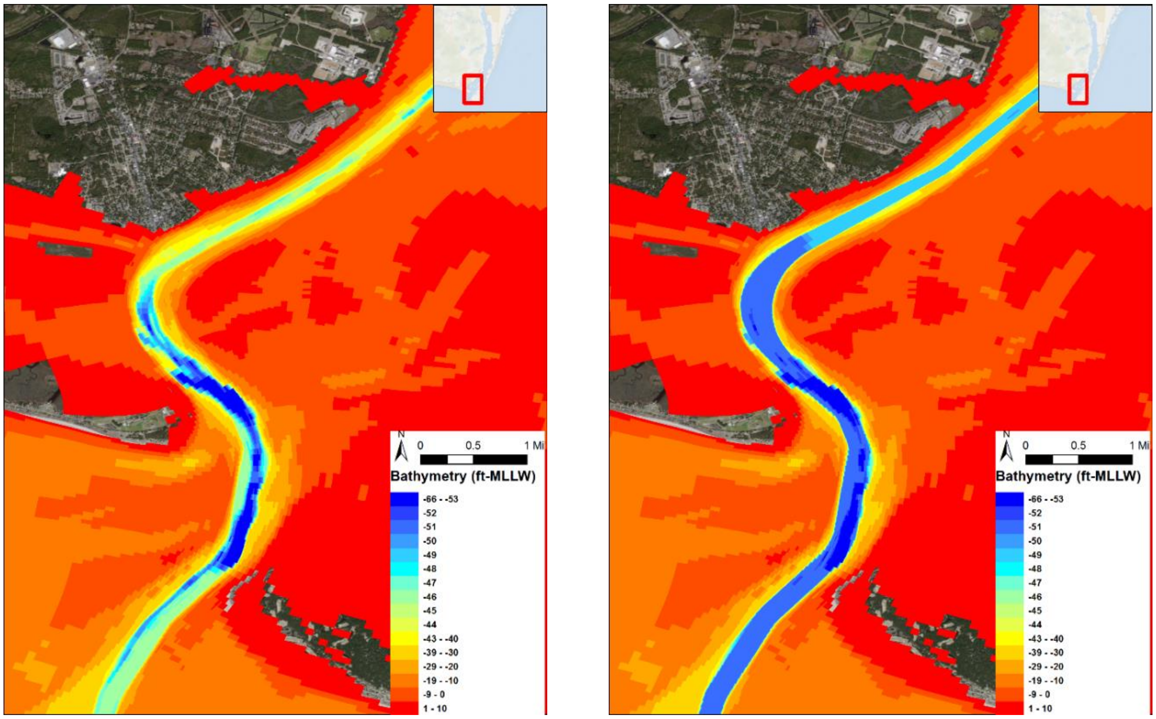

Figure 8-1: Bathymetry near Battery Island (left: FwoP, right: FwP)

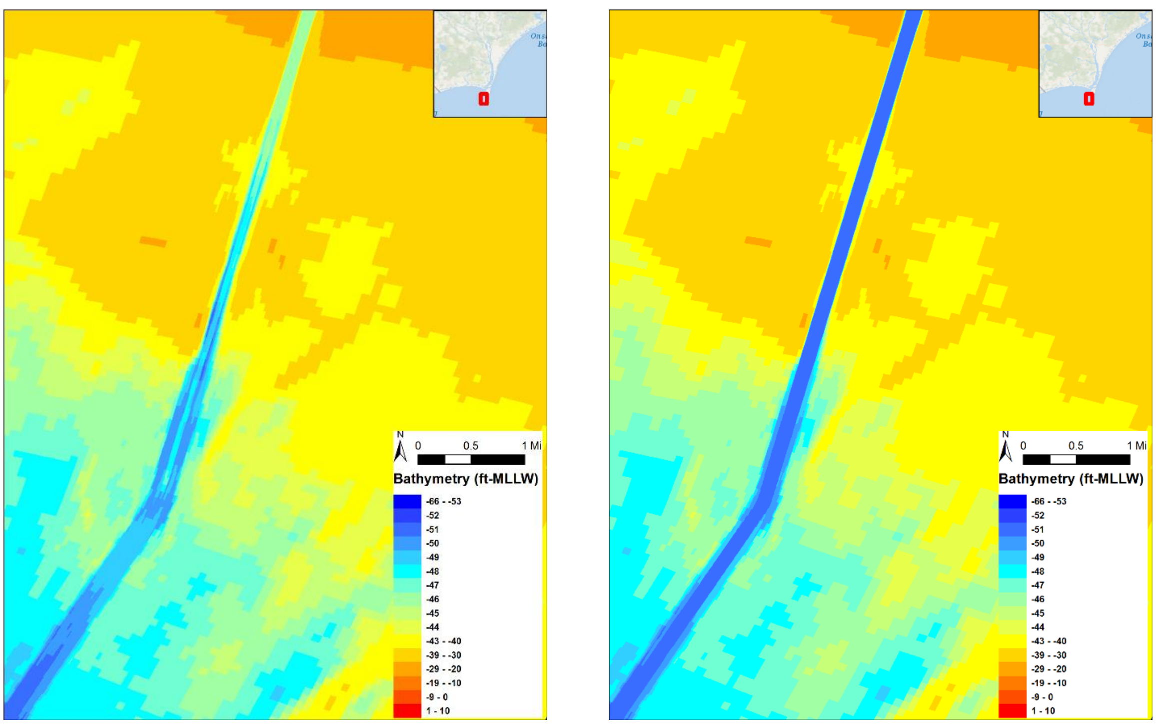

Figure 8-2: Bathymetry offshore (left: FwoP, right: FwP)

8.1.2. Sea Level Rise Scenarios

For the shoreline and entrance channel morphological modeling, only the Low RSLR scenario discussed previously (see Table 8-1) was used.

Table 8-1: Relative Sea Level Change to 2077 for Wilmington, NC

RSLR Scenario	RSLR (ft)
Low	0.34
Medium	0.88
High	2.57

8.2. Nearshore Waves

Any potential nearshore wave climate changes caused by the Project could impact the adjacent shorelines and the entrance channel shoaling rates. Thus, the long term wave climate modeling was conducted first. The development of the wave model and the results are discussed below.

8.2.1. Offshore Wave Boundary Condition

The measured wave data from 2004 to 2017 at the NOAA NDBC Buoy station 41013 were the primary source for the long term nearshore wave climate investigation. The data gaps in the buoy data were filled with available USACE WIS hindcast data and NOAA WW3 hindcast data at locations close to Station 41013. The WIS hindcast data were only available to 2014, so WW3 data were used to fill the data gaps afterwards. The combined wave data were in an hourly time interval.

Figure 8-3 shows the annual percentage of exceedance of the significant wave height from the combined offshore wave data. The annual mean significant wave height at the offshore location is about 4.4 ft.

Figure 8-4 shows the wave rose for the significant wave height at the offshore boundary from the combined wave records. It indicates that the dominant wave direction in the offshore region of the project area is from the ESE. However, the largest waves are more frequently from the ENE and S. The wave rose for the peak wave period and the wind rose are presented in Figure 8-5 and Figure 8-6, respectively.

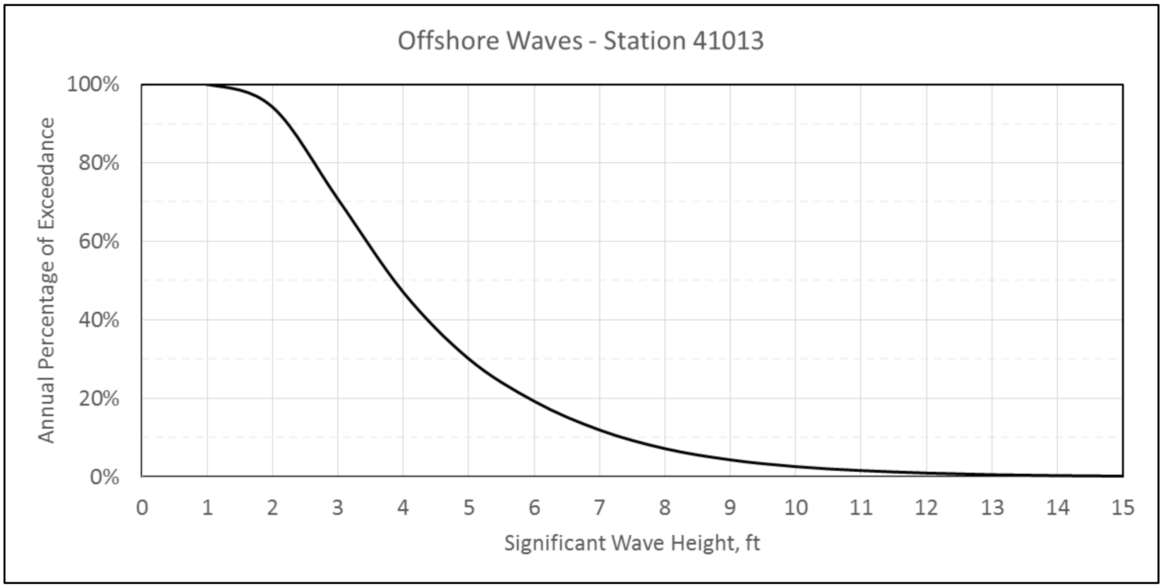

Figure 8-3: Annual percentage of exceedance of significant wave height at the offshore boundary (2004 – 2017)

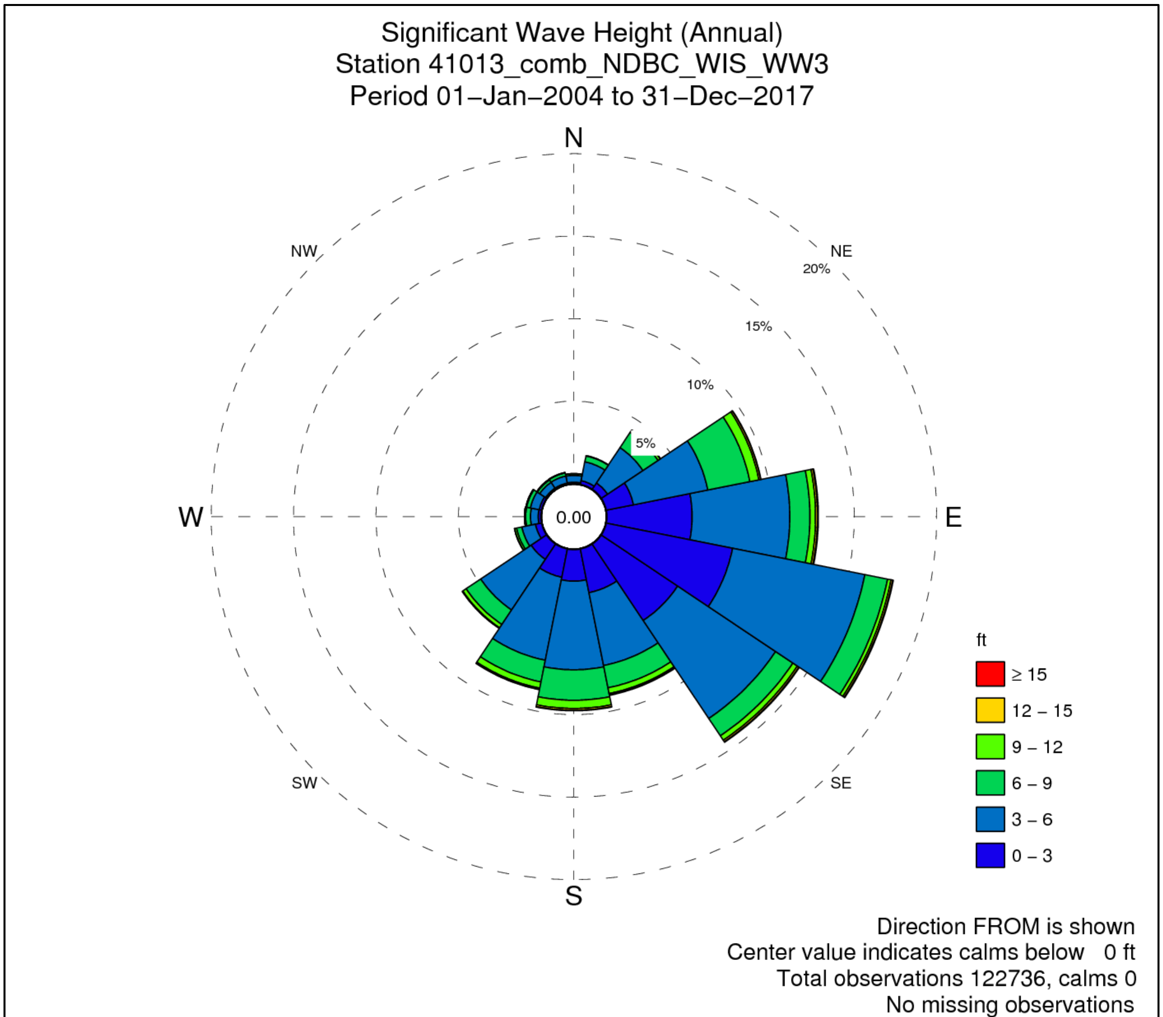

Percentage of Occurrence

Significant Wave Height, ft	N	NNE	NE	ENE	E	ESE	SE	SSE	S	SSW	SW	WSW	W	WNW	NW	NNW	Total
Total	0.61	1.77	4.31	9.56	12.83	17.75	14.45	9.04	9.76	8.69	6.14	1.67	1.00	0.97	0.71	0.73	100.00
≥ 15																	0.22
12 – 15				0.11	0.12	0.11	0.11		0.11								0.78
9 – 12			0.15	0.56	0.35	0.22	0.33	0.35	0.50	0.39	0.24	0.12					3.37
6 – 9	0.10	0.36	1.11	2.60	1.22	1.40	1.26	1.38	1.85	1.34	1.06	0.33	0.30	0.24	0.17	0.20	14.92
3 – 6	0.42	1.17	2.58	4.60	5.92	8.18	7.14	4.50	5.37	5.13	3.68	0.84	0.47	0.55	0.43	0.43	51.43
0 – 3		0.22	0.45	1.68	5.17	7.81	5.57	2.69	1.91	1.74	1.12	0.38	0.16	0.14			29.28

Figure 8-4: Wave rose of significant wave height at the offshore boundary (2004 – 2017)

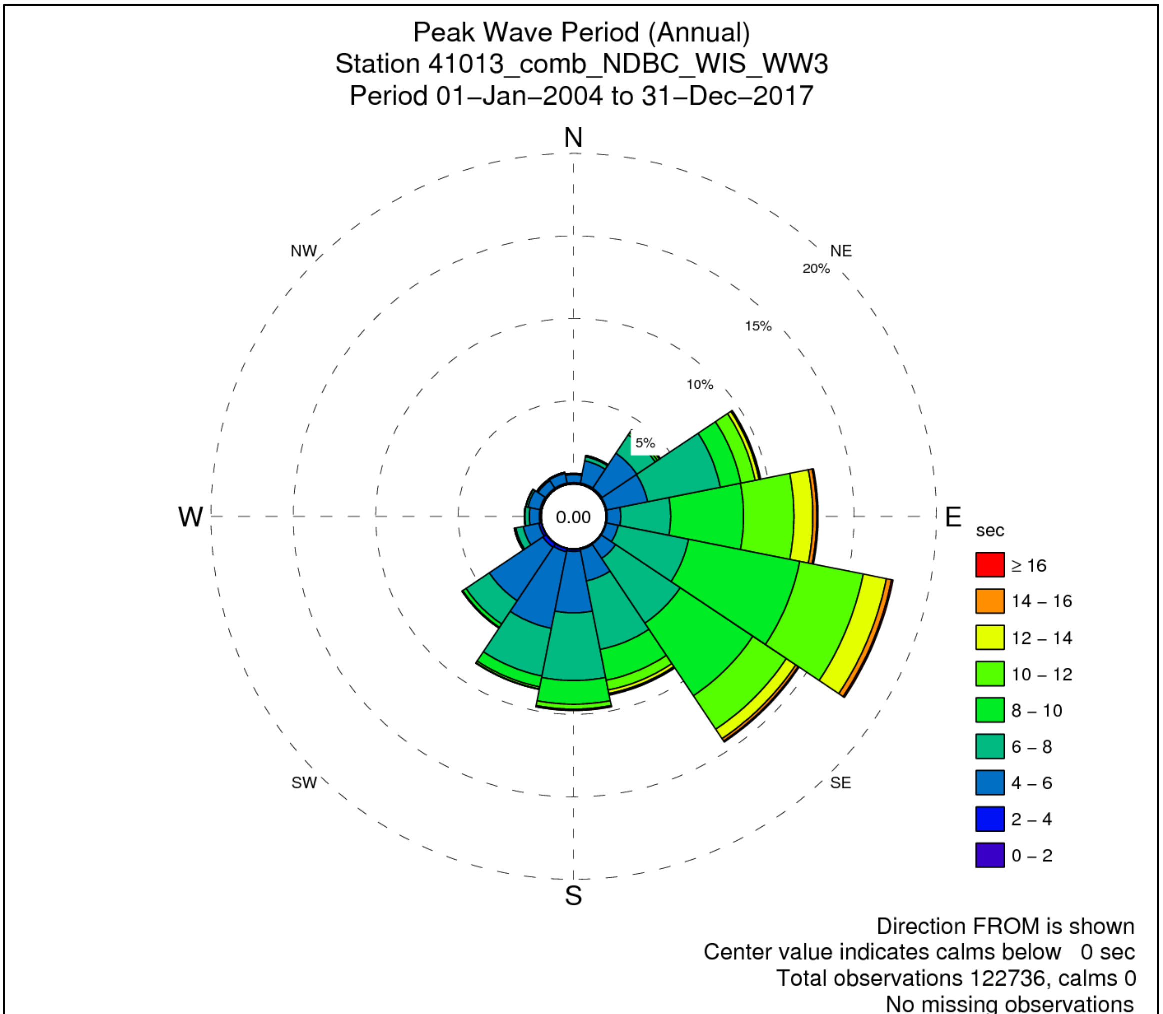

Percentage of Occurrence

Peak Wave Period, sec	N	NNE	NE	ENE	E	ESE	SE	SSE	S	SSW	SW	WSW	W	WNW	NW	NNW	Total
Total	0.61	1.77	4.31	9.56	12.83	17.75	14.45	9.04	9.76	8.69	6.14	1.67	1.00	0.97	0.71	0.73	100.00
≥ 16																	0.33
14 – 16					0.23	0.32	0.18										0.96
12 – 14				0.25	1.15	1.43	0.68	0.21									3.87
10 – 12			0.15	0.88	3.05	3.92	2.44	0.60	0.30	0.13							11.61
8 – 10			0.16	1.27	4.42	6.88	5.30	1.90	1.44	0.67	0.24						22.42
6 – 8		0.25	1.34	4.50	3.03	4.35	4.71	4.24	4.10	2.94	1.70	0.46	0.27	0.12			32.16
4 – 6	0.49	1.37	2.54	2.53	0.83	0.74	1.04	1.94	3.73	4.73	3.90	0.97	0.61	0.74	0.55	0.59	27.30
2 – 4									0.12	0.19	0.25	0.15					1.34
0 – 2																	

Figure 8-5: Wave rose of peak wave period at the offshore boundary (2004 – 2017)

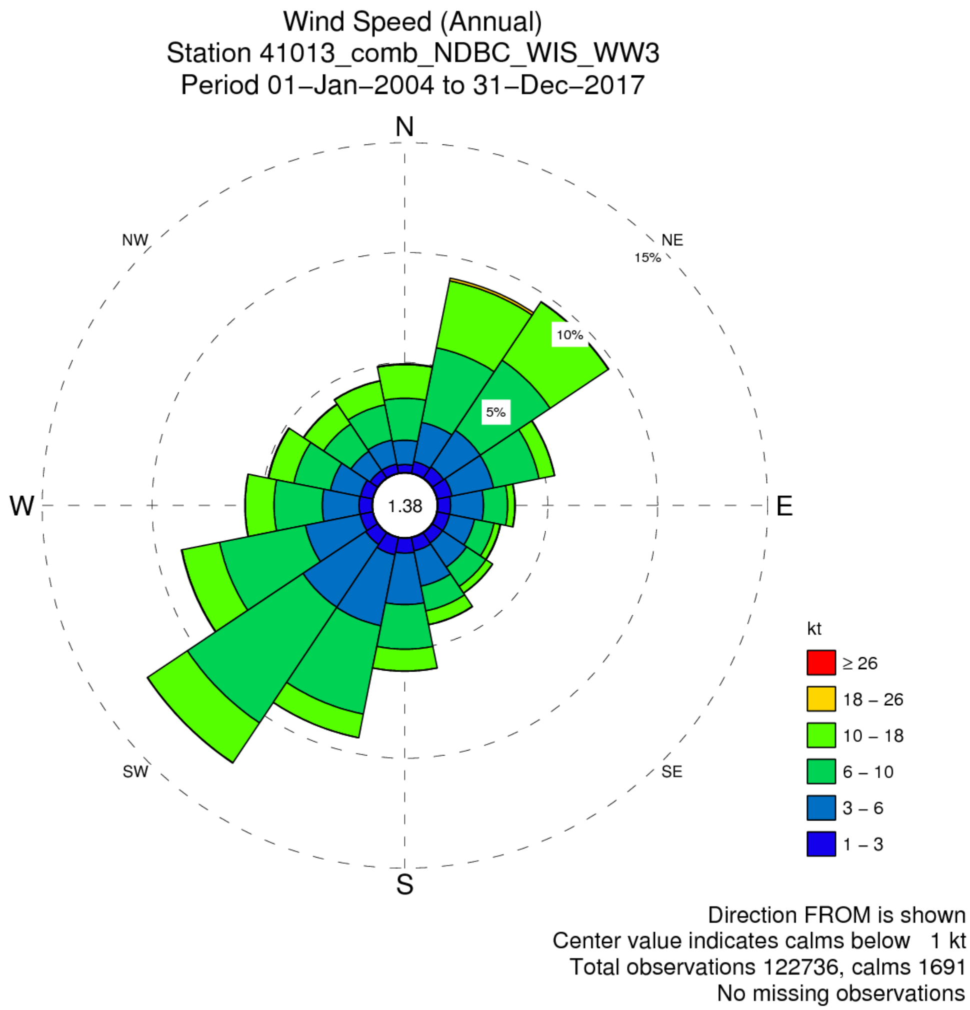

Percentage of Occurrence

Wind Speed, kt	N	NNE	NE	ENE	E	ESE	SE	SSE	S	SSW	SW	WSW	W	WNW	NW	NNW	Total
Total	4.94	9.04	9.65	5.45	3.52	2.94	3.30	4.04	6.04	9.28	12.60	8.87	5.78	4.85	4.06	4.28	98.62
26 and above																	
18 – 26		0.12															0.40
10 – 18	1.53	3.10	3.18	0.71	0.33	0.29	0.36	0.63	0.99	1.09	2.18	1.75	1.31	1.17	1.08	1.10	20.79
6 – 10	1.91	3.46	3.83	2.11	1.10	0.91	1.06	1.15	2.03	4.10	6.33	3.98	2.19	1.69	1.49	1.64	38.98
3 – 6	1.10	1.82	2.00	1.92	1.50	1.16	1.32	1.64	2.34	3.29	3.43	2.54	1.67	1.39	1.05	1.12	29.29
1 – 3	0.36	0.53	0.62	0.68	0.58	0.57	0.56	0.61	0.67	0.80	0.64	0.57	0.59	0.56	0.41	0.41	9.16

Figure 8-6: Wind rose at the offshore boundary (2004 – 2017)

8.2.2. Nearshore Wave Climate Results

The calibrated wave model was utilized to determine the potential nearshore wave climate impacts due to the Project. Only the low RSLR scenario was investigated.

The nearshore wave conditions at the GenCade "wave gage" locations as shown in Figure 8-7 were extracted from the long term wave climate modeling results.

Figure 8-7: Nearshore wave locations for GenCade shoreline model

Figure 8-8 through Figure 8-22 present wave roses for the significant wave heights at the GenCade "wave gage" locations, while Figure 8-23 through Figure 8-37 present the annual percentage of exceedance of significant wave heights. The wave roses illustrate the sheltering capacity of Frying Pan Shoals to efficiently filter out wave energy from the northeast and east-. Table 8-2 presents the statistics of significant wave heights for both without and with Project conditions at these locations. The impact of the Project on nearshore wave heights at all locations is less than 0.1ft for the 25%, 50%, 75% and 99% wave heights with the vast majority of the differences less than 0.02 ft. The model results indicate that the Project will have minimal impact on the nearshore wave climates.

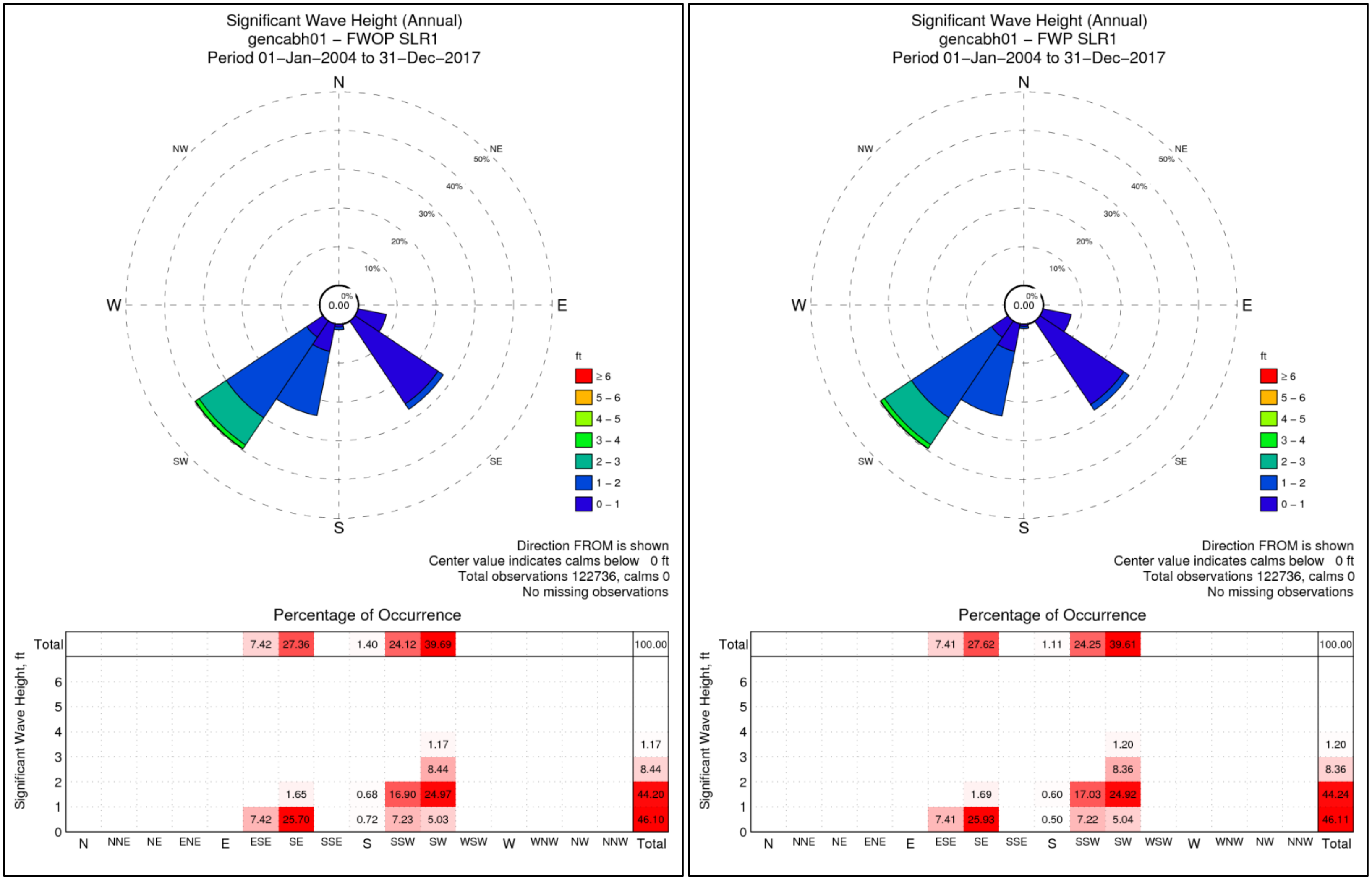

Figure 8-8: Wave height rose comparisons between FWOP and FWP at Bald Head Island nearshore location gencabh01 (approximate local shoreline azimuth 115º)

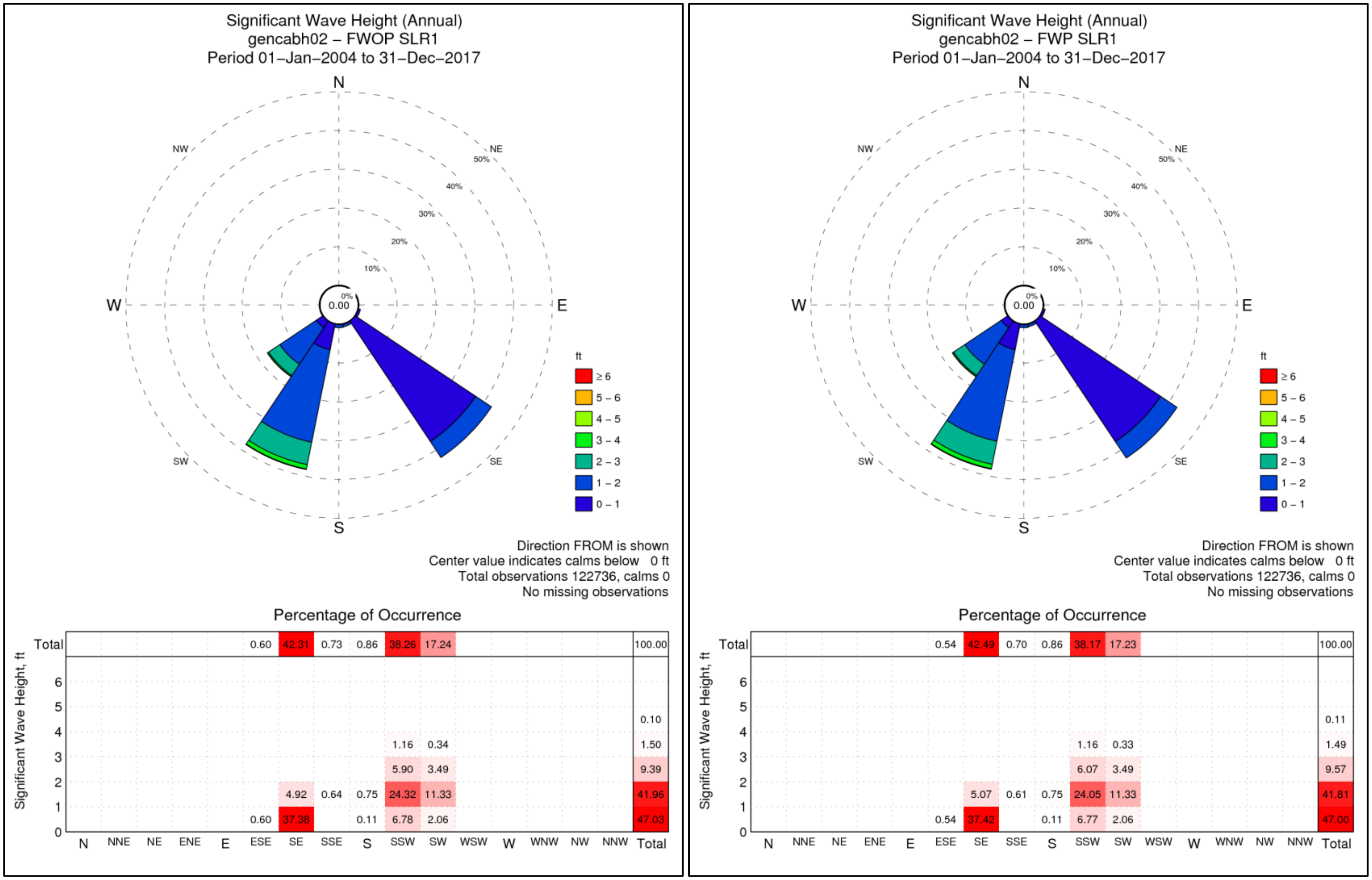

Figure 8-9: Wave height rose comparisons between FWOP and FWP at Bald Head Island nearshore location gencabh02 (approximate local shoreline azimuth 115º)

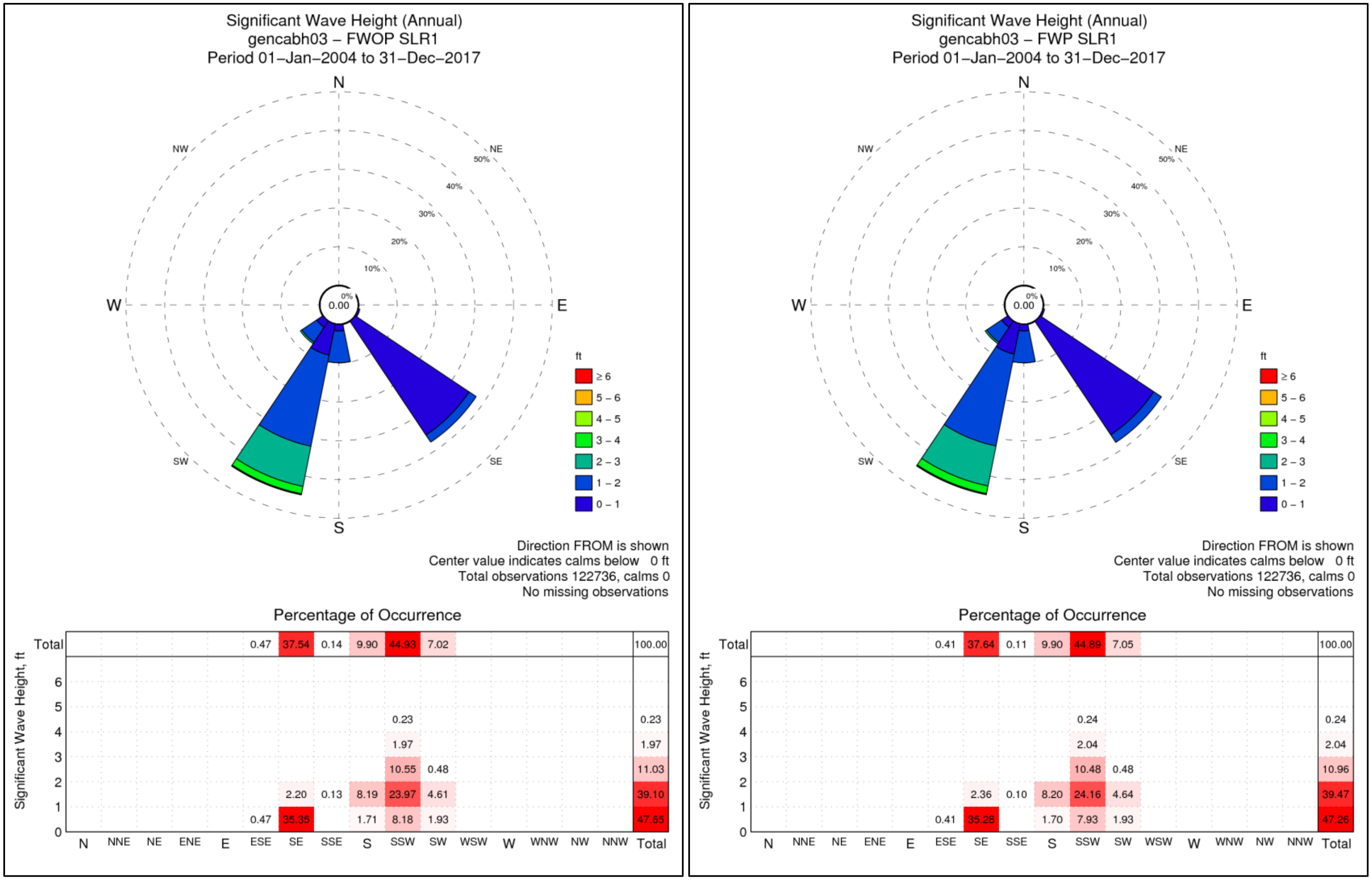

Figure 8-10: Wave height rose comparisons between FWOP and FWP at Bald Head Island nearshore location gencabh03 (approximate local shoreline azimuth 110º)

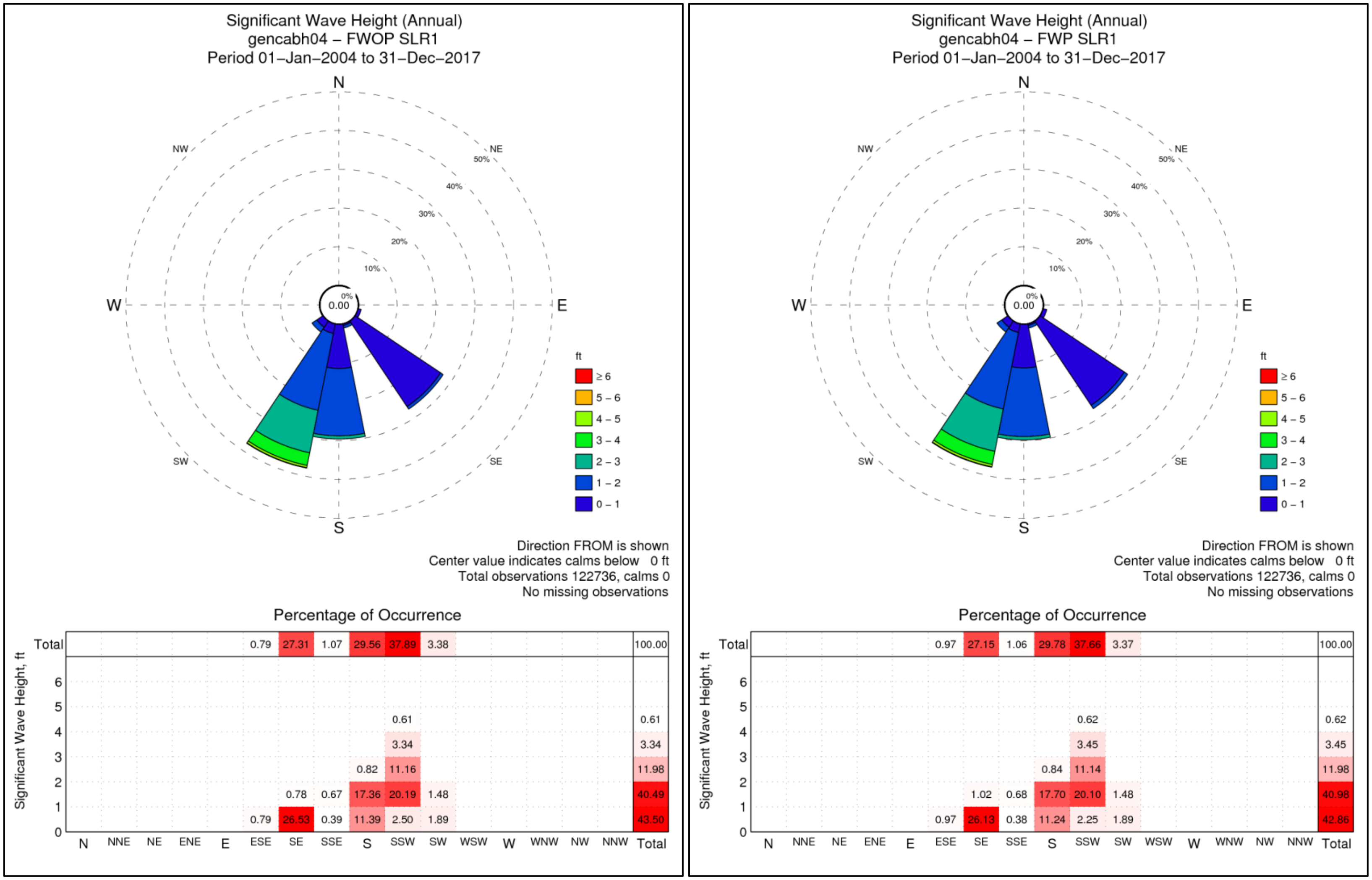

Figure 8-11: Wave height rose comparisons between FWOP and FWP at Bald Head Island nearshore location gencabh04 (approximate local shoreline azimuth 110º)

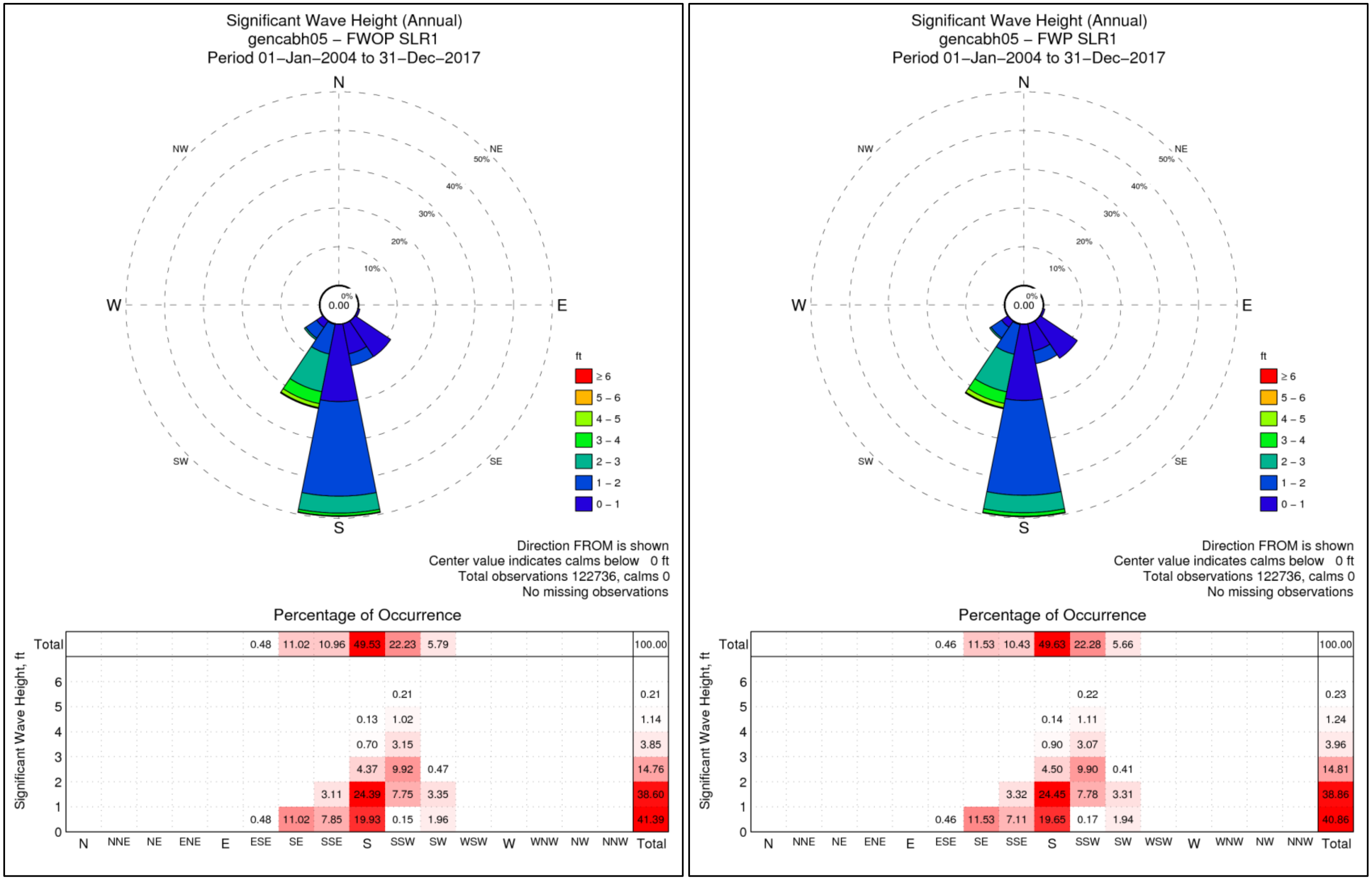

Figure 8-12: Wave height rose comparisons between FWOP and FWP at Bald Head Island nearshore location gencabh05 (approximate local shoreline azimuth 120º)

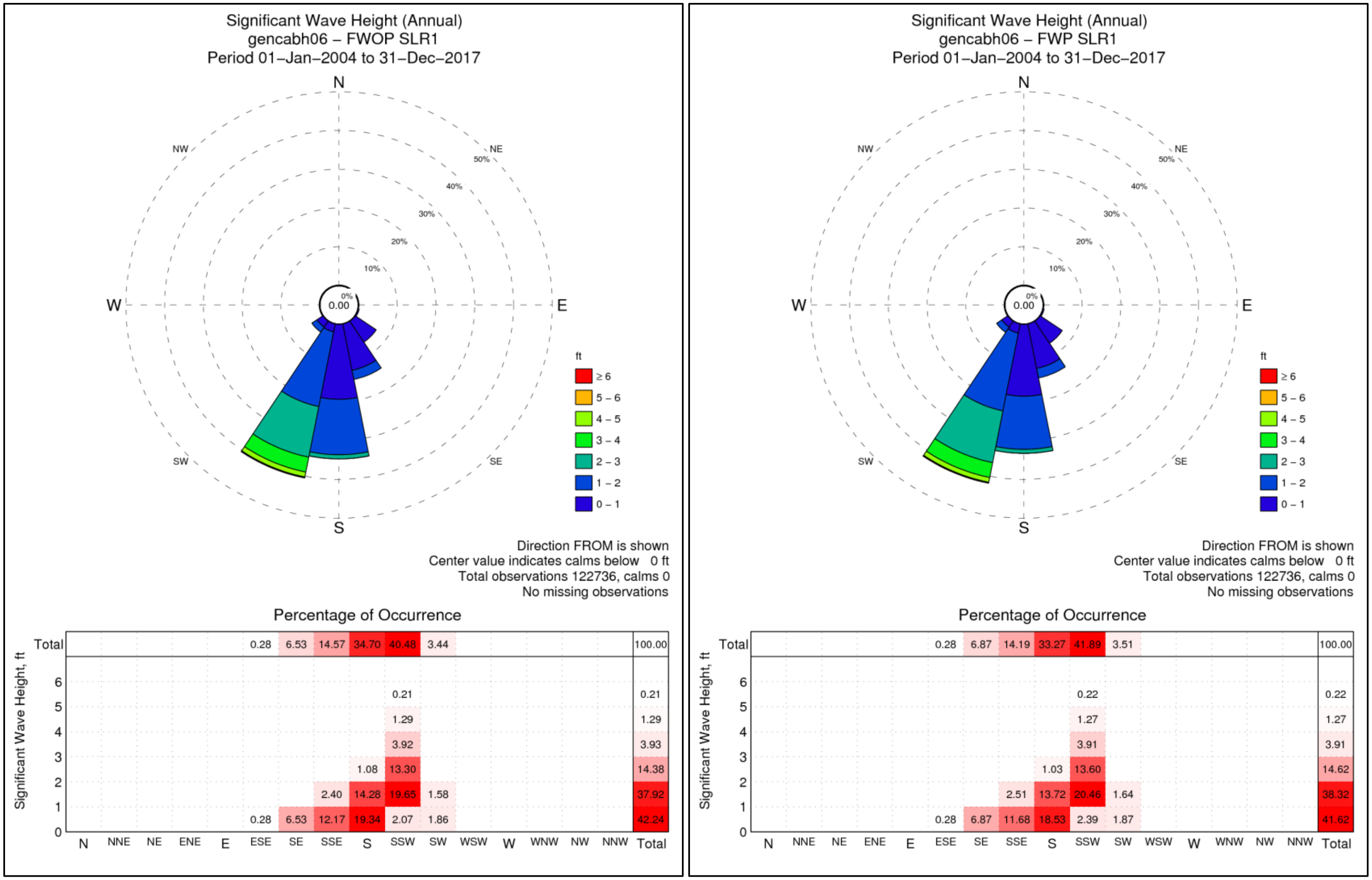

Figure 8-13: Wave height rose comparisons between FWOP and FWP at Bald Head Island nearshore location gencabh06 (approximate local shoreline azimuth 130º)

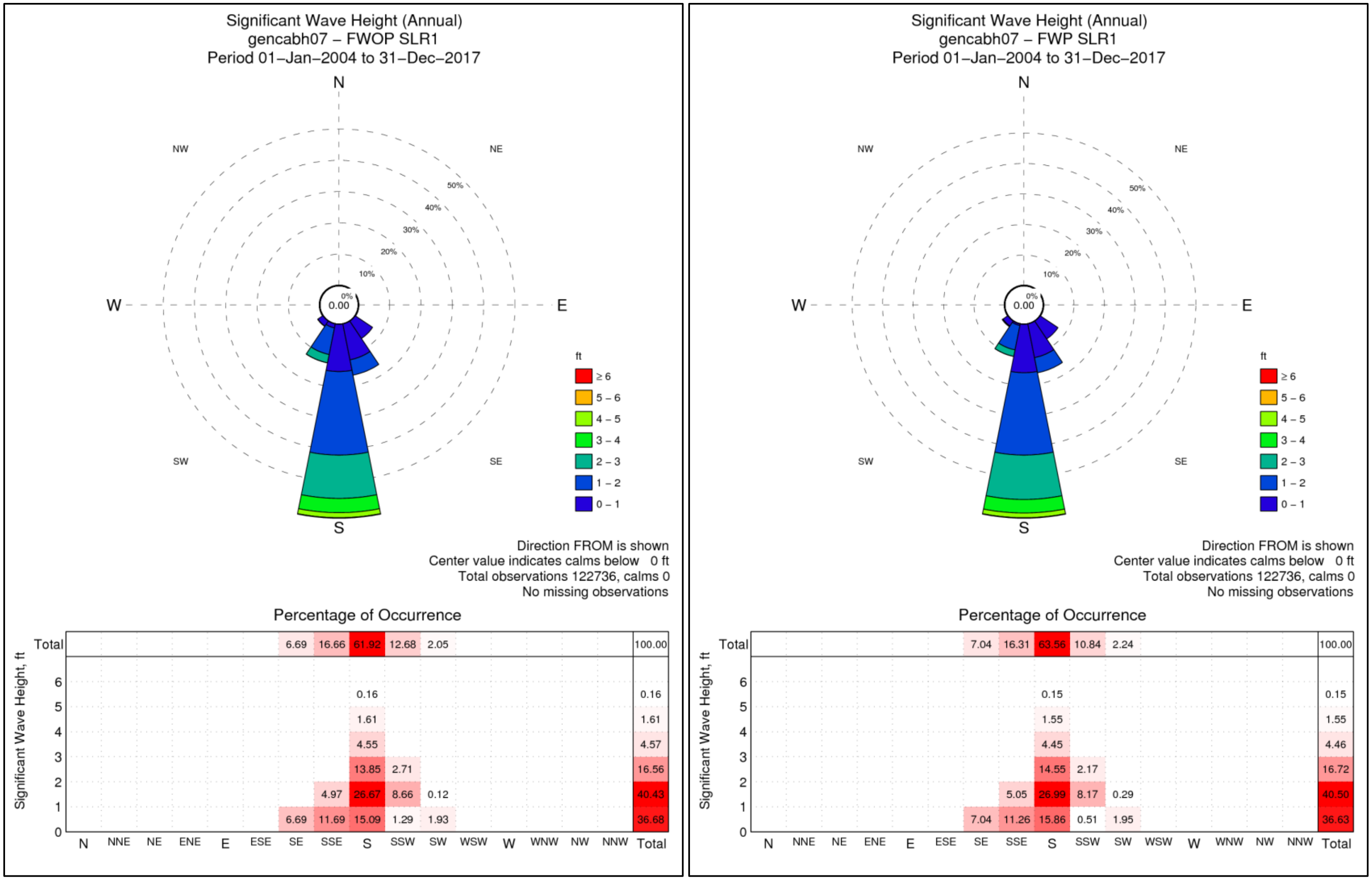

Figure 8-14: Wave height rose comparisons between FWOP and FWP at Bald Head Island nearshore location gencabh07 (approximate local shoreline azimuth 140°)

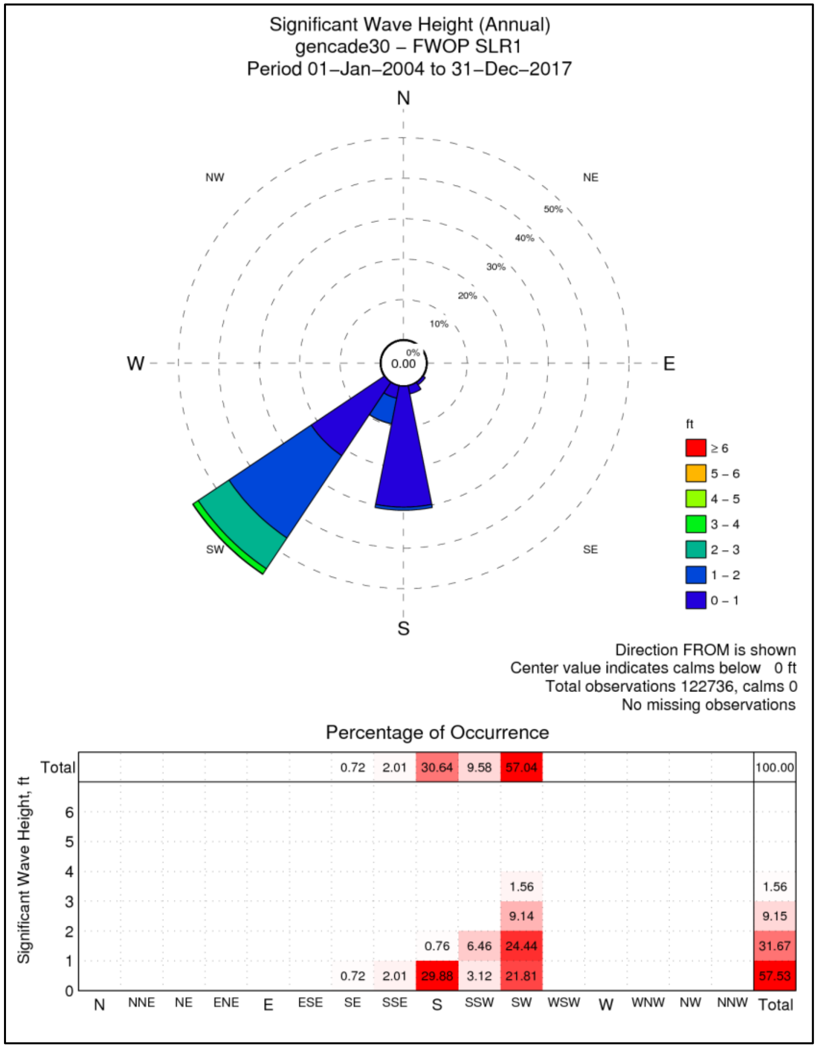

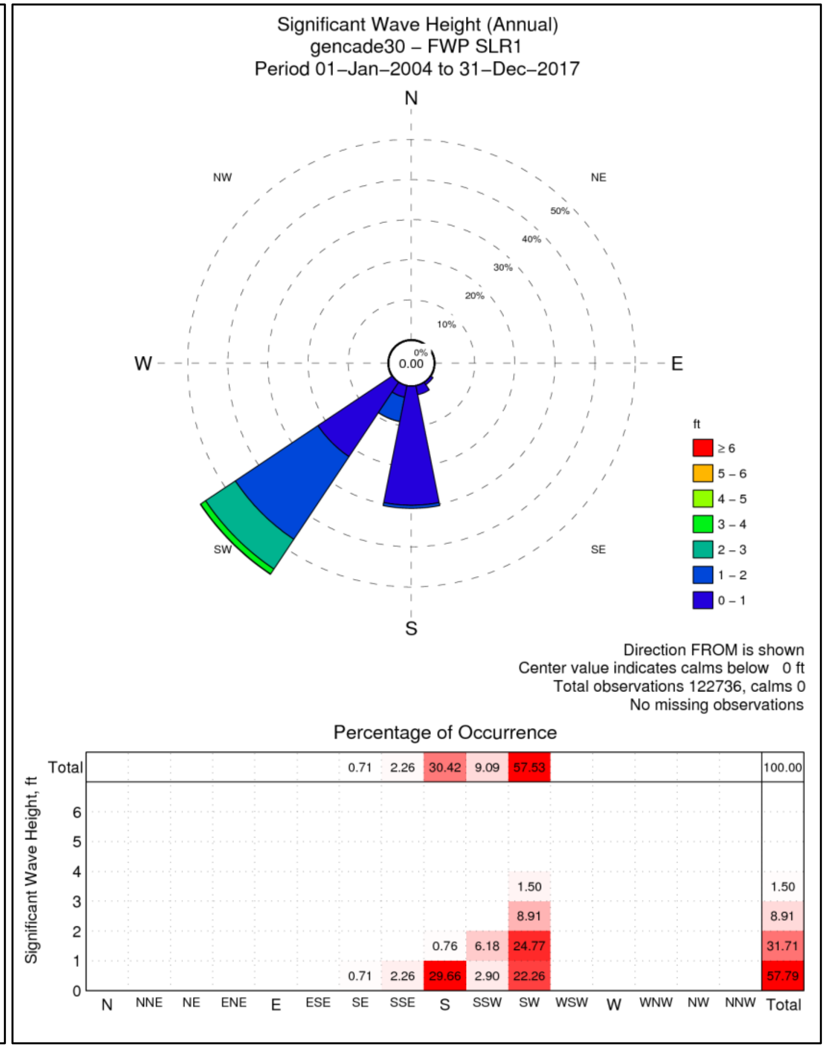

Figure 8-15: Wave height rose comparisons between FWOP and FWP at Caswell Beach nearshore location gencade30 (approximate local shoreline azimuth 105º)

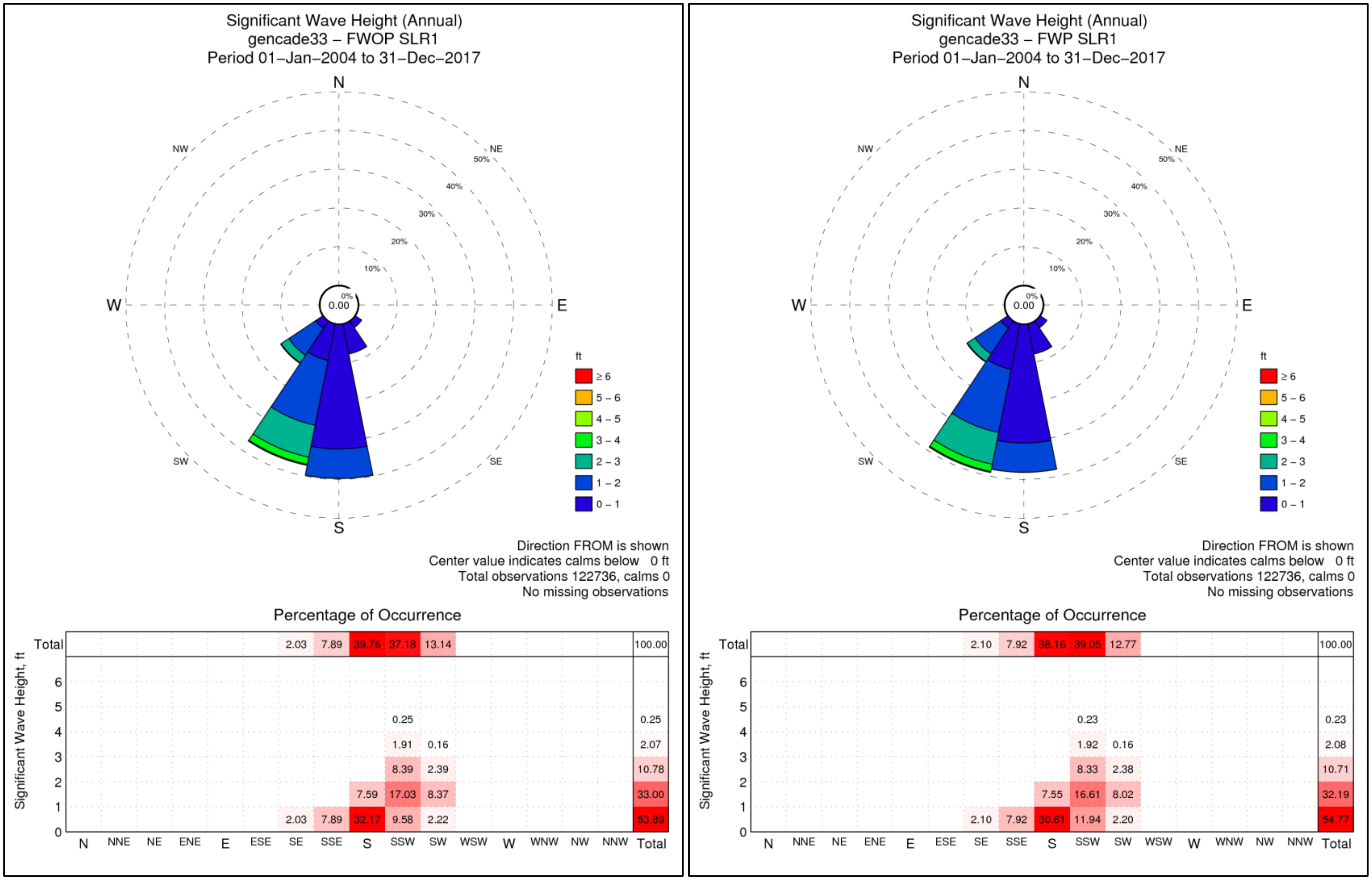

Figure 8-16: Wave height rose comparisons between FWOP and FWP at Caswell Beach nearshore location gencade33 (approximate local shoreline azimuth 110º)

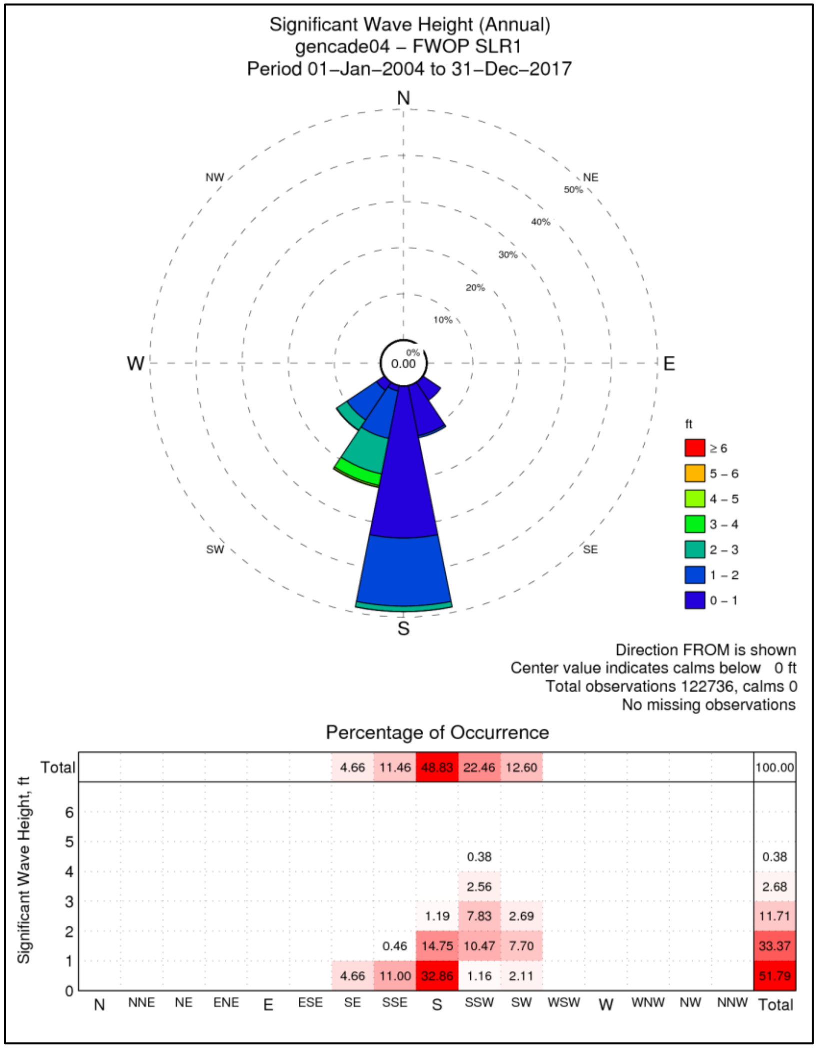

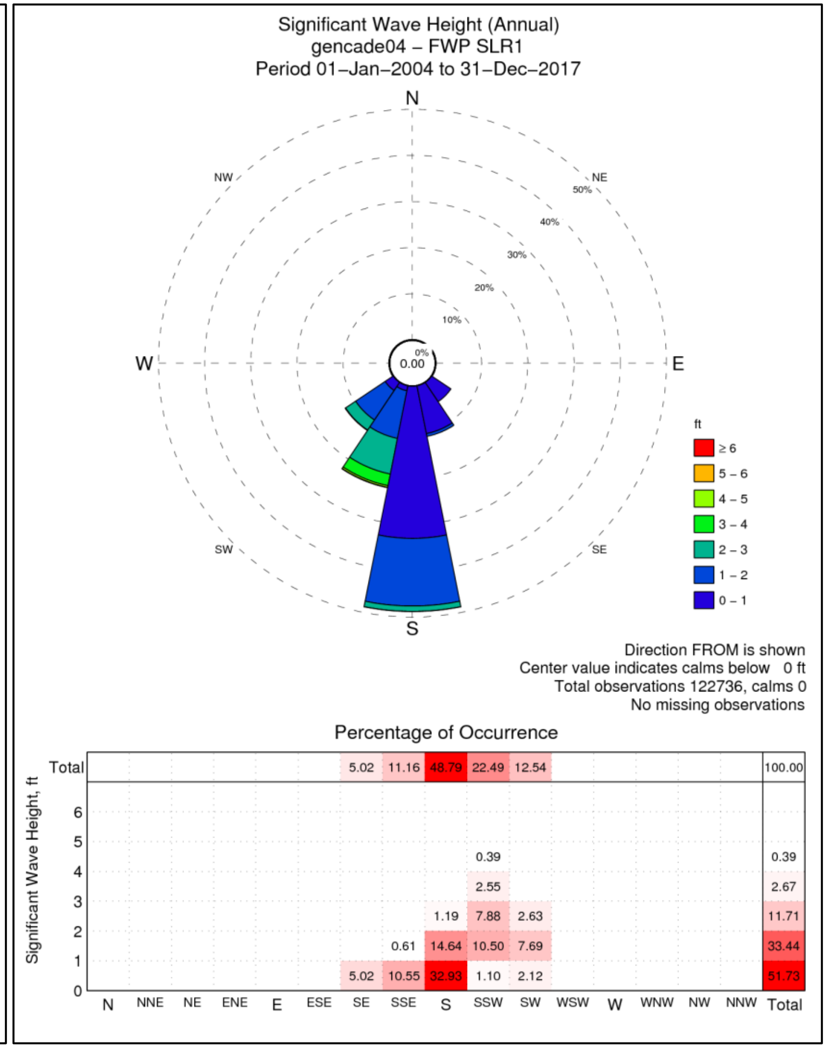

Figure 8-17: Wave height rose comparisons between FWOP and FWP at Caswell Beach nearshore location gencade04 (approximate local shoreline azimuth 110°)

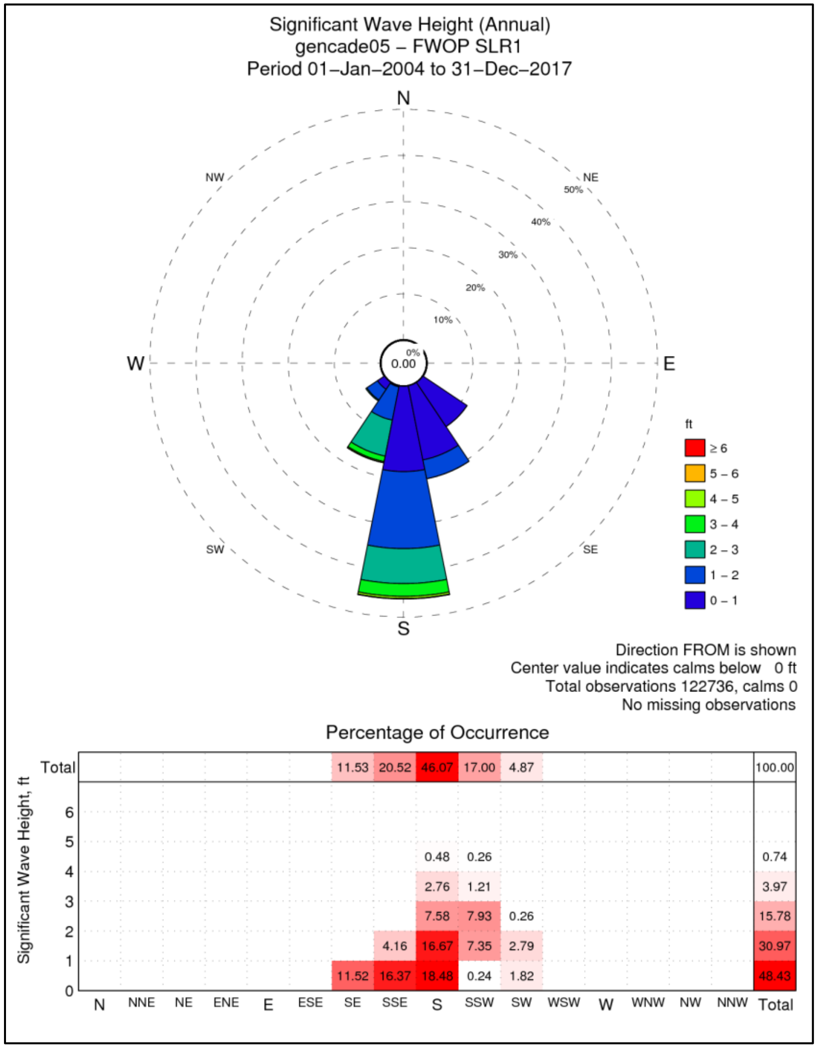

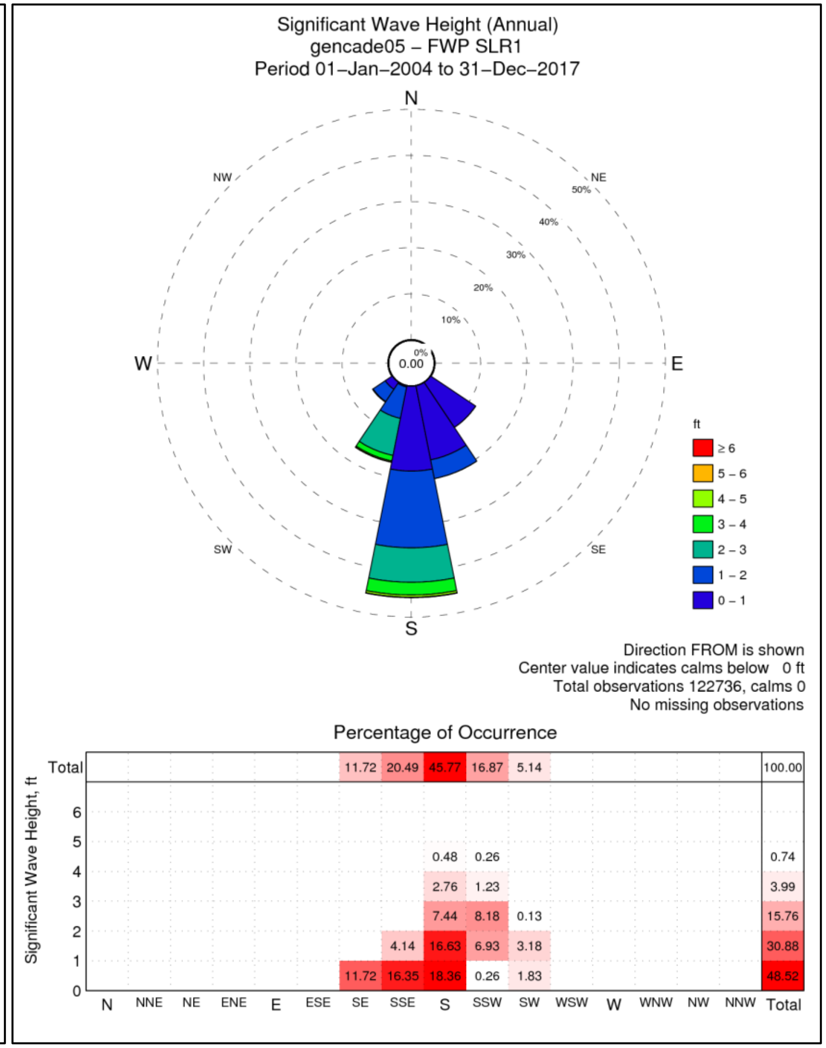

Figure 8-18: Wave height rose comparisons between FWOP and FWP at Oak Island nearshore location gencade05 (approximate local shoreline azimuth 100º)

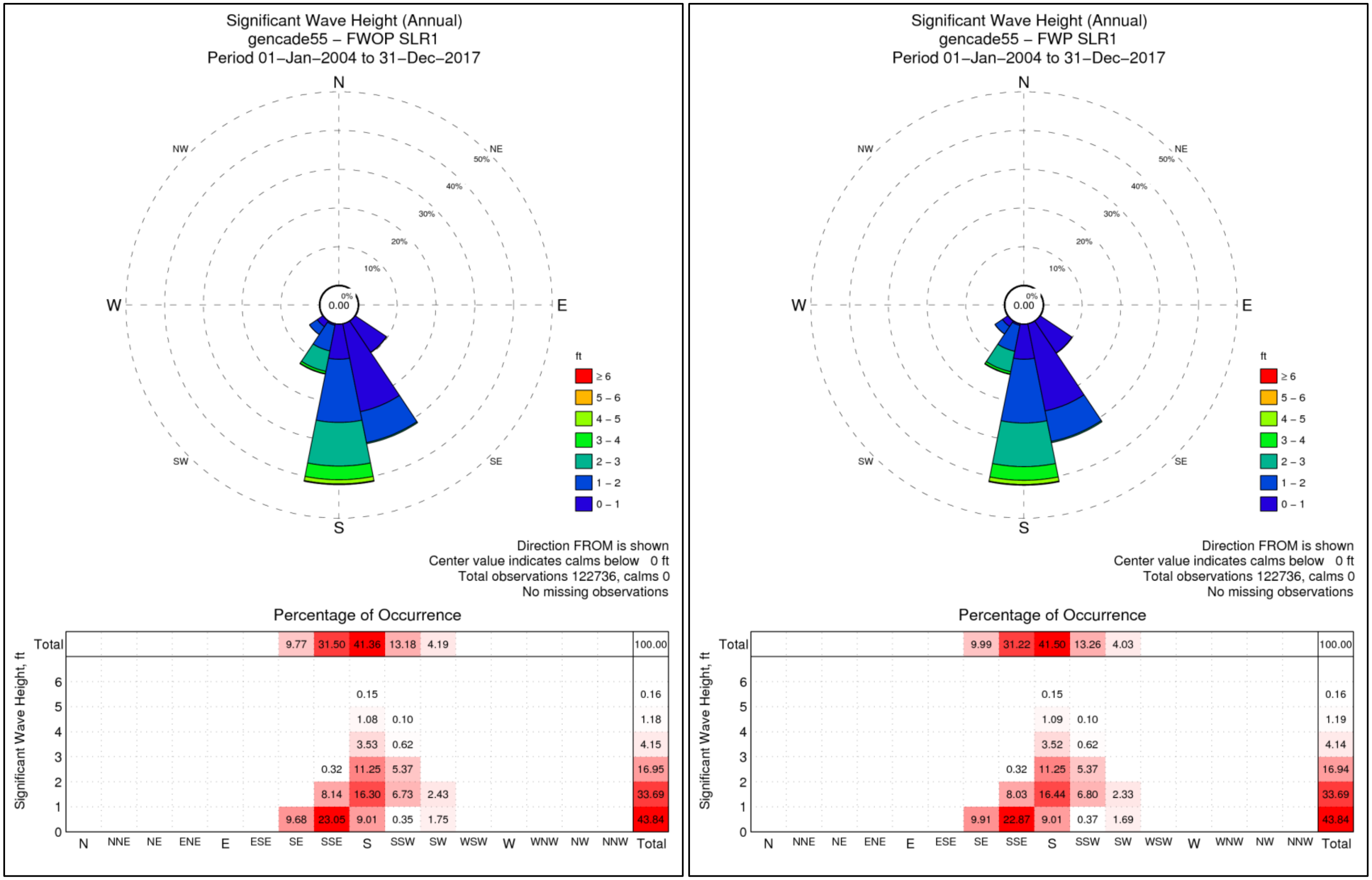

Figure 8-19: Wave height rose comparisons between FWOP and FWP at Oak Island nearshore location gencade55 (approximate local shoreline azimuth 100º)

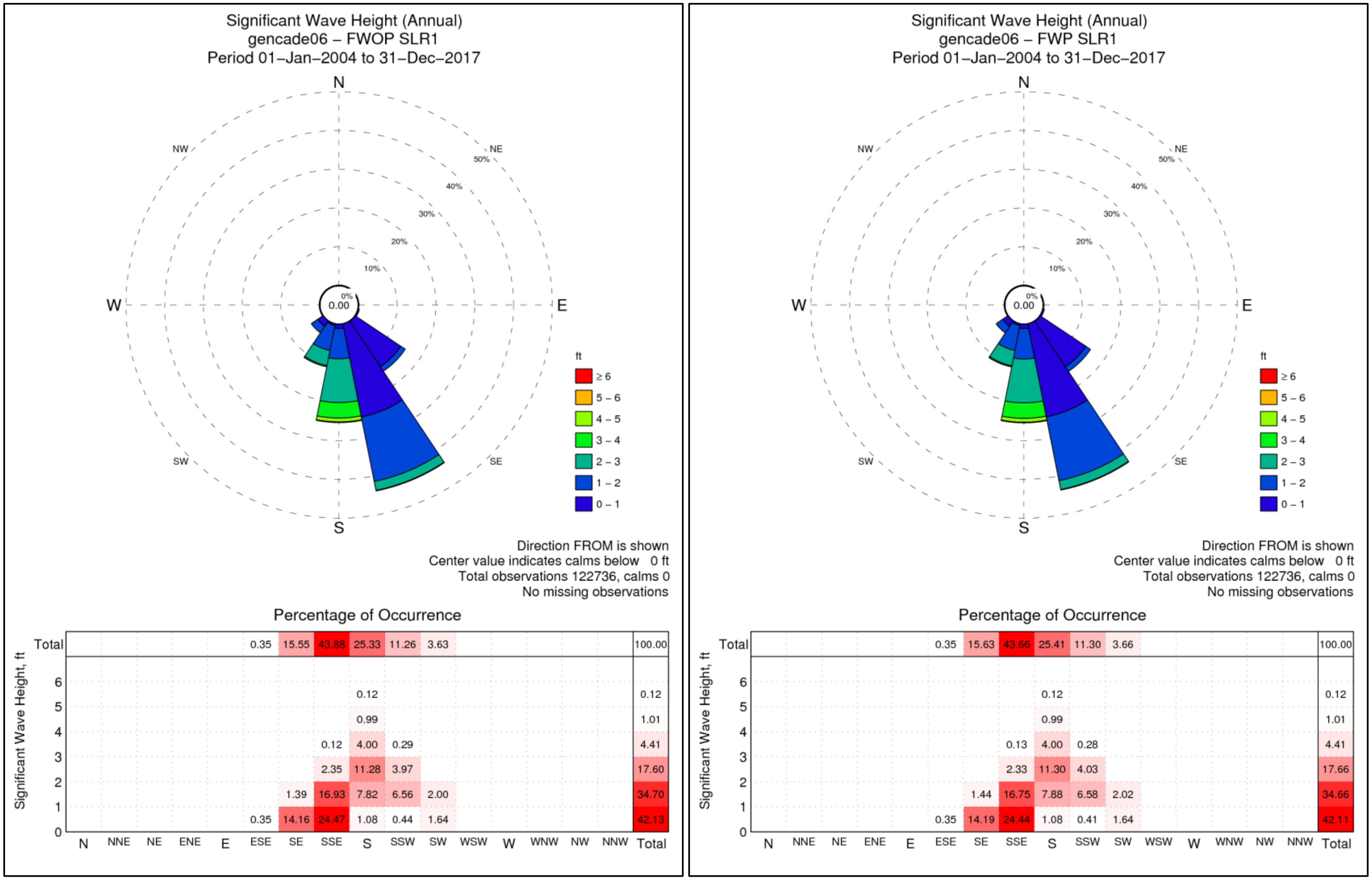

Figure 8-20: Wave height rose comparisons between FWOP and FWP at Oak Island nearshore location gencade06 (approximate local shoreline azimuth 95º)

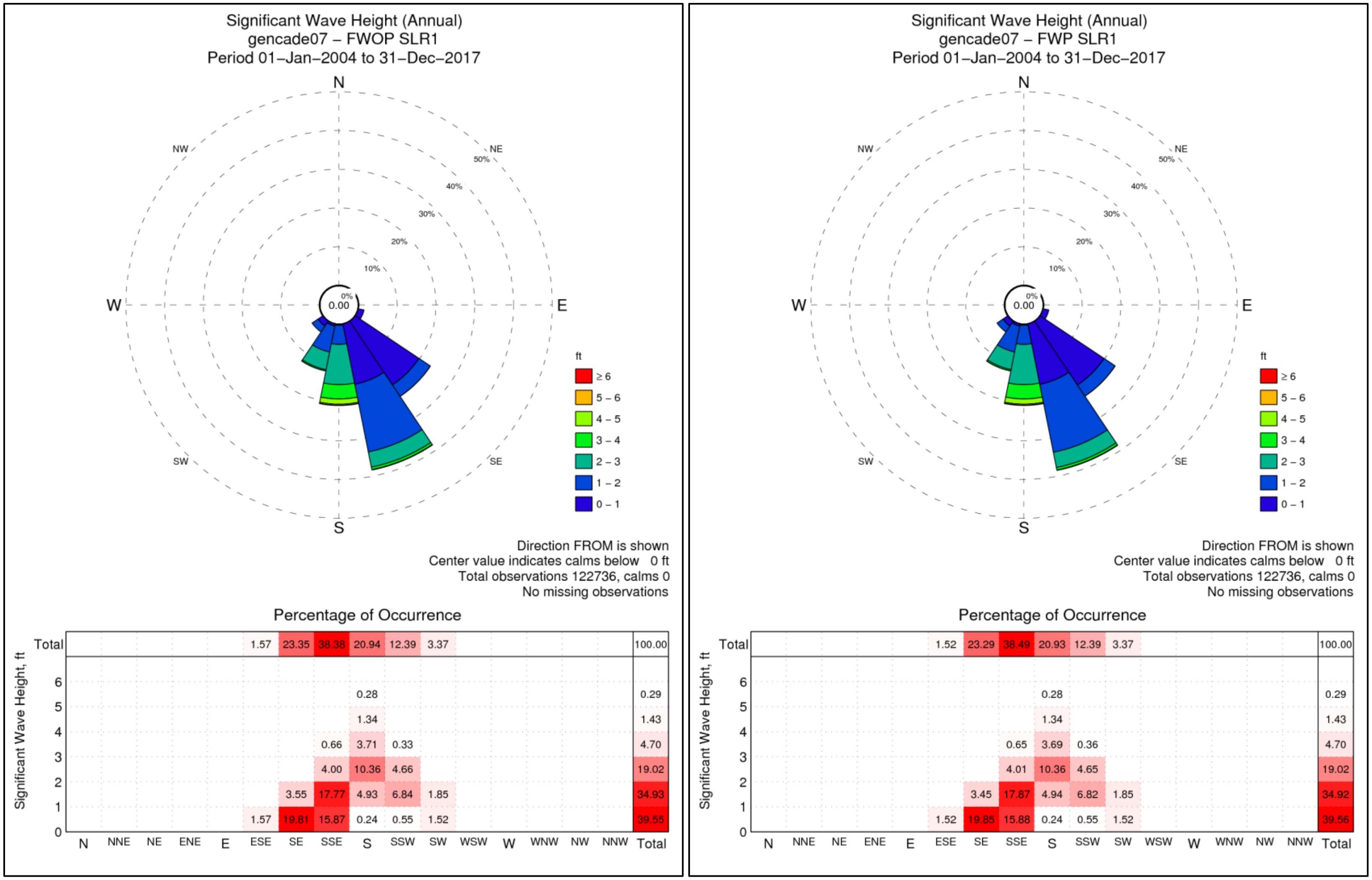

Figure 8-21: Wave height rose comparisons between FWOP and FWP at Oak Island nearshore location gencade07 (approximate local shoreline azimuth 90º)

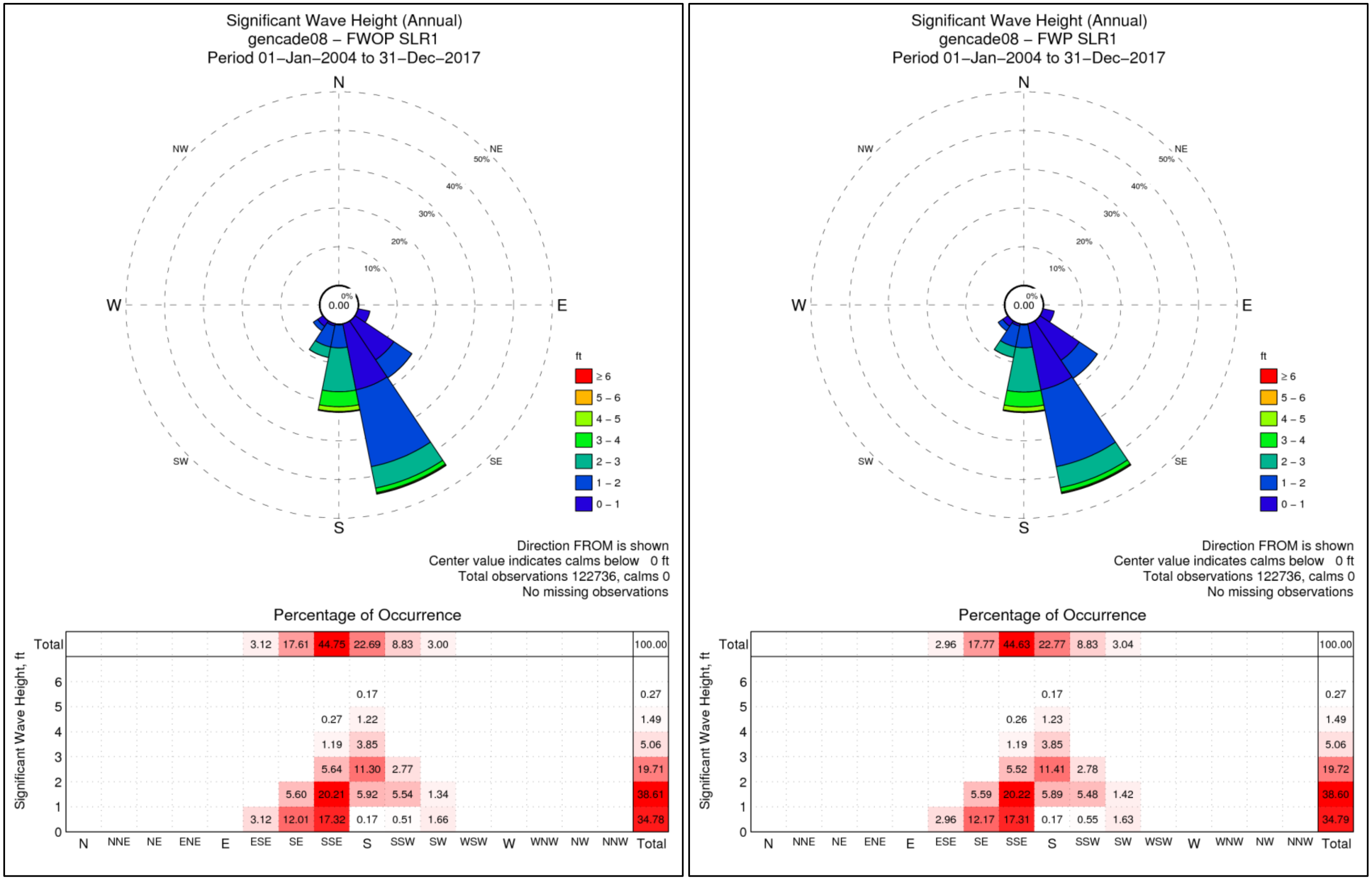

Figure 8-22: Wave height rose comparisons between FWOP and FWP at Oak Island nearshore location gencade08 (approximate local shoreline azimuth 85º)

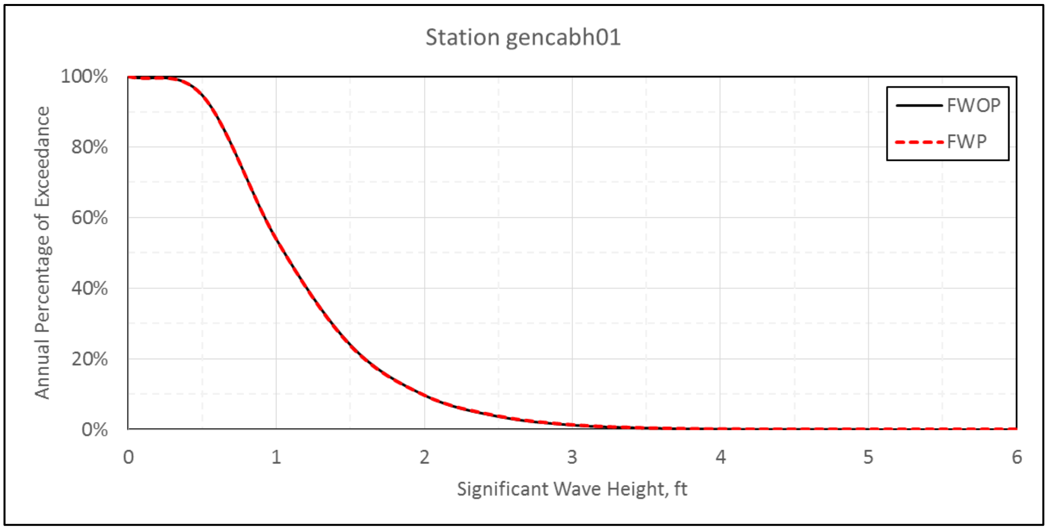

Figure 8-23: Annual percentage of exceedance of significant wave height at Bald Head Island nearshore location gencabh01 (2004 – 2017)

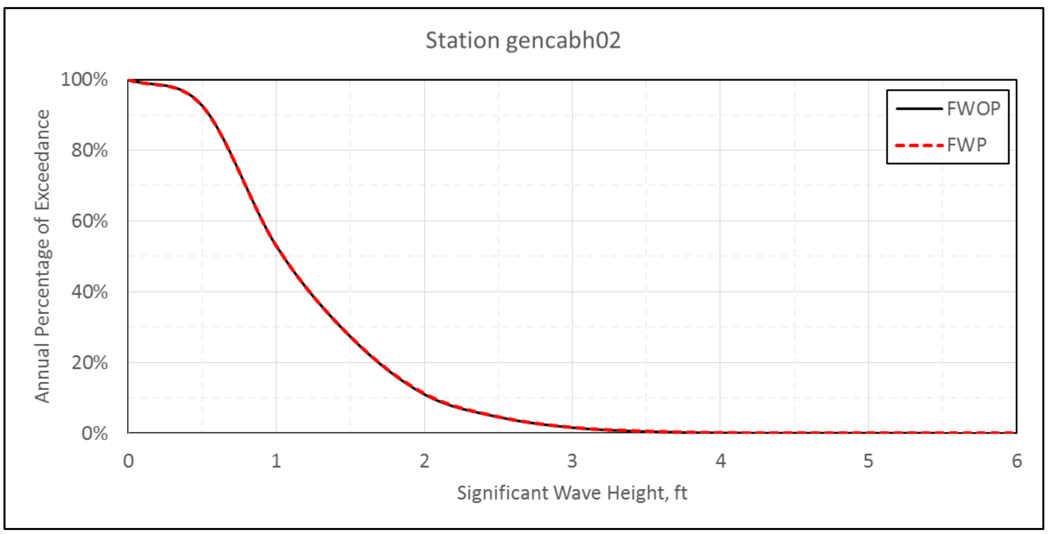

Figure 8-24: Annual percentage of exceedance of significant wave height at Bald Head Island nearshore location gencabh02 (2004 – 2017)

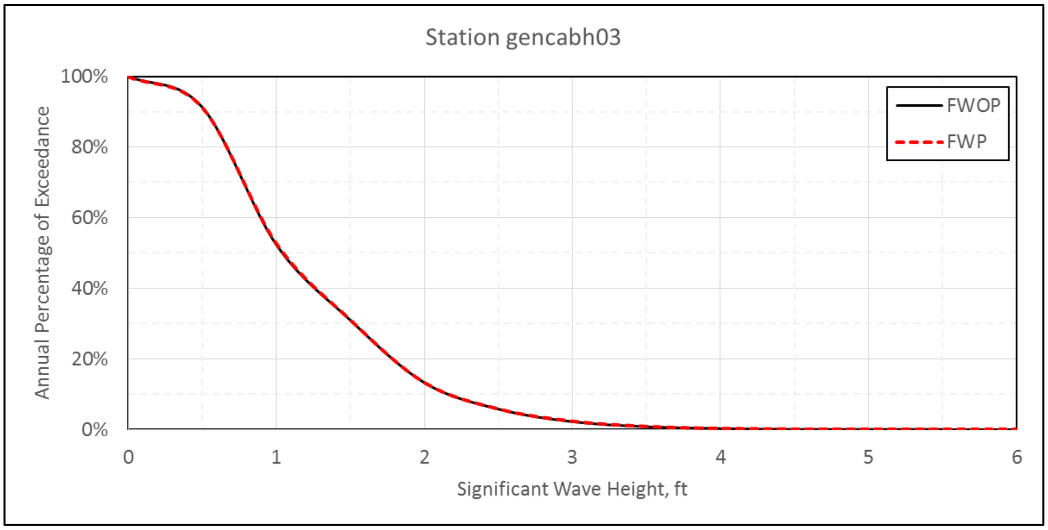

Figure 8-25: Annual percentage of exceedance of significant wave height at Bald Head Island nearshore location gencabh03 (2004 – 2017)

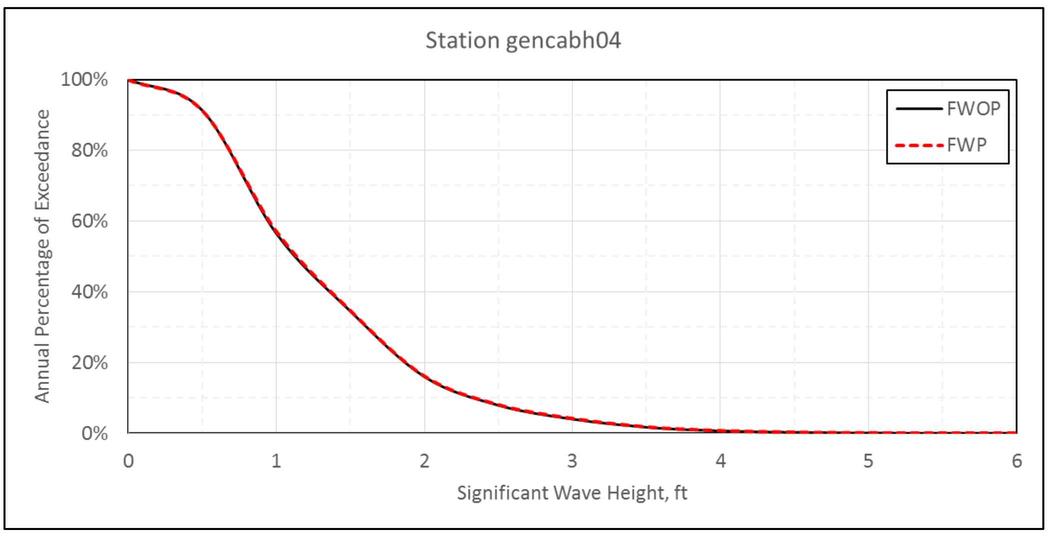

Figure 8-26: Annual percentage of exceedance of significant wave height at Bald Head Island nearshore location gencabh04 (2004 – 2017)

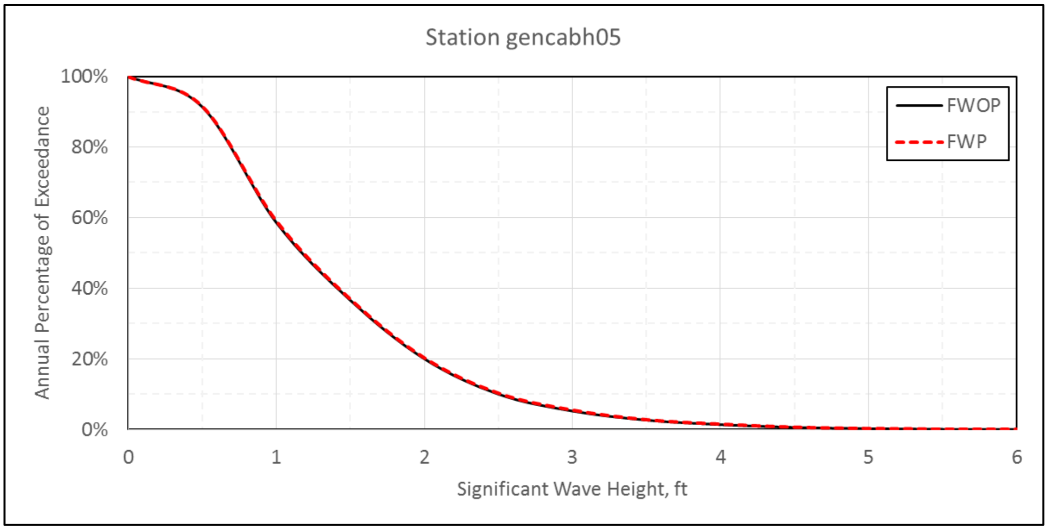

Figure 8-27: Annual percentage of exceedance of significant wave height at Bald Head Island nearshore location gencabh05 (2004 – 2017)

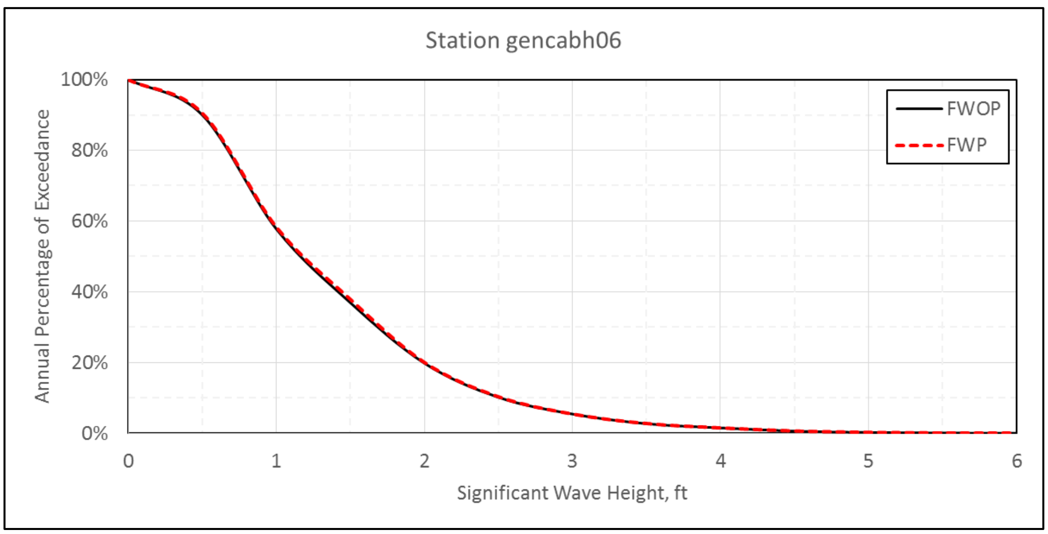

Figure 8-28: Annual percentage of exceedance of significant wave height at Bald Head Island nearshore location gencabh06 (2004 – 2017)

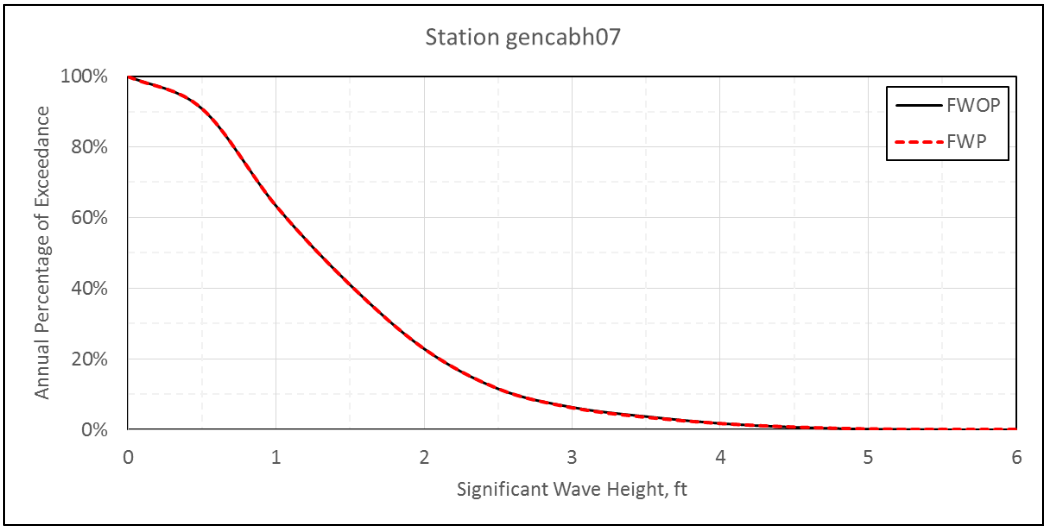

Figure 8-29: Annual percentage of exceedance of significant wave height at Bald Head Island nearshore location gencabh07 (2004 – 2017)

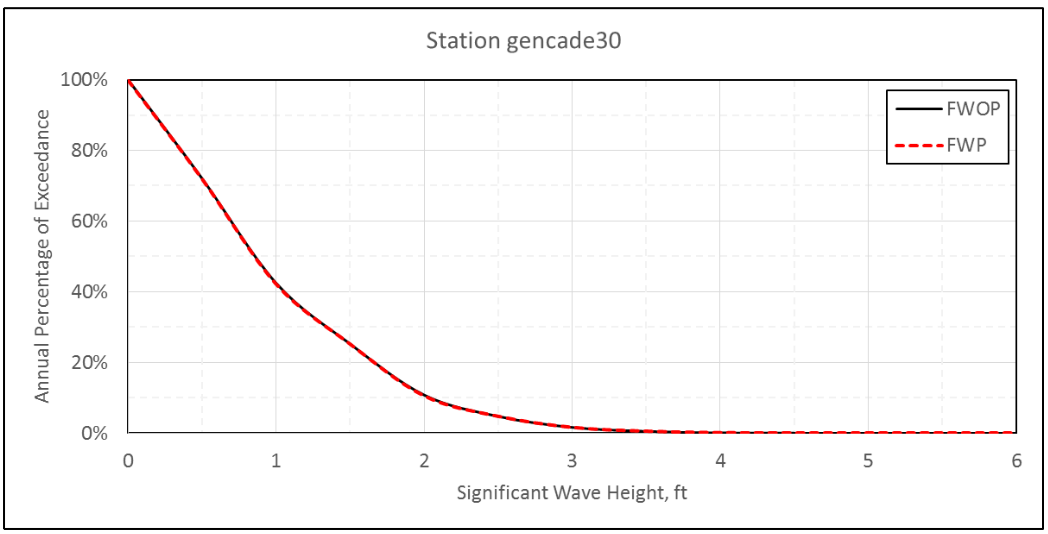

Figure 8-30: Annual percentage of exceedance of significant wave height at Caswell Beach nearshore location gencade30 (2004 – 2017)

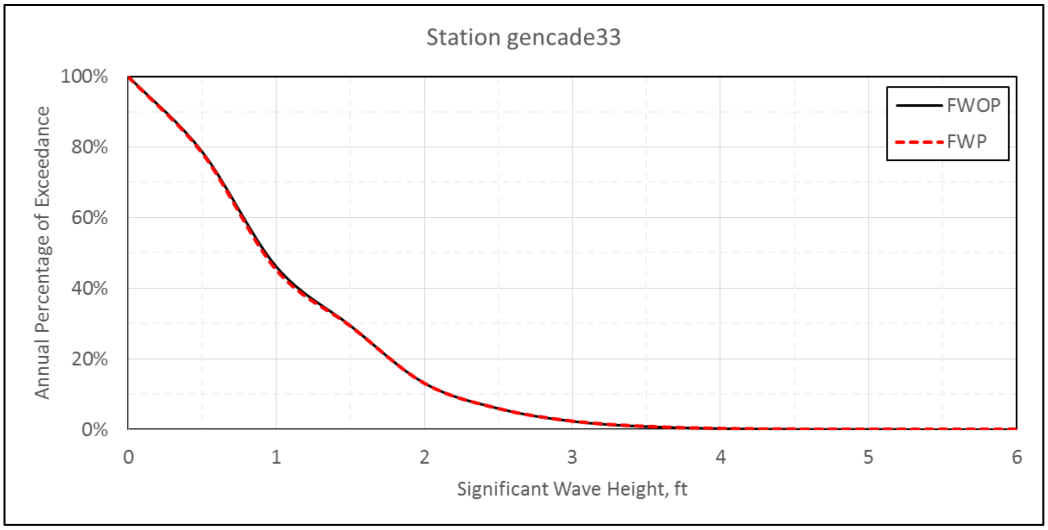

Figure 8-31: Annual percentage of exceedance of significant wave height at Caswell Beach nearshore location gencade33 (2004 – 2017)

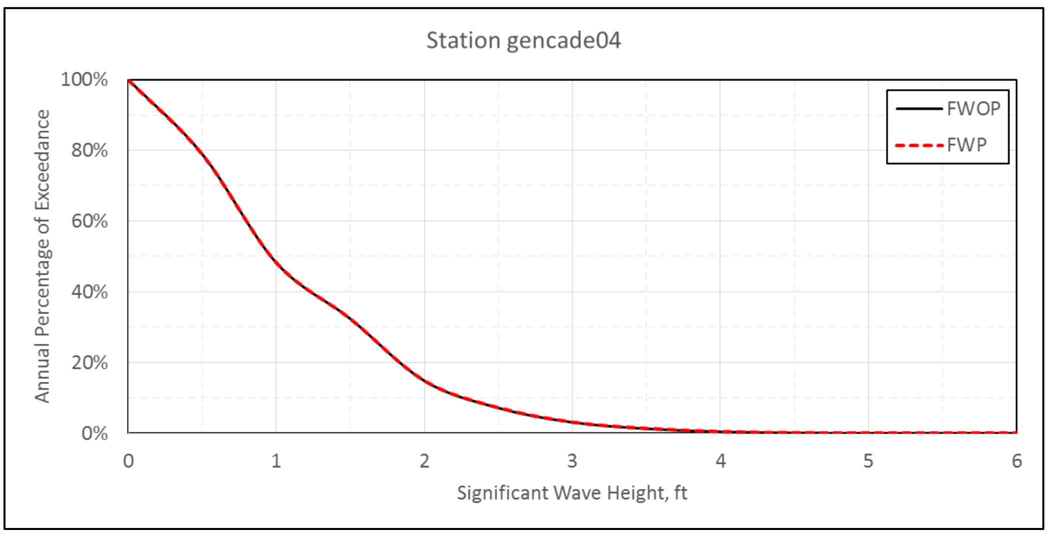

Figure 8-32: Annual percentage of exceedance of significant wave height at Caswell Beach nearshore location gencade04 (2004 – 2017)

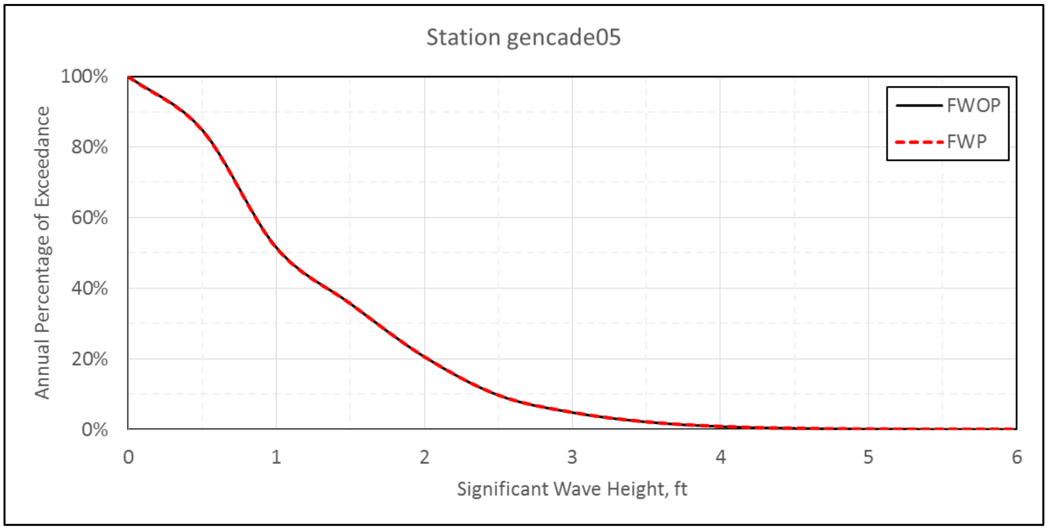

Figure 8-33: Annual percentage of exceedance of significant wave height at Oak Island nearshore location gencade05 (2004 – 2017)

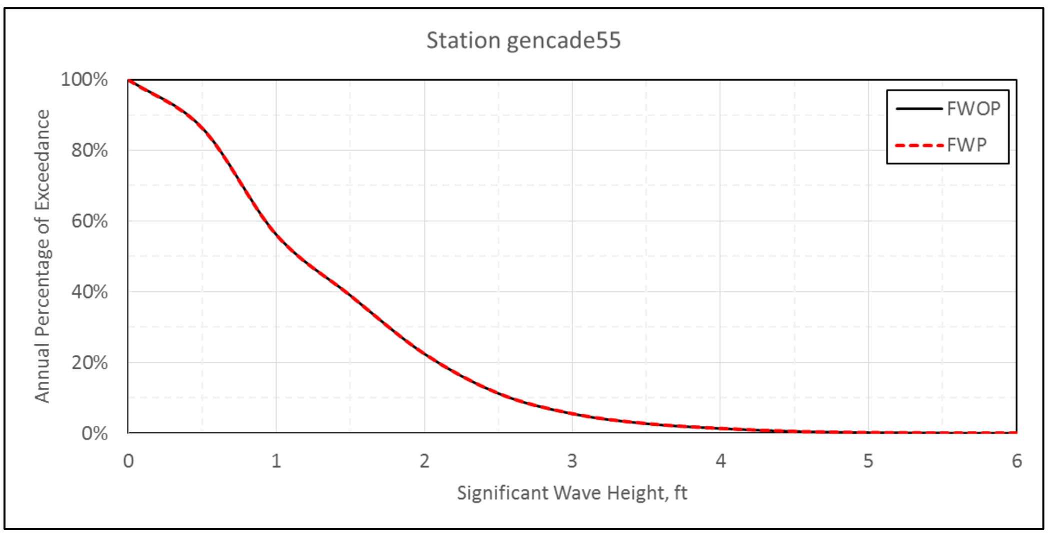

Figure 8-34: Annual percentage of exceedance of significant wave height at Oak Island nearshore location gencade55 (2004 – 2017)

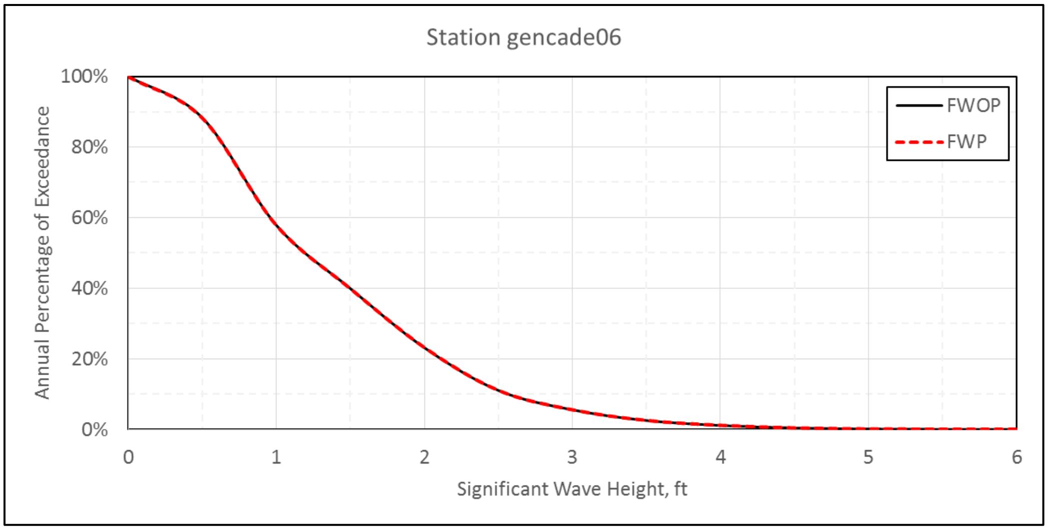

Figure 8-35: Annual percentage of exceedance of significant wave height at Oak Island nearshore location gencade06 (2004 – 2017)

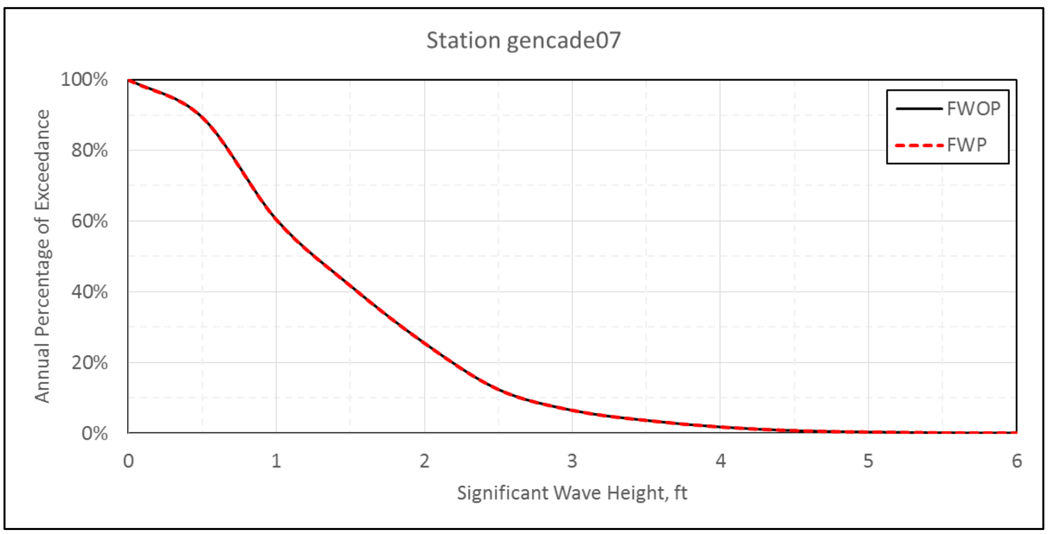

Figure 8-36: Annual percentage of exceedance of significant wave height at Oak Island nearshore location gencade07 (2004 – 2017)

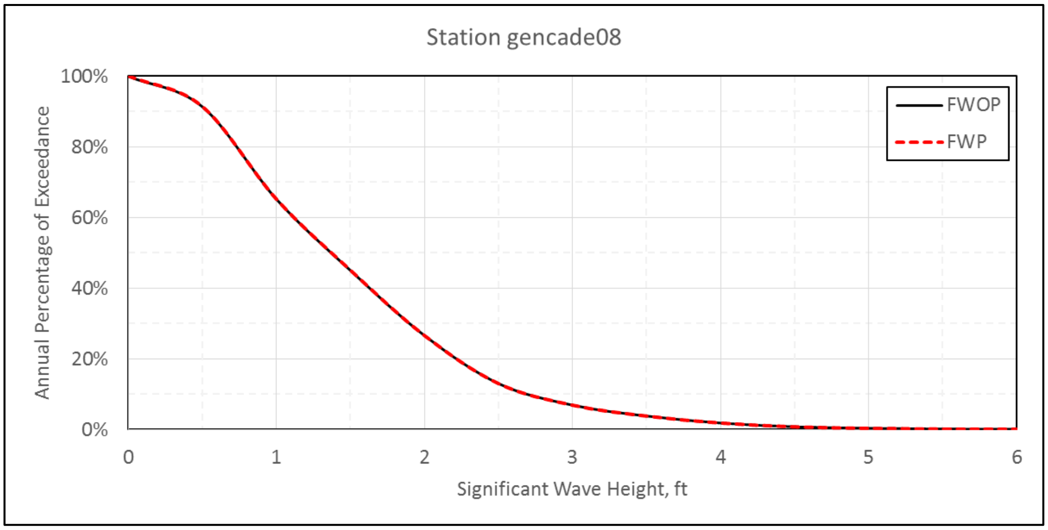

Figure 8-37: Annual percentage of exceedance of significant wave height at Oak Island nearshore location gencade08 (2004 – 2017)

Table 8-2: Significant wave height (H_s) statistics at nearshore locations

Station	25% H_s			50% H_s (mean)			75% H_s			99% H_s		
	FwoP	FwP	FwP-FwoP	FwoP	FwP	FwP-FwoP	FwoP	FwP	FwP-FwoP	FwoP	FwP	FwP-FwoP
gencabh01	0.76	0.76	0.00	1.04	1.05	0.01	1.49	1.49	0.00	3.09	3.10	0.01
gencabh02	0.71	0.72	0.01	1.06	1.06	0.00	1.55	1.56	0.01	3.22	3.23	0.01
gencabh03	0.70	0.70	0.00	1.06	1.06	0.00	1.63	1.63	0.00	3.40	3.42	0.02
gencabh04	0.73	0.73	0.00	1.13	1.13	0.00	1.75	1.75	0.00	3.80	3.83	0.03
gencabh05	0.76	0.77	0.01	1.18	1.20	0.02	1.83	1.84	0.01	4.11	4.18	0.07
gencabh06	0.75	0.75	0.00	1.18	1.20	0.02	1.85	1.86	0.01	4.16	4.16	0.00
gencabh07	0.80	0.81	0.01	1.27	1.27	0.00	1.90	1.90	0.00	4.28	4.26	-0.02
gencade30	0.46	0.46	0.00	0.81	0.80	-0.01	1.51	1.52	0.01	3.23	3.22	-0.01
gencade33	0.53	0.52	-0.01	0.91	0.91	0.00	1.60	1.61	0.01	3.41	3.41	0.00
gencade04	0.55	0.55	0.00	0.96	0.95	-0.01	1.69	1.69	0.00	3.60	3.61	0.01
gencade05	0.61	0.61	0.00	1.06	1.06	0.00	1.84	1.84	0.00	3.95	3.95	0.00
gencade55	0.67	0.67	0.00	1.13	1.13	0.00	1.91	1.91	0.00	4.10	4.09	-0.01
gencade06	0.69	0.69	0.00	1.17	1.17	0.00	1.94	1.94	0.00	4.04	4.04	0.00
gencade07	0.74	0.73	-0.01	1.25	1.25	0.00	2.02	2.02	0.00	4.33	4.33	0.00
gencade08	0.83	0.83	0.00	1.35	1.35	0.00	2.06	2.06	0.00	4.34	4.34	0.00

8.3. Shoreline Impacts

The near-term potential Project impacts on the adjacent Bald Head Island and Oak Island shorelines under the Low RSLR scenario were investigated using the calibrated GenCade models. However, annual shoreline retreats attributable to RSLR were not included in the model results since the focus of the current study is simply on the differences between FwoP and FwP conditions. The nearshore wave modeling results did account for the low RSLR water levels. The GenCade version (v1r6) used for this study does not have the functionality to incorporate sea level rise directly yet. The shoreline retreats due to sea level rise could be estimated by the Bruun rule (Bruun, 1962) and linearly added to the GenCade results. The annual shoreline retreats under the low RSLR scenario would be in the order of 0.5 ft/yr following the Bruun rule:

$$R = \frac{W_*}{h+B} S \qquad (31)$$

where R is the shoreline recession rate, S is the sea level change rate, W_* is the width of the active profile which is in the order of 2,000 ft in the study area, h is the depth of closure which is about 20 – 25 ft, and B is the beach berm crest elevation which is about 6 ft. It is considered to be relatively small comparing to the shoreline change rates caused by waves.

8.3.1. Initial Shoreline

The initial shoreline for the long-term shoreline change modeling was the February 2016 shoreline digitized by NCDCM based upon 2016 NC Imagery. This shoreline was the latest available shoreline during this study and had been applied as the final shoreline for the GenCade model validation process.

8.3.2. Coastal Structures

The terminal groin and the sixteen geo-textile sand tube groins on the Bald Head Island shorelines were included in the GenCade model at their current locations. Their characteristics were discussed in detail previously and were kept the same for the long term shoreline modeling.

8.3.3. Beach Fills

Any potential beach fill project in the future, either Federal or locally sponsored, was not included in this study due to the uncertainty of the placement schedule and extent.

8.3.4. Inlet Shoal Volumes

The inlet shoal volumes (ebb shoal, bypassing bars, attachment bars and flood shoal) used for the GenCade calibration and validation were kept the same for the long-term shoreline modeling.

8.3.5. Regional Contour

The regional contour is one of the many adjustment tools within GenCade that allows the model to more realistically represent the behavior of the prototype. The use of a regional contour allows the modeler to specify the underlying shoreline shape that the model will evolve towards, rather than having the model evolve toward a straight line. It is the result of all the large-scale, alongshore forcing-function non-homogeneities and underlying geology that are not accounted for in GenCade and that, in combination, cause the real-world shoreline to attain a non-straight, long-term equilibrium planform shape. The developed regional contour in the GenCade model calibration was applied.

8.3.6. Boundary Conditions

For the seaward boundary conditions, the 2004 – 2017 nearshore wave climates discussed previously were applied as the input wave conditions for the near-term shoreline change modeling in 14 years.

For the model left (east) lateral boundary, the long-term shoreline erosion rate (11.7 ft/yr) at the eastern end of the South Beach determined by NCDCM (2012) was adopted to mimic the long-term trend. This is different than the erosion rate for the model calibration/validation where a measured shoreline erosion rate of 62 ft/yr during the calibration period (2008 – 2012) was used to match the final shoreline position at the boundary. The short-term shoreline change rate used for model calibration/validation was not representative of the long-term shoreline change trend. The shoreline has been fluctuating back and forth as shown in Figure 8-38.

For the model right (west) lateral boundary, a pinned boundary condition which implies no shoreline change at this location, was applied. This is the same as in the GenCade model calibration/validation.

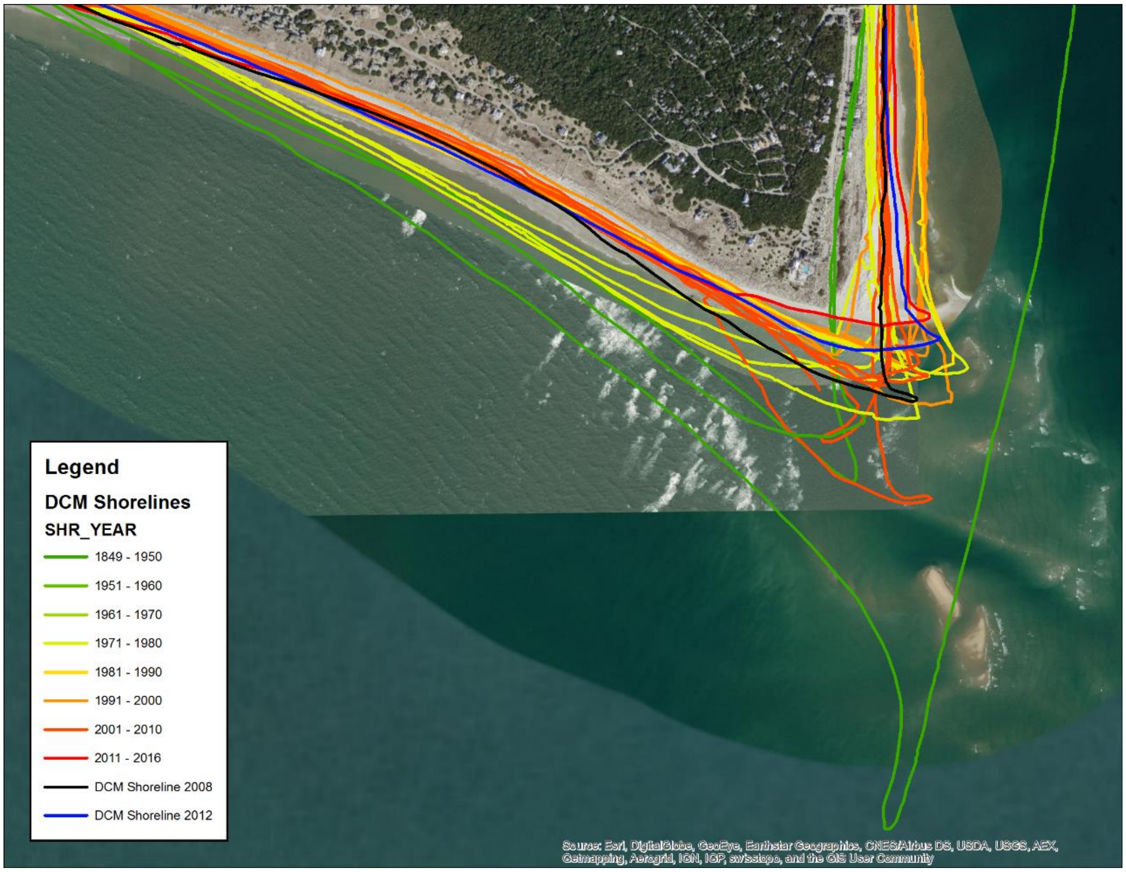

Figure 8-38: Historical shoreline positions at east end of South Beach, Bald Head Island

8.3.7. Sediment and Beach Characteristics

The sediment size, berm height, depth of closure, and sediment transport parameters (K_1 and K_2) were the same as those used in the GenCade model calibration/validation. The transport rate coefficient, K1, is used to control the time-scale and magnitude of the simulated shoreline change, while K2 is used to control shoreline change and longshore sand transport in the vicinity of structures.

8.3.8. Model Results

The shoreline changes and annual longshore sediment transport rates after 14 years based on the wave data from 2004 to 2017 were calculated by the GenCade model for both FWOP and FWP conditions.

8.3.8.1. Bald Head Island Shoreline

Figure 8-39 presents the calculated Bald Head Island annual shoreline change rates for both FWOP and FWP conditions under the low RSLR scenario. The GenCade model results indicate that the Project could have minimal impacts on the central South Beach shoreline reaches between 92+15 and 170+02 as compared to the baseline erosion rates; with rates only as much as 0.6 ft/yr higher than without Project conditions. The model results also suggest the Project could have minimal favorable impacts on the western end of the South Beach shoreline, with an average of 1.3ft/yr less erosion than without Project conditions.

The calculated annual net longshore sediment transport rates along the South Beach shoreline are presented in Figure 8-40. The Project could result in westerly longshore transport rate increases by as much as 3,800 cy/yr comparing to without Project conditions. However, given the model uncertainties, these potential changes should be considered minimal at best.

8.3.8.2. Oak Island/Caswell Beach Shoreline

The long-term shoreline change rates and annual net longshore sediment transport rates along Oak Island/Caswell Beach are presented in Figure 8-41 and Figure 8-42, respectively.

The model results indicate that the Project impacts on the Oak Island/Caswell Beach shoreline change rates (including existing "hot spots") would be negligible as compared to the baseline erosion rates; less than 0.1ft/yr difference over most of the island and a slight reduction of 0.2 ft/yr in erosion at the eastern end of Caswell Beach. The longshore sediment transport rate results also suggest minimal impacts due to the Project.

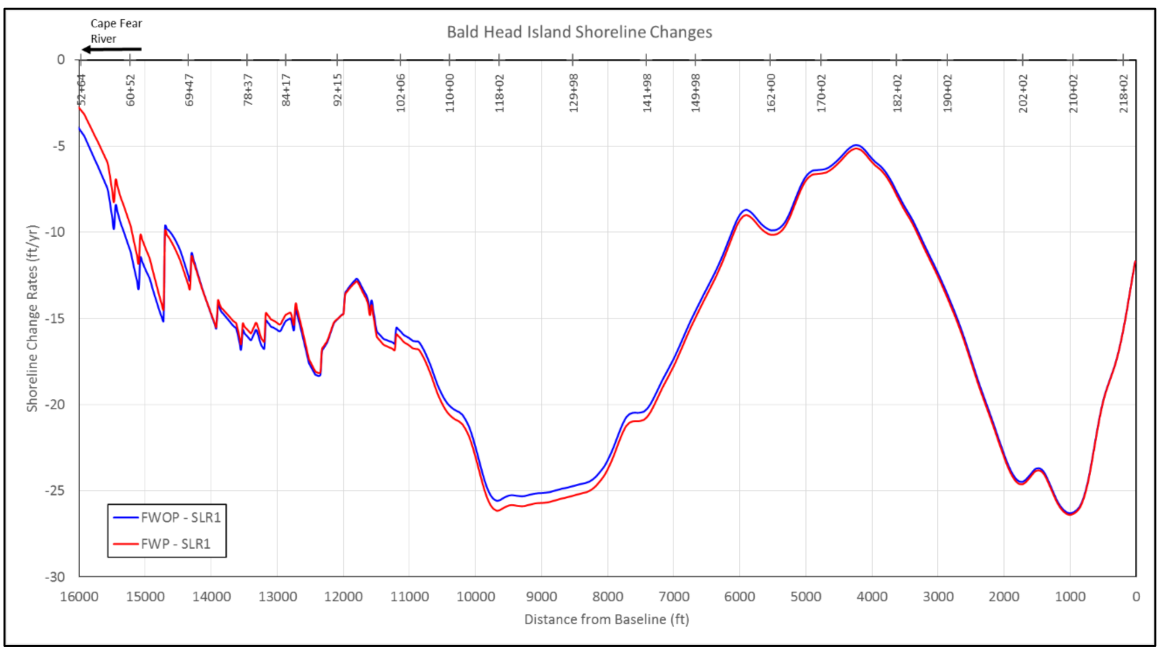

Figure 8-39: Calculated long-term shoreline impacts along Bald Head Island

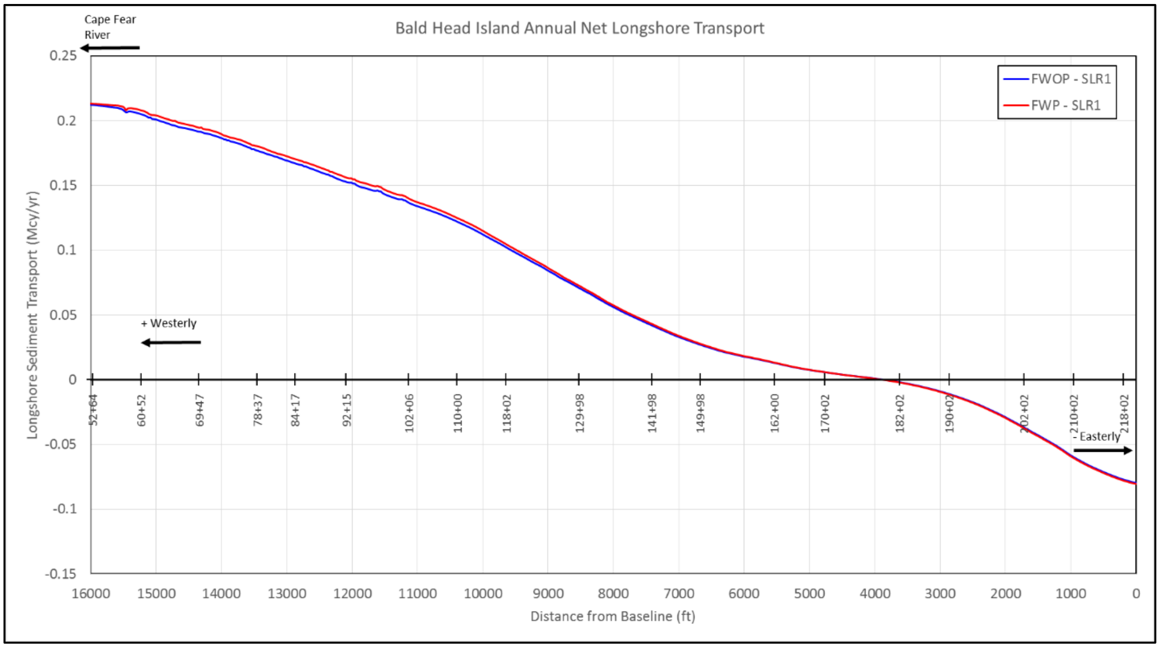

Figure 8-40: Calculated long-term net longshore transport rates along Bald Head Island

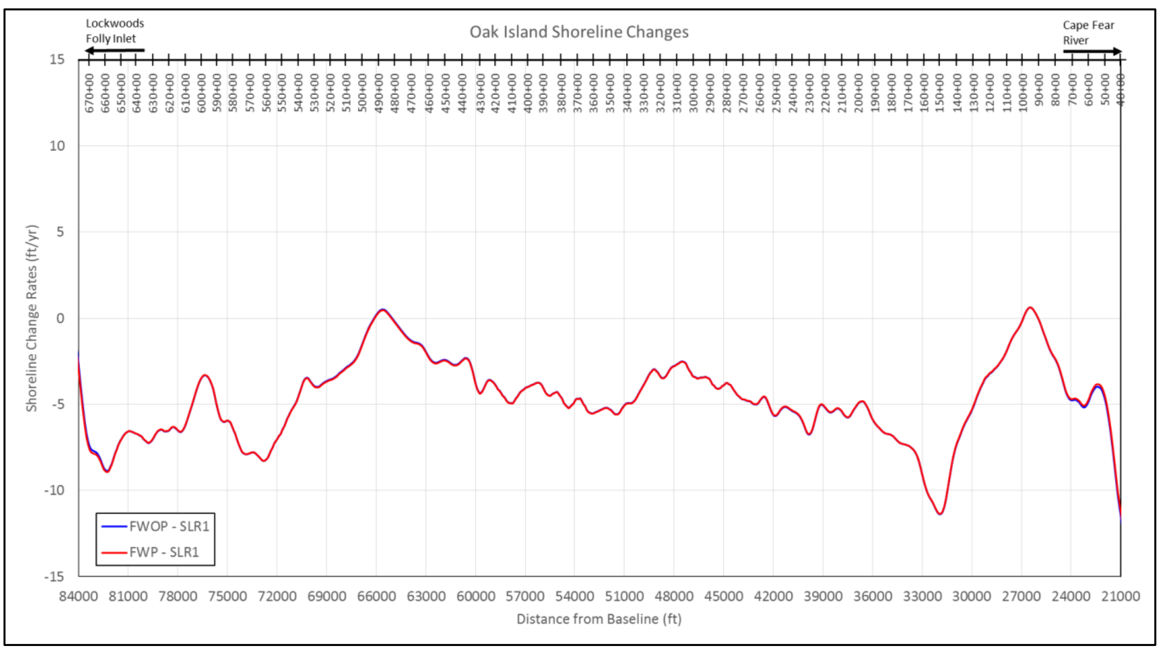

Figure 8-41: Calculated long-term shoreline impacts along Oak Island/Caswell Beach

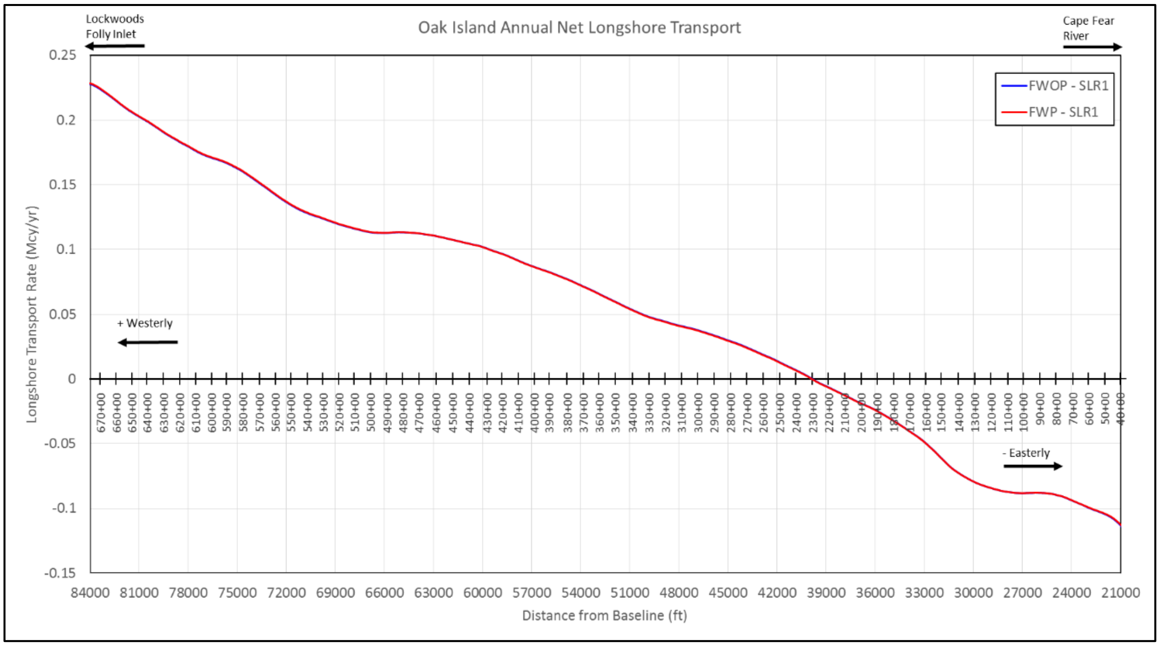

Figure 8-42: Calculated long-term net longshore transport rates along Oak Island/Caswell Beach

8.4. Entrance Channel Morphology

The potential Project impacts on the entrance channel annual shoaling volumes under the Low RSLR scenario were investigated using the calibrated entrance channel morphology model.

The model setups were the same as the model calibration except for the initial model bathymetries which incorporated the FWOP and FWP channel conditions including accurately representing the proposed channel widening and deepening and the resulting side slopes. The shoaling volumes in the entrance channels were calculated after a 1-year simulation of sediment transport and morphology changes under annual average wave conditions. Tide and wave schematizations were the same as those used during model calibration.

Table 8-3 presents the shoaling volumes in the three ocean inner bar entrance channel reaches for three different sediment grain sizes: 0.15mm, 0.20mm and 0.25mm. The shoaling volumes were computed between the channel setback lines based on the modeled cumulative sedimentation in the channels. The USACE setback distance is ~150 ft for the existing Cape Fear River entrance navigation channels, and it is assumed to be the same for the Project design channels for shoaling volume calculation purposes.

The results generally indicate that the Project could cause slightly more shoaling in all three channel ranges, especially in Baldhead Shoal Reach 1 where the shoaling volume could increase between 7% and 25% depending on the grain size. In both Smith Island and Baldhead Shoal Reach 2, the shoaling volume increases would be about 5% or less.

However, based on the recommendations from the calibration report, it is assumed that the grain size for Smith Island and Baldhead Shoal Reach 1 is 0.25mm; and for Baldhead Shoal Reach 2, an average between 0.15mm and 0.20mm. Thus, the total shoaling volume increase for these three reaches potentially caused by the Project, as shown in Table 8-4, would be about 8%.

Table 8-3: Shoaling volumes in the entrance channels (cy/yr)

Channel range	**0.15mm**		**0.20mm**		**0.25mm**	
	FWOP	FWP	FWOP	FWP	FWOP	FWP
Baldhead Shoal Reach 1	483,000	517,700	207,570	237,520	126,270	158,450
Baldhead Shoal Reach 2	429,540	444,890	176,730	186,350	130,250	134,960
Smith Island	508,600	515,010	395,760	401,410	292,630	304,760
Total	1,421,140	1,477,600	780,060	825,280	549,150	598,170
% total increase		4%		6%		9%

Table 8-4: Potential Changes in shoaling volumes due to the Project (cy/yr)

Channel Reach		
	FWOP	FWP
Baldhead Shoal Reach 1	126,270	158,450
Baldhead Shoal Reach 2	303,140	315,620
Smith Island	292,630	304,760
Total	722,040	778,830
% total increase		8%

9. Groundwater and Vessel Wake Modeling

9.1. Groundwater

9.1.1. Background

Groundwater Management Associates, Inc. (GMA) developed a three-dimensional, steady-state, seven-layer groundwater flow model to evaluate the potential effects of the proposed deepening on regional and local groundwater flow patterns and the potential for saltwater intrusion into fresh water aquifers (see Appendix E-1 and Appendix E-2 for complete reports). The groundwater flow model was constructed using the Groundwater Modeling System interface (GMS 10.3.7) with the United States Geological Survey (USGS) groundwater model, MODFLOW-NWT. MODFLOW is a modular, three-dimensional groundwater-flow model code that simulates groundwater flow using a finite-difference method applied to a block-centered rectangular grid.

Previous channel modifications for the Port of Wilmington were modeled by Jeff Lautier with the North Carolina Department of Environment and Natural Resources, Division of Water Resources using the 3D finite element model, FEMWATER. GMA initially attempted to update the original FEMWATER model to simulate the proposed channel modifications. Due to the age of the NCDWR model, software changes over the last 10 years, and limitations of the original modeling code, this effort proved unsuccessful. GMA then constructed and calibrated a finite difference MODFLOW model to encompass the area potentially affected by the proposed channel modifications. This modeling effort has incorporated the results of field exploration and data collection, aquifer testing, groundwater-level monitoring, as well as geographic and geologic data.

The focus of the modeling program was to evaluate the potential for saltwater intrusion into the groundwater system as a result of deepening and widening of the existing Cape Fear River channel. GMA's model predicts hydraulic head in four aquifers potentially affected by the channel deepening – the Surficial, the Castle Hayne, the Upper Peedee, and the Lower Peedee - under steady state conditions based on regional water-level information from 2017.

9.1.2. Model Assumptions

- The model area covers 1,134 square miles and encompasses most of New Hanover and Brunswick Counties.
- Grid cell dimensions are 1000 feet by 1000 feet (almost 23 acres per cell).
- The model includes 7 layers that simulate the Surficial Aquifer (SA), the Castle Hayne Confining Layer (CHCL), the Castle Hayne Aquifer (CHA), the Upper Peedee Confining Layer (UPCL), the Upper Peedee Aquifer (UPDA), the Lower Peedee Confining Layer (LPCL), and the Lower Peedee Aquifer (LPDA). These layers represent all hydraulic units that are locally in contact with, or are hydraulically influenced by, the Cape Fear River channel. In addition, the model includes a deeper aquifer (the LPDA) that is not hydraulically influenced by the Cape Fear River Channel.

- The model area encompasses the region and layers modeled by the NCDWR in 1998. The NCDWR framework study and model assumptions were the foundation of the input parameters incorporated by GMA into the MODFLOW model.
- The NCDWR model framework and input assumptions were updated to incorporate results from drilling at three new monitoring well stations adjacent to the Cape Fear River channel. The framework was further modified to incorporate subdivisions of the Peedee Aquifer into upper and lower units based upon available new data from other regional drilling programs. GMA's model also incorporated updated data (since 1998) on expanded groundwater usage within the model domain.
- Moffatt & Nichol provided the existing channel dimensions and river bathymetry from the Wilmington Harbor Deepening Survey of 2018. The channel is currently 42 feet deep relative to Mean Lower Low Water (MLLW).
- Channel modifications within the model were based upon a proposed deepening to a 47-foot deep channel relative to MLLW level. This channel depth was provided by Moffatt & Nichol as the selected channel modification. To simulate channel deepening, GMA modified grid elevations within the channel to match the proposed 47-foot deep channel.
- GMA calibrated the model relative to available water-level data from 2017.
- Hydraulic boundaries assigned to the model included:
    - Ocean set constant at zero (feet MSL).
    - Cape Fear River set constant at zero (feet MSL).
    - Intracoastal Waterway set constant at zero (feet MSL).
    - General head boundaries established along the western and northern margins of the model area and along the shoreline (for the LPDA) to account for hydraulic influence of areas outside the model domain.
    - Drains were incorporated along major streams to simulate loss of groundwater to local discharge features (such as creeks, rivers, and swamps) within the model domain.

9.1.3. Model Calibration

GMA adjusted recharge rates, hydraulic conductivities, and boundary conditions to achieve a close match of simulated heads with observed head data from 2017. Most adjustments were made manually to establish a close correlation between known hydraulic data and model assigned properties. Final calibration was accomplished using PEST, a model-independent parameter estimation and uncertainty analysis, to achieve an optimal match between known and simulated head values. All recharge and hydraulic conductivity values were within the range of published values for the model domain. A comparison between modeled and observed groundwater levels indicate a good fit ($r^2 = 0.98$). A mean absolute residual error of 1.61 feet and a root mean squared residual of 2.07 feet were achieved.

9.1.4. Baseline Simulations of Existing Conditions

A baseline groundwater flow model was initially developed using current channel geometry to simulate existing conditions. Results from the model of existing conditions indicates the following:

- The Cape Fear River serves primarily as a discharge area for the Surficial Aquifer. Heads in the Surficial Aquifer adjacent to the river channel are higher than the head in the River, and groundwater flow is toward the River.

- The Cape Fear River also acts as a discharge area for both the Castle Hayne and the Upper Peedee Aquifers except in local areas where production well pumping has depressurized those units.

- The Upper Peedee Aquifer is unconfined throughout much of the western portion of the model domain, and groundwater flow patterns within this unit mimic the patterns seen in the Surficial Aquifer.

- The Lower Peedee Aquifer is well-confined, and it appears to be uninfluenced by the Cape Fear River channel.

- Model simulations show two areas relatively close to the dredge channel where groundwater pumping has lowered groundwater heads beneath sea level. This pumping has created the *potential* for surface water to migrate downward into the groundwater system. Two identified areas proximal to the navigation channel have a downward-directed head potential. These areas include Southport in the vicinity of the Capital Power Corporation withdrawal, and the area near Carolina Beach and Kure Beach water-supply wells.

- Model results indicate that the cone of depression from the Capital Power Corporation withdrawal from the Upper Peedee Aquifer extends beneath the Cape Fear River. However, the Upper Peedee Aquifer is well confined in this region, and any downward migration of surface water would be slow. The newly constructed monitoring well station at Southport includes an Upper Peedee Aquifer monitoring well placed adjacent to the Cape Fear River, between the river channel and the Capital Power Corporation wellfield. Groundwater heads in this monitoring well are consistently about 4 feet below mean sea level as a result of pumping from the Capital Power Corporation wellfield. Despite the downward directed head gradient relative to the River, groundwater samples collected from this well are fresh, which suggests that the UPDA is well confined in this region. Furthermore, tidal variation of water levels in the UPDA monitoring well is muted, indicating that the aquifer is not directly connected to tidal surface water in the Cape Fear River.

- The Carolina Beach wellfield exists in close proximity to a paleochannel where erosion has removed the Castle Hayne Confining Layer, thereby exposing the Castle Hayne Aquifer to enhanced local recharge from the Surficial Aquifer. This paleochannel was described by the US Geological Survey, and the feature was incorporated into the NCDWR model and into the current MODFLOW model. The lack of effective confinement of the Castle Hayne Aquifer near Carolina Beach makes the area vulnerable to saltwater intrusion from the ocean and from the Cape Fear River. Furthermore, this region also exhibits thinning or absence of the confining layer between the Castle Hayne and the Upper Peedee Aquifers. Groundwater withdrawals from the Upper Peedee and Castle Hayne Aquifers at Carolina Beach and at Kure Beach have locally lowered the potentiometric surfaces within these aquifers to below sea level, thereby allowing water from the Surficial Aquifer, and from adjacent surface water bodies (the Ocean and the Cape Fear River), to move downward into the Castle Hayne and Peedee Aquifers. Existing localized saltwater intrusion in the vicinity of Carolina Beach has been an ongoing challenge to the Carolina Beach public water system. The groundwater flow model predicts groundwater levels below sea level in the vicinity of Carolina Beach. This prediction is consistent with existing known saltwater intrusion issues. The area of saltwater intrusion potential near Carolina Beach is intrinsic to the existing geological conditions (i.e., poor confinement of the Castle Hayne and Upper Peedee Aquifers) and to the groundwater withdrawal patterns that have lowered the equipotential surface below sea level. The existing localized saltwater intrusion issues at Carolina Beach appear to be unrelated to the existing navigation channel of the Cape Fear River, because the depressurization below sea level does not extend beneath the current river to the navigation channel position.

9.1.5. Simulations of Proposed Sea Level Rise and Channel Modifications

GMA used bathymetry data for the planned 47-foot deep channel improvement provided by Moffatt & Nichol to adjust the elevation of the top of layer one in the calibrated groundwater flow model. GMA identified areas where the proposed channel deepening would incise into a different aquifer or confining unit. GMA changed the model parameters in those model cells, as appropriate, to reflect the direct connection between the deepened channel with the newly exposed aquifer or confining layer materials. GMA then re-ran the calibrated model to evaluate the effects of the channel deepening. To evaluate the potential effects of sea-level rise, GMA also performed simulations of both the existing and the modified channel geometry under a projected 2.56 foot rise in sea level. This corresponds to the Army Corps of Engineers' "high" estimate for projected sea-level rise for the year 2077 (50 years after construction is completed) and is the "worst" case SLR scenario with respect to potential project impacts on groundwater resources; thereby bracketing these potential impacts. GMA's groundwater simulations of the modified channel and sea-level rise effects indicate the following:

- The proposed channel deepening project does not significantly influence groundwater flow patterns. In fact, groundwater flow patterns for all four modeled aquifers (SA, CHA, UPDA, and the LPDA) were virtually identical under the proposed channel modification simulations.

- The proposed channel deepening adjacent to Southport does not breach or thin the Upper Peedee Confining Layer, and therefore the proposed channel does not increase the potential for saltwater intrusion into the Upper Peedee Aquifer in that area. Model simulations reveal no effect on the groundwater flow patterns near Southport in response to proposed channel modifications.

- Simulations also indicate that the planned channel improvement will not increase the potential for saltwater migration in the vicinity of the Carolina Beach or Kure Beach municipal water-supply wells. The predicted depressurized area around these well fields impinges upon the shoreline of the Cape Fear River, but does not extend to the navigational channel, located more than a mile away on the west side of the river. If future groundwater withdrawals from this area are excessive, especially from wells placed closest to the river, salinity may increase as salty surface water migrates towards the wellfield. Model results suggest, however, that the channel deepening is too far removed from the pumping wells at Carolina Beach and Kure Beach to affect saltwater intrusion in this semiconfined area.

- Simulations for sea level rise, both with and without channel modifications, showed very little changes to the patterns of groundwater flow and discharge. Model results suggest that sea-level rise will not increase the potential for saltwater intrusion associated with proposed channel modifications.

In summary, groundwater modeling indicates that the proposed channel modifications will not increase the potential for saltwater intrusion above what currently exists within the system. Modeling indicates that the cone of depression from pumping in the Southport area extends beneath the Cape Fear River, and this pumping has created the *potential* for downward migration of salty surface water into the Upper Peedee Aquifer. Importantly, however, the Upper Peedee Aquifer in this area is well confined, and the aquifer exists approximately 50 feet *below* the proposed channel bottom. Thus, the proposed channel deepening near Southport would not impact the degree of confinement of the Upper Peedee Aquifer beneath the channel. Likewise, the proposed channel modifications near Carolina Beach are not projected to affect the potential for saltwater intrusion in that area. The naturally poor confinement of the Castle Hayne and Peedee Aquifers near Carolina Beach, and the existing groundwater withdrawal conditions have resulted in localized saltwater intrusion under existing conditions. Model results indicate that the proposed channel modifications do not alter these existing groundwater conditions.

9.2. Vessel Wakes

An evaluation was made of the effect of ship generated waves with regards to bed shear stress in the vicinity of Southport, Battery Island, and Orton Point, NC as a result of the deepened and widened channel and larger design vessel, 12,400 TEU container ships. The current channel design vessel is an 8,000 TEU container ship.

9.2.1. Ship-Generated "Waves"

This section describes the characteristics of ship-generated effects in narrow channel. The following section is adapted from several sources including PIANC (1987), Sorensen (1997), and Schiereck (2004).

9.2.1.1. Primary Wave

From a hydrodynamic point of view, flow near a moving ship is similar to flow around a fixed body such as bridge abutment. As the ship moves along the channel, there is water flow past the vessel hull opposite the direction of travel, known as the return current. The velocity head of the water flowing past the vessel causes the water level along the vessel's length to fall to maintain the total head constant. The water level around the vessel is thus lowered. This water level depression is also referred to as the primary wave, Figure 9-1.

The transition between the undisturbed water level in front of the vessel and the water level depression takes the form of a sloping water surface referred to as the front wave. The water surface immediately ahead of the vessel is elevated by the approaching ship and so the total height of the front wave is slightly greater than the water level depression.

The transversal stern wave is the transition between the water level depression and the normal water level behind the ship.

The combination of water level depression, front wave and transversal stern wave will hereafter be referred to as the primary wave. The primary wave behaves like long solitary wave with a length similar to that of the ship. Therefore, the primary wave is not easily observed in the field, other than in the case of relatively large vessels sailing in confined channels. The primary wave does not "break" at the shoreline as "normal" waves do. It is more like a tidal "pulse", slowly rising and falling as the vessel passes.

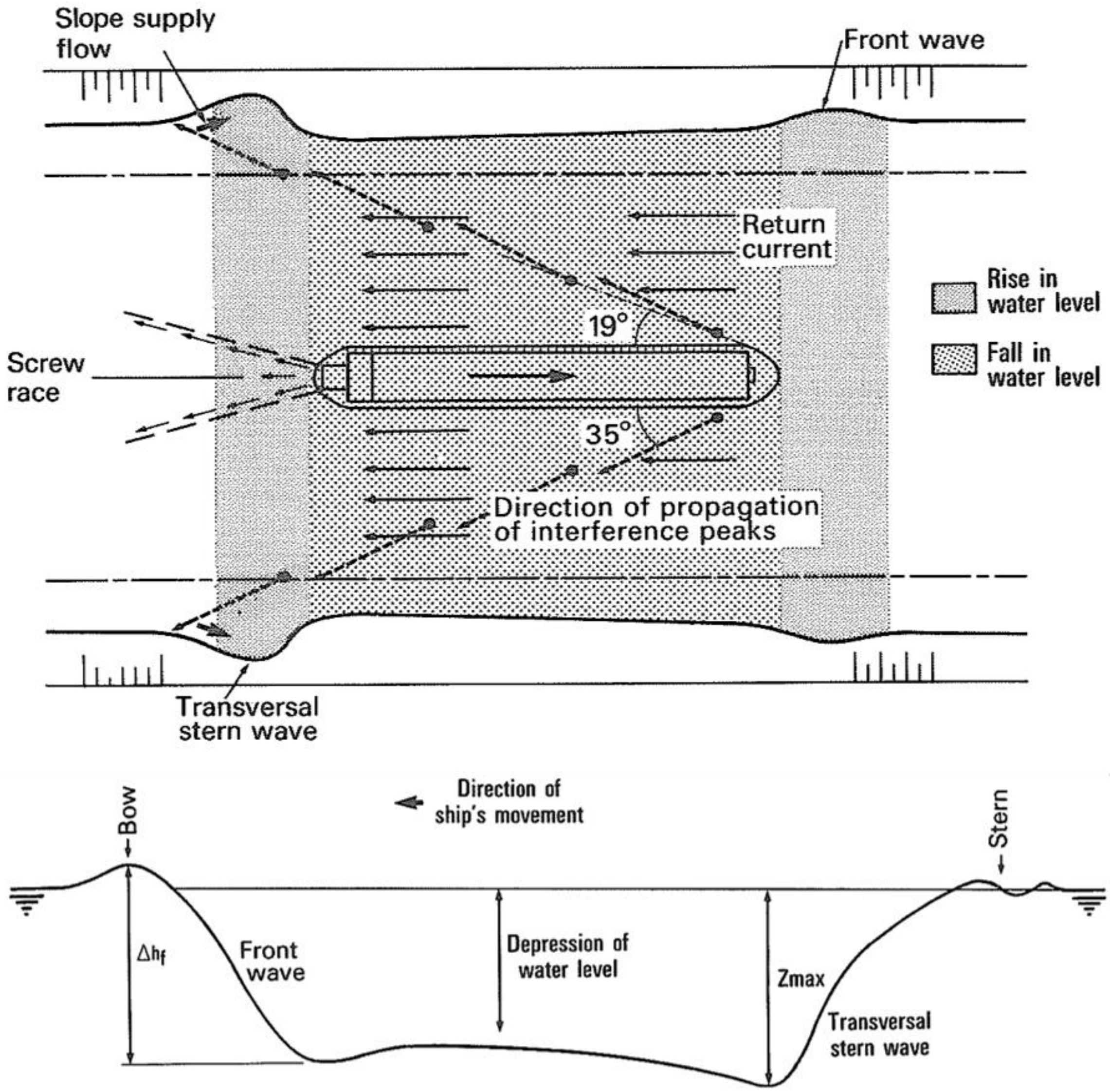

(adapted from PIANC 1987)

Figure 9-1: Components of Ship Induced Water Motions

9.2.1.2. Secondary Wave

When responding to the sharp rise and fall in the water surface at the bow and the stern, inertia causes the water surface to lag behind its equilibrium position and produces a surface oscillation. This, in turn, produces the pattern of free surface waves generally called secondary waves that propagate from the vessel, Figure 9-2. The pattern spreads out from the vessel with decreasing wave amplitudes due to diffraction. The pattern consists of symmetrical sets of diverging waves that move obliquely out from the sailing line and a single set of transverse waves that move in the direction of the sailing line. The transverse and diverging waves meet to form cusps, also called interference peaks, located along a pair of lines that form an angle of 19.5 degrees with the sailing line. The highest wave in the pattern are found along the cusp locus line. A similar pattern of waves, but typically with much lower amplitudes, is generated at the vessel stern and superimposed on the pattern generated out from the bow. These secondary waves are the ones that are generally visible in the field. Secondary waves are always "short" and behave like "normal" waves, which means that the general linear wave theory relations for wave length, celerity etc. are valid. They also break as the approach the bank shoreline and breaking type is dictated by the same slope and wavelength relationship as other "normal" waves.

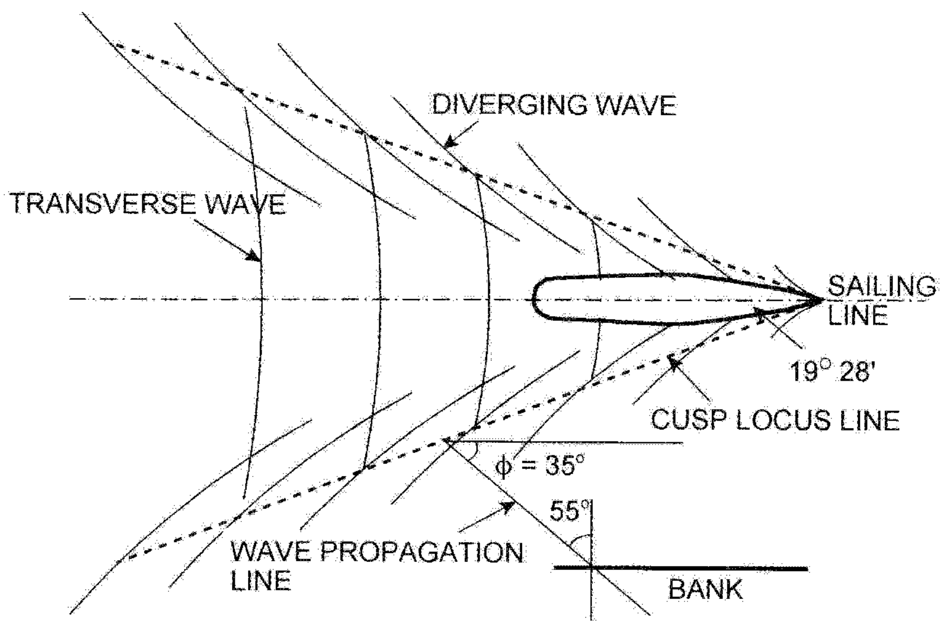

Figure 9-2: Secondary Wave Pattern

9.2.2. Ship Wake Modeling

This section focuses on prediction and analysis of ship generated primary and secondary waves including the effect of the proposed channel deepening and widening project in the Cape Fear River. To evaluate the primary ship generated wave the XBeach model (Roelvink, et al., 2015) was used. However, XBeach cannot accurately represent the secondary ship generated waves, so an analytical approach was used to evaluate the secondary waves.

9.2.2.1. Primary Wave Modeling

The XBeach model (Roelvink, et al., 2015) was used to evaluate the primary wave induced by the design and current container vessel used in the Cape Fear River Navigation Channel. XBeach was originally developed as a two-dimensional shallow-water flow model to simulate morphological change in the nearshore environment. XBeach has two modes, a hydrostatic mode and a non-hydrostatic model. The hydrostatic mode solves the short-wave amplitude variation separate from the long wave transformation, currents, and morphological change. While the non-hydrostatic mode no longer requires the short-wave action balance and instead solves all processes including the short-wave motions and a non-hydrostatic pressure. As a result, the non-hydrostatic mode has the ability to resolve both the short and long waves which is needed to simulate ship wakes.

The non-hydrostatic mode of XBeach has a specific application of generating and propagating ship wake that was implemented by (Zhou, 2013) and calibrated in several studies (e.g. De Jong et. al., 2013, Zhou et al., 2014). A moving ship is introduced into model domain as a pressure head that creates a water level depression equal to the vessel displacement. The vessel moves throughout the model domain along a pre-defined track that moves the area of increased pressure simulating the passing ship. This application of XBeach was applied to the Cape Fear River in the vicinity of Southport, Battery Island, and Orton Point, N.C.

9.2.2.2. Model Domain

Two base XBeach models were used for this analysis, one in the vicinity of Southport and Battery Island and another one in the vicinity of Orton Point. The Southport & Battery Island and Orton Point Models will be known as the SPBI and OP models, respectively, hereinafter.

The SPBI model domain covered an area of 3,500 m x 6,000 m and was composed of a rectilinear grid with 5 m x 5 m resolution. A grid with 2 m x 2 m spacing was tested and resulted in no significant differences, indicating the original grid resolution was sufficient to resolve the ship wake. The SPBI model domain is shown in Figure 9-3. The SPBI model covers Southport Channel, Battery Channel, and Lower Swash Channel Ranges and portions of Bald Head Caswell and Snows Marsh Channel Ranges.

The OP model domain covered an area of 3,000 m x 5,300 m and was composed of a rectilinear gird with 5 m x 5 m resolution. The OP mode domain is shown in Figure 9-4. The OP model covers portions of Upper Midnight Channel and Lower Lilliput Ranges.

Figure 9-3: Southport and Battery Island Model Domain

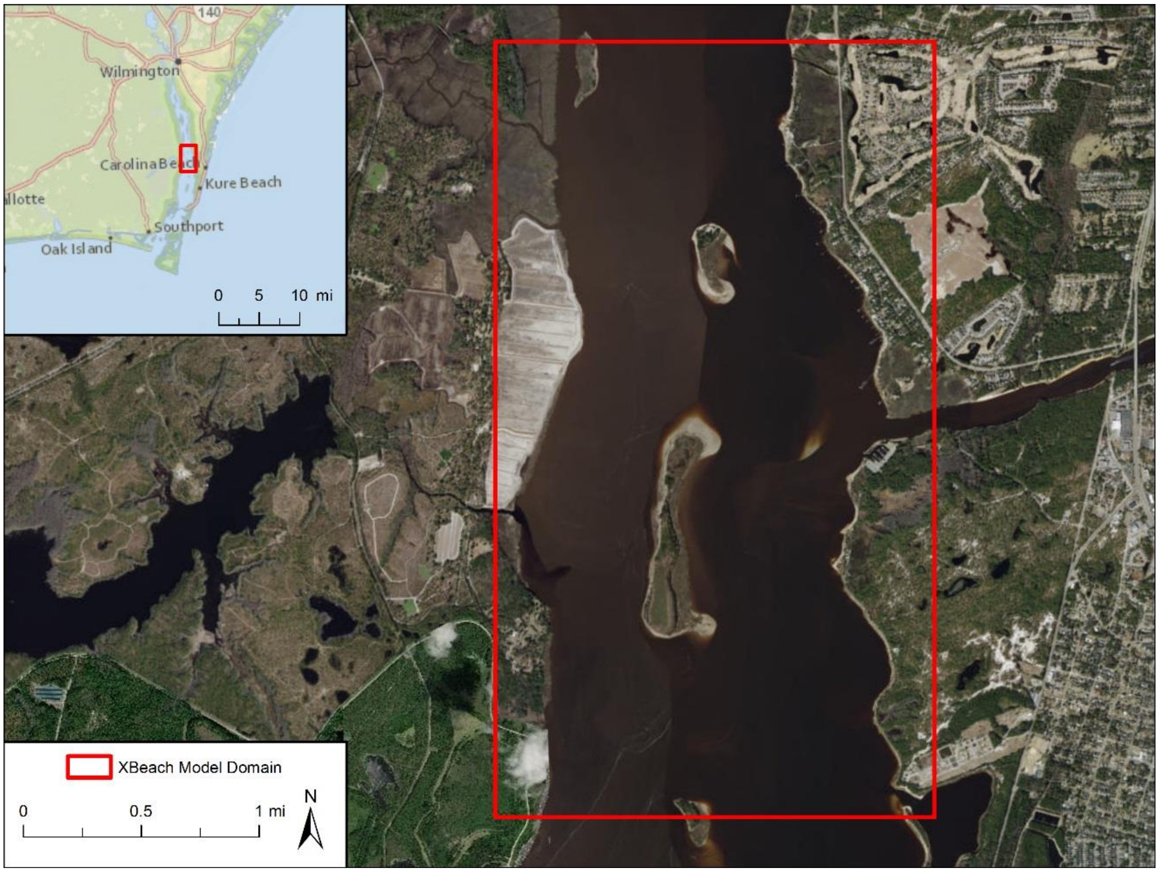

Figure 9-4: Orton Point Model Domain

9.2.2.3. Channel Geometry

For the SPBI two channel geometries were evaluated with the XBeach model, the existing navigation channel and the proposed design navigation channel, Figure 9-5. For the OP model there are no proposed changes to the navigation channel other than the deepening, and therefore only one geometry was evaluated with the Xbeach model, Figure 9-6.

Figure 9-5: Southport and Battery Island Proposed and Existing Navigation Channels

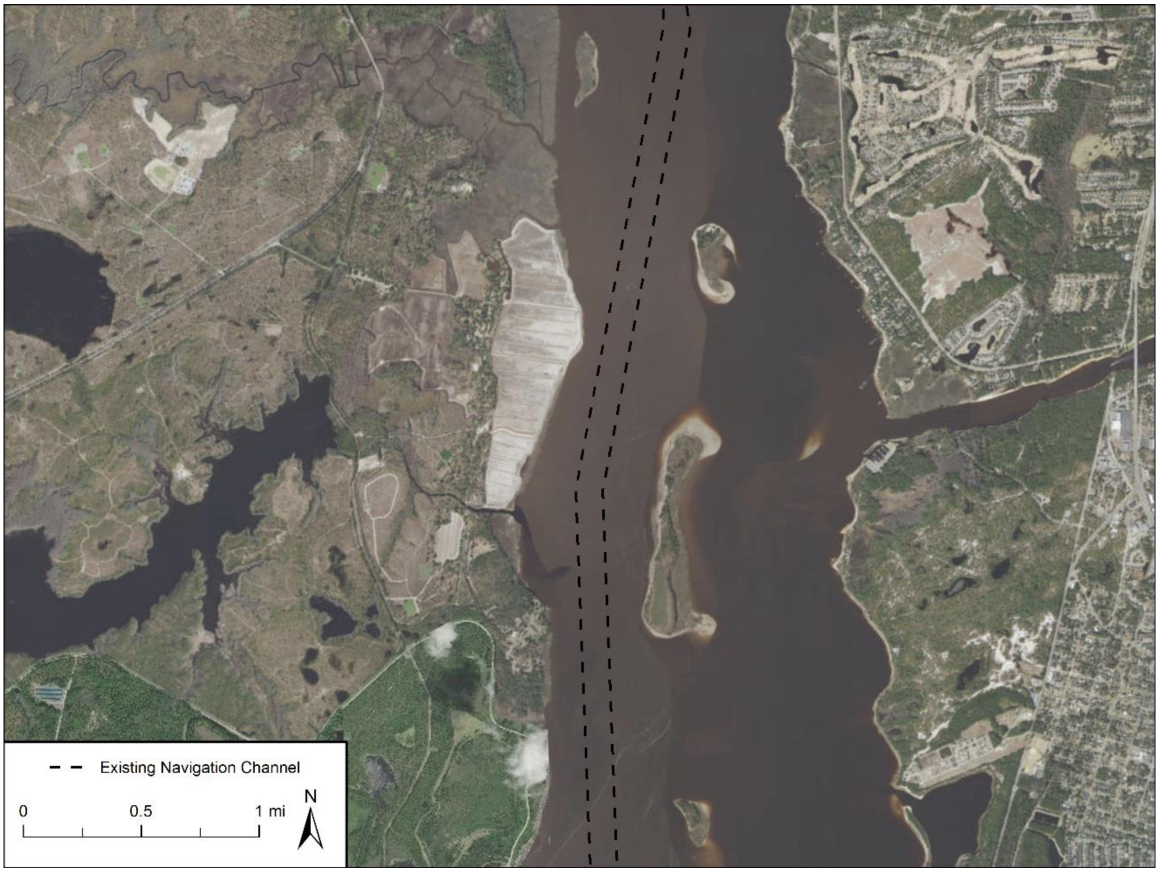

Figure 9-6: Orton Point Existing Navigation Channel

9.2.2.4. Model Bathymetry

The design project navigation channel depth is -47 ft MLLW, with an additional 2 ft of depth from Battery Island Turn to the pilot station to allow for adequate under keel clearance in areas affected by ocean waves. Additionally, there is an over dredge allowance of 2 ft for the entire navigation channel. The existing channel is permitted for -42 ft MLLW with an additional 2 ft of depth from Battery Island Turn to the pilot station and 2 ft of over dredge for the entire channel. For the model bathymetry the over dredge allowance was included. A slope of 1:3 (vertical: horizontal) or 1:5 was assumed for the channel side slopes for both the existing and design channels. A slope of 1:5 was assumed for Baldhead Shoal Reach 3 to Battery Island, for the remainder of the ranges a 1:3 slope was assumed.

Outside of the navigation channel bathymetry and ground elevations were combined from seven datasets, which are listed below. The datasets are listed in order of increasing priority as datasets overlap in some areas.

- Navigational charts from C-MAP by Jeppesen for offshore areas
- North Carolina Department of Public Safety (NCDPS) ADCIRC grid data for upstream river channels and wetlands
- Topography from Flood Risk Information System (FRIS) for the wetlands adjoining Cape Fear river downstream of Wilmington harbor
- United Stated Army Corps of Engineers (USACE) survey data for the navigation channel
- National Ocean Service (NOS) estuarine bathymetry for the area outside the navigation channel
- Bathymetric survey from FUGRO for navigation channel bank and slope
- Bathymetric survey from FUGRO for navigation channel in the offshore area

For combining, all datasets were converted to reference UTM Zone 17N. Vertical reference was converted to MLLW in meters using VDatum. In total four different bathymetry sets were used for this analysis:

- Southport/ Battery Island Model Design Channel (47 ft/49 ft MLLW + 2 ft over dredge), Figure 9-7,
- Southport/ Battery Island Model Existing Channel (42 ft/44 ft MLLW + 2 ft over dredge), Figure 9-8,
- Orton Point Model Design Channel (47 ft MLLW + 2 ft over dredge), Figure 9-9,
- Orton Point Model Existing Channel (42 ft MLLW + 2 ft over dredge), Figure 9-10.

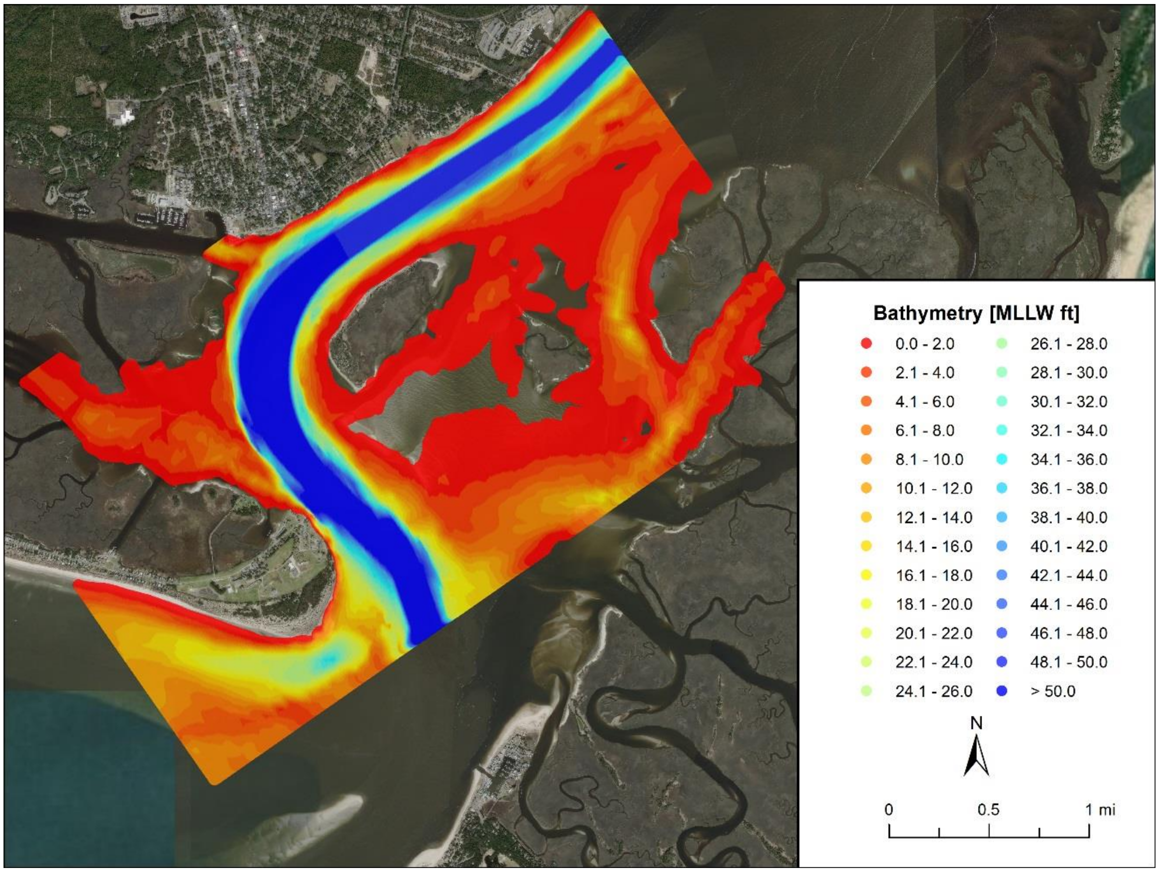

Figure 9-7: Southport and Battery Island Model Design Channel Bathymetry

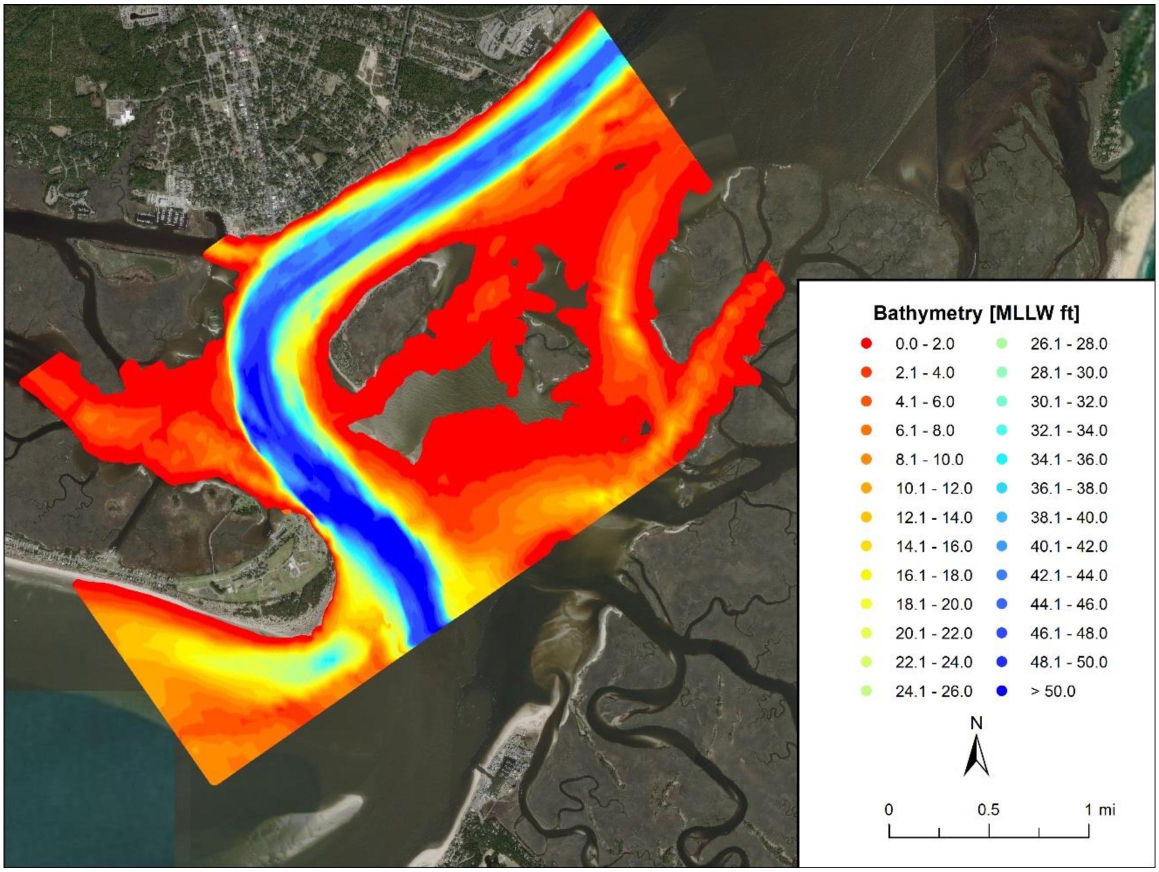

Figure 9-8: Southport and Battery Island Model Existing Channel Bathymetry

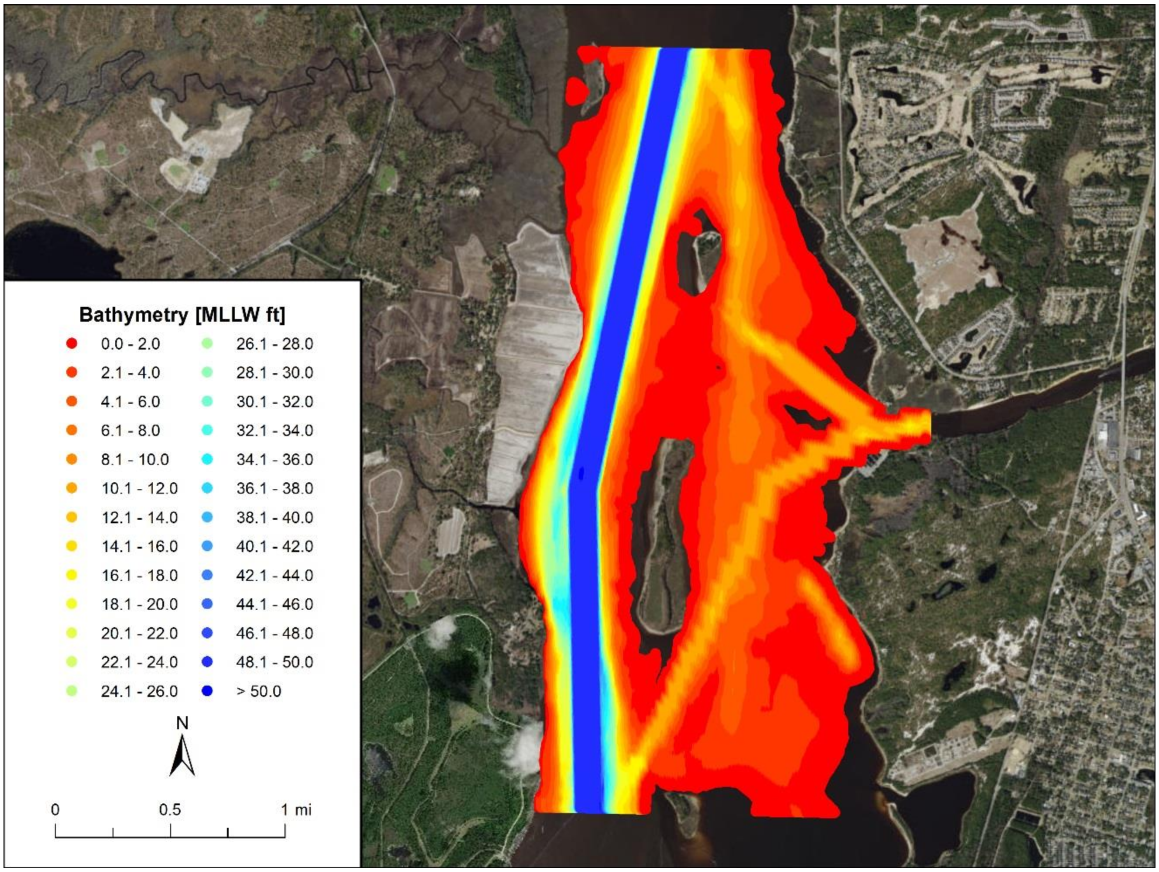

Figure 9-9: Orton Point Model Design Channel Bathymetry

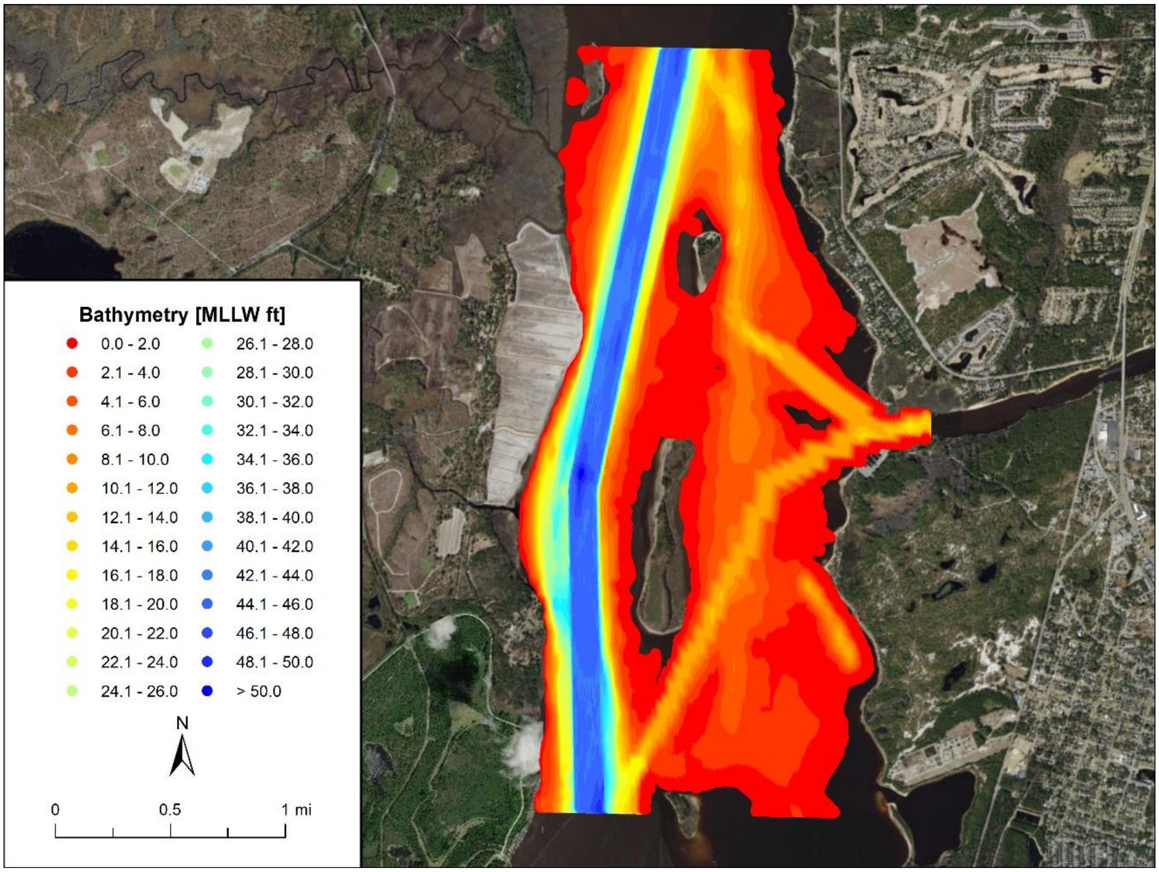

Figure 9-10: Orton Point Model Existing Channel Bathymetry

9.2.3. Boundary Conditions

XBeach requires a single boundary condition type along each of the four domain boundaries. Two different boundary conditions were used for this analysis, a two-dimensional weakly reflective boundary and a closed boundary (shorelines). The weakly reflective boundary allows waves to propagate out of the computational domain. Boundary conditions were defined as documented in Figure 9-11, Figure 9-12, and Table 9-1. Due to the bend in the navigation channel the boundary conditions for the SPBI model were dependent on the direction of the vessel transit to limit the influence of the boundary condition on the model results. The boundary conditions remained the same independent of the direction of transit for the OP model.

The model water level was set to a constant level of zero and it was forced by the ship pressure field discussed later herein. The zero-water level represents MLLW.

Figure 9-11: Southport and Battery Island Model Boundaries

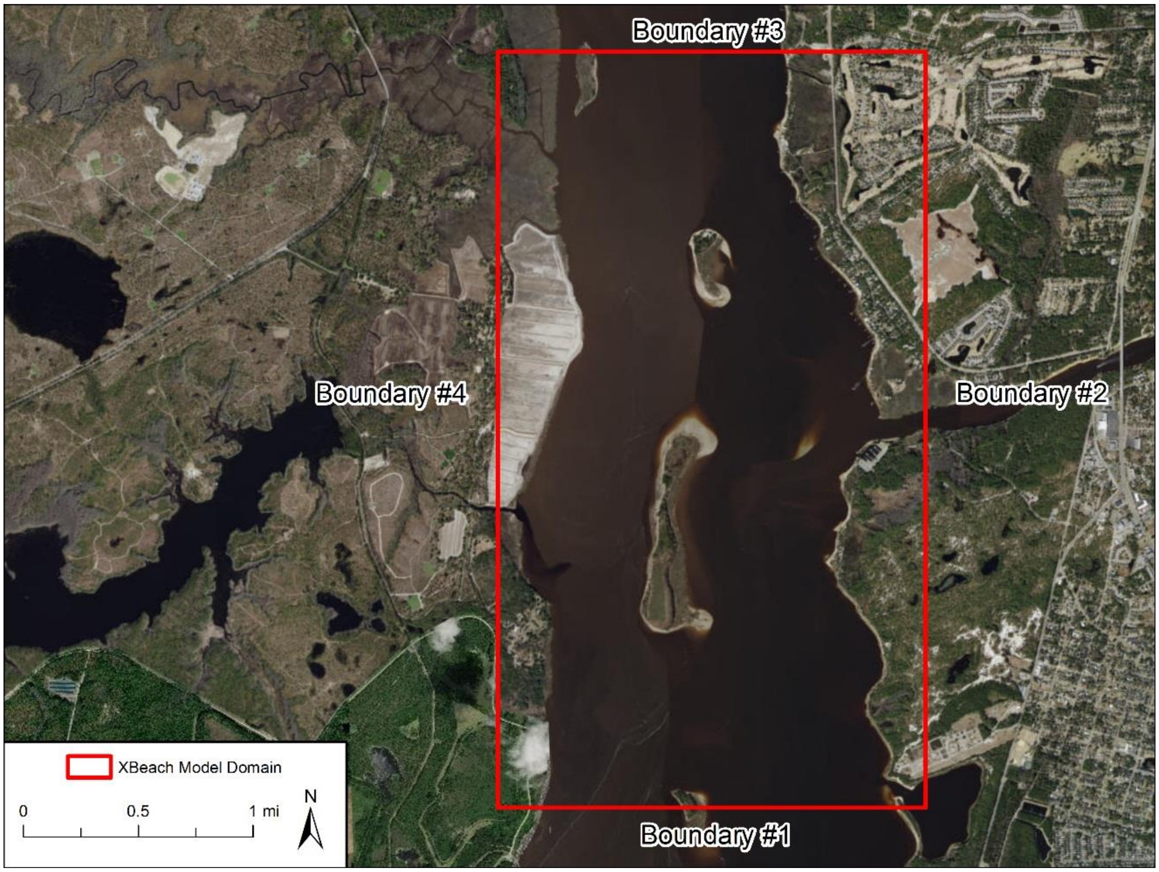

Figure 9-12: Orton Point Model Boundaries

Table 9-1: Model Boundaries

	Boundary #1	Boundary #2	Boundary #3	Boundary #4
SPBI Inbound Model	Weakly Reflective	Closed	Weakly Reflective	Closed
SPBI Outbound Model	Closed	Weakly Reflective	Closed	Weakly Reflective
OP Model	Weakly Reflective	Closed	Weakly Reflective	Closed

9.2.4. XBeach Model Runs

In total eight XBeach model runs were simulated, four for the SPBI model and four for the OP model. The performed runs are listed in Table 9-2. This run matrix serves the purpose of this study to evaluate the differences in ship generated waves with regards to bed shear stress as a result of the deepened and widened channel and larger design vessel.

Table 9-2: XBeach Run Matrix.

Run	Area	Channel Geometry	Transiting Vessel	Transiting Direction
1	Southport / Battery Island	Existing	8,000 TEU	Inbound
2		Design	12,400 TEU	
3		Existing	8,000 TEU	Outbound
4		Design	12,400 TEU	
5	Orton Point	Existing	8,000 TEU	Inbound
6		Design	12,400 TEU	
7		Existing	8,000 TEU	Outbound
8		Design	12,400 TEU	

9.2.4.1. Vessel Model Parameters

The design vessel for this ship generated wave analysis was the MSC Lauren, a 12,400 TEU container vessel. The vessel used to represent the existing channel design vessel was the CMA CGM Hugo, an 8,000 TEU container vessel. The particulars of these two design vessels are summarized in Table 9-3. It should be noted that the maximum draft allowed to transit Cape Fear River in the existing -42 ft MLLW channel without tide restrictions is 38 ft. As a result, the draft of CMA CGM Hugo in the existing channel model was limited to 38 ft. The draft of MSC Lauren was 43 ft.

Table 9-3: Deep Draft Design Vessels

Attribute	12,400 TEU Container Vessel	8,000 TEU Container Vessel
Design Vessel	MSC Lauren	CMA CGM Hugo
LOA (ft)	1,200	1,096
LBP (ft)	1,148	1,047
Beam (ft)	158.8	140.4
Loaded Draft [ft]	49	48
Modeled Draft [ft]	43	38

The moving vessel is represented in the model as a pressure head that moves along a user-defined track. For this study, both an inbound and outbound ship track were evaluated. The track for the inbound and outbound simulations for the SPBI model for the design conditions were taken from a desktop navigation simulation study performed in January 2018. The track for the existing conditions for the SPBI model is a synthetic track, representing the path of highest traffic density based on historic data. The three tracks used for the SPBI model are shown in Figure 9-13.

For the OP model the same ship track was used for inbound and outbound transits for the existing and design channels. This track for the OP model was a synthetic track, representing the highest traffic density based on historic data and is shown in Figure 9-14.

To avoid a spurious disturbance wave in the model, the Xbeach manual recommends gradually introducing the ship effect into the model. The ship was gradually brought to the target velocity over a certain duration of simulation time depending on the model domain and target velocity, Table 9-4. The target velocity is based on typical speeds of historical vessel traffic and the results from a desktop navigation simulation study performed in January 2018.

Table 9-4: Transiting Vessel Speeds and Simulation Time to Reach Target Speed

Model Domain	Direction of Transit	Vessel Speed [kts]	Simulation Time to Reach Target Transiting Speed [minutes:seconds]
Southport / Battery Island	Inbound	10	5:00
Southport / Battery Island	Outbound	9	4:30
Orton Point	Inbound	11	5:30
Orton Point	Outbound	11	2:50

Figure 9-13: Ship track for XBeach simulations for Southport / Battery Island

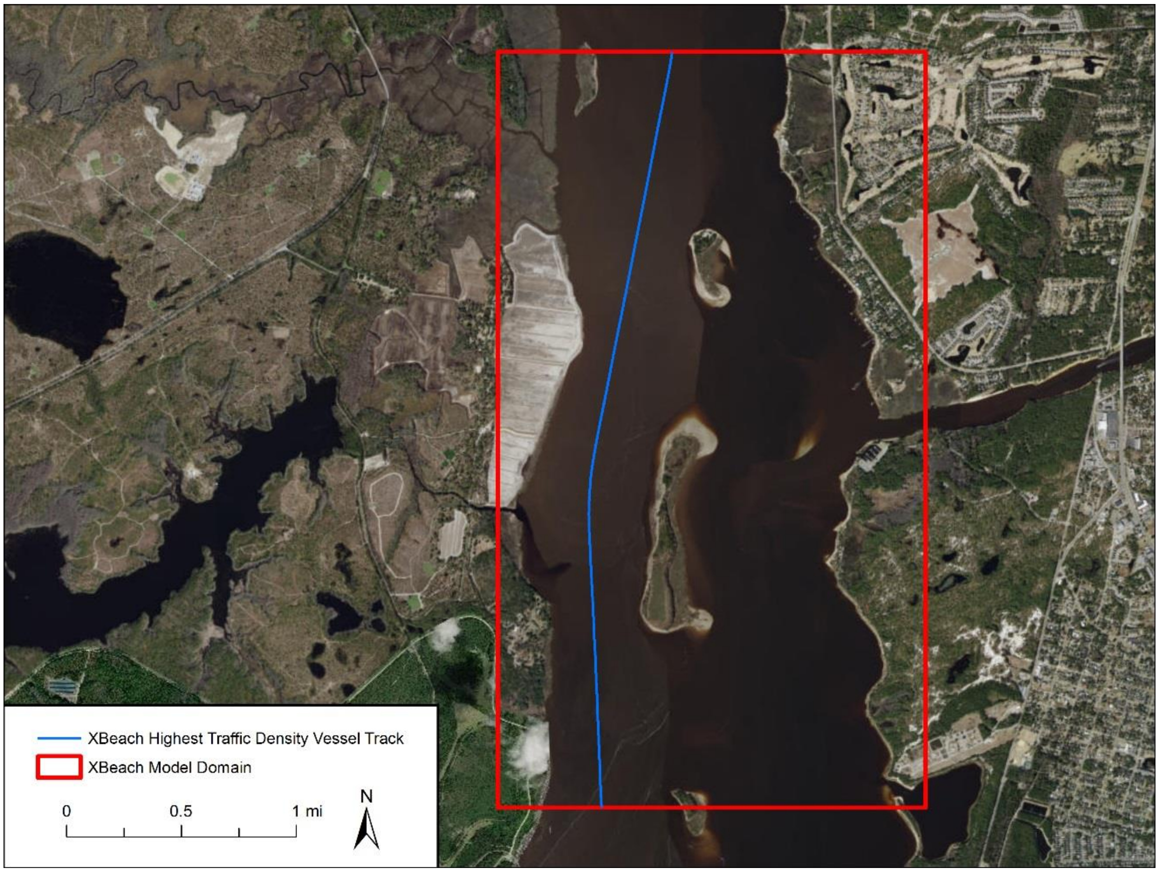

Figure 9-14: Ship track for XBeach simulations for Orton Point

The shape of the vessel is input to Xbeach on a separate grid from the computational grid. This grid resolution defines the level of detail of ship. One hull depth point can be specified for each grid cell on this auxiliary grid. As previously stated, for this study two different container vessels (8,000 TEU and 12,400 TEU) were input into the model simulations. The ship grid and draft at each cell for the two container vessels is shown in Figure 9-15. The 8,000 TEU maximum draft was limited to 38 ft (11.58 m) due to the existing dredged navigational channel of -42 ft MLLW.

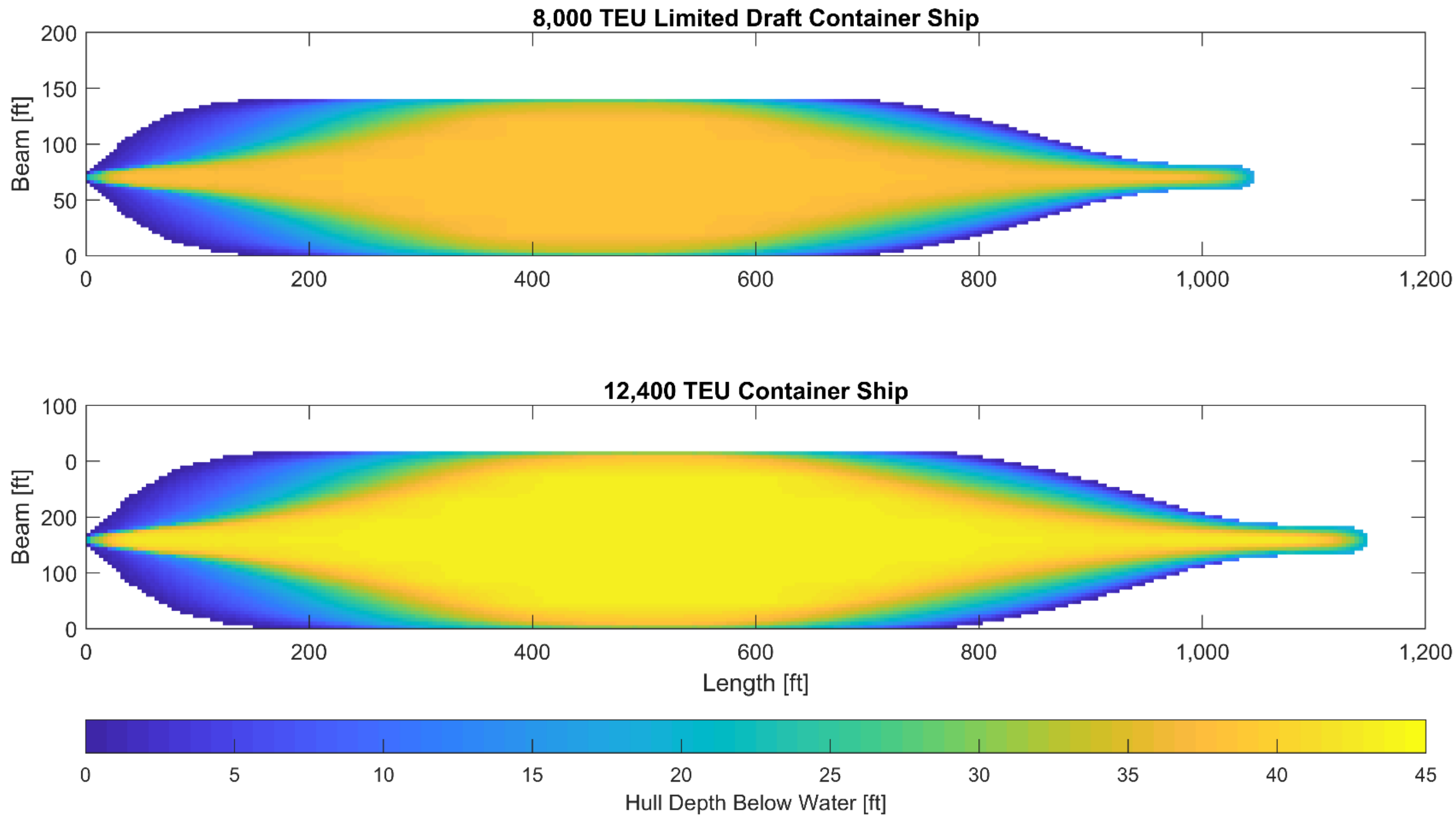

Figure 9-15: XBeach container vessel grids and draft.

9.2.5. Model Calibration

No calibration of the XBeach models was conducted due to lack of measured data. However, since this analysis is taking a comparative approach between the channel geometry and larger vessels, the relative differences should still be valid.

9.2.6. Model Results

For this study eight model simulations were evaluated as outlined previously to assess the environmental conditions created from each ship. Water levels and currents were obtained from the model results. Figure 9-16 shows an example of the primary wave propagation for the 12,400 TEU vessel at three different times throughout the inbound simulation for SPBI following the inbound design track shown in Figure 9-13.

For both the SPBI and OP models three observation point time series were extracted of the water surface elevation and current velocity for the two modeled vessels for both the inbound and outbound simulations. For the SPBI model Points A, B, and C were evaluated and are shown geographically in Figure 9-17. The time series for Points A, B, and C are shown in Figure 9-19 to Figure 9-24. The differences in magnitude at the observation points between the 8,000 TEU and 12,400 TEU vessels are shown in Table 9-5. Comparatively, at the three observation points with the increase in vessel size the primary wave height and current velocities generally increase or remain the same.

For the OP model Points D, E, and F were evaluated and are shown geographically in Figure 9-18. The time series for Points D, E, and F are shown in Figure 9-25 to Figure 9-30. The differences in magnitude at the observation points between the 8,000 TEU and 12,400 TEU vessels are shown in Table 9-6. Comparatively, with the increase in vessel size the primary wave height and current velocities generally increase.

To evaluate the vessels' impact on the bed throughout the river the bottom shear stress was determined. The XBeach Manual (Roelvinki, 2015) gives the following equations for bottom shear stress (τ_b)

$$\tau_{bx}^{E} = c_f \rho u_E \sqrt{(1.16u_{rms})^2 + (u_E + v_E)^2}$$
$$\tau_{by}^{E} = c_f \rho v_E \sqrt{(1.16u_{rms})^2 + (u_E + v_E)^2}$$

where:

$$c_f = \text{ Dimensionless friction coefficient}$$
$$\rho = \text{ Density of water, } 1{,}025\,\frac{\text{kg}}{\text{m}^3}$$
$$u_E = \text{ X} - \text{component eulerian velocity, }\frac{\text{m}}{\text{s}}$$
$$v_E = \text{ Y} - \text{component eulerian velocity, }\frac{\text{m}}{\text{s}}$$
$$u_{rms} = \text{wave orbitial velcity, }\frac{\text{m}}{\text{s}}$$

All variables needed to calculate the bottom shear stress excluding the density of water were directly taken from the XBeach model output. The time series and difference from the 8,000 TEU at the observation points for the SPBI and OP models are shown in Table 9-5 and Table 9-6, respectively. Similar trends were found with the bottom shear stress as the primary wave height and current magnitude with an increase in vessel size.

Table 9-5: Difference in magnitude between the 8,000 TEU and 12,400 TEU Vessels - Southport Battery Island Simulations

Point	Transit Direction	Change in Maximum Primary Wave Height^ $[\mathrm{ft}]$	Change in Maximum Current Velocity^ $\left[\frac{\mathrm{ft}}{\mathrm{s}}\right]$	Change in Maximum Bed Shear Stress^ $\left[\frac{\mathrm{lbf}}{\mathrm{ft}^2}\right]$
A	Inbound	+0.2	+1.1	+0.3
B		0.0	+0.8	+0.1
C		0.0	+1.0	+0.1
A	Outbound	+0.4	+2.5	+0.3
B		+0.1	+0.7	+0.2
C		+0.2	+0.3	0.0
^ Values reported are the 12,400 TEU minus the 8,000 TEU				

Table 9-6: Difference in magnitude between the 8,000 TEU and 12,400 TEU Vessels - Orton Point Simulations

Point	Transit Direction	Change in Maximum Primary Wave Height^ $[\mathrm{ft}]$	Change in Maximum Current Velocity^ $\left[\frac{\mathrm{ft}}{\mathrm{s}}\right]$	Change in Maximum Bed Shear Stress^ $\left[\frac{\mathrm{lbf}}{\mathrm{ft}^2}\right]$
D	Inbound	0.0	+4.5	+1.5
E		+0.2	+3.3	+1.1
F		+0.2	+0.7	+0.1
D	Outbound	+0.6	+3.0	+0.5
E		0.0	+2.3	+0.6
F		-0.1	+3.5	+0.8
^ Values reported are the 12,400 TEU minus the 8,000 TEU				

The maximum water surface elevation and bed shear stress at each node throughout the simulations were determined and compared. The maximum water surface elevation and bed shear stress for the SPBI and OP inbound and outbound simulations are shown in Figure 9-31 to Figure 9-38. The difference in bed shear stress between the two vessels for SPBI and OP inbound and outbound simulations are shown in Figure 9-39 to Figure 9-42.

For both the SPBI inbound and outbound simulations, minimal differences were seen along the Southport shoreline as a result of the increased vessel size and the change in the vessel swept path (which is closer to Southport on the inbound transit). However, the shoreline northeast of Southport, which is denoted by the blue rectangles in Figure 9-32 and Figure 9-34, saw an increase in the magnitude of water level and significant bed shear stress as a result of the increasing vessel size and the vessel swept path closer to this shoreline on both inbound and outbound transits.

For the inbound simulation, the shoreline of Battery Island saw minimal differences with the exception of its northernmost shoreline where a decrease in magnitude of water level and bed shear stress occurred as a result of the increasing vessel size due to the existing swept path being approximately 200 feet closer to the Battery Island shoreline. For the outbound simulations minimal differences were seen along the shoreline of Battery Island with the exception of its southern coastline where there was an increase in magnitude of water level and bed shear stress as a result of the increasing vessel size.

For the OP inbound and outbound simulations, the increasing vessel size resulted in a corresponding increase in the magnitude of water level and significant bed shear stress along the Orton Point coastline on both sides of the navigation channel.

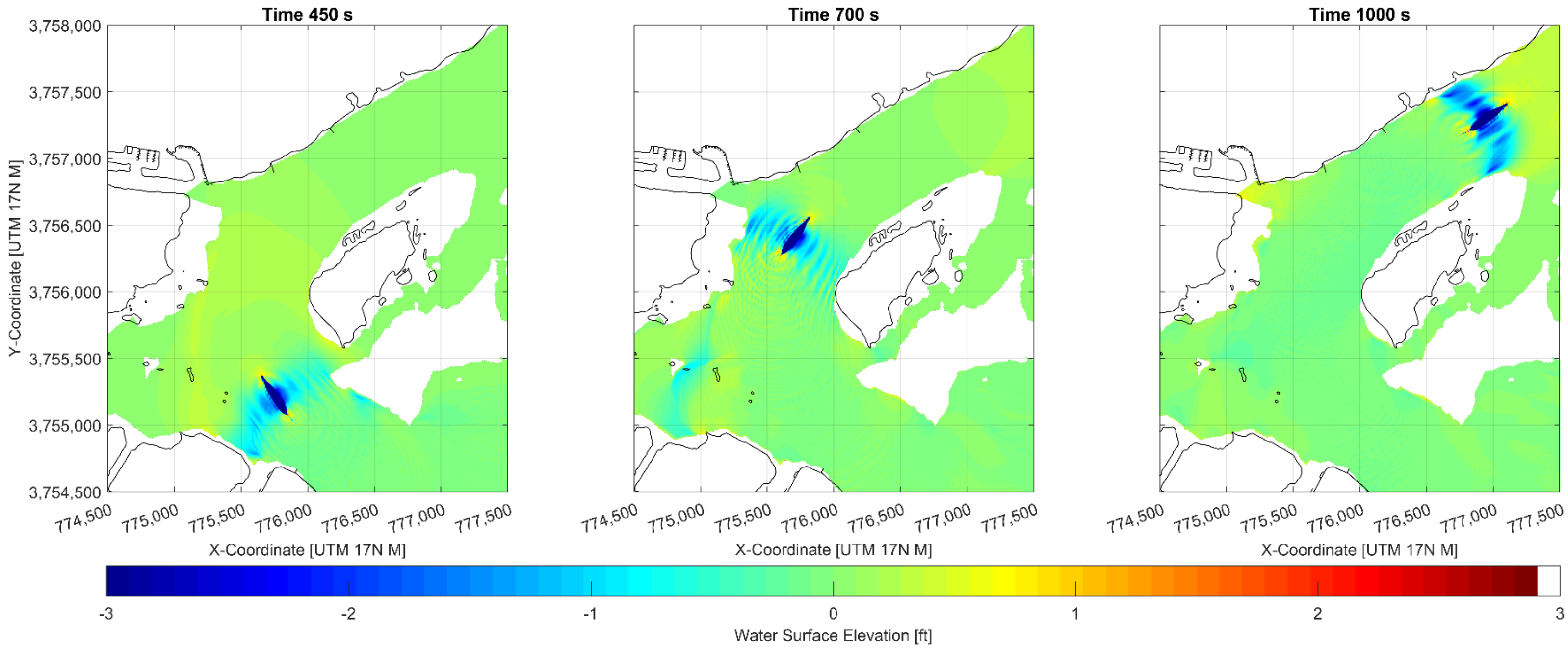

Figure 9-16: Water surface elevation at varying timesteps of the 12,400 TEU XBeach inbound design simulation for SPBI.

Figure 9-17: Map location of Point A, B, and C.

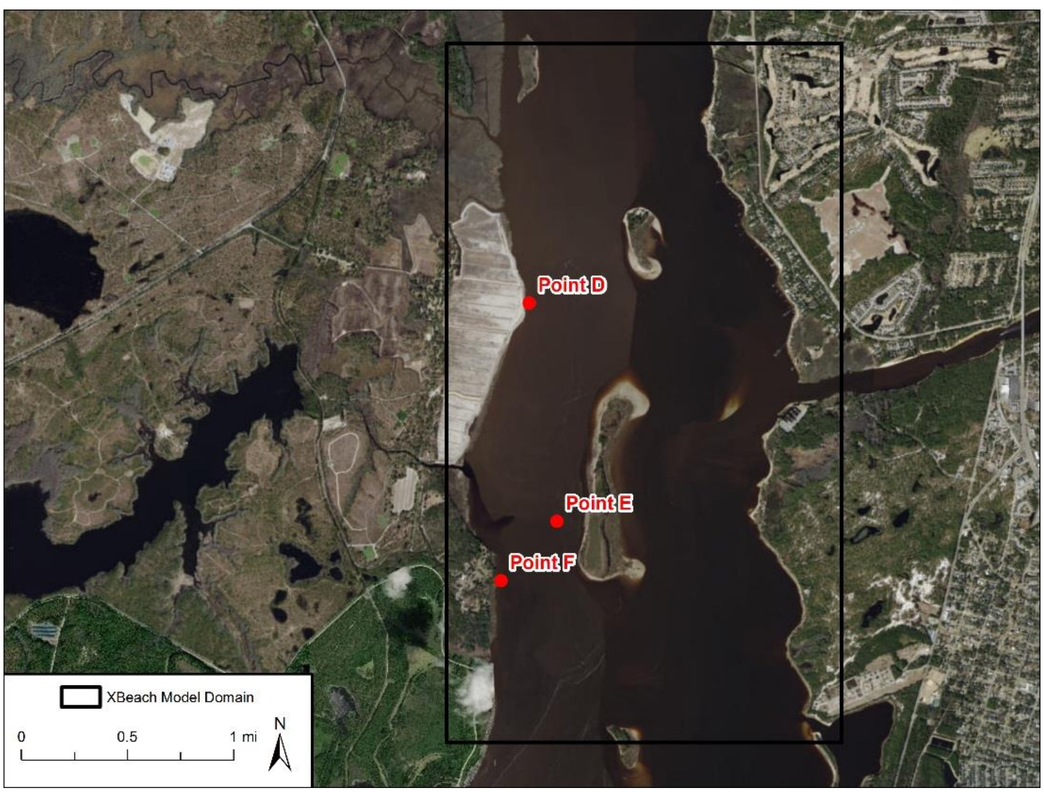

Figure 9-18: Map location of Point D, E, and F.

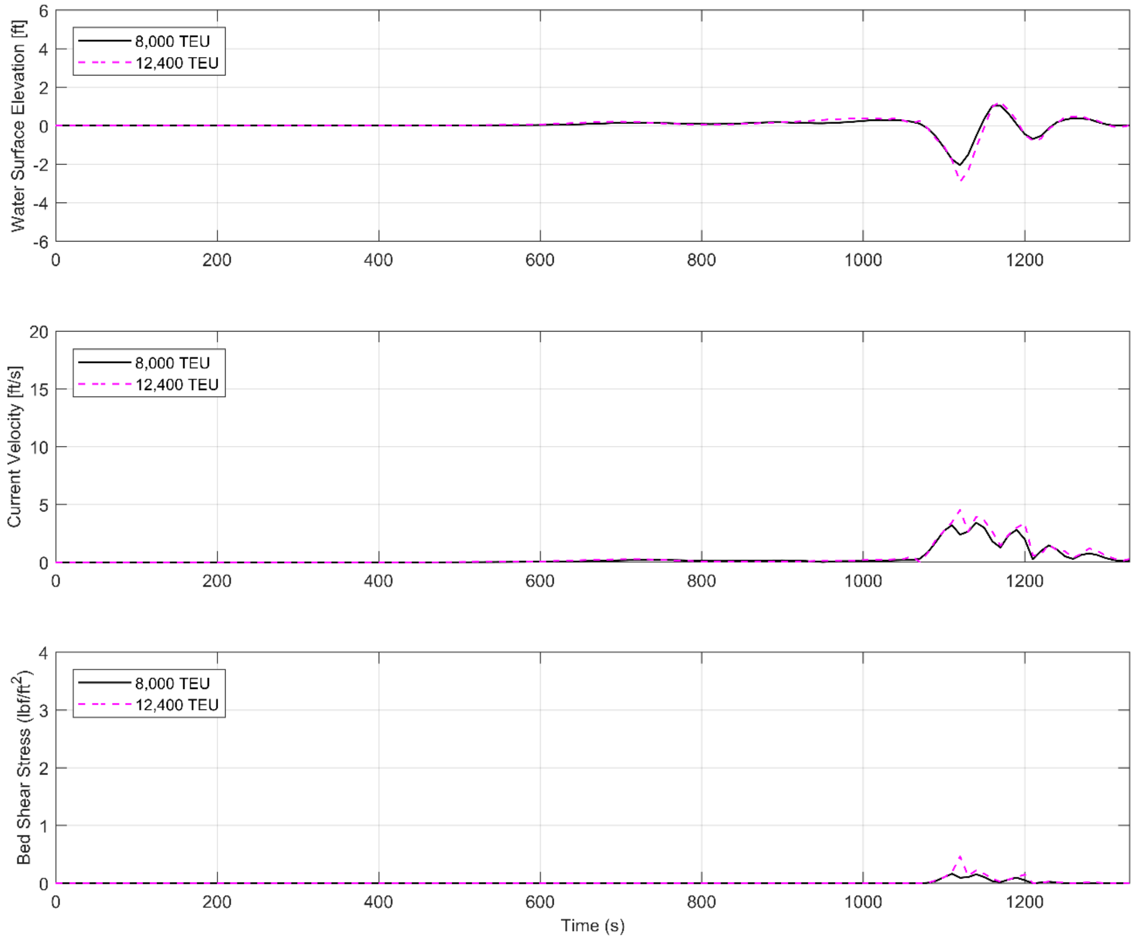

Figure 9-19: Timeseries of water surface elevation, current velocity, and bed shear stress at Point A for the inbound simulation.

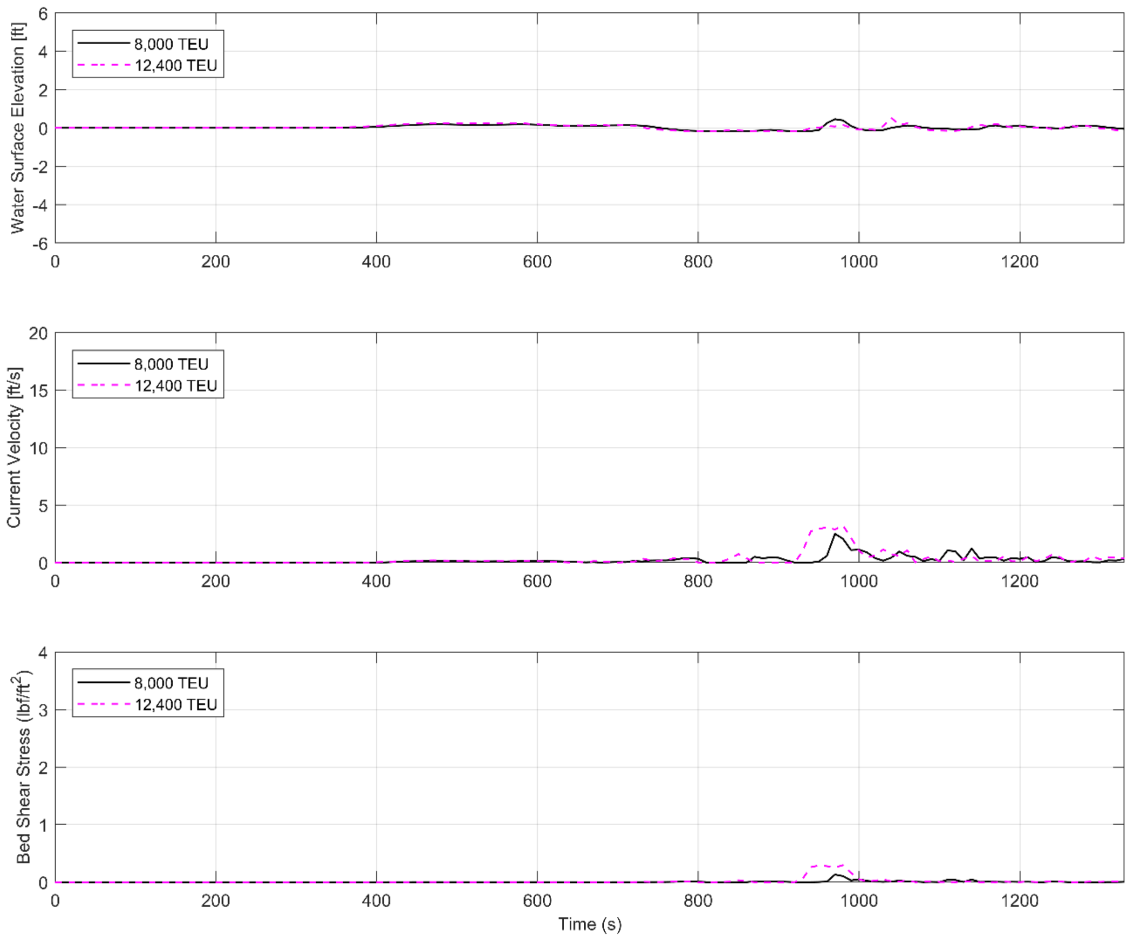

Figure 9-20: Timeseries of water surface elevation, current velocity, and bed shear stress at Point B for the inbound simulation.

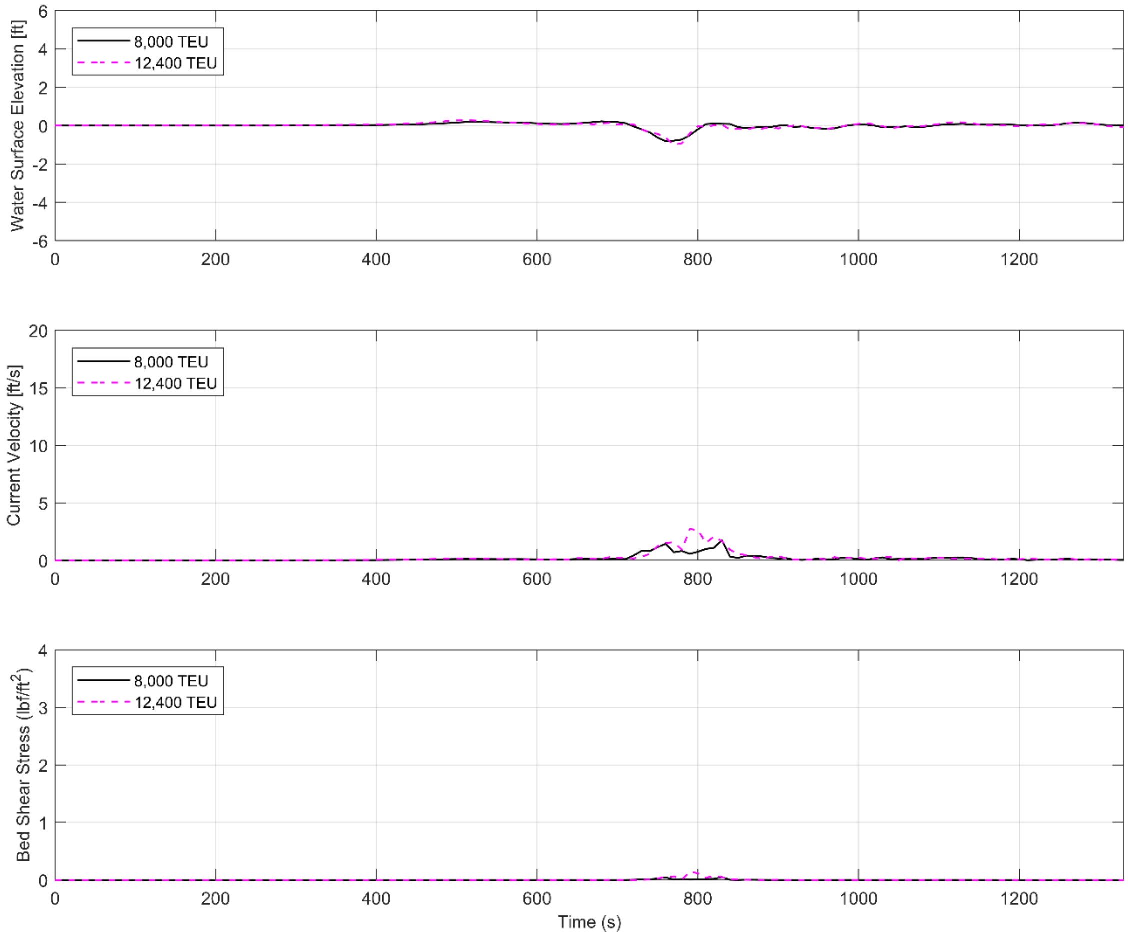

Figure 9-21: Timeseries of water surface elevation, current velocity, and bed shear stress at Point C for the inbound simulation.

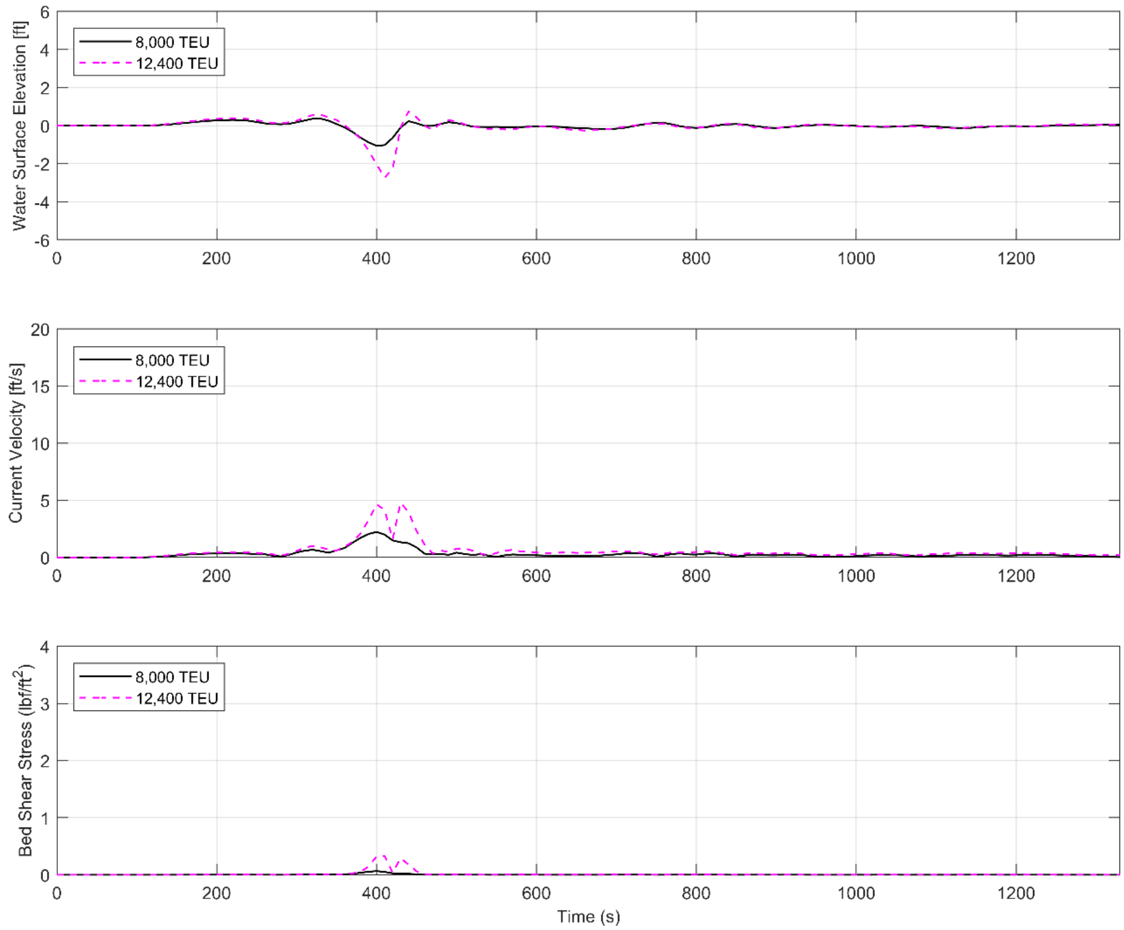

Figure 9-22: Timeseries of water surface elevation, current velocity, and bed shear stress at Point A for the outbound simulation.

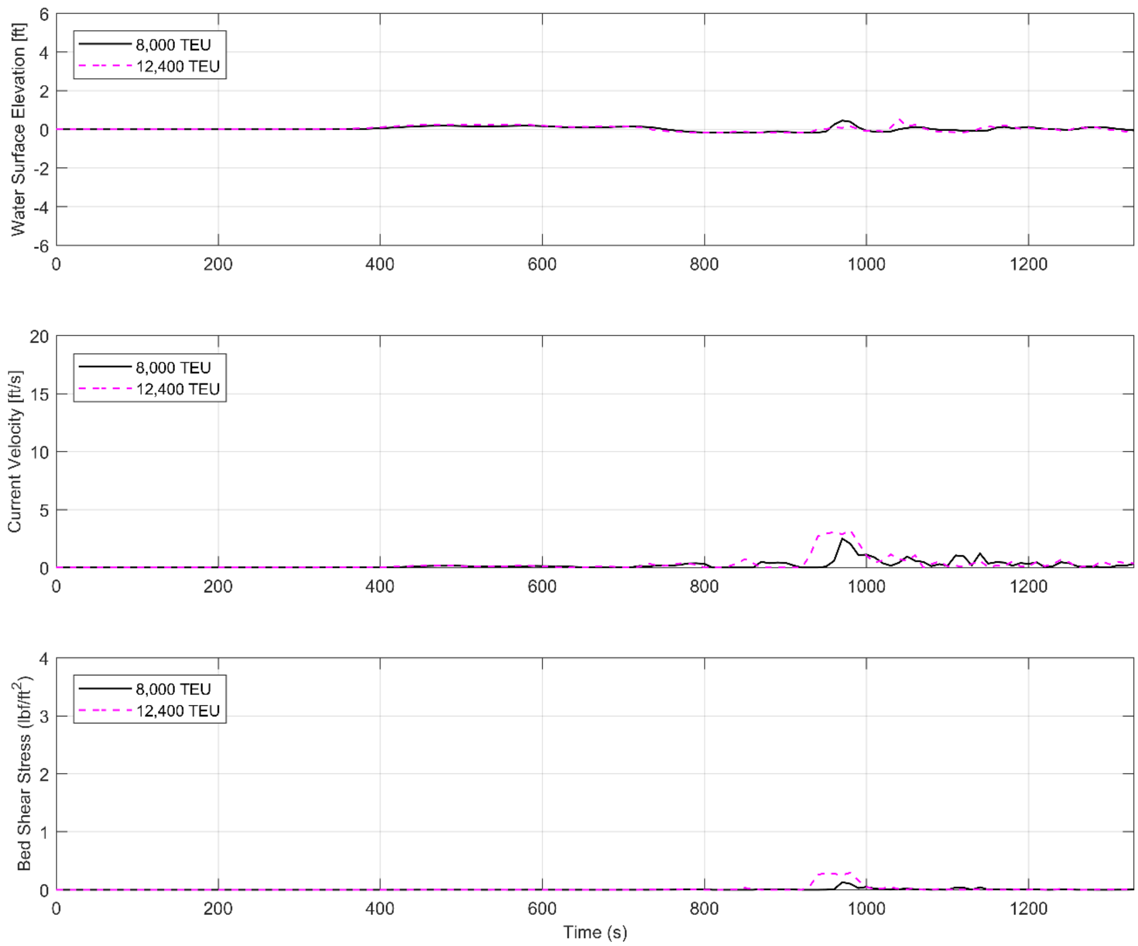

Figure 9-23: Timeseries of water surface elevation, current velocity, and bed shear stress at Point B for the outbound simulation.

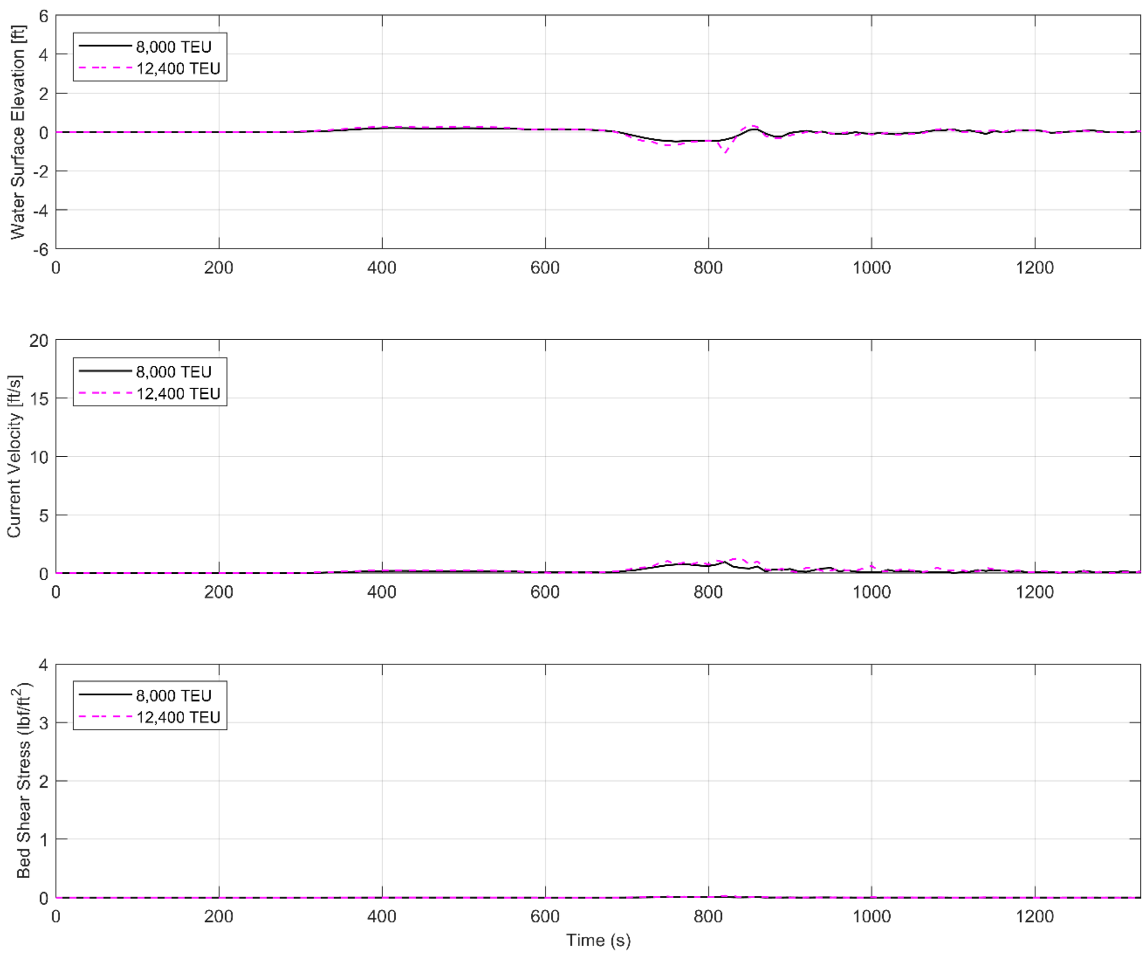

Figure 9-24: Timeseries of water surface elevation, current velocity, and bed shear stress at Point C for the outbound simulation.

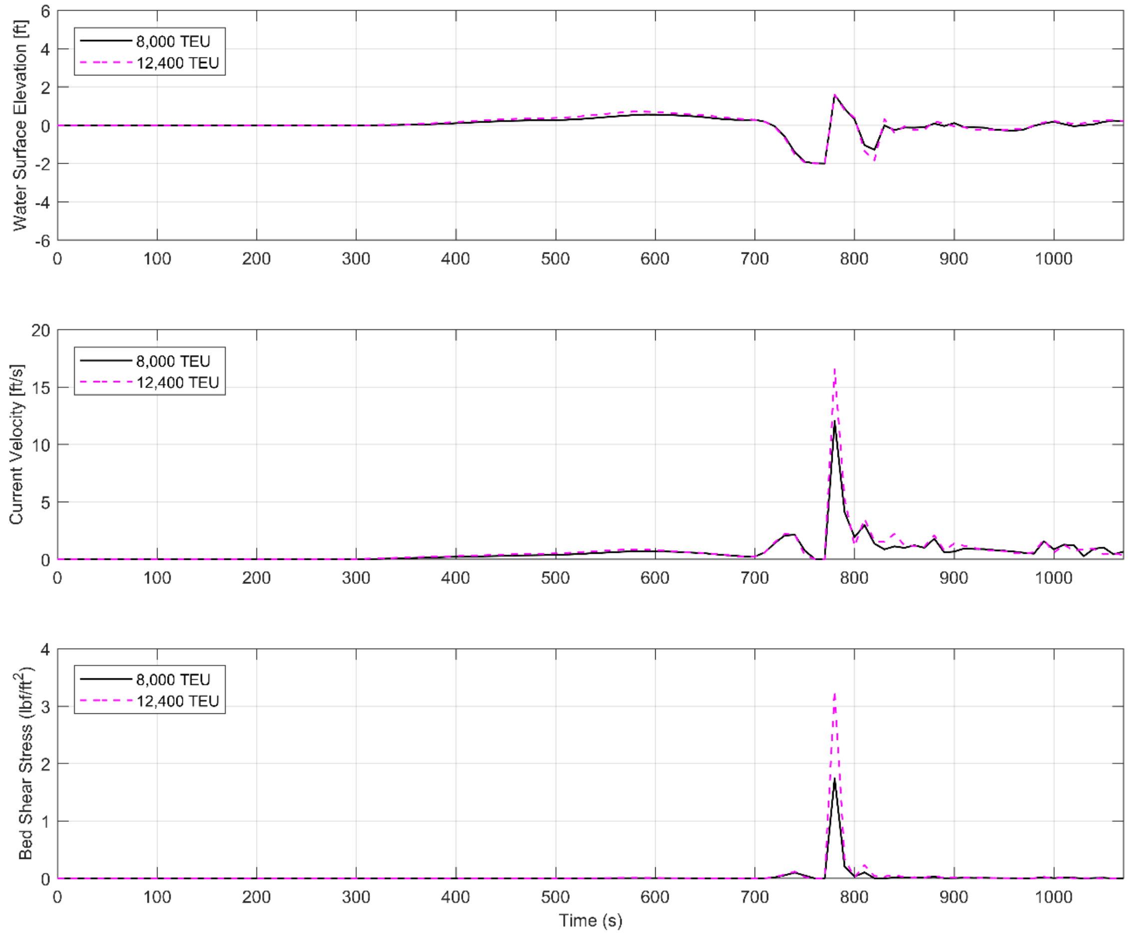

Figure 9-25: Timeseries of water surface elevation, current velocity, and bed shear stress at Point D for the inbound simulation.

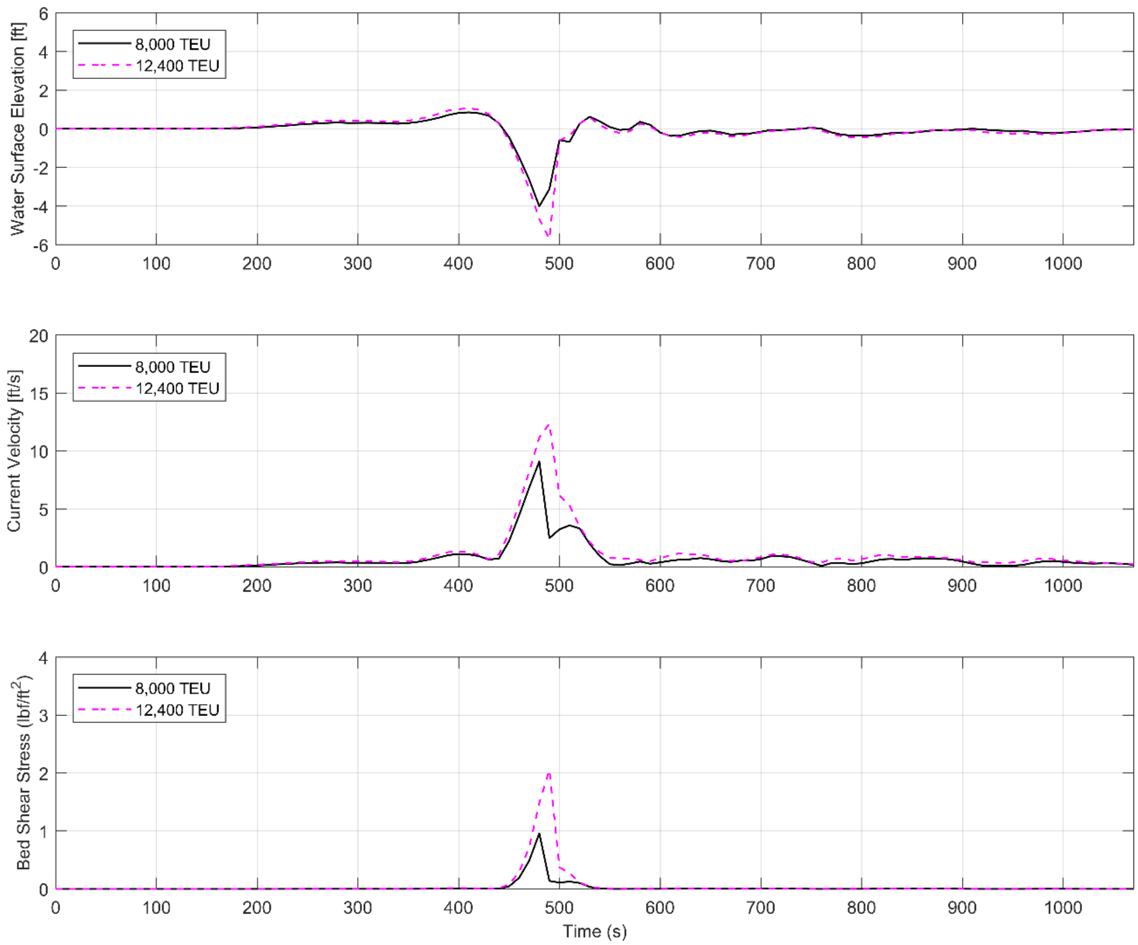

Figure 9-26: Timeseries of water surface elevation, current velocity, and bed shear stress at Point E for the inbound simulation.

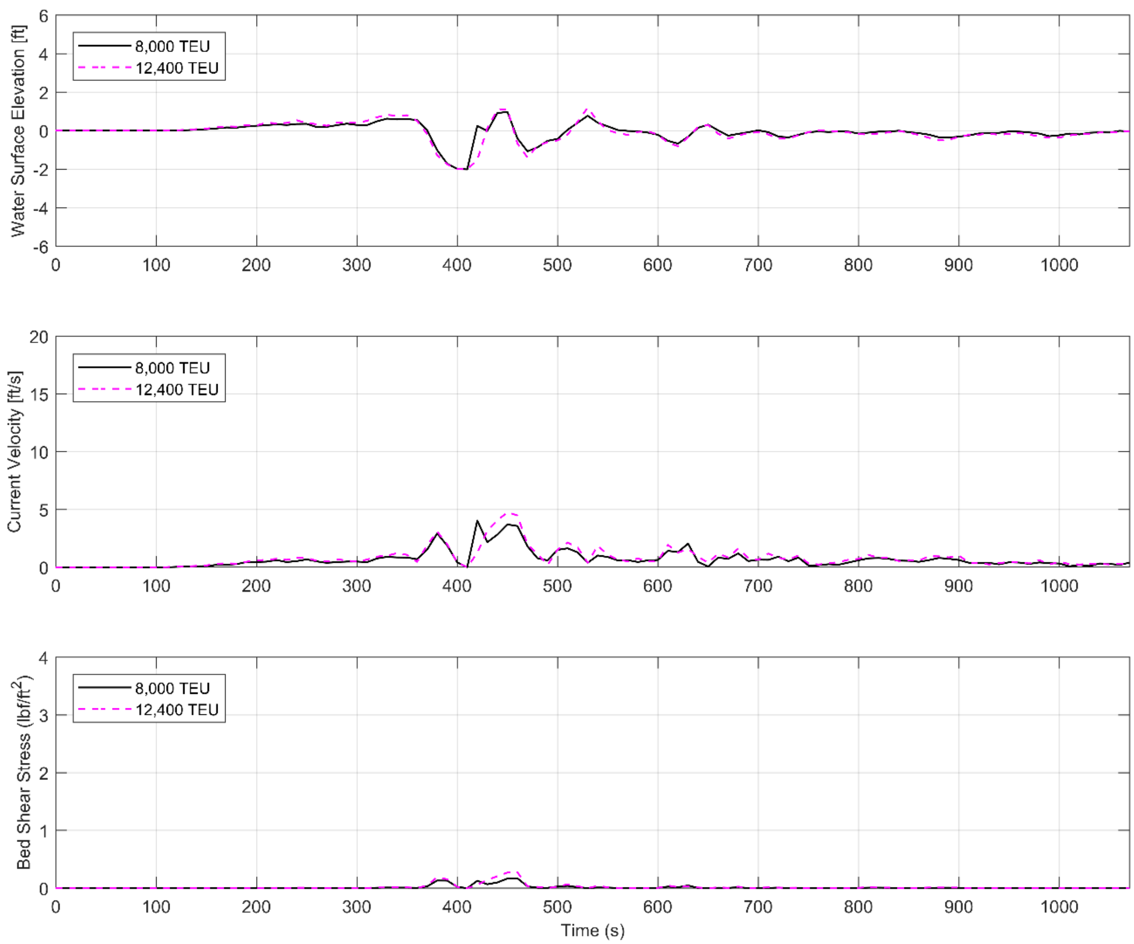

Figure 9-27: Timeseries of water surface elevation, current velocity, and bed shear stress at Point F for the inbound simulation.

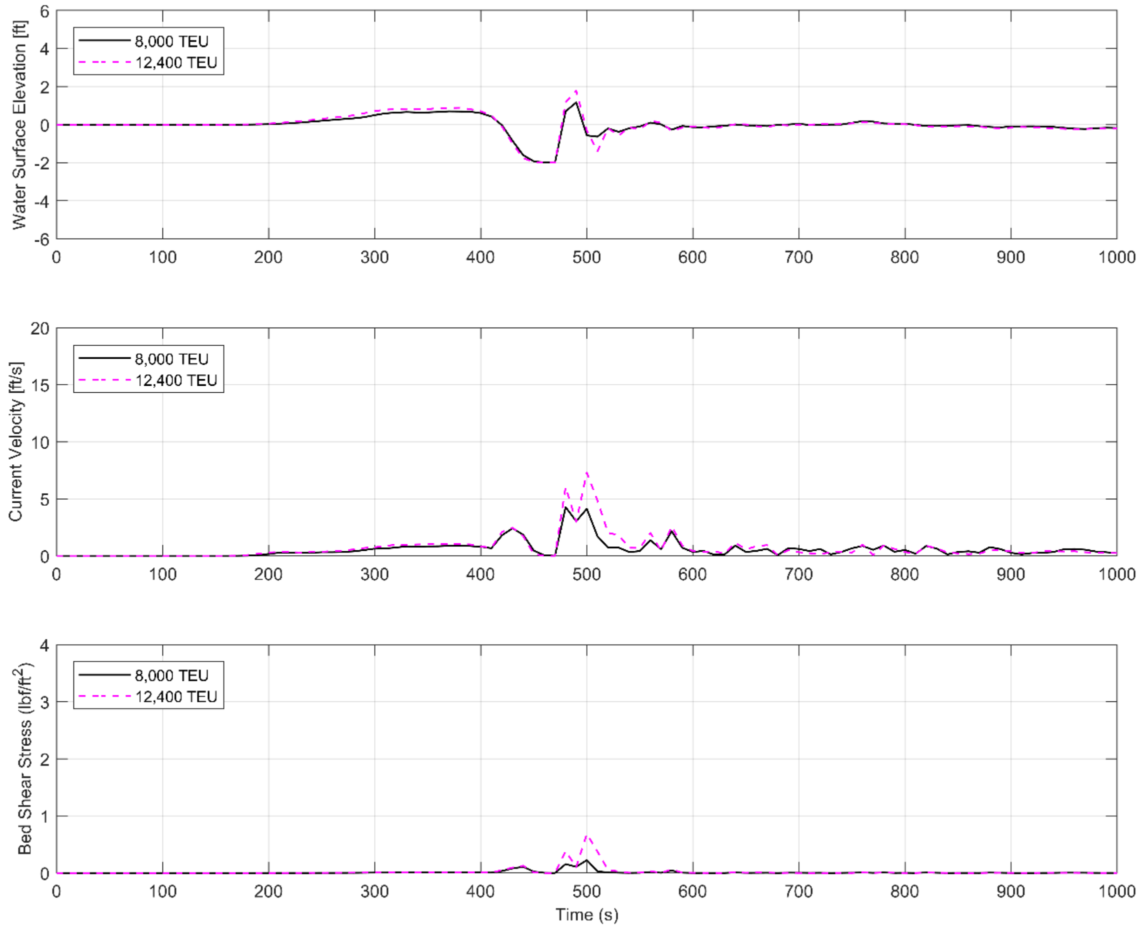

Figure 9-28: Timeseries of water surface elevation, current velocity, and bed shear stress at Point D for the outbound simulation.

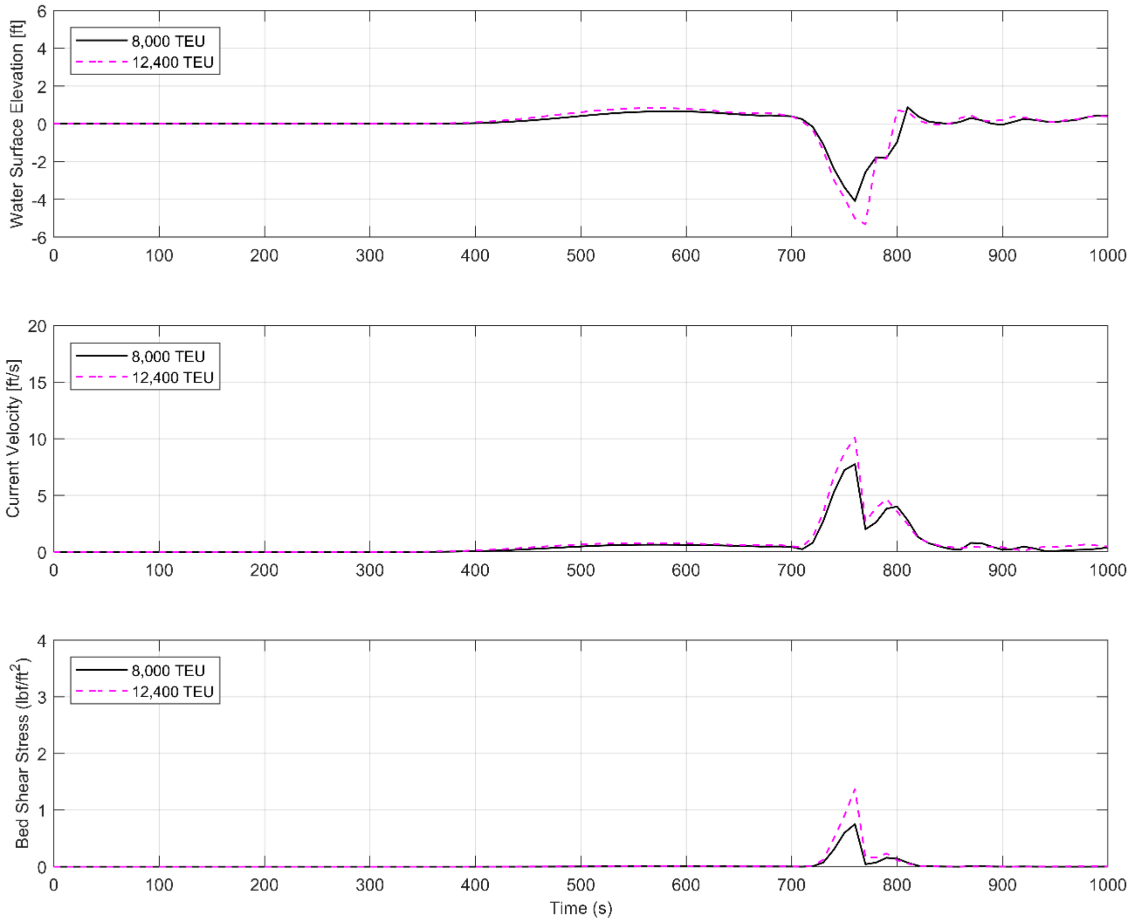

Figure 9-29: Timeseries of water surface elevation, current velocity, and bed shear stress at Point E for the outbound simulation.

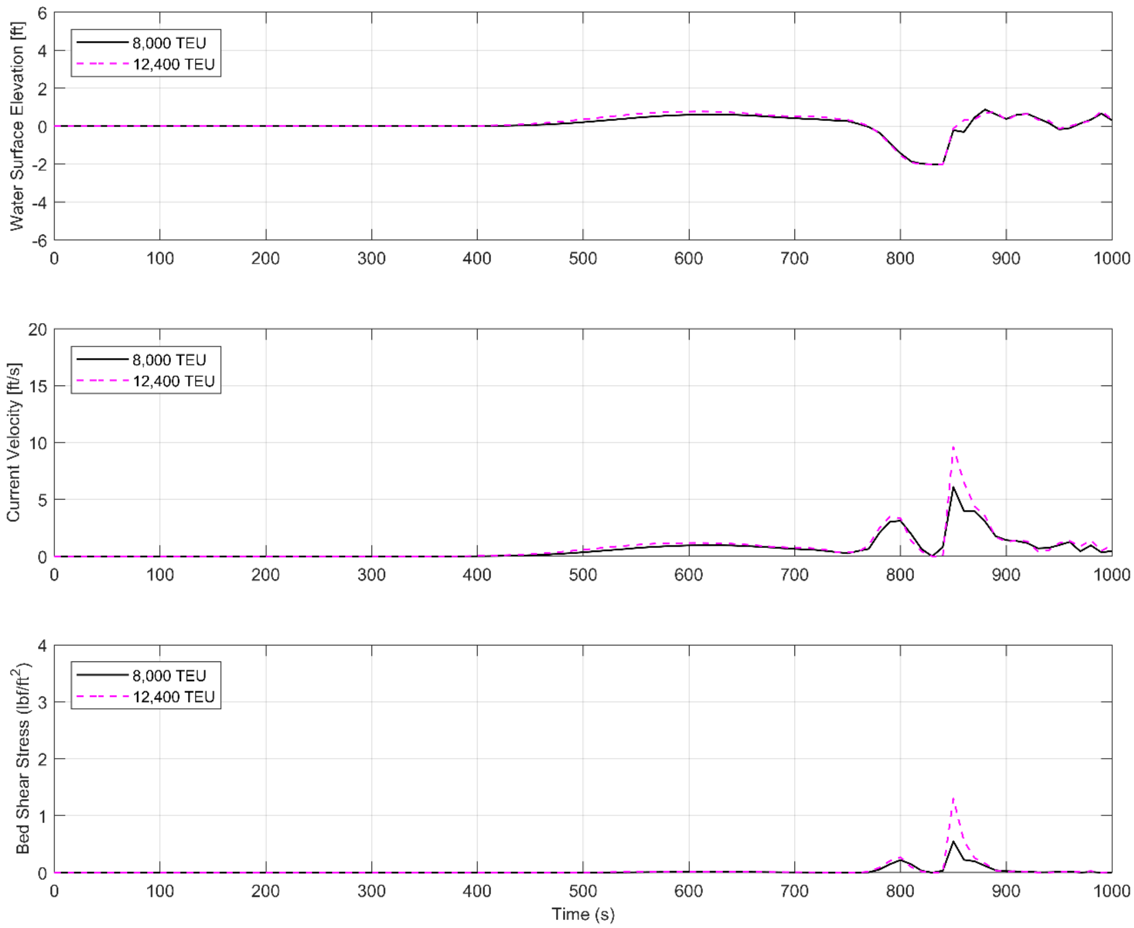

Figure 9-30: Timeseries of water surface elevation, current velocity, and bed shear stress at Point F for the outbound simulation.

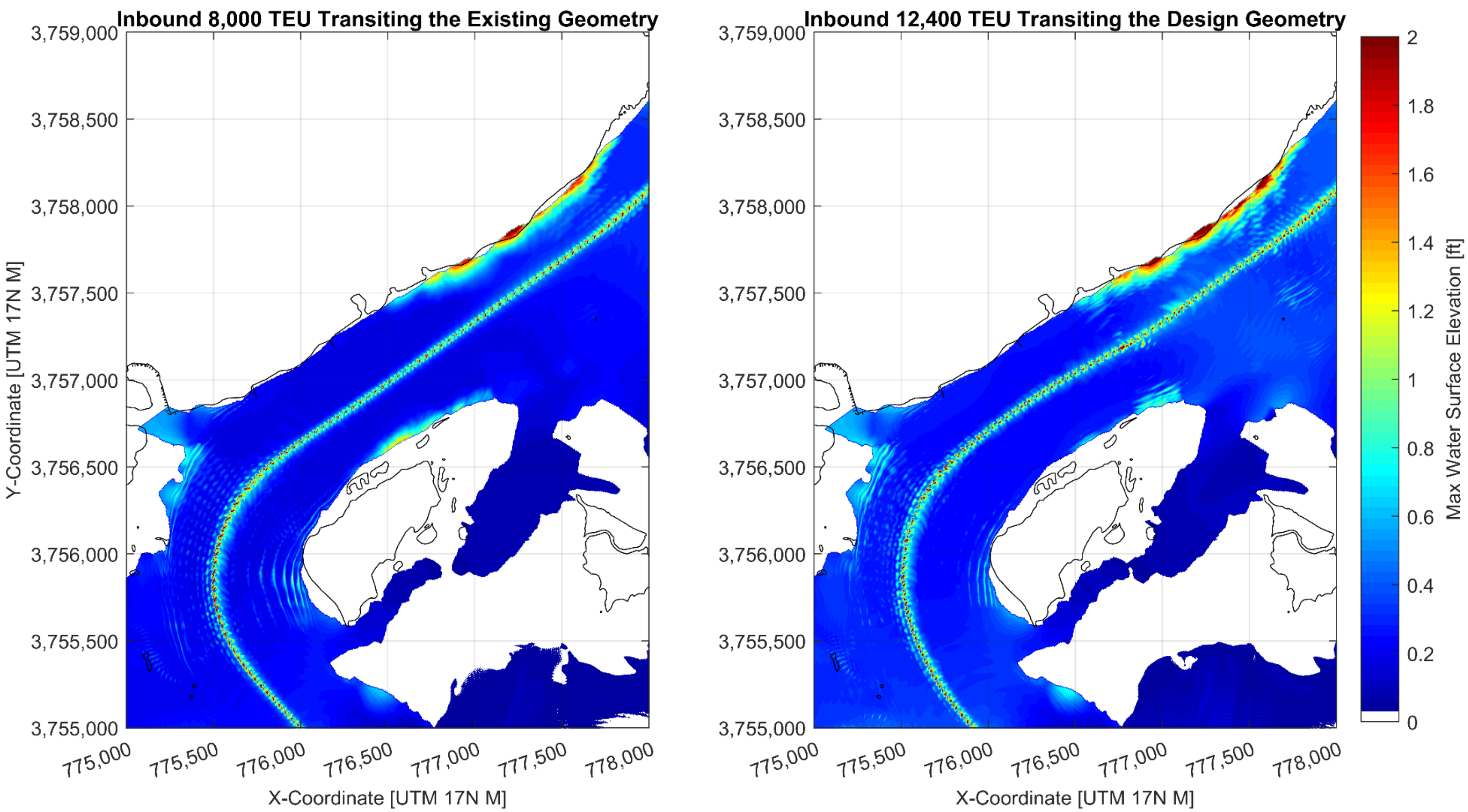

Figure 9-31: Maximum Water Surface Elevation for the Typical (left) and Design Vessels (right) for Inbound Southport Battery Island Simulations.

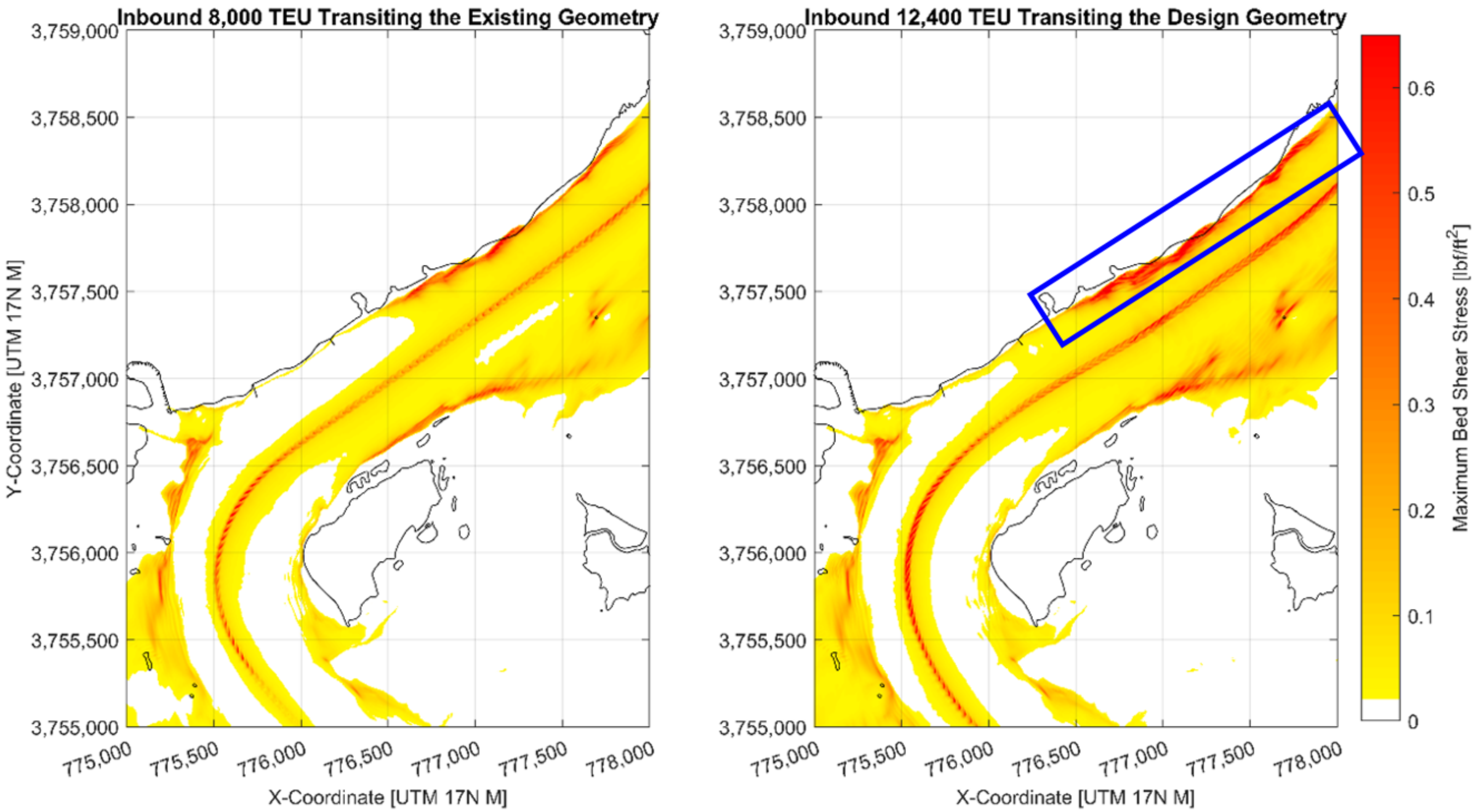

Figure 9-32: Maximum Bed Shear Stress for the Typical (left) and Design Vessels (right) for Inbound Southport Battery Island Simulations.

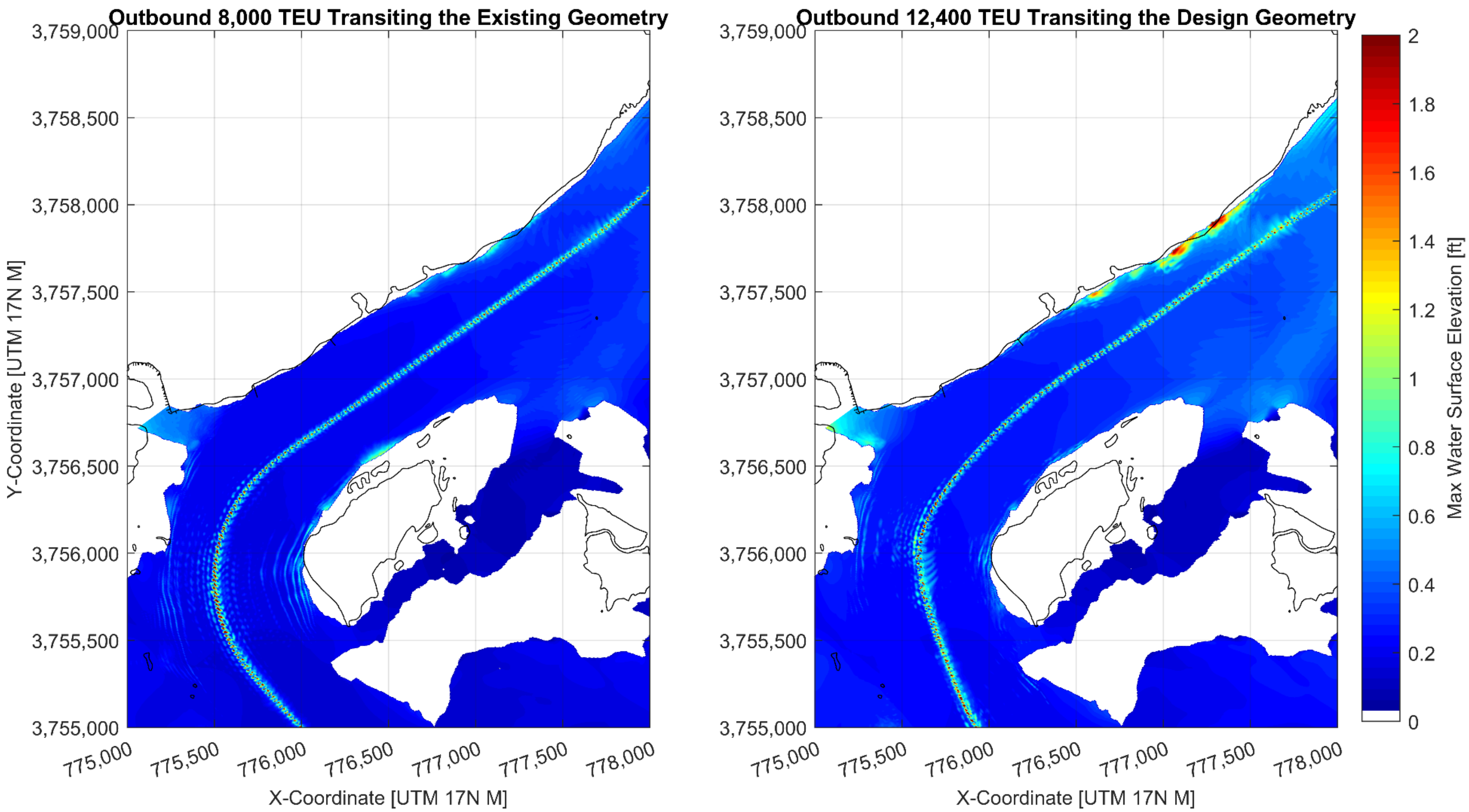

Figure 9-33: Maximum Water Surface Elevation for the Typical (left) and Design Vessels (right) for Outbound Southport Battery Island Simulations.

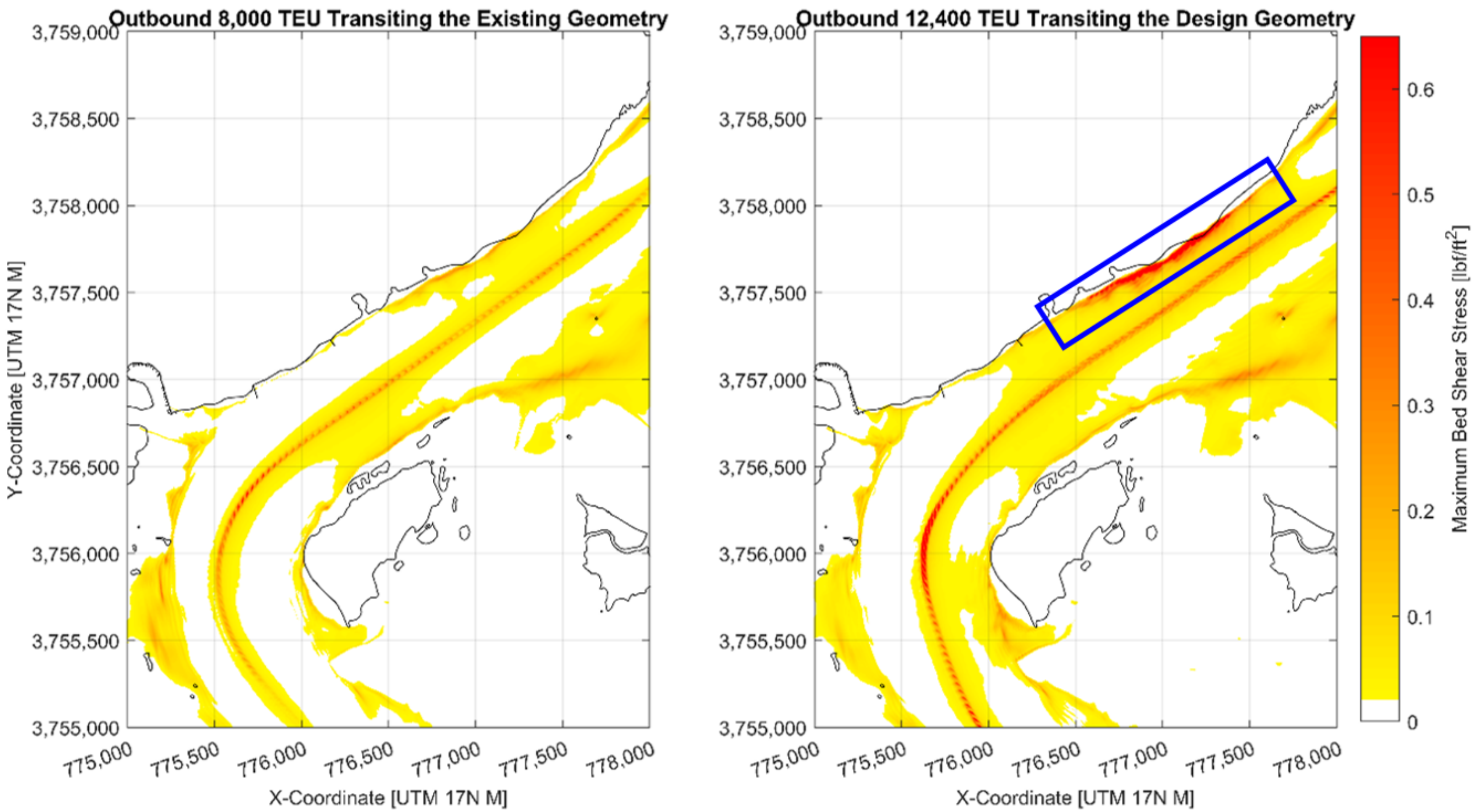

Figure 9-34: Maximum Bed Shear Stress for the Typical (left) and Design Vessels (right) for Outbound Southport Battery Island Simulations.

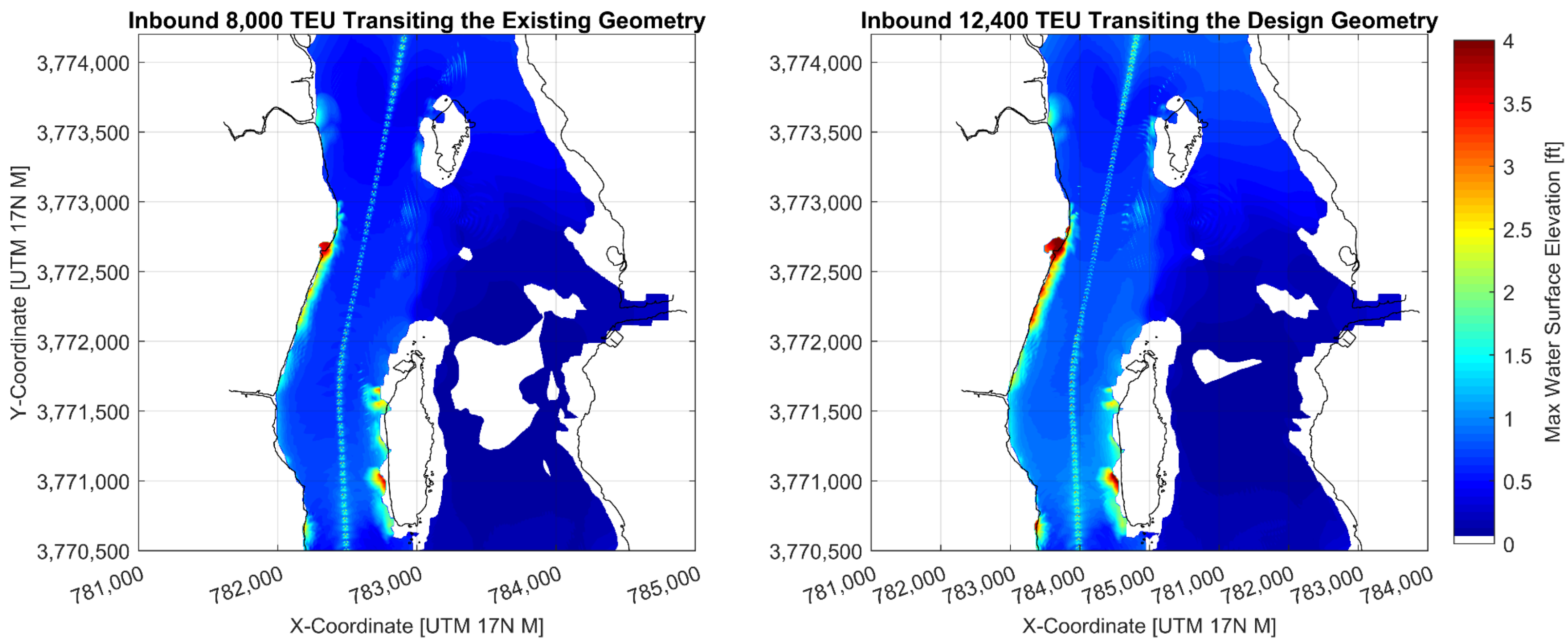

Figure 9-35: Maximum Water Surface Elevation for the Typical (left) and Design Vessels (right) for Inbound Orton Point Simulations.

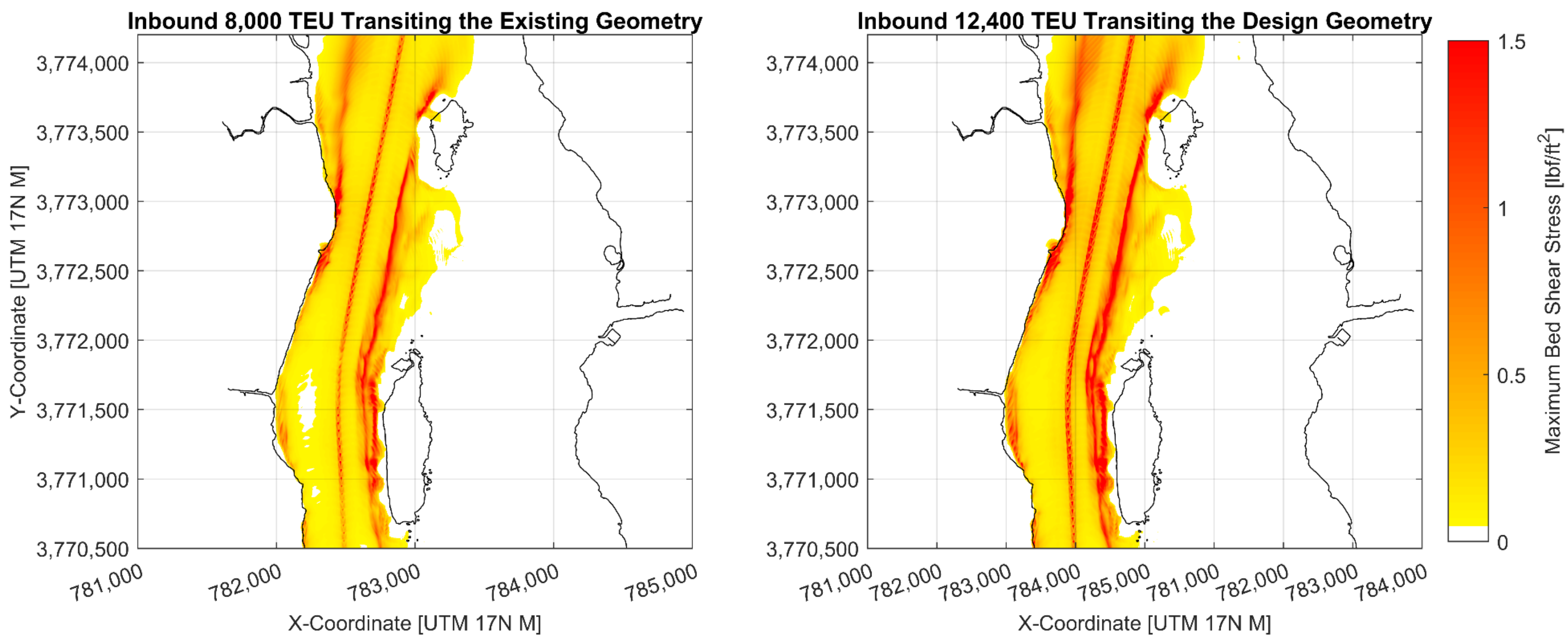

Figure 9-36: Maximum Bed Shear Stress for the Typical (left) and Design Vessels (right) for Inbound Orton Point Simulations.

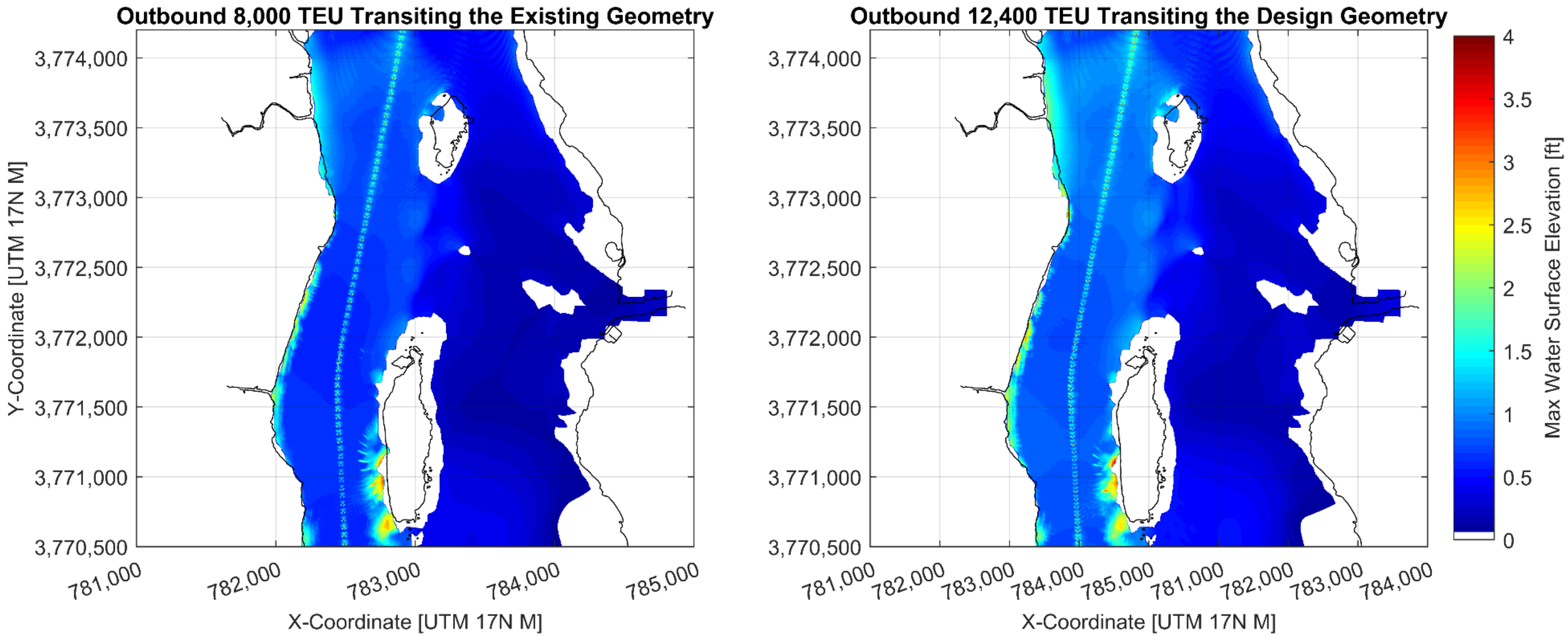

Figure 9-37: Maximum Water Surface Elevation for the Typical (left) and Design Vessels (right) for Outbound Orton Point Simulations.

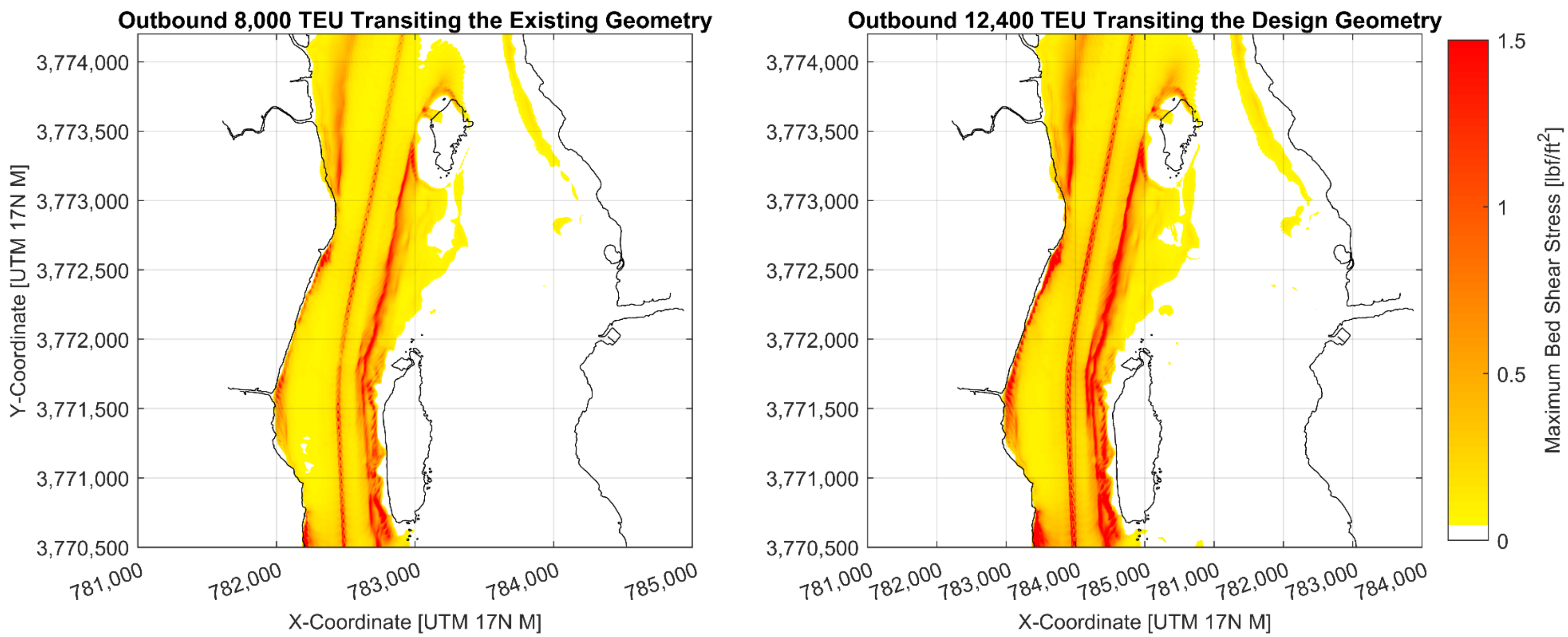

Figure 9-38: Maximum Bed Shear Stress for the Typical (left) and Design Vessels (right) for Outbound Orton Point Simulations.

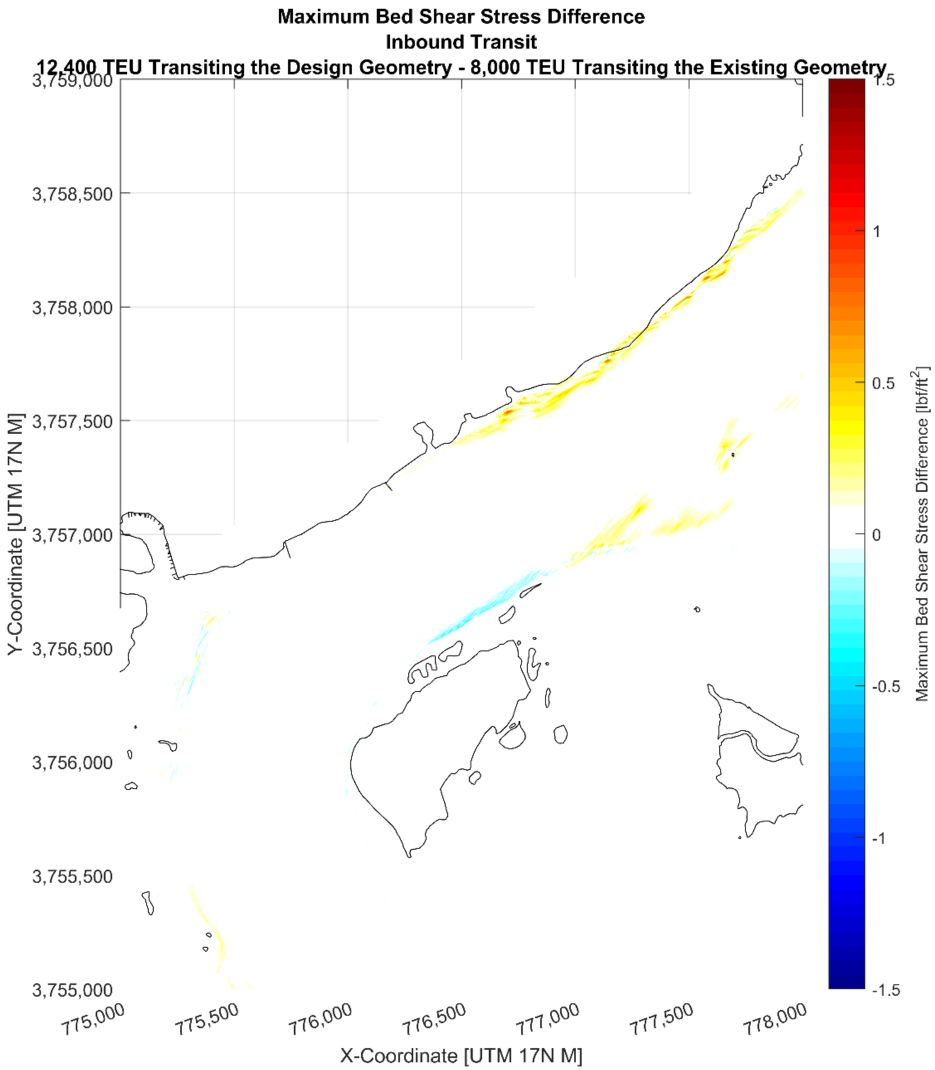

Figure 9-39: Maximum bed shear stress difference between the 12,400 TEU and 8,000 TEU vessels for inbound Southport Battery Island transits. A positive value implies a greater stress from the 12,400 TEU vessel than the 8,000 TEU vessel.

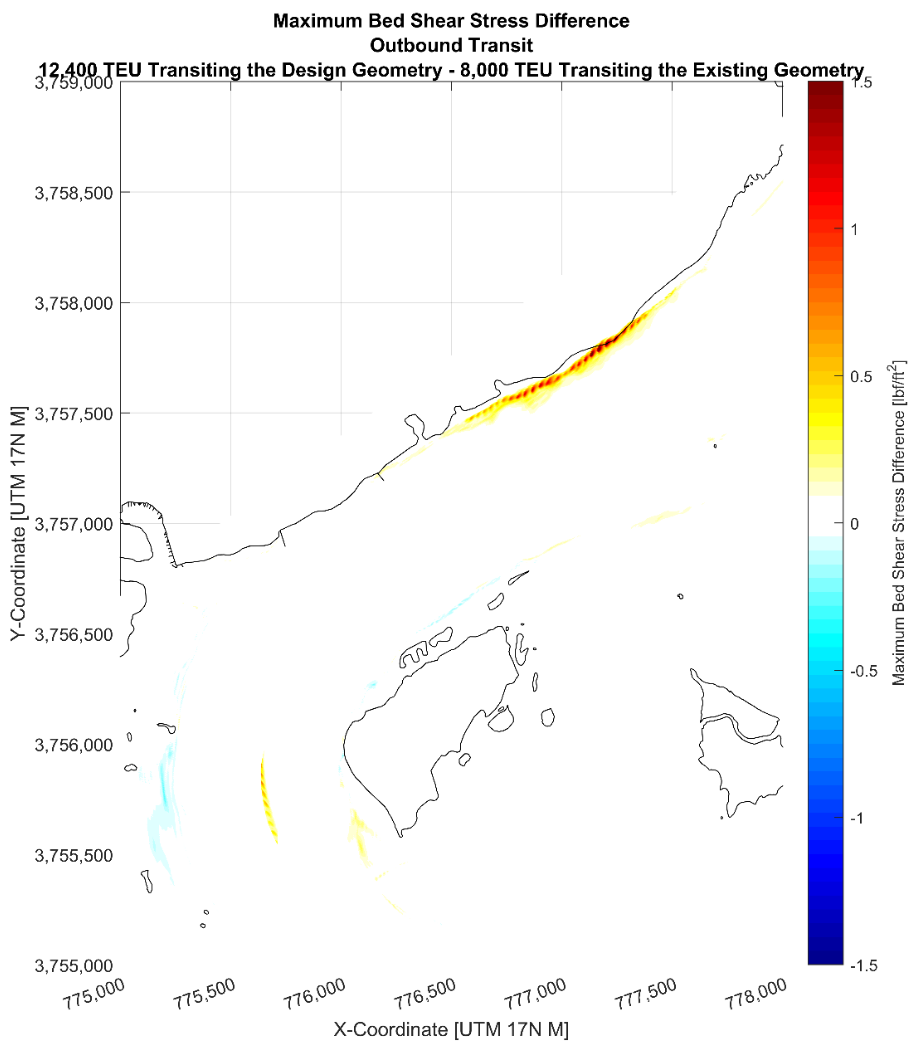

Figure 9-40: Maximum bed shear stress difference between the 12,400 TEU and 8,000 TEU vessels for outbound Southport Battery Island transits. A positive value implies a greater stress from the 12,400 TEU vessel than the 8,000 TEU vessel.

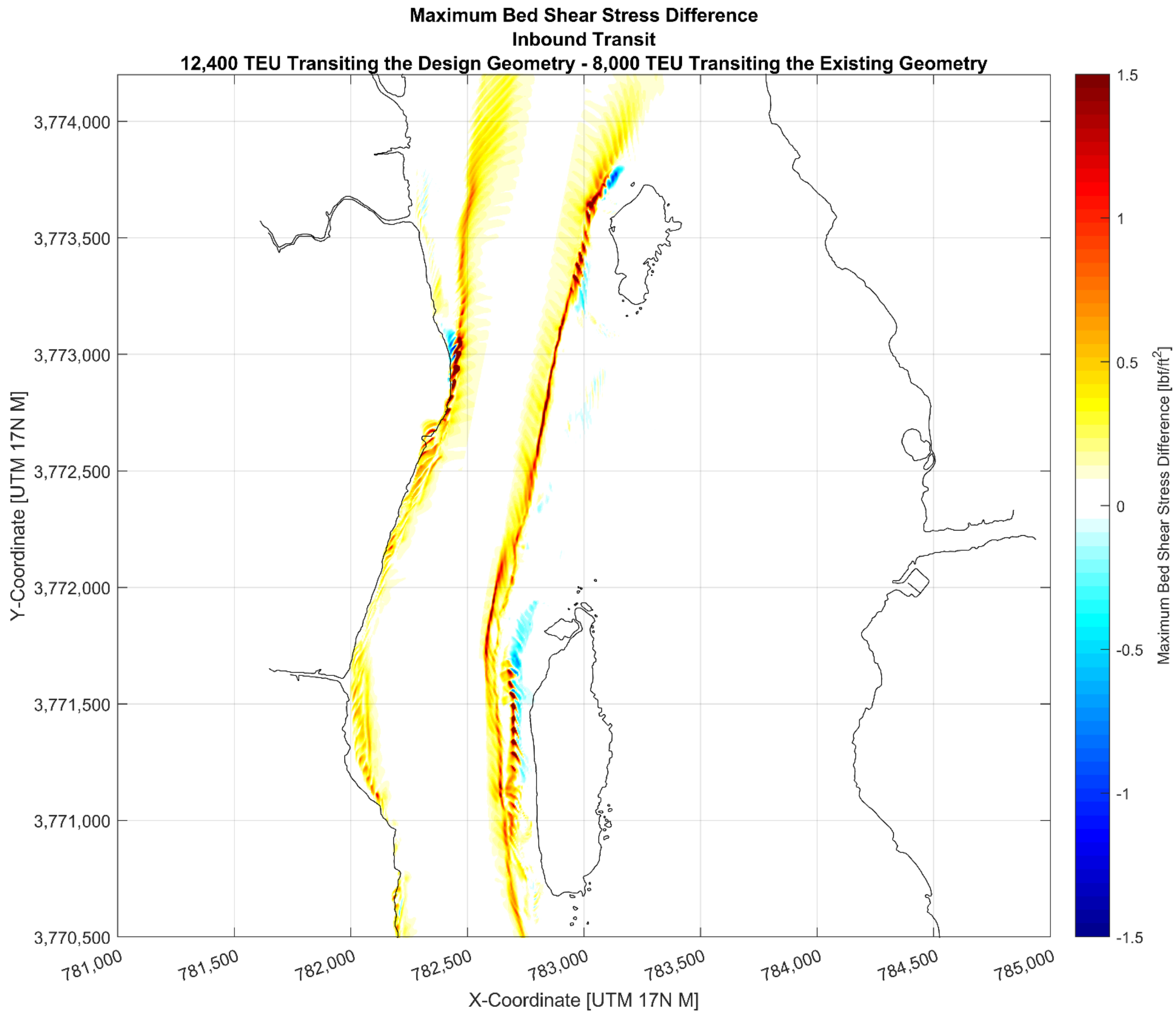

Figure 9-41: Maximum bed shear stress difference between the 12,400 TEU and 8,000 TEU vessels for inbound Orton Point transits. A positive value implies a greater stress from the 12,400 TEU vessel than the 8,000 TEU vessel.

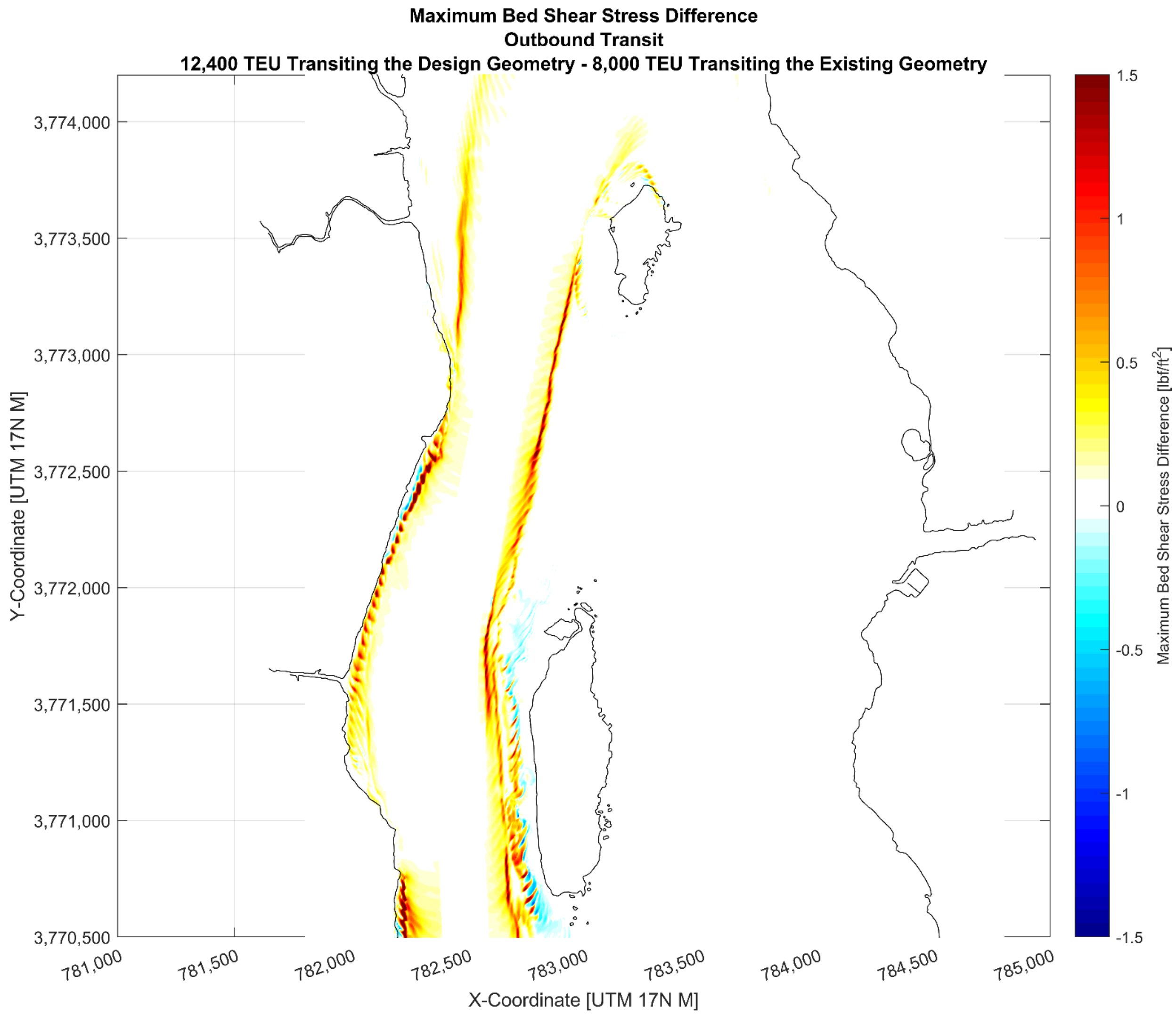

Figure 9-42: Maximum bed shear stress difference between the 12,400 TEU and 8,000 TEU vessels for outbound Orton Point transits. A positive value implies a greater stress from the 12,400 TEU vessel than the 8,000 TEU vessel.

9.2.7. Secondary Wave Prediction

The secondary waves are typically deep or intermediate water waves, which would require a 3D profile to accurately simulate. According to the literature in principle, the non-hydrostatic XBeach model should be able to reproduce the secondary wave created from the passing ship. However, as noted in numerous studies (e.g., De Jong et. al., 2013, Zhou et al., 2014) and from above XBeach results the secondary short waves induced by the ship are not correctly produced from the model as the short waves do not propagate towards the shoreline. Therefore, to evaluate the secondary waves induced from the two different vessels an analytical approach was used.

A Permanent International Association of Navigation Congress (PIANC) working group report on the design of canal revetments (1987) gives the following equations for secondary waves generated by passing vessels.

$$H = h\alpha_1 \left(\frac{s}{h}\right)^{-\frac{1}{3}} F_s^4$$

$$T_p = \cos 35° \, v_s \frac{2\pi}{g}$$

where:

$$H = \text{height of ship wave}$$
$$T_p = \text{ship wave period}$$
$$F_s = \text{Ship Froude number. } F_s = \frac{v_s}{\sqrt{gh}}$$
$$h = \text{channel depth}$$
$$v_s = \text{vessel speed}$$
$$g = \text{acceleration due to gravity}$$
$$\alpha_1 = \text{ship geometry coefficient.} \, \alpha_1 = \alpha_2 \frac{T}{L_e}$$
$$T = \text{ship draft}$$
$$L_e = \text{Distance from the ship's bow to the beginning of the parallel midship section}$$
$$\alpha_2 = \text{coefficient based on vessel type}$$
$$s = \text{distance between the ship's side and the point of interest}$$

Verhey and Bogaerts (1989) give a conservative value of 4.0 for the α_2 coefficient based on laboratory and field test in deep water (i.e., $F_s < 0.7$, which is the case for this study). The distance between the vessel and the point of interest was assumed to be the shortest distance between the vessel track line and the shoreline. Table 9-7 and Table 9-8 show the resulting wave heights and periods for the secondary ship wake for the existing channel with the 8,000 TEU and the design channel with the 12,400 TEU for the three areas of interest, Battery Island, Southport, and Orton Point for the inbound and outbound transits, respectively. The table shows metric units as required by the equations.

The two compared vessels were assumed to have the same ship shape and traveling at the same transiting speed which are justified assumptions for this analysis. The distance from the shoreline was determined based of the track of the vessel and direction of transit of interest. The ship shape and traveling speed of the vessel primarily control the secondary wave calculations and therefore result in little to no difference between the secondary wave height and period with the increased ship size and deepened channel.

Table 9-7: Secondary Ship Wake Height and Period for the Design Vessels for the Inbound Simulations

Component	Battery Island		Southport		Orton Point	
	8,000 TEU	12,400 TEU	8,000 TEU	12,400 TEU	8,000 TEU	12,400 TEU
$\boldsymbol{g}$, gravity [m/s^2]	9.8	9.8	9.8	9.8	9.8	9.8
$\boldsymbol{h}$, channel depth [m]	13.4	14.9	13.4	14.9	13.4	14.9
$\boldsymbol{v_s}$, vessel speed [m/s]	5.1	5.1	5.1	5.1	5.7	5.7
$\boldsymbol{F_s}$, Ship Froude Number [-]	0.5	0.4	0.5	0.4	0.5	0.5
$\boldsymbol{T}$, ship draft [m]	11.6	13.1	11.6	13.1	11.6	13.1
$\boldsymbol{L_e}$, distance from Ship's Bow to the Beginning of the Parallel Midship Section [m]	129.7	142.3	129.7	142.3	129.7	142.3
$\boldsymbol{\alpha_2}$, coefficient based on vessel type [-]	4.00	4.00	4.00	4.00	4.00	4.00
$\boldsymbol{\alpha_1}$, ship Shape Coefficient [-]	0.36	0.37	0.36	0.37	0.36	0.37
$\boldsymbol{s}$, distance from ship’s side and the point of interest [m]	342.0	400.0	378.0	316.0	194.0	191.0
$\boldsymbol{H}$, Ship Wake Height [m]	**0.07**	**0.06**	**0.06**	**0.06**	**0.12**	**0.11**
$\boldsymbol{T_p}$, Ship Wake Period [s]	**2.7**	**2.7**	**2.7**	**2.7**	**3.0**	**3.0**

Table 9-8: Secondary Ship Wake Height and Period for the Design Vessels for the Outbound Simulations

Component	**Battery Island**		**Southport**		**Orton Point**	
	8,000 TEU	12,400 TEU	8,000 TEU	12,400 TEU	8,000 TEU	12,400 TEU
$\boldsymbol{g}$, gravity [m/s^2]	9.8	9.8	9.8	9.8	9.8	9.8
$\boldsymbol{h}$, channel depth [m]	13.4	14.9	13.4	14.9	13.4	14.9
$\boldsymbol{v_s}$, vessel speed [m/s]	5.1	5.1	5.1	5.1	5.7	5.7
$\boldsymbol{F_s}$, Ship Froude Number [-]	0.5	0.4	0.5	0.4	0.5	0.5
$\boldsymbol{T}$, ship draft [m]	11.6	13.1	11.6	13.1	11.6	13.1
$\boldsymbol{L_e}$, distance from Ship's Bow to the Beginning of the Parallel Midship Section [m]	129.7	142.3	129.7	142.3	129.7	142.3
$\boldsymbol{\alpha_2}$, coefficient based on vessel type [-]	4.00	4.00	4.00	4.00	4.00	4.00
$\boldsymbol{\alpha_1}$, ship Shape Coefficient [-]	0.36	0.37	0.36	0.37	0.36	0.37
$\boldsymbol{s}$, distance from ship's side and the point of interest [m]	500.0	396.0	337.0	399.0	194.0	191.0
$\boldsymbol{H}$, Ship Wake Height [m]	**0.06**	**0.06**	**0.06**	**0.06**	**0.12**	**0.11**
$\boldsymbol{T_p}$, Ship Wake Period [s]	**2.7**	**2.7**	**2.7**	**2.7**	**3.0**	**3.0**

9.2.8. Model Simulations for Smaller Vessels

An additional analysis was performed to evaluate the effects of ship wakes resulting from smaller capacity vessels traversing the proposed navigation channel in the vicinity of Southport and Battery Island. Four model simulations were executed to evaluate ship wake effects of the two channel geometries (design and existing) at the two areas of interest (Southport and Battery Island). The model simulation matrix is listed in Table 9-9. This run matrix serves the purpose of this study to evaluate the effects of ship wake with regards to bed shear stress as a result of smaller capacity vessels traversing close to Southport and Battery Island in the deepened and widened channel.

Table 9-9: Model simulation matrix

Simulation No.	Area of Interest	Channel Geometry
1	Southport	Design
2		Existing
3	Battery Island	Design
4		Existing

9.2.8.1. Model Vessel Parameters

The design vessel for this analysis was the Independent Pursuit, a 2,500 TEU container vessel. Geometry details of the Independent Pursuit are listed in Table 9-10. This vessel was used for all model simulations.

Table 9-10: Design vessel geometry

Attribute	Independent Pursuit
Capacity (TEU)	2,500
LOA (ft)	685.2
LBP (ft)	645.8
Beam (ft)	98.4
Draft (ft)	38.0

XBeach represents a sailing vessel as a moving pressure head that follows a user-defined track. Each model simulation had a different vessel track that was dependent on the channel geometry and the area of interest (Figure 9-43). Model simulations that incorporated the proposed design navigation channel geometry (Simulations 1 and 3) used a “worst case” vessel track that was 150 ft inward of the proposed design navigation channel boundary (herein referred to as Idealized track) that was closest to the area of interest; whereas model simulations that incorporated the existing navigation channel geometry (Simulations 2 and 4) used a vessel track obtained from the Automatic Identification System (AIS) for marine traffic (herein referred to as AIS track) that was closest to the area of interest. All simulated vessel tracks were generated in the inbound (south to north) direction.

It can be seen from Figure 9-43 that the Battery Island Idealized and AIS tracks converge north of Battery Island. This was done due to the selected AIS track coming within 150 ft of the proposed design navigation channel boundary.

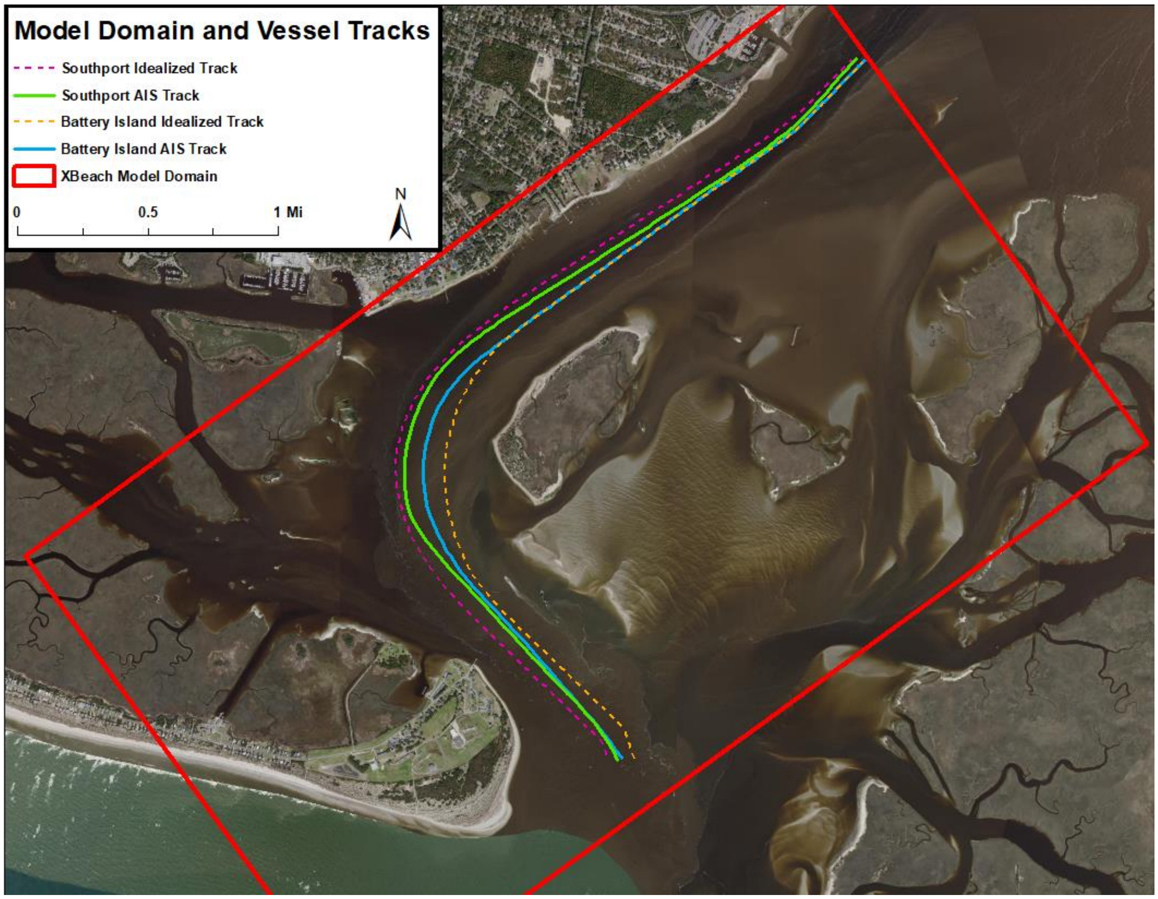

Figure 9-43: Model simulation vessel tracks

The XBeach manual recommends to gradually accelerate the vessel to a desired sailing velocity to avoid unwanted spurious water surface elevation disturbances. In all model simulations, the vessel was accelerated at 2 knots/s until the desired sailing velocity of 10 knots was reached.

The vessel shape is inputted into XBeach on a separate grid from the computational grid. One hull depth point can be specified for each grid cell on this auxiliary grid. The vessel draft is interpolated to the global model grid at every timestep while the vessel volume remains constant. The vessel draft for the smaller capacity (2,500 TEU) vessel used in this study is shown in comparison to the larger capacity (8,000 and 12,400 TEU) vessels used prevously (Figure 9-44).

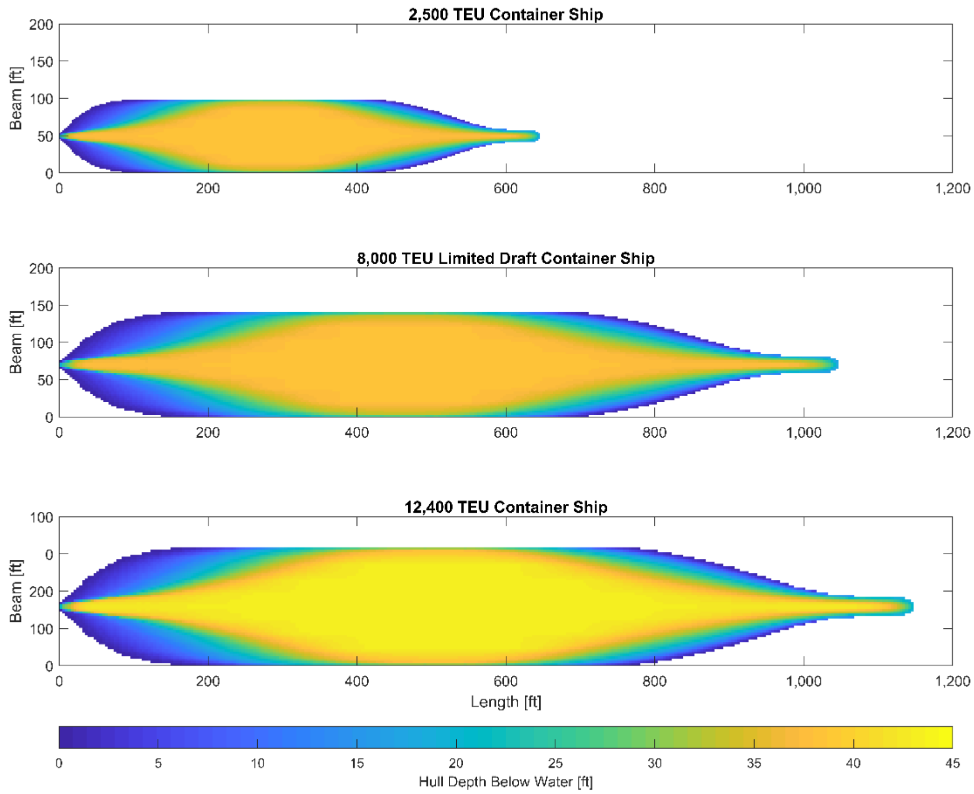

Figure 9-44: Vessel grids and drafts

9.2.8.2. Model Calibration

As previously discussed, calibration of the XBeach models was not conducted due to lack of measured field data. However, the relative differences evaluated between the different vessel tracks are still valid due to the comparative approach that was taken during this study.

9.2.8.3. Model Results

The four model simulations were executed to assess the change in environmental conditions from smaller capacity vessels sailing closer to Southport and Battery Island due to the proposed design navigation channel.

Model output data of water surface elevation and current velocity were extracted at three observation points (Figure 9-45) for all model simulations. Time series of the extracted model output data are shown in Figure 9-46 through Figure 9-51. The differences in maximum water surface elevation, current velocity magnitude, and bed shear stress magnitude at each observation point are given in Table 9-11. In Table 9-11 a positive sign implies a greater model output value during the Idealized track simulation as compared to the AIS track simulation. Comparing all model simulations, the greatest change in maximum water surface elevation and current velocity magnitude occurred at Point A for the vessel tracks closest to Southport. Comparing only the vessel tracks closest to Battery Island, the greatest change in maximum water surface elevation and current velocity magnitude occurred at Point C.

The ship wake impact on the bed at the areas of interest was evaluated through the bed shear stress. All variables required to calculate bed shear stress, excluding the density of sea water, were taken directly from the XBeach model output. Comparing all model simulations, the greatest change in maximum bed shear stress magnitude occurred at Point A for the vessel tracks closest to Southport. Comparing only the vessel tracks closest to Battery Island, the greatest change in maximum bed shear stress magnitude occurred at Point B.

Figure 9-45: Geographic location of observation points

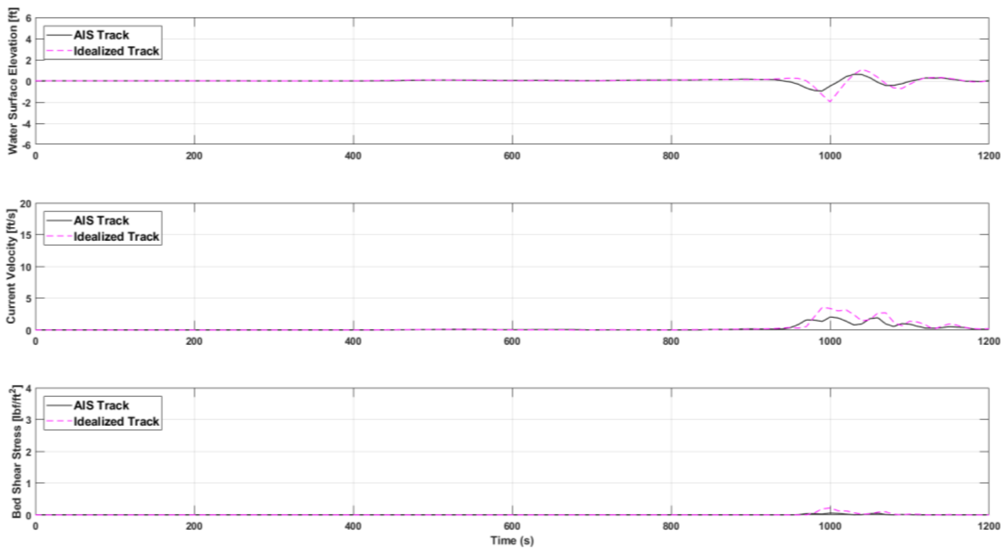

Figure 9-46: Timeseries of water surface elevation (top), current velocity (middle), and bed shear stress (bottom) at Point A for vessel tracks closest to Southport

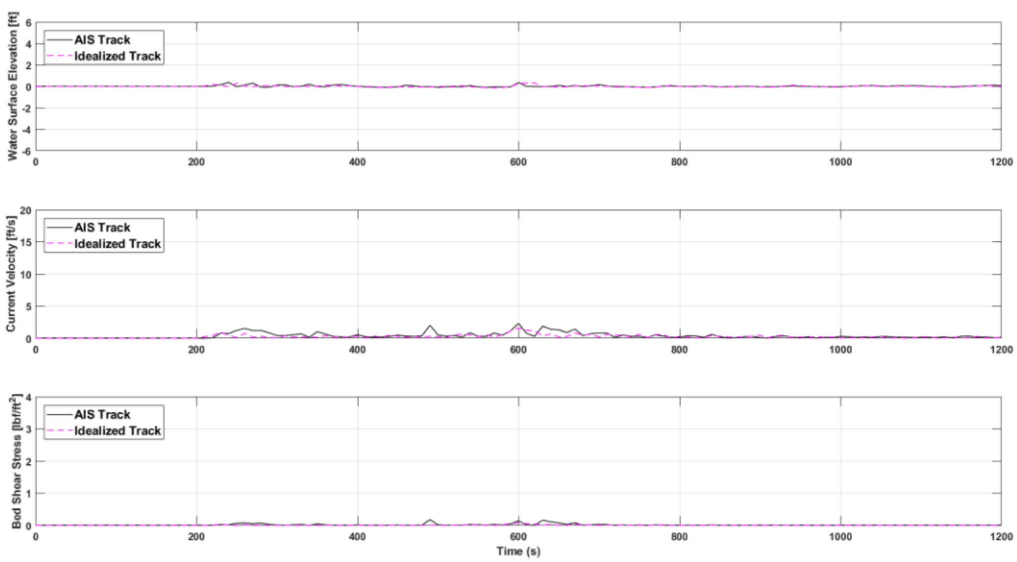

Figure 9-47: Timeseries of water surface elevation (top), current velocity (middle), and bed shear stress (bottom) at Point B for vessel tracks closest to Southport

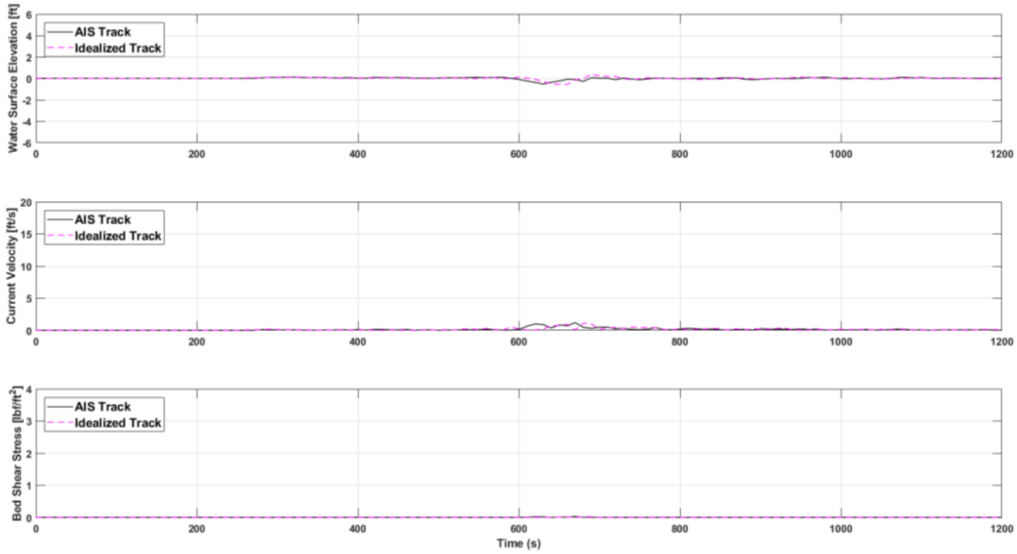

Figure 9-48: Timeseries of water surface elevation (top), current velocity (middle), and bed shear stress (bottom) at Point C for vessel tracks closest to Southport

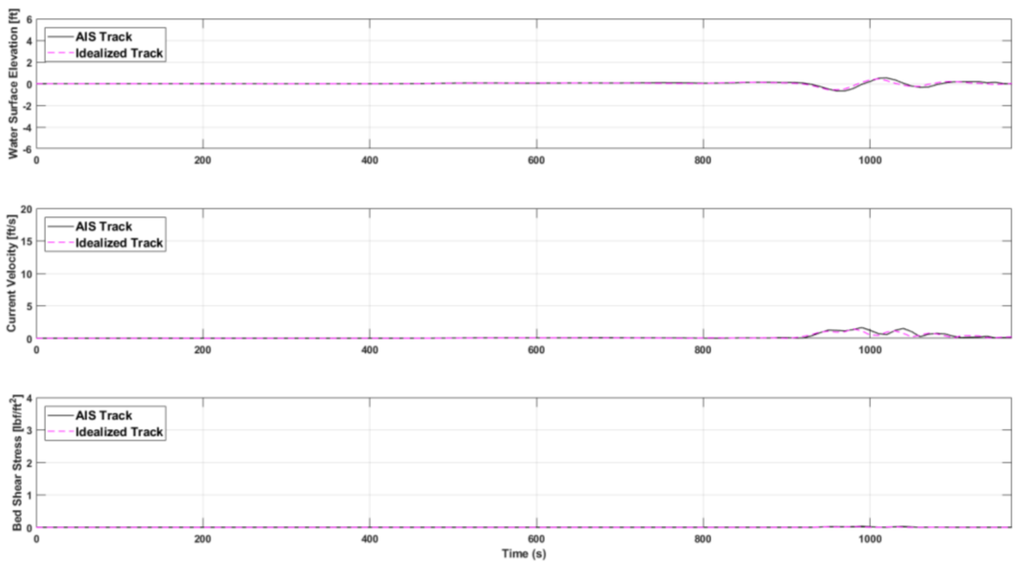

Figure 9-49: Timeseries of water surface elevation (top), current velocity (middle), and bed shear stress (bottom) at Point A for vessel tracks closest to Battery Island

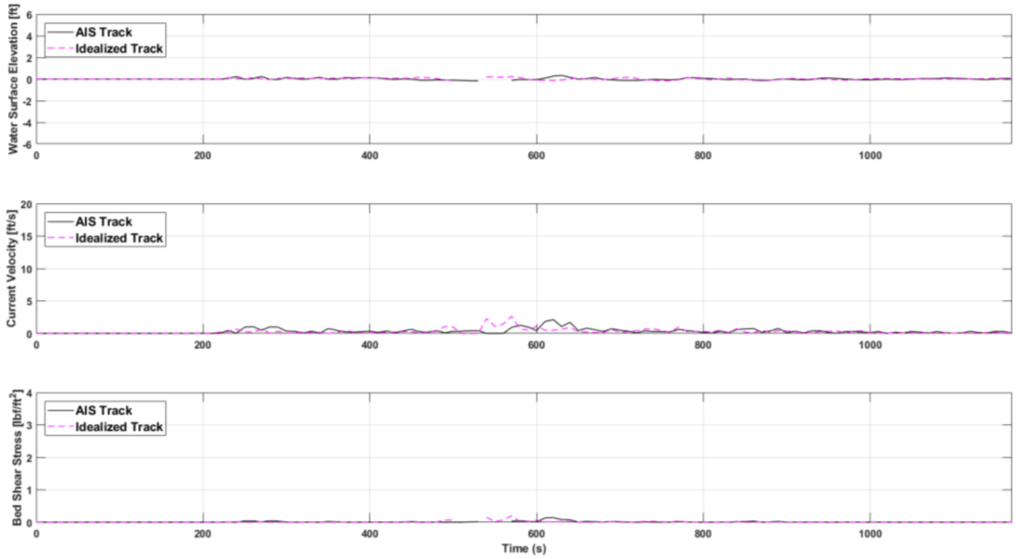

Figure 9-50: Timeseries of water surface elevation (top), current velocity (middle), and bed shear stress (bottom) at Point B for vessel tracks closest to Battery Island

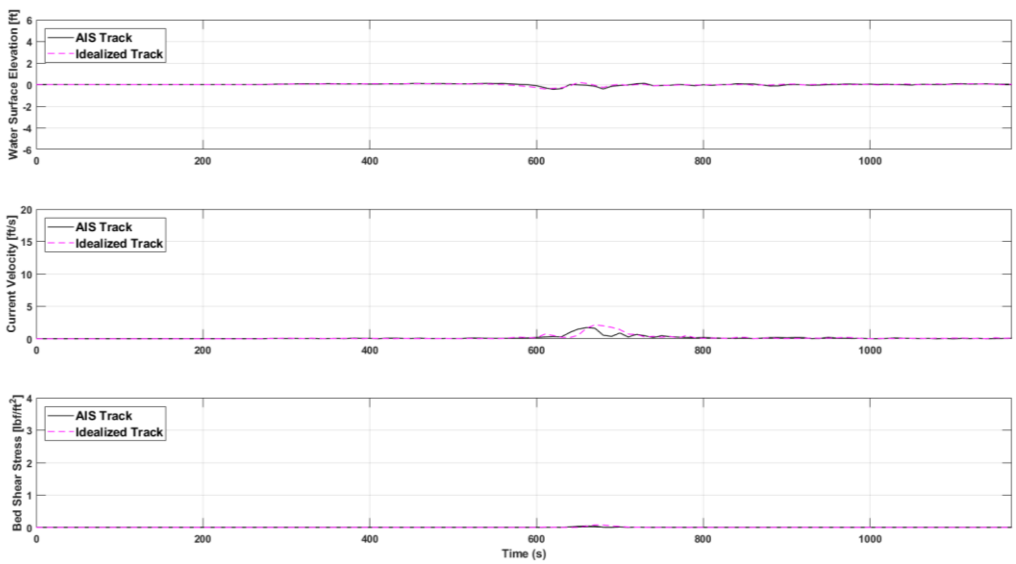

Figure 9-51: Timeseries of water surface elevation (top), current velocity (middle), and bed shear stress (bottom) at Point C for vessel tracks closest to Battery Island

Table 9-11: Difference in maximum model outputs between Idealized track and AIS track for Southport and Battery Island simulations

Area of Interest	Point	Change in Maximum Water Surface Elevation^ [ft]	Change in Maximum Current Velocity Magnitude^ [$\frac{ft}{s}$]	Change in Maximum Bed Shear Stress Magnitude^ [$\frac{lbf}{ft^2}$]
Southport	A	+0.5	+1.5	+0.2
	B	-0.1	-0.7	-0.1
	C	+0.3	-0.1	0.0
Battery Island	A	-0.1	-0.2	0.0
	B	-0.1	+0.5	+0.1
	C	+0.1	+0.4	+0.0
^ Values reported are Idealized track results minus AIS track results				

The maximum water surface elevation and bed shear stress magnitude at each grid cell throughout the model domain were determined and compared. The maximum water surface elevation and bed shear stress magnitude resulting from the AIS and Idealized tracks closest to Southport are shown in Figure 9-52 and Figure 9-53, respectively. The maximum water surface elevation and bed shear stress magnitude resulting from the AIS and Idealized tracks closest to Battery Island are shown in Figure 9-54 and Figure 9-55, respectively.

For comparative purposes, the difference in the maximum bed shear stress magnitude for the tracks closest to Southport (Figure 9-56) and Battery Island (Figure 9-57) are shown. As in Table 9-11, positive values imply a greater model output for the Idealized track simulation compared to the AIS track simulation. From Figure 9-56, there was a significant increase in maximum bed shear stress magnitude along the northeastern coast of Southport (blue box) due to the more landward vessel track. Along Battery Island there was minimal increase in maximum bed shear stress magnitude due to the more landward vessel track, Figure 9-57. However, it should be noted along the northern coast of Battery Island there was actually a decrease in maximum bed shear stress magnitude, meaning that the design channel should create less impact to this shoreline under the tested conditions.

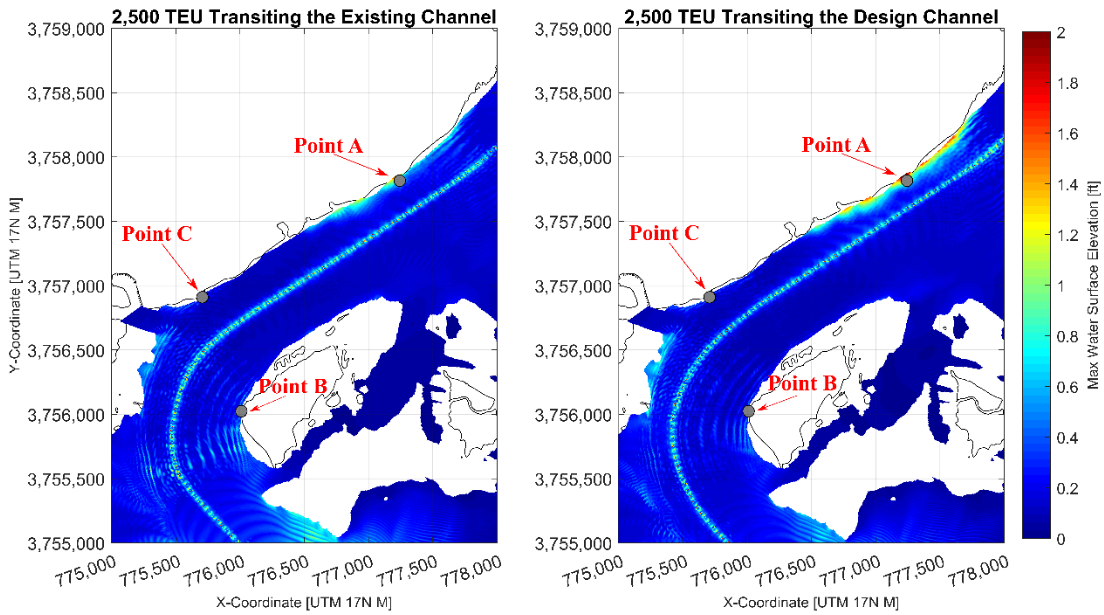

Figure 9-52: Maximum water surface elevation resulting from the AIS track (left) and Idealized track (right) close to Southport

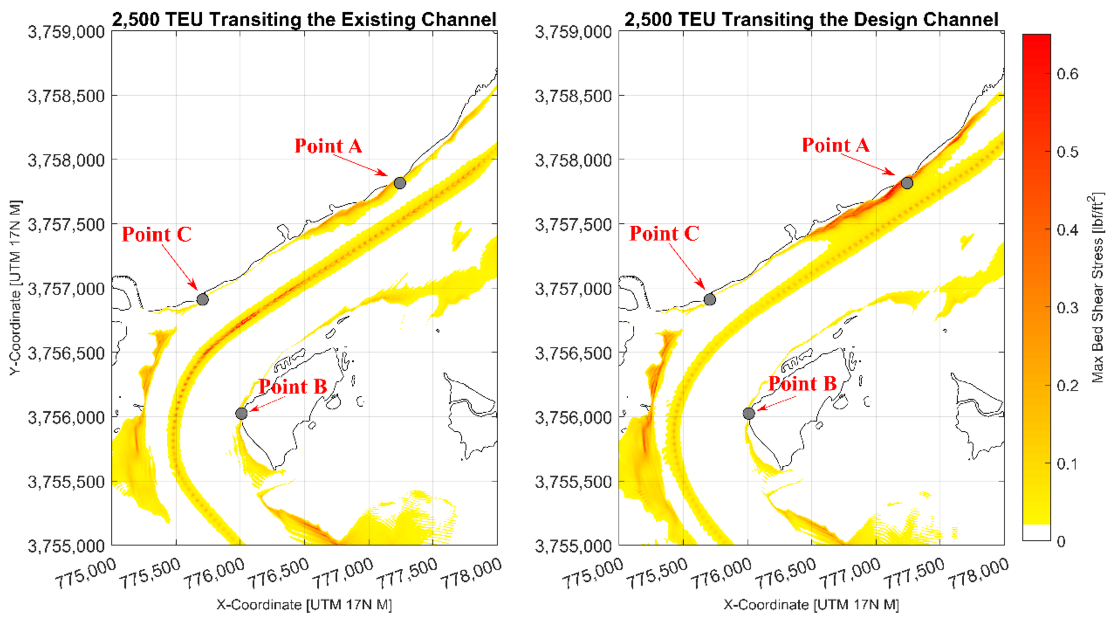

Figure 9-53: Maximum bed shear stress magnitude resulting from the AIS track (left) and Idealized track (right) close to Southport

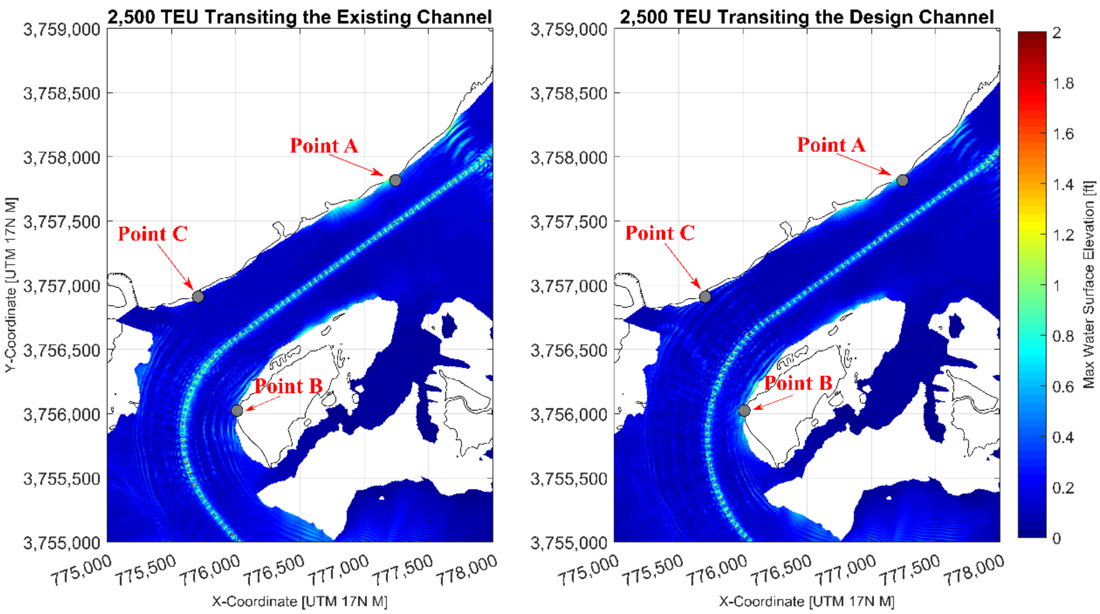

Figure 9-54: Maximum water surface elevation resulting from the AIS track (left) and Idealized track (right) close to Battery Island

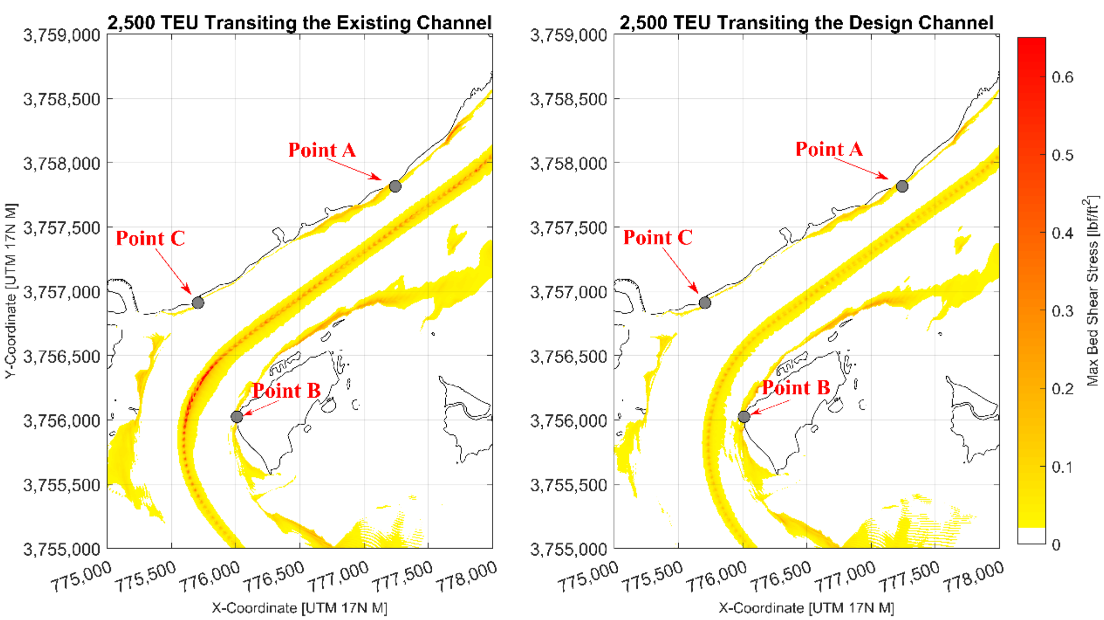

Figure 9-55: Maximum bed shear stress magnitude resulting from the AIS track (left) and Idealized track (right) close to Battery Island

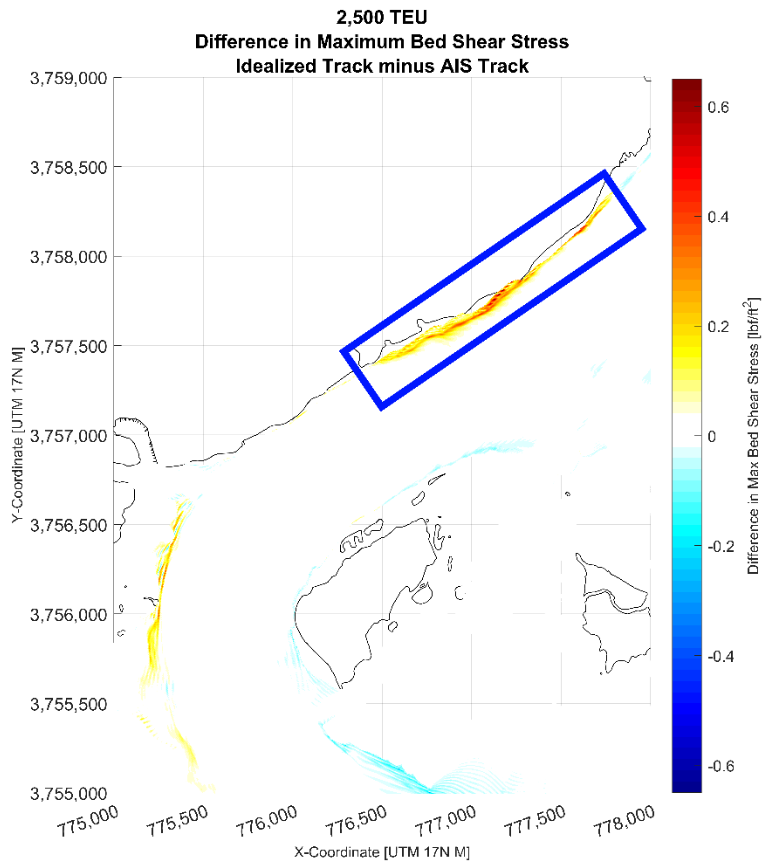

Figure 9-56: Difference in maximum bed shear stress magnitude for tracks close to Southport

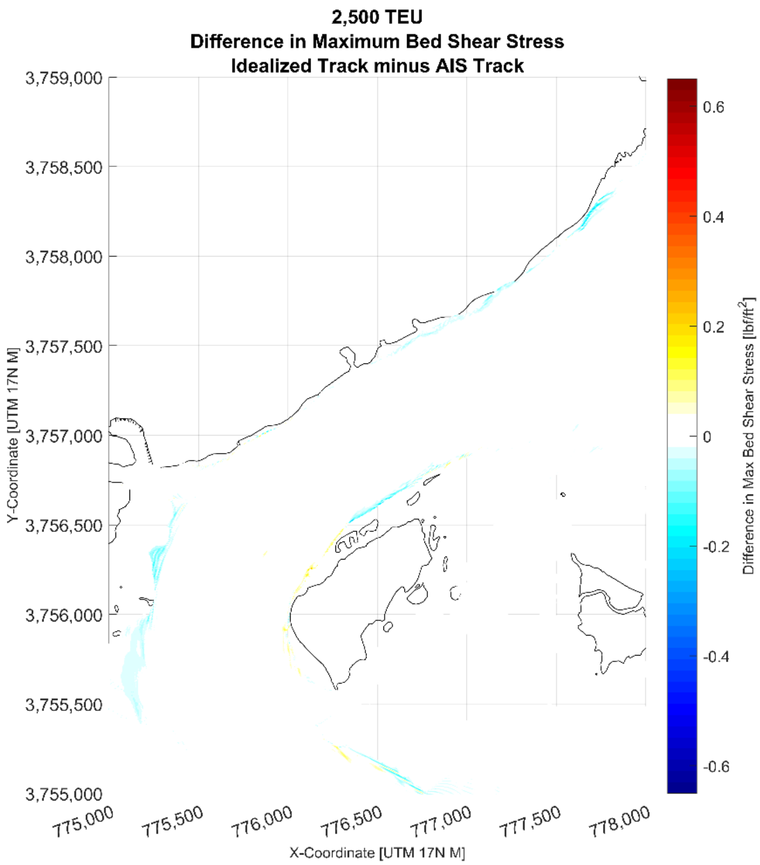

Figure 9-57: Difference in maximum bed shear stress magnitude for tracks close to Battery Island

9.2.9. Adjacent Islands

To evaluate the potential for vessel impacts to the smaller "bird" island located adjacent to the channel due to widening and larger vessels, model results were extracted at Points G and H (Figure 9-58). Since the channel width and depth is constant through this reach of the river (with the except of the passing lanes), and the distance from the channel to these islands is similar, these results are representative of the potential effects the proposed project may have on these islands.

The results show a slight increase in water surface elevation and an increase in bed shear stress for the larger capacity vessels. The increased bed shear stress magnitude showed to be geographically dependent, as the increase at Point H was much greater than at Point G (Figure 9-59 and Figure 9-60).

The difference in maximum water surface elevation, current velocity, and bed shear stress at Point G and Point H are shown (Table 9-12). Varied results with respect to the maximum water surface elevation were observed, as Point G experienced a decrease in maximum water surface elevation for the larger capacity vessel. However, an increase in maximum current velocity and maximum bed shear stress at Point G and Point H was experienced due to the larger capacity vessel.

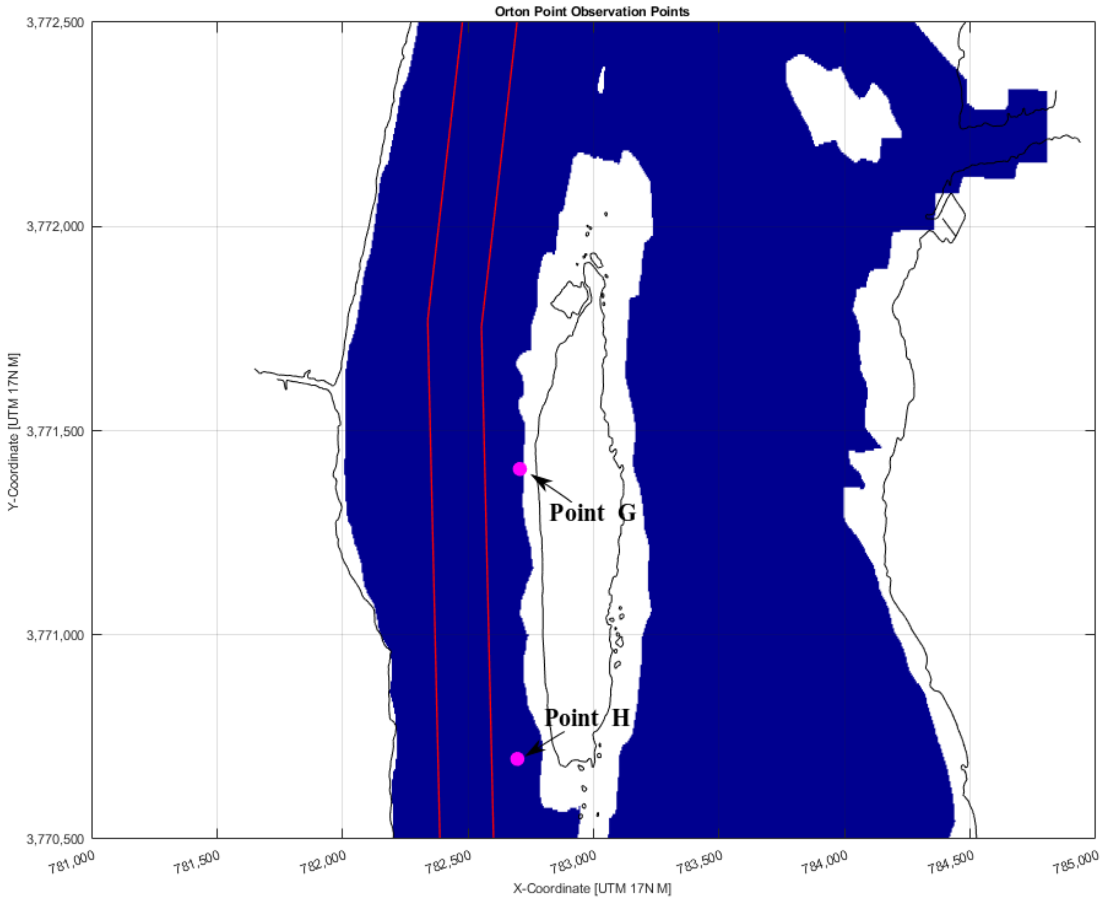

Figure 9-58: Observation points (magenta circles) where model output data was extracted during inbound Orton Point simulations. The solid red line represents the proposed design channel.

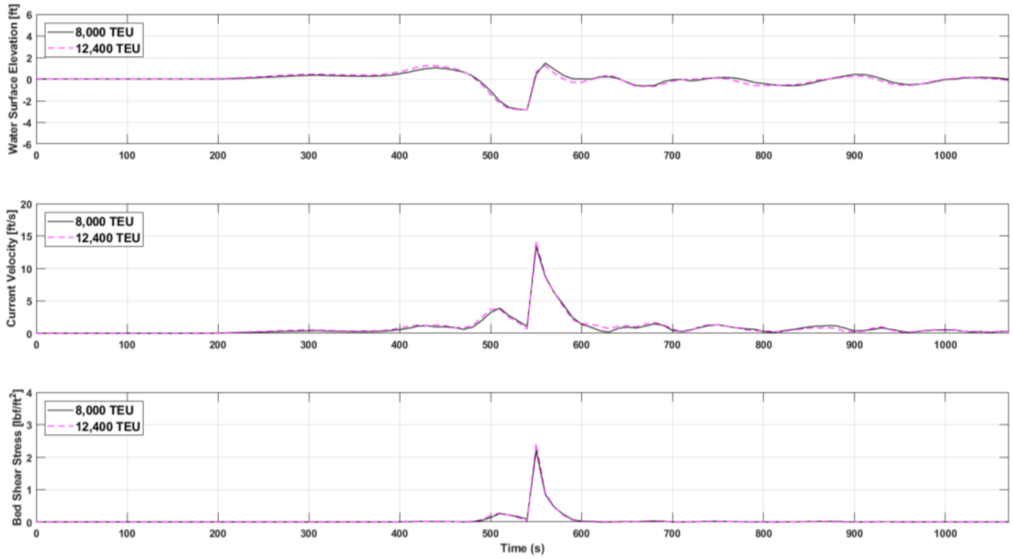

Figure 9-59: Timeseries of water surface elevation (top), current velocity (middle), and bed shear stress (bottom) at Point G for inbound Orton Point simulation.

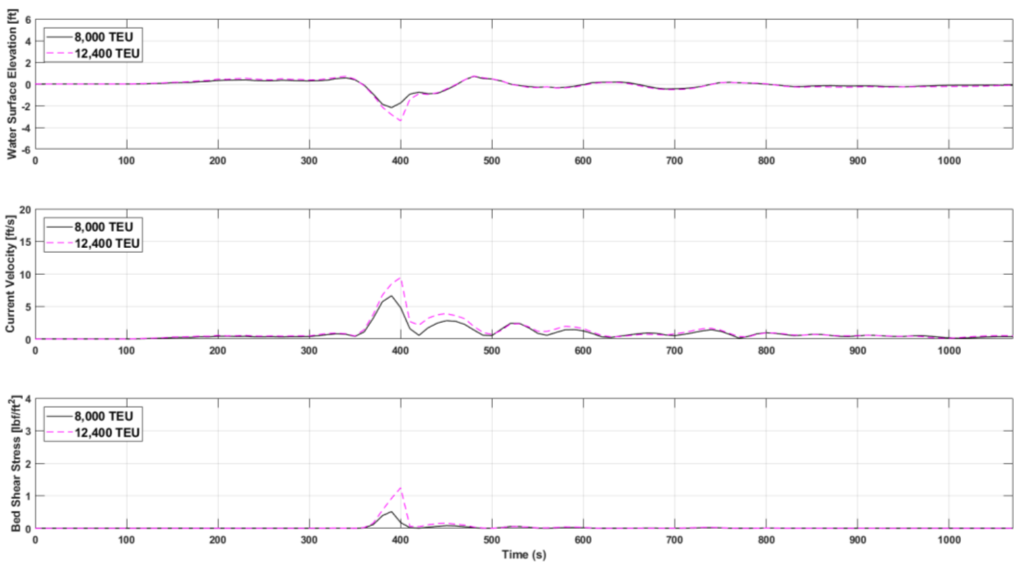

Figure 9-60: Timeseries of water surface elevation (top), current velocity (middle), and bed shear stress (bottom) at Point H for inbound Orton Point simulation.

Table 9-12: Difference in magnitude between the 8,000 TEU and 12,400 TEU Vessels - Adjacent Island Simulations.

Point	Change in Maximum Primary Wave Height^ $[\mathbf{ft}]$	Change in Maximum Current Velocity^ $[\frac{\mathbf{ft}}{\mathbf{s}}]$	Change in Maximum Bed Shear Stress $[\frac{\mathbf{lbf}}{\mathbf{ft^2}}]$
G	- 0.2	+0.9	+0.2
H	0.0	+2.8	+0.7
^ Values reported are the 12,400 TEU minus the 8,000 TEU			

9.2.10. Throughput Comparison

With the increased TEU capacity of the larger vessels, fewer vessels will need to call at the Port of Wilmington to meet the same throughput. Thus, an analysis was made assuming every three 8,000 TEU container vessels will be replaced by two 12,400 TEU container vessels with the single transit primary wave bed shear stress for each of the vessels being tripled or doubled, respectively, and the differences between the two vessels' summations then normalized. This results in differences in maximum bed shear stresses (erosion potential) for the areas of interests due to the increased vessel size and channel changes only.

Figure 9-61 through Figure 9-64 show the normalized differences in maximum bed shear stress for the 12,400 and 8,000 TEU vessels. From, Figure 9-61, in the vicinity of Southport and Battery Island, overall the annual total bed shear stress will remain the same or decrease due to the proposed project for the inbound transits. However, for outbound transits, see Figure 9-62, the annual total bed shear stress will increase along the shoreline northeast of Southport along River Drive as a result of the proposed project. Figure 9-63 and Figure 9-64 show the bed shear stresses for Orton Point for inbound and outbound transits, respectively, and overall they remain unchanged or decrease due to the proposed project except for few localized areas of higher stresses at Orton Point.

The normalized bed shear stress shown in Figure 9-63 was extracted at Points D and E to evaluate the annual total bed shear stress expected to impact the "bird" islands. There was a significant decrease (-0.17 lbf/ft^2) and a minimal increase (0.09 lbf/ft^2) in normalized bed shear stress at Points D and E, respectively.

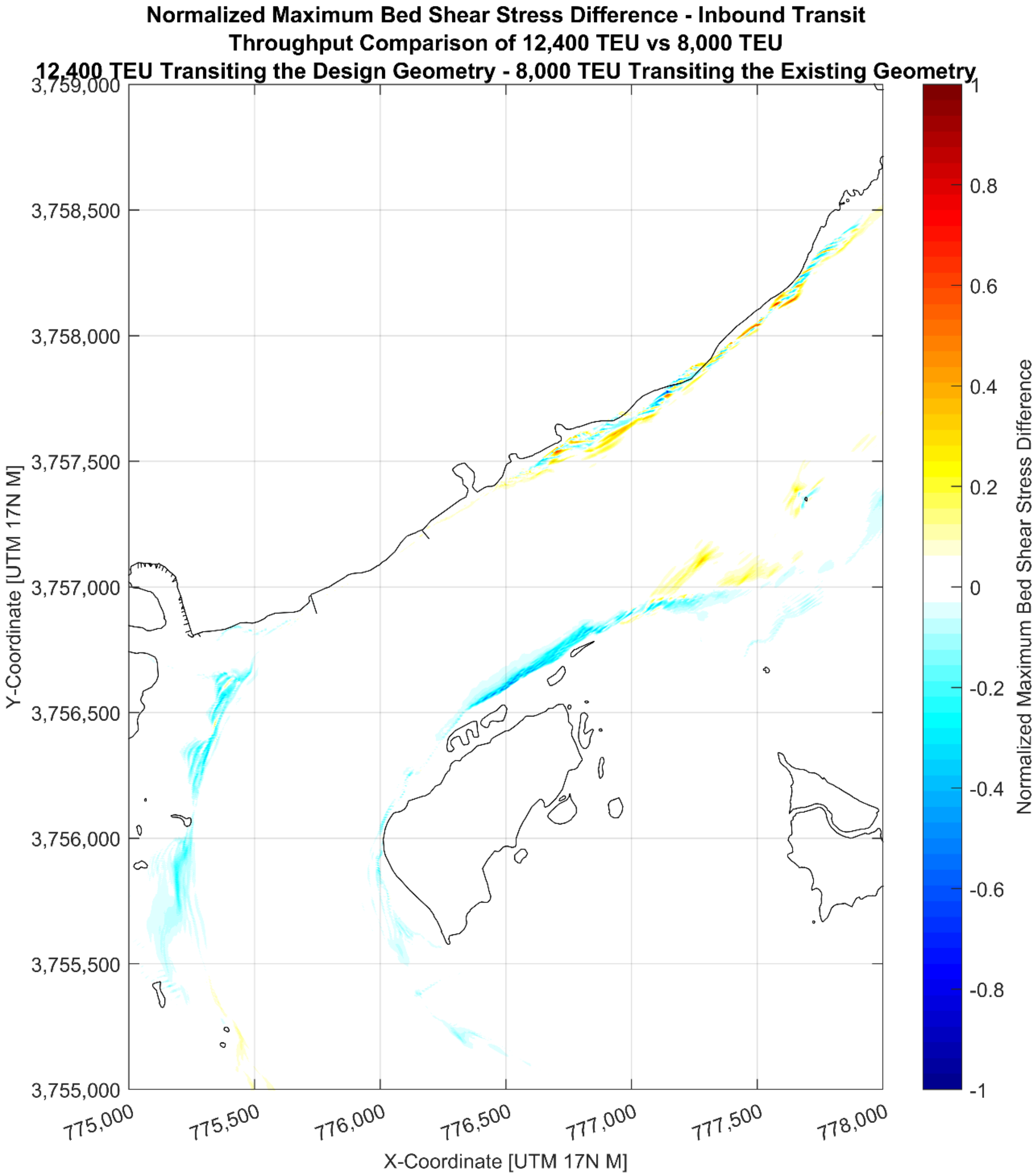

Figure 9-61: Throughput comparison of normalized maximum bed shear stress difference between the 12,400 TEU and 8,000 TEU vessels for inbound Southport Battery Island transits.

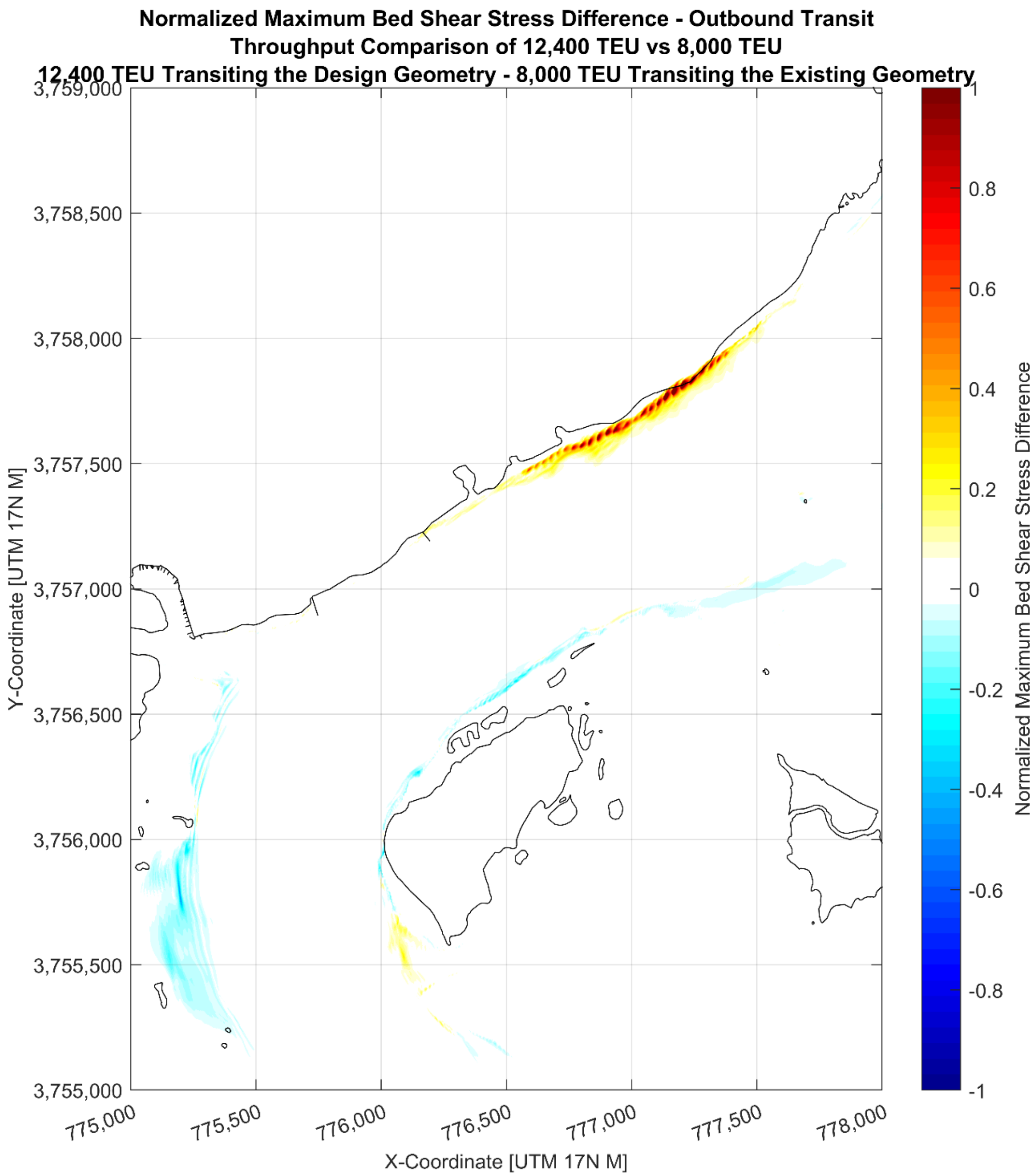

Figure 9-62: Throughput comparison of normalized maximum bed shear stress difference between the 12,400 TEU and 8,000 TEU vessels for outbound Southport Battery Island transits.

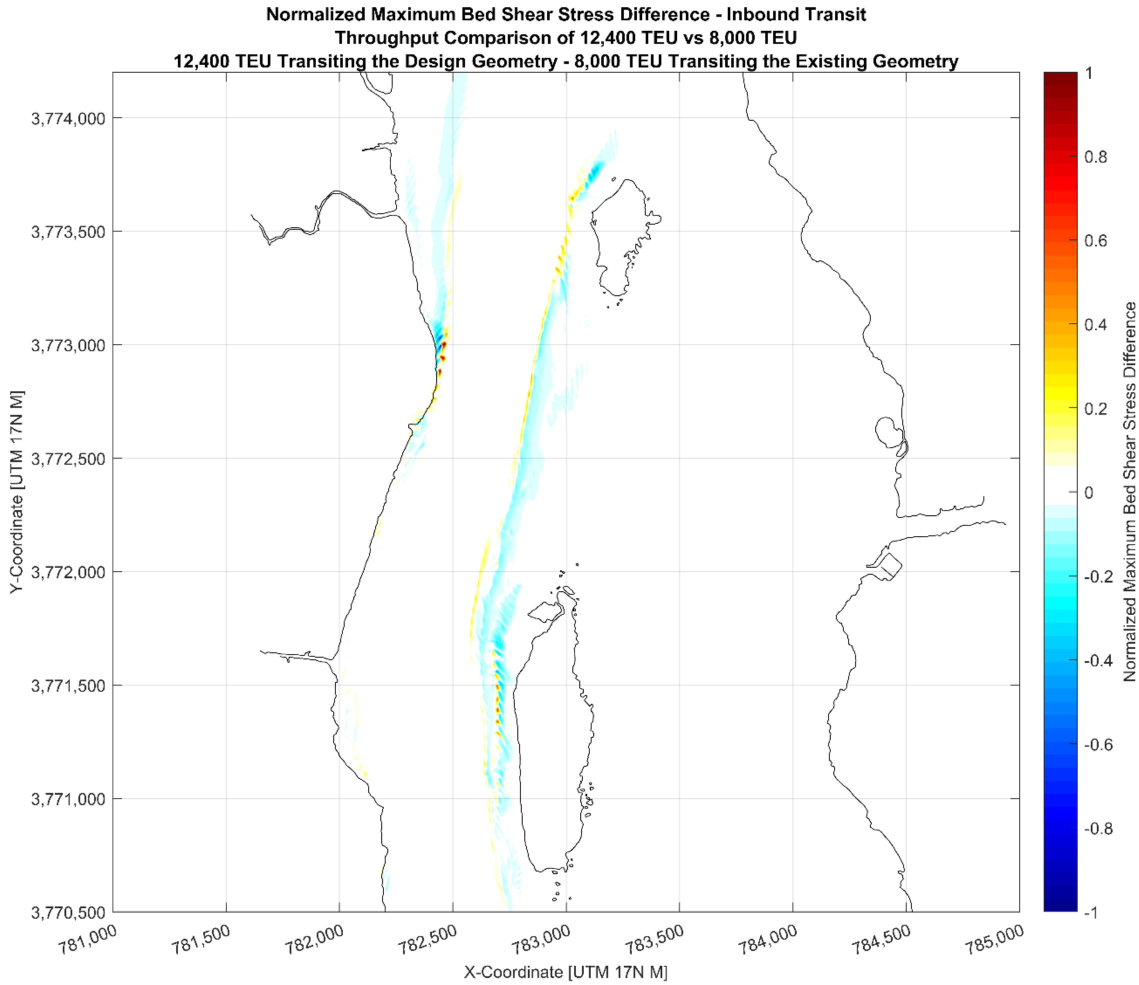

Figure 9-63: Throughput comparison of normalized maximum bed shear stress difference between the 12,400 TEU and 8,000 TEU vessels for inbound Orton Point transits.

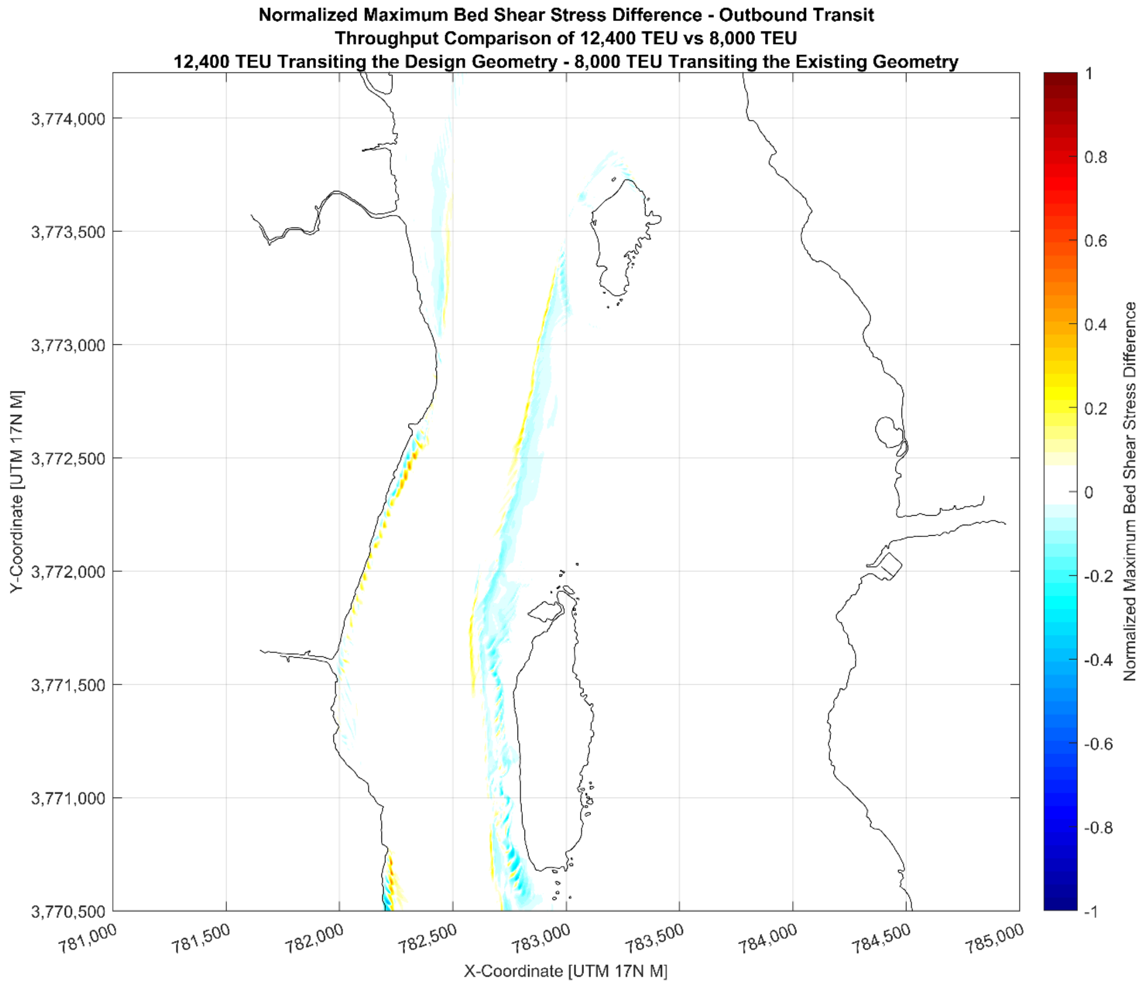

Figure 9-64: Throughput comparison of normalized maximum bed shear stress difference between the 12,400 TEU and 8,000 TEU vessels for outbound Orton Point transits.

9.2.11. Summary

From the primary wave modeling two main conclusions can be drawn. First, the primary wave effects increase with increasing vessel size, for ships travelling at the same speed, except for localized areas where the vessel track for the existing channel is closer to a particular shoreline than the new design channel track.

The secondary wave analysis resulted in wave heights that did not vary significantly from ship to ship traveling at the same speed and of the same shape. Thus, based on this analysis with a widened / deepened channel, the secondary wave heights did not increase. Therefore, with the widening and deepening and larger vessel this analysis showed that the difference in energy is a result of the primary wave rather than the secondary wave.

Secondly, the bed shear stress due to the primary waves may increase significantly between the 8,000 TEU and the 12,400 TEU vessels, and likely represents the primary difference in erosion potential due to the widened / deepened channel and concomitant increased vessel size. Thus, for this analysis, bed shear stress was used as a proxy for erosion. This study does not aim to address the level at which the bed shear stress will actively entrain the sediment, but rather focuses on the potential difference in energy in the system as a result of the widened / deepened channel and larger vessel.

Specifically, for the areas of interest the following conclusions can be drawn when comparing the model domain water levels and bed shear stresses between the existing conditions with the 8,000 TEU vessel and the proposed design conditions with a 12,400 TEU vessel or a smaller 2,500 TEU vessel transiting closer to the widened channel edge.

<u>12,400 TEU Vessel (Proposed Channel) vs 8,000 TEU Vessel (Existing Channel)</u>

- Southport
    - Minimal differences occurred in water levels and bed shear stresses for Southport’s shoreline.
    - Increases in water levels and bed shear stresses occurred along the shoreline northeast of Southport.
- Battery Island
    - For inbound transits, minimal differences occurred in the water levels and bed shear stresses with the exception of its northernmost shoreline.
    - For inbound transits there was a decrease in water levels and bed shear stresses along the northernmost shoreline due to the new design track being further from this shoreline.
    - For outbound transits there was a slight increase in bed shear stresses along the southern most coastline of Battery Island.

- Orton Point
    - There was an increase in water levels and bed shear stresses along the shorelines adjacent to the navigation channel.
- "Bird" Islands Adjacent to the Channel
    - A general increase in bed shear stress occurred but was geographically dependent.

<u>2,500 TEU Vessel Proposed Channel vs Existing Channel</u>

- Southport:
    - An increase in the water levels and maximum bed shear stress magnitude occurred along the northeastern coast of Southport due to the more landward vessel track.
    - A slight increase in water levels and minimal to no increase in maximum bed shear stress magnitude occurred along the southern coast of Southport.
- Battery Island:
    - A minimal increase in maximum bed shear stress magnitude occurred along the western coast of Battery Island.
    - A decrease in maximum bed shear stress magnitude occurred along the northern coast of Battery Island where the Idealized and AIS vessel tracks converged.

<u>(2) 12,400 TEU Vessels vs (3) 8,000 TEU Vessels (Equivalent Throughput)</u>

- Southport
    - Minimal differences occurred in water levels and bed shear stresses for Southport's shoreline for inbound transits.
    - Increases in water levels and bed shear stresses occurred along the shoreline northeast of Southport for outbound transits.
- Battery Island
    - Minimal differences occurred in the water levels and bed shear stresses.

- Orton Point
  - Very localized increases in water levels and bed shear stresses along the shorelines adjacent to the navigation channel.
- "Bird" Islands Adjacent to the Channel
  - A significant decrease (Point D) and minimal increase (Point E) in bed shear stress occurred.

9.2.12. Conclusions

Orton Point and the shoreline northeast of Southport remain areas of concern. The modeling results indicate that there will be potential impacts to these areas due to the larger vessels and proposed channel design. Additionally, the frequency of occurrence will increase as the port's capacity grows over the 50 year project life. Therefore, additional more detailed analyses will be performed during the EIS and / or Pre-Construction Engineering and Design (PED) phases of the project to collect field data and document the existing conditions and further quantify impacts. These analyses will then be incorporated into the design of mitigative measures for these two locations.

Minimal or no impacts are expected due to the proposed project to Battery Island or the "Bird" Islands. However, given the concern over previous erosion along these shorelines, additional detailed analyses will also be performed for these areas during the EIS and / or Pre-Construction Engineering and Design (PED) phases of the project to collect field data, document the existing conditions and further quantify impacts. These analyses will then be incorporated into the design of mitigative measures for these two locations, if necessary.

10. References

Arhonditsis, G. B., and M. T. Brett. (2004). Evaluation of the current state of mechanistic aquatic biogeochemical modeling, *Mar. Ecol. Prog. Ser.*, 271, 13–26.

Benoit, M., Frigaard, Peter, and H.A. Schäffer (1997) "Analyzing Multidirectional Wave Spectra", Proceedings of the 27th IAHR Congress, San Francisco, 10–15 August 1997, IAHR Seminar "Multidirectional Waves and their Interaction with Structures", Mansard, Etienne (ed.), Canadian Government Publishing, Benoit.

Birkemeier, W.A. (1985). "Field data on seaward limit of profile change". Journal of Waterway, Port, Coastal and Ocean Engineering 111(3):598–602.

Bowen, J.D., S. Negusse, J.M. Goodman, B. Duclaud, M. Robin, and J. Williams. (2009). Development and use of a three-dimensional water quality model to predict dissolved oxygen concentrations in the lower Cape Fear River Estuary, North Carolina. University of North Carolina at Charlotte.

Brekke, L.D., J.E. Kiang, J.R. Olsen, R.S. Pulwarty, D.A. Raff, D.P. Turnipseed, R.S. Webb, and K.D. White. 2009. Climate change and water resources management – a federal perspective. US Geological Survey Circular 1331, 65 p.

Brutsché, K. E., Rosati, J., Pollock, C. E., and McFall, B. C. (2016). "Calculating depth of closure using WIS hindcast data". ERDC/CHL CHETN-VI-45. Vicksburg, MS: U.S. Army Engineer Research and Development Center.

Bruun, P., (1962). "Sea-level rise as a cause of shore erosion." Journal of Waterway. Harbours Div. 88, 117– 130.

Carr de Betts, E.E. (1999). "An examination of flood tidal deltas at Florida's tidal inlets". M.S. Thesis, Coastal and Oceanographic Eng. Dept., U. of Florida, Gainesville, FL.

Carr de Betts, E.E., and Mehta, A.J. (2001). "An assessment of inlet flood deltas in Florida". Proc. Coastal Dynamics '01, ASCE, 252-262.

Cerco, C.F. and M.R. Noel. (2017). The 2017 Chesapeake Bay Water Quality and Sediment Transport Model. A Report to the US Environmental Protection Agency Chesapeake Bay Program. May 2017 Draft. US Army Engineer Research and Development Center, Vicksburg MS.

Chow, V.T. (1959). "Open-channel hydraulics: New York, McGraw-Hill, 680 p."

de Jong, M.P.C, and D., Reijmerink, S.P., Breederveld, C. Roelvink. (2013). Numerical Modeling of Passing-Ship Effects in Complex Geometries and on Shallow Water. Smart Rivers Conference 2013.

Deltares, (2016). D-Water Quality, versatile water quality modelling in 1D, 2D or 3D systems including physical, (bio)chemical and biological processes, user manual, version 4.99, released for Delft3D Suite 4.02.03, Delft, The Netherlands.

Deltares, (2016a). Delft3D-FLOW User Manual. Deltares 3.15 Ed.

Deltares, (2017). D-Waq DIDO, Interactive grid editor for coupling FLOW with WAQ models, user manual, version 4.00, released for Delft3D Suite 4.02.03, Delft, The Netherlands.

Deltares, (2018). Processes library description, technical reference manual, version 5.01, released for Delft3D FM Suite 2018, D-Hydro Suite 2018, SOBEK Suite 3.7, WAQ Suite 2018, Delft, The Netherlands.

Dial Cordy and Associates Inc. (2017), "Surficial sediment sampling and analysis of the Wilmington Harbor Outer Entrance Channel Extension, Wilmington Harbor Section 203 Improvement Study", Technical Memorandum, September 7, 2017.

Earle, M.D, K.E. Steele, and D.W.C. Wang (1999), "Use of advanced directional wave spectra analysis methods", Ocean Engineering, Volume 26, Issue 12, December 1999, Pages 1421–1434.

Egbert, G., Bennett, A., and Foreman, M. (1994). "TOPEX/Poseidon tides estimated using a global inverse model." *Journal of Geophysical Research*, vol. 99, No C12, pp. 24,821–24,852, 1994.

Frey, A.E. (2016), "Applications of dredging and beach fills in GenCade". ERDC/CHL CHETN-IV-109, Vicksburg, MS: U.S. Army Engineer Research and Development Center.

Frey, A.E., Connell, K.J., Hanson, H., Larson, M., Thomas, R.C., Munger, S., and Zundel, A. (2012a). "GenCade version 1: Model theory and user's guide". ERDC/CHL TR-12-25. Vicksburg, MS: U.S. Army Engineer Research and Development Center.

Frey, A.E., Munger, S., Williams, G.L., Wutkowski, M.J., and Conner, K.B. (2012b), "GenCade application at Onslow Bay, North Carolina". ERDC/CHL CHETN-IV-85, Vicksburg, MS: U.S. Army Engineer Research and Development Center.

Friedman, D., J. Schechter, Sant-Miller, A.M., C. Mueller, G. Villarini, K.D. White, and B. Baker. (2018), US Army Corps of Engineers Nonstationarity Detection Tool User Guide. US Army Corps of Engineers: Washington, DC.

Hallermeier, R. J. (1981). "A profile zonation for seasonal sand beaches from wave climate". Coastal Engineering 4:253–277.

Kraus, N.C. (2008a). "Engineering of tidal inlets and morphologic consequences". U.S. Army Engineer Research and Development Center, Coastal and Hydraulics Laboratory, Vicksburg, MS.

Kraus, N.C. (2008b). “Regional analysis for beach nourishment planning, Brunswick County, North Carolina”. Memorandum for Record, October 8, 2008. U.S. Army Engineer Research and Development Center, Coastal and Hydraulics Laboratory, Vicksburg, MS.

Lesser, G.R., (2009). “An Approach to Medium-term Coastal Morphological Modelling.” PhD Thesis, TU Delft, Delft, Holland.

Limber, P.W., List, J.H., and Warren, J.D. (2004). “Investigating methods of Mean High Water shoreline extraction from Lidar data and the relationship between photo-derived and datum-based shorelines in North Carolina”. North Carolina Division of Coastal Management.

Mallin, M. A., L. Cahoon, M.R. McIver, D.C. Parsons, and G. Shank. (1999). Alternation of Factors Limiting Phytoplankton Production in the Cape Fear River Estuary. Estuaries. 22. 825-836. 10.2307/1353064.

Moffatt & Nichol (2016). “Post hurricane Joaquin shoreline mapping and storm damage assessment”. Prepared for the Town of Oak Island, North Carolina.

Mol A.C.S. (2007), “R&D Kustwaterbouw Reductie Golfrandvoorwaarden OPTI Manual.” Research report H4959.10. WL|Delft Hydraulics, the Netherlands.

National Oceanic and Atmospheric Administration (NOAA) National Centers for Environmental Information https://www.nodc.noaa.gov

National Oceanic and Atmospheric Administration (NOAA) National Data Buoy Center http://www.ndbc.noaa.gov

National Oceanic and Atmospheric Administration (NOAA) Tides & Currents https://tidesandcurrents.noaa.gov

National Research Council’s 1987 report, Responding to Changes in Sea Level: Engineering Implications.

North Carolina Division of Coastal Management (NCDCM), (2012). “North Carolina 2011 Long-Term Average Annual Oceanfront Erosion Rate Update Study, Methods Report.”

North Carolina Ports. (2018). Accessed October 2018. https://ncports.com/.

Offshore and Coastal Technologies Inc. (2008). “Brunswick data compilation, analysis and sediment budget, Phase I”. Prepared for US Army Corps of Engineers, Wilmington District.

Olsen Associates, Inc. (2011). “Bald Head Island, N.C. beach monitoring program, monitoring report No.9 (May 2010 to May 2011)”. Prepared for the Village of Bald Head Island, North Carolina.

Olsen Associates, Inc. (2012). "Calibration of a Delft3D model for Bald Head Island and the Cape Fear River Entrance, Phase I". Prepared for the Village of Bald Head Island, North Carolina.

Olsen Associates, Inc. (2013), "Shoreline stabilization analysis, Bald Head Island, N.C.", prepared for Village of Bald Head Island, July 2013.

Olsen Associates, Inc. (2015). "Bald Head Island, N.C. beach monitoring program, monitoring report No.13 (May 2014 to April 2015)". Prepared for the Village of Bald Head Island, North Carolina.

Olsen Associates, Inc. (2016). "Bald Head Island, N.C. beach monitoring program, monitoring report No.14 (April 2015 to April 2016)". Prepared for the Village of Bald Head Island, North Carolina.

Olsen Associates, Inc. (2017), "Bald Head Island, N.C. beach monitoring program, monitoring report No.15 (April 2016 to May 2017)", prepared for Village of Bald Head Island, July 2017.

Olsen Associates, Inc. (2018), "Bald Head Island, N.C. beach monitoring program, monitoring report No.16 (May 2017 to May 2018)", prepared for Village of Bald Head Island, July 2018.

Permanent International Association of Navigation Congress (PIANC). (1987). Guidelines for the Design and Construction of Flexible Revetments Incorporating Geotextiles for Inland Waterways. Supplement to Bulletin No.57, Report of Working Group 4 of the Permanent Technical Committee I.

Rijn, L. C. van, J. A. Roelvink and W. T. Horst, (2012), "Approximation formulae for sand transport by currents and waves and implementation in DELFT-MOR", Tech. Rep. Z3054.40, WL|Delft Hydraulics, Delft, The Netherlands.

Roelvink, Dano, Ap van Dongeren, Robert McCall, Bas Hoonhout, Arnold van Rooijen, Pieter van Geer, Lodewijk de Vet, Kees Nederhoff, and Ellen Quataert. (2015). XBeach Technical Reference: Kingsday Release. Deltares.

Schiereck, Gerrit J. (2004). Introduction to Bed, Bank and Shore Protection. London: Spon Press.

Simmons, C.E. (1993). "Sediment Characteristics of North Carolina Streams, 1970-79"

Sorensen, R.M. (1997). "Prediction of Vessel-Generated Waves with Reference to Vessels Common to the Upper Mississippi River System." Prepared for US Army Corps of Engineers.

Thompson, E.F., Lin L., and Jones, D.L. (1999). "Wave climate and littoral sediment transport potential, Cape Fear River Entrance and Smith Island to Ocean Isle Beach, North

Carolina". Technical Report CHL-99-18, Vicksburg, MS: U.S. Army Engineer Research and Development Center.

U.S. Army Corps of Engineers, and Land Management Group, Inc. (2014), "Village Bald Head Island shoreline project, final environmental impact statement", August 2014.

United States Army Corps of Engineers (USACE) guidance ER 1100-2-8162, Incorporating Sea Level Changes in Civil Works Programs,

United States Army Corps of Engineers (USACE). (2007). "Wilmington Harbor Cape Fear River, NC, Dredged Material Management Plan, Alternative Formulation Briefing, Preconference Materials." US Army Corps of Engineers, Wilmington District

United States Army Corps of Engineers (USACE). (2014). "Wilmington Harbor Navigation Improvements Feasibility Report and Environmental Assessment." US Army Corps of Engineers, Wilmington District.

United States Geological Survey (USGS) https://waterdata.usgs.gov

United States Geological Survey (USGS) StreamStats https://streamstats.usgs.gov/ss/

USACE (2000), "Wilmington Harbor Sand Management Plan, Ocean Entrance Channels and Inner Harbor from Snows Marsh through Horseshoe Shoal Channels", U.S. Army Corps of Engineers, Wilmington District Document, February 2000.

USACE (2010). "Physical Monitoring Wilmington Harbor Navigation Project, Report 7: October 2008 – September 2009". US Army Corps of Engineers, Wilmington District.

USACE (2011), "Draft reevaluation report – sand management plan Wilmington Harbor Navigation Project", U.S. Army Corps of Engineers, Wilmington District, January 2011.

USACE (2012), "Draft integrated general reevaluation report and environmental impact statement, coastal storm damage reduction, Brunswick County beaches, North Carolina", U.S. Army Corps of Engineers, Wilmington District, October 2012.

USACE (2012a). "Storm damage reduction Carolina Beach and Kure Beach, maintenance dredging Wilmington Harbor Inner Ocean Bar, New Hanover and Brunswick Counties, North Carolina". IFB No. W912PM-12-B-011. US Army Corps of Engineers, Wilmington District.

USACE (2013). "Physical Monitoring Wilmington Harbor Navigation Project, Report 9: October 2010 – September 2012". US Army Corps of Engineers, Wilmington District.

USACE (2015). Recent US Climate Change and Hydrology Literature Applicable to US Army Corps of Engineers Missions - South Atlantic-Gulf Region 3. Civil Works Technical Report CWTS 2015-03, USACE, Washington, DC.

USACE (2019a). Climate Hydrology Assessment Tool. http://corpsmapu.usace.army.mil/cm_apex/f?p=313:2:0::NO. Accessed online September 6, 2019.

USACE (2019b). Nonstationarity Detection Tool http://corpsmapu.usace.army.mil/cm_apex/f?p=257:2:0::NO:::. Accessed online September 6, 2019.

USACE Surv & Map http://navigation.usace.army.mil/Survey/

USACE, Sea-Level Change Curve Calculator (Version 2017.55) http://corpsmapu.usace.army.mil/rccinfo/slc/slcc_calc.html

USEPA (Environmental Protection Agency). 2013 Watershed modeling to assess the sensitivity of streamflow, nutrient, and sediment loads to potential climate change and urban development in 20 U.S. watersheds. National Center for Environmental Assessment, Washington, DC; EPA/600/R-12/058F.

USGCRP (Global Climate Research Program), 2018: Impacts, Risks, and Adaptation in the United States: Fourth National Climate Assessment, Volume II: Report-in-Brief [Reidmiller, D.R., C.W. Avery, D.R. Easterling, K.E. Kunkel, K.L.M. Lewis, T.K. Maycock, and B.C. Stewart (eds.)]. U.S. Global Change Research Program, Washington, DC, USA, 186 pp.

Verhey, H.J. and Bogaerts, M.P. (1989). "Ship Waves and the Stability of Armour Layers Protecting Slopes." Publication No. 428.

Walton, T.L., and Adams, W.D. (1976). "Capacity of inlet outer bars to store sand". Proceedings of the 15th Coastal Engineering Conference, ASCE, pp1919-1937.

Weather Underground https://www.wunderground.com

Willmott, C.J. "Some comments on the evaluation of model performance." Bulletin American Meteorological Society 63.11 (1982): 1309-1313.

Willmott, C.J., Ackleson, S.G., Davis, R.E., Feddema, J.J., Klink, K.M., Legates, D.R., O'Donnell, J., and Rowe, C.M. "Statistics for the evaluation and comparison of models." Journal of Geophysical Research 90.C5 (1985): 8995-9005.

WL | Delft Hydraulics. (2014). Hydro-Morphodynamics Flow Model User Manual.

Zhou, Minggui, Dano Roelvink, Henk Verheij, and Han. Ligteringen. (2013). Study of Passing Ship Effects along a Bank by Delft3D-FLOW and XBeach. Delft, The Netherlands: International Workshop on Next Generation Nautical Traffic Models 2013.

Zhou, Minggui, Zaojian Zou, and Dano Roelvink. (2014). Prediction of Ship-Ship Interactions in Ports by a Non-Hydrostatic Model. Journal of Hydrodynamics.